STUDIES OF HEXAARYL[3]RADIALENE LIGANDS: SYNTHESIS, COORDINATION CHEMISTRY AND ANION INTERACTIONS

A thesis
submitted in fulfilment
of the requirements for the degree
of
Doctor of Philosophy in Chemistry
in the
School of Chemistry and Physics
in the
University of Adelaide
by

Courtney A. Hollis

THE UNIVERSITY of ADELAIDE

Adelaide
Australia
2013

Declaration

This thesis contains no material which has been accepted for the award of any other degree or diploma in any university or other tertiary institution and, to the best of my knowledge and belief, contains no material previously published or written by another person, except where due reference has been made in the text. In addition, I certify that no part of this work will, in the future, be used in a submission for any other degree or diploma in any university or other tertiary institution without the prior approval of the University of Adelaide and where applicable, any partner institution responsible for the joint-award of this degree.

I give consent to this copy of my thesis, when deposited in the University Library, being made available for loan and photocopying, subject to the provisions of the Copyright Act 1968. I also give permission for the digital version of my thesis to be made available on the web, via the University's digital research repository, the Library catalogue and also through web search engines, unless permission has been granted by the University to restrict access for a period of time.

Courtney A. Hollis
18th June 2013

Acknowledgements

First and foremost I wish to thank my supervisor, Assoc. Prof. Chris Sumby, for sharing his wealth of knowledge and providing much appreciated guidance throughout the past four years. This thesis would not have eventuated without his encouragement and support.

I would also like to thank Dr Antonio Avellaneda for his skilful synthetic work in the development of the synthesis of hexakis(3,4-dicyanophenyl)[3]radialene. Thanks also to Jack Evans and Alex Gentleman for their computational study of the anion interactions of hexaaaryl[3]radialenes. I would like to express my gratitude to Prof. Stuart Batten and Prof. Michaele Hardie for their assistance in the determination of complex structure topologies. Thanks also to Prof. Richard Keene for helpful discussions and excellent advice. Dr Sandra Hack is acknowledged for her expertise in the operation of the Orbitrap mass spectrometer. I also wish to thank Phil Clements and Gino Farese for the maintenance of the many instruments which were used throughout this study.

To the past and present members of the Sumby group: Rachel, Maisara, Marie, Herbert, Wit, Jenny, Damien, Necky, Steph, Antonio, Jack, Jesse, Michael, Jason, Tony, Alex, Pete and Cam; thanks for all the good times shared within the lab and without.

Lastly, I wish to thank my Mum, without whose love and support this thesis would not have become a reality, and to my dear friends, Anton, Jade and Claire, who have travelled this long and winding road by my side, I look forward to graduating with you in September!

Table of Contents

Abbreviations

$\sum_{vdw}$	sum of the van der Waals radii
bpy	4,4’-bipyridine
n-BuLi	n-butyllithium
Cp	cyclopentadiene
Cp*	pentamethyl-cyclopentadiene
CSD	Cambridge Structural Database
DCM	dichloromethane
DFT	density functional theory
dppe	1,2-bis(diphenylphosphino)ethane
DMF	N,N’-dimethylformamide
DMSO	dimethylsulfoxide
EI-MS	electron impact mass spectroscopy
en	1,2-ethylenediamine
ESI-HRMS	electrospray ionisation high resolution mass spectrometry
ESI-MS	electrospray ionisation mass spectrometry
EtOAc	ethyl acetate
EtOH	ethanol
h	hour/s
HAT	1,4,5,8,9,12-hexaazatriphenylene
HOMO	highest occupied molecular orbital
IR	infrared
LUMO	lowest unoccupied molecular orbital
M	molar
MeOH	methanol
min	minutes
NCE	normalised collision energy
NDI	napthalenediimide
NMR	nuclear magnetic resonance
ppm	parts per million
Q_{zz}	quadropole moment along the z-axis
RCSR	Reticular Chemistry Structure Resource
tccp	tetrachlorocyclopropene
TEBB	1,3,5-tris(4-ethynylbenzonitrile)benzene
THF	tetrahydrofuran
TLC	thin layer chromatography
UV-Vis	ultra violet-visible

Abstract

This thesis describes the synthesis and study of three nitrile substituted hexaaaryl[3]radialene ligands, two of which are new compounds, and three new flexible bis-pyridyl ligands produced as precursors in the attempted synthesis of extended hexaaryl[3]radialenes. The coordination and metallo-supramolecular chemistry of these compounds were investigated with a variety of different metal atoms, primarily silver(I) and copper(I) due to the nature of the soft nitrile donors. Five different coordination modes were observed for hexakis(4-cyanophenyl)[3]radialene with silver(I) and copper(I) including bidentate, tetradentate, and also the first example of this compound acting as a hexadentate ligand. The flexible bis-pyridyl ligands were observed to form predominantly 1-D coordination polymers but also on occasion led to the production of 2-D networks.

Mononuclear ruthenium(II) complexes of hexakis(4-cyanophenyl)[3]radialene and hexakis(3-cyanophenyl)[3]radialene are also described, although di- and tri-nuclear complexes were unable to be obtained and thus the nature of any metal-metal interactions within such complexes were unable to be examined. Visible absorption and fluorescence spectroscopy, as well as cyclic voltammetry, were used to examine the properties of the mononuclear radialene complexes as well as dinuclear ruthenium(II) complexes of the [3]radialene precursors 4,4'-dicyanodiphenylmethane and 3,3'-dicyanodiphenylmethane.

Close contacts between anions and the [3]radialene core were first observed in solid-state structures of hexakis(4-cyanophenyl)[3]radialene and silver(I). In order to determine whether these interactions were predominately due to anion-hydrogen bonding, or whether anion-π interactions with the [3]radialene core were also involved, a three pronged study involving computational, mass spectrometric, and X-ray crystallographic techniques was undertaken. The combined evidence from each of these methods provides a strong case for the existence of anion-π interactions between anions and the [3]radialene core in both the gas phase and the solid-state.

In conjunction with infrared spectroscopy and elemental analysis, X-ray crystallography was used to characterise the majority of metal complexes and coordination polymers produced during the course of this work. The crystal structures of six precursor compounds or ligands and 25 complexes are described.

Chapter 1

Introduction

Chapter 1

1. Introduction

1.1. Background

The synthesis of the first coordination complex, $[Co(NH_3)_6]Cl_3$, is credited to the 18th century French chemist Tassaert (Figure 1.1 (a)).[1] Even though Prussian Blue, $Fe_4[Fe(CN)_6]_3$, was reported beforehand in 1704 by Diesbach, Tassaert's 1798 discovery was the first time that it was realised that such compounds belonged to a new class. Throughout the following century many other examples of coordination complexes were prepared; however it was not until 1893 and the advent of Alfred Werner's famous *Coordination Theory* that a satisfactory rationale for the formation and identity of such compounds was proposed.[2,3]

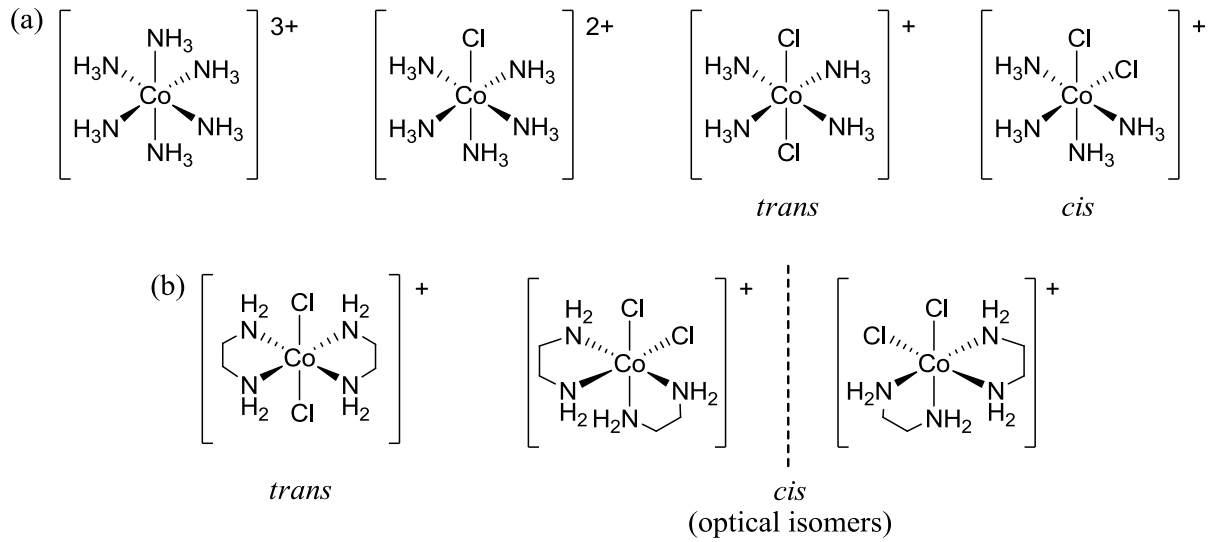

Figure 1.1. The cobalt(III) complexes studied by Alfred Werner.

Based on a series of careful conductivity measurements made on the cobalt(III) complexes $[Co(NH_3)_6]Cl_3$, $[CoCl(NH_3)_5]Cl_2$ and $[CoCl_2(NH_3)_4]Cl$ (Figure 1.1 (a)) Werner proposed an octahedral arrangement of ligands around the cobalt(III) metal centre which also agreed with the experimental observation of two isomers for $[CoCl_2(NH_3)_4]Cl$ (the *cis*-isomer is green and the *trans*-isomer is violet). To further support his theory Werner went on to separate the optical isomers of *cis*-$[CoCl_2(en)_2]Cl$ and measure their specific rotation (Figure 1.1 (b)). In 1913 Werner was awarded the Nobel Prize for his groundbreaking work in coordination chemistry.

In the century since, coordination chemistry has developed from its inorganic roots to include complicated multidentate organic ligands that has allowed the extension of simple complexes into discrete metallo-supramolecular structures and infinite coordination polymers. These structures are based around the metal-ligand coordinate bond but also utilise an array of other weak intermolecular interactions, commonly used in the cognate field of supramolecular chemistry, to promote the self-assembly of pre-organised components into metallo-supramolecular structures. The types of ligands utilised in this area, which combines traditional coordination chemistry with supramolecular chemistry to become the new field known as metallo-supramolecular chemistry, include nitrogen-containg heterocycles, carboxylates and nitriles. These ligands often possess extended conjugated π-systems which can allow for interaction to occur between adjacent metal centres. Conversely, the inclusion of ligands with alternative modes of π-electron communication, such as cross-conjugation or omniconjugation, in metallo-supramolecular assemblies has not been studied as extensively.

1.2. Cross Conjugation and the Chemistry of Radialenes

Conjugated organic compounds, the most common of which are carbon-rich frameworks with linearly conjugated π-systems and cyclic aromatic structures, have been widely studied due to their optical and electronic properties.[4,5] Alternative modes of π-electron communication, such as cross-conjugation and omniconjugation,[6] have been studied to a lesser extent but these systems also exhibit interesting properties. Cross-conjugated compounds by definition "contain three unsaturated groups, two of which though conjugated to a third unsaturated centre are not conjugated to each other".[7,8] Some examples of cross-conjugated systems include the acyclic dendralene compounds[9-11] and their cyclic analogues the radialenes,[12-15] as well as fulvalenes,[16-18] quinones,[19,20] and fused aromatics[21,22] (Figure 1.2).

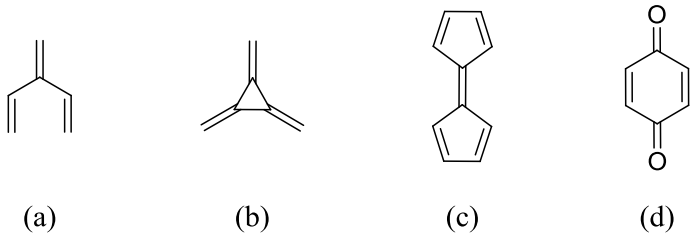

Figure 1.2. The parent structures: (a) [3]dendralene, (b) [3]radialene, (c) pentafulvalene and (d) 1,4-benzoquinone of various cross-conjugated systems.

Radialenes are cyclic cross-conjugated polyenes which exhibit the general formula $C_{2n}H_{2n}$ and contain *n* ring atoms and *n* exocyclic double bonds.[15] A historical perspective on the synthesis of the parent members of the radialene family, the smallest of which being [3]radialene (Figure 1.2 (b)), is given in Chapter 2 (section 2.1.1). One limiting factor in the study of the parent radialenes is their inherent instability with polymerisation upon exposure to air being a common problem.[23-25] To combat this, focus was shifted to derivatives of the parent species, in particular [3]radialenes containing aryl and heteroaryl moieties, due to their increased stability.

Hexaaryl[3]radialenes, first reported by Oda in 1997,[14] could be accessed via the reaction of stabilised carbanions with tetrachlorocyclopropene based on the work of Fukunaga.[26,27] A detailed examination of the synthetic method is given in Chapter 2 (section 2.1.2). Interestingly, the basic hexaphenyl[3]radialene (**1.1**) was unable to be synthesised using this technique and instead had to be accessed via lithiation and subsequent protonation of its derivative hexakis(4-iodophenyl)[3]radialene (**1.2**).[14] Compound **1.2** was able to be synthesised via the general procedure of Fukunaga. These developments were closely followed by the synthesis of the first hexaheteroaryl[3]radialenes including hexa(2-pyridyl)[3]radialene (**1.3**) and hexa(4-pyridyl)[3]radialene (**1.4**).[28-30]

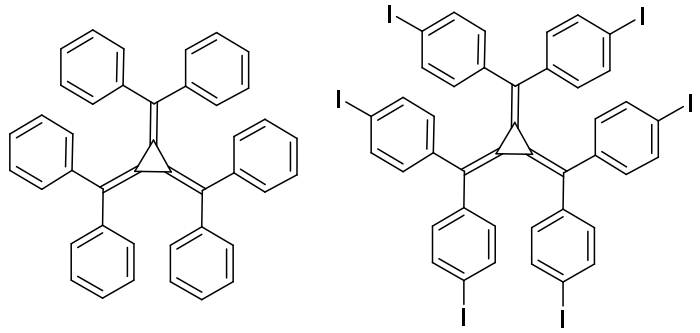

1.1 **1.2**

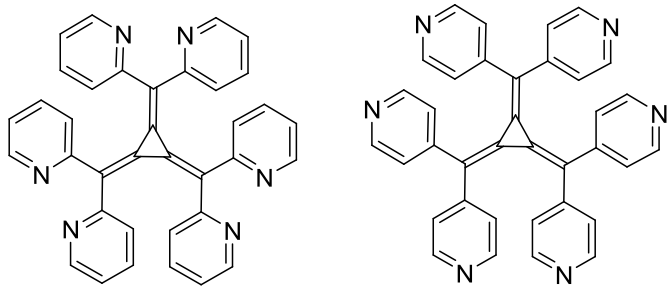

1.3 **1.4**

Figure 1.3. The [3]radialenes: hexaphenyl[3]radialene (**1.1**), hexakis(4-iodophenyl)[3]-radialene (**1.2**), hexa(2-pyridyl)[3]radialene (**1.3**), and hexa(4-pyridyl)[3]radialene (**1.4**).

Hexaaryl- and hexaheteroaryl[3]radialenes make interesting ligands for incorporation into metallo-supramolecular assemblies for a number of reasons. Firstly, these compounds adopt a propeller conformation in solution and in the solid-state which provides a scaffold with a degree of pre-organisation for the formation of extended structures.[12,14,28,29,31,32] Secondly, they have interesting photophysical properties including an intrinsic fluorescence and exhibit large Stokes shifts of approximately 130 nm.[32,33] Finally, most derivatives of **1.1** are electron deficient and have been shown to undergo two stepwise reductions to form the radical anion and the dianion respectively.[30] Despite this, the literature currently contains very few examples of hexaaryl- and hexaheteroaryl[3]radialene derivatives involved in metallo-supramolecular assemblies.[12,28,29,31,34]

1.3. Metallo-supramolecular Chemistry

Traditional synthetic chemistry is based on the formation of covalent bonds between atoms to produce larger molecular structures. Due to the strength of these covalent bonds their formation is generally irreversible and as such a conventional synthetic reaction, unless specifically controlled, can produce numerous by-products which require intensive purification. Supramolecular chemistry, drawing on nature for inspiration, involves the combination of preformed components via weaker intermolecular interactions.[35,36] The components are designed so that there is steric and electronic complementarity between their binding sites.[37] This promotes spontaneous self-organisation and the assembly of the components into a single structure via molecular recognition processes. As the intermolecular forces which drive assembly are primarily non-covalent, and therefore reversible, the lowest energy structure is formed in accordance with the principles of thermodynamics. This inherent reversibility allows error correction and reorganisation of the system upon environmental change.

The intermolecular forces commonly utilised in supramolecular chemistry include hydrogen bonds, halogen bonding, electrostatic interactions, π-stacking interactions, van der Waals forces, and hydrophobic or hydrophilic effects. Hydrogen bonding interactions occur between a proton donor bonded to an electronegative atom or electron deficient atom (D-H) and another such acceptor atom (A). Figure 1.4 (a) provides a general representation of a hydrogen bond between such atoms which usually range in strength from 5-50 kJ.mol^{-1}.[38-40] Weak hydrogen bonds, typically observed in supramolecular assemblies, exhibit D-H···A bond lengths (represented by *d* in Figure 1.4 (a)) of 2.2-3.2 Å and D-H···A bond angles of 90-150°. Various hydrogen bonding arrangements are also depicted in Figure 1.4; the most common being a linear arrangement with a D-H···A bond angle of approximately 180°

(Figure 1.4 (b)). A three centre arrangement with one hydrogen atom interacting with two acceptor atoms (Figure 1.4 (c)) can also be observed, whilst a third situation with one acceptor atom interacting with two donor hydrogen atoms (Figure 1.4 (d)) occurs less frequently.[40]

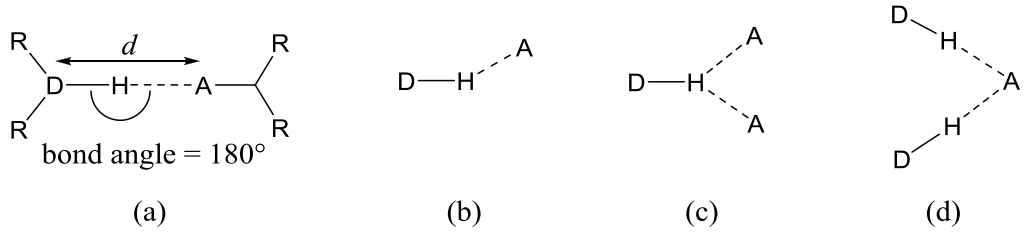

Figure 1.4. (a) A general representation of a hydrogen bonding interaction where D is the donor atom and A is the acceptor atom and different hydrogen bonding arrangements: (b) approximately linear, (c) donating bifurcated and (d) accepting bifurcated.

Weak interactions between the π-systems of aromatic rings are also often observed in supramolecular assemblies. These π-π interactions are primarily electrostatic in nature and typically range in strength from 1-5 kJ.mol^{-1}.[41-43] π-π Interactions occur between two aryl rings which are slip stacked, i.e. parallel displaced, with an angle between the ring normal and the vector between the ring centroids of approximately 20° (Figure 1.5 (a)). Within this arrangement the distance between the ring centroids can range from 3.3 to 3.8 Å for a significant interaction.[43] A second conformation, which is better described as a C-H···π interaction, involves an edge-to-face arrangement of two aryl rings (Figure 1.5 (b)). A C-H···π interaction is classified as significant if it exhibits a hydrogen atom to ring centroid distance between 2.5 and 3.4 Å.[44-46]

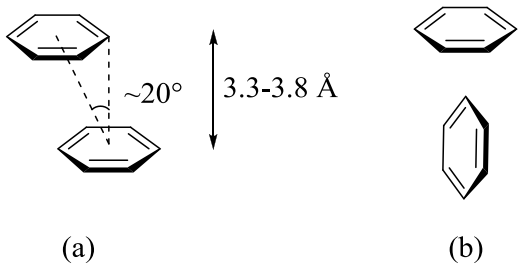

Figure 1.5. (a) Parallel displaced π-stacking with a ring centroid-centroid distance ranging from 3.3 to 3.8 Å. (b) An edge-to-face C-H···π interaction.

Metallo-supramolecular chemistry utilises the intermolecular interactions described above in conjunction with metal-ligand coordinate bonds.[47-49] These bonds occur between metal ions

and donor groups in organic molecules (ligands) such as nitrogen-containing heterocycles, carboxylates and nitriles. Together with the other non-covalent interactions previously mentioned, these metal-ligand coordinate bonds are used to promote the self-assembly of preformed components into discrete or infinite metallo-supramolecular structures. In the context of infinite polymeric structures metal-ligand coordinate bonds can be considered as intermolecular interactions.[47]

Metal-ligand coordinate bonds vary in strength from the equivalent of a hydrogen bond through to that of a weak covalent bond depending upon the identity of the metal and organic ligand donor group involved in the interaction. The majority of these interactions are reversible or labile, which allows for a degree of error correction, therefore the most stable product is often formed, generally in high yields. The diversity of possible structure topologies is virtually endless as metal ions can adopt a wide variety of geometries including, but not limited to, linear, trigonal planar, tetrahedral, square planar, trigonal bipyramidal and octahedral. The rational design of organic bridging ligands can also greatly affect the complexity of the final structure by changing the number and identity of the donor groups, the separation and angle between the donor groups and the flexibility or rigidity of the ligand itself.

1.4. Discrete Complexes versus Coordination Polymers

The type of metallo-supramolecular structure formed upon self-assembly depends on both the geometry of the metal and the coordinating moieties of the ligand. Divergent components favour infinite polymeric structures whereas convergent components favour discrete assemblies. Certain metal ions are also predisposed to forming one type of structure over another with particularly labile transition metals, such as silver(I) and copper(I), more likely to form polymeric structures and more inert metals, such as palladium(II) and ruthenium(II), being able to be tailored towards discrete complexes through the use of capping ancillary ligands.

The donor sites of palladium(II) and ruthenium(II) can be pre-organised via the use of ancillary ligands, which are difficult to displace. The geometry of palladium(II) is primarily square planar and two monodentate ligands or one chelating ligand can be used to fix the arrangement of its free binding sites to a *trans* or *cis* conformation respectively (Figure 1.6 (a)). The *cis* arrangement, where the ancillary ligand is ethylenediamine, was used by Fujita in the formation of a seminal molecular square structure, which uses 4,4’-bipyridine as the bridging ligand.[50,51] Ruthenium(II), which has an octahedral geometry, can also be tailored towards a *cis*-bidentate arrangement of free biding sites as well as meridonial (*mer*) and facial

(*fac*) tripodal conformations as seen in Figure 1.6 (b). Ruthenium(II) was employed in this project and thus ruthenium(II) complexes, particularly those involving a bridging ligand, are further discussed in Chapter 3 (section 3.1.1).

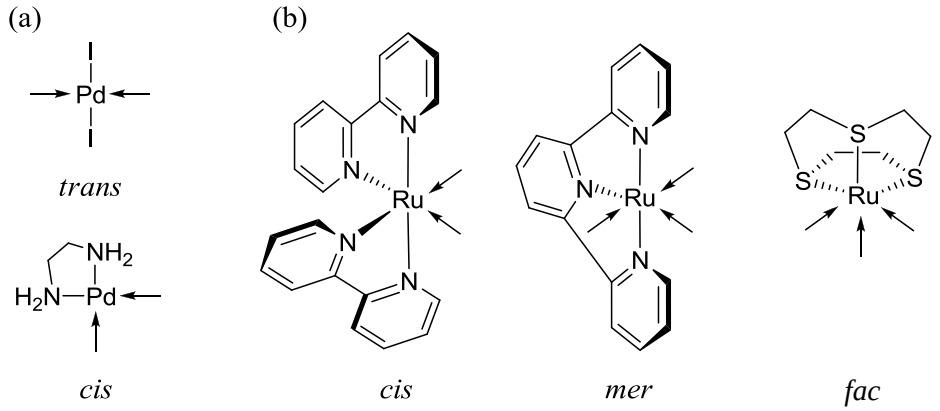

Figure 1.6. Examples of the use of ancillary ligands and anions to control the geometry of the transition metals (a) palladium(II) and (b) ruthenium(II).

Silver(I) and copper(I) are labile transition metals, which can adopt a variety of geometries, and as such are often incorporated into coordination polymers. Silver(I) is a d^{10} transition metal and although it is most comfortable in two-coordinate (linear or bent) and three-coordinate (trigonal planar or T-shaped) geometries, it has also been observed in four-coordinate (tetrahedral or square planar) and six-coordinate (octahedral) conformations.[52-55] Copper(I) is less versatile than silver(I) and prefers four coordinate (tetrahedral) geometries.[56] Both of these metal ions are widely used in this study for the production of coordination polymers, which are further discussed in Chapter 4 (section 4.1.1).

1.5. Applications of Discrete and Infinite Metallo-supramolecular Assemblies

Discrete, multinuclear ruthenium complexes have been shown to exhibit metal-metal interactions when connected by a ligand or ligands which possess conjugated π-systems. Such complexes also possess interesting electrochemical, photophysical and magnetic properties, which could be utilised in the formation of molecular devices capable of such functions as molecular switching, information storage and solar energy conversion.[57-60] Multinuclear ruthenium complexes bridged by cross-conjugated ligands may exhibit a facile interaction between two metal centres through the linearly conjugated segment of the π-system but not with a third due to cross-conjugation. This may furnish complexes with interesting electronic properties.

Coordination polymers, including the subset of materials called metal-organic frameworks, are widely studied as new materials which, depending upon their substituent parts, exhibit interesting physical properties that could be utilised for application in catalysis, conductivity, luminescence and magnetism.[61-64] Another property of such materials is permanent porosity which could be directed towards the storage of gasses as fuels or the separation of greenhouse gasses from large point sources.[62] Metal-organic frameworks which possess permanent porosity are generally rigid structures, however flexible ligands have been utilised in these compounds due to their potential for gated absorption.[65-68] The flexible ligands described in Chapter 6 could potentially be targeted towards such applications.

As previously mentioned, only a few metallo-supramolecular assemblies involving hexaaryl- and hexaheteroaryl[3]radialenes have been reported in the literature; however within the majority of these structures close contacts with anions have been observed with the [3]radialene core.[28,29,31] These potential anion-π interactions, which are further discussed in Chapter 5 (section 5.1.1), may aid in the development of discrete metallo-supramolecular cages, composed of two hexaaryl[3]radialene ligands and three or six metal ions, as anion sensors.

1.6. Thesis Coverage

This thesis presents the study of three hexaaryl[3]radialene ligands with a particular focus on both their coordination chemistry and the fundamentals of their interactions with anions. As the thesis presents diverse aspects of radialene chemistry, each chapter is commenced with a brief introduction. Chapter 2 reports the synthesis and study of known and new hexaaryl[3]radialenes with nitrile substituents. Also several attempts at producing extended hexaaryl[3]radialene structures are described. The physical properties of these compounds were examined via cyclic voltammetry, UV-visible and fluorescence spectroscopy, and X-ray crystallography.

Chapter 3 examines the formation of discrete metal ligand complexes of the nitrile substituted hexaaryl[3]radialenes with ruthenium(II); the aim being to produce multinuclear complexes and examine any metal-metal communication, or lack thereof, due to the cross-conjugated π-system of the [3]radialene ligands. The isolation of multinuclear compounds with nitrile-substituted hexaaryl[3]radialenes was challenged by the formation of intractable mixtures. Chapter 4 presents further study into the coordination chemistry of these radialenes, in particular the formation of coordination polymers observed upon reaction of radialenes with silver(I) and copper(I) salts. It was within such structures that close contacts between charge balancing anions and the [3]radialene core were first observed.[28,29,31] Taking into

account the electron deficiency of the core, it was proposed that the radialenes could be exhibiting anion-π interactions.

Chapter 5 investigates whether the close [3]radialene core-anion contacts seen in the coordination polymers are in fact true anion-π interactions. This study includes the analysis of further solid-state structures of hexaaryl[3]radialenes, coupled with computational modelling of such radialenes with various anions and observation of anion-radialene complexes in the gas phase via mass spectrometry. Finally, chapter 6 presents coordination polymers of the flexible bidentate ligands bis(4-(pyridin-2-ylethynyl)phenyl)methane, bis(4-(pyridin-3-ylethynyl)phenyl)-methane and bis(4-(pyridin-4-yl)phenyl)methane; precursors produced in the attempted synthesis of extended [3]radialenes.

1.7. References

1 J. R. Gispert, *Coordination Chemistry*, Wiley-WCH, Weinheim, 2008.

2 A. Werner, *Anorg. Chem.*, **1893**, *3*, 267.

3 A. Werner, *Ber.*, **1914**, *47*, 3087.

4 H. Meier, *Angew. Chem. Int. Ed.*, **2005**, *44*, 2482.

5 R. E. Martin and F. Diederich, *Angew. Chem. Int. Ed.*, **1999**, *38*, 1350.

6 M. H. van der Veen, M. T. Rispens, H. T. Jonkman, and J. C. Hummelen, *Adv. Funct. Mater.*, **2004**, *14*, 215.

7 N. F. Phelan and M. Orchin, *J. Chem. Educ.*, **1968**, *45*, 633.

8 M. Gholami and R. R. Tykwinski, *Chem. Rev.*, **2006**, *106*, 4997.

9 H. Hopf, *Angew. Chem. Int. Ed.*, **2001**, *40*, 705.

10 S. Fielder, D. D. Rowan, and M. S. Sherburn, *Angew. Chem. Int. Ed.*, **2000**, *39*, 4331.

11 H. Hopf, *Angew. Chem. Int. Ed. Engl.*, **1984**, *23*, 948.

12 P. J. Steel and C. J. Sumby, *Inorg. Chem. Commun.*, **2002**, *5*, 323.

13 T. Enomoto, N. Nishigaki, H. Kurata, T. Kawase, and M. Oda, *Bull. Chem. Soc. Jpn.*, **2000**, *73*, 2109.

14 T. Enomoto, T. Kawase, H. Kurata, and M. Oda, *Tetrahedron Lett.*, **1997**, *38*, 2693.

15 H. Hopf and G. Maas, *Angew. Chem. Int. Ed. Engl.*, **1992**, *31*, 931.

16 B. Halton, *Eur. J. Org. Chem.*, **2005**, *2005*, 3391.

17 M. Iyoda, M. Hasegawa, and Y. Miyake, *Chem. Rev.*, **2004**, *104*, 5085.

18 A. Gorgues, P. Hudhomme, and M. Sallé, *Chem. Rev.*, **2004**, *104*, 5151.

19 C. G. Pierpont, *Coord. Chem. Rev.*, **2001**, *216–217*, 99.

20 C. G. Pierpont, *Coord. Chem. Rev.*, **2001**, *219–221*, 415.

21 N. Kobayashi and T. Fukuda, *J. Am. Chem. Soc.*, **2002**, *124*, 8021.

22 I. Y. Bagryanskaya, Y. V. Gatilov, A. M. Maksimov, V. E. Platonov, and A. V. Zibarev, *J. Fluorine Chem.*, **2005**, *126*, 1281.

23 G. W. Griffin and L. I. Peterson, *J. Am. Chem. Soc.*, **1963**, *85*, 2268.

24 E. A. Dorko, *J. Am. Chem. Soc.*, **1965**, *87*, 5518.

25 P. Schiess and M. Heitzmann, *Helv. Chim. Acta*, **1978**, *61*, 844.

26 T. Fukunaga, *J. Am. Chem. Soc.*, **1976**, *98*, 610.

27 T. Fukunaga, M. D. Gordon, and P. J. Krusic, *J. Am. Chem. Soc.*, **1976**, *98*, 611.

28 P. J. Steel and C. J. Sumby, *Chem. Commun.*, **2002**, 322.

29 K. Matsumoto, Y. Harada, N. Yamada, H. Kurata, T. Kawase, and M. Oda, *Cryst. Growth Des.*, **2006**, *6*, 1083.

30 K. Matsumoto, Y. Harada, T. Kawase, and M. Oda, *Chem. Commun.*, **2002**, 324.

31 C. A. Hollis, L. R. Hanton, J. C. Morris, and C. J. Sumby, *Cryst. Growth Des.*, **2009**, *9*, 2911.

32 A. Avellaneda, C. A. Hollis, X. He, and C. J. Sumby, *Beil. J. Org. Chem.*, **2012**, *8*, 71.

33 M. Iyoda, N. Nakamura, M. Todaka, S. Ohtsu, K. Hara, Y. Kuwatani, M. Yoshida, H. Matsuyama, M. Sugita, H. Tachibana, and H. Inoue, *Tetrahedron Lett.*, **2000**, *41*, 7059.

34 D. M. D'Alessandro, F. R. Keene, P. J. Steel, and C. J. Sumby, *Aust. J. Chem.*, **2003**, *56*, 657.

35 J.-M. Lehn, *Supramolecular Chemistry*, Wiley VCH, Weinheim, 1995.

36 J. W. Steed and J. L. Atwood, *Supramolecular Chemistry*, John Wiley & Sons Ltd, New York, 2000.

37 J.-M. Lehn, *Proc. Nat. Acad. Sci.*, **2002**, *99*, 4763.

38 G. R. Desiraju, *Acc. Chem. Res.*, **2002**, *35*, 565.

39 G. R. Desiraju, *Acc. Chem. Res.*, **1996**, *29*, 441.

40 T. Steiner, *Angew. Chem. Int. Ed.*, **2002**, *41*, 48.

41 C. A. Hunter, K. R. Lawson, J. Perkins, and C. J. Urch, *J. Chem. Soc., Perkin Trans. 2*, **2001**, *0*, 651.

42 C. A. Hunter and J. K. M. Sanders, *J. Am. Chem. Soc.*, **1990**, *112*, 5525.

43 C. Janiak, *J. Chem. Soc., Dalton Trans.*, **2000**, 3885.

44 T. Steiner, E. B. Starikov, A. M. Amado, and J. J. C. Teixeira-Dias, *J. Chem. Soc., Perkin Trans. 2*, **1995**, *0*, 1321.

45 N. N. L. Madhavi, G. R. Desiraju, A. K. Katz, H. L. Carrell, and A. Nangia, *Chem. Commun.*, **1997**, *0*, 1953.

46 C. Janiak, S. Temizdemir, S. Dechert, W. Deck, F. Girgsdies, J. Heinze, Mario J. Kolm, Tobias G. Scharmann, and Oliver M. Zipffel, *Eur. J. Inorg. Chem.*, **2000**, *2000*, 1229.

47 E. C. Constable, *Chem. Ind. (London)*, **1994**, 56.

48 P. J. Steel, *Chemistry in NZ*, **2003**, *67*, 57.

49 P. J. Steel, *Chemistry in NZ*, **2011**, *75*, 194.

50 M. Fujita, J. Yazaki, and K. Ogura, *J. Am. Chem. Soc.*, **1990**, *112*, 5645.

51 M. Fujita, O. Sasaki, T. Mitsuhashi, T. Fujita, J. Yazaki, K. Yamaguchi, and K. Ogura, *Chem. Commun.*, **1996**, *0*, 1535.

52 A. N. Khlobystov, A. J. Blake, N. R. Champness, D. A. Lemenovskii, A. G. Majouga, N. V. Zyk, and M. Schroder, *Coord. Chem. Rev.*, **2001**, *222*, 155.

53 S. O. Kang, R. A. Begum, and K. Bowman-James, *Angew. Chem. Int. Ed.*, **2006**, *45*, 7882.

54 A. G. Young and L. R. Hanton, *Coord. Chem. Rev.*, **2008**, *252*, 1346.

55 R. Meijboom, R. J. Bowen, and S. J. Berners-Price, *Coord. Chem. Rev.*, **2009**, *253*, 325.

56 N. Armaroli, G. Accorsi, F. Cardinali, and A. Listorti In *Photochemistry and Photophysics of Coordination Compounds I*, Balzani, V., Campagna, S., Eds., Springer Berlin Heidelberg, 2007, Vol. 280, p 69.

57 F. R. Keene, *Coord. Chem. Rev.*, **1997**, *166*, 121.

58 P. L. Boulas, M. Gómez-Kaifer, and L. Echegoyen, *Angew. Chem. Int. Ed.*, **1998**, *37*, 216.

59 V. Balzani, S. Campagna, G. Denti, A. Juris, S. Serroni, and M. Venturi, *Acc. Chem. Res.*, **1998**, *31*, 26.

60 V. Balzani, A. Credi, F. M. Raymo, and J. F. Stoddart, *Angew. Chem. Int. Ed.*, **2000**, *39*, 3348.

61 C. Janiak, *Dalton Trans.*, **2003**, 2781.

62 C. Janiak and J. K. Vieth, *New J. Chem.*, **2010**, *34*, 2366.

63 C.-T. Chen and K. S. Suslick, *Coord. Chem. Rev.*, **1993**, *128*, 293.

64 W. Lin, W. J. Rieter, and K. M. L. Taylor, *Angew. Chem. Int. Ed.*, **2009**, *48*, 650.

65 S. K. Ghosh and S. Kitagawa, *CrystEngComm*, **2008**, *10*, 1739.

66 J. Yang, J.-F. Ma, Y.-Y. Liu, and S. R. Batten, *CrystEngComm*, **2009**, *11*, 151.

67 S. K. Henninger, H. A. Habib, and C. Janiak, *J. Am. Chem. Soc.*, **2009**, *131*, 2776.

68 W. M. Bloch and C. J. Sumby, *Chem. Commun.*, **2012**, *48*, 2534.

Chapter 2

Synthesis of [3]Radialenes

Chapter 2

2. Synthesis of [3]Radialenes

2.1. Introduction

2.1.1. Historical Perspective

Cross-conjugated compounds, as previously mentioned, are compounds with "three unsaturated groups, two of which although conjugated to a third unsaturated centre are not conjugated to each other".[1,2] This class of compounds has received limited attention compared to the more common linearly conjugated systems.[3,4] The primary reasons for this are a combination of synthetic challenge and product stability. Dendralenes (Figure 2.1) are a series of acyclic cross-conjugated polyenes which typify these challenges.

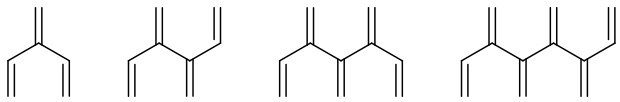

2.1 **2.2** **2.3** **2.4**

Figure 2.1. The parent dendralenes: [3]- (**2.1**), [4]- (**2.2**), [5]- (**2.3**), and [6]dendralene (**2.4**).

[3]Dendralene, **2.1**, was first synthesised in 1955 via ester pyrolysis of 3-methylenepentane-1,5-diyl diacetate, **2.5**, or the corresponding triacetate, **2.6**, in yields of 26-45% (Scheme 2.1).[5,6] Relatively large quantities of **2.1** (*ca*. 5 g) were able to be obtained in this manner, however the product was highly reactive and prone to dimerisation upon standing at room temperature or exposure to air.[5] The preparation of [4]dendralene, **2.2**, followed in 1962, in a similar manner to that of **2.1**, via ester pyrolysis of 2-(1,4-diacetoxybutan-2-yl)butane-1,4-diyl diacetate, **2.7**, in 25% yield (Scheme 2.1).[7]

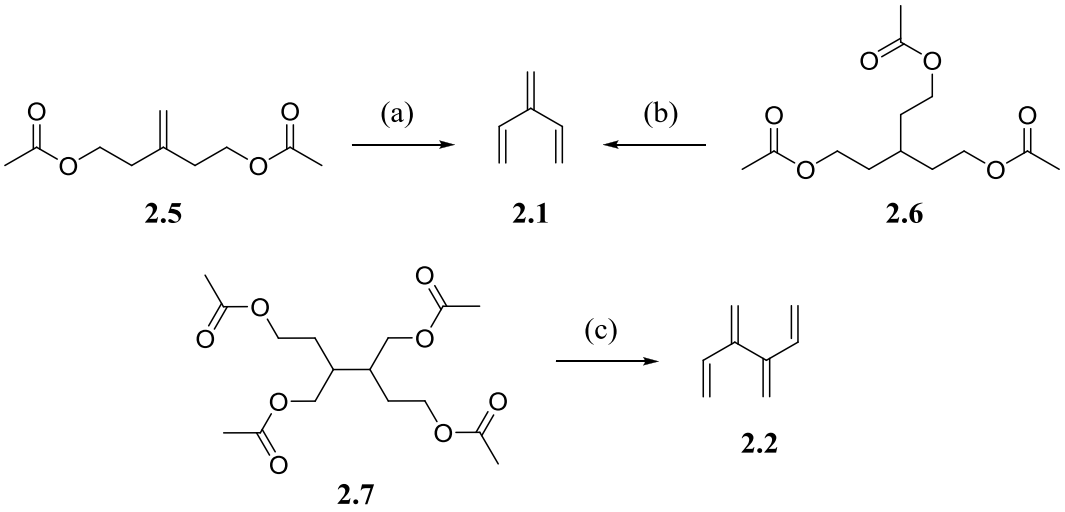

(a) 485°C, 26%; (b) 540°C, 47%; (c) 590°C, 50 mm Hg, 25%.

Scheme 2.1

Extension of the dendralene series to [5]dendralene, **2.3**, and beyond proved very difficult and this goal was not attained until the turn of the century. Sherburn and colleagues approached the problem of instability by first synthesising "masked" dendralenes where the terminal butadiene groups exist as their 3-sulfolene derivatives (**2.8**-**2.12**).[8] The masked dendralenes are crystalline solids which are stable at room temperature, under nitrogen atmosphere, for a number of months. Upon heating these derivatives at 450°C sulfur dioxide is easily eliminated leaving the desired dendralene product (Scheme 2.2). In this manner the first four parent dendralenes (Figure 2.1), as well as [8]dendralene, **2.13**, were able to be prepared in yields ranging from 52 to 89%.[8] This breakthrough in the synthesis of the parent dendralenes has allowed further in depth study into their properties, stability and reactivity; and in particular as dienes for use in Diels-Alder chemistry.[9-13]

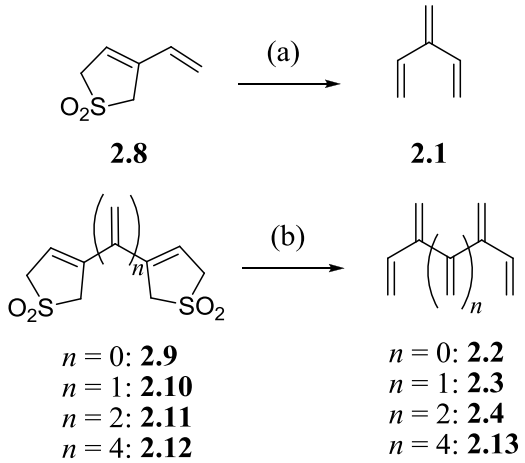

(a) 450°C, 89%; (b) 450°C, **2.2** 85%, **2.3** 65%, **2.4** 52%, **2.13** 64%.

Scheme 2.2

Radialenes are cyclic cross-conjugated polyenes which exhibit a general formula of $C_{2n}H_{2n}$ and contain *n* ring atoms and *n* exocyclic double bonds (Figure 2.2).[4] Like their acyclic dendralene analogues, radialenes have proven to be a significant synthetic challenge. [4]Radialene, **2.15**, was the first of the parent compounds to be obtained in 1962 via HBr elimination from 1,2,3,4-tetrakis(bromomethyl)cyclobutane, **2.18**, in 50% yield (Scheme 2.3).[14,15] It was noted that on exposure to air, **2.15** polymerised rapidly to form an intractable mixture of oxygen-containing polymers.[15] To prevent this, although not very practically, it was stored at -78°C as a dilute solution.

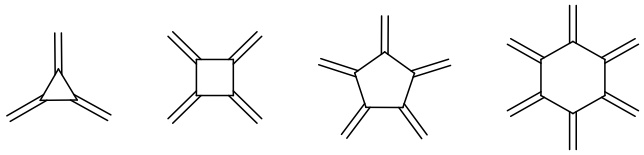

2.14 **2.15** **2.16** **2.17**

Figure 2.2. The parent radialenes: [3]- (**2.14**), [4]- (**2.15**), [5]- (**2.16**), and [6]radialene (**2.17**).

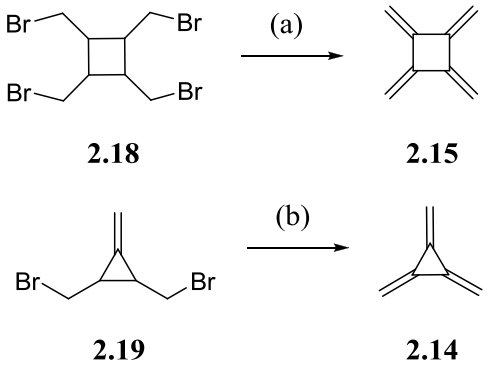

2.18 **2.15**

2.19 **2.14**

(a) NaOEt, EtOH, 0°C, 50%; (b) KOH, 150°C, 47%.

Scheme 2.3

The preparation of [3]radialene, **2.14**, followed in 1965, in a similar manner to that of **2.15**, via HBr elimination from 1,2-bis(bromomethyl)-3-methylenecyclopropane, **2.19**, in 47% yield (Scheme 2.3).[16] [5]Radialene, **2.16**, has proven a particularly difficult synthetic target, and remains unreported to this day. On the other hand the synthesis of [6]radialene, **2.17**, was reported concurrently by Heitzmann and Bokelheide in 1978.[17,18] Early research into the parent radialenes progressed further than that of the dendralenes; however they have not experienced a similar recent resurgence and development. Focus has instead shifted to derivatives of the parent species, in particular [3]radialenes containing aryl and heteroaryl moieties, due to their increased stability.

2.1.2. General Synthesis of Hexaaryl[3]radialenes

Fukunaga's method, reported in 1976, of reacting stabilised carbanions with tetrachlorocyclopropene (tccp) was originally used to synthesise the hexacyano[3]radialene dianion salt, **2.21** (Scheme 2.4).[19,20] The precursor for this reaction, malononitrile, **2.20**, has very acidic methyl hydrogens and is easily deprotonated with sodium hydride. The resultant carbanion is stabilised by resonance delocalisation of the negative charge onto the two nitrile nitrogen atoms. The ease of production, low steric bulk, and high stability of the carbanion is reflected in the near quantitative yield of **2.21**, upon reaction of the carbanion with tetrachlorocyclopropene. Radialene **2.21** is stable as a dianion, with oxidation potentials of +0.34 and +1.13 V, and was isolated as its bis(tetrabutylammonium) salt.[19]

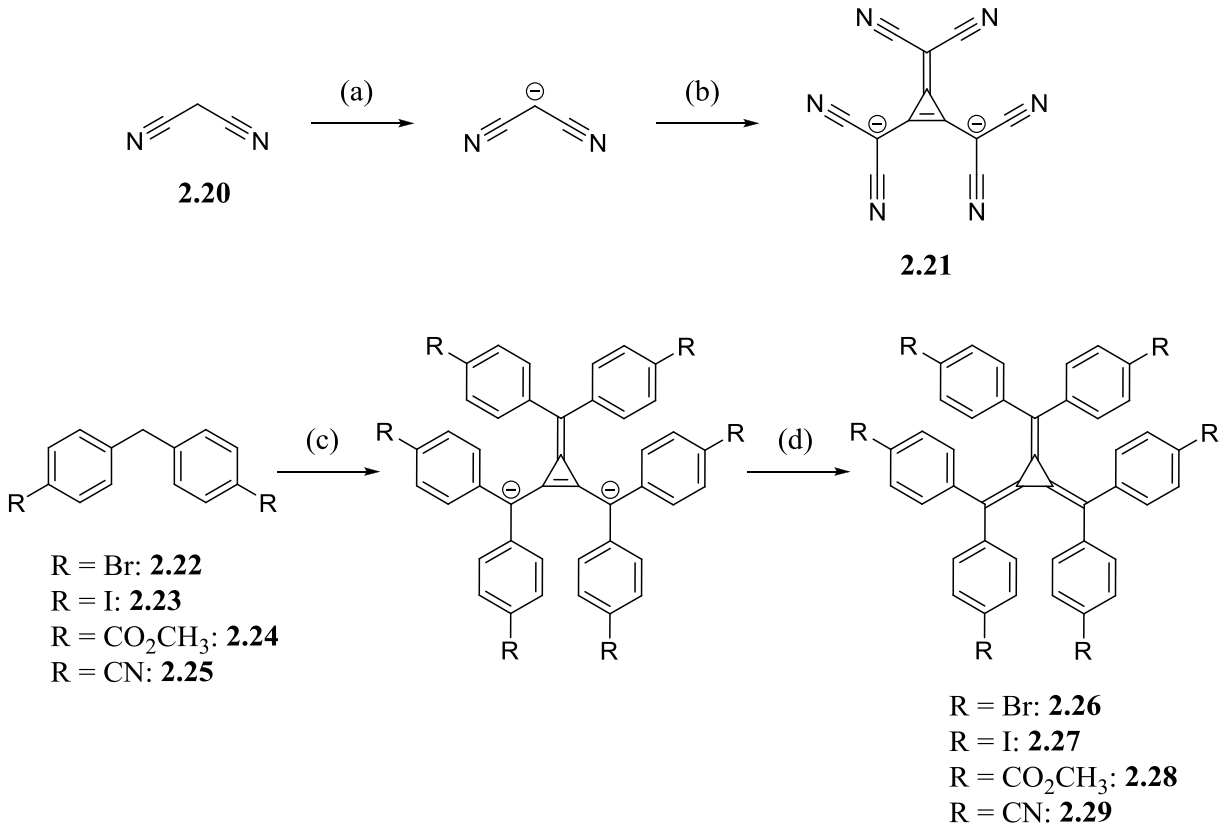

(a) 6 equiv. NaH, glyme; (b) ⅓ equiv. tccp, 94%; (c) i) 1.1 equiv. nBuLi, THF, -78°C, ii) ⅙ equiv. tccp; (d) O_2, 0°C, **2.26** 25-35%, **2.27** 30%, **2.28** 21%, **2.29** 73%.

Scheme 2.4

Fukunaga's method was further developed by Oda, in 1997, for the synthesis of hexaaryl[3]radialenes, which could be accessed via oxidation of the dianion species (Scheme 2.4).[21,22] As the methyl hydrogens of the diaryl species **2.22-2.25** are not as acidic as those of **2.20**, a stronger base, n-BuLi, was used instead of sodium hydride. After nucleophilic substitution of three equivalents of the carbanion onto tetrachlorocyclopropene the

intermediate requires deprotonation to form the dianion. In the case of Fukunaga's method six equivalents of sodium hydride are used and so it is available to deprotonate both **2.20** and the intermediate species. n-BuLi is such a strong base that use of more than one equivalent could led to non-specific deprotonation of the diaryl species, therefore, in Oda's modification six equivalents of the aryl species are used and act as both a nucleophile and a room temperature-stable base during the reaction. Unlike **2.21**, the hexaaryl[3]radialene dianion species are not stable but can be oxidised with molecular oxygen to form the neutral species, **2.26-2.29**. Hexapyridyl[3]radialenes were obtained using an analogous procedure, with the synthesis of hexa(2-pyridyl)[3]radialene (**1.3**) being reported simultaneously by Oda and Steel.[23,24]

Amongst the first hexaaryl[3]radialenes synthesised, those with electron withdrawing groups in the 4-position of the aryl ring, such as hexakis(4-cyanophenyl)[3]radialene, **2.29**, were produced in the highest yields (73% as opposed to 21% for **2.28**).[21] This can be attributed to the increased stability of the 4,4'-dicyanodiphenylmethane, **2.25**, carbanion as the negative charge can be delocalised via resonance onto the nitrile group nitrogen atoms. Unlike the parent [3]radialene, hexaaryl[3]radialenes are robust materials which are not prone to polymerisation and exhibit melting points greater than 300°C.[21,22] These compounds also possess many properties which make them interesting synthetic targets such as intrinsic electron deficiency,[22,23] intense fluorescence emission,[25,26] and a propeller-like three dimensional structure.[24,26-29] Ideally, the combination of these attributes could be utilised in the development of fluorescent anion sensors via the extension of the pre-organised propeller structure provided by the hexaaryl[3]radialene scaffold.

2.2. Synthesis of Hexakis(cyanophenyl)[3]Radialenes

*2.2.1. Hexakis(4-cyanophenyl)[3]radialene **2.29***

At the time this research commenced compound **2.29** was both the easiest hexaaryl[3]radialene to access and the most electron deficient, with reduction potentials of -0.63 and -1.03 V in dichloromethane, which led us to pursue it in regard to developing anion sensors.[21,22,26] The nitrile functional group was also the most interesting present in the hexaaryl[3]radialenes reported by Oda as it has the potential to coordinate metals to produce discrete metal-ligand complexes or coordination polymers. Radialene **2.29** was prepared via the reaction of 4,4'-dicyanodiphenylmethane, **2.25**, with tetrachlorocyclopropene (tccp) as described in section 2.1.2 (Scheme 2.5). The radialene reaction proceeded in good yields of 68-71%.

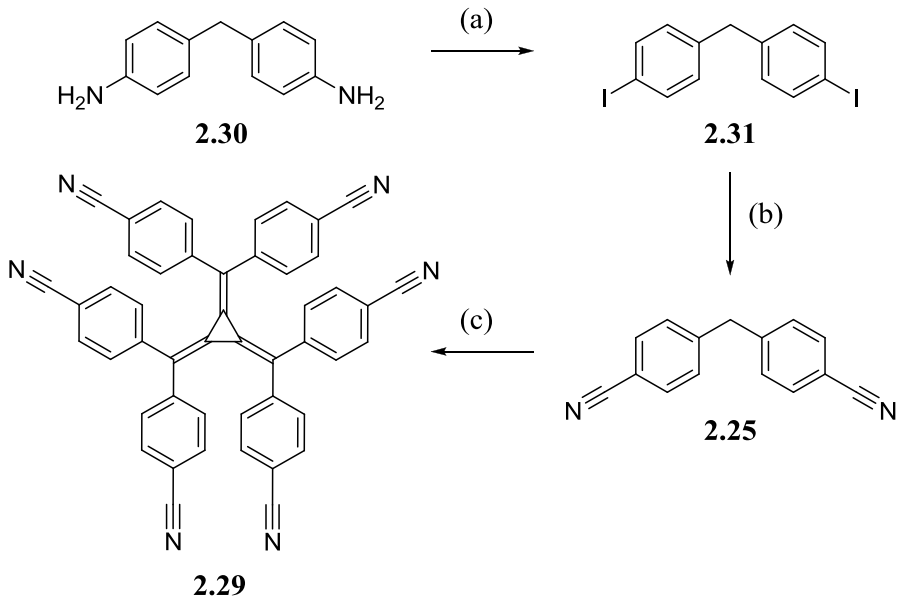

(a) i) H_2SO_4, $NaNO_2$, ii) KI, 62%; (b) CuCN, DMF, 95%; (c) i) 1.1 equiv. nBuLi, THF, -78°C, ii) ⅙ equiv. tccp, iii) O_2, 0°C, 71%.

Scheme 2.5

Compound **2.25** was produced in two steps from the commercially available 4,4'-diaminodiphenylmethane, **2.30**. The first step entailed the diazotisation of the amine via reaction with sulfuric acid and sodium nitrite. The resultant diazonium salt was then reacted with potassium iodide to afford 4,4'-diiododiphenylmethane, **2.31**, in 62% yield.[30] Treatment of **2.31** with copper cyanide, in DMF at 100°C for two days, gave **2.25** in 95% yield.[29,31] This route provided access to **2.25** in a higher yield (59% over two steps) than the one step literature procedure referenced by Oda, which used commercially available 4,4'-dibromodiphenylmethane instead of the diiodo equivalent with a resulting yield of 39%.[32] The increase in yield of **2.25** from 39% to 59% can be explained by the fact that the iodide anion is a better leaving group than the bromide anion.

Compounds **2.31** and **2.25** were characterised via ^{1}H and ^{13}C NMR spectroscopy, IR spectroscopy, EI-MS and melting point analysis. Characteristic peaks for the CH_2 groups were observed for **2.31** and **2.25** at δ 3.85 and 4.09 respectively and their molecular ions (MH^+) were observed at *m/z* 419.8 and 218.1 in their mass spectra. Compound **2.25** also exhibited a characteristic C≡N peak at 2225 cm^{-1} in the IR spectrum. Single crystals of **2.25** suitable for X-ray crystallography were obtained via slow evaporation from methanol. The compound crystallises in the orthorhombic space group *Fdd*2 with half a molecule of **2.25** in the asymmetric unit. The structure was refined to R_1 3.78% with no disorder problems. A perspective view of the structure is depicted in Figure 2.3. The bond lengths and angles are

consistent with normal aromatic rings; the aromatic C-C bond lengths range from 1.381(2) to 1.3969(19) Å.

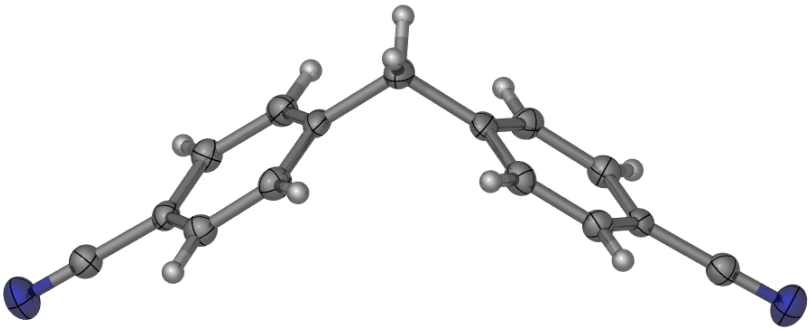

Figure 2.3. A perspective view of compound **2.25** with anisotropic displacement parameters represented as ellipsoids at the 50% probability level.

Radialene **2.29** was characterised via melting point, IR spectroscopy, ESI-MS, ^{1}H and ^{13}C NMR spectroscopy and elemental analysis. The characteristic C≡N peak in the IR spectra of **2.29** appeared at 2224 cm^{-1}, which is very similar that of the precursor **2.25** (2225 cm^{-1}). Of particular interest are the aryl proton shifts of **2.25** and **2.29** in the ^{1}H NMR spectra. The precursor, **2.25**, exhibits aryl proton shifts of δ 7.27 and 7.61, which are then significantly upfield shifted in the corresponding radialene at δ 6.97 and 7.41. This is due to the propeller conformation that the radialene adopts in order to prevent steric clash of its substituents, which positions the aryl protons above and below the plane of the ring, where they experience considerable shielding by the adjacent aryl rings. This double three-bladed propeller conformation has been observed in the solid-state with the crystal structure of a dichloromethane solvate of **2.29** being reported by Oda.[21] In this case the aryl rings are twisted by an average of 42° from the [3]radialene plane. To allow comparison in different solvents, we have also determined the crystal structure of a nitromethane solvate of **2.29**.

Single crystals of **2.29** suitable for X-ray crystallography were obtained via slow evaporation from nitromethane. The compound crystallises in the monoclinic space group $P2_1/c$ with one molecule of **2.29** and four nitromethane solvate molecules in the asymmetric unit. The structure was refined to R_1 8.13% with disorder of one nitromethane molecule, which was modelled over two positions (*ca.* 65:35). A perspective view of the asymmetric unit is depicted in Figure 2.4.

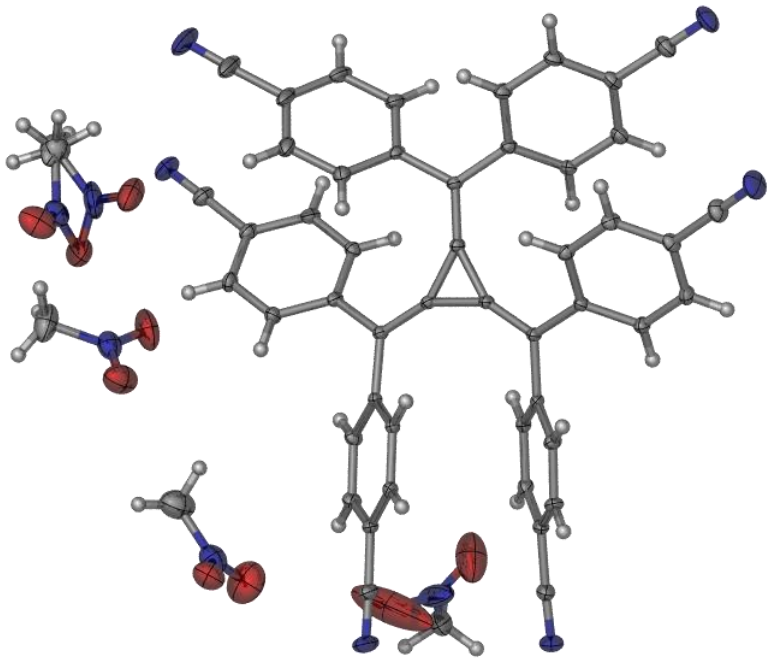

Figure 2.4. The asymmetric unit of **2.29·4(CH_3NO_2)** with anisotropic displacement parameters represented as ellipsoids at the 50% probability level. There is disorder of one of the nitromethane solvent molecules, which was modelled over two positions *ca.* 65:35.

In this structure, the [3]radialene core is planar and the "arms" extend in a double-bladed propeller conformation with torsion angles of *ca.* 38° on average which is common for hexaaryl[3]radialenes and similar to that observed in the dichloromethane solvate of **2.29**.[21,24,27-29] Bond lengths and angles about the central core are consistent with a [3]radialene derivative with the C-C bonds of the propane ring ranging from 1.428(2) to 1.432(3) Å and the exocyclic double bonds ranging from 1.357(2) to 1.361(3) Å.

In the extended packing of this structure there are two nitromethane solvate molecules which are positioned above and below the [3]radialene core. One is situated almost directly over the core and exhibits close contacts between an oxygen atom and a core carbon atom of 3.40 Å and between the same oxygen atom and an exocyclic carbon atom of 3.30 Å. A single hydrogen bond is also present between the first nitromethane molecule and a radialene aryl hydrogen atom with an O···H bond length of 2.52 Å. The second nitromethane molecule is situated slightly off centre in respect to the [3]radialene core and so only exhibits a close contact between an oxygen atom and an exocyclic carbon atom of 3.21 Å. This nitromethane molecule also exhibits one hydrogen bond with a radialene aryl hydrogen atom of 2.68 Å. In other solid-state hexaaryl- and hexapyridyl[3]radialene structures similar close contacts have been observed with anions,[24,28,29] which will be further discussed in Chapter 5.

*2.2.2. Hexakis(3-cyanophenyl)[3]radialene **2.38***

To produce capsule-like metallo-supramolecular anion sensors, ideally, the hexaaryl[3]radialene scaffold should be extended in the 3-position of the aryl rings. This would lead to the positioning of the substituents on one face or above and below the plane of the electron deficient [3]radialene core to form either a single anion binding site or two binding cavities. In contrast, extension of substituents in the 4-position, as for **2.29**, would produce more divergent structures; i.e. coordination polymers. The first radialene target substituted in the 3-position was hexakis(3-cyanophenyl)[3]radialene, **2.38**, as it was proposed that it could be generated following an analogous synthesis to that of **2.29** (Scheme 2.6).

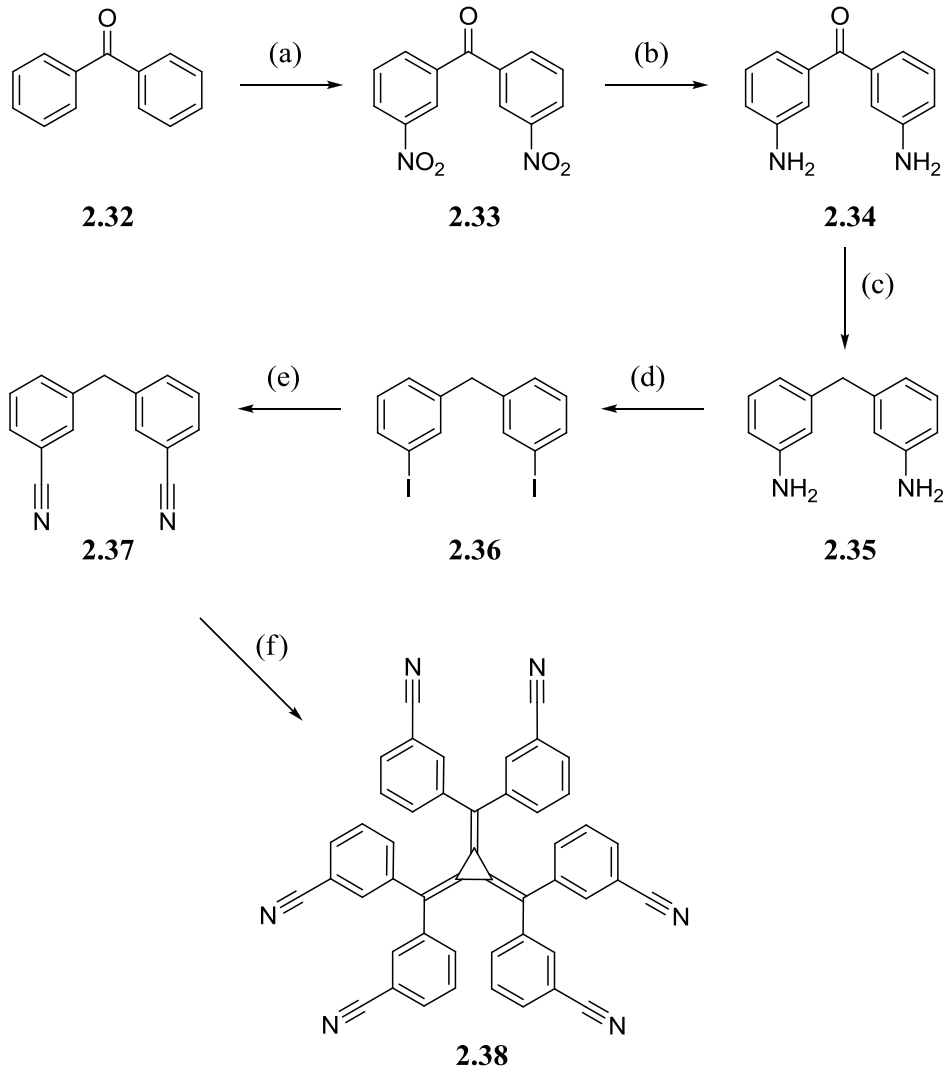

(a) HNO_3/H_2SO_4, 43%; (b) $SnCl_2$, H_2SO_4, 99%; (c) KOH, ethylene glycol, $NH_2NH_2.H_2O$, 63%; (d) i) H_2SO_4, $NaNO_2$, ii) KI, 55%; (e) CuCN, DMF, 90%; (f) i) 1.1 equiv. nBuLi, THF, -78°C, ii) ⅙ equiv. tccp, iii) O_2, 0°C, 16%.

Scheme 2.6

3,3'-Diaminodiphenylmethane, **2.35**, is difficult to obtain commercially and is much more expensive than its 4-substituted analogue **2.30**, thus it was decided to synthesise it in-house from readily available starting materials. Nitration of the common reagent benzophenone, **2.32**, with nitric acid proceeded in a low yield, though comparable to that reported in the literature.[33,34] The reduction of 3,3'-dinitrobenzophenone, **2.33**, with stannous chloride to produce 3,3'-diaminobenzophenone, **2.34**, was much more efficient proceeding in near quantitative yield.[35,36] Characterisation of **2.33** and **2.34** via melting point analysis and ^{1}H NMR spectroscopy produced data consistent with that reported in the literature.[33-36]

A number of approaches for the conversion of **2.34** to **2.35** were investigated. A Clemmenson reduction of **2.34**, using zinc/mercury amalgam and dry hydrogen chloride gas, gave a reported yield of 80%.[35,36] However, we endeavoured to avoid the use of hydrogen chloride gas where possible. Performing the Clemmenson reduction using freshly prepared zinc-mercury amalgam and concentrated hydrochloric acid gave a low yield of 30%. Other methods of reduction were also trialled, but were ultimately unsuccessful. These were a hypophosphorous acid/iodine reducing system[37] and direct hydrogenation using Pd/C catalyst and hydrogen gas in a Parr hydrogenation apparatus or using a ThalesNano H-cube continuous flow hydrogenation reactor.

The method which proved most convenient and effective was the Wolff-Kishner reduction where **2.34** was reacted with hydrazine hydrate in ethylene glycol to give **2.35** in 63% yield.[38] Compound **2.35** was isolated as an oil, although it has been reported to be a solid with a melting point of 85-87°C.[36] This may be due to a small amount of residual ethylene glycol, however the ^{1}H NMR spectrum of **2.35** was consistent with the literature and showed no impurities. The mass spectra of **2.35** showed the molecular ion M^{+} at *m/z* 198.1 with fragmentation to $(M\text{-}NH_2)^{+}$ at *m/z* 182.1, $[M\text{-}(NH_2)_2]^{+}$ at *m/z* 167.0, and $(M\text{-}PhNH_2)^{+}$ at *m/z* 106.1. This was acceptable for our purposes as **2.35** was only an intermediary compound.

Conversion of **2.35** to 3,3'-diiododiphenylmethane, **2.36**, and subsequently to the key intermediate 3,3'-dicyanodiphenylmethane, **2.37**, proceeded in good yields analogous to those seen for the 4-substituted compounds. **2.36** and **2.37**, being new compounds, were characterised via ^{1}H and ^{13}C NMR spectroscopy, IR spectroscopy, ESI-MS, and melting point analysis. Characteristic peaks for the CH_2 groups were observed for **2.36** and **2.37** at δ 3.85 and 4.05 respectively and their molecular ions (MH^{+}) were observed at *m/z* 420.1 and 218.2 in the mass spectra. Compound **2.37** also exhibited a characteristic C≡N peak at 2224 cm^{-1} in the IR spectrum.

Single crystals of **2.37** suitable for X-ray crystallography were obtained via slow evaporation from methanol. The compound crystallises in the chiral orthorhombic space

group $P2_12_12$ with half a molecule of **2.37** in the asymmetric unit (due to the absence of heavy atoms the Flack parameter of 2(6) is essentially meaningless). This compound is only chiral in the solid-state as in solution free rotation around the methylene group would be allowed. The structure was refined to R_1 4.21% with no disorder problems. A perspective view of the structure is depicted in Figure 2.5. The bond lengths and angles are consistent with normal aromatic rings; the aromatic C-C bond lengths range from 1.378(2) to 1.399(2) Å. It is interesting to note that rotation around the C-CH_2 bonds has positioned the nitrile groups on opposite sides of the molecule in order to prevent steric clash.

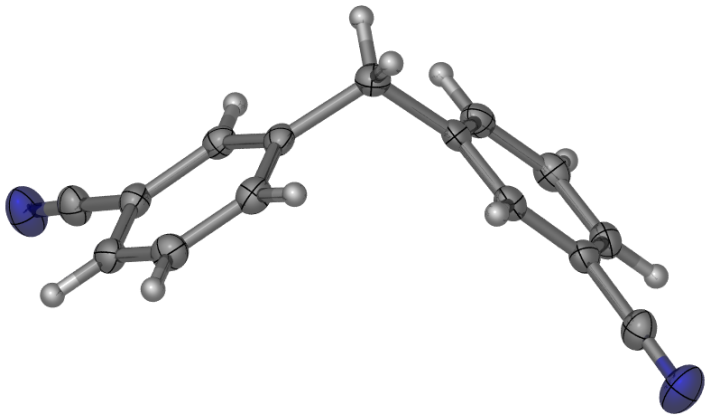

Figure 2.5. A perspective view of compound **2.37** with anisotropic displacement parameters represented as ellipsoids at the 50% probability level.

Radialene **2.38** was obtained from **2.37** in 16% yield via the general procedure described in section 2.1.2. However, yields of **2.38** could be variable and were often as low as 3%. The distinct difference in yield between **2.38** and **2.29** (71% isolated yield) is a consequence of the relative stability of the carbanions of the two dicyanodiphenylmethane precursors. The negative charge of the carbanion can be delocalised onto the nitrile nitrogen when the nitrile group is in the 4-position, however when the nitrile is moved to the 3-position it is no longer conjugated to the carbanion at the methylene group and thus can no longer stabilise it via resonance.

Radialene **2.38** was characterised via ^{1}H and ^{13}C NMR spectroscopy, IR spectroscopy, ESI-HRMS, elemental and melting point analysis. The molecular ion (MH^+) was observed at *m/z* 685.21196 in the high resolution mass spectrum, which is very close to that calculated (*m/z* 685.21352). The characteristic C≡N peak was seen in the IR spectrum at 2228 cm^{-1}. The upfield shift of the radialene aryl hydrogen atoms compared to that of the diarylmethane precursor, observed in **2.29**, is apparent for H2 (δ 7.41-7.48 to 6.96), H5 (δ 7.41-7.48 to 7.23) and H6 (δ 7.56 to 7.30) in **2.38** but not H4 (δ 7.41-7.48 to 7.59) as it extends directly out from

the [3]radialene core and so is not shielded by the propeller arrangement of the aryl rings. Unfortunately no crystals of **2.38** suitable for X-ray crystallography were able to be grown, in order to confirm the propeller conformation of the radialene in the solid-state, despite multiple attempts.

*2.2.3. Hexakis(3,4-dicyanophenyl)[3]radialene **2.44***

In order to maintain a high yielding synthesis whilst investigating substitution in the 3-position, a new strategy was developed which involved retention of an electron withdrawing group in the 4-position whilst incorporating new substituents at the 3-position. The natural progression of this work was to use this strategy to synthesise hexakis(3,4-dicyanophenyl)[3]radialene, **2.44**. Initial work towards **2.44**, by honours student Xin He,[39] progressed via successful diazotisation and iodination of 3,3'-dichloro-4,4'-diaminodiphenylmethane followed by attempted reaction with copper cyanide. However, chloride is a poor leaving group compared to iodide and so complete conversion of all four halogens to nitrile groups was unsuccessful. The synthesis of the tetracyanomethane precursor, **2.43**, and the subsequent radialene (Scheme 2.7) was developed by Dr Antonio Avellaneda during his time as a postdoctoral fellow with the Sumby group.[26]

4,4'-Carbonyldiphthalic acid, **2.39**, was obtained via hydrolysis of commercially available 3,3',4,4'-benzophenone tetracarboxylic anhydride in quantitative yield. Hydrogenation of **2.39** with 5% Pd/C gave 4,4'-methyldiphthalic acid, **2.40**,[40] which was then reacted with formamide to yield the corresponding diimide, **2.41**.[41] Treatment of **2.41** with aqueous ammonia solution gave the tetraamide, **2.42**.[41] Finally, **2.42** was dehydrated to the tetranitrile, **2.43**, using thionyl chloride.[42,43] Compounds **2.40**-**2.43** were isolated in good yields of at least 85% and were characterised via ^{1}H and ^{13}C NMR spectroscopy, IR spectroscopy, ESI-MS, and melting point analysis. Characteristic CH_2 peaks were observed in the ^{1}H NMR spectrum for **2.40**-**2.43** at δ 4.09, 4.33, 4.01 and 4.45 respectively. Carbonyl stretches were seen in the IR spectrum of **2.40**-**2.42** at 1656, 1770 and 1712, and 1693 and 1649 cm^{-1} respectively. The nitrile stretch of **2.43** appeared at 2233 cm^{-1} in the IR spectrum. The molecular ions ($[M\text{-}H^{+}]^{-}$) for **2.40**, **2.42**, and **2.43** were observed in the mass spectra in negative ion mode at *m/z* 343.0, 340.8, and 267.1 respectively. Whereas the molecular ion of **2.41** (MH^{+}) was able to be observed in positive ion mode in the mass spectrum at *m/z* 307.4.

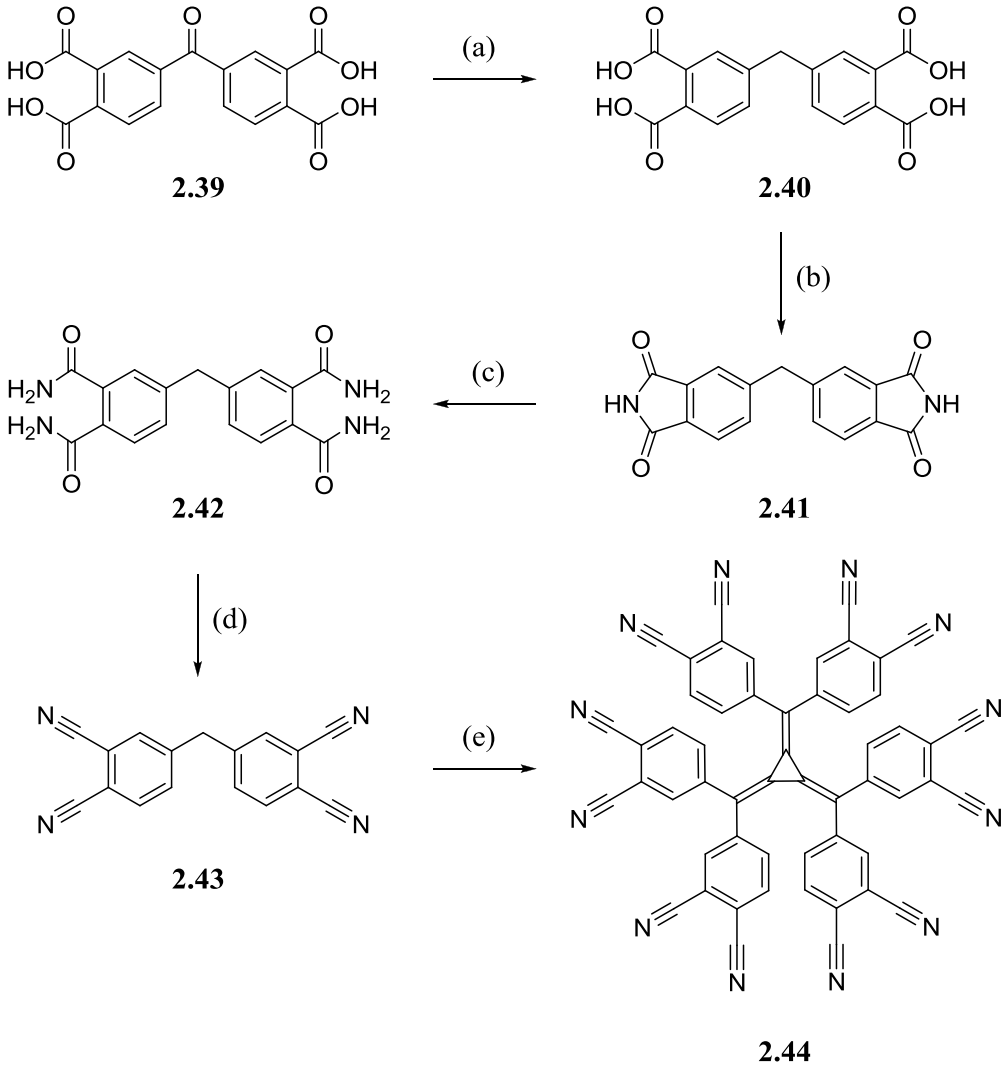

2.39 **2.40** **2.41** **2.42** **2.43** **2.44**

(a) Pd/C, H_2, EtOH, 95%; (b) formamide, 85%; (c) $NH_4OH_{(aq)}$, 85%; (d) $SOCl_2$, DMF, 89%; (e) i) 1.1 equiv. NaH, DMF, 0°C, ii) ⅙ equiv. tccp, iii) air, iv) sat $NH_4Cl_{(aq)}$, 76%.

Scheme 2.7

Single crystals of **2.43** suitable for X-ray crystallography were obtained via slow evaporation from acetonitrile. The compound crystallises in the chiral orthorhombic space group $P2_12_12$ with half a molecule of **2.43** in the asymmetric unit (Flack parameter of 8(10)). This compound is only chiral in the solid-state as in solution free rotation around the methylene group would be allowed. The structure was refined to R_1 7.82% with no disorder problems. A perspective view of the structure is depicted in Figure 2.6. The bond lengths and angles are consistent with normal aromatic rings; the aromatic C-C bond lengths range from 1.382(8) to 1.397(7) Å. As in the structure of **2.37**, the nitrile groups in the 3-position are located on opposite sides of the molecule in order to prevent steric clash.

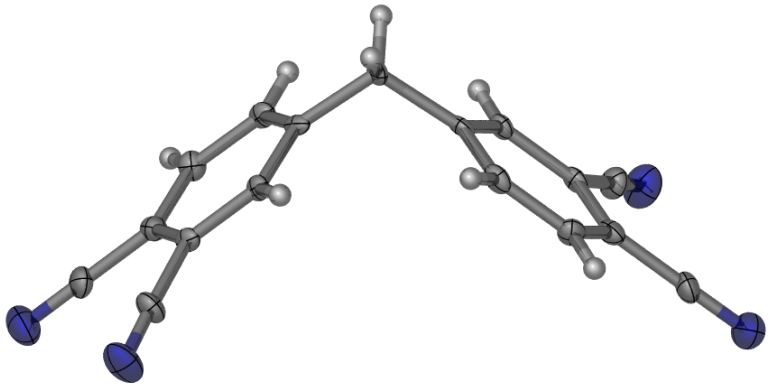

Figure 2.6. A perspective view of compound **2.43** with anisotropic displacement parameters represented as ellipsoids at the 50% probability level.

Initial attempts to synthesise radialene **2.44** using the standard procedure, outlined in section 2.1.2, were unsuccessful. The deprotonation of **2.43** using n-BuLi proceeded successfully as indicated by a colour change of the reaction mixture from colourless to dark blue. Upon addition of tetrachlorocyclopropene another colour change to dark purple/black implied that a reaction was taking place. Oxidation with gaseous oxygen led to a brown solution which showed no intense red/orange coloured spots on the TLC plates. Observation of intensely coloured spots, which fluoresce orange under UV light, are indicative of hexaaryl[3]radialenes. It appeared that decomposition of the dianion species was occurring during the oxidation step.

It was found that due to the greater acidity of **2.43** (compared to **2.25** and **2.37**) it was able to be deprotonated by the weaker base sodium hydride instead of n-BuLi. The tetranitrile carbanion itself is also more stable than that of **2.25** and **2.37** due to the increased stabilisation imparted by the four nitrile groups, which allowed the reaction to take place at 0°C instead of -78°C and hence the use of DMF instead of THF as a solvent. Different methods of oxidation were trialled, including bubbling oxygen and air directly through the solution, but these were ultimately unsuccessful. Finally it was discovered that slow oxidation of the dianion, by fitting the reaction vessel with a potassium hydroxide drying tube and allowing it to stir for two days, produced the desired product. Compound **2.44** was then able to be isolated via precipitation in saturated aqueous ammonium chloride solution and purified by silica gel chromatography in 76% yield.

The difficulty experienced during the oxidation step may be attributed to the electron deficiency of the final product. The first reduction step for **2.44** occurs at +0.06 V which, when the measurement error of ±0.02 V is taken into account, is very close to zero. This would suggest that the dianion of **2.44** is relatively stable making it resistant to oxidation;

however, if this is entirely the case then vigorous oxidation would be preferable to slow oxidation. Another possibility is that the dianion is unstable in the presence of large amounts of oxygen and vigorous oxidation leads to side reactions. For example if even a small amount of water was present the nitrile groups could be oxidised back to the aryl amides.[44]

Radialene **2.44** was characterised via ^{1}H and ^{13}C NMR spectroscopy, IR, ESI-HRMS, elemental and melting point analysis. The molecular ion (M^-) was observed at *m/z* 834.17629 in negative ion mode in the high resolution mass spectrum, which is very close to that calculated (*m/z* 834.17829). The characteristic C≡N peak was seen in the IR spectrum at 2235 cm^{-1}. The upfield shift of the radialene aryl hydrogen atoms compared to that of the diarylmethane precursor, observed in **2.29** and **2.38**, is apparent for H2 (δ 8.04 to 7.56), H5 (δ 7.92 to 7.30) and H6 (δ 8.04 to 7.82).

Radialene **2.44** was also characterised by X-ray crystallography as small red crystals were able to be obtained by slow evaporation from acetonitrile. The compound crystallises in the monoclinic space group $P2_1/c$ and the asymmetric unit contains one molecule of the radialene ligand and an acetonitrile solvate molecule. The small crystals were weakly diffracting but the structure refined to R_1 6.82% with no significant disorder problems. A perspective view of the asymmetric unit is depicted in Figure 2.7.

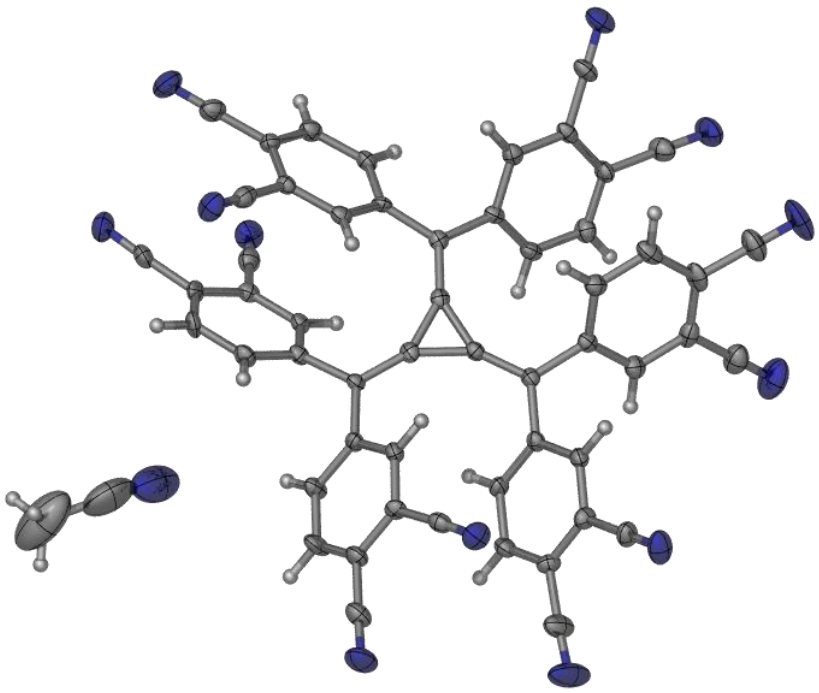

Figure 2.7. The asymmetric unit of the acetonitrile solvate of radialene **2.44** with anisotropic displacement parameters represented as ellipsoids at the 50% probability level.

As expected, the [3]radialene core is planar and the "arms" extend in a double-bladed propeller conformation with torsion angles of *ca* 39° on average which is common for hexaaryl[3]radialenes.[21,24,27-29] The nitrile substituents in the 4-position extend directly out from the structure in approximately the same plane as the core, whereas those in the 3-position are situated above and below the plane. In the conformation observed, four are up and two are directed down. This type of conformation is less commonly encountered as symmetrical arrangements of multi-armed compounds, those with no net dipole, are more favoured.[45] Bond lengths and angles about the central core are consistent with a [3]radialene derivative with the C-C bonds of the propane ring ranging from 1.425(5) to 1.436(5) Å and the exocyclic double bonds ranging from 1.351(5) to 1.355(5) Å.

2.2.4. Electrochemistry and Physical Properties

[3]Radialene compounds have been shown to undergo two one electron reductions to yield the radical anion and dianion species.[23-26] These reduction steps can be measured via a technique called cyclic voltammetry. Cyclic voltammetry involves the immersion of a working electrode, a reference electrode and an auxiliary electrode in a solution of the analyte and supporting electrolyte.[46] The potential applied between the working electrode and the reference electrode, by a potentiostat, is increased over time and the current is measured between the working and auxiliary electrodes.[46] As opposed to linear sweep voltammetry, where the potential is increased in one direction and stops at a set point, in cyclic voltammetry the potential is inverted when the set point is reached. This allows the observation of the oxidation, in the forward scan, and reduction, in the reverse scan, of a redox couple. The data are plotted as current *vs*. potential to produce a cyclic voltammogram like that of radialene **2.44** shown in Figure 2.8. If the reduction and oxidation peaks have a similar shape and absolute current this indicates that the reduction is reversible, as observed in Figure 2.8. On the other hand, if the oxidation peak is smaller than the reduction peak the reduction is said to be quasi-irreversible; or if no oxidation peak is observed the reduction is irreversible.

Up until recently the most electron deficient hexaaryl[3]radialene reported, **2.29**, recorded reduction potentials of −0.63 and −1.03 V in dichloromethane (Table 2.1).[23,26] Radialene **2.38** is slightly harder to reduce than **2.29**, with potentials of −0.80 and −1.32 V in dichloromethane. This is due to the inability of the nitrile groups in the 3-position to stabilise the anion by resonance delocalisation. A similar effect on the reduction potentials is observed for the pyridyl series,[24,28,47] whereby the change from a 2-substituted pyridine to a 3-substituted pyridine ring system results in a compound that is 0.10 V more difficult to reduce.

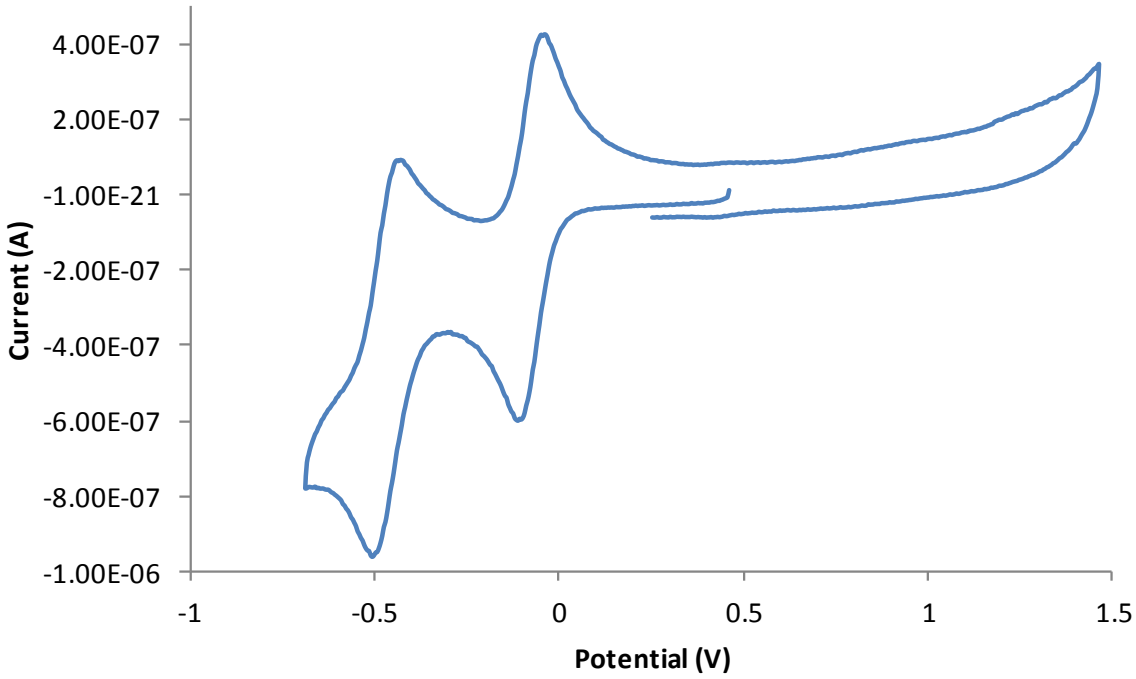

Figure 2.8. Cyclic voltammogram of radialene **2.44** (1mM in dichloromethane/0.1M $[(n\text{-}C_4H_9)_4]NPF_6$, platinum working electrode and ferrocene internal standard).

Conversely, radialene **2.44** is very easy to reduce. This is shown by its reduction potentials of −0.06 and −0.45 V, respectively, and is attributed to the combined electron-withdrawing effect of the twelve nitrile substituents. While **2.44** is considerably more electron deficient than other hexaaryl[3]radialenes, it still exists in its neutral form, which makes it ideal for investigating anion-π interactions. In contrast, other related [3]radialene compounds, such as hexacyano[3]radialene, **2.21**,[19] exist as stable dianions. Chapter 5 reports an investigation into anion-π interactions of the three nitrile radialene species, **2.29**, **2.38**, and **2.44**.

Table 2.1. Reduction potentials for radialenes **2.29**, **2.38** and **2.44** and related compounds.

Compound	$\mathbf{E_{red(1)}}^{\mathbf{a,b}}$	$\mathbf{E_{red(2)}}^{\mathbf{a,b}}$
Hexakis(3,4-dicyanophenyl)[3]radialene, **2.44**	-0.06	-0.45
Hexakis(4-cyanophenyl)[3]radialene, **2.29**	-0.63	-1.03
Hexakis(3-cyanophenyl)[3]radialene, **2.38**	-0.80	-1.32[c]
Hexa(2-pyridyl)[3]radialene[47]	-0.93	-1.29
Hexa(3-pyridyl)[3]radialene[47]	-1.03	-1.48[c]
Hexa(4-pyridyl)[3]radialene[47]	-1.02	-1.33[c]

[a] Potentials (V) measured in DCM/0.1 mol.L^{-1} $[(n\text{-}C_4H_9)_4]NPF_6$ (in DCM the ferrocene/ferrocenium couple occurred at +0.46 V vs. Ag/Ag^+).

[b] Uncertainty in $E_{1/2}$ values *ca.* ± 0.02 V.

[c] Irreversible (approximate value estimated from anodic half-scan).

Most hexaaryl[3]radialenes are orange or red in colour with UV–visible absorption maxima in the range of 460–490 nm in dichloromethane (Table 2.2, Figure 2.9 (a)), with **2.29** and **2.38** being consistent with this observation. The absorption properties of **2.44** had to be measured in acetone due to its limited solubility in dichloromethane (Table 2.2, Figure 2.9 (b)). The UV-visible absorption maxium for **2.44** in acetone was 493 nm which is consistent with the general absorption range for hexaaryl[3]radialenes. The UV-visible absorption maxima for **2.29** and **2.38** do not change significantly when measured in acetone or dichloromethane (Table 2.2).

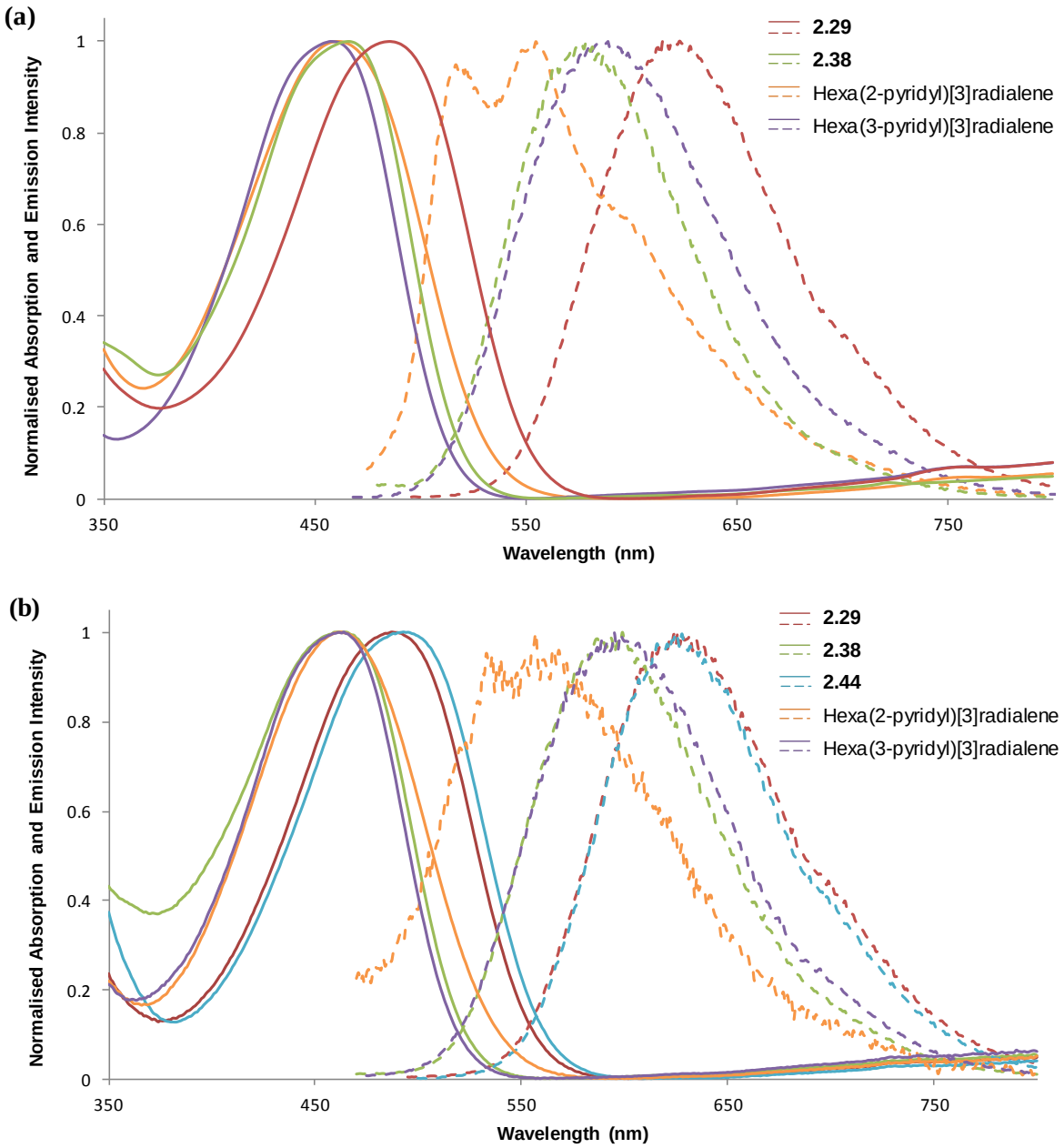

Figure 2.9. (a) UV–visible (solid line) and fluorescence (dashed line) spectra of various hexaaryl[3]radialene species in dichloromethane. (b) UV–visible (solid line) and fluorescence (dashed line) spectra of various hexaaryl[3]radialene species in acetone.

Table 2.2. Visible absorption maxima, molar extinction coefficient ε, and fluorescence emission maxima for various hexaaryl[3]radialene compounds.

Compound	**λ_{max} (nm)**	**log ε**	**Fluorescence max (nm)**	**Stokes shift**
Hexakis(3-cyanophenyl)[3]radialene, **2.38**	461[a]	4.21	576[a]	115
	461[b]	4.24	595[b]	134
Hexakis(4-cyanophenyl)[3]radialene, **2.29**	489[a]	4.42	620[a]	131
	487[b]	4.37	626[b]	139
Hexakis(3,4-dicyanophenyl)[3]radialene, **2.44**	493[b]	4.39	625[b]	132
Hexa(2-pyridyl)[3]radialene	464[a]	4.53	555[a]	91
	463[b]	4.25	564[b]	101
Hexa(3-pyridyl)[3]radialene	465[a]	4.48	585[a]	120
	464[b]	4.16	598[b]	134
Hexa(4-pyridyl)[3]radialene[47]	463[a]	4.62	not reported	
Hexakis(3,5-dimethylpyrazolyl)[3]radialene[26]	443[a]	4.33	467[a]	24
	440[b]	4.13	468[b]	28
Hexakis(4-chlorophenyl)[3]radialene[25]	483[a]	4.68	606[a]	123
Hexaphenyl[3]radialene[25]	467[a]	4.42	617[a]	150

[a]UV-Visible and fluorescence spectra measured in dichloromethane.

[b]UV-Visible and fluorescence spectra measured in acetone.

The nitrile derivatives **2.29**, **2.38** and **2.44**, along with the previously synthesised compounds, hexa(2-pyridyl)[3]radialene and hexa(3-pyridyl)[3]radialene, show a weak absorption in the near infrared (around 800 nm) in both dichloromethane and acetone. This is consistent with spectra observed for the radical anions reported by Oda, which show absorption maxima at 794 and 841 nm respectively for the hexa(2-pyridyl)[3]radialene and hexa(3-pyridyl)[3]radialene radical anions.[23]

The fluorescence of hexaaryl[3]radialenes has not been widely studied.[25] Radialenes **2.29**, **2.38** and **2.44** exhibit large Stokes shifts, of at least 130 nm, for their fluorescence maxima in acetone. The large Stokes shifts are consistent with the HOMO of the [3]radialene being located predominantly on the exocyclic double bonds.[48] As a consequence, the electronic structure of the excited state is considerably more polar than that of the ground state.[25] This is also consistent with the Stokes shift being 10–20 nm larger for the spectra measured in acetone, compared to those measured in dichloromethane, and with calculations that show intramolecular charge transfer character in the lowest excited states for hexaaryl[3]radialene derivatives.[25] In the excited state, rotation about the exocyclic bonds of the cyclopropane ring is also possible. The fluorescence emission of the hexaaryl[3]radialenes, coupled with the large Stokes shifts, suggests that these compounds could be useful as sensor components.

2.3. Attempted Synthesis of Extended [3]Radialenes

*2.3.1. Bis(4-(pyridin-2-ylethynyl)phenyl)methane **2.51** and Bis(4-(pyridin-3-ylethynyl)phenyl)methane **2.52***

The first extended hexaaryl[3]radialenes we began working towards were those with an extra aryl ring, in this case pyridine, attached to the first via an alkyne. The precursors for these radialenes could be synthesised via a Sonogashira coupling of 4,4'-diiododiphenylmethane, **2.31**, and 3,3'-diiododiphenylmethane, **2.36**, with ethynylpyridines. As previously mentioned, substitution in the 3-position is desired in order to position the substituents above and below the [3]radialene core. However, as **2.31** is more readily available than **2.36** (produced via one reaction as opposed to four) it was used for the initial study. Compound **2.31** was reacted with 2-ethynylpyridine, **2.49**, and 3-ethynylpyridine, **2.50**, to produce the precursors bis(4-(pyridin-2-ylethynyl)phenyl)methane, **2.51**, and bis(4-(pyridin-3-ylethynyl)phenyl)methane, **2.52** (Scheme 2.8).

Compounds **2.49** and **2.50** were generated from the Sonogashira coupling of 2-bromopyridine, **2.45**, and 3-bromopyridine, **2.46**, respectively with 2-methyl-3-butyn-2-ol followed by subsequent deprotection of the resulting compounds (**2.47** and **2.48**) with sodium hydroxide (Scheme 2.8).[49,50] Ethynylpyridine compounds are known to be quite volatile and so the low yields of 65% and 54% are attributed to loss of product during isolation.[50] Compounds **2.47-2.50** were characterised via ^{1}H NMR spectroscopy and melting point analysis and produced data consistent with that reported in the literature.[49,50]

Early attempts at Sonagashira coupling of **2.31** and **2.49** were performed in triethylamine/acetonitrile and produced the desired di-substituted product (**2.51**). However, the ^{1}H NMR spectra revealed that the mono-substituted intermediate and the symmetrical diyne, 1,4-di(pyridine-2-yl)buta-1,3-diyne, were also present, reducing the yield of the desired product to 15%. The mono-substituted intermediate was able to be removed via silica gel chromatography; however the di-substituted product and 1,4-di(pyridine-2-yl)buta-1,3-diyne coeluted and **2.51** was only able to be obtained cleanly via subsequent washing with hot hexane. 1,4-Di(pyridine-2-yl)buta-1,3-diyne is formed via an oxidative homocoupling of the ethynyl pyridine reagent, known as Glaser coupling, which can occur if oxygen is not excluded completely from the reaction. Thorand and Krause have reported that Glaser coupling can be minimised if the reaction is performed in tetrahydrofuran, instead of the traditional triethylamine, and the alkyne is added dropwise.[51] Repeating the Sonogashira coupling of **2.31** with **2.49** and **2.50**, basing the synthesis on the procedures outlined by Thorand and Krause,[51] gave **2.51** and **2.52** in 60% and 47% yield respectively.

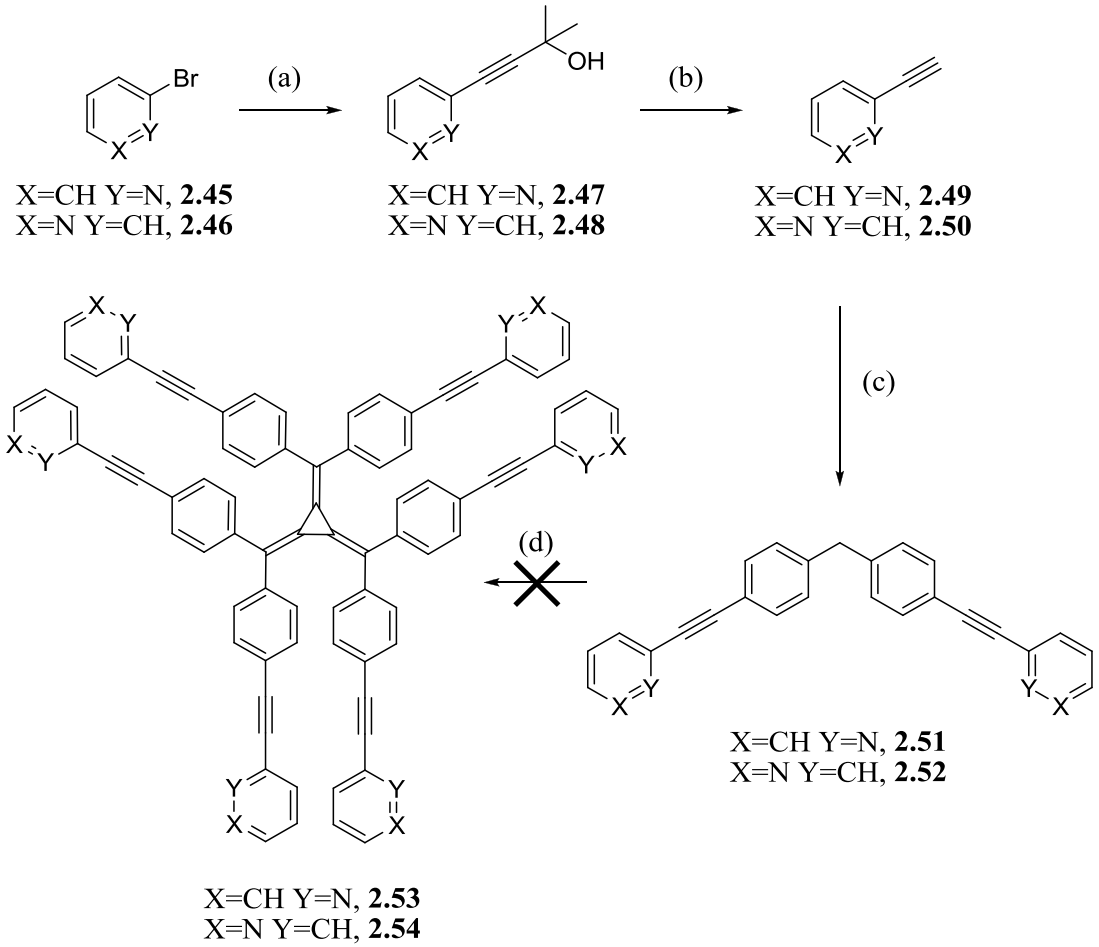

(a) 2-methyl-3-butyn-2-ol, $Pd(PPh_3)_2Cl_2$, CuI, triethylamine/THF 5:2, **2.47** 88%, **2.48** 71%; (b) NaOH, toluene, **2.49** 65%, **2.50** 54%; (c) **2.31** 0.5 equiv, $Pd(PPh_3)Cl_2$, CuI, triethylamine, THF, **2.51** 60%, **2.52** 47%; (d) i) 1.1 equiv. nBuLi, THF, -78°C, ii) ⅙ equiv. tccp, iii) O_2, 0°C.

Scheme 2.8

Compounds **2.51** and **2.52** were characterised via ^1H and ^{13}C NMR spectroscopy, IR spectroscopy, ESI-MS, elemental and melting point analysis. The molecular ions (MH^+) were observed at *m/z* 373.3 and 373.4 respectively in the mass spectrum. The characteristic C≡C peak was seen in the IR spectrum at 2222 cm^{-1} for **2.51** and at 2219 cm^{-1} for **2.52**. The methane hydrogen atoms were observed in the ^1H NMR spectrum at δ 4.01 and 4.02 for **2.51** and **2.52** respectively.

Attempts to synthesise radialene **2.53** from **2.51** using the standard procedure were unsuccessful. Deprotonation with n-BuLi at -78°C was straightforward and yielded a dark green solution. Addition of tetrachlorocyclopropene at -78°C also appeared to react appropriately turning the solution deep purple. However upon warming the reaction mixture to 0°C the solution turned brown and after subsequent oxidation no product was obtained. The incremental warming of the reaction mixture after tetrachlorocyclopropene is added is

necessary to allow the subsequent substitutions of the carbanion onto tetrachlorocyclopropene to occur. The first substitution occurs at -78°C, the second at 0°C and the third at room temperature; however it appears that the carbanion of **2.51** is not stable at 0°C and thus the reaction to form the radialene is unable to go to completion. It was hypothesised that the pyridyl nitrogen atom would be able to stabilise the carbanion via resonance but as the compound is not planar its role in stabilisation is likely to be inductive only.

It is also possible that the synthesis of this extended hexaaryl[3]radialene was not successful due to the steric bulk of the methane precursor, **2.51**, preventing the substitution of a second and third molecule onto tetrachlorocyclopropene; however, this explanation is less likely as a radialene with a high degree of steric bulk, hexakis(3,5-dimethlypyrazolyl)-[3]radialene, has been previously reported by our group.[26] As the pyridyl nitrogen in **2.52** is not conjugated to the carbanion and its inductive stabilisation of the anion would be even weaker than that of **2.51** due to it being further removed from the methylene group, the conversion of **2.52** to the [3]radialene was not attempted.

*2.3.2. Bis(4-(pyridin-4-yl)phenyl)methane **2.55***

Taking into account the problems encountered in the synthesis of extended hexaaryl[3]radialenes **2.53** and **2.54** the next radialene precursor, bis(4-(pyridin-4-yl)phenyl)methane, **2.55**, was designed with the pyridyl nitrogen closer to the methylene group by removing the alkyne linker. Compound **2.55** was produced in one step via a Suzuki coupling of **2.31** and 4-pyridineboronic acid in 38% yield (Scheme 2.9).[52,53] The nitrogen atom of the pyridine ring is in the 4-position and as such could stabilise the carbanion via resonance and induction.

Compound **2.55** was characterised via ^{1}H and ^{13}C NMR spectroscopy, IR spectroscopy, ESI-MS, elemental and melting point analysis. The molecular ion (MH^{+}) was observed at *m/z* 323.4 in the mass spectrum and the C=C peak was seen in the IR spectrum at 1594 cm^{-1}. The methane hydrogen atoms were observed in the ^{1}H NMR spectrum as a singlet at δ 4.10.

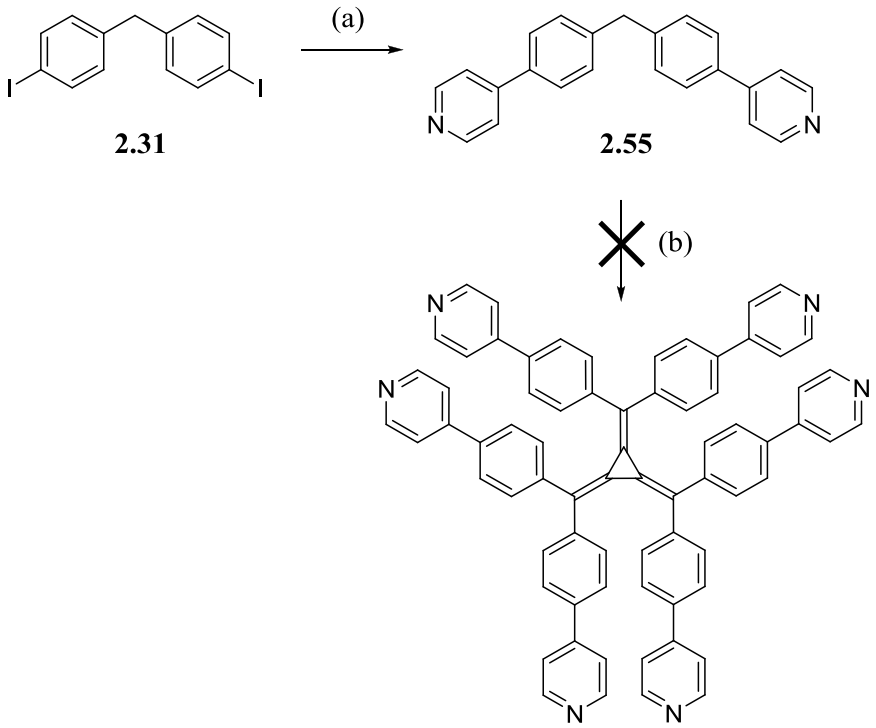

2.31 **2.55** **2.56**

(a) 2 equiv. 4-pyridineboronic acid, $Pd(PPh_3)_4$, Na_2CO_3, EtOH/benezene 5:2, 38%;
(b) i) 1.1 equiv. nBuLi, THF, -78°C, ii) ⅙ equiv. tccp, iii) O_2, 0°C.

Scheme 2.9

Attempts to synthesise radialene **2.56** from **2.55** using the standard procedure were unsuccessful. As previously noted for the alkyne precursors, the deprotonation of **2.55** with n-Buli at -78°C proceeded smoothly with a colour change from colourless to bright green. Addition of tetrachlorocyclopropene at -78°C also caused a colour change to orange indicative of reaction with the carbanion. However upon warming the reaction mixture to 0°C the solution turned brown and after subsequent oxidation no product was able to be observed. Again it appears that the carbanion is not stable at 0°C. This is likely due to rotation around the single bond connecting the aryl ring to the pyridyl ring, in order to avoid steric clash of the pyridyl and aryl protons, meaning that the pyridyl nitrogen is not in the same plane as the methylene preventing resonance stabilisation.

Attempts to synthesise extended hexaaryl[3]radialenes from **2.51**, **2.52**, and **2.56** were all unsuccessful. Subsequently, these three compounds have been studied as ligands for the synthesis of coordination polymers and the results from these investigations are presented in Chapter 6.

2.4. Attempted Synthesis of a Fluorinated [3]Radialene

2.4.1. 4,4'-Methylenebis(2,3,5,6-tetrafluorobenzonitrile) ***2.58***

Previous investigations into coordination polymers of **2.29** have found that close radialene core π-anion contacts are generally accompanied by anion-hydrogen bonds.[29] To determine whether these anion-π interactions are significant in their own right, or simply a consequence of the positioning of acidic aryl hydrogen atoms, a derivative of **2.29** with fluorine atoms replacing the hydrogens was designed. It is also possible that the fluorine atoms may enhance the observed radialene-anion interactions by participating in halogen bonding.[54,55] Fluorinated compounds have also received recent interest due to their possible application in organic electronics and crystal engineering.[56] Fortunately, the methane precursor for this radialene could be synthesised in one step from commercially available 2,3,4,5,6-pentafluorobenzonitrile, **2.57** (Scheme 2.10).[57]

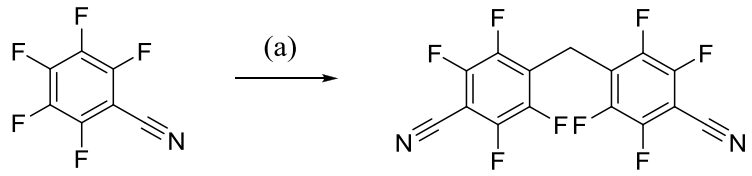

2.57 **2.58**

(a) 2 equiv. CH_3MgCl, THF, -20°C, 31%.

Scheme 2.10

Treatment of **2.57** with methyl magnesium chloride in THF under argon at -20°C gave the desired product, 4,4'-methylenebis(2,3,5,6-tetrafluorobenzonitrile), **2.58**, as well as the intermediate, 2,3,5,6-tetrafluoro-*p*-toluonitrile, as a crude yellow oil. The oil crystallised over one week and recrystallisation from methanol provided **2.58** as a pure crystalline solid in 31% yield. The precursor was characterised by ^{1}H NMR spectroscopy, where one CH_2 peak was observed at δ 4.29, ^{19}F NMR spectroscopy, which displayed two peaks for the aryl fluorine atoms at δ -139.17 and -132.08, as well as IR spectroscopy, the characteristic nitrile peak was observed at 2248 cm^{-1}, and ESI-MS, the molecular ion (MH^+) appeared at *m/z* 361.9.

Single crystals of **2.58** suitable for X-ray crystallography were obtained via recrystallisation of the crude product from methanol. The compound crystallises in the monoclinic space group $P2_1/c$ with one complete molecule in the asymmetric unit. The structure was refined to R_1 6.77% with no disorder problems. A perspective view of the asymmetric unit is depicted in Figure 2.10.

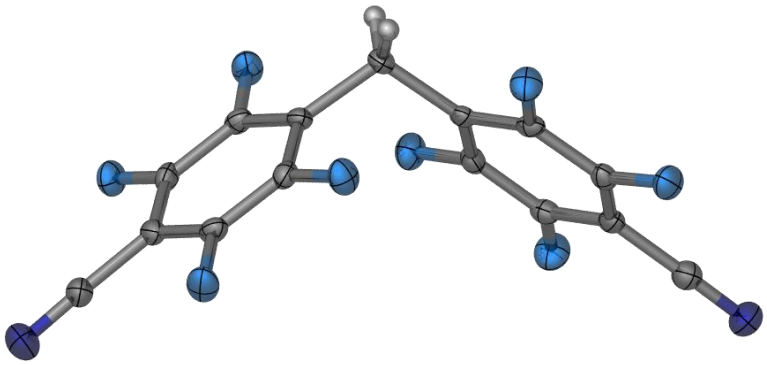

Figure 2.10. The asymmetric unit of compound **2.58** with anisotropic displacement parameters represented as ellipsoids at the 50% probability level.

The bond lengths and angles are consistent with normal aromatic rings; the C-C bond lengths range from 1.371(5)-1.394(6) Å. There is quite a pronounced twist of the aromatic rings in structure **2.58** in order to prevent steric clash of the fluorine substituents. This is demonstrated by the torsion angles of the aryl rings around the CH_2 linker being 65.5 and 71.8°. In the hydrogenated derivative, **2.25**, there is no twist of the aryl rings as shown by torsion angles of 85.5 and 94.5°.

*2.4.2. Attempted Synthesis of Hexakis(2,3,5,6-tetrafluoro-4-cyanophenyl)[3]radialene **2.59***

Successful and relatively efficient synthesis of the methane precursor, **2.58**, allowed multiple attempts at producing the desired [3]radialene, **2.59** (Scheme 2.11). Deprotonation of **2.58** with n-BuLi at -78°C was successful with the production of a bright orange solution of the carbanion. Addition of tetrachlorocyclopropene caused a colour change to a deep red solution, which was maintained during warming through 0°C to room temperature. However issues were again encountered at the oxidation step. Direct oxidation via bubbling gaseous oxygen and air thorough the solution and indirect aerial oxidation all led to intractable brown mixtures with no fluorescent spots observed via TLC. Attempts to isolate the product directly from the reaction mixture, bypassing the oxidation step, led to the separation of a small amount of yellow oil. The desired product peak of 1115 *m/z* was not observed in the negative ion mass spectrum and the ^{19}F NMR spectrum exhibited no discernible peaks.

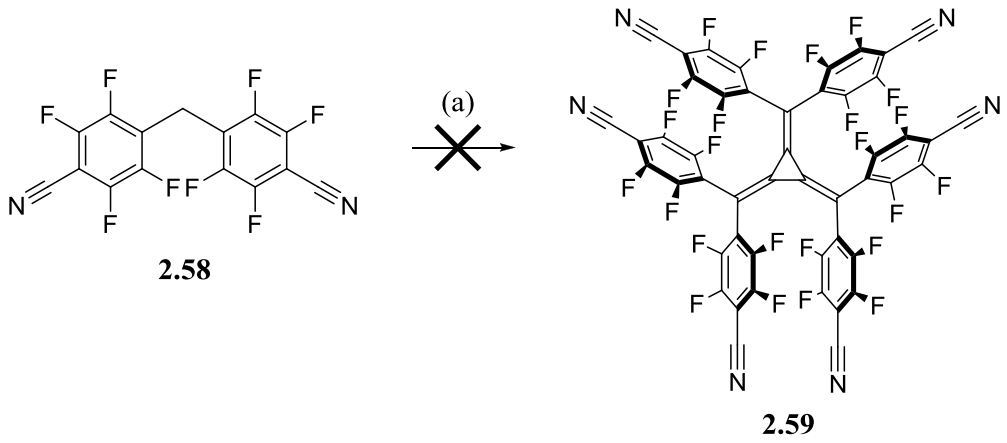

2.58 **2.59**

(a) various conditions (see text).

Scheme 2.11

Similar to **2.43**, the methane hydrogen atoms of **2.58** are so acidic that it is able to be deprotonated by the weaker base sodium hydride (in fact a small degree of deprotonation, indicated by a colour change, is observed upon addition of DMF as a solvent). When performed in DMF at 0°C using sodium hydride as the base the reaction proceeds in a fashion analogous that described above with colour changes upon addition of reactants that initially appeared promising. Again upon oxidation the reaction mixture seemed to decompose. This led us to hypothesise that the desired radialene, **2.59**, was too electron deficient to be stable as the neutral species. This was followed by attempts to trap the anion as its tetrabutylammonium salt. Addition of tetrabutylammonium hexafluorophosphate as a solution in THF to the reaction mixture caused the precipitation of colourless crystals. However, upon analysis of these crystals by ^{19}F NMR spectroscopy it was found that only peaks corresponding to the hexafluorophosphate anion were present. After much synthetic effort the synthesis of **2.59** was abandoned as indications of the desired product were not observed in mass spectra or ^{19}F NMR spectra of the isolated fractions or the reaction mixtures produced under a wide range of reaction conditions and using various purification procedures.

2.5. Summary

This chapter has outlined the progression of the chemistry of selected cross-conjugated compounds since the 1950's and highlighted that the field remains underdeveloped, particularly the study of radialenes. The synthesis of three nitrile substituted hexaaryl[3]radialenes, **2.29**, **2.38**, and **2.44**, have been described, two of which are new compounds. During the development of these synthetic routes it has been noted that the position of the electron withdrawing substituents on the methane precursor plays an important role in the overall success of the radialene reaction.

When the nitrile group is in the 4-position of the aryl ring it is able to withdraw electron density from the methylene position via induction and resonance. This leads to an increased acidity of the methylene protons making specific deprotonation at this position easier. The resultant carbanion is then stabilised via resonance delocalisation onto the electronegative nitrogen atom of the nitrile substituent. Increased stability of the carbanion results in a high yield of the hexaaryl[3]radialene product as observed for **2.29**, 71%, and **2.44**, 76%.

Conversely, when the nitrile group is in the 3-position of the aryl ring it is only able to withdraw electron density from the methane position via induction, which results in less acidic methylene protons. This could possibly lead to non-specific deprotonation of the aryl rings upon addition of a strong base. The resultant carbanion can no longer be stabilised via resonance as it is not conjugated to the nitrile group in the 3-position as it was when the nitrile group was in the 4-position. Decreased acidity of the methylene protons and stabilisation of the carbanion results in a much lower yield of the hexaaryl[3]radialene product, 16% for **2.38**.

The electrochemical and physical properties of these radialenes have been investigated and the attributes which make them promising anion sensor components - intrinsic electron deficiency, intense fluorescence emission and propeller-like 3-D structure - have been highlighted. The solid-state structures of radialenes **2.29** and **2.44** have both exhibited the double-bladed propeller conformation with the "arms" of the radialene at an average torsion angle of 39° to the core plane. The nitrile groups in the 3-position of radialene **2.44** have been shown to reside above and below the plane of the core, interestingly not in a symmetrical arrangement (four directed to one side and two to the other), which would be required to produce metallo-supramolecular cage assemblies from these compounds. The propeller structure is also maintained in solution as shown by the upfield shift of the aryl protons of the [3]radialene compared to those of the methylene precursor in the ^{1}H NMR spectrum. This is due to the shielding of these protons by aryl rings on adjacent radialene "arms".

The increasing electron deficiency of the radialenes along the series **2.38** < **2.29** < **2.44** has been shown via the determination of their respective reduction potentials by cyclic

voltammetry. Hexaaryl[3]radialenes undergo two stepwise reductions to form the radical anion and the dianion respectively and radialene **2.44** was shown to have the lowest reduction potentials of -0.06 and -0.45 V. The increased electron deficiency of **2.44** is due to the combined electron withdrawing potential of its twelve nitrile substituents and this also results in increased acidity of the aryl protons. The electron deficient radialene core and the acidic aryl protons are favourable motifs for anion interactions, making anions a possible target for radialene based sensors.

The series of nitrile radialenes are all brightly coloured with **2.38** being bright orange, whereas **2.29** and **2.44** are red in colour. They are also highly fluorescent and exhibit large Stokes shifts; the difference between the excitation and emission maxima. A fluorescent sensor ideally possesses a large Stokes shift as this allows the emission photons to be detected against a low background signal, isolated from the excitation photons, which enhances the sensitivity of the technique. Interaction of the radialene based sensors with anions may produce a shift in the emission maxima or a change in intensity of the fluorescent signal, which could be measured qualitatively or quantitatively.

Despite considerable synthetic effort, the acquisition of extended hexaaryl[3]radialenes, with the aim of utilising these as components in metallo-supramolecular capsules, was unsuccessful. This was largely proposed to be due to the instability of the methane carbanions of **2.51**, **2.52**, and **2.55**. Electron-withdrawing groups were present in the methane precursors in the form of pyridine rings yet it was presumed that bond rotation placing the pyridyl nitrogen in a different plane to the methylene resulted in reduced resonance stabilisation. However, these methane precursors, **2.51**, **2.52**, and **2.55**, make interesting ligands for metal coordination in their own right and the results from these studies are detailed in Chapter 6.

A recent study, published during the course of this work, by Matsumoto and colleagues reported the synthesis of extended hexaaryl[3]radialenes via post-synthetic modification of hexakis(4-bromophenyl)[3]radialene.[58] This was effected via a cross-coupling reaction with various lithium diarylamides according to Hartwig's procedure. Post-synthetic modification of pre-existing hexaaryl[3]radialenes may provide a more effective route for the formation of the desired extended hexaaryl[3]radialenes.

Finally, attempts to produce a fluorinated derivative of radialene **2.29**, hexakis(2,3,5,6-tetrafluoro-4-cyanophenyl)[3]radialene **2.59**, were unsuccessful. The required precursor, **2.58**, was synthesised and fully characterised, however numerous attempts at conversion to the [3]radialene provided no indication of the desired product in the mass spectra or ^{19}F NMR spectra. Isolation of the dianion as its tetrabutylammonium salt was also ineffective.

2.6. Experimental

2.6.1. General Experimental

Melting points were determined using a Gallenkamp variable heat melting point apparatus and are uncorrected. UV–visible absorption spectra were recorded on a Varian CARY 5000 spectrophotometer. Samples were dissolved in dichloromethane or acetone at a concentration of approximately 0.03 mM. Fluorescence spectra were recorded on a Varian CARY Eclipse spectrophotometer. Samples were dissolved in dichloromethane or acetone at a concentration of approximately 0.01 mM. Infrared spectra were recorded using a Perkin Elmer Spectrum 100 FTIR spectrometer with a universal attenuated total reflectance (UATR) sampling accessory. The Campbell microanalytical laboratory at the University of Otago performed the elemental analyses.

Low resolution mass spectra were acquired using either electrospray ionisation on a Finnigan LCQ mass spectrometer (ESI-MS) or electron impact on a Shimadzu GCMS-QP5050A gas chromatograph mass spectrometer (EI-MS). Samples were dissolved in HPLC grade methanol or acetonitrile with a concentration of 0.01 mg/cm^3. Electrospray ionisation, high resolution mass spectroscopy (ESI-HRMS) was performed by the Adelaide Proteomics Centre using an LTQ Orbitrap XL ETD spectrometer.

^{1}H NMR spectra were recorded on a Varian Gemini 300 MHz spectrometer (75 MHz for ^{13}C NMR, 121 MHz for ^{19}F) or a Varian Inova 600 MHz spectrometer (150 MHz for ^{13}C NMR). ^{1}H NMR spectra recorded in $CDCl_3$ were referenced to the internal standard Me_4Si (0 ppm). ^{1}H NMR spectra recorded in DMSO-d_6 and acetone-d_6 were referenced to the solvent peaks 2.50 ppm and 2.05 ppm, respectively. ^{13}C NMR spectra recorded in $CDCl_3$, DMSO-d_6 and acetone-d_6 were referenced to the solvent peaks 77.0 ppm, 39.5 ppm and 29.9 ppm, respectively. ^{19}F NMR recorded in $CDCl_3$ were referenced to external C_6F_6.

Unless otherwise stated, reagents were obtained from commercial sources and used as received. Solvents were dried by literature procedures[59] and freshly distilled as required. 2-Methyl-4-(2-pyridyl)-3-butyn-2-ol (**2.47**),[49,60] 2-methyl-4-(3-pyridyl)-3-butyn-2-ol (**2.48**),[49,60] 2-ethynylpyridine (**2.49**),[50] and 3-ethynylpyridine (**2.50**)[50] were synthesised following literature procedures.

2.6.2. Synthetic Procedures

4,4'-Diiododiphenylmethane (2.31). 4,4'-Diaminodiphenylmethane (5.00 g, 25.2 mmol) in concentrated sulfuric acid (30 mL) was stirred at 0°C. Sodium nitrite (5.00 g, 72.4 mmol) in water (20 mL) was added dropwise over a period of 15 min. The resultant solution was

stirred at 0°C for 30 min followed by the addition of potassium iodide (29.2 g, 176 mmol) in water (100 mL). The reaction mixture was heated at 60°C for 1 h then cooled to room temperature and basified with 40% sodium hydroxide solution (60 mL). The mixture was extracted with dichloromethane (6×50 mL). The organic fractions were combined and washed with 1M hydrochloric acid solution (150 mL), 1M aqueous sodium thiosulfate solution (150 mL), dried ($MgSO_4$), and the solvent evaporated under vacuum to yield a brown solid. Purification via silica chromatography, eluting with petroleum spirit, yielded **2.31** as white needles (6.55 g, 62%). Mp 84-86°C (lit.[30] 85-86°C); ^{1}H NMR (300 MHz, $CDCl_3$): δ 3.85 (s, 2H, CH_2); 6.90 (d, 4H, [J = 8.2 Hz], H2, H6); 7.60 (d, 4H, [J = 8.2 Hz], H3, H5); ^{13}C NMR (150 MHz, $CDCl_3$): δ 41.1, 91.8, 131.1, 137.8, 140.3; EI-MS: *m/z* 419.8 (M^+); FT-IR v_{max}/cm^{-1}: 1581 (C=C).

4,4'-Dicyanodiphenylmethane (2.25). A mixture of **2.31** (1.00 g, 2.38 mmol) and copper cyanide (0.66 g, 7.37 mmol) in dry DMF (15 mL) was heated at 100°C for 2 days. The cooled reaction mixture was diluted with EtoAc (40 mL) and the resultant solution washed with concentrated ammonia solution (30 mL), water (20 mL), brine (20 mL), dried ($MgSO_4$) and the solvent evaporated under vacuum to yield **2.25** as an off white solid (0.50 g, 95%). Mp 165-167°C (lit.[32]166-167°C); ^{1}H NMR (300 MHz, $CDCl_3$): δ 4.09 (s, 2H, CH_2); 7.27 (d, 4H, [J = 8.2 Hz], H2, H6); 7.61 (d, 4H, [J = 8.2 Hz], H3, H5); ^{13}C NMR (150 MHz, $CDCl_3$): δ 42.1, 111.0, 118.8, 129.9, 132.8, 145.0; EI-MS: *m/z* 218.1 (M^+); FT-IR v_{max}/cm^{-1}: 2225 (C≡N). Crystals of **2.25** suitable for X-ray crystallography were obtained via slow evaporation from methanol. Anal. calcd for $C_{15}H_{10}N_2$ C 82.54, H 4.63, N 12.84; found, C 82.30, H 4.55, N 12.80%.

Hexakis(4-cyanophenyl)[3]radialene (2.29). Compound **2.25** (1.20 g, 5.50 mmol) was placed in a dry two-necked flask under argon. Dry THF(40 mL) was added and the solution was cooled to -78 °C. n-BuLi (2.40 mL of a 2.48 M solution in hexane) was added slowly and the reaction mixture stirred for 30 min. Tetrachlorocyclopropene (100 μL, 0.92 mmol) was added and the solution stirred at -78 °C for 1 h, 0 °C for 30 min and room temperature for 30 min. The mixture was again cooled to 0 °C and oxygen bubbled through it for 30 min at 0 °C and then 1 h at room temperature. The resultant red/brown solution was quenched with water (40 mL) and extracted with DCM (60 mL) followed by further DCM (5×20 mL). The organic extracts were combined, dried ($MgSO_4$), and the solvent evaporated to yield a dark red solid. Purification via silica chromatography eluting with 24:1 $CHCl_3$/MeOH yielded **2.29** as a dark red solid (0.45 g, 71%). Mp >300°C (lit.[21] 400-402°C); ^{1}H NMR (600 MHz, DMSO-d_6): δ 6.92 (d, 12H, [J = 8.1 Hz], H2, H6); 7.35 (d, 12H, [J = 8.1 Hz], H3, H5); ^{13}C NMR (150 MHz, $CDCl_3$): δ 110.7, 118.3, 120.7, 123.2, 130.5, 130.9, 143.4; ESI-MS (-ve mode): *m/z* 683.3

([M-H]$^-$); FT-IR v_{max}/cm^{-1}: 2224 (C≡N), 1599 (C=C). Crystals of **2.29** suitable for X-ray crystallography were obtained via slow evaporation from nitromethane. Anal. calcd for $C_{48}H_{24}N_6.CH_3NO_2$ C 78.90, H 3.66, N 13.15; found, C 79.45, H 3.50, N 12.97%; FT-IR υ_{max}/cm^{-1}: 2224 (C≡N str., vs), 1598 (C=C, str., vs), 1556 and 1379 (N-O, str.).

3,3'-Dinitrobenzophenone (2.33). Benzophenone (20.0 g, 110 mmol) was dissolved in concentrate sulphuric acid (110 mL) at room temperature. A mixture of concentrated nitric acid (12 mL) and concentrated sulfuric acid (28 mL) was added and the reaction mixture heated slowly to 75°C then stirred at 75°C for 45 min. After cooling to room temperature the mixture was poured over crushed ice. The yellow gummy mass produced hardened overnight and was ground into a powder, which was washed with water until the washings were neutral. The resultant pale yellow solid was air dried and recrystallised from butanone to yield **2.33** as a cream coloured solid (12.9 g, 43%). Mp 150-154°C (lit.[34] 144-146°C); ^{1}H NMR (300 MHz, $CDCl_3$): δ 7.78 (t, 2H,[J = 8.0 Hz], H5); 8.15 (dd, 2H, [J = 8.0, 1.2 Hz], H4); 8.44 (dd, 2H, [J = 8.0, 1.2 Hz], H6); 8.64 (s, 2H, H2); EI-MS: *m/z* 272.0 (M^+); FT-IR v_{max}/cm^{-1}: 1659 (C=O), 1615 (C=C), 1541 and 1348 (N-O).

3,3'-Diaminobenzophenone (2.34). A mixture of **2.33** (5.00 g, 18.4 mmol) and stannous chloride (25.0 g, 132 mmol) in concentrated hydrochloric acid (100 mL) was stirred at 70°C for 6 h. The pale yellow precipitate which formed was isolated and taken up in water (100 mL), to which 1 M sodium hydroxide solution (200 mL) was added. The resultant suspension was extracted with EtOAc (3×200 mL) and the extracts dried (Na_2SO_4), and the solvent evaporated under vacuum to yield **2.34** as a yellow solid (3.85 g, 99%). Mp 149-152°C (lit.[35] 148-149°C); ^{1}H NMR (300 MHz, DMSO-d_6): δ 5.40 (s, 4H, br, 2(NH_2)); 6.84 (d, 4H, [J = 7.6 Hz], H4, H6); 6.95 (s, 2H, H2); 7.19 (t, 2H, [J = 7.6 Hz], H5); EI-MS: *m/z* 212.1 (M^+); FT-IR v_{max}/cm^{-1}: 3393 and 3300 (N-H), 1743 (C=O), 1595 (C=C).

3,3'-Diaminodiphenylmethane (2.35). Compound **2.34** (1.00 g, 4.71 mmol) was added to a solution of potassium hydroxide (0.53 g, 9.45 mmol) in ethylene glycol (20 mL) resulting in a bright yellow suspension. Hydrazine hydrate (0.34 mL, 10.83 mmol) was added and the resultant mixture heated at reflux for 4 h. The reaction mixture was then cooled to room temperature and extracted with benzene (6×20 mL) and the extracts washed with water (20 mL), brine (20 mL), dried ($MgSO_4$), and the solvent evaporated under vacuum to yield **2.35** as a yellow oil (0.59 g, 63%). ^{1}H NMR (300 MHz, $CDCl_3$): δ 3.59 (s, 4H, br, 2(NH_2)); 3.79 δ(s, 2H, CH_2); 6.52 (m, 4H, overlapped singlet and doublet, H2, H6); 6.61 (d, 2H, [J = 7.5 Hz], H4); 7.07 (t, 2H, [J = 7.5 Hz], H5), EI-MS: *m/z* 198.1 (M^+); FT-IR v_{max}/cm^{-1}: 3423 and 3346 (N-H), 1598 (C=C).

3,3'-Diiododiphenylmethane (2.36). Compound **2.35** (0.62 g, 3.13 mmol) in concentrated sulfuric acid (10 mL) was stirred at 0°C. Sodium nitrite (0.62 g, 8.99 mmol) in water (6 mL) was added dropwise over a period of 10 min. The resultant solution was stirred at 0 °C for 30 min followed by the addition of potassium iodide (3.62 g, 21.8 mmol) in water (40 mL). The reaction mixture was heated at 50 °C for 1 h then cooled to room temperature and neutralized with aqueous sodium hydroxide solution (50% w/v, 5 mL). The mixture was extracted with DCM (6×10 mL). The organic fractions were combined and washed with 1M hydrochloric acid solution (20 mL), 1 M sodium thiosulfate solution (20 mL), dried ($MgSO_4$), and the solvent evaporated under vacuum to yield a brown solid. Purification via silica chromatography eluting with hexane yielded **2.36** as white needles (0.73 g, 55%). Mp 63-65°C; ^{1}H NMR (300 MHz, $CDCl_3$): δ 3.85 (s, 2H, CH_2), 7.03 (t, 2H, [J = 7.8 Hz], H5), 7.12 (d, 2H, [J = 7.8 Hz], H6), 7.53-7.70 (overlapped d and s, 4H, H2, H4); ^{13}C NMR (75 MHz, $CDCl_3$): δ 40.9, 94.7, 128.2, 130.3, 135.5, 137.8, 142.6; ESI-MS: *m/z* 420.1 (MH^+); FT-IR ν_{max}/cm^{-1}: 1582 (C=C).

3,3'-Dicyanodiphenylmethane (2.37). A mixture of **2.36** (0.71 g, 1.69 mmol) and copper cyanide (0.47 g, 5.25 mmol) in dry DMF (15 mL) was heated at 100 °C for 2 days. The cooled reaction mixture was diluted with EtOAc (40 mL) and the resultant solution washed with concentrated ammonia solution (30 mL), water (20 mL), brine (20 mL), dried ($MgSO_4$), and the solvent evaporated under vacuum to yield **2.37** as an off-white solid (0.33 g, 90%). Mp 151-153°C; ^{1}H NMR (300 MHz, $CDCl_3$): δ 4.05 (s, 2H, CH_2), 7.41-7.48 (m, 6H, H2, H4, H5), 7.56 (d, 2H, [J = 7.8 Hz], H6); ^{13}C NMR (75 MHz, $CDCl_3$): δ 40.8, 112.9, 118.5, 129.6, 130.5, 132.3, 133.3, 140.9; ESI-MS: *m/z* 218.2 (MH^+); FT-IR ν_{max}/cm^{-1}: 2224 (C≡N), 1597 (C=C). Crystals of **2.37** suitable for X-ray crystallography were obtained via slow evaporation from methanol. Anal. calcd for $C_{15}H_{10}N_2$ C 82.54, H 4.63, N 12.84; found, C 81.82, H 4.52, N 12.77%.

Hexakis(3-cyanophenyl)[3]radialene (2.38). Compound **2.37** (0.50 g, 2.29 mmol) was placed in a dry two-necked flask under argon. Dry THF (20 mL) was added and the solution was cooled to -78 °C. n-BuLi (1.04 mL of a 2.20 M solution in hexane) was added slowly and the reaction mixture stirred for 30 min. Tetrachlorocyclopropene (46.0 μL 0.38 mmol) was added and the solution stirred at -78 °C for 1 h, 0 °C for 30 min and room temperature for 30 min. The mixture was again cooled to 0 °C and oxygen bubbled through it for 30 min at 0 °C and then 1 h at room temperature. The resultant brown solution was quenched with water (40 mL) and extracted with DCM (30 mL) followed by further DCM (5×10 mL). The organic extracts were combined, dried ($MgSO_4$), and the solvent evaporated to yield a brown oil. Purification via silica chromatography eluting with 1:2 EtOAc/hexane yielded **2.38** as an

orange solid (40.0 mg, 16%). Mp 321°C (dec.); ^{1}H NMR (300 MHz, $CDCl_3$): δ 6.96 (s, 6H, H2); 7.23 (d, 6H, [J = 7.9 Hz], H6), 7.30 (t, 6H, [J = 7.9 Hz], H5); 7.59 (d, 6H, [J = 7.9 Hz], H4); ^{13}C NMR (75 MHz, $CDCl_3$): δ 112.5, 117.9, 118.9, 123.0, 129.5, 132.3, 134.0, 140.6; ESI-HRMS: (MH^+) calcd for $C_{48}H_{25}N_6$ *m/z* 685.21352; found 685.21196; FT-IR v_{max}/cm^{-1} 2228 (C≡N); Anal. calcd for $C_{48}H_{24}N_6 \cdot H_2O$ C 82.03, H 3.74, N 11.96; found, C 81.54, H 4.31, N 10.90%.

4,4'-Methyldiphthalic acid (2.40). 4,4'-Carbonyldiphthalic acid (4.40 g, 12.3 mmol) was dissolved in EtOH (100 mL). 5% Pd/C (0.88 g) was added and the resultant mixture heated at reflux under a hydrogen atmosphere for 1 week. After cooling the mixture was filtered and the filtrate concentrated under reduced pressure. The residue was dissolved in water (30 mL), basified with sodium hydroxide (4.00 g, 100 mmol) and heated at reflux for 1 h. Upon cooling the solution was acidifed with dilute sulfuric acid and concentrated to 30 mL under reduced pressure, which resulted in the precipitation of a white solid. Filtration and subsequent drying in a desiccator overnight yielded **2.40** as a white solid (4.06 g, 95%). Mp 255°C; ^{1}H NMR (300 MHz, DMSO-d_6): δ 4.09 (s, 2H, CH_2); 7.39 (d, 2H, [J = 8.0 Hz], H5); 7.81 (s, 2H, H3); 7.91 (d, 2H, [J = 8.0 Hz], H6); ^{13}C NMR (75 MHz, DMSO-d_6): δ 130.7, 131.0, 131.4, 131.8, 134.6, 143.3, 168.0, 168.3, DMSO peak obscures CH_2 carbon; ESI-MS (-ve mode): *m/z* 343.0 ($[M-H]^-$); FT-IR v_{max}/cm^{-1} 3435 (O-H), 1656 (C=O) 1572 (C=C).

4,4'-Methyldiphthalimide (2.41). Compound **2.40** (4.00 g, 11.6 mmol) was suspended in formamide (35 mL) and stirred at 190°C for 2 h, then 150°C for 1 h, before being cooled to room temperature. The resultant precipitate was collected via filtration and washed thoroughly with water. Drying in a desiccator overnight yielded 4,4'-methyldipthalimide as a white powder (3.01 g, 85%). Mp >280°C. ^{1}H NMR (300 MHz,DMSO-d_6): δ 4.33 (s, 2H, CH_2); 7.77-7.80 (m, 6H); 11.27 (s, 2H, NH); ^{13}C NMR (75 MHz, DMSO-d_6): δ 40.6, 123.2, 123.3, 130.8, 133.3, 134.7, 147.4, 169.0, 169.1; ESI-MS: *m/z* 307.4 (MH^+); FT-IR: v_{max}/cm^{-1} 3185 (N-H), 1770 and 1712 (C=O), 1603 (C=C).

4,4'-Methyldiphthalamide (2.42). Compound **2.41** (2.98 g, 9.73 mmol) was finely crushed and suspended in 28% concentrated ammonia solution (40 mL). The flask was stoppered and the mixture stirred for 2 days at room temperature. The resultant mixture was filtered and the precipitate washed thoroughly with water. Drying in a desiccator overnight yielded **2.42** as a white powder (2.82 g, 85%). Mp >280°C; ^{1}H NMR (300 MHz, DMSO-d_6): δ 4.01 (s, 2H, CH_2); 7.29-7.43 (m, 10H); 7.67-7.69 (m, 4H); ^{13}C NMR (75 MHz, DMSO-d_6): δ 127.9, 129.3, 133.8, 136.7, 142.0, 169.9, 170.2, DMSO peak obscures CH_2 carbon; ESI-MS (-ve mode): *m/z* 340.8 ($[M-H^+]^-$); FT-IR: v_{max}/cm^{-1} 3329 and 3176 (N-H), 1693 and 1649 (C=O), 1603 (C=C).

4,4'-Methyldiphthalonitrile (2.43). Compound **2.42** (2.78 g, 8.17 mmol) was suspended in DMF (40 mL) and the mixture cooled to -20°C. Sulfonyl chloride (20 mL) was added dropwise ensuring the temperature remained below 0°C. The resultant mixture was stirred at 0°C for 2 h and then allowed to warm to room temperature overnight. The reaction mixture was slowly poured onto crushed ice (400 g) and stirred until the ice was completely melted. The resultant precipitate was collected via filtration, washed thoroughly with water, and dried in a desiccator. Purification via silica chromatography eluting with DCM yielded **2.43** as a white powder (1.96 g, 89%). Mp 205°C; ^{1}H NMR (300 MHz, acetone-d_6): δ 4.45 (s, 2H, CH_2); 7.92 (m, 2H, H6); 8.04 (m, 4H, H2, H5); ^{13}C NMR (75 MHz, acetone-d_6): δ 41.5, 114.7, 116.4 (two signals overlapped), 116.8, 135.1, 135.4 (two signals overlapped), 146.9; ESI-MS (-ve mode): *m/z* 267.1 ([M-H$^+$]$^-$); FT-IR: v_{max}/cm^{-1} 2233 (C≡N), 1596 (C=C). Crystals of **2.43** suitable for X-ray crystallography were obtained via slow evaporation from acetonitrile. Anal. calc. for $C_{17}H_8N_4$ C 76.10, H 3.01, N 20.89%; found C 75.82, H 3.01, N 21.10%.

Hexakis(3,4-dicyanophenyl)[3]radialene (2.44). 60% Sodium hydride (50.0 mg, 1.26 mmol) was placed in a dry two-necked flask under argon. Degassed DMF (3 mL) was added and the suspension stirred for 15 min. The mixture was then cooled to 0°C and a solution of **2.43** (322 mg, 1.20 mmol) in degassed DMF (12 mL) was added dropwise via cannula. The resultant deep blue solution was stirred at 0°C for 30 min and then at room temperature for 1 hr. The reaction mixture was again cooled to 0°C and tetrachlorocyclopropene (23.0 μL, 0.20 mmol) was added slowly. The flask was hermetically sealed and allowed to warm to room temperature then stirred for 2 days. The mixture was then cooled back to 0°C and fitted with a potassium hydroxide drying tube. The solution was then warmed slowly back to room temperature and stirred for a further two days. The deep red solution was then poured onto cold saturated ammonium chloride solution (200 mL) and stirred overnight. After dilution with water (300 mL) the mixture was filtered to yield a brown solid. Purification by silica chromatography eluting with MeOH/acetone/DCM 0.5:1:9 until one red spot was observed and then further elution with acetone yielded **2.44** as a red solid (127 mg, 76%). Mp >280°C; ^{1}H NMR (600 MHz, DMSO-d_6/TFA): δ 7.30 (d, 6H, [J = 7.8 Hz], H5); 7.56 (s, 6H, H2); 7.82 (d, 6H, [J = 7.8 Hz], H6); ^{13}C NMR (150 MHz, DMSO-d_6/TFA): δ 114.4, 114.6, 115.5, 115.7 122.1, 122.4, 133.7, 135.3, 135.6, 143.7; ESI-HRMS (-ve mode): (M$^-$) calcd for $C_{54}H_{18}N_{12}$ *m/z* 834.17829; found 834.17629; FT-IR: v_{max}/cm^{-1} 2235 (C≡N), 1595 (C=C). Crystals of **2.44** suitable for X-ray crystallography were obtained via slow evaporation from acetonitrile. Anal. calcd for $C_{54}H_{18}N_{12}.H_2O$ C 76.04, H 2.37, N 19.71; found C 75.67, H 2.37, N 19.21%.

Bis(4-(pyridin-2-ylethynyl)phenyl)methane (2.51). To a stirred mixture of **2.31** (2.92 g, 6.95 mmol), copper iodide (106 mg, 0.56 mmol), and $[Pd(PPh_3)_2Cl_2]$ (205 mg, 0.28 mmol) in THF (25 mL) was added triethylamine (3.87 mL, 20.85 mmol) at room temperature under nitrogen. A solution of **2.49** (1.51 g, 14.6 mmol) in THF (10 mL) was then added over 30 min. The resultant solution was stirred at room temperature for 2 days. The reaction mixture was filtered and the precipitate washed with THF (20 mL). The filtrate and washings were then evaporated under vacuum to yield a brown oil. Purification via silica chromatography, eluting with 1:1 EtOAc/hexane, yielded **2.51** as a tan coloured solid (1.53 g, 60%). Mp 148-150°C; ^{1}H NMR (600 MHz, $CDCl_3$): δ 4.01 (s, 2H, CH_2); 7.18 (d, 4H, [J = 8.1 Hz], H2, H6); 7.23 (td, 2H, [J = 5.4 and 1.6 Hz], H4'); 7.51 (d, 2H, [J = 8.1 Hz], H6'); 7.54 (d, 4H, [J = 8.1 Hz], H3, H5); 7.67 (td, 2H, [J = 8.1 and 1.8 Hz], H5'); 8.62 (d, 1H, [J = 4.2 Hz], H3'); ^{13}C NMR (150 MHz, $CDCl_3$): δ 41.78, 88.49, 89.18, 120.2, 122.6, 127.1, 129.0, 132.3, 136.1, 141.5, 143.5, 150.4; ESI-MS: *m/z* 371.3 (MH^+); FT-IR: ν_{max}/cm^{-1} 2222 (C≡C), 1580 (C=C); Anal. calcd for $C_{27}H_{18}N_2$ C 87.53, H 4.91, N 7.56; found C 87.12, H 4.89, N 7.77%.

Bis(4-(pyridin-3-ylethynyl)phenyl)methane (2.52). To a stirred mixture of **2.31** (1.20 g, 2.86 mmol), copper iodide (43.0 mg, 0.23 mmol), and $[Pd(PPh_3)_2Cl_2]$ (84.0 mg, 0.11 mmol) in THF (25 mL) was added triethylamine (1.59 mL, 8.55 mmol) at room temperature under argon. A solution of **2.50** (0.62 g, 6.01 mmol) in THF (10 mL) was then added over 30 min. The resultant solution was stirred at room temperature for 4 days. The reaction mixture was filtered and the precipitate washed with THF (20 mL). The filtrate and washings were then evaporated under vacuum to yield an orange solid. Purification via silica chromatography, eluting with 1:1 EtOAc/hexane, yielded **2.52** as a yellow solid (0.45 g, 42%). Mp 145-147°C; ^{1}H NMR (600 MHz, $CDCl_3$): δ 4.02 (s, 2H, CH_2); 7.19 (d, 4H, [J = 8.1 Hz], H2, H6); 7.28 (dd, 2H, [J = 7.8 and 4.7 Hz], H5'); 7.48 (d, 4H, [J = 8.1 Hz], H3, H5); 7.79 (dt, 2H, [J = 7.8 and 1.6 Hz], H6'); 8.54 (dd, 2H, [J = 4.7 and 1.6 Hz], H4'); 8.76 (s, 2H, H2'); ^{13}C NMR (150 MHz, $CDCl_3$): δ 41.73, 85.8, 92.5, 120.5 (two peaks overlapped), 123.0, 129.1, 131.9, 138.3, 141.4, 148.5, 152.2; ESI-MS: *m/z* 371.4 (MH^+); FT-IR: ν_{max}/cm^{-1} 2219 (C≡C), 1582 (C=C); Anal. calcd for $C_{27}H_{18}N_2 \cdot ½(H_2O)$ C 85.45, H 5.06, N 7.38; found C 85.45, H 4.94, N 7.25%.

Bis(4-(pyridin-4-yl)phenyl)methane (2.55). To a suspension of 4-pyridine boronic acid (1.30 g, 10.5 mmol) in EtOH (100 mL) was added a solution of **2.31** (2.00 g, 4.76 mmol) in benzene (40 mL) followed by a solution of sodium carbonate (3.20 g, 30.1 mmol) in water (20 mL). The mixture was then degassed with nitrogen for 20 min followed by the addition of $[Pd(PPh_3)_4]$ (0.60 g, 0.52 mmol). The reaction was then heated at reflux under nitrogen overnight. The resultant suspension was cooled to room temperature and filtered. The filtrate was then evaporated under vacuum. The residue was taken up in DCM (75 mL) and washed

with water, brine, dried (Na_2SO_4) and the solvent removed under vacuum to yield a brown oil. Purification via silica chromatography, eluting with 1:4 EtOAc/hexane, yielded **2.55** as cream coloured crystals (0.58 g, 38%). Mp 180-183°C; ^{1}H NMR (600 MHz, $CDCl_3$): δ 4.10 (s, 2H, CH_2); 7.34 (d, 4H, [J = 8.4 Hz], H2, H6); 7.49 (dd, 4H, [J = 4.4 and 1.8 Hz], H2', H6'); 7.60 (d, 4H, [J = 8.4 Hz], H3, H5); 8.65 (dd, 2H, [J = 4.4 and 1.8 Hz], H3', H5'); ^{13}C NMR (150 MHz, $CDCl_3$): δ 41.30, 121.4, 127.2, 129.7, 136.2, 141.8, 147.9, 150.2; ESI-MS: *m/z* 323.4 (MH^+); FT-IR: v_{max}/cm^{-1} 1594 (C=C); Anal. calcd for $C_{23}H_{18}N_2$ C 85.67, H 5.64, N 8.69; found C 85.74, H 5.68, N 8.54%.

4,4'-Methylenebis(2,3,5,6-tetrafluorobenzonitrile) (2.58). A 3 M solution of methyl magnesium chloride in THF (6.94 mL 20.8 mmol) was added dropwise to a stirred solution of 2,3,4,5,6-pentafluorobenzonitrile (1.30 mL, 10.3 mmol) in THF (40 mL) under argon at -20°C. The reaction mixture was stirred for 1 h at approximately -20 to -15°C. To this solution was slowly added THF:H_2O (1:1, 30 mL), followed by 4 M HCl solution (30 mL), and the resultant mixture stirred at room temperature until all solids dissolved. The solution was then extracted with DCM (3×30 mL) and the extracts washed with saturated sodium bicarbonate solution (20 mL), 2 M hydrochloric acid solution (20 mL), brine (20 mL), dried ($MgSO_4$) and evaporated under vacuum to give a yellow oil. The oil crystallised over 1 week and was recrystallised from methanol to yield **2.58** as colourless crystals which were suitable for X-ray crystallography (0.57 g, 31%). Mp 105-107°C; ^{1}H NMR (600 MHz, $CDCl_3$): δ 4.29 (s, 2H, CH_2); ^{19}F NMR (121 MHZ, $CDCl_3$): δ -139.17 (s, 4F, F2, F6); -132.08 (s, 4F, F3, F5); ^{13}C NMR (150 MHz, $CDCl_3$): δ 17.4 (s, 2C, CH_2), 94.4 (t, 2C, [J = 17.1 Hz], C1), 106.9 (s, 2C, C≡N), 121.2 (t, 2C [J = 12.5 Hz], C4), 144.9 (dd, 4C, [J = 252.1 and 13.2 Hz], C2, C6), 147.1 (dd, 4C, [J = 263.0 and 14.9 Hz], C3, C5); EI-MS: *m/z* 361.9 (M^+); FT-IR: v_{max}/cm^{-1} 2248 (C≡N), 1502 (C=C); Anal. calcd for $C_{15}H_2N_2F_8$ C 49.74, H 0.56, N 7.74; found C 49.76, H 0.66, N 7.70%.

2.6.3. Cyclic Voltammetry

Cyclic voltammetry measurements were performed on a PAR Model 263A potentiostat under nitrogen. Measurements were recorded on 1 mM solutions in dichloromethane/0.1 M [(n-$C_4H_9)_4$]NPF_6 solution using a platinum working electrode, platinum wire auxiliary and pseudo-reference electrodes. Ferrocene was added as an internal standard on completion of each experiment and tabulated potentials are given *vs.* the saturated calomel electrode [$E_0(Fc/Fc^+)$ = 460 mV vs SCE (dichloromethane)]. Cyclic voltammetry was performed with a sweep rate of 100 mVs^{-1}.

2.6.4. X-Ray Crystallography

Crystals were mounted under oil on a loop and X-ray diffraction data was collected at 150(2) K with Mo Kα radiation (λ = 0.71073 Å) using an Oxford Diffraction X-Calibur Diffractometer fitted with an Eos CCD detector or a Bruker-AXS single crystal diffraction system fitted with an Apex II CCD detector. The data sets were corrected for absorption using a multi-scan method. Structures were solved by direct methods using SHELXS-97[61] and refined by full-matrix least squares on F^2 by SHELXL-97,[62] interfaced through the program X-Seed.[63] In general, all non-hydrogen atoms were refined anisotropically and hydrogen atoms were included as invariants at geometrically estimated positions.

2.6.5. Crystallographic Data

Table 2.3. Crystal data and X-ray experimental data for **2.25**, **2.29·4(CH_3NO_2)**, **2.37**, **2.43**, and **2.44·CH_3CN**.

Compound	**2.25**	**2.29·4(CH_3NO_2)**	**2.37**	**2.43**	**2.44·CH_3CN**
Empirical formula	$C_{15}H_{10}N_2$	$C_{52}H_{36}N_{10}O_8$	$C_{15}H_{10}N_2$	$C_{17}H_8N_4$	$C_{56}H_{21}N_{13}$
Formula weight	218.25	928.91	218.25	268.27	875.86
Radiation source	Mo Kα	Mo Kα	Mo Kα	Mo Kα	Mo Kα
Crystal system	Orthorhombic	Monoclinic	Orthorhombic	Orthorhombic	Monoclinic
Space group	*Fdd*2	$P2_1/c$	$P2_12_12$	$P2_12_12$	$P2_1/c$
a (Å)	19.4362(8)	9.4964(11)	16.4875(9)	7.7456(11)	13.7345(13)
b (Å)	13.6628(6)	19.218(2)	7.8530(5)	20.319(4)	12.6611(9)
c (Å)	8.7151(4)	26.352(3)	4.3079(2)	4.3323(9)	25.128(2)
α (°)	90	90	90	90	90
β (°)	90	98.503(6)	90	90	93.942(8)
γ (°)	90	90	90	90	90
Volume ($Å^3$)	2314.32(18)	4756.4(10)	557.77(5)	681.8(2)	4359.3(6)
Z	8	4	2	2	4
D_{calc} (mg/m^3)	1.253	1.297	1.300	1.307	1.335
Absorption coefficient (mm^{-1})	0.075	0.091	0.078	0.082	0.084
F(000)	912	1928	228	276	1792
Crystal size (mm^3)	0.62 × 0.41 × 0.20	0.50 × 0.37 × 0.22	0.39 × 0.37 × 0.23	0.40 × 0.10 × 0.04	0.15 × 0.13 × 0.04
Theta range for data (°)	2.96 to 30.02	1.32 to 28.89	2.47 to 28.91	2.81 to 29.47	2.67 to 23.26
Reflections collected	5615	88392	3119	3825	28680
Independent reflections [R(int)]	1509 [0.0304]	12409 [0.0357]	1271 [0.0299]	1598 [0.0816]	6241 [0.1149]
Completeness to theta full (%)	99.9	99.8	98.9	99.6	99.9
Observed reflections [I>2σ(I)]	1322	9184	1084	915	3667
Data / restraints / parameters	1509 / 0 / 78	12409 / 0 / 662	1271 / 0 / 78	1598 / 0 / 96	6241 / 0 / 623
Goodness-of-fit on F2	1.047	1.048	1.052	1.389	1.025
R_1 [I>2σ(I)]	0.0378	0.0813	0.0421	0.0782	0.0682
wR_2 (all data)	0.0898	0.2580	0.1036	0.3033	0.1608
Largest diff. peak and hole ($e.Å^{-3}$)	0.164 and -0.194	1.77 and -1.21	0.144 and -0.180	0.388 and -0.401	0.362 and -0.320

Table 2.4. Crystal data and X-ray experimental data for **2.58**.

Compound	**2.58**
Empirical formula	$C_{15}H_2N_2F_8$
Formula weight	362.19
Radiation source	Mo Kα
Crystal system	Monoclinic
Space group	$P2_1/c$
a (Å)	7.5512(7)
b (Å)	18.9667(18)
c (Å)	9.2507(8)
α (°)	90
β (°)	91.618(9)
γ (°)	90
Volume (Å^3)	1324.4(2)
Z	4
D_{calc} (mg/m^3)	1.816
Absorption coefficient (mm^{-1})	0.189
F(000)	712
Crystal size (mm^3)	0.40 × 0.21 × 0.15
Theta range for data (°)	2.45 to 29.30
Reflections collected	11768
Independent reflections [R(int)]	3181 [0.0662]
Completeness to theta full (%)	99.5
Observed reflections [I>2σ(I)]	2025
Data / restraints / parameters	3181 / 0 /226
Goodness-of-fit on F2	1.118
R_1 [I>2σ(I)]	0.0677
wR_2 (all data)	0.1996
Largest diff. peak and hole (e.Å^{-3})	0.399 and -0.348

Additional refinement details for 2.29·4(CH_3NO_2). There is disorder of one nitromethane solvate molecule, which is modelled over two major positions *ca.* 65:35.

Additional refinement details for 2.44·CH_3CN. This crystal was weakly diffracting with a theta range of 2.67 to 23.26°. High angle data was not observed for **2.44·CH_3CN** and thus the data was omitted above 46° in order to provide a reasonable completeness.

2.7. References

1 N. F. Phelan and M. Orchin, *J. Chem. Educ.*, **1968**, *45*, 633.

2 M. Gholami and R. R. Tykwinski, *Chem. Rev.*, **2006**, *106*, 4997.

3 H. Hopf, *Angew. Chem. Int. Ed. Engl.*, **1984**, *23*, 948.

4 H. Hopf and G. Maas, *Angew. Chem. Int. Ed. Engl.*, **1992**, *31*, 931.

5 A. T. Blomquist and J. A. Verdol, *J. Am. Chem. Soc.*, **1955**, *77*, 81.

6 W. J. Bailey and J. Economy, *J. Am. Chem. Soc.*, **1955**, *77*, 1133.

7 W. J. Bailey and N. A. Nielsen, *J. Org. Chem.*, **1962**, *27*, 3088.

8 S. Fielder, D. D. Rowan, and M. S. Sherburn, *Angew. Chem. Int. Ed.*, **2000**, *39*, 4331.

9 A. D. Payne, A. C. Willis, and M. S. Sherburn, *J. Am. Chem. Soc.*, **2005**, *127*, 12188.

10 T. A. Bradford, A. D. Payne, A. C. Willis, M. N. Paddon-Row, and M. S. Sherburn, *Org. Lett.*, **2007**, *9*, 4861.

11 G. Bojase, A. D. Payne, A. C. Willis, and M. S. Sherburn, *Angew. Chem. Int. Ed.*, **2008**, *47*, 910.

12 A. D. Payne, G. Bojase, M. N. Paddon-Row, and M. S. Sherburn, *Angew. Chem. Int. Ed.*, **2009**, *48*, 4836.

13 T. A. Bradford, A. D. Payne, A. C. Willis, M. N. Paddon-Row, and M. S. Sherburn, *J. Org. Chem.*, **2010**, *75*, 491.

14 G. W. Griffin and L. I. Peterson, *J. Am. Chem. Soc.*, **1962**, *84*, 3398.

15 G. W. Griffin and L. I. Peterson, *J. Am. Chem. Soc.*, **1963**, *85*, 2268.

16 E. A. Dorko, *J. Am. Chem. Soc.*, **1965**, *87*, 5518.

17 P. Schiess and M. Heitzmann, *Helv. Chim. Acta*, **1978**, *61*, 844.

18 L. G. Harruff, M. Brown, and V. Boekelheide, *J. Am. Chem. Soc.*, **1978**, *100*, 2893.

19 T. Fukunaga, *J. Am. Chem. Soc.*, **1976**, *98*, 610.

20 T. Fukunaga, M. D. Gordon, and P. J. Krusic, *J. Am. Chem. Soc.*, **1976**, *98*, 611.

21 T. Enomoto, T. Kawase, H. Kurata, and M. Oda, *Tetrahedron Lett.*, **1997**, *38*, 2693.

22 T. Enomoto, N. Nishigaki, H. Kurata, T. Kawase, and M. Oda, *Bull. Chem. Soc. Jpn.*, **2000**, *73*, 2109.

23 K. Matsumoto, Y. Harada, T. Kawase, and M. Oda, *Chem. Commun.*, **2002**, 324.

24 P. J. Steel and C. J. Sumby, *Chem. Commun.*, **2002**, 322.

25 M. Iyoda, N. Nakamura, M. Todaka, S. Ohtsu, K. Hara, Y. Kuwatani, M. Yoshida, H. Matsuyama, M. Sugita, H. Tachibana, and H. Inoue, *Tetrahedron Lett.*, **2000**, *41*, 7059.

26 A. Avellaneda, C. A. Hollis, X. He, and C. J. Sumby, *Beil. J. Org. Chem.*, **2012**, *8*, 71.

27 P. J. Steel and C. J. Sumby, *Inorg. Chem. Commun.*, **2002**, *5*, 323.

28 K. Matsumoto, Y. Harada, N. Yamada, H. Kurata, T. Kawase, and M. Oda, *Cryst. Growth Des.*, **2006**, *6*, 1083.

29 C. A. Hollis, L. R. Hanton, J. C. Morris, and C. J. Sumby, *Cryst. Growth Des.*, **2009**, *9*, 2911.

30 W. B. Austin, N. Bilow, W. J. Kelleghan, and K. S. Y. Lau, *J. Org. Chem.*, **1981**, *46*, 2280.

31 L. Friedman and H. Shechter, *J. Org. Chem.*, **1961**, *26*, 2522.

32 J. J. Young, G. R. Stevenson, and N. L. Bauld, *J. Am. Chem. Soc.*, **1972**, *94*, 8790.

33 E. B. Barnett and M. R. Matthews, *J. Chem. Soc.*, **1924**, 767.

34 H. A. M. Hejaz, L. W. L. Woo, A. Purohit, M. J. Reed, and B. V. L. Potter, *Bioorg. Med. Chem.*, **2004**, *12*, 2759.

35 L. H. Klemm, R. Mann, and C. D. Lind, *J. Org. Chem.*, **1958**, *23*, 349.

36 P. N. Preston, V. B. Jigajinni, I. Soutar, B. Woodfine, N. J. Stewart, and J. N. Hay, *Polymer*, **1994**, *35*, 2378.

37 L. D. Hicks, J. K. Han, and A. J. Fry, *Tetrahedron Lett.*, **2000**, *41*, 7817.

38 A. Canty and N. Minchin, *Aust. J. Chem.*, **1986**, *39*, 1063.

39 X. He, *Coordination of Electron Deficient Ligands to Ruthenium Complexes*, **2009**, Honours Thesis, The University of Adelaide, Adelaide, Australia.

40 D. G. Hawthorne, J. H. Hodgkin, M. B. Jackson, J. W. Loder, and T. C. Morton, *High Perform. Polym.*, **1994**, *6*, 287.

41 E. F. Ellis and J. G. D. Schulz, Nitrogen-containing diaryl compounds, U.S. Patent 3,275,651, Feb 27, 1966.

42 S. Vagin and M. Hanack, *Eur. J. Org. Chem.*, **2004**, *2004*, 600.

43 G. Schultz, Á. Szabados, G. Tarczay, and K. Zauer, *Struct. Chem.*, **1999**, *10*, 149.

44 K. L. Reed, J. T. Gupton, and T. L. Solarz, *Synth. Commun.*, **1990**, *20*, 563.

45 D. A. McMorran and P. J. Steel, *Tetrahedron*, **2003**, *59*, 3701.

46 F. Marken, A. Neudack, and A. M. Bond In *Electroanalytical Methods, Guide to Experiments and Applications*, 2nd ed., Scholz, F., Ed., Springer Berlin Heidelberg, 2010, p 57.

47 C. J. Sumby, *The Synthesis and Study of Bridging Heterocyclic Ligands*, **2003**, PhD Thesis, The University of Canterbury, Christchurch, New Zealand.

48 C. Domene, P. W. Fowler, L. W. Jenneskens, and E. Steiner, *Chem. Eur. J.*, **2007**, *13*, 269.

49 K. Sonogashira, Y. Tohda, and N. Hagihara, *Tetrahedron Lett.*, **1975**, *16*, 4467.

50 L. Yu and J. S. Lindsey, *J. Org. Chem.*, **2001**, *66*, 7402.

51 S. Thorand and N. Krause, *J. Org. Chem.*, **1998**, *63*, 8551.

52 N. Miyaura and A. Suzuki, *Chem. Rev.*, **1995**, *95*, 2457.

53 Y. Wang, D. L. Frattarelli, A. Facchetti, E. Cariati, E. Tordin, R. Ugo, C. Zuccaccia, A. Macchioni, S. L. Wegener, C. L. Stern, M. A. Ratner, and T. J. Marks, *J. Phys. Chem. C*, **2008**, *112*, 8005.

54 G. Cavallo, P. Metrangolo, T. Pilati, G. Resnati, M. Sansotera, and G. Terraneo, *Chem. Soc. Rev.*, **2010**, *39*, 3772.

55 P. Politzer, J. S. Murray, and T. Clark, *Phys. Chem. Chem. Phys.*, **2010**, *12*, 7748.

56 J.-M. Vincent, *Chem. Commun.*, **2012**, *48*, 11382.

57 L. A. Hartmann and J. F. Stephen, Difunctional polyfluoroaromatic derivatives and a process of preparing the same, U.S. Patent 4,965,394, Oct 23, 1990.

58 K. Matsumoto, N. Yamada, T. Enomoto, H. Kurata, T. Kawase, and M. Oda, *Chem. Lett.*, **2011**, *40*, 1033.

59 W. L. F. Armarego and C. L. L. Chai, *Purification of Laboratory Chemicals*, 5th ed., Butterworth-Heinemann, Cornwall, U.K., 2003.

60 Z. Novák, A. Szabó, J. Répási, and A. Kotschy, *J. Org. Chem.*, **2003**, *68*, 3327.

61 G. M. Sheldrick, *Acta Crystallogr., Sect. A*, **1990**, *46*, 467.

62 G. M. Sheldrick, *SHELXL-97*, University of Gottingen, Gottingen, Germany 1997.

63 L. J. Barbour, *J. Supramol. Chem.*, **2001**, *1*, 189.

Chapter 3

Discrete Complexes of [3]Radialenes

Chapter 3

3. Discrete Complexes of [3]Radialenes

3.1. Introduction

3.1.1. Ruthenium Complexes

Ruthenium complexes of polypyridyl ligands with the ability to bridge multiple metals have been extensively studied.[1-7] These complexes exhibit interesting photophysical and electrochemical properties; and often possess the ability to facilitate metal-metal interactions through their conjugated bridges.[8-17] One of the earliest examples of a dinuclear ruthenium complex bridged by a nitrogen-containing heterocycle is that of the Creutz-Taube ion, which was first reported in 1969.[18,19] The Creutz-Taube ion is a $Ru^{II}Ru^{III}$ mixed-valence species that consists of two ruthenium pentaamine groups bridged by a pyrazine ring (Figure 3.1(a)). The two ruthenium centres can communicate through the bridging ligand as demonstrated by a separation of the oxidation and reduction potential, of the Ru^{II} centre and the Ru^{III} centre respectively, of 390 mV.[19,20] Another dinuclear ruthenium complex reported by Meyer utilises the bis-bidentate chelating ligand 2,2'-bipyrimidine as a bridging ligand between two ruthenium di-bipyridine groups (Figure 3.1(b)).[21] This complex also exhibits metal-metal interactions as shown by the 170 mV difference in oxidation potential of the two Ru^{II} centres.

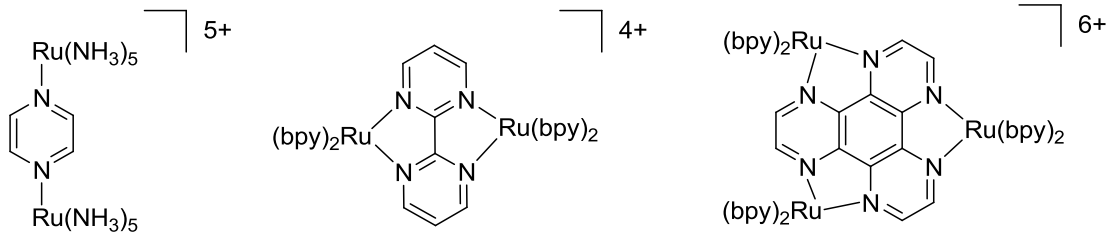

(a) (b) (c)

Figure 3.1. (a) The dinuclear Cruetz-Taube ion. (b) A dinuclear ruthenium complex of 2,2'-bipyrimidine. (c) A trinuclear ruthenium complex of 1,4,5,8,9,12-hexaazatriphenylene (HAT).

A trinuclear ruthenium polypyridyl complex incorporating 1,4,5,8,9,12-hexaazatriphenylene (HAT) has also been reported by Masschelein and colleagues.[22] The HAT ligand has three bidentate binding sites available for chelating ruthenium and forms the complex $\{[Ru(bpy)_2]_3(\mu_3\text{-HAT})\}^{6+}$ when reacted with $[Ru(bpy)_2Cl_2]\cdot 2H_2O$ (Figure 3.1 (c)).

There is a separation of approximately 255 mV between each of the three consecutive Ru^{II} oxidation steps (+1.61, +1.87 and +2.12 V), which demonstrates that metal-metal communication exists between the three ruthenium centres through the conjugated HAT ligand. Keene also demonstrated that the homochiral (Δ^3/Λ^3) and heterochiral ($\Delta^2\Lambda/\Lambda^2\Delta$) diastereoisomers of this trinuclear complex could be separated and that they maintain the same electrochemical properties.[23]

An even more complicated polypyridyl structure is that of the tetranuclear ruthenium complex (Figure 3.2. (a)) investigated by Serroni and co-workers, which contains both electron deficient 2,3-bis(2-pyridyl)pyrazine (2,3-dpp) and electron rich 3,5-bis(pyridin-2-yl)-1,2,4-triazolate (bpt^-) polypyridyl bridging ligands.[24] The complex exhibits two reversible redox events which correspond to the one electron oxidation of Ru_A and the simultaneous two-electron oxidation of the Ru_B metal centres, which demonstrates that there is no metal-metal communication between the Ru_B metal centres (the oxidation potential of Ru_C fell outside the anodic potential window). On the other hand the mixed-valence species, where only Ru_A is oxidised, exhibits metal-metal communication between Ru_C^{II} and Ru_A^{III}.

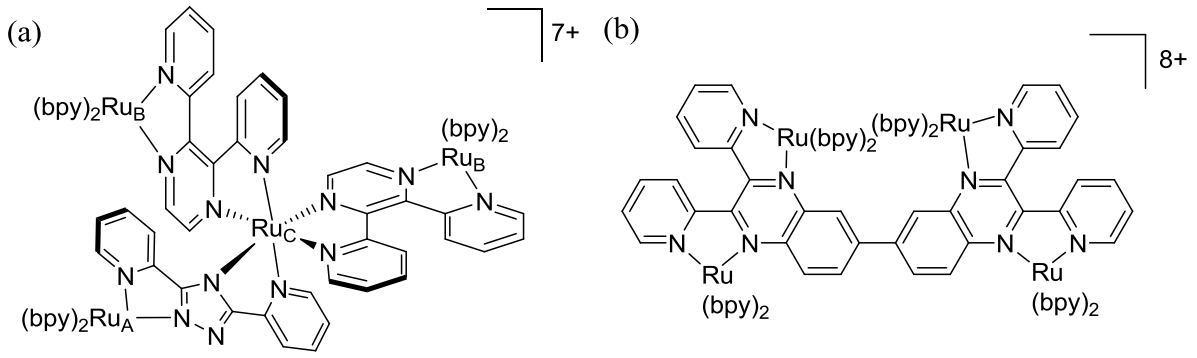

Figure 3.2. (a) Tetranuclear complex $\{(bpy)_2Ru_A(\mu\text{-}bpt^-)Ru_C[(\mu\text{-}2,3\text{-}dpp)Ru_B(bpy)_2]_2\}^{7+}$.
(b) Tetranuclear ruthenium complex of 2,2',3,3'-tetrakis(2-pyridyl)-6,6'-biquinoxaline.

The tetranuclear ruthenium complex of the polypyridyl bridging ligand 2,2',3,3'-tetrakis(2-pyridyl)-6,6'-biquinoxaline (Figure 3.2 (b)) also exhibits intervalence charge transfer but only between the ruthenium centres at the same end of the ligand.[25] In essence, the complex behaves as two doubly-bidentate bridging ligands, held together by the bond between the two quinoxaline moieties, and as such no long range communication is observed.

Similar studies have been accomplished for carbon based molecular wires which show excellent metal-metal interactions over quite large distances that are again facilitated through their linearly π-conjugated systems.[26-30] For instance, the metal centres in the dinuclear ruthenium complex, $\{Ru(dppe)Cp^*\}_2(\mu\text{-}C_8)$, reported by Bruce and co-workers (Figure 3.3

(a)) are linked by an 8-carbon chain of alternating single and alkyne bonds, which spans over 1 nm, and yet still experience a degree of electronic communication as demonstrated by the different oxidation potentials, separated by 350 mV, observed for the two metals.[31] A similar trinuclear structure (Figure 3.3 (b)) containing [Ru(dppe)$_2$] as the central linking group has recently been described.[31] Theoretical DFT calculations and electrochemical data provide evidence for a delocalised electronic structure over the Ru-C_4-Ru-C_4-Ru chain with a separation in energy of the first two oxidation events of 380 mV. This suggests that there is communication between the terminal [Ru(dppe)Cp*] groups through the C4 chains and the [Ru(dppe)$_2$] centre.

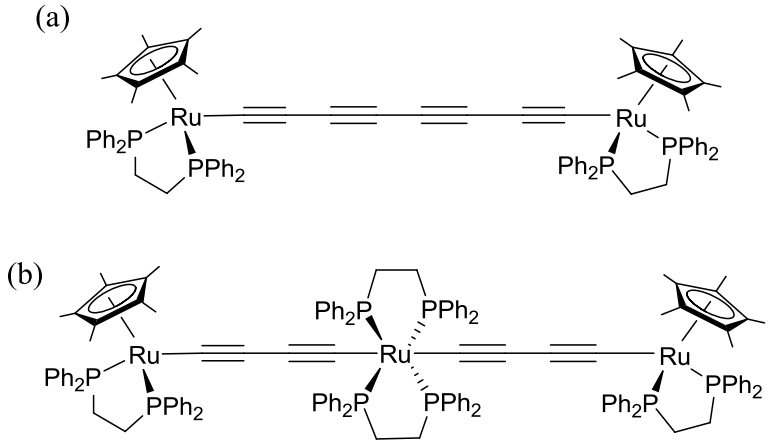

Figure 3.3. (a) Dinuclear ruthenium complex {Ru(dppe)Cp*}$_2$(μ-C_8). (b) Trinuclear ruthenium complex *trans*-Ru{C≡CC≡C[Ru(dppe)Cp*]}$_2$(dppe)$_2$.

In contrast, the nature of interactions that result from other modes of π-electron communication, in particular cross-conjugation,[32] have been less frequently studied.[33-35] A dinuclear ruthenium complex which contains a cross-conjugated tri-nitrile bridging ligand (Figure 3.4) has also been reported by Bruce.[36] There is some metal-metal communication between the two ruthenium centres as the two oxidation events are separated by 230 mV. It is unknown whether a third ruthenium centre would be involved in this communication as all attempts to add a third [Ru(PPh$_3$)$_2$Cp] group to the ligand were unsuccessful.

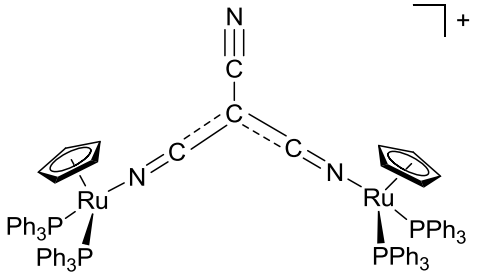

Figure 3.4. Dinuclear ruthenium complex {[Ru(PPh$_3$)$_2$Cp]$_2$[(NC)$_2$C(CN)]}$^+$.

Bridging ligands incorporating a cross-conjugated [3]radialene core may enable a metal atom in a multinuclear complex to interact in a facile manner with a second metal through the linearly conjugated segment of the π-system but not in the same manner with a third due to cross-conjugation.

3.1.2. Coordination Chemistry of Radialenes

The synthetic advances pioneered by Oda[37,38] have led to an increase in the availability of [3]radialene derivatives, with a particular focus on compounds able to coordinate transition metals, such as hexa(2-pyridyl)[3]radialene (**1.3**),[39,40] hexa(4-pyridyl)[3]radialene (**1.4**),[41] and hexakis(4-cyanophenyl)[3]radialene (**2.29**).[37,38] These compounds possess six metal binding sites and have the potential to be involved in bridging multiple metal centres. As noted, this is particularly relevant as the unique electronic properties of the cross-conjugated [3]radialene core may confer interesting properties upon multinuclear complexes containing such ligands.

The coordination chemistry of hexaaryl- and hexa-heteroaryl[3]radialenes has been studied to a limited extent.[40-43] Radialene **1.3** has received particular attention, displaying three modes of coordination with Ag(I); hexadentate in a discrete M_6L_2 cage,[40] a 1-D coordination polymer composed of M_3L_2 cages bridged by linear silver atoms (pentadentate), and a second 1-D coordination polymer where the radialene ligand acts as a tetradentate bridge.[40,42] Radialene **1.4** has also been observed to act as a bridging ligand in a 3-D coordination polymer with $AgClO_4$,[41] whilst two isomorphous 2-D (6,3) networks were obtained upon reaction of **2.29** with $AgPF_6$ and $AgClO_4$.[43] One feature of note within the 2-D (6,3) nets is the chelation of a silver atom by two nitrile groups on adjacent arms of the [3]radialene to form a 17-membered chelate ring (Figure 3.5 (a)). This observation led us to consider the synthesis of complexes of **2.29** whereby the metal is chelated in a similar fashion. The ultimate extension of this being a discrete, tris(bidentate), trinuclear metal complex of **2.29**, where all six nitrile groups are involved in coordination (Figure 3.5 (b)).

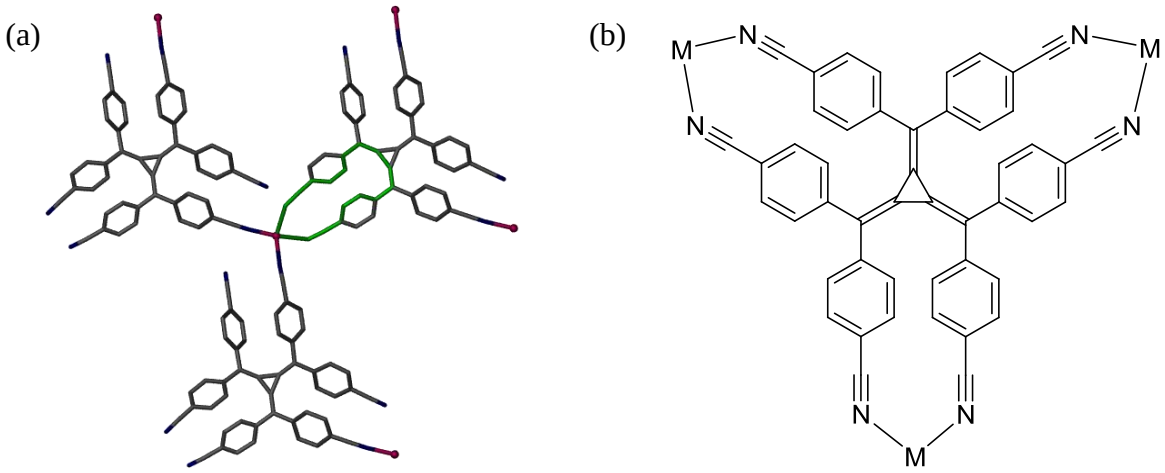

Figure 3.5. (a) A perspective view, from the crystal structure, of the coordination chemistry around a single Ag(I) centre in 2-D coordination polymers of **2.29**. The 17-membered chelate ring is highlighted in this image with green bonds. (b) The structure of a potential trinuclear complex of **2.29** displaying this coordination mode, where M = metal.

Two isomers (*rac* and *meso*) of a ruthenium(II) complex incorporating a hexapyridyl[3]radialene bridging ligand have been reported.[44] Radialene **1.3** has been shown to form a dinuclear ruthenium complex where the radialene ligand acts as a bridge between two [Ru(bpy)$_2$] subunits (Figure 3.6).[44] However, in this complex no metal-metal interactions were observed as indicated by a single, two electron, ruthenium oxidation step at +1.24 V.[44] This lack of interaction was attributed in part to the conformation of the dinuclear complex where both ruthenium centres were thought to lie out of the plane of the [3]radialene core due to the boat conformation that the chelate ring adopts.

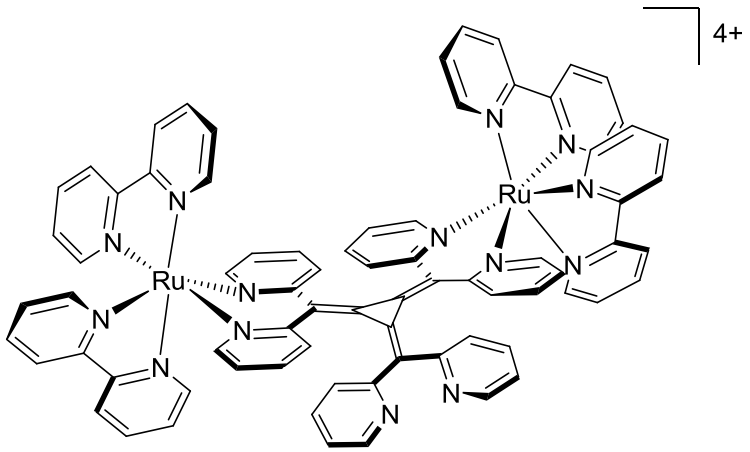

Figure 3.6. Diagram of the dinuclear ruthenium complex of **1.3**.

By synthesising ruthenium complexes with the nitrile substituted hexaaryl[3]radialene ligands **2.29** and **2.38**, which have more divergent donor atoms than **1.3**, complexes where the ruthenium atoms are within the plane of the [3]radialene core may be achievable. Also by using peripheral ligands that are less rigid than bipyridine, such as triphenylphosphine and cyclopentadienyl ligands (Cp and Cp*), an overall more conformationally flexible complex, which has a greater likelihood of exhibiting the required conformation for metal-metal communication, may result.

3.2. Synthesis of Discrete [3]Radialene Complexes

3.2.1 $RuCp(PPh_3)_2$ Complexes

In order to establish suitable reaction conditions and produce model dinuclear ruthenium complexes, the hexaaryl[3]radialene precursors 4,4'-dicyanodiphenylmethane (**2.25**) and 3,3'-dicyanodiphenylmethane (**2.37**) were used as ligands to instigate this study. Based on the synthesis of related compounds by Bruce [45] and Low,[46] treatment of **2.25** and **2.37** with two equivalents of $[RuCp(PPh_3)_2]Cl$ and ammonium hexafluorophosphate in dichloromethane, heating at reflux for 3 h, led to the formation of the expected dinuclear complexes **3.1** and **3.2** in good yields (Scheme 3.1).

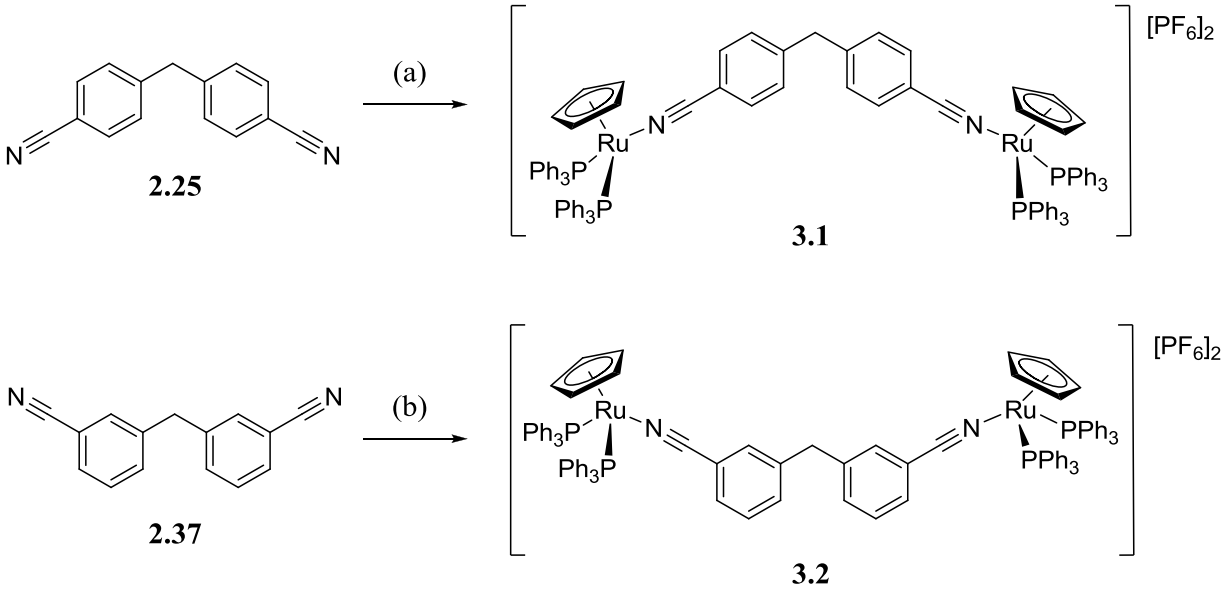

2.25 **3.1**

2.37 **3.2**

(a) 2 equiv. $[RuCp(PPh_3)_2]Cl$, NH_4PF_6, DCM, 74%. (b) 2 equiv. $[RuCp(PPh_3)_2]Cl$, NH_4PF_6, DCM, 83%.

Scheme 3.1

Characteristic peaks for the cyclopentadienyl ligand (δ 4.53 for **3.1**, 4.58 for **3.2**) and triphenylphosphine ligands (δ 40.79 for **3.1**, 41.00 for **3.2**) were seen in the ^{1}H and ^{31}P NMR spectra, respectively (Table 3.1). The PF_6 counter-ion was also observed in the ^{31}P NMR spectra at δ -144.58 (J_{PF} = 712 Hz) for **3.1** and -144.73 (J_{PF} = 713 Hz) for **3.2**, while the methylene spacers of the ligands **2.25** and **2.37** were observed with integrals in the correct ratio for the formation of the expected dinuclear products. The IR spectra showed strong nitrile absorption bands at 2226 and 2229 cm^{-1} for **3.1** and **3.2** respectively, compared with the free ligands at 2225 and 2224 cm^{-1}. Electrospray ionisation, high resolution mass spectrometry and elemental analysis further confirmed the identity and purity of the complexes (see experimental section 3.5.2.)

Table 3.1. Selected spectroscopic data for compounds PhCN, **2.25**, **2.29**, **2.37**, and **2.38**, and complexes $[Ru(NCPh)(PPh_3)_2Cp]PF_6$ and **3.1-3.4**.

Compound	$\nu_{C\equiv N}$ **(cm^{-1})**	ν_{P-F} **(cm^{-1})**	**Cp δ_H (ppm)**	**CH_2 δ_H (ppm)**	**PR_3 δ_P (ppm)**
PhCN[47]	2232				
2.25	2225			4.10	
2.37	2224			4.05	
2.29	2224				
2.38	2228				
$[Ru(NCPh)(PPh_3)_2Cp]PF_6$[46]	2233	not reported	4.55		42.9
3.1	2226	839	4.53	4.01	40.79
3.2	2229	833	4.58	4.01	41.00
3.3	2227	830	4.66		39.56, 39.69
3.4	2231	836	4.58		40.95

Synthesis of $[RuCp(PPh_3)_2]$ complexes of the multidentate radialene ligands proved more problematic. For reactions involving either **2.29** and **2.38** multiple products were observed when high metal to ligand ratios (between 3:1 and 5:1) were used in an attempt to synthesise the targeted trinuclear complex. For the reaction involving **2.29**, these products were identified as a mixture of complexes, specifically a mononuclear complex **3.3** (Scheme 3.2) and three different dinuclear complexes via ^{31}P and ^{1}H NMR spectroscopy, and mass spectrometry. As well as observing a mixture of dinuclear complexes with *m/z* 2211.7 and the mononuclear complex with *m/z* 1375.5 in the mass spectrum, a third peak was seen with *m/z*

1112.8. This last peak corresponds to the loss of one triphenylphosphine ligand from complex **3.3** and possibly chelation by **2.29** to the single metal centre (**3.3c**). As noted, chelation of a metal by this radialene ligand has been observed in the form of a seventeen membered chelate ring within two isomorphous 2-D coordination polymers (Figure 3.5 (a)). This product appears to form in the mass spectrum but is not present in detectable amounts in the product mixture, particularly on heating. Dinuclear complexes with loss of one (*m/z* 1948.7) and two (*m/z* 1685.9) triphenylphosphine ligands were also observed (Figure 3.7).

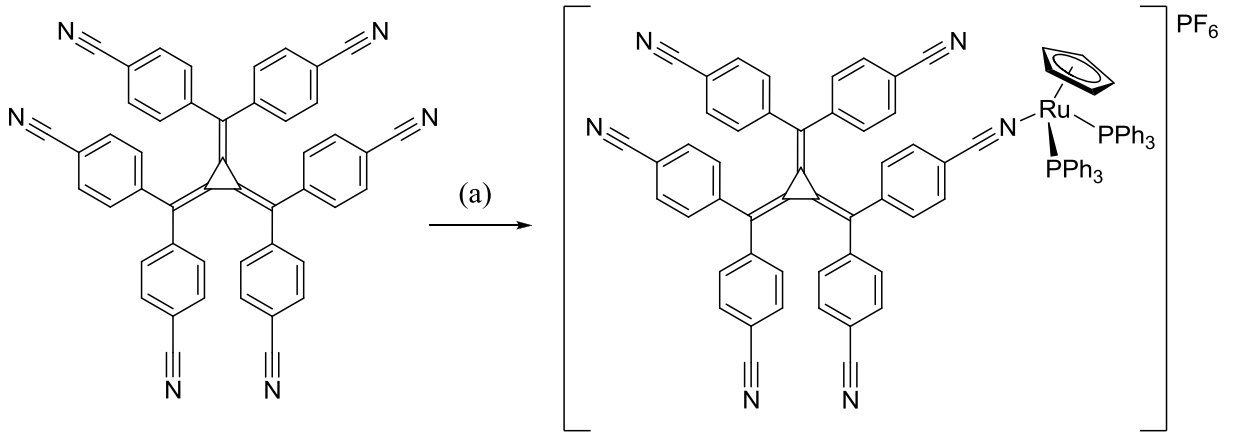

2.29 **3.3**

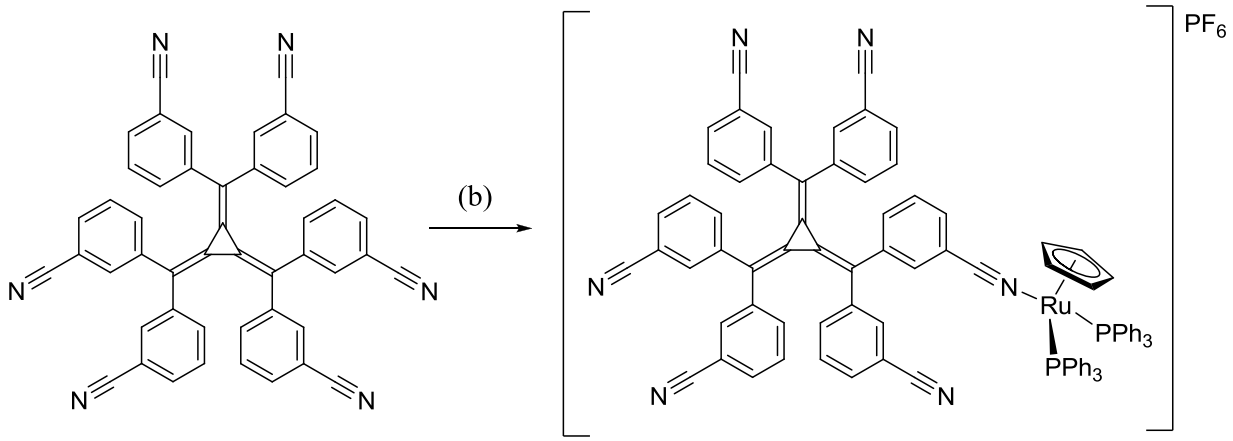

2.38 **3.4**

(a) 1 equiv. $[RuCp(PPh_3)_2]Cl$, NH_4PF_6, MeOH, 62%. (b) 1 equiv. $[RuCp(PPh_3)_2]Cl$, NH_4PF_6, DCM, 76%.

Scheme 3.2

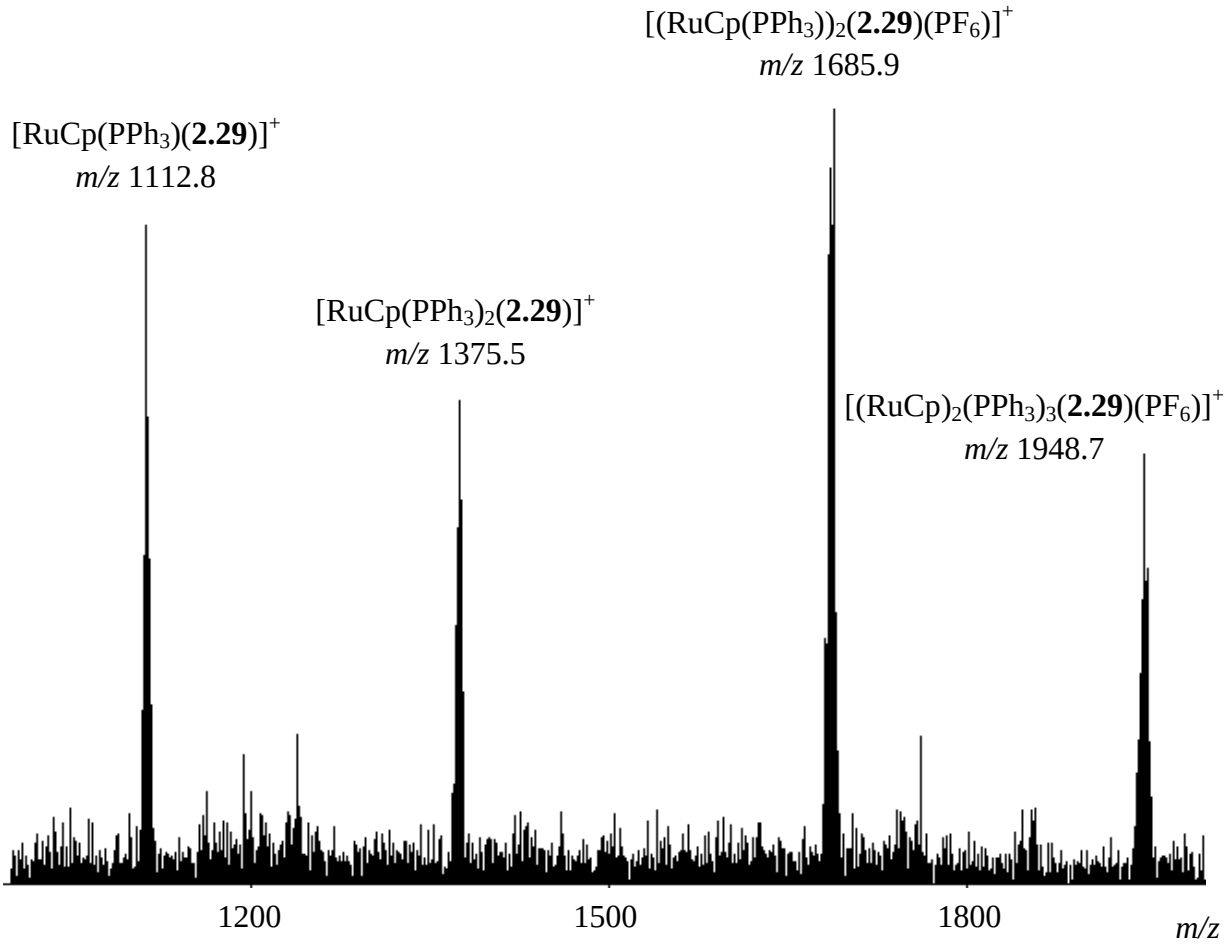

Figure 3.7. The mass spectrum of the products of the reaction of **2.29** with three equivalents of $[RuCp(PPh_3)_2]Cl$.

The synthesis of **3.3** as the sole product in 62% yield was accomplished by reaction of **2.29** with only one equivalent of $[RuCp(PPh_3)_2]Cl$ and heating at reflux overnight (Scheme 3.2). The ^1H NMR spectrum revealed a single characteristic peak for the cyclopentadienyl ligand (δ 4.66), and elemental analysis indicated the product was pure **3.3** (Anal. found, C 66.02, H 4.01, N 4.48; calc. for $C_{89}H_{59}N_6Ru_1P_3F_6 \cdot 1½(CH_2Cl_2)$ C 65.69, H 3.80, N 5.10). In the mass spectrum both **3.3** and **3.3c** were again observed and this provides evidence for the loss of one triphenylphosphine ligand and subsequent formation of **3.3c** in the mass spectrometer. The ^{31}P NMR spectrum exhibits two peaks at δ 39.56 and 39.69 which were assigned to the two triphenylphosphine ligands of **3.3** due to restricted rotation around the Ru-N≡C bond in the complex (Table 3.1). This restricted rotation is due to the considerable steric bulk of the ligand, **2.29**, and the triphenylphosphine ligands.

In a deliberate attempt to form **3.3c,** copper(I) iodide was added to the reaction to promote the loss of triphenylphosphine[48] and subsequent chelation to form **3.3c** (Figure 3.8). Thus heating **2.29**, $[RuCp(PPh_3)_2]Cl$ and copper iodide (1:1:2 ratio) in methanol at reflux for three

days led to a poorly soluble purple precipitate. Suspension of this precipitate in chloroform caused dissolution of any **3.3** and unreacted **2.29**. The insoluble material was then isolated, further washed with chloroform and air dried. Unfortunately this substance was insoluble in common solvents for NMR spectroscopy or mass spectrometry. Furthermore elemental analysis revealed that the material did not have an analysis consistent with the expected product and this was not pursued further. Attempts to synthesise the desired trinuclear complex involved increased ratios of ligand to metal (typically 1:3), use of high boiling point solvents, and increased reaction times without success. For example, heating **2.29**, $[RuCp(PPh_3)_2]Cl$ and copper iodide (1:3:4 ratio) in dimethylformamide at reflux overnight lead to the formation of a similar insoluble purple precipitate.

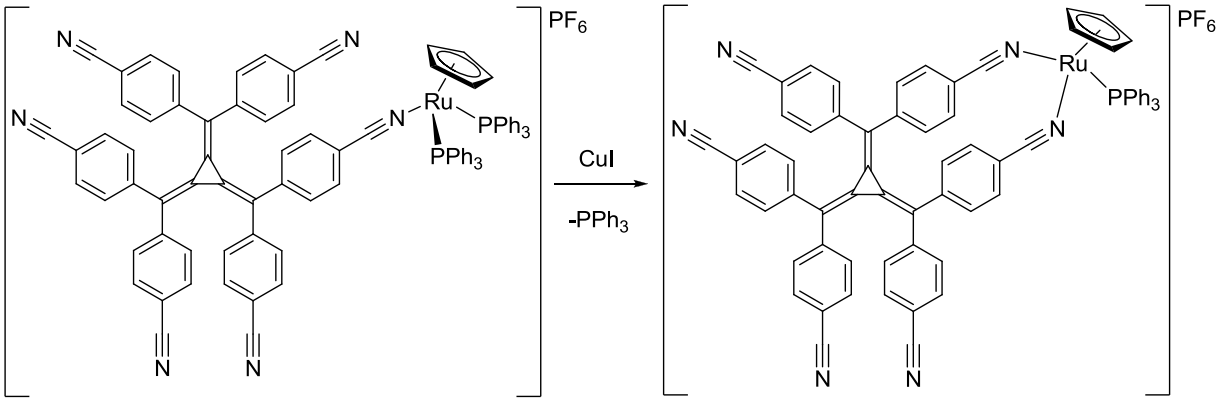

3.3 **3.3c**

Figure 3.8. Possible route to the formation of **3.3c**.

In a similar manner to the synthesis of **3.3**, reaction of **2.38** with one equivalent of $[RuCp(PPh_3)_2]Cl$, heating at reflux overnight, gave **3.4** in 76% yield (Scheme 3.2). The ^{1}H and ^{31}P NMR spectrum of **3.4** is similar to that of **3.3** with characteristic peaks for the cyclopentadienyl (δ 4.59) and triphenylphosphine ligands (δ 40.95) (Table 3.1). However only one signal is observed in the ^{31}P NMR spectrum, which suggests that the two triphenylphosphine groups are equivalent and thus that free rotation around the ruthenium centre can occur. This is consistent with the structures of the ligands as the nitrile groups of **2.38** are more divergent than those of **2.29** and can be located on opposing faces of the [3]radialene core. ESI-HRMS was used to confirm the formation of **3.4** which gives a molecular ion $[\mathbf{3.4\text{-}PF_6}]^+$ at *m/z* 1375.33637 (calc. *m/z* 1375.33145). In a similar manner to **3.3**, compound **3.4** also loses a triphenylphosphine ligand in the mass spectrometer. Again, this potentially chelated product could not be isolated from reactions using copper(I) iodide.

The difficulty in producing multinuclear complexes of both [3]radialenes **2.29** and **2.38**, coupled with the possibility of chelated products in the synthesis of mononuclear complexes of **2.29**, led to the broadening of this work to include [3]radialene **2.44**, which has 12 nitrile substituents, to be abandoned. With such a large number of possible coordination modes the likelihood of producing a single complex from a reaction involving compound **2.44** was considered remote.

3.2.2. RuCp(dppe) Complexes*

In order to eliminate the potential for chelation and to provide direct routes to monodentate hexaaryl[3]radialene monoruthenium species, [RuCp*(dppe)]Cl was used instead of $[RuCp(PPh_3)_2]Cl$. As reported,[49] this chelating phosphine is difficult to displace and thus strictly only one nitrile group can be accommodated within its coordination sphere. Treatment of the two diaryl compounds, **2.25** and **2.37**, with two equivalents of [RuCp*(dppe)]Cl and NH_4PF_6 in dichloromethane gave dinuclear complexes **3.5** and **3.6** respectively in good yields (Scheme 3.3).

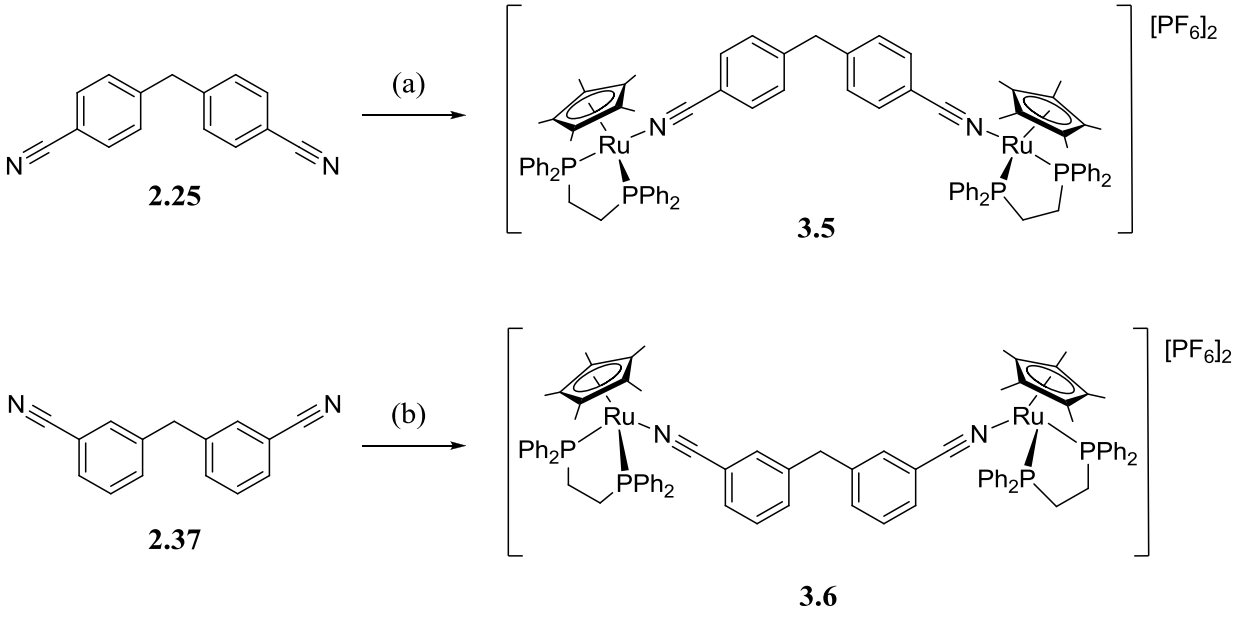

(a) 2 equiv. [RuCp*(dppe)]Cl, NH_4PF_6, DCM, 76%. (b) 2 equiv. [RuCp*(dppe)]Cl, NH_4PF_6, DCM, 62%.

Scheme 3.3

Characteristic peaks for the pentamethylcyclopentadienyl (Cp*) (δ 1.49 for **3.5**, 1.51 for **3.6**) and 1,2-bis(diphenylphosphino)ethane (dppe) ligands (δ 74.09 for **3.5**, 74.01 for **3.6**) were seen in the ^1H and ^{31}P NMR spectra respectively (Table 3.2). The PF_6 counterion was also observed in the ^{31}P NMR spectra at δ -144.78 (J_{PF} = 712 Hz) for **3.5** and -144.79 (J_{PF} =

711 Hz) for **3.6**. The methylene spacers of the ligands **2.25** and **2.37** were also observed with integrals in the correct ratio for the formation of the expected dinuclear products. Evidence for **3.5** and **3.6** was also provided by the IR spectra which revealed strong nitrile absorption bands at 2227 and 2229 cm^{-1} respectively. This compares with 2225 and 2224 cm^{-1} in the free compounds **2.25** and **2.27**. Electrospray ionisation, high resolution mass spectrometry and elemental analysis further confirmed the identity and purity of the complexes (see experimental section 3.5.2).

Table 3.2. Selected spectroscopic data for compounds PhCN, **2.25**, **2.29**, **2.37**, and **2.38**, and complexes [Ru(NCPh)(dppe)Cp*]PF_6 and **3.5-3.8**.

Compound	$\nu_{C\equiv N}$ (cm^{-1})	ν_{P-F} (cm^{-1})	Cp* δ_H (ppm)	CH_2 δ_H (ppm)	PR_3 δ_P (ppm)
PhCN[47]	2232				
2.25	2225			4.10	
2.37	2224			4.05	
2.29	2224				
2.38	2228				
[Ru(NCPh)(dppe)Cp*]PF_6[46]	2227	not reported			76.2
3.5	2227	835	1.49	3.88	74.06
3.6	2229	833	1.51	3.77	74.09
3.7	2227	830	1.51		74.01
3.8	2229	836	1.49		74.42

A small number of yellow rod-shaped crystals of **3.6** suitable for X-ray crystallography were recovered from the microcrystalline precipitate of this product. The dinuclear complex crystallises in the monoclinic space group $P2_1/n$ with an asymmetric unit (Appendix 1, Figure A1.1) that contains half a molecule of the 3,3'-dicyanodiphenylmethane ligand (**2.37**), a [RuCp*(dppe)] moiety, one hexafluorophosphate anion, and one half occupied dichloromethane solvate molecule. The structure was refined with significant disorder of the ligand (disordered over two positions with *ca.* 65:35 occupancy) and the dichloromethane solvate molecule (Figure 3.9).

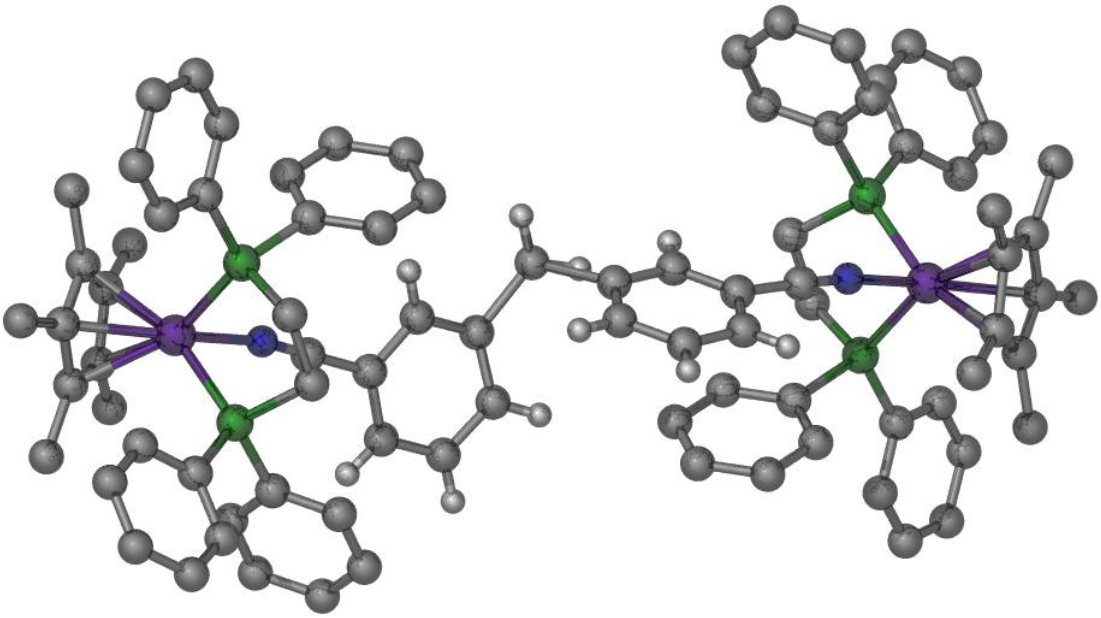

(a)

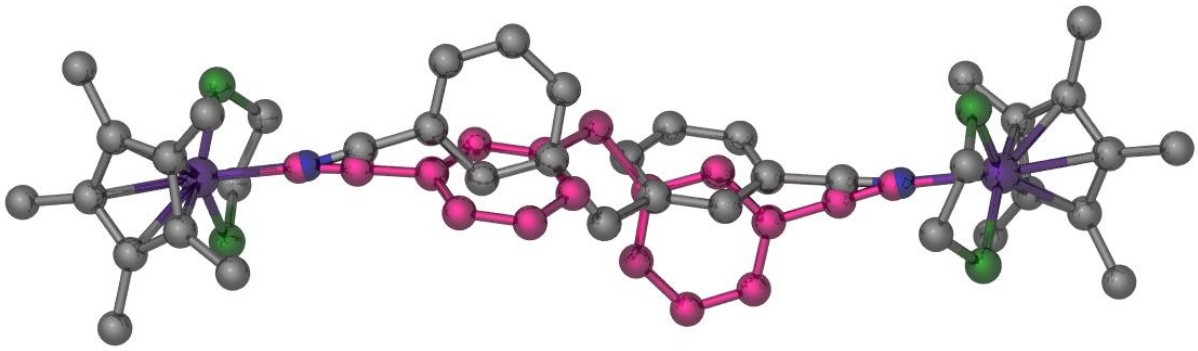

(b)

Figure 3.9. (a) A perspective view of the dinuclear complex **3.6**. Ligand disorder, hydrogen atoms, except those of the ligand, anions and solvate molecules are not shown. (b) Another perspective view of the dinuclear complex **3.6** displaying the minor component of the disordered ligand in pink. Hydrogen atoms, anions, solvate molecules and the triphenylphosphine phenyl rings have been omitted for clarity.

The bond lengths and angles of **3.6** are comparable to those of [Ru(NCPh)(dppe)Cp*]PF_6 (Table 3.3), the structure of which has been previously reported by the Low group.[46] The average bonds lengths of the disorder model of **2.37** have been quoted. One phenyl ring of **2.37** is involved in weak face-to-face π-stacking with the dppe ligand of one ruthenium metal centre (phenyl ring centroid-to-centroid distance of 4.07 Å), whilst the second is involved in an edge-to-face C-H···π interaction with the dppe ligand of the other ruthenium atom (hydrogen atom-to-centroid distance of 2.90 Å).

Table 3.3. Selected bond lengths (Å) and angles (°) for **3.6** and [Ru(NCPh)(dppe)Cp*]PF_6.

Compound	Ru-N	C≡N	Ru-P(1)	Ru-P(2)	P-Ru-P	Ru-N≡C
3.6	2.034(7)	1.141(13)	2.306(1)	2.312(1)	83.65(3)	172.5(17)
[Ru(NCPh)(dppe)Cp*]PF_6[46]	2.027(5)	1.146(7)	2.315(1)	2.315(1)	83.50(5)	173.6(4)

Attempts to grow crystals of the other complexes were unsuccessful as the diphenylmethane complexes **3.1**, **3.2** and **3.5** yielded microcrystalline samples directly from the reaction and, if left in solution for extended periods of time, slowly decompose, while in general complexes of [3]radialene ligands are difficult to crystallise.

Synthesis of the equivalent [RuCp*(dppe)] complexes of both **2.29** and **2.38**, complexes **3.7** and **3.8** respectively, proved straightforward and the compounds were isolated in good yields of 71 and 78% (Scheme 3.4). Characteristic peaks for the Cp* ligand (δ 1.51 for **3.7**, 1.49 for **3.8**) and dppe ligand (δ 74.01 for **3.7**, 74.42 for **3.8**) were seen in the ^{1}H and ^{31}P NMR spectra respectively (Table 3.2). The PF_6 counterion was also observed in the ^{31}P NMR spectra at δ -145.12 (J_{PF} = 713 Hz) for **3.7** and -145.06 (J_{PF} = 712 Hz) for **3.8**. The IR spectra confirmed the presence of strong nitrile absorption bands at 2227 and 2229 cm^{-1} for **3.7** and **3.8** respectively. Electrospray ionisation, high resolution mass spectrometry and elemental analysis further confirmed the identity and purity of the complexes (see experimental section 3.5.5).

As only one ^{31}P NMR signal was observed for both of these complexes it is apparent that free rotation around the ruthenium centre can occur. This is consistent with observations of the Tolman cone angles for the ligands. The substitution of two triphenylphosphine ligands (Tolman cone angle θ = 145°) for the bidentate ligand dppe (θ = 125° for half of the chelate) decreases the steric bulk around the ruthenium.[50] Conversely, the exchange of the Cp ligand (θ = 88.2°) for its pentamethylated derivative, Cp*, (θ = 122.4°) increases the steric bulk.[51] Thus, while the Tolman cone angle of a ligand does not take into account the other ligands present around a metal centre, and the relative orientation of these ligands, we may assume that [Ru(PPh_3)$_2$Cp] is a more bulky complex than [Ru(dppe)Cp*]. This is consistent with observations in the ^{31}P NMR spectra for the radialene ruthenium complexes **3.3**, **3.4**, **3.7** and **3.8** that would suggest that [Ru(PPh_3)$_2$Cp] is the more bulky complex as it is present in **3.3**, the only species for which we see two differentiated phosphorous signals for the phosphine ligands.

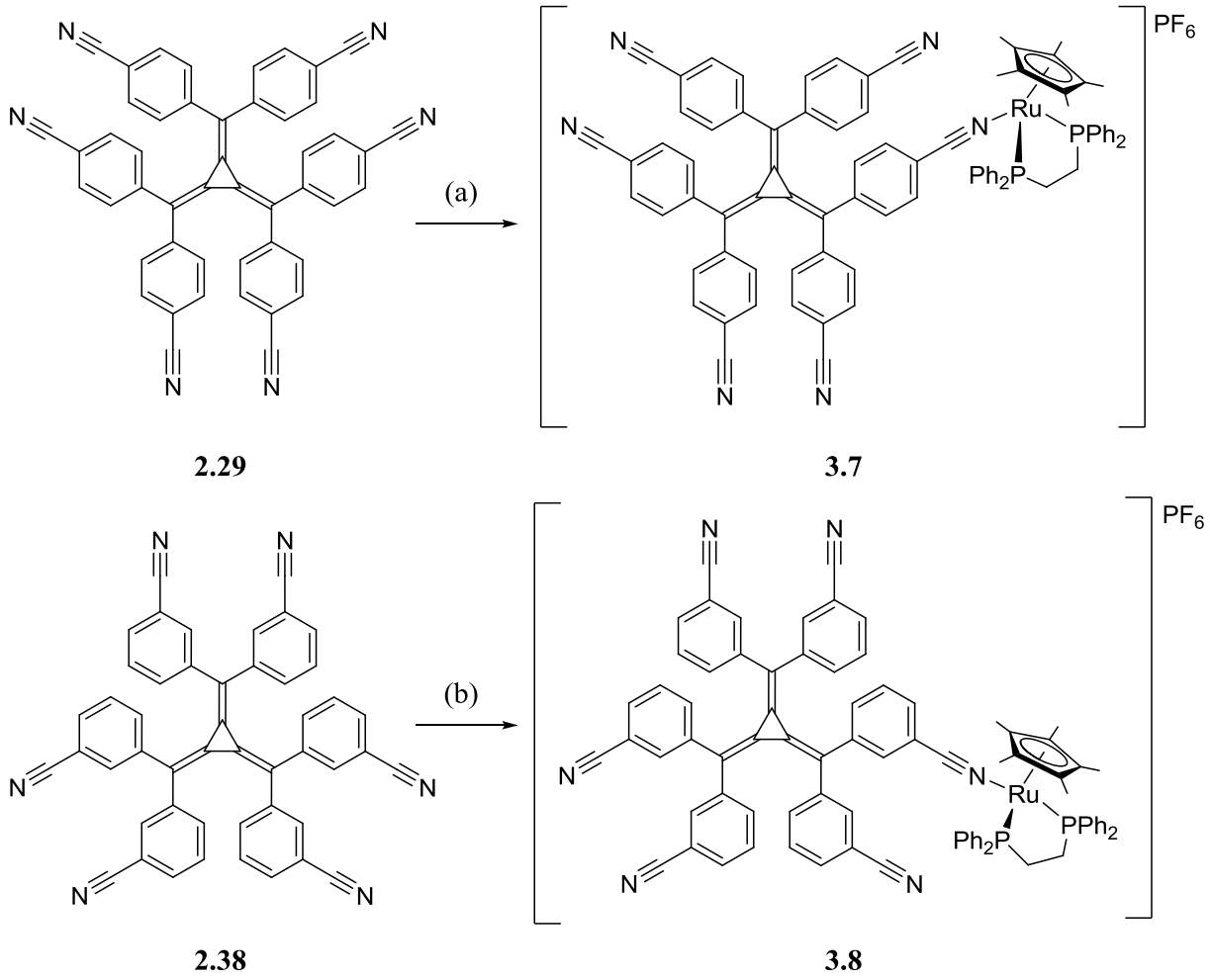

2.29 **3.7**

2.38 **3.8**

(a) 1 equiv. [RuCp*(dppe)]Cl, NH_4PF_6, DCM, 78%. (b) 1 equiv. [RuCp*(dppe)]Cl, NH_4PF_6, DCM, 71%.

Scheme 3.4

In summary eight ruthenium complexes have been synthesised. Four of these are dinuclear complexes of diaryl methanes **2.25** and **2.37** with [Ru$(PPh_3)_2$Cp] and [Ru(dppe)Cp*]. However, only mononuclear complexes of radialenes **2.29** and **2.38** with [Ru$(PPh_3)_2$Cp] and [Ru(dppe)Cp*] were able to be obtained cleanly. One of these, **3.3**, may lose a phosphine ligand in the mass spectrometer or upon heating to produce an interesting bidentate chelate complex, **3.3c**, although an inability to isolate this has prevented in-depth characterisation and study of its physical properties.

3.3. Physical Properties

3.3.1. Electrochemistry

Cyclic voltammetry of all complexes (Table 3.4) were performed for 1 mM solutions in dichloromethane, containing 0.1 M $[(n\text{-}C_4H_9)_4]NPF_6$, with potentials referenced against an internal ferrocene standard (Fc/Fc^+ = +0.46 V *vs* SCE). This technique can be used to determine whether there is any communication between two metals in a multinuclear complex via the calculation of the comproportionation constant, K_c. If a mixed-valence form of a complex exists it will be subject to the comproportionation equilibrium

$$[2,2] + [3,3] \rightleftharpoons 2[2,3]$$

where [2,3] represents the mixed-valence form, which was designated such to indicate Ru^{II}-Ru^{III} metal centres, [2,2] represents the fully reduced form and [3,3] represents the fully oxidised form.[20,52] From this equilibrium K_c can be derived as

$$K_c = [2,3]^2/[2,2][3,3]$$

When no communication exists between the two metal centres K_c = 4 (the statistical value). However, if there is a significant interaction between the two metal centres the value of K_c will be much higher; generally in the region of 10^3 to 10^5.[53,54] It was determined by Creutz that K_c can be ascertained using electrochemical data as

$$K_c = 10^{\Delta E/59\ mV}$$

where ΔE is the difference in potential of the two successive oxidation processes in mV.[20] The comproportionation constant has been used to compare the stability of mixed-valence species for dinuclear complexes where the most stable complexes, those with the greatest degree of metal-metal communication, have the highest K_c value.

It has been demonstrated that care should be taken when comparing electrochemical measurements performed under different conditions as the identity of the electrolyte anions can lead to a shift in oxidation potential as they can associate with positive species.[53,56] This must be considered as the oxidation potentials of two literature examples, $[Ru(NCPh)(PPh_3)_2Cp]PF_6$ and $[Ru(NCPh)(dppe)Cp^*]PF_6$, which will be used for comparison were collected in dichloromethane using $[(n\text{-}C_4H_9)_4]NBF_4$ as the electrolyte,[46,55] whereas the measurements made here, although the solvent is the same, used $[(n\text{-}C_4H_9)_4]NPF_6$ as the electrolyte.

Table 3.4. Electrochemical properties of the [3]radialenes **2.29** and **2.38**, and complexes $[Ru(NCPh)(PPh_3)_2Cp]PF_6$, $[Ru(NCPh)(dppe)Cp^*]PF_6$, and **3.1-3.8**.

Compound	$E_{ox(1)}$[c] (V)	$E_{red(1)}$[c] (V)	$E_{red(2)}$[c] (V)
$[Ru(NCPh)(PPh_3)_2Cp]PF_6$[55]	+1.30[b]		
3.1	+1.30 ($2e^-$)[a]		
3.2	+1.30 ($2e^-$)[a]		
$[Ru(NCPh)(dppe)Cp^*]PF_6$[46]	+1.10[b]		
3.5	+1.08 ($2e^-$)[a]		
3.6	+1.07 ($2e^-$)[a]		
2.29		-0.63[a]	-1.03[a]
3.3	+1.27[a,e]	-0.55[a]	-0.95[a]
3.7	+1.09[a]	-0.55[a]	-0.93[a]
2.38		-0.80[a]	-1.32[a,d]
3.4	+1.32[a]	-0.69[a]	-1.11[a,d]
3.8	+1.07[a]	-0.66[a]	-1.08[a,d]

[a] Potentials (V) measured in DCM/0.1 $mol.L^{-1}$ $[(n\text{-}C_4H_9)_4]NPF_6$ (in DCM the ferrocene/ferrocenium couple occurred at +0.46 V vs. Ag/Ag^+).

[b] Potentials (V) measured in DCM/0.1 $mol.L^{-1}$ $[(n\text{-}C_4H_9)_4]NBF_4$.

[c] Uncertainty in $E_{1/2}$ values *ca.* ± 0.02 V.

[d] Irreversible (approximate value estimated from anodic half-scan).

[e] Irreversible (approximate value estimated from cathodic half-scan).

The oxidation potential of ruthenium complexes **3.1** and **3.2** were identical at +1.30 V (Figure 3.10). These oxidation potentials correlate exactly with that of the benzonitrile complex $[Ru(NCPh)(PPh_3)_2Cp]PF_6$,[55] which shows that the extension of the benzonitrile ligand via a methylene group has no effect on the electronic properties of the adjacent ruthenium centre. In the cyclic voltammogram, only one oxidation wave is observed for these complexes confirming that no communication occurs between the metal centres due to the insulating methylene spacer of the dinitrile ligands **2.25** and **2.37**. A similar observation is noted for complexes **3.5** and **3.6** which exhibit oxidation potentials within the margin of error of that of the benzonitrile complex $[Ru(NCPh)(dppe)Cp^*]PF_6$ (+1.10 V).[46] Again, only one oxidation wave is observed corresponding to the simultaneous oxidation of both ruthenium metal centres (Figure 3.10).

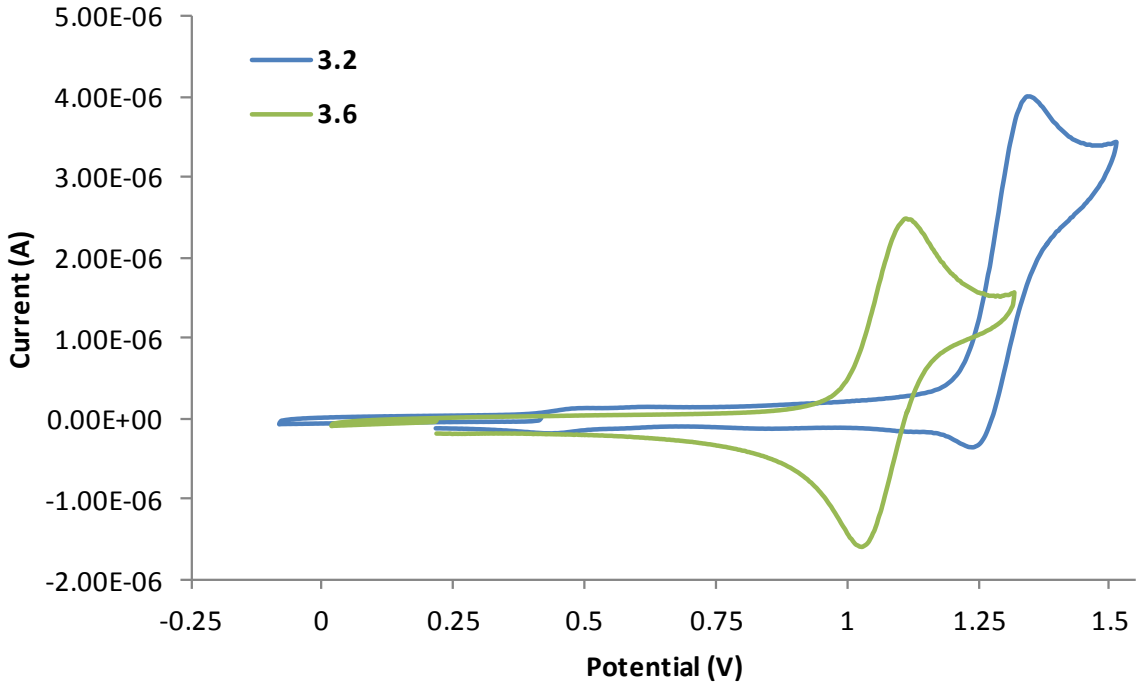

Figure 3.10 Cyclic voltammogram of complexes **3.2** and **3.6** (1mM in dichloromethane/0.1M $[(n\text{-}C_4H_9)_4]NPF_6$, platinum working electrode and ferrocene internal standard).

The [3]radialene ligands **2.29** and **2.38** both undergo two one electron reduction steps to form the radical anion and dianion respectively[32] and this was observed in the voltammograms of the complexes along with the ruthenium(II/III) oxidation band. Complex **3.3** shows no significant change in the ruthenium oxidation potential (although the potential is slightly lower) when compared to $[Ru(NCPh)(PPh_3)_2Cp]PF_6$, however the two potentials at which **3.3** is reduced decrease by approximately 0.08 V over that of the free radialene (Appendix 2, Figure A2.1). A similar observation is noted for complex **3.7**, which shows no significant change in the ruthenium oxidation potential when compared to $[Ru(NCPh)(dppe)Cp^*]PF_6$, but the two potentials at which **3.7** is reduced also decrease by 0.09 V on average (Figure 3.11).

This indicates that in **3.3** and **3.7**, where the radialene is *para*-substituted, there is an interaction between the ruthenium centre and the radialene that allows the stabilisation of the reduced forms of the radialene. As shown previously, *para*-substituted nitrile groups have the ability to stabilise the radical anion and dianion forms of the radialene via resonance delocalisation[57] and, in this case, it appears that coordination of the ruthenium complex to the radialene ligand is enhancing this effect. It is interesting to note that there is no significant change between the radialene reduction potentials of **3.3** and **3.7**, even though Cp* is a much more electron donating group than Cp[58] and should make it more difficult for the ruthenium centre to accept electrons in the reduced form of the complex.

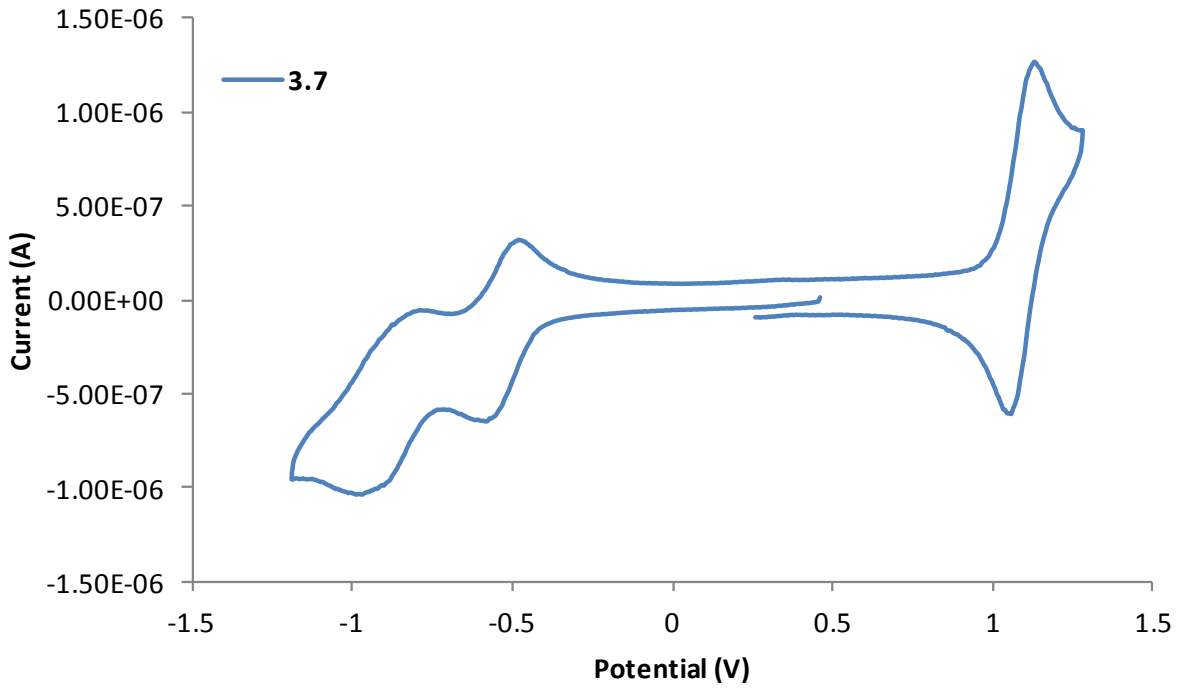

Figure 3.11 Cyclic voltammogram of complex **3.7** (1mM in dichloromethane/0.1M $[(n\text{-}C_4H_9)_4]NPF_6$, platinum working electrode and ferrocene internal standard).

A similar set of observations were made for complexes **3.4** and **3.8** (Appendix 2, Figures A2.2 and A2.3 respectively). Again, while the oxidation potential does not change significantly (it is slightly reduced in complex **3.8**), the reduction of the compound is easier than the radialene itself (-0.69 and -1.11 V for **3.4** and -0.66 and -1.08 V for **3.8** compared with -0.80 and -1.32 V for **2.38**). This indicates that despite the lack of direct conjugation in the *meta* isomer **2.38**, the ruthenium centre still acts to stabilise the radical and, to a lesser extent, the dianion. Similar electrochemical behaviour and a lack of conjugation has been observed with other *meta*-substituted derivatives.[59,60]

Unlike complexes **3.3** and **3.7** there is a noticeable difference between the reduction potentials of the radialene ligands in complexes **3.4** and **3.8**. Therefore, the phosphine and cyclopentadienyl ligands must be exerting some electronic effect. Triphenylphosphine and dppe possess similar electron donating abilities[50,61,62] so the change in phosphine ligand is unlikely to be the cause. On the other hand Cp* is a more electron donating ligand than Cp[58] thus there should be greater electron density available for induction into the radialene system in **3.8** than in **3.4**. However, this is not what we observe as the radialene ligand in complex **3.8** is easier to reduce than that in **3.4**. This may be a result of the geometry of the complexes, with the radialene ligand in **3.4** possibly existing at a less acute angle to the ruthenium centre than that in **3.8** allowing for more direct induction. This may also explain the small decrease

in oxidation potential of the ruthenium centre in **3.8** as the electron density donated to the metal by the Cp* ligand is not withdrawn onto the nitrile ligand.

In general, each of the radialene ruthenium complexes possess a 1+ charge and as **2.29** and **2.38** are neutral ligands it would be expected that the radialene reduction occurs at a slightly less cathodic potential (ie. more easily).[63,64]

3.3.2. UV-Vis Absorbance and Fluorescence

UV-visible absorption spectra of each of the complexes were recorded in dichloromethane at a concentration of approximately 0.03 mM (Table 3.5). The absorption maxima for **3.1** and **3.2**, 324 and 315 nm respectively, are fairly consistent with that of $[Ru(NCPh)(PPh_3)_2Cp]PF_6$, 307 nm, with only a slight red shift observed. This band has previously been attributed for $[Ru(NCPh)(PPh_3)_2Cp]PF_6$ as an overlapping of the $Ru_{d\pi}$-Cp MLCT and $Ru_{d\pi}$-NCR_{π^*} MLCT transitions.[46] In $[Ru(NCPh)(dppe)Cp^*]PF_6$ these two transitions can be differentiated as absorption maxima at 310 and 346 nm.[46] These bands can be observed in complexes **3.5** and **3.6** as absorption maxima at 321 and 309 nm with shoulders at 347 and 343 nm respectively (Figure 3.12).

Table 3.5. Visible absorption maxima, log of the molar absorptivity, ε, and fluorescence emission maxima of the [3]radialenes **2.29** and **2.38**, and complexes $[Ru(NCPh)(PPh_3)_2Cp]PF_6$, $[Ru(NCPh)(dppe)Cp^*]PF_6$, and **3.1**-**3.8**.

Compound	λ_{max} (nm)	log ε	Fluorescence max (nm)	Stokes shift
$[Ru(NCPh)(PPh_3)_2Cp]PF_6$[55]	307	4.13		
3.1	324	3.89		
3.2	315	3.87		
$[Ru(NCPh)(dppe)Cp^*]PF_6$[46]	310, 346	3.74		
3.5	321, 347 sh	3.77		
3.6	309, 343 sh	3.72		
2.29	302, 489	4.42	620	131
3.3	304, 499	4.49	619	120
3.7	302, 495	4.52	617	122
2.38	291, 461	4.21	576	115
3.4	278, 320, 449	4.23	581	132
3.8	278, 314 sh, 455	4.19	578	123

sh = shoulder

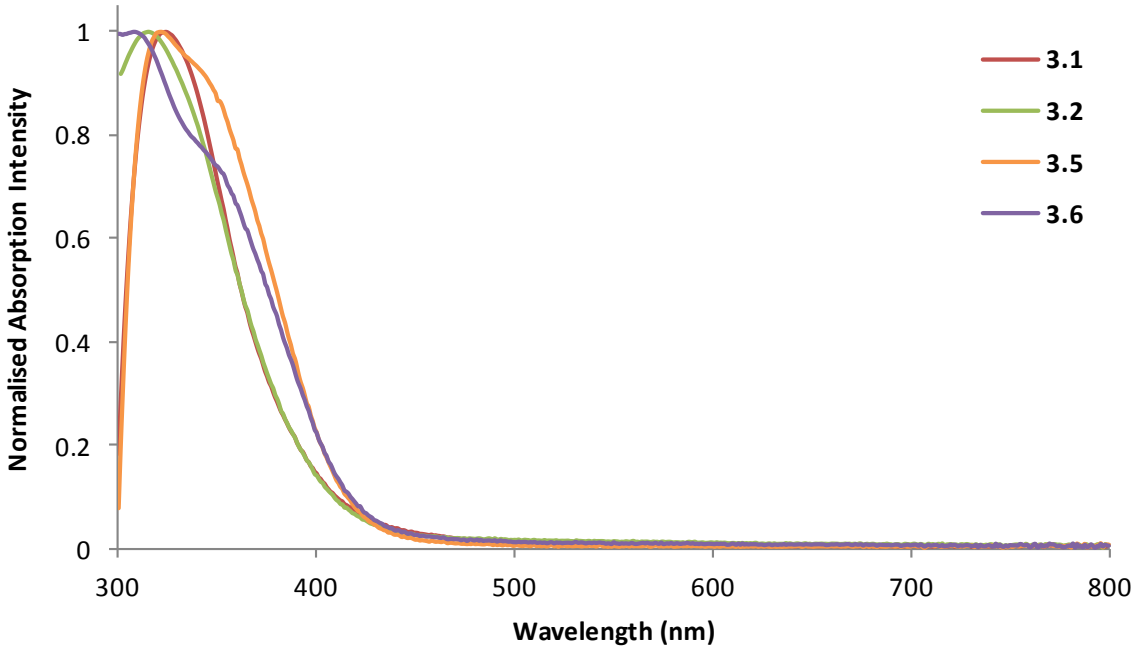

Figure 3.12. UV-Vis spectra of ruthenium complexes of **2.25** and **2.37** in dichloromethane.

Hexaaryl[3]radialene compounds have strong absorption bands between 460-490 nm, attributed to the π-π* transition, which account for their intense orange or red colouring. Coordination to ruthenium affects this absorption band slightly with a red shift seen for complexes **3.3** and **3.7** (absorption maxima of 495 and 499 nm respectively compared to 486 nm for **2.29**) and a blue shift seen for complexes **3.4** and **3.8** (absorption maxima of 455 and 449 nm respectively compared to 466 nm for **2.38**) (Figure 3.13).

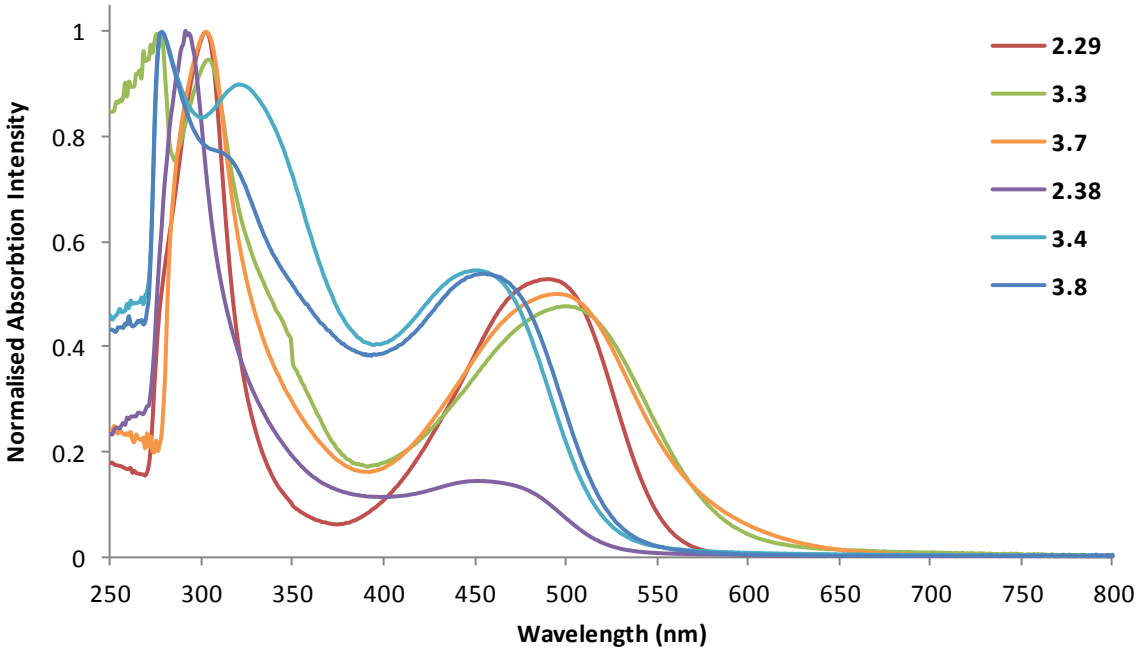

Figure 3.13. UV-Vis spectra of [3]radialenes **2.29** and **2.38** and their ruthenium complexes in dichloromethane.

The red shift of complexes **3.3** and **3.7** is as expected due to the stabilisation imparted by coordination to the ruthenium complex as observed electrochemically where the complexes are reduced more easily than the free radialenes. An additional reason for the observed red shift of complexes **3.3** and **3.7** is that the *para* configuration of the donor nitrile groups on the propeller-like radialene scaffold positions the coordinated ruthenium metal centre close in space to the nitrile group on an adjacent arm of the radialene which may result in a degree of intramolecular charge transfer. This interaction has been observed to produce a red shift in extended hexaaryl[3]radialenes with appended triarylamine moieties (λ_{max} ~600 nm) compared to their precursor hexakis(4-bromophenyl)[3]radialene (λ_{max} 485 nm).[65]

Conversely the blue shift of complexes **3.4** and **3.8** is unexpected as the electrochemical measurements also suggest a stabilisation imparted by the incorporation of the ruthenium complex. Blue shifts of ligand π-π* transitions are often due to reduced conjugation or a distortion in the ligand structure. Examination of the ^{1}H NMR spectra of complexes **3.4** and **3.8** may aid in the determination of whether this is the case, although the complex itself is asymmetrical which complicates the matter. Unfortunately, the signals within the aromatic region of the ^{1}H NMR spectra of these complexes are too complicated to ascertain whether distortion of the radialene ligand is present.

The free radialenes **2.29** and **2.38** also exhibit absorption peaks in the ultraviolet region at 302 and 291 nm respectively. These peaks overlap with the $Ru_{d\pi}$-Cp MLCT and $Ru_{d\pi}$-NCR_{π^*} MLCT transitions in the absorption spectra of the ruthenium complexes of **2.29**, **3.3** and **3.7**, as indicated by a broadening of the peaks although no significant shift in absorption maxima is observed. For the ruthenium complexes of **2.38** two distinct peaks are observed in the ultraviolet region. Complex **3.4** exhibits a broad absorption envelope between 275 and 400 nm with two clear maxima at 278 and 320 nm. These peaks can be assigned to the $Ru_{d\pi}$-Cp MLCT and $Ru_{d\pi}$-NCR_{π^*} MLCT transitions which are shifted in opposite directions compared the simple benzonitrile complex $[Ru(NCPh)(PPh_3)_2Cp]PF_6$ where they overlap at 307 nm. This broad absorption envelope also includes the radialene ultraviolet peak. The ultraviolet region in the absorption spectrum of complex **3.8** has a similar structure to that of complex **3.4** with a sharp peak at 278 nm, however the second peak at 314 nm is less well defined. These can also be assigned to the $Ru_{d\pi}$-Cp MLCT and $Ru_{d\pi}$-NCR_{π^*} MLCT transitions and are both blue shifted in comparison to the related peaks in $[Ru(NCPh)(dppe)Cp^*]PF_6$, which occur at 310 and 346 nm.

Hexaaryl[3]radialene compounds are also highly fluorescent and exhibit large Stokes shifts of up to 130 nm. The fluorescence of each of the radialene complexes was recorded in dichloromethane at a concentration of approximately 0.01 mM (Figure 3.14). A subtle shift in

fluorescence maxima were observed for complexes **3.3** and **3.7** (subtle decreases from 620 to 619 and 617 nm respectively, compared to **2.29**) as well as complexes **3.4** and **3.8** (similarly subtle increases from 576 to 581 and 578 nm respectively, compared to **2.38**). A red shift is expected, as seen for **3.4** and **3.8**, as the energy of the LUMO is lower in the complexes than in the free radialenes as shown by the electrochemistry where the complexes are reduced more easily. Complexes **3.3** and **3.7** show a blue shift however the change in wavelength is around 1-3 nm, but given the broadeness of the maxima and the accuracy of the peak finding functions of the software, this is not particularly significant. The Stokes shifts for the radialene containing complexes are 120, 122, 132, 123 nm for **3.3**, **3.7**, **3.4**, and **3.8** respectively (compared with 131 and 115 nm for **2.29** and **2.38**). The Stokes shifts for complexes **3.3** and **3.7** decrease due to the red shift of their respective UV-Vis absorption maxima as discussed above, whereas the opposite is observed for complexes **3.4** and **3.8**.

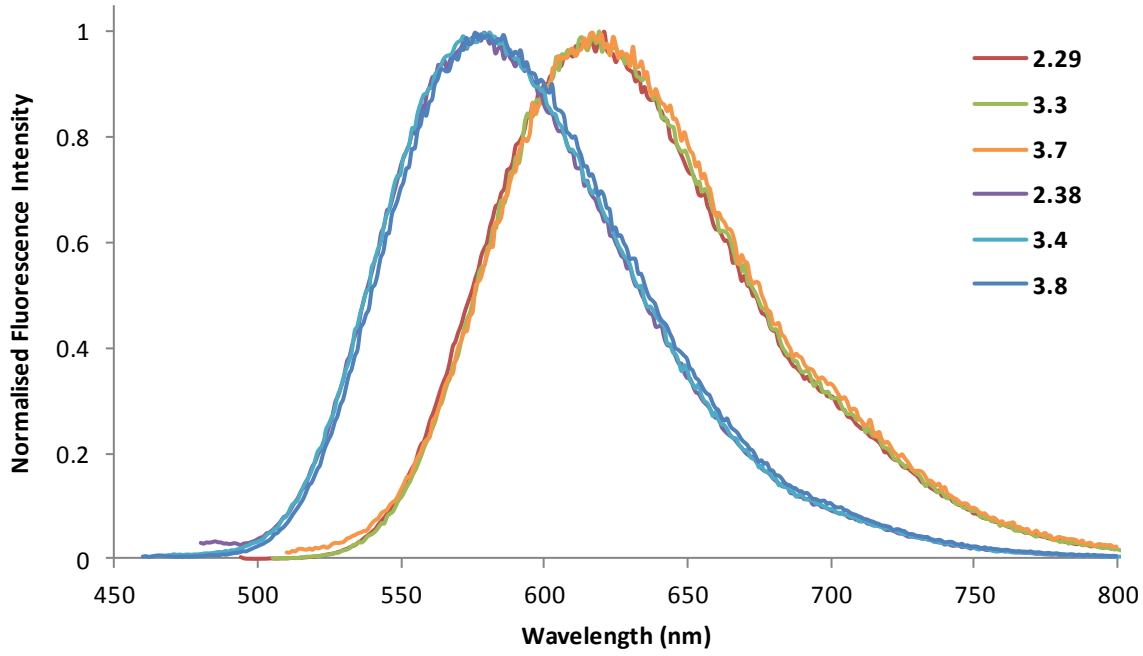

Figure 3.14. Fluorescence spectra of [3]radialenes **2.29** and **2.38** and their ruthenium complexes in dichloromethane.

3.4. Summary

This chapter has provided a brief introduction to multinuclear ruthenium complexes involving conjugated bridging ligands, the majority of which exhibit metal-metal interactions. It has also highlighted the relative lack of research into similar structures containing cross-conjugated bridging ligands. One such complex incorporating the cross-conjugated ligand hexa(2-pyridyl)[3]radialene has been reported, however no metal-metal interactions were observed due to its proposed non-planar conformation.[44] The observation of a chelating binding motif in coordination polymers of hexakis(4-cyanophenyl)[3]radialene (**2.29**) led to the conception of a discrete, tris(bidentate), trinuclear metal complex where all six nitrile groups are involved in coordination. It was also proposed that a metal atom in such a complex may interact in a facile manner with a second metal through the linearly conjugated segment of the π-system but not in the same manner with a third due to cross-conjugation. However, such a species was found to be unattainable using the approaches explored in this work.

The synthesis of four dinuclear ruthenium complexes, **3.1**, **3.2**, **3.5** and **3.6**, containing the [3]radialene precursor ligands 4,4'-dicyanodiphenylmethane (**2.25**) and 3,3'-dicyanodiphenyl-methane (**2.37**) have been described. The oxidation potentials of these complexes correlate closely with those of the corresponding benzonitrile complexes $[Ru(NCPh)(PPh_3)_2Cp]PF_6$[55] and $[Ru(NCPh)(dppe)Cp^*]PF_6$[46] which shows that the extension of the benzonitrile ligand via a methylene group has no effect on the electronic properties of the adjacent ruthenium centre. No metal-metal communication is observed for these complexes, as shown by the presence of only one oxidation wave in the cyclic voltammogram, due to the insulating methylene spacer.

The synthesis of multinuclear ruthenium complexes of the radialene ligands **2.29** and **2.38** proved to be problematic. Reaction with these ligands with more than one equivalent of $[RuCp(PPh_3)_2]Cl$ lead to the formation of multiple products including the mononuclear species and three isomeric dinuclear species. Successful synthesis of the pure mononuclear species **3.3** and **3.4** was achieved via reaction with one equivalent of $[RuCp(PPh_3)_2]Cl$ in dichloromethane heating at reflux overnight. The identity of these products was confirmed by elemental analysis and ESI-HRMS respectively, however a peak at 1112.8 *m/z* was observed for both complexes in the mass spectrum. This corresponded to the loss of one triphenylphosphine ligand from the ruthenium and possibly chelation by the ligand to the single metal centre in a similar fashion to that observed in coordination polymers of **2.29**. The attempted synthesis and isolation of such a species, via addition of copper(I) iodide to the reaction mixture to extract a triphenylphosphine ligand, was unsuccessful.

In order to eliminate the potential for chelation and to provide direct routes to the mononuclear complexes **2.29** and **2.38** were reacted with [RuCp*(dppe)]Cl as the chelating phosphine ligand is difficult to displace. The resultant mononuclear complexes **3.7** and **3.8** were obtained in good yields. The electronic properties of each of the mononuclear radialene ruthenium complexes were investigated via cyclic voltammetry. Hexaaryl[3]radialenes undergo two stepwise reductions to form the radical anion and the dianion respectively and these were observed along with the ruthenium oxidation wave. For complexes **3.3** and **3.7** the ruthenium oxidation potential does not change significantly from that observed for the corresponding benzonitrile complexes. However the radialene reduction potentials are reduced by an average of 0.09 V from the free radialene which indicates that where the radialene is *para*-substituted, there is an interaction between the ruthenium centre and the radialene that allows the stabilisation of the reduced forms of the radialene. Interestingly, a similar scenario is seen for complexes **3.4** and **3.8** where the radialene is *meta*-substituted. This indicates that despite the lack of direct conjugation in the *meta* isomer **2.38**, the ruthenium centre still acts to stabilise the radical and, to a lesser extent, the dianion. In general, each of the radialene ruthenium complexes possess a 1+ charge and as **2.29** and **2.38** are neutral ligands it would be expected that the radialene reduction occurs at a slightly less cathodic potential (ie. more easily).[63,64]

In the UV-Vis spectra of complexes **3.1**, **3.2**, **3.5** and **3.6** the $Ru_{d\pi}$-Cp MLCT and $Ru_{d\pi}$-NCR_{π^*} MLCT transitions were observed and these correlated well with the analogous transitions in the model complexes $[Ru(NCPh)(PPh_3)_2Cp]PF_6$[55] (for **3.1** and **3.2**) and $[Ru(NCPh)(dppe)Cp^*]PF_6$[46] (for **3.5** and **3.6**). These transitions were also observed in the [3]radialene containing complexes **3.3**, **3.4**, **3.7** and **3.8** along with the radialene π-π* transitions. A red shift was observed for the *para* substituted radialene complexes, **3.3** and **3.7**, compared to the free radialene, **2.29**. This was expected due to the stabilisation of the ligand imparted by the positive ruthenium metal centre as shown by the radialene reduction potentials. Another contributing factor is potential intramolecular charge transfer from the ruthenium ion to the radialene ligand due to its close positioning in space to the adjacent radialene arm. Conversely, the blue shift observed for the *meta* substituted radialene complexes, **3.4** and **3.8**, compared to the free radialene, **2.38**, was unexpected. This may be due to a loss of conjugation within the system or a distortion of the structure of the ligand.

Hexaaryl[3]radialene compounds are highly fluorescent and subtle shifts were observed in the fluorescence maxima for complexes **3.3**, **3.4**, **3.7** and **3.8** compared to the free radialenes, however the changes were very small and cannot be considered significant.

3.5. Experimental

3.5.1. General Experimental

Melting points were determined using a Gallenkamp variable heat melting point apparatus and are uncorrected. UV-visible absorption spectra were recorded on a Varian CARY 5000 spectrophotometer. Samples were dissolved in dichloromethane at a concentration of approximately 0.03 mM. Fluorescence spectra were recorded on a Varian CARY eclipse spectrophotometer. Samples were dissolved in dichloromethane at a concentration of approximately 0.01 mM. Infrared spectra were recorded using a Perkin Elmer Spectrum 100 FT-IR spectrometer with a universal attenuated total reflectance (UATR) sampling accessory. The Campbell microanalytical laboratory at the University of Otago performed elemental analyses.

Electrospray ionisation, high resolution mass spectroscopy (ESI-HRMS) was performed by the Adelaide Proteomics Centre using an LTQ Orbitrap XL ETD spectrometer. Samples were dissolved in HPLC grade acetonitrile or methanol at a concentration of 0.01 mg/cm^3. ^{1}H and ^{31}P NMR spectra were recorded on a Varian Gemini 300 MHz spectrometer (121 MHz for ^{31}P NMR). ^{1}H NMR spectra recorded in $CDCl_3$ were referenced to the internal standard Me_4Si, 0 ppm. ^{31}P NMR spectra recorded in $CDCl_3$ were referenced to external H_3PO_4. Unless otherwise stated, reagents were obtained from commercial sources and used as received. $[RuCp(PPh_3)_2Cl]$[66] and $[RuCp^*(dppe)Cl]$[27,67] were synthesised following literature procedures.

3.5.2. Synthetic Procedures

$[\{RuCp(PPh_3)_2\}_2$(2.25)$](PF_6)_2$ (3.1). Compound **2.25** (20.0 mg, 91.6 μmol), $[RuCp(PPh_3)_2]Cl$ (133 mg, 183 μmol) and NH_4PF_6 (59.7 mg, 366 μmol) in DCM (10 mL) was heated at reflux for 3 h. The resultant yellow solution was cooled to room temperature and MeOH (10 mL) was added. The DCM was removed under reduced pressure and the suspension refrigerated overnight. The resultant precipitate was isolated and air dried to yield **3.1** as a yellow solid (137 mg, 74%). Mp: 142-145 °C; ^{1}H NMR (300 MHz, $CDCl_3$): δ 4.01 (s, 2H, CH_2), 4.53 (s, 10H, Cp), 7.07-7.41 (m, 68H, Ar); ^{31}P NMR (121 MHz, $CDCl_3$): δ 40.79 (s, PPh_3), -144.58 (septet, J = 712 Hz, PF_6); ESI-HRMS (*m/z*): ($[M\text{-}PF_6^-]^+$) calcd for $C_{97}H_{80}N_2Ru_2P_5F_6$, 1745.30412; found 1745.30633; FT-IR: ν_{max}/cm^{-1} 2226 (C≡N), 839 (PF_6); Anal. found, C 61.45, H 4.39, N 1.53; calc. for $C_{97}H_{80}N_2Ru_2P_6F_{12}$ C 61.65, H 4.27, N 1.48.

$[\{RuCp(PPh_3)_2\}_2$(2.37)$](PF_6)_2$ (3.2). Compound **2.37** (20.0 mg, 91.6 μmol), $[RuCp(PPh_3)_2]Cl$ (133 mg, 183 μmol) and NH_4PF_6 (59.7 mg, 366 μmol) in DCM (10 mL)

was heated at reflux for 3 h. The resultant yellow solution was cooled to room temperature and MeOH (10 mL) was added. The DCM was removed under reduced pressure and the suspension refrigerated overnight. The resultant precipitate was isolated and air dried to yield **3.2** as a yellow solid (143 mg, 83%). Mp: 157-159 °C; ^{1}H NMR (300 MHz, $CDCl_3$): δ 4.01 (s, 2H, CH_2), 4.58 (s, 10H, Cp), 6.70 (d, 2H, J = 9.0 Hz, ligand Ar), 7.08-7.37 (m, 62H, Ar), 7.46 (d, 2H, J = 9.0 Hz, ligand Ar), 7.66 (s, 2H, ligand Ar); ^{31}P NMR (121 MHz, $CDCl_3$): δ 41.00 (s, PPh_3), -144.73 (septet, J = 713 Hz PF_6); ESI-HRMS (*m/z*): ($[M\text{-}PF_6^-]^+$) calcd for $C_{97}H_{80}N_2Ru_2P_5F_6$, 1745.30412; found 1745.30517; FT-IR: v_{max}/cm^{-1} 2229 (C≡N), 833 (PF_6); Anal. found, C 60.87, H 4.13, N 1.79; calc. for $C_{97}H_{80}N_2Ru_2P_6F_{12}\cdot$½($CH_2Cl_2$) C 60.61, H 4.23, N 1.45.

[RuCp(PPh$_3$)$_2$(2.29)]PF$_6$ (3.3). Radialene **2.29** (25.0 mg, 36.5 μmol), [RuCp(PPh_3)$_2$]Cl (26.5 mg, 36.5 μmol) and NH_4PF_6 (11.9 mg, 73.0 μmol) in MeOH (15mL) was heated at reflux overnight. The dark red solution was refridgerated overnight and the resultant precipitate was isolated and air dried to yield **3.3** as a red solid (31 mg, 62%). Mp: 205-207 °C; ^{1}H NMR (300 MHz, $CDCl_3$): δ 4.66 (s, 5H, Cp), 6.90 (d, 4H, J = 9.0 Hz, ligand Ar), 7.03-7.44 (m, 50H, Ar); ^{31}P NMR (121 MHz, $CDCl_3$): δ 39.56 (s, PPh_3), 39.69 (s, PPh_3), -145.72 (septet, J = 711 Hz, PF_6); ESI-HRMS (*m/z*): ($[M\text{-}PF_6^-]^+$) calcd for $C_{89}H_{59}N_6Ru_1P_2$, 1375.33145; found 1375.33711; FT-IR: v_{max}/cm^{-1} 2227 (C≡N), 830 (PF_6); Anal. found, C 66.02, H 4.01, N 4.48; calc. for $C_{89}H_{59}N_6RuP_3F_6\cdot1$½($CH_2Cl_2$) C 65.69, H 3.80, N 5.10.

[RuCp(PPh$_3$)$_2$(2.38)]PF$_6$ (3.4). Radialene **2.38** (5.0 mg, 7.3 μmol), [RuCp(PPh_3)$_2$]Cl (5.3 mg, 7.3 μmol) and NH_4PF_6 (2.4 mg, 15 μmol) in DCM (5mL) was heated at reflux overnight. The resultant orange solution was cooled to room temperature the solvent reduced to approximately 1 mL. MeOH (5 mL) was added and the suspension refrigerated overnight. The resultant precipitate was isolated and air dried to yield **3.4** as an orange solid (7.6 mg, 76%). Mp: 200-204 °C; ^{1}H NMR (300 MHz, $CDCl_3$): δ 4.58 (s, 5H, Cp), 6.62-7.79 (m, 54H, Ar); ^{31}P NMR (121 MHz, $CDCl_3$): δ 40.95 (s, PPh_3), -144.59 (septet, J = 710 Hz, PF_6); ESI-HRMS (*m/z*): ($[M\text{-}PF_6^-]^+$) calcd for $C_{89}H_{59}N_6RuP_2$, 1375.33145; found 1375.33637; FT-IR: v_{max}/cm^{-1} 2231 (C≡N), 836 (PF_6). Due to only having a limited amount of this compound no elemental analysis was performed.

[{RuCp*(dppe)}$_2$(2.25)](PF$_6$)$_2$ (3.5). Compound **2.25** (5.0 mg, 23 μmol), [RuCp*(dppe)]Cl (28.0 mg, 46 μmol) and NH_4PF_6 (15 mg, 92 μmol) in DCM (10 mL) was heated at reflux overnight. The resultant yellow solution was cooled to room temperature the solvent reduced to approximately 1 mL. MeOH (10 mL) was added and the suspension refrigerated overnight. The resultant precipitate was isolated and air dried to yield **3.5** as a yellow solid (31 mg, 76%). Mp: 207-210 °C; ^{1}H NMR (300 MHz, $CDCl_3$): δ 1.49 (s, 30H,

Cp^*), 2.34-2.56 (m, 8H, 4×CH_2) 3.88 (s, 2H, CH_2), 6.50 (d, 4H, *J* = 8.2 Hz, ligand Ar), 7.11 (d, 4H, *J* = 8.2 Hz, ligand Ar), 7.46-7.54 (m, 40H, Ar); ^{31}P NMR (121 MHz, $CDCl_3$): δ 74.06 (s, dppe), -144.78 (septet, *J* = 712 Hz, PF_6); ESI-HRMS (*m/z*): ($[M\text{-}PF_6^-]^+$) calcd for $C_{87}H_{88}N_2Ru_2P_5F_6$, 1633.36672; found 1633.36709; FT-IR: v_{max}/cm^{-1} 2227 (C≡N), 835 (PF_6); Anal. found, C 58.55, H 4.89, N 1.64; calc. for $C_{87}H_{88}N_2Ru_2P_6F_{12}$ C 58.78, H 4.99, N 1.58.

[{RuCp*(dppe)}$_2$(2.37)](PF$_6$)$_2$ (3.6). Compound **2.37** (5.0 mg, 23 μmol), [RuCp*(dppe)]Cl (28.0 mg, 46 μmol) and NH_4PF_6 (15 mg, 92 μmol) in DCM(10 mL) was heated at reflux overnight. The resultant yellow solution was cooled to room temperature the solvent reduced to approximately 1 mL. Methanol (10 mL) was added and the suspension refrigerated overnight. The resultant precipitate was isolated and air dried to yield **3.6** as a yellow solid (25 mg, 62%) with a small number of crystals suitable for X-ray crystallography recovered. Mp: 232-235 °C; ^{1}H NMR (300 MHz, $CDCl_3$): δ 1.51 (s, 30H, Cp^*), 2.39-2.59 (m, 8H, 4×CH_2), 3.77 (s, 2H, CH_2), 6.42-6.47 (m, 4H, Ar), 7.07-7.63 (m, 44H, Ar); ^{31}P NMR (121 MHz, $CDCl_3$): δ 74.09 (s, dppe), -144.79 (septet, *J* = 711 Hz, PF_6); ESI-HRMS (*m/z*): ($[M\text{-}PF_6^-]^+$) calcd for $C_{87}H_{88}N_2Ru_2P_5F_6$, 1633.36672; found 1633.37059; FT-IR: v_{max}/cm^{-1} 2229 (C≡N), 833 (PF_6); Anal. found, C 57.48, H 4.99, N 1.78; calc. for $C_{87}H_{88}N_2Ru_2P_6F_{12}\cdot CH_2Cl_2$ C 57.03, H 4.84, N 1.49.

[{RuCp*(dppe)}(2.29)]PF$_6$ (3.7). Radialene **2.29** (20.0 mg, 29.2 μmol), [RuCp*(dppe)]Cl (18.0 mg, 29.2 μmol) and NH_4PF_6 (9.6 mg, 58.4 μmol) in DCM (10 mL) was heated at reflux overnight. The resultant purple solution was cooled to room temperature the solvent reduced to approximately 1 mL. MeOH (10 mL) was added and the suspension refrigerated overnight. The resultant precipitate was isolated and air dried to yield **3.7** as a purple solid (30 mg, 78%). Mp: 239 °C dec.; ^{1}H NMR (300 MHz, $CDCl_3$): δ 1.51 (s, 15H, Cp^*), 2.25-2.81 (m, 4H, 2×CH_2), 6.09-6.14 (m, 2H, Ar), 6.81-6.97 (m, 9H, Ar), 7.14-7.25 (m, 13H, Ar), 7.43-7.68 (m, 20H, Ar); ^{31}P NMR (121 MHz, $CDCl_3$): δ 74.01 (s, dppe), -145.12 (septet, *J* = 713 Hz, PF_6); ESI-HRMS (*m/z*): ($[M\text{-}PF_6^-]^+$) calcd for $C_{84}H_{63}N_6RuP_2$, 1319.36275; found 1319.37170; FT-IR: v_{max}/cm^{-1} 2227 (C≡N), 830 (PF_6); Anal. found, C 66.12, H 4.29, N 5.08; calc. for $C_{84}H_{63}N_6RuP_3F_6\cdot CH_2Cl_2$ C 65.89, H 4.23, N 5.42.

[{RuCp*(dppe)}(2.38)]PF$_6$ (3.8). Radialene **2.38** (10 mg, 16 μmol), [RuCp*(dppe)]Cl (9.0 mg, 16 μmol) and NH_4PF_6 (4.8 mg, 29 μmol) in DCM (5 mL) was heated at reflux overnight. The resultant orange solution was cooled to room temperature the solvent reduced to approximately 1 mL. MeOH (5 mL) was added and the suspension refrigerated overnight. The resultant precipitate was isolated and air dried to yield **3.8** as an orange solid (14 mg, 71%). Mp: 187-190 °C; ^{1}H NMR (300 MHz, $CDCl_3$): δ 1.49 (s, 15H, Cp^*), 2.23-2.65 (m, 4H, 2×CH_2), 7.14-7.72 (m, 44H, Ar); ^{31}P NMR (121 MHz, $CDCl_3$): δ 74.42 (s, dppe), -145.06

(septet, J = 712 Hz, PF_6); ESI-HRMS (m/z): ($[M\text{-}PF_6^-]^+$) calcd for $C_{84}H_{63}N_6RuP_2$, 1319.36275; found 1319.37107; FT-IR: ν_{max}/cm^{-1} 2229 (C≡N), 836 (PF_6); Anal. found, C 65.73, H 4.50, N 5.03; calc. for $C_{84}H_{63}N_6RuP_3F_6 \cdot CH_2Cl_2$ C 65.89, H 4.23, N 5.42.

3.5.3. Cyclic Voltammetry

Cyclic voltammetry measurements were performed on a PAR Model 263A potentiostat under nitrogen. Measurements were recorded on 1 mM solutions in dichloromethane/0.1 M $[(n\text{-}C_4H_9)_4]NPF_6$ solution using a platinum working electrode, platinum wire auxiliary and pseudo-reference electrodes. Ferrocene was added as an internal standard on completion of each experiment and tabulated potentials are given vs the saturated calomel electrode [$E_0(Fc/Fc^+)$ = 460 mV vs SCE (dichloromethane)]. Cyclic voltammetry was performed with a sweep rate of 100 mVs^{-1}.

3.5.4. X-Ray Crystallography

Crystals were mounted under oil on a loop and X-ray diffraction data collected at 150(2) K with synchrotron radiation (λ = 0.7107 Å) using the Macromolecular Crystallography beamline (MX1) at the Australian Synchrotron.[68] The data set was corrected for absorption using a multi-scan method, and structures were solved by direct methods using SHELXS-97[69] and refined by full-matrix least squares on F^2 by SHELXL-97,[70] interfaced through the program X-Seed.[71] All non-hydrogen atoms were refined anisotropically and hydrogen atoms were included as invariants at geometrically estimated positions.

3.5.5. Crystallographic Data

Table 2.4. Crystal data and X-ray experimental data for **3.6**.

Compound	**3.6**
Empirical formula	$C_{44}H_{45}NRuP_3F_6Cl$
Formula weight	931.24
Temperature (K)	150(2)
Radiation source	Synchrotron
Crystal system	Monoclinic
Space group	$P2_1/n$
a (Å)	11.715(2)
b (Å)	17.841(4)
c (Å)	20.230(4)
α (°)	90
β (°)	93.55(3)
γ (°)	90
Volume ($Å^3$)	4220.1(15)
Z	4
D_{calc} (mg/m^3)	1.466
Absorption coefficient (mm^{-1})	0.608
F(000)	1904
Crystal size (mm^3)	0.28 × 0.19 × 0.14
Theta range for data (°)	2.28 to 28.88
Reflections collected	73124
Independent reflections [R(int)]	10691 [0.0459]
Completeness to theta full (%)	97.6
Observed reflections [I>2σ(I)]	9753
Data / restraints / parameters	10691 / 7 / 539
Goodness-of-fit on F2	1.022
R_1 [I>2σ(I)]	0.0587
wR_2 (all data)	0.1649
Largest diff. peak and hole ($e.Å^{-3}$)	1.35 and -1.84

Additional refinement details for 3.6. There is disorder of the 3,3'-dicyanodiphenyl-methane ligand and of the dichloromethane solvate molecule. The ligand was modeled over two major positions with *ca.* 65:35 occupancy. Five restraints were used to maintain chemically sensible bond lengths within the ligand for the nitrile substituents and the methane bridge. Two restraints were used to maintain chemically sensible bond lengths within the dichloromethane solvate molecule.

3.6. References

1 C. Kaes, A. Katz, and M. W. Hosseini, *Chem. Rev.*, **2000**, *100*, 3553.

2 Y. X. Wang, W. J. Perez, G. Y. Zheng, D. P. Rillema, and C. L. Huber, *Inorg. Chem.*, **1998**, *37*, 2227.

3 C. J. Sumby, *Aust. J. Chem.*, **2008**, *61*, 894.

4 E. C. Constable, *Adv. Inorg. Chem.*, **1989**, *34*, 1.

5 C. J. Sumby, *Coord. Chem. Rev.*, **2011**, *255*, 1937.

6 J. G. Vos and J. M. Kelly, *Dalton Trans.*, **2006**, 4869.

7 D. M. D'Alessandro and F. R. Keene, *Pure Appl. Chem.*, **2008**, *80*, 1.

8 M. D. Ward, *Chem. Soc. Rev.*, **1995**, *24*, 121.

9 V. Balzani, A. Juris, M. Venturi, S. Campagna, and S. Serroni, *Chem. Rev.*, **1996**, *96*, 759.

10 J. W. Slater, D. M. D'Alessandro, F. R. Keene, and P. J. Steel, *Dalton Trans.*, **2006**, 1954.

11 D. M. D'Alessandro and F. R. Keene, *Chem. Soc. Rev.*, **2006**, *35*, 424.

12 D. M. D'Alessandro and F. R. Keene, *Chem. Rev.*, **2006**, *106*, 2270.

13 D. M. D'Alessandro and F. R. Keene, *Chem. Phys.*, **2006**, *324*, 8.

14 F. R. Keene, *Chem. Soc. Rev.*, **1998**, *27*, 185.

15 W. R. Browne, R. Hage, and J. G. Vos, *Coord. Chem. Rev.*, **2006**, *250*, 1653.

16 W. Kaim and G. K. Lahiri, *Angew. Chem. Int. Ed.*, **2007**, *46*, 1778.

17 W. Kaim and B. Sarkar, *Coord. Chem. Rev.*, **2007**, *251*, 584.

18 C. Creutz and H. Taube, *J. Am. Chem. Soc.*, **1969**, *91*, 3988.

19 C. Creutz and H. Taube, *J. Am. Chem. Soc.*, **1973**, *95*, 1086.

20 C. Creutz, *Prog. Inorg. Chem.*, **1983**, *30*, 1.

21 K. A. Goldsby and T. J. Meyer, *Inorg. Chem.*, **1984**, *23*, 3002.

22 A. Masschelein, A. K.-D. Mesmaeker, C. Verhoeven, and R. Nasielski-Hinkens, *Inorg. Chim. Acta*, **1987**, *129*, L13.

23 T. J. Rutherford, O. Van Gijte, A. Kirsch-De Mesmaeker, and F. R. Keene, *Inorg. Chem.*, **1997**, *36*, 4465.

24 S. Serroni, S. Campagna, G. Denti, T. E. Keyes, and J. G. Vos, *Inorg. Chem.*, **1996**, *35*, 4513.

25 D. P. Rillema, R. W. Callahan, and K. B. Mack, *Inorg. Chem.*, **1982**, *21*, 2589.

26 F. Paul and C. Lapinte, *Coord. Chem. Rev.*, **1998**, *178*, 431.

27 M. I. Bruce, B. G. Ellis, P. J. Low, B. W. Skelton, and A. H. White, *Organometallics*, **2003**, *22*, 3184.

28 J. L. Humphrey, K. M. Lott, M. E. Wright, and D. Kuciauskas, *J. Phys. Chem. B*, **2005**, *109*, 21496.

29 M. Akita and T. Koike, *Dalton Trans.*, **2008**, 3523.

30 M. I. Bruce, P. J. Low, K. Costuas, J.-F. Halet, S. P. Best, and G. A. Heath, *J. Am. Chem. Soc.*, **2000**, *122*, 1949.

31 M. I. Bruce, B. Le Guennic, N. Scoleri, N. N. Zaitseva, and J.-F. Halet, *Organometallics*, **2012**, *31*, 4701.

32 M. Gholami and R. R. Tykwinski, *Chem. Rev.*, **2006**, *106*, 4997.

33 Y. M. Zhao, K. Campbell, and R. R. Tykwinski, *J. Org. Chem.*, **2002**, *67*, 336.

34 D. A. Shultz, *Polyhedron*, **2001**, *20*, 1627.

35 A. B. Ricks, G. C. Solomon, M. T. Colvin, A. M. Scott, K. Chen, M. A. Ratner, and M. R. Wasielewski, *J. Am. Chem. Soc.*, **2010**, *132*, 15427.

36 M. I. Bruce, M. A. Buntine, K. Costuas, B. G. Ellis, J. F. Halet, P. J. Low, B. W. Skelton, and A. H. White, *J. Organomet. Chem.*, **2004**, *689*, 3308.

37 T. Enomoto, T. Kawase, H. Kurata, and M. Oda, *Tetrahedron Lett.*, **1997**, *38*, 2693.

38 T. Enomoto, N. Nishigaki, H. Kurata, T. Kawase, and M. Oda, *Bull. Chem. Soc. Jpn.*, **2000**, *73*, 2109.

39 K. Matsumoto, Y. Harada, T. Kawase, and M. Oda, *Chem. Commun.*, **2002**, 324.

40 P. J. Steel and C. J. Sumby, *Chem. Commun.*, **2002**, 322.

41 K. Matsumoto, Y. Harada, N. Yamada, H. Kurata, T. Kawase, and M. Oda, *Cryst. Growth Des.*, **2006**, *6*, 1083.

42 P. J. Steel and C. J. Sumby, *Inorg. Chem. Commun.*, **2002**, *5*, 323.

43 C. A. Hollis, L. R. Hanton, J. C. Morris, and C. J. Sumby, *Cryst. Growth Des.*, **2009**, *9*, 2911.

44 D. M. D'Alessandro, F. R. Keene, P. J. Steel, and C. J. Sumby, *Aust. J. Chem.*, **2003**, *56*, 657.

45 G. S. Ashby, M. I. Bruce, I. B. Tomkins, and R. C. Wallis, *Aust. J. Chem.*, **1979**, *32*, 1003.

46 R. L. Cordiner, D. Albesa-Jove, R. L. Roberts, J. D. Farmer, H. Puschmann, D. Corcoran, A. E. Goeta, J. A. K. Howard, and P. J. Low, *J. Organomet. Chem.*, **2005**, *690*, 4908.

47 R. J. Jakobsen, *Spectrochim. Acta*, **1965**, *21*, 127.

48 V. Farina, S. Kapadia, B. Krishnan, C. Wang, and L. S. Liebeskind, *J. Org. Chem.*, **1994**, *59*, 5905.

49 T. Appleby and J. Derek Woollins, *Coord. Chem. Rev.*, **2002**, *235*, 121.

50 C. A. Tolman, *Chem. Rev.*, **1977**, *77*, 313.

51 A. Glockner, H. Bauer, M. Maekawa, T. Bannenberg, C. G. Daniliuc, P. G. Jones, Y. Sun, H. Sitzmann, M. Tamm, and M. D. Walter, *Dalton Trans.*, **2012**, *41*, 6614.

52 D. E. Richardson and H. Taube, *Coord. Chem. Rev.*, **1984**, *60*, 107.

53 D. M. D'Alessandro and F. R. Keene, *Dalton Trans.*, **2004**, 3950.

54 W. Kaim, A. Klein, and M. Glöckle, *Acc. Chem. Res.*, **2000**, *33*, 755.

55 R. L. Cordiner, D. Corcoran, D. S. Yufit, A. E. Goeta, J. A. K. Howard, and P. J. Low, *Dalton Trans.*, **2003**, 3541.

56 Brett D. Yeomans, Laurence S. Kelso, Peter A. Tregloan, and F. R. Keene, *Eur. J. Inorg. Chem.*, **2001**, *2001*, 239.

57 A. Avellaneda, C. A. Hollis, X. He, and C. J. Sumby, *Beil. J. Org. Chem.*, **2012**, *8*, 71.

58 D. M. Tellers, S. J. Skoog, R. G. Bergman, T. B. Gunnoe, and W. D. Harman, *Organometallics*, **2000**, *19*, 2428.

59 A. D'Aléo, S. Welter, E. Cecchetto, and L. De Cola, *Pure Appl. Chem.*, **2005**, *77*, 1035.

60 F. Weldon, L. Hammarström, E. Mukhtar, R. Hage, E. Gunneweg, J. G. Haasnoot, J. Reedijk, W. R. Browne, A. L. Guckian, and J. G. Vos, *Inorg. Chem.*, **2004**, *43*, 4471.

61 S. O. Grim, W. L. Briggs, R. C. Barth, C. A. Tolman, and J. P. Jesson, *Inorg. Chem.*, **1974**, *13*, 1095.

62 D. R. Anton and R. H. Crabtree, *Organometallics*, **1983**, *2*, 621.

63 W. Kaim and S. Kohlmann, *Inorg. Chem.*, **1990**, *29*, 2909.

64 E. Amouyal, A. Homsi, J.-C. Chambron, and J.-P. Sauvage, *J. Chem. Soc., Dalton Trans.*, **1990**, 1841.

65 K. Matsumoto, N. Yamada, T. Enomoto, H. Kurata, T. Kawase, and M. Oda, *Chem. Lett.*, **2011**, *40*, 1033.

66 M. I. Bruce and N. J. Windsor, *Aust. J. Chem.*, **1977**, *30*, 1601.

67 F. Morandini, A. Dondana, I. Munari, G. Pilloni, G. Consiglio, A. Sironi, and M. Moret, *Inorg. Chim. Acta*, **1998**, *282*, 163.

68 T. M. McPhillips, S. E. McPhillips, H.-J. Chiu, A. E. Cohen, A. M. Deacon, P. J. Ellis, E. Garman, A. Gonzalez, N. K. Sauter, R. P. Phizackerley, S. M. Soltis, and P. Kuhn, *J. Synchrotron Radiat.*, **2002**, *9*, 401.

69 G. M. Sheldrick, *Acta Crystallogr., Sect. A*, **1990**, *46*, 467.

70 G. M. Sheldrick, *SHELXL-97*, University of Gottingen, Gottingen, Germany 1997.

71 L. J. Barbour, *J. Supramol. Chem.*, **2001**, *1*, 189.

Chapter 4

Coordination Polymers of [3]Radialenes

Chapter 4

4. Coordination Polymers of [3]Radialenes

4.1. Introduction

4.1.1. Coordination Polymers

Coordination polymers are infinite 1-, 2- and 3-D networks composed of metal ion (nodes) and organic ligands (linkers).[1-4] Access to a virtually endless structural diversity of such materials can be achieved by employing varying metal salts (coordination numbers and geometries, coordinating or non-coordinating anions) and linkers (donor nature, number and arrangement). For simple 2-connecting ligands, a typical 1-D coordination polymer can be formed when the metal has a linear or bent geometry and is coordinated by two ligand molecules leading to the formation of a simple chain (Figure 4.1). Generally, 2-D frameworks are obtained when the metal or ligand has a trigonal planar or square planar geometry and is coordinated by three or four ligand molecules, which allow its extension in two directions, and 3-D networks are formed via the inclusion of metal ions with higher coordination numbers, which can act as tetrahedral or octahedral nodes (Figure 4.1).

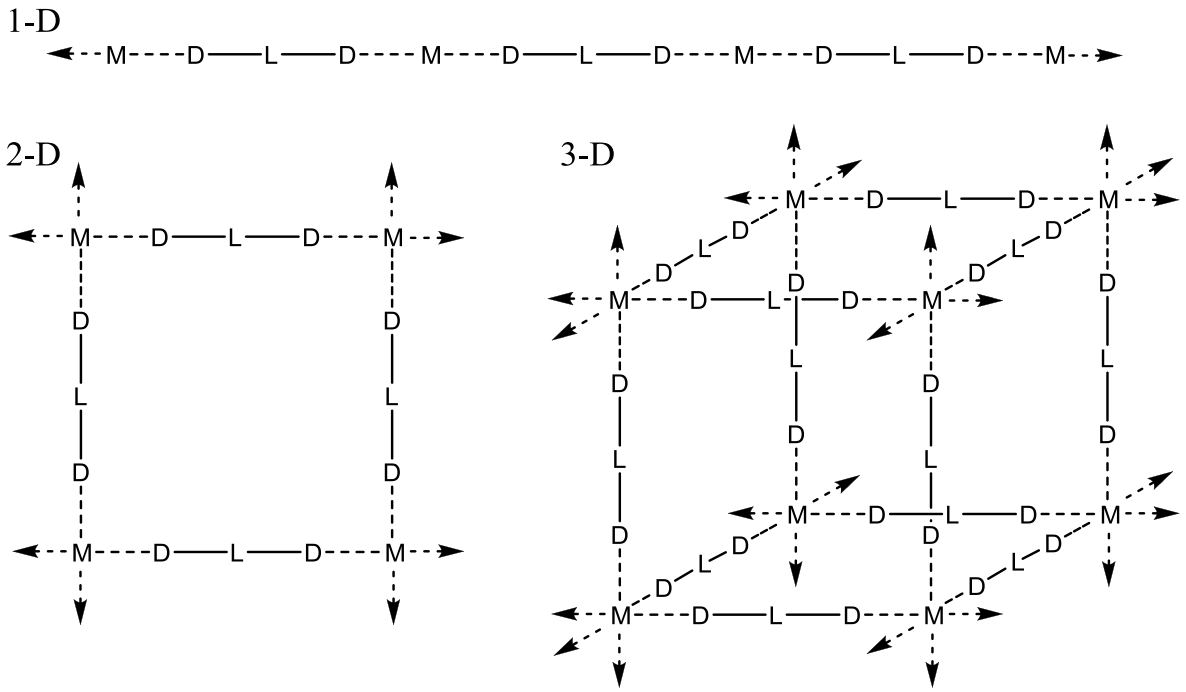

Figure 4.1. A schematic of the dimensionality of coordination polymers where M represents the metal ions, L represents the ligands, and D represents the ligand donor groups.

By definition, a coordination polymer contains metal nodes and organic linkers connected by coordinate bonds and thus this classification excludes polymeric structures connected by other interactions such as covalent, ionic and hydrogen bonds. However, these interactions are often observed as secondary interactions in the solid-state packing of coordination polymers. The ligands themselves must be organic in nature with such species as halides, oxides, sulfides and phosphates being considered 'inorganic'.[1] The metals utilised are generally the transition metals and the lanthanide series, as the alkali and alkaline earth metals exhibit ionic bonding and the main group metals are more covalent in nature.[1]

Metal-ligand coordinate bonds are strong compared to other non-covalent interactions such as hydrogen bonds and it is this factor coupled with their lability which makes them ideal for the formation of networks with long-range order. Purely organic polymers are covalently bonded and, as covalent bonds are largely irreversible, if an error is made during the polymer construction it is permanent. Conversely, the reversibility of metal-ligand coordinate bonds allows error correction during the formation of the coordination polymer resulting in a highly ordered, crystalline structure. This property of coordination polymer construction allows the determination of their structure via X-ray crystallography.

As noted, the most commonly used metal ions in coordination polymer synthesis are the transition metals, in particular those in the first-row[5-10] as well as silver(I)[11-13] and cadmium(II).[14] This is largely due to their lability and stability coupled with their predictable coordination geometries (Figure 4.2) Metals from the lanthanide series are also employed,[15-19] however their higher connectivity can lead to varied and complex structures. During synthesis these metals are utilised as their salts with, preferably non-coordinating, anions such as perchlorate, tetrafluoroborate, hexafluorophosphate and hexafluoroantimonate.

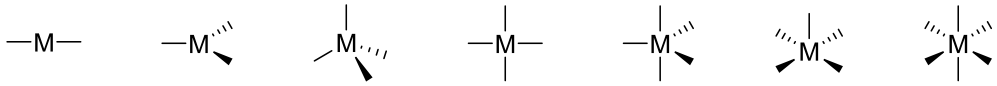

Figure 4.2. Common coordination geometries of transition metals.

Multitopic organic bridging ligands used in the synthesis of coordination polymers can contain a range of functional groups with metal coordinating ability; these are commonly nitrogen-containing heterocyclic,[20-25] carboxylate,[7,26-31] and nitrile donors.[32-35] Figure 4.1 assumes the use of linear organic ligands; however these linker molecules can also affect the overall network structure of the resultant coordination polymer by possessing a higher degree of connectivity (Figure 4.3). Modification of these components also imbues the framework with useful properties such as magnetism, conduction and porosity.[36-39]

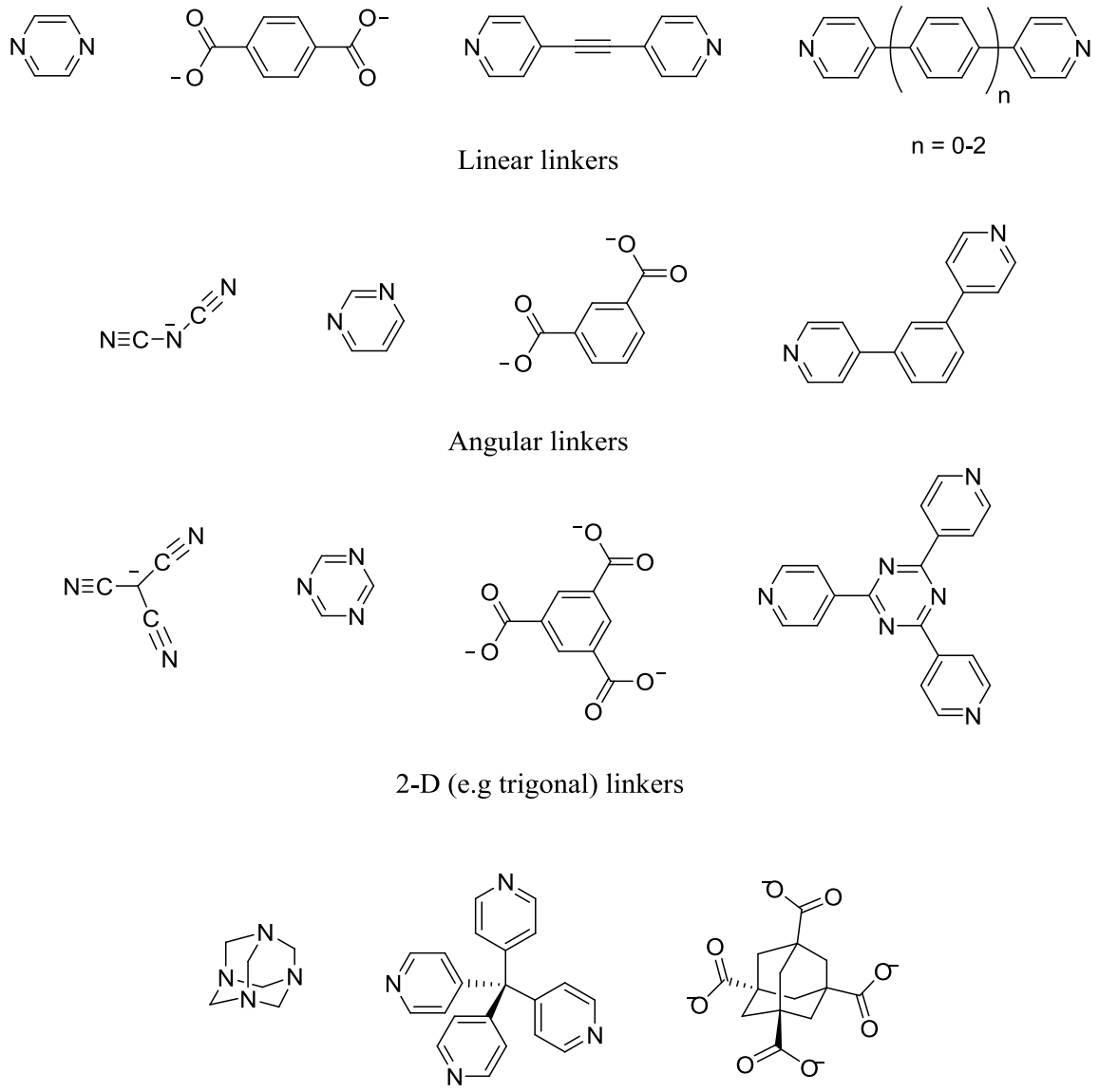

Figure 4.3. Examples of multitopic organic bridging ligands.

The coordination chemistry of linearly conjugated and aromatic polynitrile ligands has been widely studied and many coordination polymers, predominantly containing silver(I) and copper(I) due to the soft neutral nitrile donors, have been reported.[40-48] Simple benzene based ligands with varying numbers of nitrile donors have been used to synthesise a range of different network topologies. 1,3-Dicyanobenzene forms a (4,4)-connected 2-D net upon reaction with $[Cu(CH_3CN)_4]PF_6$ in a solvent mixture of acetone and pentane (Figure 4.4 (a)).[46] On the other hand, the tri-substituted derivative 1,3,5-tricyanobenzene yielded a 2-D (6,3) net upon reaction with $AgCF_3SO_3$ as both the silver(I) metal atoms and the ligands act as 3-connecting nodes (Figure 4.4 (b)).[47] A 3-D net with a **pts** type topology was produced upon reaction of 1,2,4,5-tetracyanobenezene with $[Cu(CH_3CN)_4]PF_6$ (Figure 4.4 (c)).[44] In this

structure the ligand acts as a square planar 4-connecting node while the copper(I) metal atoms act as tetrahedral 4-connecting nodes. Although the ligand is tetradentate in this network it has also been observed to exhibit bidentate[48] and tridentate[44] coordination modes.

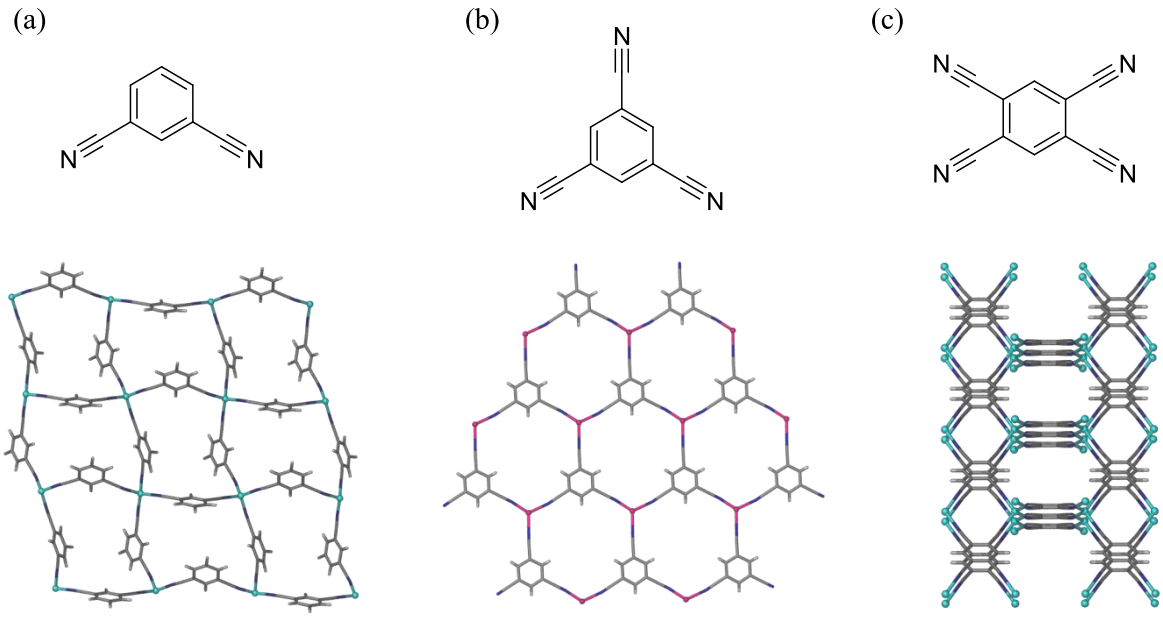

Figure 4.4. Polynitrile ligands (a) 1,3-dicyanobenzene, (b) 1,3,5-tricyano-benzene and (c) 1,2,4,5-tetracyanobenzene and examples of their polymer networks.

Further examples involving more complex ligands include the work of Hoskins and Robson who produced colourless crystals via the slow evaporation of 4,4',4",4'"-tetracyanophenylmethane and $[Cu(CH_3CN)_4]BF_4$ from a mixture of nitrobenzene and acetonitrile (Figure 4.5).[41] The structure of this coordination polymer was determined to be a 3-D diamond-like net due to the preferred geometry of copper(I), as well as the fixed arrangement of the nitrile donors, being tetrahedral.

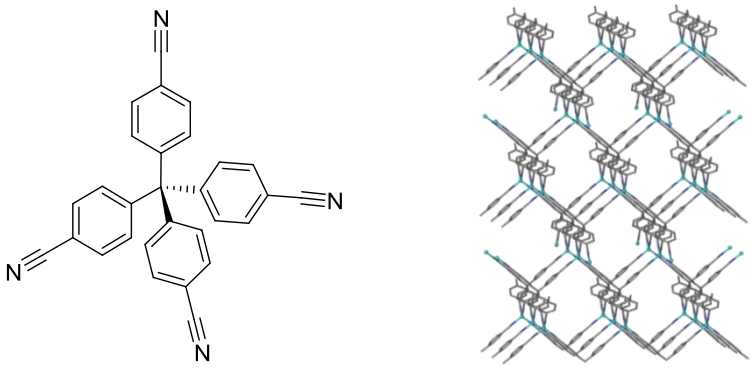

Figure 4.5. The structure of 4,4',4",4'"-tetracyanophenylmethane and its 3-D diamond-like net with copper(I).

Another example is that of the aromatic trinitrile ligand, 1,3,5-tris(4-ethynylbenzonitrile)-benzene (TEBB) reported by Moore and colleagues (Figure 4.6).[43] Reaction of TEBB and $AgCF_3SO_3$ in benzene yielded a 2-D (6,3) network of trigonal planar silver(I) atoms coordinated to three separate nitrile ligands reminiscent of a honeycomb with large solvent accessible voids.

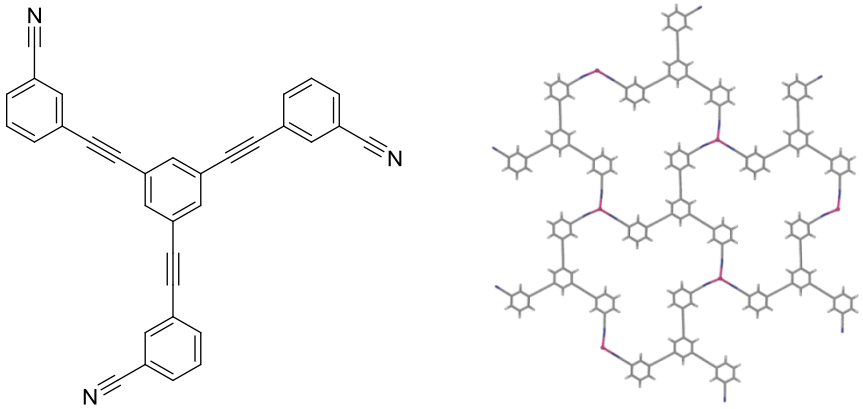

Figure 4.6. The structure of 1,3,5-tris(4-ethynylbenzonitrile)benzene (TEBB) and the 2-D network of $\{[Ag(TEBB)(CF_3SO_3)]\cdot 2(C_6H_6)\}_n$.

In contrast, the coordination chemistry of non-aromatic cross-conjugated polynitrile ligands has been investigated to a limited extent.[49-51] Recent work by Murray and Batten has yielded a number of coordination polymers of the hexacyano[3]radialene anion (Figure 4.7 (a)).[50,51] The first is a 2-D (6,3) net formed via reaction of $Mn(NO_3)_2\cdot 4H_2O$ with the hexacyano[3]radialene sodium salt (Figure 4.7 (b)).[51] Within this structure the hexacyano[3]radialene ligand acts as a 3-connecting node whilst the manganese(II) metal atoms are topologically trivial. An interesting feature is that molecules of the free anionic radialene are situated within the voids in the net acting as counter ions. The second structure is a (4,4)-connected 2-D net produced via reaction of the tetra-butyl ammonium salt of hexacyano[3]radialene with $Fe(BF_4)_2\cdot 6H_2O$ (Figure 4.7 (c)).[51] Within this structure the iron(II) metal atoms act as 4-connecting nodes whilst the hexacyano[3]radialene ligands are topologically trivial. These two examples show hexacyano[3]radialene acting as a tridentate and bidentate ligand, however it has also been observed to act as a monodentate ligand in a discrete complex with cobalt(II).[50] Even though hexacyano[3]radialene has the potential to be a hexadentate ligand it tends to remain hypodentate in its coordination compounds.

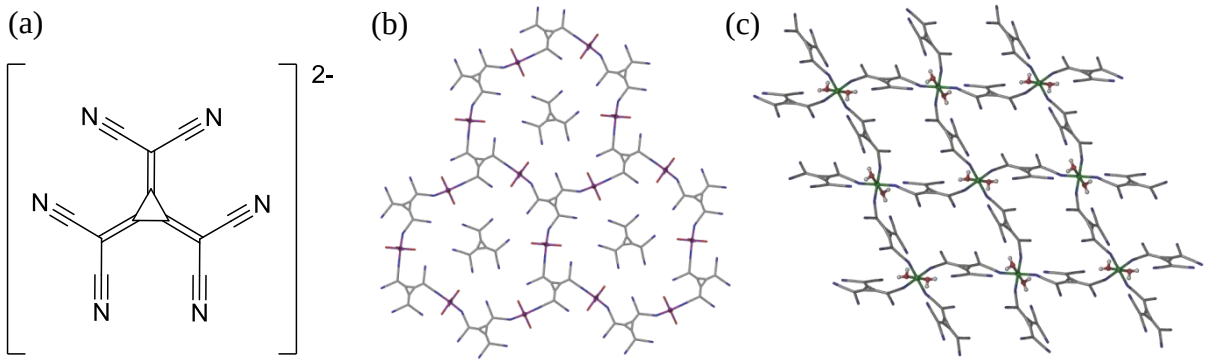

Figure 4.7. Representations of (a) hexacyano[3]radialene, (b) a 2-D (6,3) net with manganese(II) and (c) a (4,4)-connected 2-D net with iron(II).

4.1.2. Known Coordination Polymers of [3]Radialenes

Functionalised hexaaryl and hexa-heteroaryl derivatives of the parent [3]radialene make attractive ligands for use in coordination polymers due to their unusual propeller-like 3-D structures, interesting optical properties, and potential to coordinate multiple metal atoms in a variety of coordination modes. Two coordination polymers with silver(I) have been observed for hexa(2-pyridyl)[3]radialene (**1.3**). The first is a 1-D coordination polymer composed of M_3L_2 cages bridged by linear silver(I) atoms, which has the formula $\{[Ag_2(\mathbf{1.3})](PF_6)_2 \cdot CH_3CN\}_n$ (**4.1**) (Figure 4.8).[52] In this structure the radialene **1.3** acts as a pentadentate ligand to four coordinated silver(I) atoms; one silver(I) atom is chelated by pyridyl rings on the same "arm" of the radialene. The outer silver(I) atoms of the M_3L_2 cages have a distorted trigonal planar geometry whereas the silver(I) atom in the centre of the cage has a linear geometry.

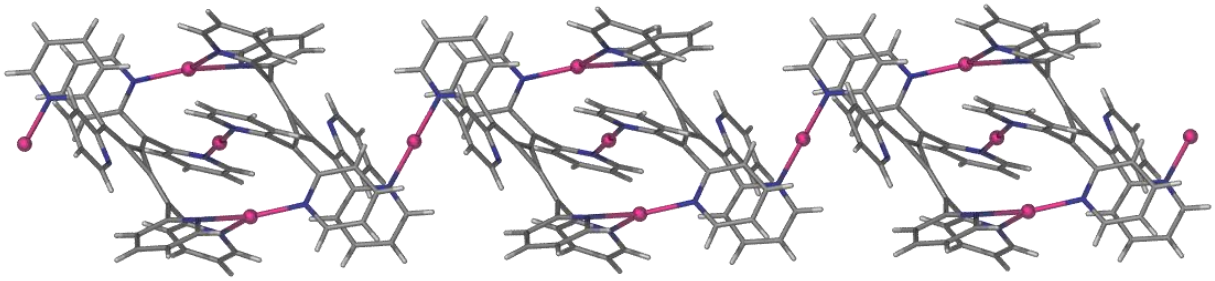

Figure 4.8. A perspective view of the cationic 1-D coordination polymer network of **4.1**.

The second structure is also a 1-D coordination polymer, with the formula $\{[Ag_2(\mathbf{1.3})](NO_3)_2 \cdot 4(H_2O)\}_n$ (**4.2**), where the radialene ligand, **1.3**, acts as a tetradentate bridge (Figure 4.9).[52] Chelation is not observed in this structure instead four pyridyl rings coordinate four separate silver(I) atoms, with one "arm" of the radialene not involved in

coordination. The silver(I) atoms maintain a distorted trigonal planar geometry as they are coordinated by two adjacent radialene ligands and one nitrate anion. There is a helical twisting arrangement of the ligands present along the coordination polymer.

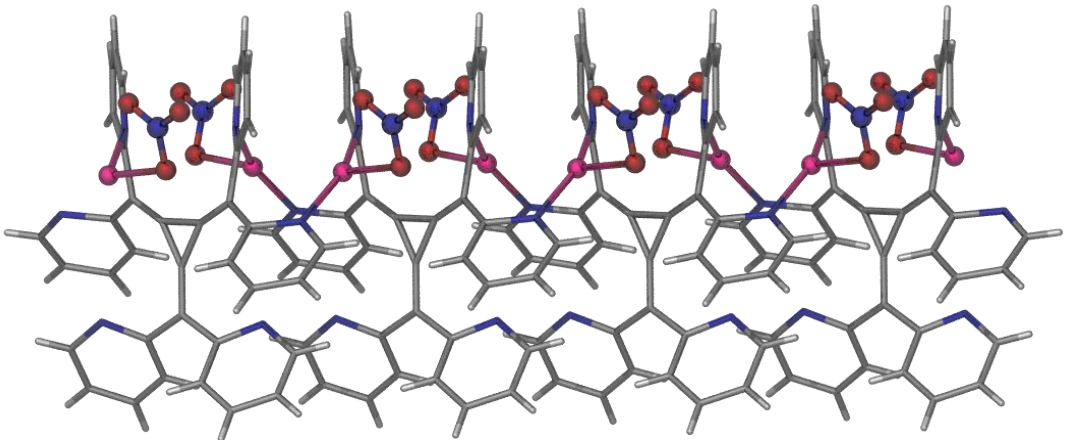

Figure 4.9. A perspective view of the 1-D coordination polymer **4.2.** Solvate molecules have been omitted for clarity.

Hexa(4-pyridyl)[3]radialene (**1.4**) has also been observed to act as a 4-connecting bridging ligand in a complex 3-D coordination polymer with $AgClO_4$, which has the formula $\{[Ag(\mathbf{1.4})]ClO_4 \cdot DMSO \cdot MeOH\}_n$ (**4.3**).[53] Within this structure the silver(I) atoms are coordinated by pyridyl rings from four separate radialenes and can be said to have a distorted tetrahedral geometry. The extended structure is rather complicated but can be reduced to a dimeric unit, $[Ag_2(\mathbf{1.4})_2]^{2+}$, where two radialene ligands are bridged by two silver(I) atoms. The dimers are then linked by a third pyridyl ring to form a 1-D chain along the *a* axis (Figure 4.10), which is connected via a fourth pyridyl ring to form the 3-D network.

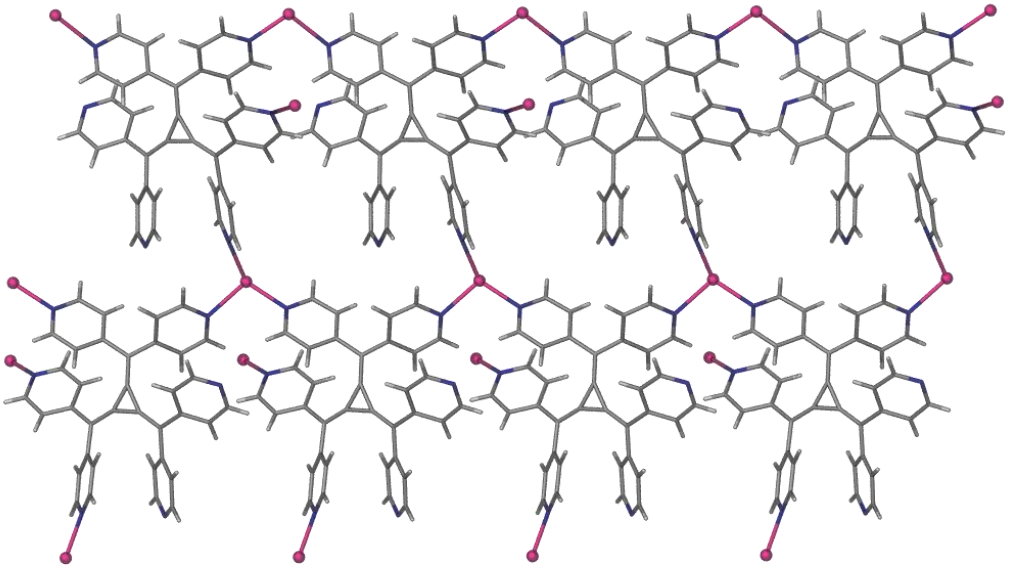

Figure 4.10. A perspective view of the cationic 1-D polymeric chain of **4.3** down the *c*-axis.

It is interesting to note that of these three hexapyridyl[3]radialene coordination polymers none exhibit complete coordination of silver(I) by all six nitrogen donor atoms. Hypodentate coordination, where multidentate ligands are coordinated through less than the maximum number of donor atoms, is relatively common although it is more usual to observe complete coordination due to the Chelate Effect in cases where a chelate ring can form.[54] Multitopic ligands with amine,[55] pyridine,[56] and pyrazole[57] donor groups have all been observed to form discrete hypodentate complexes, however hypodentate coordination polymers appear to be less common. Only one coordination complex of an hexaaryl- or hexapyridyl[3]radialene exhibiting full coordination has been reported. This structure is a discrete M_6L_2 cage of **1.3** and silver(I), which encapsulates a fluoride anion, with the formula $\{[Ag_6(\mathbf{1.3})_2F](BF_4)_5 \cdot 11(H_2O)\}$ (**4.4**) (Figure 4.11).[58] The lack of coordination polymers where [3]radialenes act as hexadentate ligands is possibly due to the acute torsion angles required to maintain such interactions.

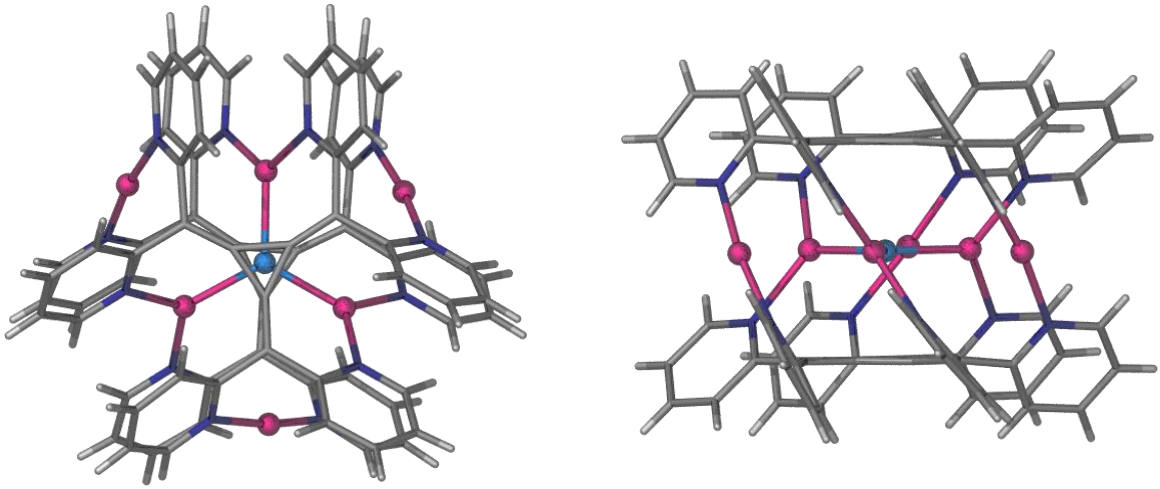

Figure 4.11. Two perspective views of the discrete cage structure of **4.4**.

The only coordination polymers of hexaaryl[3]radialenes that have been reported so far are those of two isomorphous 2-D (6,3) nets obtained upon reaction of hexakis(4-cyanophenyl)[3]radialene (**2.29**) with $AgClO_4$ (**4.5**) and $AgPF_6$ (**4.6**) (see scheme 4.1, section 4.2.1).[49] In both these materials **2.29** acts as a 3-connecting tetradentate ligand (structures **4.5** and **4.6** will be further discussed in section 4.2.1). It is also interesting to note that to date hexaaryl[3]radialenes have only been shown to form coordination complexes with silver(I). This may be due to the versatility of silver(I), it being a d^{10} species and a soft Lewis acid, and its multiple coordination geometries, which include linear, T-shaped, tetrahedral, and octahedral.[13,59-61]

4.2. Coordination Polymers of Hexakis(4-cyanophenyl)[3]radialene (2.29)

4.2.1. Silver(I) Coordination Polymers

The 2-D coordination polymers **4.5** and **4.6** mentioned earlier are the only examples of coordination polymers featuring cross-conjugated polynitrile ligands reported thus far. They were synthesised via slow evaporation of nitromethane solutions of the ligand and metal salt in 1:1 to 1:3 ratios.[49] Scheme 4.1 shows the asymmetric unit of these two structures and those of the new silver(I) coordination polymers reported herein.

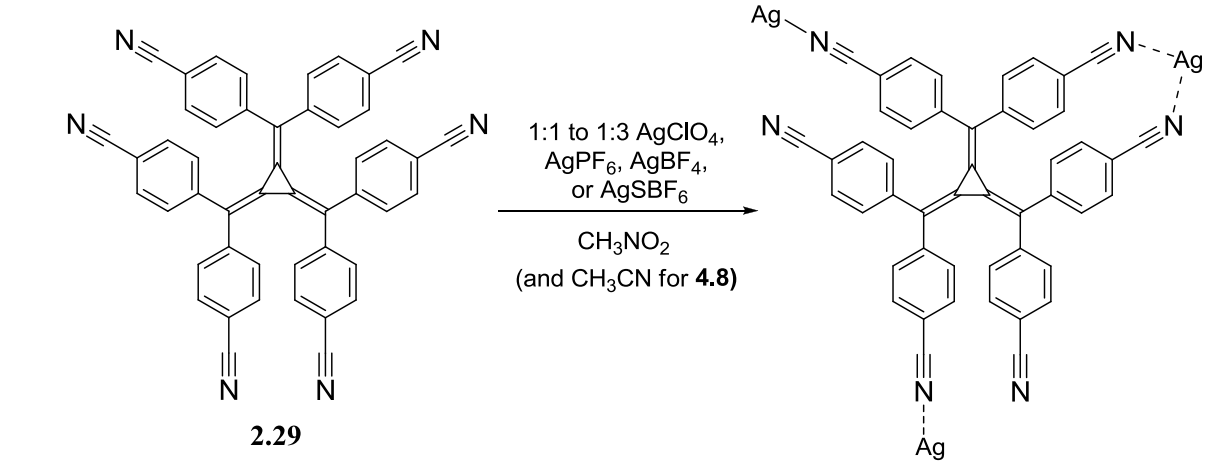

2.29

$\{[Ag(\mathbf{2.29})]ClO_4 \cdot 2(CH_3NO_2)\}_n$ **4.5**

$\{[Ag(\mathbf{2.29})]PF_6 \cdot 2(CH_3NO_2)\}_n$ **4.6**

$\{[Ag(\mathbf{2.29})]BF_4 \cdot 2(CH_3NO_2)\}_n$ **4.7**

$\{[Ag(\mathbf{2.29})]SbF_6 \cdot 2(CH_3NO_2)\}_n$ **4.8**

$\{[Ag_3(\mathbf{2.29})](ClO_4)_3 \cdot CH_3NO_2\}_n$ **4.9**

Scheme 4.1

Complexes **4.7** and **4.8** were prepared via slow evaporation of nitromethane solutions of **2.29** with $AgBF_4$ and $AgSbF_6$ respectively in ratios of 1:1 to 1:3 (**4.8** required 2 drops of acetonitrile to redissolve a small amount of initial precipitate). Bright red, diamond-shaped crystals of both $\{[Ag(\mathbf{2.29})]BF_4 \cdot 2(CH_3NO_2)\}_n$ **4.7** and $\{[Ag(\mathbf{2.29})]ClO_4 \cdot 2(CH_3NO_2)\}_n$ **4.8**,

obtained from crystallisations carried out in a 1:1 metal to ligand ratio, were found to be most suitable for X-ray crystallography.

Nitromethane has been found to be a good solvent for the growth of X-ray quality crystals of hexaaryl[3]radialenes. It has a fairly high boiling point of 101°C and thus a slow evaporation rate which leads to the growth of larger and higher quality crystals. Nitromethane is also a non-coordinating solvent and so does not compete with the radialene nitrile donor groups. Acetonitrile on the other hand does compete with the ligands and as mentioned above redissolves initial precipitate in nitromethane solutions of **2.29** and silver(I) presumably by displacing the radialene from the silver(I) coordination sphere. Hardie routinely uses another unusual crystallisation solvent, trifluoroethanol,[62-65] possibly due to its increased hydrogen bond donor ability promoting aggregation.[66,67] Nitromethane may play a similar role as a hydrogen bond acceptor, with twice the number of acceptor sites as acetonitrile.

The structures of complexes **4.7** and **4.8** are 2-D (6,3) sheets that are isomorphous to **4.5** and **4.6**, which further shows that the cationic coordination polymer units are not affected by the change in anion. Both coordination polymers crystallise in the triclinic space group *P*-1, with an asymmetric unit (Appendix 1, Figures A1.2 and A1.3) that contains one molecule of the ligand, one silver(I) atom, one anion and two nitromethane solvate molecules. The structures were refined with some disorder problems of the silver(I) atom (disordered over two positions, with *ca*. 55:45 occupancy in **4.7** and *ca.* 80:20 occupancy in **4.8**), the tetrafluoroborate anion in compound **4.7**, the hexafluoroantimonate anion in compound **4.8**, and one nitromethane solvate molecule in each structure.

In both structures, the silver(I) atom has a flattened tetrahedral coordination geometry, with bond angles in the range 87.4(2)-129.22(19)°. Houser and co-workers have developed a four coordinate geometry index, τ_4, whereby a value of unity indicates a tetrahedral four-coordinate geometry and a value of zero a square planar geometry.[68] The τ_4 values for the silver(I) atoms in **4.7** and **4.8** are 0.75 and 0.77, respectively. Hanton and Young have recently published a review of square planar silver(I) complexes where they included all four coordinate silver(I) structures in the CSD with *trans*-bond angles in the range of 175±5° and 165±15°.[13] The silver(I) atoms in **4.7** and **4.8** are distorted towards square planar as shown by their τ_4 values, however their *trans*-bond angles are outside of this range and so, as the τ_4 value indicates, they are closer to tetrahedral. The metal coordination environment in **4.7** and **4.8** involves chelation of the silver(I) atom by two nitrogen donor atoms of adjacent arms of one ligand and monodentate coordination by two nitrogen donor atoms from two neighbouring ligands to connect three different ligands in total (Figure 4.12). The coordination by the nitrile moieties involved in chelating the silver(I) atom is rather unusual,

with a 17-membered chelate ring being formed in which there are N-Ag-N bond angles of 92.43(16) and 89.4(2)°, and non-linear C≡N-Ag bond angles between 138.1 and 139.3°.

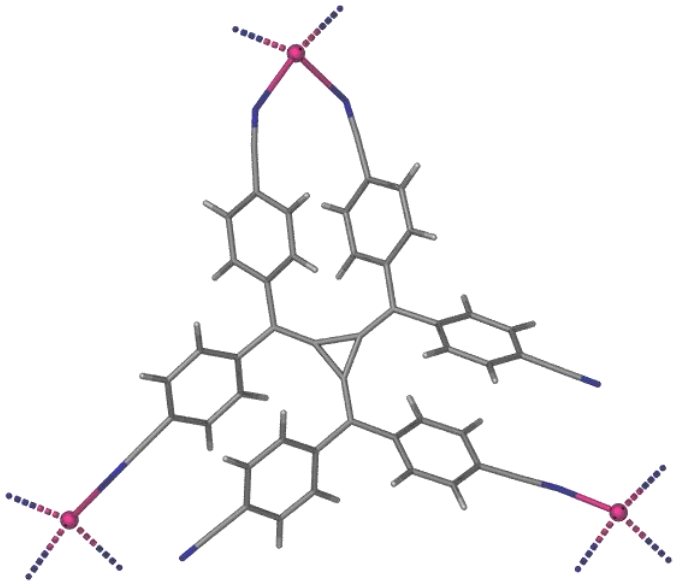

Figure 4.12. A perspective view of polymers **4.5-4.8** showing the coordination environment around a single hexakis(4-cyanophenyl)[3]radialene ligand.

This type of coordination to silver(I), and other transition metals, has been observed for nitrile groups in a number of structures where the nitrile is capping[69] or μ_2-bridging.[70] The Ag-N bond lengths in structures **4.7** and **4.8** range from 2.166(12) to 2.391(4) Å. Within both coordination polymers **2.29** is hypodentate; only four out of six of the ligand donor atoms are involved in the coordination of the silver(I) cation. As previously noted, in section 4.1.2, this is not an uncommon situation for [3]radialene ligands. The bond lengths of the radialene core are consistent with other [3]radialenes that have been reported.[49,52,53,58,71,72] The central cyclopropane ring has bond lengths in the range of 1.430(5) to 1.439(6) Å, whereas the exocyclic double bonds range from 1.349(5) to 1.362(5) Å. In these structures the torsion angles around the "arms" of the radialene average 37.0° with the ligands in a propeller conformation, which is common for hexaaryl[3]radialenes.[49,52,53,58,71,72]

In the extended structure, each radialene ligand coordinates to three silver(I) cations and it takes six units, three silver(I) cations and three ligands, to form the hexagonal ring motif of the (6,3) coordination polymer which is repeated throughout the structure (Figure 4.13).

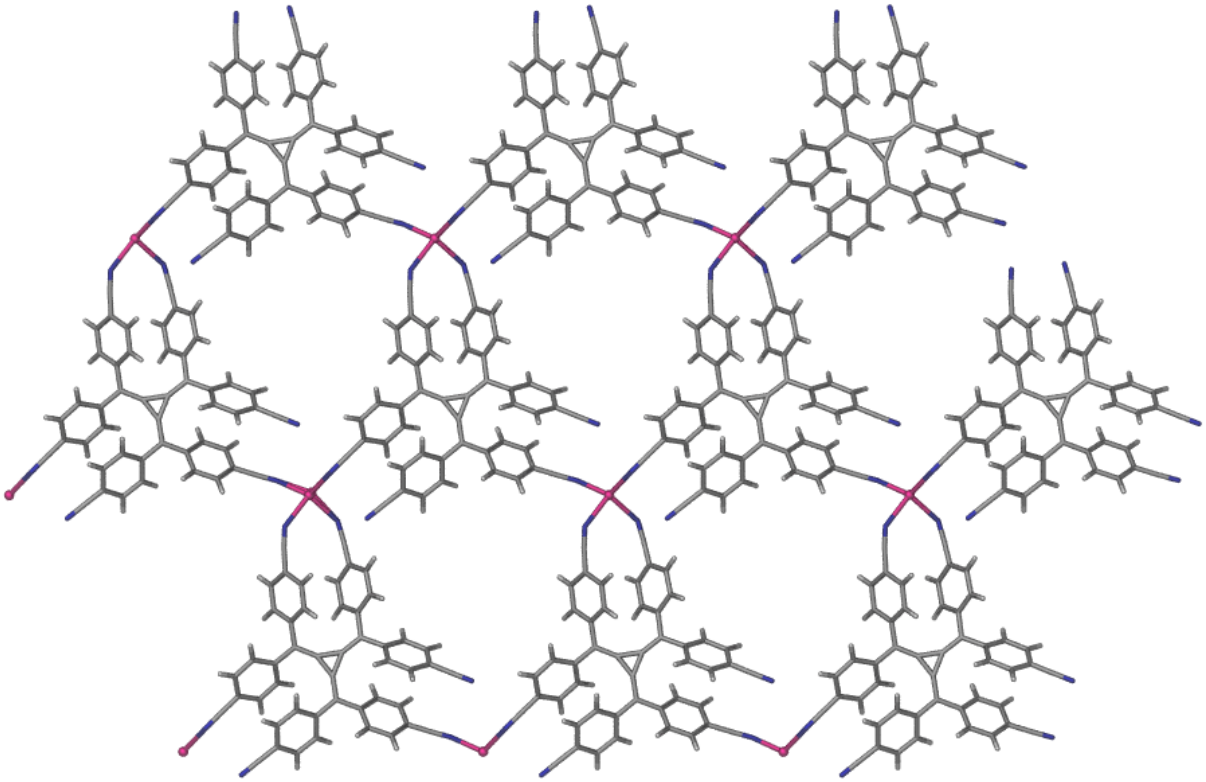

Figure 4.13. A perspective view of the cationic 2-D (6,3) polymer network from the crystal structures of compounds **4.5**-**4.8** viewed down the *a* axis of the unit cell. For clarity, the disorder of the silver(I) atom is not shown.

The 2-D (6,3) sheets are then packed in the extended crystalline lattice in discrete layers which adopt an AB repeating structure (Figure 4.14). The first layer A, shown coloured blue, is followed by layer B, shown in green, which has its [3]radialene units in the opposite orientation, related by a centre of inversion to those of A and is also offset so that its [3]radialene units do not reside directly below those of A. The anions reside between the layers both above and below the [3]radialene core of each ligand in the structure. It is worth noting, however, the anions are not equidistant between the equivalent layers; in structure **4.7**, for example, one anion ([3]radialene centroid-BF_4 centroid 4.29 Å) is located closer to the radialene core of a particular ligand than the other symmetry related anion (5.14 Å). The position of the anions within structures **4.7** and **4.8** are examined in detail in Chapter 5.

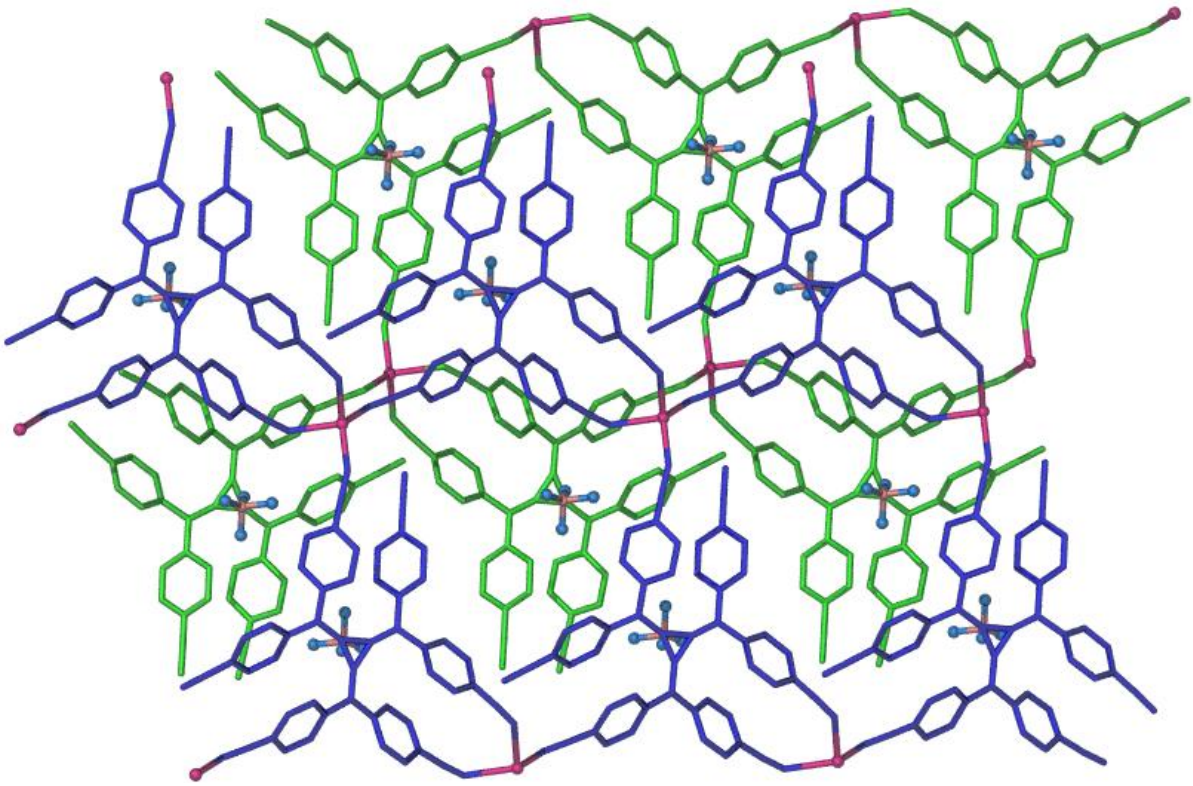

Figure 4.14. A perspective view of two layers of **4.7** showing the crystal packing and the location of the tetrafluoroborate anion sites in the crystal lattice. Layer A is coloured blue and layer B is shown in green. For clarity, solvate molecules and hydrogen atoms are not shown.

Polymers **4.7** and **4.8** bear some structural resemblance to structure **4.3**, described in section 4.1.2, which is a 3-D coordination polymer composed of hexa(4-pyridyl)[3]radialene (**1.4)** ligands and silver(I) metal nodes.[53] In structure **4.3** the radialene acts as a tetradentate ligand with four of its six pyridyl nitrogens coordinated to four different silver(I) atoms. In turn, each silver(I) atom is coordinated to four pyridyl nitrogen atoms from four different radialene ligands, rather than the three ligand molecules in the structures of **4.7** and **4.8** reported here. The difference between the two types of coordination polymer may be due to the added degrees of freedom which gives ligand **2.29** the ability to chelate to a silver(I) atom via the formation of a large chelate ring and the resulting flattened tetrahedral geometry of the silver(I) connectors.

A number of 2-D (6,3) networks were mentioned in section 4.1.1. Polymers **4.7** and **4.8** are similar in topology to the structures containing the aromatic polynitrile ligands 1,3,5-tricyanobenzene (Figure 4.4 (b))[47] and TEBB (Figure 4.6).[43] In these polymers both the polynitrile ligands and the trigonal planar silver(I) metal atoms act as 3-connecting nodes. The radialene ligands and silver(I) atoms in **4.7** and **4.8** also both act as 3-connecting nodes, however the silver(I) atoms are distorted tetrahedral as opposed to trigonal planar due to the

ability of the radialene ligand to chelate the silver with two nitrile donor groups from adjacent radialene arms. Another difference is that the tritopic nitrile ligands 1,3,5-tricyanobenzene and TEBB experience complete coordination whereas hexadentate **2.29** is hypodentate, with only four of its six nitrile donor groups involved in coordination. In this respect structures **4.7** and **4.8** are more similar to the 2-D (6,3) network of the hexacyano[3]radialene anion (Figure 4.7).[51] In that structure the hexatopic radialene ligand is also hypodentate with only three of its six nitrile donor groups involved in chelation. This structure differs in the fact that whilst the radialene ligand acts as a 3-connecting node the manganese(II) metal atoms act as 2-connecting linkers, despite their octahedral geometry, and are therefore topologically trivial.

Structure determination of coordination polymers of **2.29** and silver(I) salts from solutions with higher ligand to metal ratios than 1:3 has proven difficult. Reaction of **2.29** with $AgNO_2$, $AgPF_6$, $AgBF_4$, $AgSbF_6$, $AgNO_3$, AgSCN, and AgCl in ligand to metal ratios of 1:6 to 1:18, in the solvents nitromethane, acetonitrile, methanol and mixtures of these, generally led to no crystal growth or precipitation prior to complete evaporation of the solvent. In the case of slow evaporation with $AgNO_3$ and AgSCN in nitromethane orange, diamond shaped crystals were observed but were found to be the nitromethane solvate of the ligand, **2.29·4(CH_3NO_2)** (see Chapter 2, section 2.2.1). Reaction of **2.29** with $AgPF_6$ in a 1:18 ratio in nitromethane led to the precipitation of a red, amorphous solid. Elemental analysis of this material supported the formation of a 5:2 metal to ligand complex of the formula $\{[Ag_5(\mathbf{2.29})_2](PF_6)_5\}_n$ (calculated for C 43.78, H 1.84, N 6.38; found C 44.28, H 2.33, N 6.21). In a similar manner, numerous attempts at synthesising complexes of hexakis(3-cyanophenyl)[3]radialene (**2.38**) with various copper(I) and silver(I) salts were fruitless with no sign of crystallisation or precipitation; even crystals of the radialene itself were unable to be obtained.

Slow evaporation of a solution of **2.29** with ten equivalents of $AgClO_4$ in nitromethane, after the initial precipitate had been removed, yielded very small, red, rod-shaped crystals. These crystals were only suitable for X-ray crystallography using synchrotron radiation. Complex **4.9**, $\{[Ag_3(\mathbf{2.29})](ClO_4)_3\cdot CH_3NO_2\}_n$, is a 3-D coordination polymer of (10,3)-*b* topology and crystallises in the orthorhombic space group *Pnna* with an asymmetric unit that contains one molecule of the ligand and four silver(I) atoms (two fully occupied and two 50% occupied, Appendix 1, Figure A1.4). Unfortunately the anion and solvent molecules within the structure were disordered. Due to the disorder, the anions and solvent molecules could not be located in their entirety and the SQUEEZE routine of PLATON was applied to the data. The contents of the solvent region calculated from the result of the SQUEEZE routine (three perchlorate anions and one nitromethane solvate molecule per asymmetric unit) are represented in the unit cell contents of the crystal data.

The crystals were only obtained in trace quantities, approximately four or five individual crystals per vial, so enough material for elemental analysis was unable to be readily obtained. However, analysis of the initial precipitate, which constituted the bulk of the isolated material, gave a reasonably good fit (within 0.65%) to the formula derived from the crystal structure minus solvent (the sample was dried to constant weight under vacuum). The IR absorption value for the nitrile stretch of the crystals (2257 cm^{-1}) differed to that of the precipitate (2247 cm^{-1}), although there are a number of other well correlated peaks within the spectra including the Cl-O stretch (1059 cm^{-1} for the precipitate and 1052 cm^{-1} for the crystals).

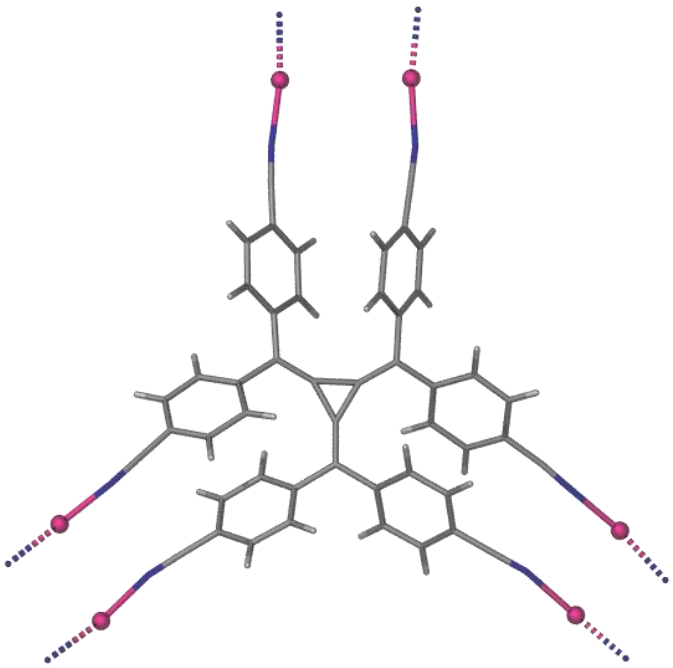

Figure 4.15. A perspective view of part of the structure of **4.9** showing the coordination environment around a single hexakis(4-cyanophenyl)[3]radialene ligand.

In complex **4.9** the silver(I) atoms have a near linear geometry and are coordinated to nitrogen donor atoms of two radialene ligands. The Ag-N bond lengths in structure **4.9** range from 2.067(7) to 2.159(7) Å. In contrast to previously reported coordination polymers of **2.29**, here all six of the nitrogen donor atoms are coordinated to a silver(I) atom (Figure 4.15). Even though **2.29** has the potential to be anything from monodentate to hexadentate, this is the first time that hexadentate coordination has been observed. The radialene core of **2.29** exhibits bond lengths which are consistent with those of other [3]radialenes reported in the literature.[49,52,53,58,71,72] The bond lengths of the central cyclopropane ring are in the range of 1.438(8) to 1.450(7) Å and the exocyclic double bonds range from 1.328(8) to 1.375(8) Å. In compound **4.9** the torsion angles around the "arms" of the radialene average 41.8° with the

ligands taking on a propeller conformation, which is common for hexaaryl- and hexapyridyl[3]radialenes.[49,52,53,58,71,72]

The topology of this network, (10,3)-*b*, was determined with assistance from Prof. Michaele Hardie of the University of Leeds, UK. The (10,3)-*b* net is characterised by crosslinked zig-zag chains[1] and the zig-zag motif of structure **4.9** can be observed in Figure 4.16. Within the extended structure **2.29** acts as a three connecting node while the 2-coordinate silver(I) centres are topologically trivial. The (10,3)-*b* net motif is then composed of a ring of ten 3-connecting radialene ligands and twenty linking silver(I) atoms (Figure 4.16).

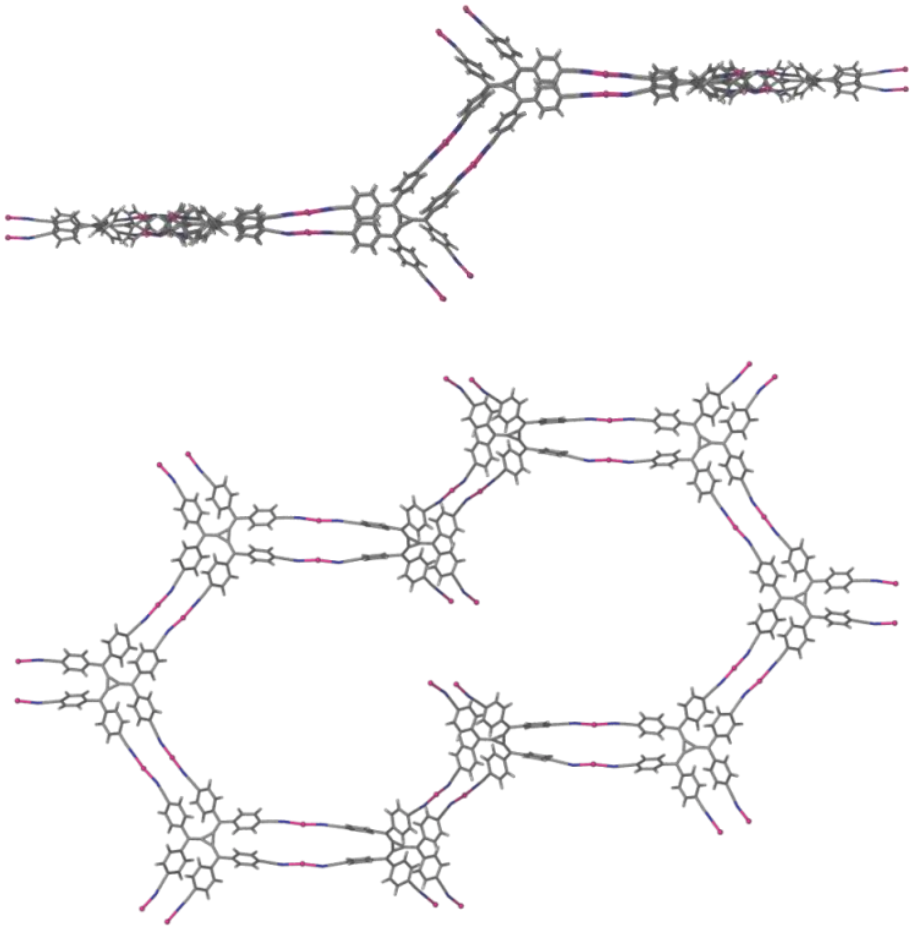

Figure 4.16. Two perspective views of the 10,3-b net motif of compound **4.9**

The (10,3)-*b* ring motif is then extended into a three dimensional network via the 3-connecting radialene nodes (Figure 4.17). The (10,3) net is the most frequently encountered 3-connected 3-D net and the (10,3)-*b* subtype is a common variation.[1] The silver(I) atoms coordinated to nitrile groups located on adjacent "arms" of the radialene are fairly close in space with a separation of 3.71 Å, however this is slightly outside the sum of the van der Waals radii for silver (3.44 Å)[73,74] and so cannot be considered a significant interaction.

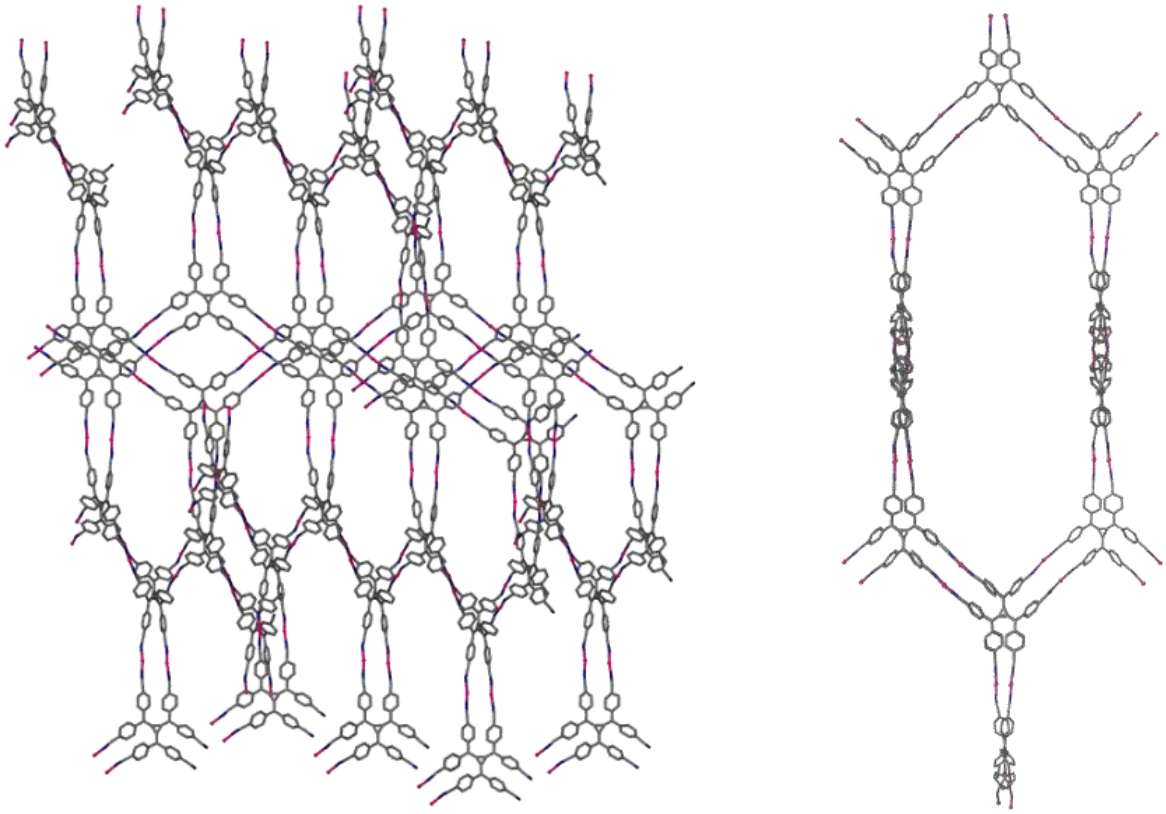

Figure 4.17. Two perspective views of the (10,3)-*b* net of **4.9** extended in three dimensions.

The 3-D structure is then 8-fold interpenetrated (Figure 4.18 (a)) in order to minimise the void space and stabilise the framework. This leads to the formation of a densely packed network with 1-D pores running down the *b*-axis (Figure 4.18 (b)). The pores along the *b*-axis are filled with disordered perchlorate anions and nitromethane solvate molecules, which were unable to be modelled, and measure approximately 12 by 7.7 Å in diameter. The SQUEEZE routine of PLATON indicated that there was 7132 $Å^3$ of solvent accessible voids within the network which represents 51% of the unit cell volume (13912(5) $Å^3$). This is a surprisingly large amount of void space for a structure which is so highly interpenetrated, but it is known that these types of calculations can over-estimate the solvent accessible volume. Weak silver-silver interactions are present between adjacent interpenetrated nets within structure **4.9** with a Ag-Ag distance of 3.34 Å, which is within the sum of the van der Waals radii for silver (3.44 Å).[73,74]

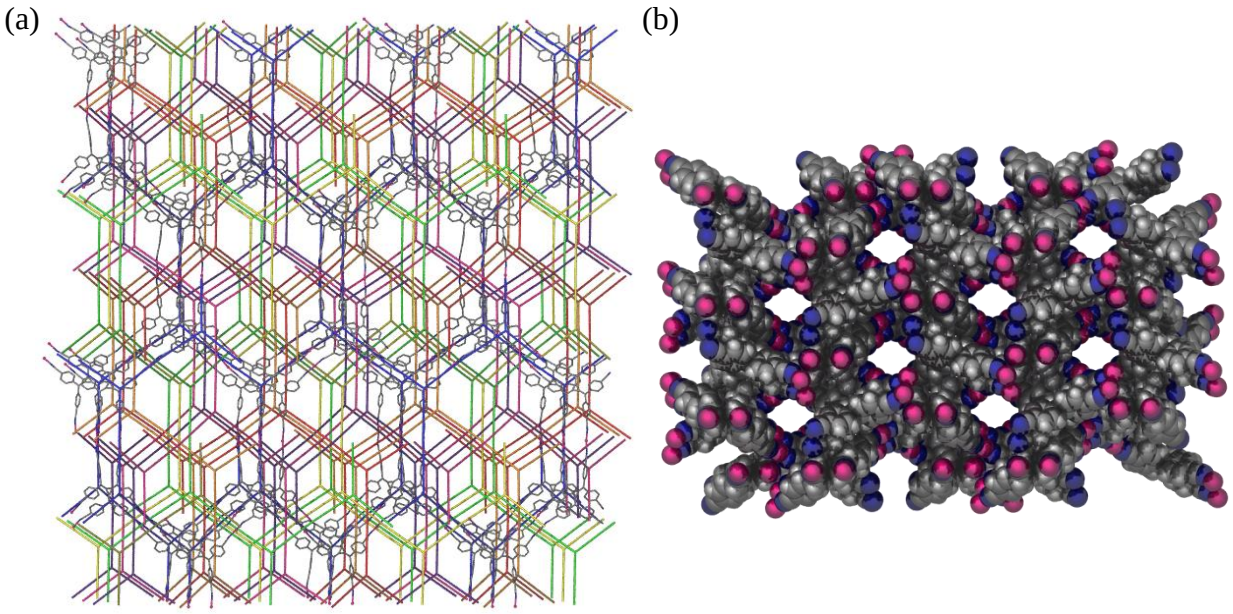

Figure 4.18. (a) A representation of the 8-fold interpenetrated structure of **4.9** with one network showing the molecular structure and the other 7 simplified for clarity (the [3]radialene centroid is treated as a node and the silver(I) centres are topologically trivial), and (b) the 1-D channels which run along the *b*-axis.

The majority of (10,3)-*b* nets reported in the literature are either 2-fold[75-78] or 3-fold[79-82] interpenetrated however there are recent examples of 4-fold[83] and 8-fold[84] interpenetration. A 4-fold interpenetrated (10,3)-*b* network reported by Sun was composed of a 5-(isonicotinamido) isophthalate ligand (Figure 4.19 (a)) and copper(II).[83] In this structure both the ligand and copper(II) metal atoms act as 3-connecting nodes to form the (10,3)-*b* net. Su and Fu reported a coordination polymer based on a ligand composed of two 2-(2-pyridyl)imidazole groups linked by a four carbon chain (Figure 4.19 (b)) which, upon hydrothermal reaction with zinc(II) acetate, formed an 8-fold interpenetrated (10,3)-*b* net.[84] Within this structure the zinc(II) atoms act as 3-connecting nodes whereas the ligands are topologically irrelevant. Interestingly, this is the opposite of what is observed in **4.9** where the ligand is 3-connecting and the silver(I) atoms act as linkers.

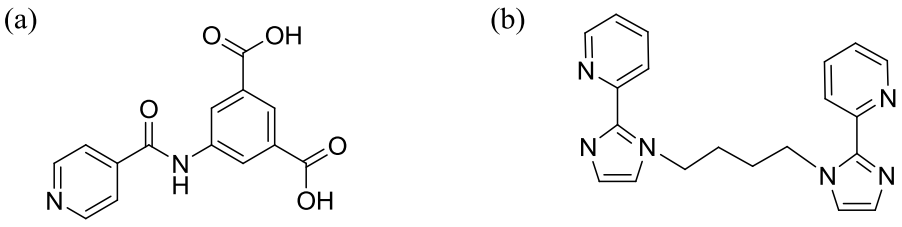

Figure 4.19. The structures of (a) 5-(isonicotinamido)isophthalic acid and (b) the linked 2-(2-pyridyl)imidazole ligand reported by Su and Fu.

4.2.2. Copper(I) Coordination Polymers

Silver(I) and copper(I) are both d^{10} species and soft Lewis acids, however they differ in size and preferred coordination number. Silver(I) is comfortable in multiple coordination geometries, which include linear, T-shaped, tetrahedral, and octahedral[13,59-61], whereas copper(I) maintains a predominantly tetrahedral geometry.[85] Silver(I) also has a significantly larger ionic radius of 129 pm compared to 91 pm for copper(I).[73,74] These fundamental differences may lead to a series of structures unlike those of silver(I) and **2.29**, discussed above.

Dissolution of **2.29** in nitromethane followed by addition of nitromethane solutions of $[Cu(CH_3CN)_4]BF_4$ and $[Cu(CH_3CN)_4]PF_6$ in stoichiometries ranging from 1:6 to 1:18 led to immediate precipitation of an orange solid. Addition of two drops of acetonitrile effectively redissolved the precipitate. Slow evaporation of both red solutions yielded two different crystal morphologies in each reaction; in both cases the first to form were large red octahedra followed by smaller orange block-shaped crystals. The variation in physical appearance of these crystals belied a dramatic difference in stability; the large red crystals being inherently solvent dependent and the smaller orange crystals being air stable. All of the complexes, $\{[Cu_2(\mathbf{2.29})_2](BF_4)_2 \cdot 20(CH_3NO_2)\}_n$ **4.10a**, $\{[Cu(\mathbf{2.29})]BF_4 \cdot 2(CH_3NO_2)\}_n$ **4.10b**, $\{[Cu_2(\mathbf{2.29})_2](PF_6)_2 \cdot 14(CH_3NO_2)\}_n$ **4.11a** and $\{[Cu(\mathbf{2.29})]PF_6 \cdot 2(CH_3NO_2)\}_n$ **4.11b**, were characterised by elemental analysis, IR spectroscopy and X-ray crystallography. Scheme 4.2 shows the coordination mode of **2.29** and the formula of these structures.

Elemental analysis of all four copper(I) complexes repeatedly produced low carbon values. As only a small number of the larger crystals, **4.10a**, were present in the mixture they were able to be separated manually from the smaller crystals, **4.10b**. These were then dried to constant weight under vacuum. The initial analysis of these samples gave carbon values which were out by 11.85% for **4.10b** and 9.20% for **4.10a**, although the hydrogen and nitrogen values were within 1%. Seeding nitromethane solutions of a 1:6 ratio of **2.29**:copper(I) salt with crystals of **4.10a** or **4.11a** led to formation of only these species which allowed for easier isolation. Unfortunately seeding of the same solutions with **4.10b** and **4.11b** still resulted in mixtures of both crystal forms in each sample. Upon separation of the initial mixtures it was noted that some blue copper(II) salts had begun precipitating. It was thought that perhaps this was the reason for the low carbon values. They were removed by floating the crystals of **4.10b** and **4.11b** on a mixture of dichloromethane and dibromomethane; the copper(II) salts remained at the bottom of the vial. These crystals and the samples of **4.10a** and **4.11a** grown by seeding were dried to constant weight under vacuum prior to analysis. Even with this careful isolation and drying of the crystals the carbon

values were still low (**4.10a** 3.85%, **4.10b** 9.56%, **4.11a** 9.45%, **4.11b** 3.86%). However, the hydrogen and nitrogen values were now within 0.4% (0.5% for **4.10a**).

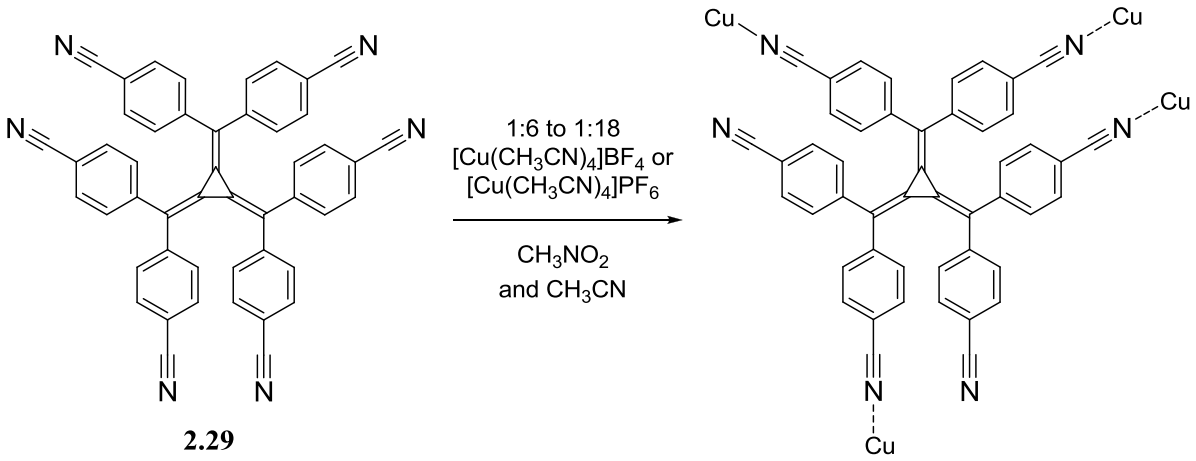

2.29

$\{[Cu_2(\mathbf{2.29})_2](BF_4)_2 \cdot 20(CH_3NO_2)\}_n$ **4.10a**

$\{[Cu_2(\mathbf{2.29})_2](PF_6)_2 \cdot 14(CH_3NO_2)\}_n$ **4.11a**

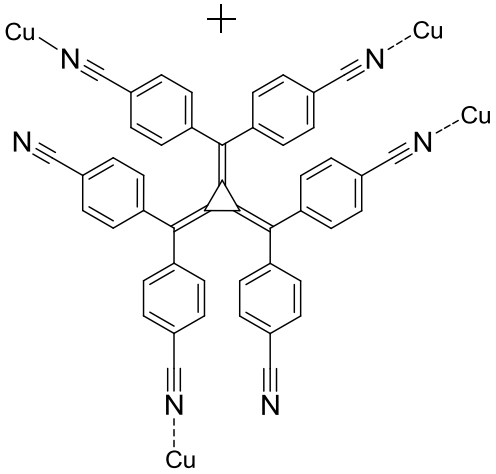

$\{[Cu(\mathbf{2.29})]BF_4 \cdot 2(CH_3NO_2)\}_n$ **4.10b**

$\{[Cu(\mathbf{2.29})]PF_6 \cdot 2(CH_3NO_2)\}_n$ **4.11b**

Scheme 4.2

It is known that samples which contain phosphorous may not combust successfully and give low carbon values although this does not explain why the BF_4 analogues also give low carbon analyses. Incomplete combustion of the ligand is another possibility; a number of examples in the literature have reported low carbon values in elemental analyses due to incomplete combustion of highly unsaturated arene structures.[86] However, this has not been an issue in previous elemental analyses of hexaaryl[3]radialene complexes.[49] The most likely reason is the formation of stable metal carbides which persist after combustion is complete.[87] The IR spectra of **4.10a** and **4.10b** correlate well except for one extra significant peak in

4.10b (1551 cm^{-1}). Complexes **4.11a** and **4.11b** also have very similar IR spectra and the spectra of all four complexes exhibit two C≡N stretches (approximately 2247 and 2224 cm^{-1}) for the coordinated and uncoordinated nitrile groups.

The structures of complexes **4.10b** and **4.11b** are 2-D coordination polymers. Both coordination polymers crystallise in the triclinic space group *P*-1, with an asymmetric unit that contains one molecule of the ligand, one copper(I) atom, one anion, and two nitromethane solvate molecules (Appendix 1, Figures A1.6 and A1.8). The structures were refined with some disorder problems of the tetrafluoroborate anion in compound **4.10b** and one of the nitromethane solvate molecules in both compounds. The crystal structures are isomorphous and the cationic coordination polymers in the two structures are isostructural.

In both structures the copper(I) atom has a distorted tetrahedral coordination geometry with bond angles in the range 92.89(14)-126.07(8)°. The τ_4 values for the copper(I) atoms in **4.10b** and **4.11b** are 0.84 and 0.83 respectively. This compares with the values in the silver(I) structures **4.7** and **4.8** which are 0.75 and 0.77. The coordination environment of the copper(I) involves monodentate binding by nitrogen donor atoms from three ligands within the same plane and one ligand in a different plane to connect four different ligands in total. The Cu-N bond lengths in structures **4.10b** and **4.11b** range from 1.912(3) to 2.168(2) Å.

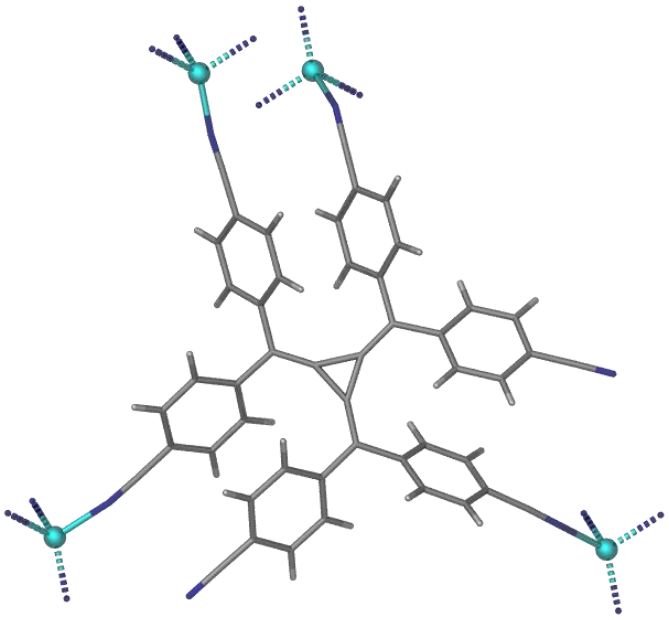

Figure 4.20. A perspective view of polymers **4.10b** and **4.11b** showing the coordination environment around a single [3]radialene ligand.

Within both coordination polymers **2.29** is hypodentate; only four out of six ligand donor atoms coordinate to the copper(I) cation (Figure 4.20). As previously mentioned, this has been

observed in quite a few coordination polymers of hexaaryl- and hexapyridyl[3]radialenes.[49,52,53] The radialene core exhibits bond lengths which are consistent with those of other radialenes reported in the literature.[49,52,53,58,71,72] The bond lengths of the central cyclopropane ring are in the range of 1.432(4) to 1.439(3) Å and the exocyclic double bonds range from 1.348(4) to 1.356(4) Å. In complexes **4.10b** and **4.11b** the torsion angles around the "arms" of the radialene average 41.6° with the ligands taking on a propeller conformation, which is common for hexaaryl[3]radialenes as previously mentioned.[49,52,53,58,71,72]

In the extended structure each radialene ligand coordinates to four copper(I) cations; with three of these cations it forms a 2-D (6,3) network, layer A, which is crosslinked by the fourth copper(I) cation to a second 2-D (6,3) sheet, B, directly below it (Figure 4.21) to create an A-B bilayer. All the 3-connecting nodes are bridged to create a 4-connected 2-D net. Layer B, shown in green has its [3]radialene units in the opposite orientation, related by a centre of inversion, to those of A, shown in blue, and is also offset so that its [3]radialene units do not reside directly below those of A. The bilayer, A-B, is then packed in the extended crystalline lattice in additional layers that adopt an A-B A-B repeating structure. The anions reside between the layers A and B but not directly above or below the [3]radialene core of **2.29**.

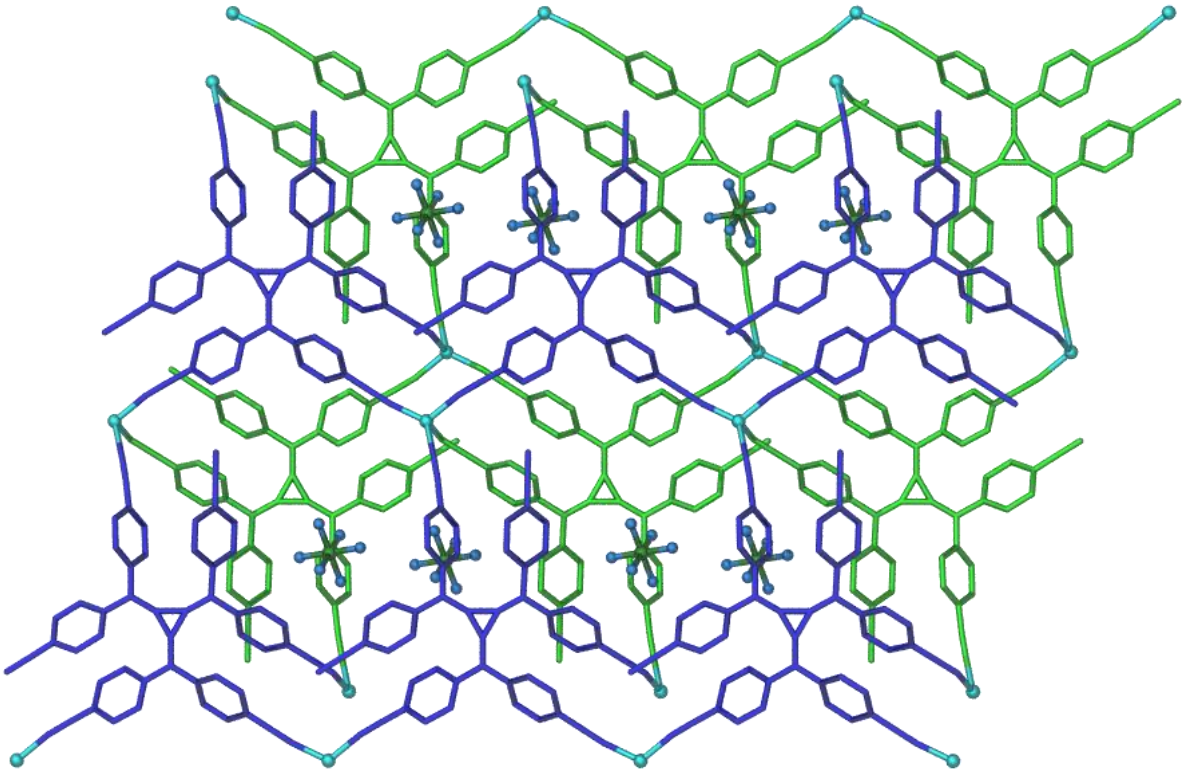

Figure 4.21. The 2-D layered packing of **4.11b** with layer A in blue and layer B in green. Hydogen atoms and solvent molecules were removed for clarity.

Another example of the bridging of (6,3) sheets to form a bilayer can be observed in the structure of $[Cu_4(\text{dicyanamide})_4(4,4'\text{-bipyridine})_3(CH_3CN)_2]_n$ reported by Batten and co-workers.[88] A point of difference is that this structure is only partially crosslinked and so forms a 3,4-connected net instead of a 4-connected net as seen here. Also the dicyanamide ligands used in this coordination polymer are anionic so no charge balancing anions are required, hence comparision of anion positions with the structures of **4.10b** and **4.11b** cannot be made. The position of the anions within coordination polymers **4.10b** and **4.11b** are examined in detail in Chapter 5.

Structures **4.10b** and **4.11b** are reminiscent of the four isomorphous 2-D (6,3) networks of **2.29** and silver(I), **4.5**-**4.8**. The defining feature of **4.5**-**4.8**, which is not observed in **4.10b/4.11b** and gives rise to the structural differences between them, is the chelation of a silver(I) atom by two nitrile groups on adjacent "arms" of the radialene ligand. Because of this chelating binding mode the radialene acts as a three connecting node as opposed to a four connecting node; thus the equivalent layers A and B in the silver(I) structure are not physically connected. Chelation is not observed in the copper(I) polymers **4.10b** and **4.11b**. This is most likely due to the smaller ionic radius of copper(I), 91 pm, compared to that of silver(I), 129 pm.[73,74]

The large red octahedral crystals, which crystallised first from nitromethane/acetonitrile solutions of **2.29** and $[Cu(CH_3CN)_4]BF_4$ or $[Cu(CH_3CN)_4]PF_6$, proved particularly difficult to investigate. Size was not an issue as they were much larger than the orange block shaped crystals, **4.10b/4.11b**, which crystallised second and so could be easily separated. Their inherent instability was readily observed upon removal from the mother liquor where the loss of solvent would cause the crystal to blacken and disintegrate in a matter of seconds. Suspension in paratone-N would lead to the same conclusion. Mounting of the crystals in a sealed glass capillary with a small amount of solvent to prevent evaporation was also attempted; however this could not be achieved quickly enough to inhibit partial decomposition. Diffraction data was obtained from the tetrafluoroborate analogue, $\{[Cu_2(\mathbf{2.29})_2](BF_4)_2 \cdot 20(CH_3NO_2)\}_n$ **4.10a**, via rapid selection of a suitable crystal and immediate mounting within a cryostream at 150 K. Data was also obtained from the hexafluorophosphate analogue, $\{[Cu_2(\mathbf{2.29})_2](PF_6)_2 \cdot 14(CH_3NO_2)\}_n$ **4.11a**, in a similar manner, however it is of considerably poorer quality.

Structures **4.10a** and **4.11a** are 3-D coordination polymers which crystallise in the orthorhombic space group *Pbca*, with an asymmetric unit that contains two molecules of the ligand, two copper(I) atoms, and in the case of **4.10a**, three tetrafluoroborate anions (two with 50% occupancy, Appendix 1, Figures A1.5 and A1.7). There was a large amount of disorder

in both structures due to large channels filled with solvent molecules which run along the *b*-axis. Due to this disorder the solvent molecules in **4.10a** could not be located in their entirety and the SQUEEZE routine of PLATON was applied to the data. The electron density removed equates to approximately 20 nitromethane molecules per asymmetric unit. This is supported by ^{1}H NMR spectroscopic analysis of crystals of **4.10a** in deuterated acetonitrile. The integration ratio of one radialene phenyl hydrogen peak, which represents 12 protons due to the symmetry of the radialene molecule, to the nitromethane methyl peak is 1:2.5. Therefore, the nitromethane methyl peak represents 30 protons and hence 10 nitromethane molecules per radialene molecule. As the asymmetric unit contains two molecules of the radialene ligand this equates to 20 nitromethane molecules per asymmetric unit.

In the case of **4.11a** both the anion and solvent molecules were unable to be located and the SQUEEZE routine of PLATON was used again. The electron count for the unit cell void was 9476 which relates to two hexafluorophosphate anions and approximately 32 nitromethane molecules per asymmetric unit. In contrast, the ^{1}HNMR spectrum of **4.11a** exhibits a radialene phenyl hydrogen to nitromethane methyl hydrogen integration ratio of 1:1.75 which equates to 21 methyl protons and thus 7 nitromethane molecules per radialene molecule and 14 per asymmetric unit. This value is a lot lower than that indicated by the electron density removed from the asymmetric unit via the SQUEEZE program. However, it would be expected that **4.11a** would have a similar and maybe even a lesser amount of solvent in its asymmetric unit than **4.10a** due to their isomorphous structures and the larger size of the PF_6 anion compared to the BF_4 anion. Thus it is likely that the number of molecules of nitromethane per asymmetric unit for complex **4.11a** indicated via ^{1}H NMR spectroscopy is more accurate than that given by the crystallographic data, and hence 14 nitromethane molecules are reported in the formula of **4.10a**.

In these structures the copper(I) atoms have a tetrahedral coordination geometry with bond angles in the range 96.55-124.50°. The τ_4 values for the copper(I) atoms in **4.10a** are 0.87 and 0.96 and those in **4.11a** are 0.85 and 0.96, demonstrating that one copper(I) atom has a more distorted tetrahedral geometry than the other. The coordination environment of the more distorted copper(I) involves monodentate binding by nitrogen donor atoms from four different ligands, two of which it shares in common with the less distorted copper(I) atom. This also displays monodentate binding to four different ligands. The Cu-N bond lengths in these structures range from 1.912(9) to 2.016(3) Å. As in coordination polymers **4.10b** and **4.11b**, **2.29** is hypodentate; only four out of six ligand donor atoms coordinate to the copper(I) cations (Figure 4.22).

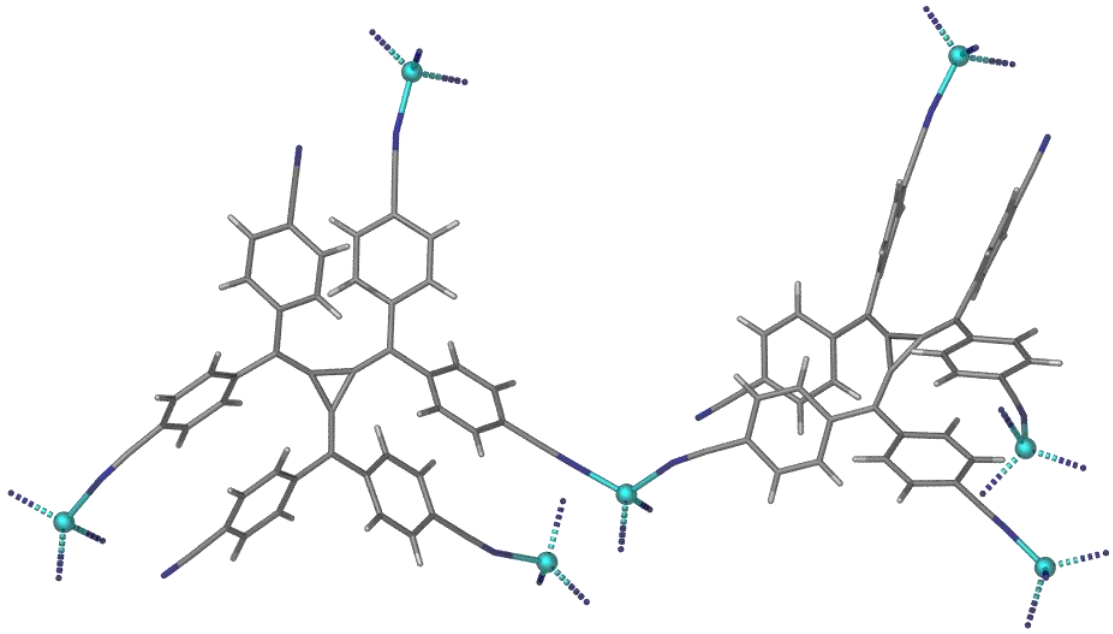

Figure 4.22. A perspective view of polymers **4.10a** and **4.11a** showing the coordination environment around the two crystallographically unique radialene ligands.

The radialene core of both molecules of **2.29** within the asymmetric unit exhibit bond lengths which are consistent with those of other [3]radialenes reported in the literature.[49,52,53,58,71,72] The bond lengths of the central cyclopropane rings in complex **4.10a** are in the range of 1.429(4) to 1.449(4) Å and the exocyclic double bonds range from 1.345(4) to 1.361(4) Å. In complex **4.10a** the torsion angles around the "arms" of the radialenes average 38.5° with the ligands taking on a propeller conformation, which is common for hexaaryl[3]radialenes.[49,52,53,58,71,72] Due to the poor quality of the data, which was omitted above 42° to provide reasonable completeness, the bond lengths of the cyclopropane ring and exocyclic double bonds for **4.11a** (1.383(9)-1.539(9) and 1.290(8)-1.399(8)) lie outside of the ranges noted above for **4.10a**. Three restraints were used to maintain chemically sensible bond lengths within the [3]radialene core, however they remained outside of the typical literature range. The average torsion angle around the "arms" of the radialenes for **4.11a** is 40.5° due to a distorted phenyl ring which exhibits a torsion angle of 64.3°, without this angle the average would be 38.1°. Restraints were also trialled to normalise the distorted phenyl ring, however this did not lead to an improved model and so were not used in the final refinement.

As previously mentioned this structure contains two crystallographically unique ligands (Figure 4.22) and two crystallographically unique copper(I) ions. Each copper(I) ion coordinates in a tetrahedral arrangement to four ligands and both ligands each coordinate to four copper ions(I). The extended structure is a complicated 3-D coordination polymer, the

topology of which was determined with assistance from Prof. Stuart Batten of Monash University, Australia. The metals and ligands, described above, are arranged such that distinct pairs of copper(I) ions, composed of two unique metal ions, are formed (Figure 4.23). These pairs are connected by two ligands, again one of each type.

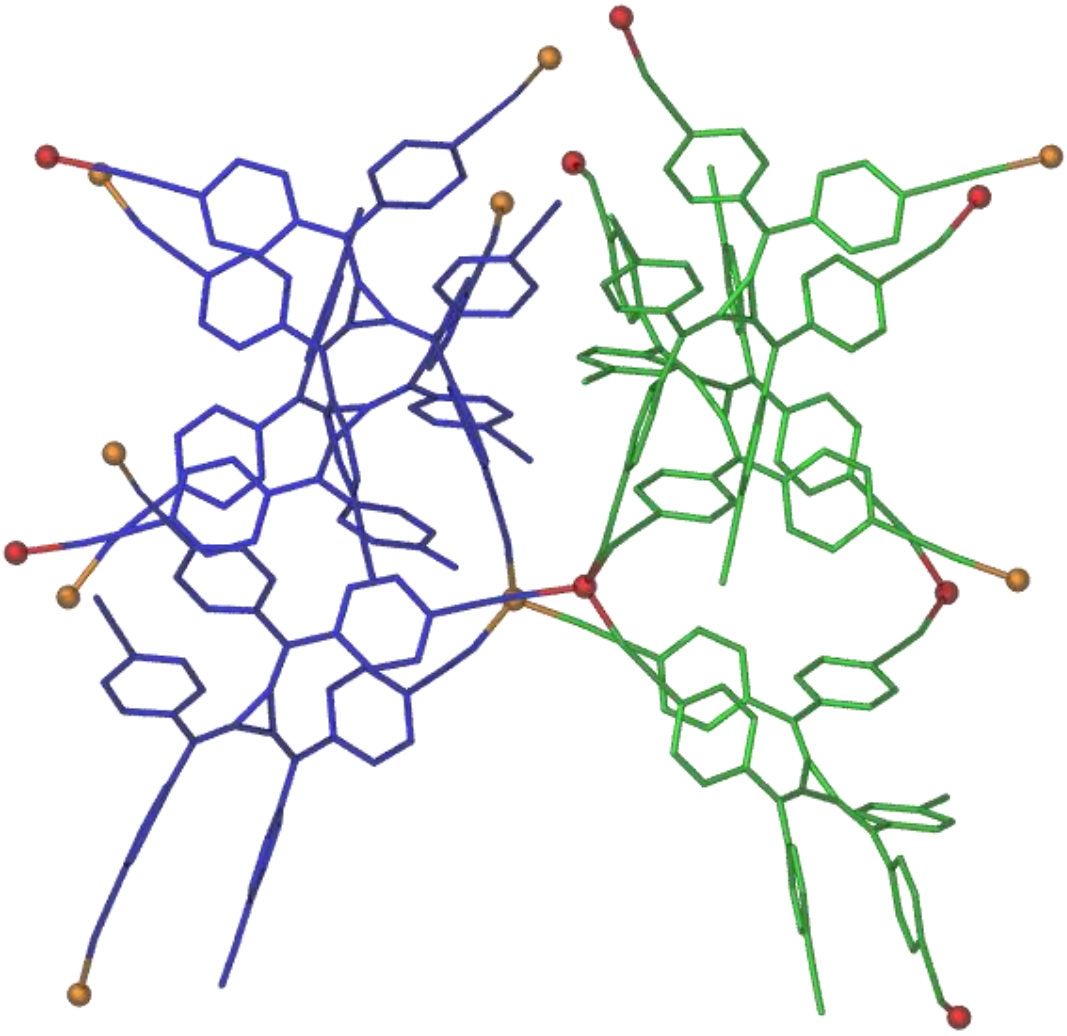

Figure 4.23. The local coordination environment of metals and ligands in **4.10a** and **4.11a**. For clarity, the crystallographically distinct metal ions and ligands have been coloured differently and the hydrogen atoms and anions omitted.

The metal ions in this pair also coordinate once to four other ligands (two of each type) to give the 3-D network. If this pair of metal ions is considered as a 6-connecting node, and each ligand considered as a 3-connecting node (each coordinates to three Cu_2 pairs), then the structure has a network with $(4.6^2)(4^2.6)(4^3.6^6.8^6)$ topology (the two 3-connecting nodes are inequivalent), as shown in Figure 4.24. This topology is closely related to (but distinct from) the **brk** net found on the Reticular Chemistry Structure Resource (RCSR) database.[89]

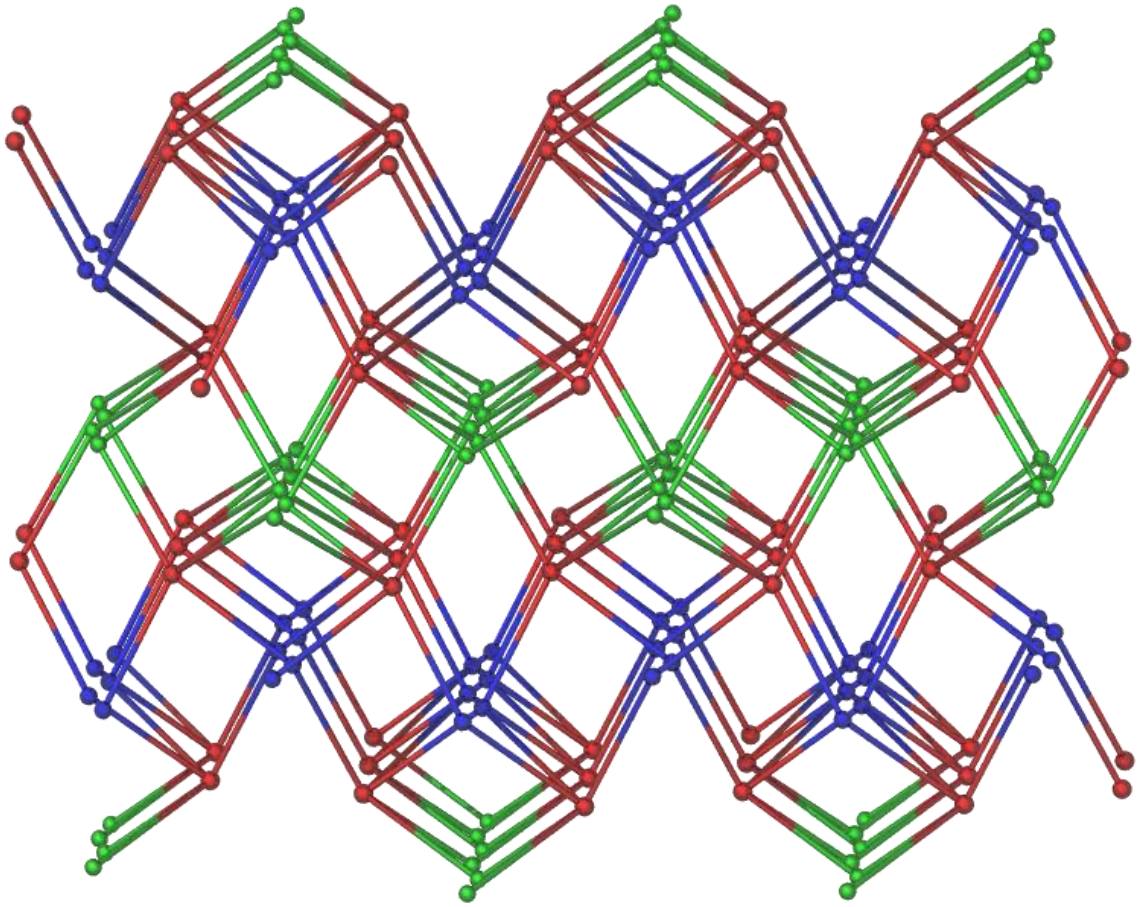

Figure 4.24. The overall network topology of **4.10a**. Red nodes represent the Cu_2 moieties, while the green and blue nodes represent the 3-connecting ligands (colours are consistent with Figure 4.23).

Similar to structure **4.9**, there are large pores (~11.4 by 8.4 Å) that run along the *b*-axis of structures **4.10a** and **4.11a** which are filled with disordered solvate molecules (Figure 4.25). The SQUEEZE routine of PLATON for **4.10a** indicated that there was 13091 $Å^3$ of solvent accessible voids within the network which represents 48% of the unit cell volume (27246(9) $Å^3$). The presence of a very large amount of solvate-filled void space explains the rapid decomposition of these crystals upon solvent removal.

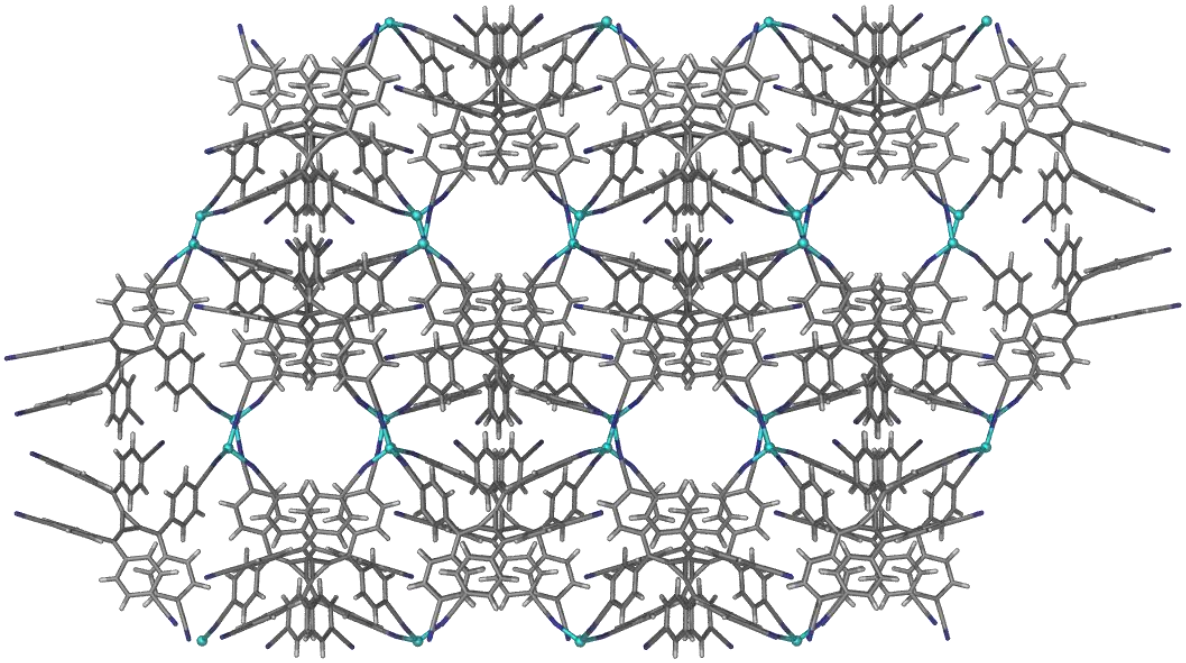

Figure 4.25. A stick representation of **4.10a** showing the channels parallel to the *b*-axis.

4.2.3. Copper(II) Coordination Polymers

All of the structures described thus far have included either silver(I) or copper(I) metal ions as these metals are soft acceptors suitable for the soft, neutral nitrile donors. Attempts at crystallisation of **2.29** with various copper(II), nickel(II), and iron(II) salts most often led to either crystallisation of the metal, in the case of $Cu(BF_4)_2{\cdot}H_2O$ and $Fe(BF_4){\cdot}6H_2O$, oiling out of the metal, as seen for $Cu(NO_3)_2{\cdot}3H_2O$ and $Ni(NO_3)_2{\cdot}6H_2O$, or crystallisation of **2.29** as a solvate, as observed for $Ni(ClO_4)_2{\cdot}6H_2O$. In fact only one example of a coordination polymer containing **2.29** and iron(II) was obtained as described in section 4.2.4.

This resistance to forming complexes in the majority of cases is most likely due to the nitrile groups of **2.29** being soft donors and the divalent, late first row transition metals (copper(II), nickel(II), and iron(II)) being borderline hard acceptors. Similarly, only one coordination polymer containing copper(II) was obtained; however it was synthesised using a copper(I) salt. Complex **4.12** was prepared via slow evaporation of a nitromethane solution of **2.29** with $[Cu(CH_3CN)_4]PF_6$ in a ratio of 1:3; after the removal of a small amount of initial precipitate (Scheme 4.3). The crystals obtained were bright red, hexagonal plates of the formula $\{[Cu(\mathbf{2.29})_2(H_2O)_2](PF_6)_2{\cdot}4(CH_3NO_2)\}_n$ (**4.12**) as determined by X-ray crystallography.

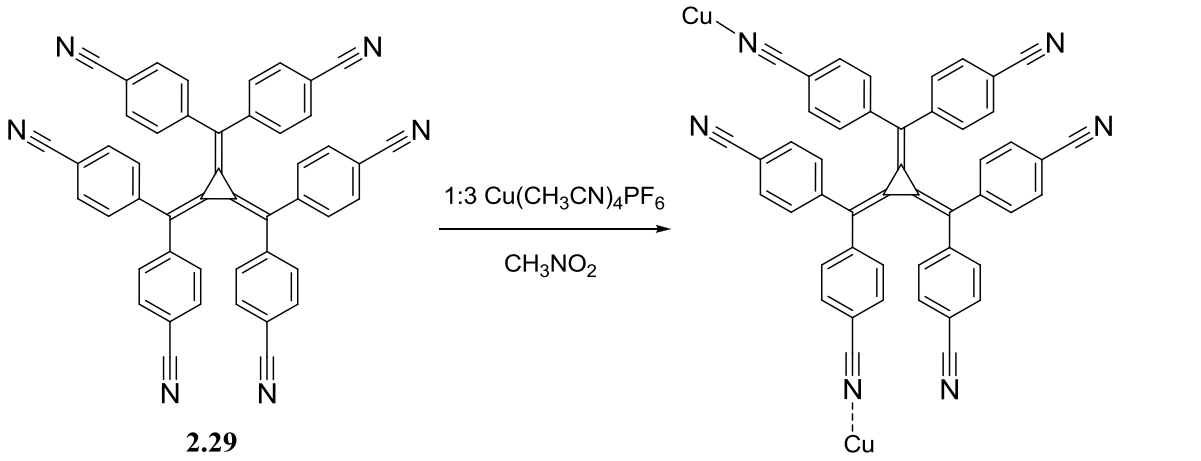

2.29

$\{[Cu(\mathbf{2.29})_2(H_2O)_2](PF_6)_2 \cdot 4(CH_3NO_2)\}_n$ **4.12**

Scheme 4.3

Complex **4.12** crystallises in the triclinic space group *P*-1, with an asymmetric unit (Appendix 1, Figure A1.9) that contains one molecule of the ligand, one copper(II) atom on a centre of inversion with a coordinated water molecule, one hexafluorophosphate anion and two nitromethane solvate molecules. The structure was refined with some disorder problems of one nitromethane molecule upon which four restraints were used to maintain chemically sensible bond lengths and angles. The hydrogen atoms of the water molecule coordinated to the copper(II) atom were found in the electron difference map. Presumably the oxidation of the copper(I) salt originally added to the crystallisation mixture has come at the expense of the reduction of some of the radialene **2.29** or through a disproportionation reaction of copper(I) as the crystals were only produced in trace quantities. In the former case this is plausible as, discussed in Chapter 2 section 2.2.4, hexaaryl[3]radialenes are electron deficient and undergo two stepwise reductions to form the radical anion and dianion respectively.

Attempts to repeat this reaction, in order to amass enough material for further characterisation, often led to precipitation. Bubbling oxygen through the solution was trialled to promote oxidation from copper(I) to copper(II), however this was also unsuccessful in producing crystals. Elemental analysis of the precipitate gave a result which fitted reasonably well to the formula of the crystal structure (calculated for $C_{96}H_{48}N_{12}P_2F_{12}Cu \cdot 3(CH_3NO_2) \cdot 8(H_2O)$ C 58.00, H 3.59, N 10.25, found C 57.77, H 2.94, N 9.75) and the IR spectrum exhibited peaks for the water O-H stretch (3424 cm^{-1}), nitrile C≡N stretch (2249 and 2224 cm^{-1}) and hexafluorophosphate P-F stretch (828 cm^{-1}).

Another example of a copper(II) coordination polymer formed via the reaction of a ligand with a copper(I) salt was recently reported by Lee.[90] The tribenzo-O_2S_2-macrocycle, depicted in Figure 4.26, and copper(I) chloride were dissolved in a mixture of dichloromethane and

acetonitrile. Slow evaporation of this solution led to the formation of crystals of a 1-D coordination polymer of the macrocyclic ligand and copper(II), Figure 4.25, in 20% yield. The copper(II) atoms have a five-coordinate geometry with a coordination sphere which includes two macrocycle donor sulfur atoms, two charge balancing chloride anions and one acetonitrile molecule. The authors do not speculate as to the cause of the copper(I) oxidation, however the low yield suggests that the macrocyclic ligand could act as the sacrificial oxidant. While copper(I) salts are often oxidised *in-situ*, it is relatively uncommon for this to result in the production of X-ray quality crystals.

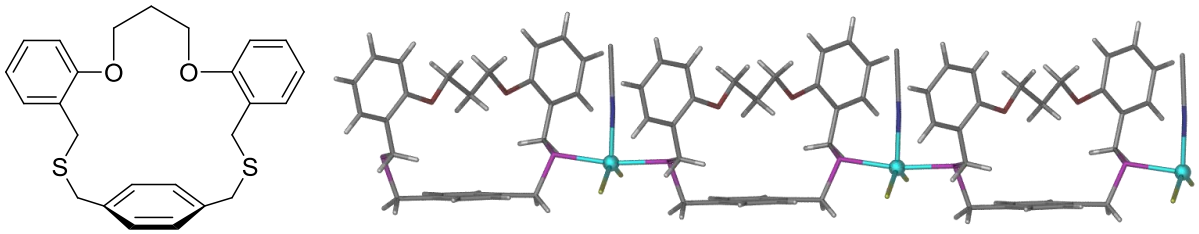

Figure 4.26. The structure of the tribenzo-O_2S_2-macrocycle and its 1-D copper(II) coordination polymer produced upon reaction with copper(I) chloride.[90]

The [3]radialene core of ligand **2.29** in complex **4.12** exhibits bond lengths which are consistent with those of other [3]radialenes reported in the literature.[49,52,53,58,71,72] The bond lengths of the central cyclopropane ring are in the range of 1.432(6) to 1.439(6) Å and the exocyclic double bonds range from 1.350(6) to 1.354(6) Å. The torsion angles around the "arms" of the radialene average 37.7° with the ligands taking on a propeller conformation, which is common for hexaaryl[3]radialenes as previously mentioned.[49,52,53,58,71,72]

Within complex **4.12** each copper(II) ion is coordinated by four separate molecules of **2.29** which in turn coordinate two different copper(II) atoms. In this structure **2.29** is bidentate, even though it has six donor nitrile groups, and connects adjacent copper(II) atoms with donor groups from different "arms" of the [3]radialene to form a 1-D linear chain (Figure 4.27). The 1-D chain is composed of loops made up of two radialene ligands and two copper(II) ions. The six-coordinate copper(II) cations experience tetragonal distortion due to the Jahn-Teller effect.[91] This is evident in the crystal structure as the two Cu-O bonds and two of the Cu-N bonds are quite short at 1.989(3) and 1.980(4) Å respectively, whereas the other two Cu-N bonds are significantly longer at 2.403(4) Å.

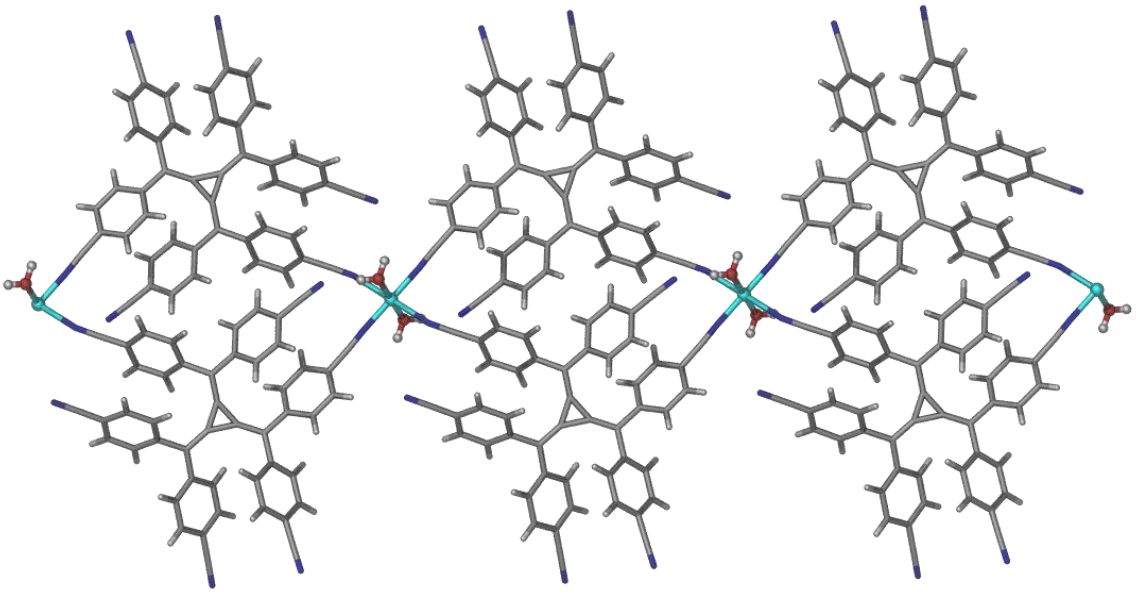

Figure 4.27. A perspective view of the cationic 1-D coordination polymer chain from the crystal structure of compound **4.12**.

The 1-D coordination polymer chains then pack in layers within the crystal lattice with the hexafluorophosphate anions sandwiched between them (Figure 4.28). Each of the chains is slightly offset from the one below it. The nitromethane solvate molecules are located in pockets between adjacent 1-D chain stacks (Figure 4.28). No π-stacking interactions are observed between radialene ligands in different chains due to the radialene propeller structure, which maintains face-to-face π-stacking interactions between phenyl rings on adjacent "arms" of a single radialene ligand. The centroid-to-centroid distances for these interactions range from 3.81-4.05 Å in structure **4.12**.

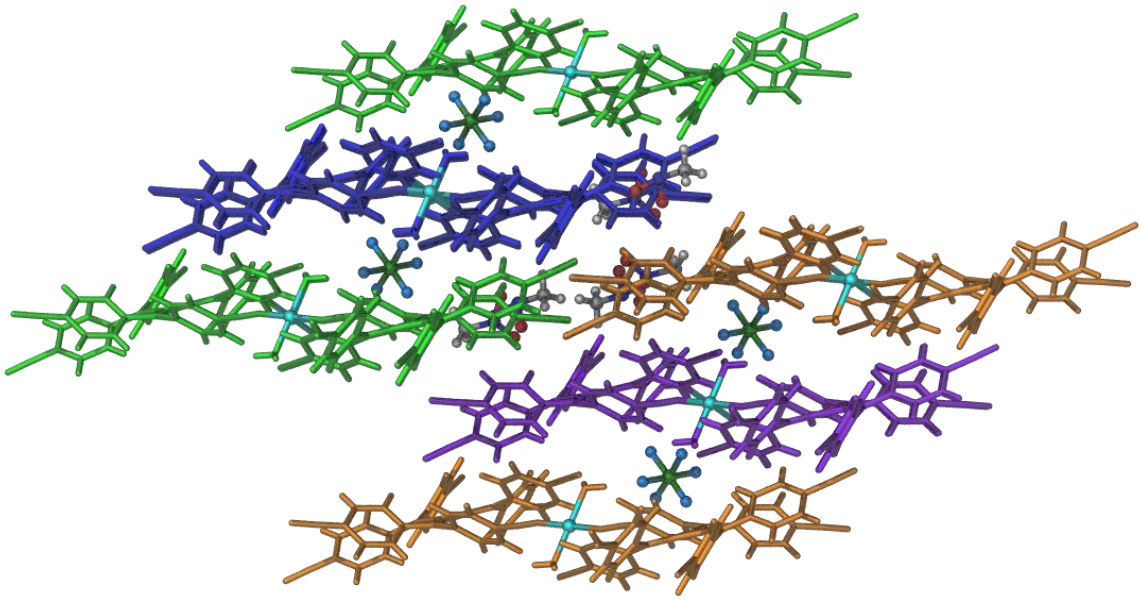

Figure 4.28. A perspective view, looking down the *b*-axis, of the layered packing of **4.12**.

4.2.4. Iron(II) Coordination Polymers

As mentioned in section 4.2.3 only one coordination polymer of **2.29** grown from a solution of the ligand and a metal(II) salt has been synthesised. Complex **4.13** was prepared via addition of $Fe(ClO_4)_2 \cdot 6H_2O$ in methanol to a nitromethane solution of **2.29** in a ligand to metal ratio of 1:10 followed by slow evaporation (Scheme 4.4). The crystals obtained were dark red rods of the formula $\{[Fe_2(\mathbf{2.29})_2(H_2O)_8](ClO_4)_4 \cdot CH_3NO_2 \cdot 2(H_2O)\}_n$ (**4.13**) as determined by X-ray crystallography.

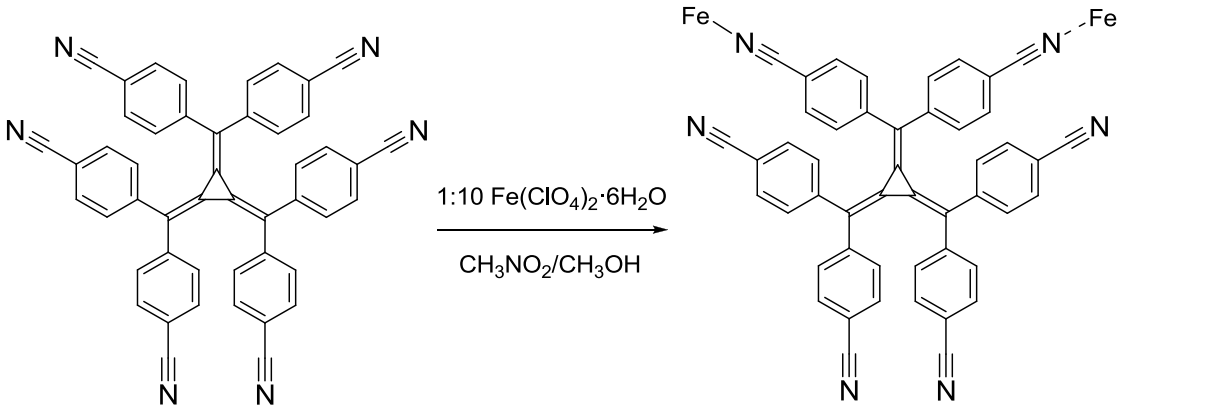

2.29 $\{[Fe_2(\mathbf{2.29})_2(H_2O)_8](ClO_4)_4 \cdot CH_3NO_2 \cdot 2(H_2O)\}_n$ **4.13**

Scheme 4.4

Complex **4.13** crystallises in the triclinic space group *P*-1 with two molecules of **2.29**, two iron(II) cations with eight coordinated water molecules and four perchlorate anions in the asymmetric unit (Appendix 1 Figure A1.10). There was disorder of one of the perchlorate anions and this was modelled over two positions with an occupancy of *ca.* 74:26. There was also disorder of the nitromethane solvate molecules which could not be located in their entirety and so the SQUEEZE routine of PLATON was applied to the data. The contents of the solvent region calculated from the result of the SQUEEZE routine (one nitromethane and two water solvate molecules per asymmetric unit) are represented in the unit cell contents in the crystal data. The hydrogen atoms of the coordinated water molecules were also unable to be located in the electron difference map but were included in the formula of the structure.

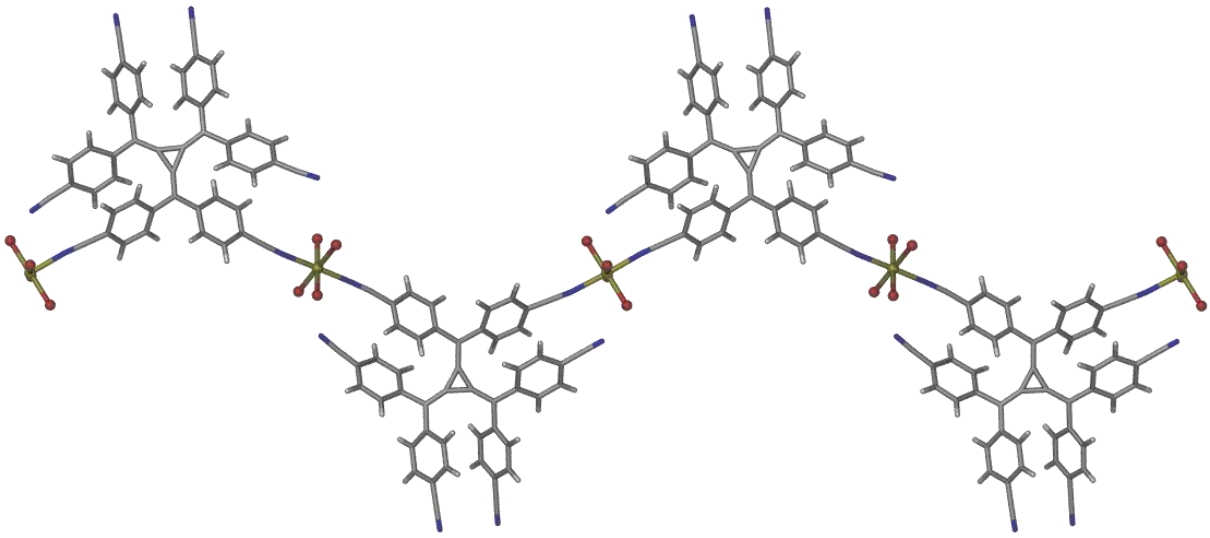

Figure 4.28. A perspective view of the cationic 1-D coordination polymer chain from the crystal structure of compound **4.13**.

Within complex **4.13** the iron(II) atoms have an octahedral geometry being coordinated by nitrile donor groups from two separate molecules of **2.29** as well as four water molecules. The Fe-O bond lengths range from 2.067(6) to 2.122(4) Å with the Fe-N bonds being slightly longer (between 2.147(6) and 2.185(6) Å). Again the radialene ligands are hypodentate in this structure, coordinating to only two iron(II) cations. Each molecule of **2.29** connects two different iron(II) metal nodes with donor groups from the same "arm" of the radialene to form a 1-D linear chain (Figure 4.29). Complex **4.13** is a simple zig-zag 1-D polymer chain in contrast to complex **4.12** which is composed of loops made up of two molecules of **2.29** and two copper(II) atoms (Figure 4.27). This is due to the fact that the iron(II) atoms in **4.13** are only coordinated by two different radialene ligands, whereas the copper(II) atoms in **4.12** are coordinated by four.

Within polymer **4.13** the bond lengths of the central cyclopropane rings of the two crystallographically unique molecules of **2.29** are in the range of 1.437(8) to 1.455(8) Å and the exocyclic double bonds range from 1.338(8) to 1.362(8) Å. The torsion angles around the "arms" of the first crystallographically unique radialene average 38.3° and those of the second radialene average 35.9°. For both radialenes the torsion angles around the two phenyl groups on the single radialene "arm" which is involved in coordination differ substantially. For the first radialene one phenyl ring has a torsion angle of 30.7° whereas the other is more twisted with a torsion angle of 41.0°. This is even more pronounced in the second radialene where one torsion angle is 40.4° and the other is 22.1°.

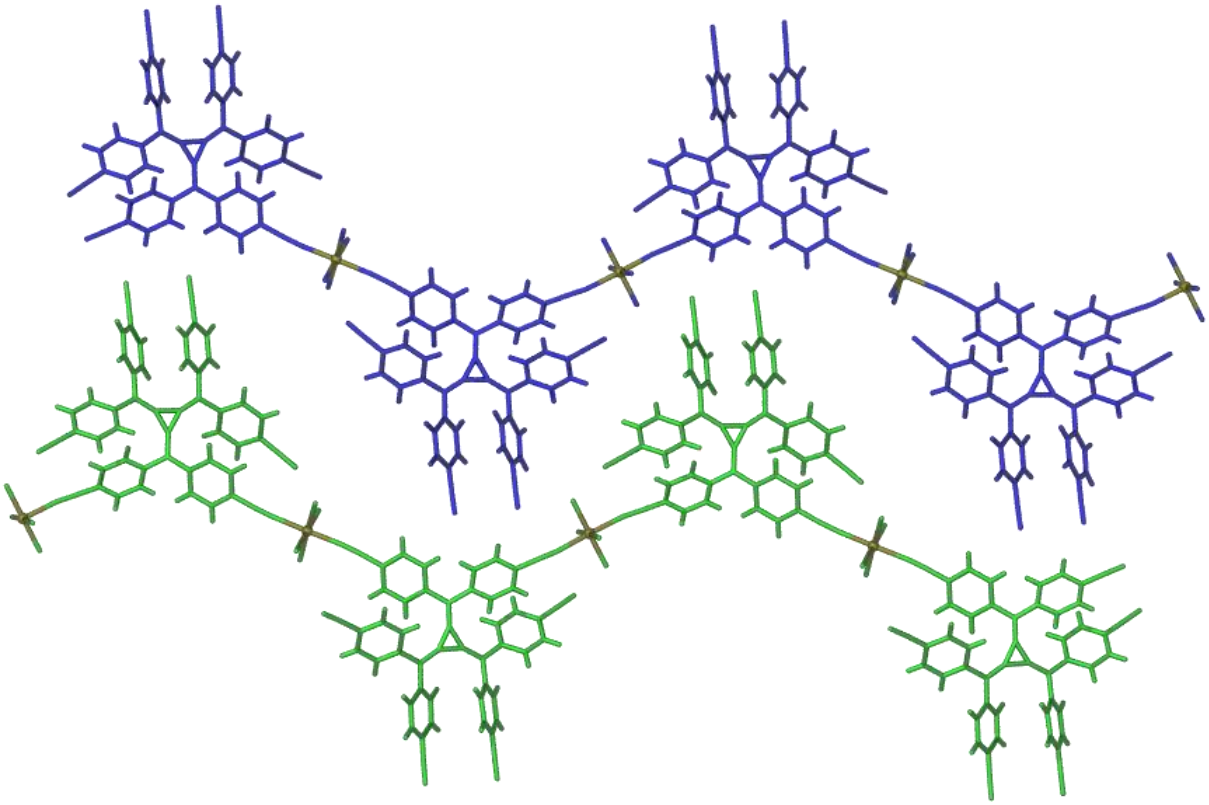

Figure 4.30. A perspective view of the packing of two 1-D polymer layers of **4.13**.

The 1-D zig-zag polymer chains pack in interdigitated layers as seen in Figure 4.30. There are no π-stacking interactions present between the polymer layers due to the propeller structure of the [3]radialene ligands. The interdigitated chains then pack in the extended crystal lattice in layers which are slightly offset to those above and below them (Figure 4.31). Two of the perchlorate anions are positioned in pockets near the iron(II) centre whereas the other two are localised above the core of the [3]radialene ligands. Anion interactions present in this structure are further discussed in Chapter 5.

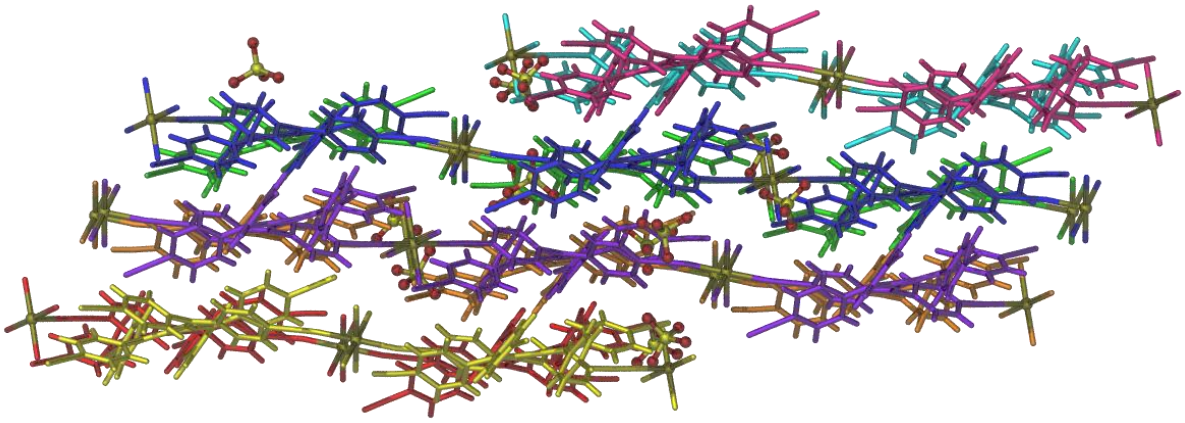

Figure 4.31. A perspective view, looking down the *c*-axis, of the extended packing of the interdigitated 1-D polymer layers of **4.13**. The disorder of the perchlorate anions is not shown.

4.3. Coordination Polymers of Hexakis(3,4-dicyanophenyl)[3]radialene (2.44)

4.3.1. Silver(I) Coordination Polymers

Attempted crystallisation of hexakis(3,4-dicyanophenyl)[3]radialene (**2.44**) with $[Cu(CH_3CN)_4]PF6$ and $[Cu(CH_3CN)_4]BF_4$ invariably led to the precipitation of the copper(I) salt and in one case crystallisation of an oxidised copper(II) salt as blue crystals. Reaction with silver(I) salts yielded slightly more success with dark red spheres being observed upon reaction of **2.44** with $AgClO_4$ in ratios of 1:1 to 1:12 in a mixture of nitromethane and acetonitrile. These were non-diffracting, however elemental analysis supported the formation of a 4:1 metal to ligand complex of the formula $\{[Ag_4(\mathbf{2.44})](ClO_4)_4 \cdot CH_3CN\}_n$ (calculated for C 39.45, H 1.24, N 10.68; found C 40.12, H 1.74, N 10.22). Finally, a 3-D coordination polymer containing $AgPF_6$ and **2.44** was obtained. Complex **4.14** was prepared via slow evaporation of a nitromethane solution of **2.44** with $AgPF_6$ in a ratio of 1:12 (Scheme 4.5). The crystals obtained were bright red, triangular rods of the formula $\{[Ag_2(\mathbf{2.44})](PF_6)_2 \cdot 7(CH_3NO_2)\}_n$ (**4.14**) as determined by X-ray crystallography.

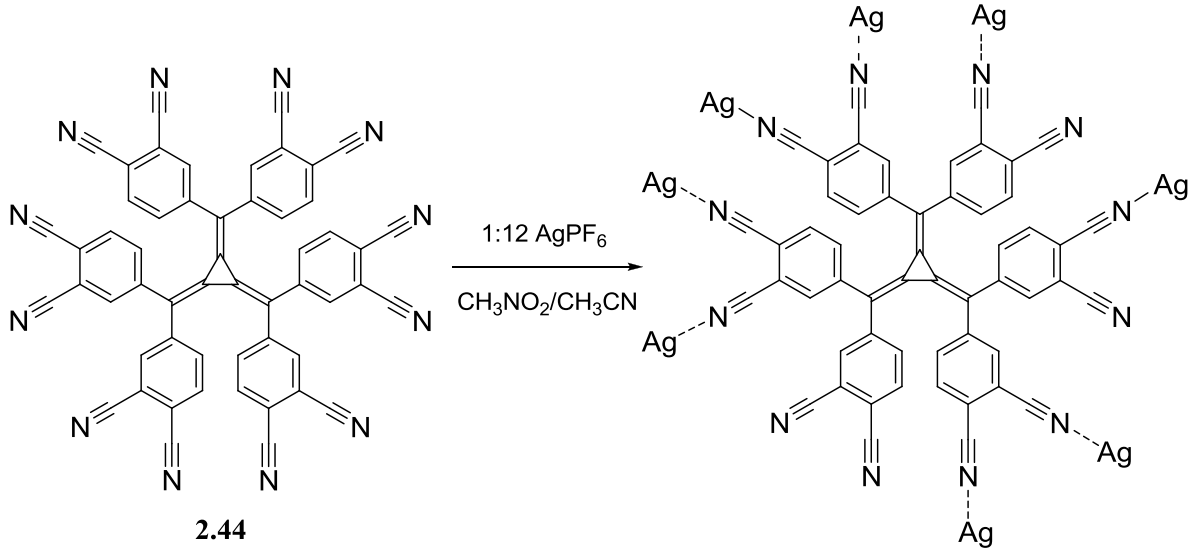

Scheme 4.5

Complex **4.14** crystallises in the monoclinic space group $P2_1/n$, with an asymmetric unit (Appendix 1, Figure A1.11) that contains one molecule of the ligand, two silver(I) atoms, three hexafluorophosphate anions (one fully occupied, one 50% occupied, and one fully occupied but on a special position) and four nitromethane solvate molecules. The structure also contained a number of diffuse electron density peaks that could not be adequately

identified and refined as solvent, thus the SQUEEZE routine of PLATON was applied to the data. The contents of the solvent region calculated from the result of the SQUEEZE routine (three nitromethane solvate molecules per asymmetric unit) are also represented in the unit cell contents in the crystal data.

In complex **4.14** the silver(I) atoms have a tetrahedral coordination geometry with bond angles in the range 88.6-140.3°. The τ_4 values for the silver(I) atoms in **4.14** are 0.71 and 0.84 demonstrating that one silver(I) atom has a more distorted tetrahedral geometry than the other. The Ag-N bond lengths in these structures range from 2.204(5) to 2.335(4) Å. As in the coordination polymers of **2.29**, the radialene ligand **2.44** is hypodentate; only eight out of twelve ligand donor atoms coordinate to the silver(I) cations (Figure 4.32). The [3]radialene core of **2.44** within the asymmetric unit exhibits bond lengths which are consistent with those of other radialenes reported in the literature.[49,52,53,58,71,72] The bond lengths of the central cyclopropane rings are in the range of 1.415(6) to 1.448(7) Å and the exocyclic double bonds range from 1.350(7) to 1.362(6) Å. In complex **4.14** the torsion angles around the "arms" of the radialene average 40.3° with the ligands taking on a propeller conformation, which is common for hexaaryl[3]radialenes.[49,52,53,58,71,72]

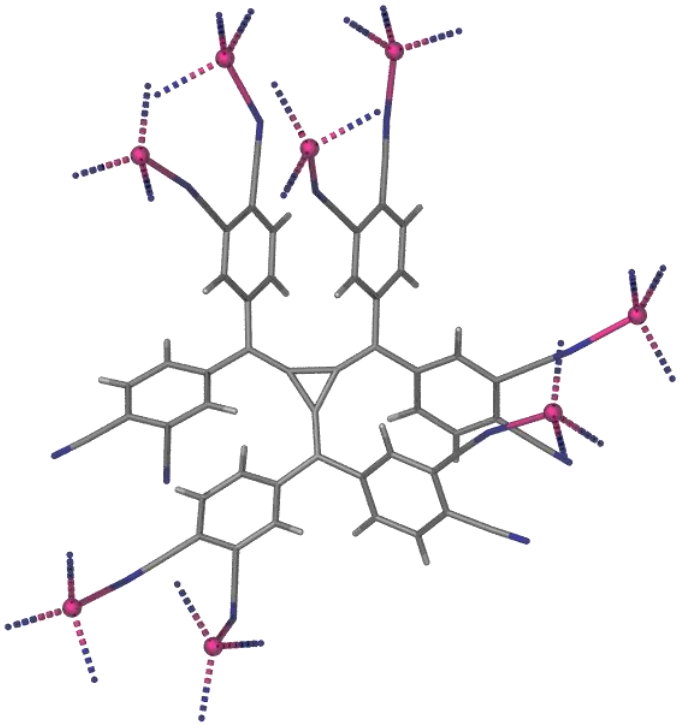

Figure 4.32. A perspective view of polymer **4.14** showing the coordination environment around a single molecule of **2.44**.

Structure **4.14** is a 3-D coordination polymer with a (3,6)-connected rutile network topology. Within this polymer the [3]radialene ligand, **2.44**, acts as a 3-connecting node and a

cluster of four silver(I) atoms acts as a 6-connecting node. Each of the four tetrahedral silver(I) atoms which make up the cluster are coordinated to four different radialene ligands for a total of six different radialene ligands when treating the cluster as a node (Figure 4.33).

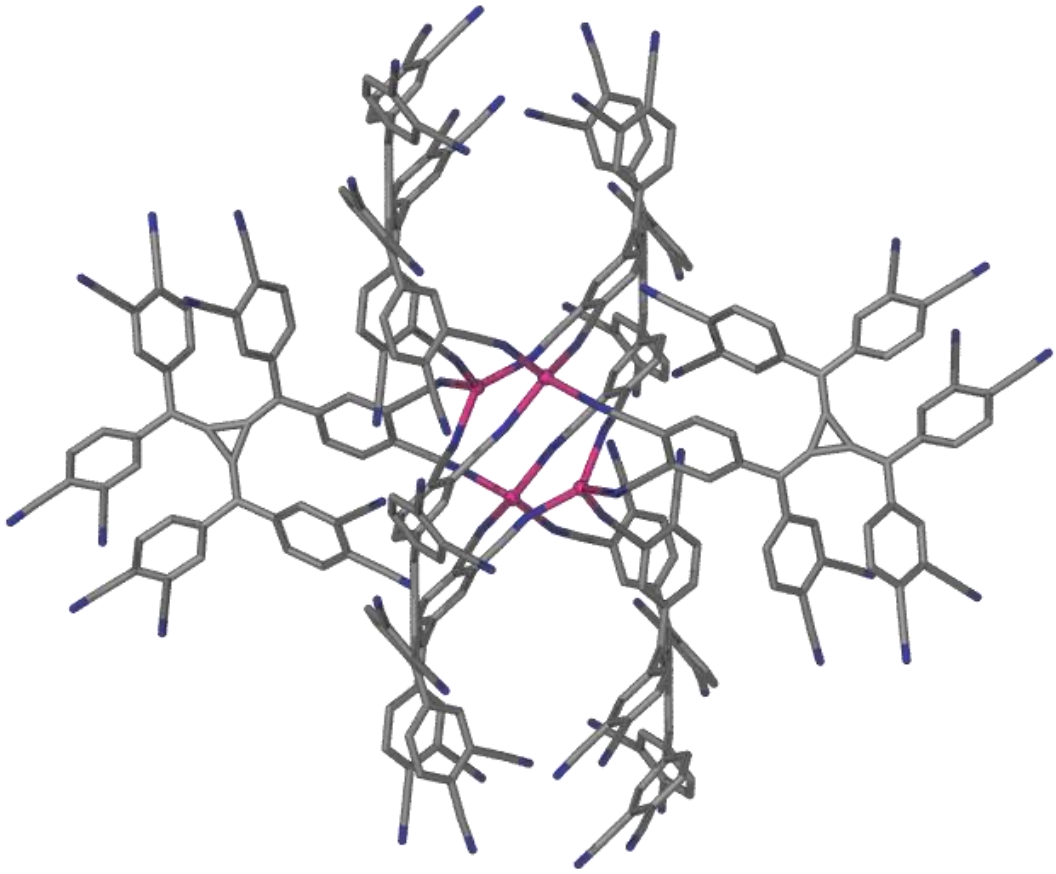

Figure 4.33. The cluster of four silver(I) atoms (pink) which acts as a 6-connecting node in the structure of **4.14**. For clarity, only the four silver(I) atoms that constitute a single node have been shown and the hydrogen atoms, anions and solvate molecules were omitted.

The radialene ligands are connected to three silver(I) clusters to form a 3-connecting node (Figure 4.34). As **2.44** acts as an octadentate ligand in this structure the coordination of the radialene to each of the three silver(I) clusters is slightly different. Figure 4.34 shows that each of the silver(I) atoms of the first cluster, coloured yellow, are coordinated by one nitrile donor group each from two phenyl rings on adjacent radialene "arms". Only two silver(I) atoms of the second cluster, coloured orange, are coordinated. These two metal ions are connected via the nitrile groups in the 3-position of two phenyl rings on adjacent radialene "arms". The third silver(I) cluster, coloured red, also only has two of its metal atoms coordinated by the 3-connecting radialene node highlighted in green in Figure 4.34. The two silver(I) atoms are connected by the two nitrile groups of one single phenyl ring, which leaves the nitrile groups of the final phenyl ring uncoordinated.

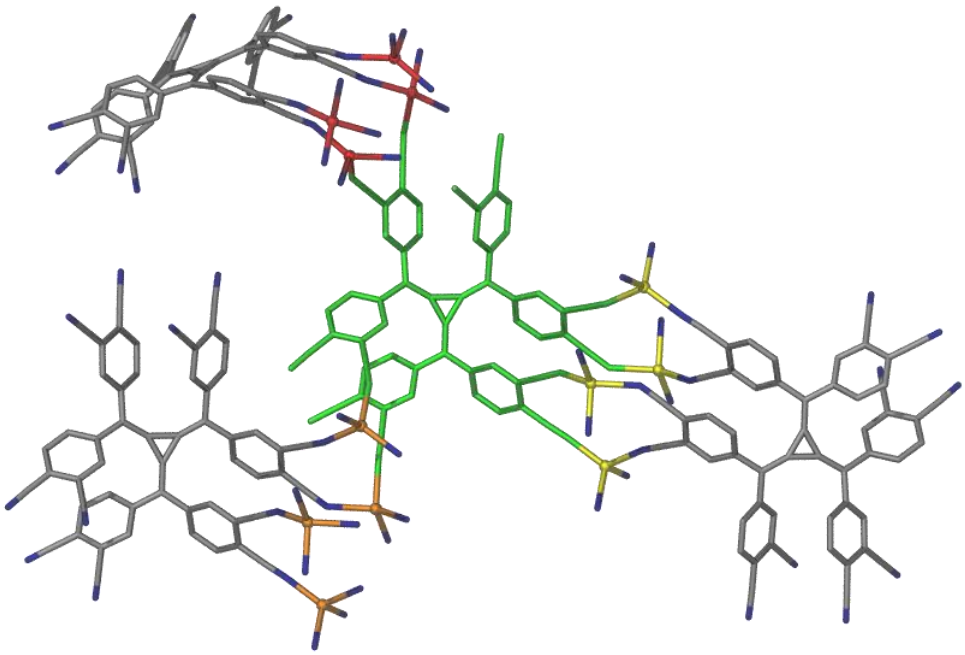

Figure 4.34. A perspective view of ligand, **2.44**, acting as a 3-connecting node (highlighted in green) in the structure of **4.14**. For clarity, the peripheral ligands have not been shown and the hydrogen atoms, anions and solvate molecules were omitted.

The combination of the 3-connecting radialene nodes and the 6-connecting Ag_4 nodes gives a 3-D network with a rutile topology (Figure 4.35 (a)), which has the Schläfli symbol $(4.6^2)_2(4^2.6^{10}.8^3)$.

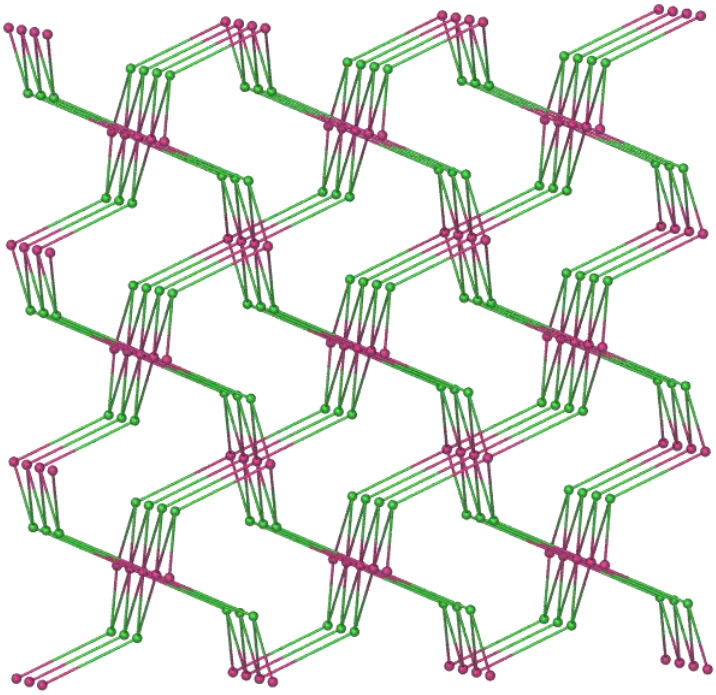

Figure 4.35. The overall network topology of **4.14**. Pink nodes represent the centroid of the Ag_4 clusters while the green nodes represent the centroid of the 3-connecting ligands.

The structure has large solvate and anion filled channels running down the *a*-axis of the unit cell (Figure 4.36 (a)). These channels are approximately 20 by 9.2 Å in diameter. There are also smaller pores running down the *b*-axis which are approximately 6.7 by 5.3 Å (Figure 4.36 (b)). Four nitromethane solvate molecules per asymmetric unit were able to be located in their entirety in the electron difference map, however there were still a number of electron density peaks which could not be refined as solvent. The SQUEEZE routine of PLATON was applied to the data and the electron density removed from the unit cell correlated to another three nitromethane solvate molecules per asymmetric unit; making seven in total.

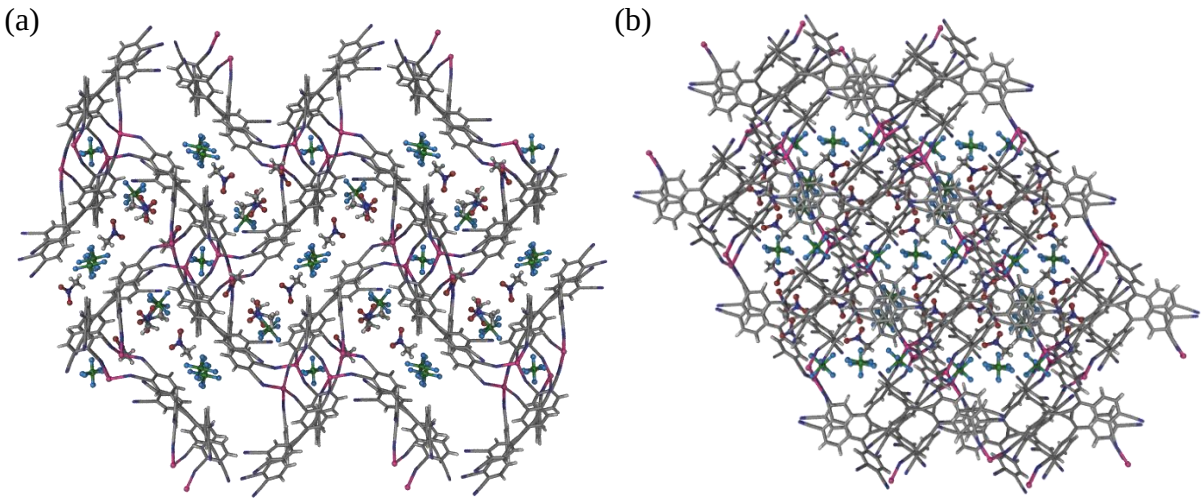

Figure 4.36. Ball and stick representations of **4.14** showing (a) the channels parallel to the *a*-axis and (b) the channels parallel to the *b*-axis.

The rutile net is typified by a polymorph of TiO_2 and is the most common topology of the (3,6)-connected networks.[1,92-97] Some characteristic examples of a rutile framework are the isomorphous structures reported by Murray and Robson which are composed of the tricyanomethanide anion (Figure 4.37 (a)) and one of a number of metal(II) centres including, but not limited to, chromium(II), copper(II), mercury(II) and zinc(II).[94] Within these relatively simple polymers the tricyanomethanide anion acts as a 3-connecting node whilst the octahedral metal(II) ions act as 6-connecting nodes. The rutile network which results is sufficiently spacious to allow the interpenetration of a second framework, unlike the single net of **4.14**.

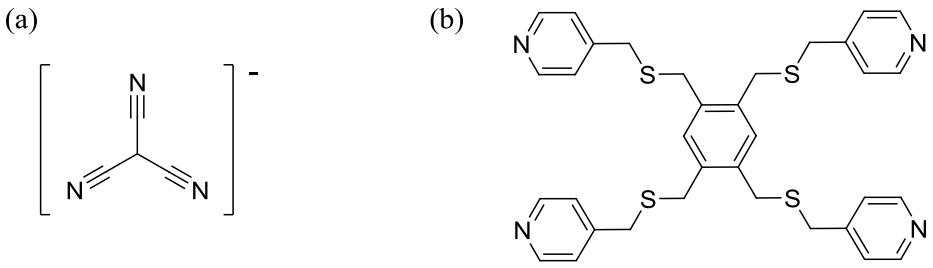

Figure 4.37. The structures of (a) the tricyanomethanide anion and (b) 1,2,4,5-tetrakis(4-pyridylmethylsulfanylmethyl)benzene.

Another (3,6)-connected rutile network of greater complexity is that reported by Hanton and Cordes.[97] Reaction of 1,2,4,5-tetrakis(4-pyridylmethylsulfanylmethyl)benzene (Figure 4.37 (b)) with $AgPF_6$ in a 1:2 ratio gave a 3-D rutile framework. Within this structure the ligand acts as a 6-connecting node via coordination to four separate silver(I) ions through its four pyridyl groups and chelation of another two silver(I) ions through its two pairs of sulfur donors. The tetrahedral silver(I) centres act as 3-connecting nodes as they are each chelated by two sulfur atoms from one ligand and then coordinated to a further two ligands through their pyridyl donors. This is in contrast to polymer **4.14** in which the ligand acts as the 3-connecting node and a cluster of four silver(I) atoms acts as the 6-connecting node.

4.4. Summary

A total of nine new coordination polymers have been synthesised from the hexatopic ligand hexakis(4-cyanophenyl)[3]radialene, **2.29,** with silver(I), copper(I)/(II) and iron(II). Within these structures five different coordination modes have been observed for **2.29** (Figure 4.38). Two different bidentate coordination modes have been observed for the polymers of **2.29** with metal(II) nodes. The first with iron(II), **4.13**, exhibits binding via two nitrile donor groups from the same arm of the radialene, which could be represented as *1,1'* (Figure 4.38 (a)) if we label the six nitrile groups of **2.29** *1, 1', 2, 2', 3* and *3'*. The second bidentate coordination mode, seen in structure **4.12**, involves binding to copper(II) via two nitrile donor groups from adjacent radialene arms, *1,2* (Figure 4.38 (b)). Both of these bidentate coordination modes led to the formation of 1-D polymer chains. In the case of **4.13** the 1-D polymer is a simple 1-D zig-zag chain, whereas the structure of **4.12** is composed of loops of two molecules of **2.29** and two copper(II) ions.

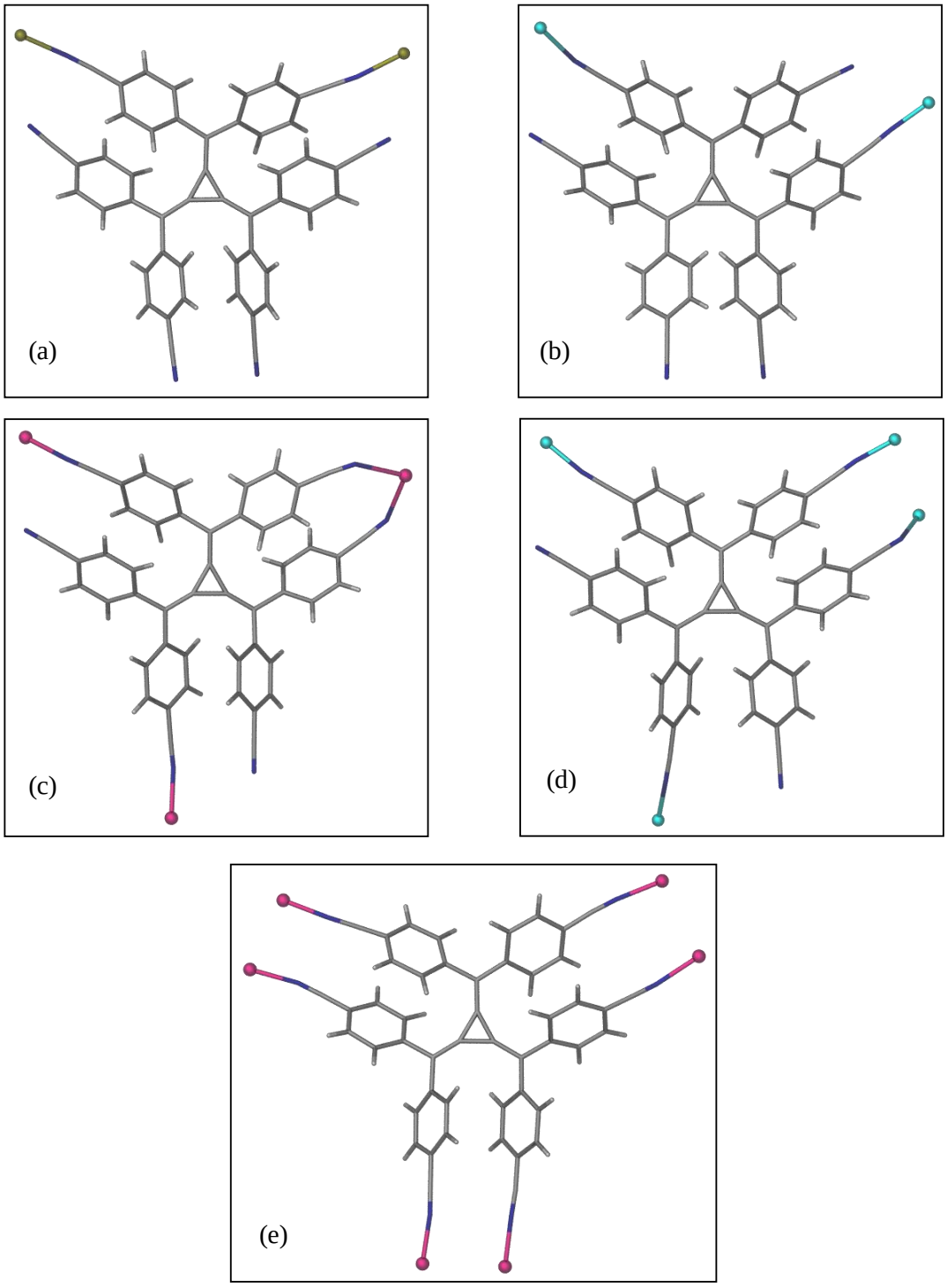

Figure 4.38. The five coordination modes observed in structures (a) **4.13**, (b) **4.12**, (c) **4.5-4.8**, (d) **4.10a/b** and **4.11a/b**, and (e) **4.9**. The metal atoms, iron(II) coloured olive, copper(I)/(II) coloured cyan, and silver(I) coloured pink, are represented as balls.

Two different tetradentate coordination modes are also observed but with metal(I) nodes. Interestingly the first tetradentate coordination mode involves binding to only three silver(I) ions. This is due to chelation via two donor nitrile groups from adjacent arms of **2.29**. This binding mode, which is observed in structures **4.5-4.8**, can be represented as *1,1'-2,3* (Figure

4.38 (c)). The 17-membered chelate ring which is formed is particularly unusual as it exhibits nonlinear C≡N-Ag bond angles between 138.1 and 139.3°. The second tetradentate coordination mode, which is observed in structures **4.10a/b** and **4.11a/b**, is a combination of the two bidentate modes with binding of two copper(I) atoms via two nitrile donor groups on the same arm of the [3]radialene and further binding to two other copper(I) atoms via one donor group from each of the remaining two [3]radialene arms, *1,1',2,3* (Figure 4.38 (d)). Chelation is not observed in the copper(I) polymers due to the smaller ionic radius of copper(I), 91 pm, compared to that of silver(I), 129 pm.[73,74]

These two tetradentate coordination modes result in 2-D coordination polymers with either a (6,3) topology, as seen in structures **4.5**-**4.8**, or a 4-connected network caused by the bridging of (6,3) sheets, as observed for **4.10b/4.11b**. The *1,1',2,3* coordination mode also results in a complex 3-D network in the case of **4.10a/4.11a**. Polymers **4.10a/b** and **4.11a/b** all form from reactions undertaken with Cu:**2.29** stoichiometries in the region of 6:1 to 18:1. Both structures are produced in each reaction and have the same stoichiometry of Cu:**2.29** despite being formed at different stages of the slow evaporation process. In this case the more open, metastable products (**4.10a** and **4.11a**) appear to form first – these are particularly solvent dependent – and over time the denser, close-packed and stable structures of **4.10b** and **4.11b** form. This observation was supported by the fact that only **4.10a** and **4.11a** could be formed exclusively from seeding reactions carried out using four sets of crystals; when **4.10b** and **4.11b** were added to a reaction mixture the more rapidly formed compounds **4.10a** and **4.11a** are isolated as well as **4.10b** and **4.11b**.

The final coordination mode which was observed for [3]radialene **2.29** involves binding by all six nitrile donor groups to six silver(I) ions, *1,1',2,2',3,3'* (Figure 4.38 (e)). Even though **2.29** has the potential to be hexadentate it prefers to be hypodentate, as shown by the other four observed coordination modes, and structure **4.9** is the first example of **2.29** acting as a hexadentate ligand. With low Ag:**2.29** stoichiometries, in the region of 1:1 to 3:1, [3]radialene **2.29** acts as a tetradentate ligand as observed for the *1,1'-2,3* binding mode seen in structures **4.5**-**4.8**. Increasing the Ag:**2.29** ratio dramatically to 10:1 allows the isolation of structure **4.9**, an 8-fold interpenetrated (10,3)-*b* net, in which **2.29** acts as a hexadentate ligand. It appears that such high Ag:**2.29** ratios are necessary to facilitate utilisation of all six nitrile donor groups of **2.29**.

The majority of coordination polymers containing [3]radialene **2.29** were produced via reaction with metal(I) salts due to the soft nitrile donors preferring soft metal(I) ions. In fact, of the two structures which contain metal(II) ions, **4.12** and **4.13**, one was generated via *in situ* oxidation of a metal(I) salt. Polymer **4.12** was produced via reaction of **2.29** with the

copper(I) salt $[Cu(CH_3CN)_4]PF_6$ in a 1:3 ratio in nitromethane. It is proposed that the oxidation of the copper(I) salt has come at the expense of the reduction of some of the radialene, as **2.29** is electron deficient and has been shown to undergo two stepwise reductions to form the radical anion and dianion respectively, or through a disproportionation reaction of copper(I) as the crystals were only produced in trace quantities. While copper(I) salts are often oxidised *in-situ*, it is not commonly reported for this to result in the production of X-ray quality crystals as shown by the discovery of only one other example of the oxidation of copper(I) to copper(II) during crystallisation.[90]

Hexaaryl[3]radialenes are generally quite difficult to crystallise with only six examples of coordination polymers containing these ligands reported to date.[49,52,53,58] Much synthetic effort was expended in the endeavour to crystallise the two new hexaaryl[3]radialene compounds **2.38** and **2.44**. [3]Radialene **2.38** proved resistant to all crystallisation attempts and not even crystals of the compound itself could be obtained. Finally, success was achieved with the generation of a 3-D coordination polymer, **4.14**, via the reaction of **2.44** with $AgPF_6$ in a ratio of 1:12. Within this structure the potentially dodecatopic ligand is hypodentate with only eight of its twelve nitrile donor groups involved in coordination. The polymer itself appears complex but the topology can be reduced to that of the rutile network via the treatment of a four silver(I) cluster as a 6-connecting node and the radialene ligands as 3-connecting nodes.

Within the coordination polymers of hexaaryl[3]radialenes previously reported, close contacts have been observed between the anions and the [3]radialene core.[49,58] This is proposed to be due to the electron deficiency of the cross-conjugated [3]radialene core and also the acidity of the aryl hydrogen atoms. Anions have also been observed to localise near the [3]radialene core in a number of the structures reported in this chapter, notably **4.7**, **4.8** and **4.13**. The presence of anion interactions in these structures is assessed in Chapter 5.

4.5. Experimental

4.5.1. General Experimental

Infrared spectra were recorded using a Perkin Elmer Spectrum 100 FT-IR spectrometer with universal attenuated total reflectance (UATR) sampling accessory. The Campbell microanalytical laboratory at the University of Otago performed elemental analyses. ^{1}H NMR spectra were recorded on a Varian Gemini 300 MHz spectrometer in CD_3CN and referenced to the solvent peak, 1.93 ppm. Unless otherwise stated, reagents were obtained from commercial sources and used as received. *Perchlorate salts are potentially explosive and should be handled with care in small amounts.*

4.5.2. Crystallisation Procedures

{[Ag(2.29)]BF_4·2(CH_3NO_2)}$_n$ (4.7). A solution of **2.29** (5.0 mg, 0.0073 mmol) in nitromethane (2 mL) was combined in a vial with a solution of $AgBF_4$ (1.4 mg, 0.0073 mmol) in nitromethane (0.5 mL). Slow evaporation of the solvent led to precipitation of **4.7** as bright red, diamond-shaped crystals (2.0 mg, 27%) that were suitable for X-ray crystallography. Analysis calcd for **4.7**: $C_{48}H_{24}N_6AgBF_4$·1½(CH_3NO_2) C 61.22, H 2.96, N 10.82; found C 61.19, H 2.87, N 10.64; FT-IR υ_{max}/cm^{-1}: 2228 (C≡N str., vs), 1048 (B-F str., vs, b). Carrying out the reaction with a **2.29**:$AgBF_4$ ratio in the range from 1:1 to 1:3 gave the same product.

{[Ag(2.29)]SbF_6·2(CH_3NO_2)}$_n$ (4.8). A solution of **2.29** (5.0 mg, 0.0073 mmol) in nitromethane (2 mL) was combined in a vial with a solution of $AgSbF_6$ (2.4 mg, 0.0073 mmol) in nitromethane (0.5 mL). Precipitation occurred immediately and the precipitate was redissolved via addition of acetonitrile (2 drops). Slow evaporation of the solvent led to precipitation of **4.8** as bright red, diamond-shaped crystals (3.2 mg, 38%) that were suitable for X-ray crystallography. Analysis calcd for **4.8**: $C_{48}H_{24}N_6AgSbF_6$·1½(CH_3NO_2) C 53.09, H 2.57, N 9.38; found C 53.01, H 2.37, N 9.34; FT-IR υ_{max}/cm^{-1}: 2226 (C≡N str., vs), 654 (Sb-F str., vs). Carrying out the reaction with a **2.29**:$AgSbF_6$ ratio in the range from 1:1 to 1:3 gave the same product.

{[Ag_3(2.29)](ClO_4)$_3$·CH_3NO_2}$_n$ (4.9). A solution of **2.29** (5.0 mg, 0.0073 mmol) in nitromethane (3 mL) was combined in a vial with a solution of $AgClO_4$ (15 mg, 0.073 mmol) in nitromethane (0.5 mL). Precipitation occurred immediately and the precipitate removed via filtration. Slow evaporation, over approximately one month, led to precipitation of **4.9** as very small, dark red, rod-shaped crystals (trace quantities) suitable for X-ray crystallography. Analysis calcd for initial precipitate $C_{48}H_{24}N_6Cl_3O_{12}Ag_3$ C 44.12, H 1.85, N 6.43; found C 43.97, H 2.50, N 5.78; FT-IR υ_{max}/cm^{-1} of initial precipitate: 2247 (C≡N str. vs), 1599, 1498, 1406, 1277, 1059 (Cl-O str. vs, b), 1018, 928, 838, 767; FT-IR υ_{max}/cm^{-1} of crystals: 2257 (C≡N str. vs), 1651, 1604, 1501, 1406, 1279, 1052 (Cl-O str. vs, b), 1019, 927, 842, 757.

{[Cu_2(2.29)$_2$](BF_4)$_2$·20(CH_3NO_2)}$_n$ (4.10a) and {[Cu(2.29)]BF_4·2(CH_3NO_2)}$_n$ (4.10b). A solution of **2.29** (5.0 mg, 0.0073 mmol) in nitromethane (3 mL) was combined in a vial with a solution of [Cu(CH_3CN)$_4$]BF_4 (41.4 mg, 0.131 mmol) also in nitromethane (0.5 mL). Precipitation occurred immediately and the precipitate was redissolved via addition of acetonitrile (2 drops). Slow evaporation of the solvent led to precipitation of **4.10a** first as bright red, octahedral crystals (trace quantities) that were solvent dependent, and **4.10b** second as bright orange block-shaped crystals (2.9 mg, 41%) that were air stable. Crystals suitable for X-ray crystallography were obtained for both products. Carrying out the reaction

with a **2.29**:$[Cu(CH_3CN)_4]BF_4$ ratio in the range from 1:6 to 1:18 gave the same two products. **4.10a** (5.6 mg, 53%) can be recovered as the sole product by seeding a 1:6 **2.29**:$[Cu(CH_3CN)_4]BF_4$ ratio nitromethane solution with crystals of **4.10a**. However, seeding of an identical solution with **4.10b** leads to equal formation of both products. Analysis calcd for **4.10a**: $C_{48}H_{24}N_6BF_4Cu$ C 69.04, H 2.90, N 10.06; found C 65.19, H 2.93, N 9.56;* FT-IR υ_{max}/cm^{-1}: 2247 (C≡N str., vs), 2225 (C≡N str., vs), 1052 (B-F str., vs, b). Analysis calcd for **4.10b**: $C_{48}H_{24}N_6BF_4Cu$ C 69.04, H 2.90, N 10.06; found C 59.48, H 2.96, N 10.40;* FT-IR υ_{max}/cm^{-1}: 2246 (C≡N str., vs), 2223 (C≡N str., vs), 1052 (B-F str., vs, b).

$\{[Cu_2(2.29)_2](PF_6)_2 \cdot 14(CH_3NO_2)\}_n$ (4.11a) and $\{[Cu(2.29)]PF_6 \cdot 2(CH_3NO_2)\}_n$ (4.11b). A solution of **2.29** (5.0 mg, 0.0073 mmol) in nitromethane (3 mL) was combined in a vial with a solution of $[Cu(CH_3CN)_4]PF_6$ (16.3 mg, 0.044 mmol) in nitromethane (0.5 mL). Precipitation occurred immediately and the precipitate was redissolved via addition of acetonitrile (2 drops). Slow evaporation of the solvent led to precipitation of **4.11a** first as bright red, octahedral crystals (trace quantities) that were solvent dependent, and **4.11b** second as bright orange block-shaped crystals (3.0 mg, 40%) that were air stable. Crystals suitable for X-ray crystallography were obtained for both products. Carrying out the reaction with a **2.29**:$[Cu(CH_3CN)_4]PF_6$ ratio in the range from 1:6 to 1:18 gave the same two products. **4.11a** (5.1 mg, 53%) can be recovered as the sole product via seeding of a 1:6 **2.29**:$[Cu(CH_3CN)_4]PF_6$ ratio nitromethane solution. However, seeding of an identical solution with **4.11b** leads to equal formation of both products. Analysis calcd for **4.11a**: $C_{48}H_{24}N_6PF_6Cu$ C 64.54, H 2.71, N 9.41; found C 55.09, H 2.88, N 9.72;* FT-IR υ_{max}/cm^{-1}: 2248 (C≡N str., vs), 2224 (C≡N str., vs), 829 (P-F str., vs). Analysis calcd for **4.11b**: $C_{48}H_{24}N_6PF_6Cu$ C 64.54, H 2.71, N 9.41; found C 60.68, H 2.76, N 9.56;* FT-IR υ_{max}/cm^{-1}: 2246 (C≡N str., vs), 2223 (C≡N str., vs), 822 (P-F str., vs).

$\{[Cu(2.29)_2(H_2O)_2](PF_6)_2 \cdot 4(CH_3NO_2)\}_n$ (4.12). A solution of **2.29** (5.0 mg, 0.0073 mmol) in nitromethane (2 mL) was combined in a vial with a solution of $[Cu(CH_3CN)_4]PF_6$ (8.2 mg, 0.022 mmol) in nitromethane (0.5 mL). After a small amount of initial amorphous precipitate was removed, slow evaporation of the solvent led to precipitation of **4.12** (trace quantities) as bright red, hexagonal plate-like crystals that were suitable for X-ray crystallography. Attempts to repeat this procedure to amass enough material for further characterisation often led to precipitation. Bubbling oxygen through the solution was trialled to promote oxidation from copper(I) to copper(II), however this was also unsuccessful in producing crystals. FT-IR υ_{max}/cm^{-1} of precipitate: 3424 (O-H str., b), 2249 (C≡N str., vs), 2224 (C≡N str., vs), 828 (P-F str., vs).

* See section 4.2.2 for a discussion of these elemental analysis results.

{[Fe_2(2.29)$_2$(H_2O)$_8$](ClO_4)$_4$·CH_3NO_2·2H_2O}$_n$ (4.13). A solution of **2.29** (5.0 mg, 0.0073 mmol) in nitromethane (2 mL) was combined in a vial with a solution of $Fe(ClO_4)_2·6H_2O$ (18.6 mg, 0.073 mmol) in MeOH (0.5 mL). Slow evaporation of the solvent led to precipitation of **4.13** as dark red, rod-shaped crystals (4.3 mg, 55%) that were suitable for X-ray crystallography. Analysis calcd for **4.13**: $C_{96}H_{48}N_{12}Fe_2Cl_4O_{16}·CH_3NO_2·11H_2O$ C 54.08, H 3.44, N 8.52; found C 54.08, H 3.31, N 8.72; FT-IR υ_{max}/cm^{-1}: 3402 (O-H str., b), 2261 (C≡N str., vs), 2237 (C≡N str., vs), 1065 (Cl-O str. vs, b).

{[Ag_2(2.44)](PF_6)$_2$·7(CH_3NO_2)}$_n$ (4.14). A solution of **2.44** (5.0 mg, 0.0060 mmol) in nitromethane (2 mL) was combined in a vial with a solution of $AgPF_6$ (18.2 mg, 0.0073 mmol) in nitromethane (0.5 mL). Precipitation occurred immediately and the precipitate was redissolved via addition of acetonitrile (2 drops). Slow evaporation of the solvent led to precipitation of **4.14** as bright red, triangular rod-shaped crystals (5.1 mg, 48%) that were suitable for X-ray crystallography. FT-IR υ_{max}/cm^{-1}: 2228 (C≡N str., vs), 836 (P-F str., vs).

4.5.3. X-Ray Crystallography

Crystals were mounted under oil on a loop and X-ray diffraction data were collected at 150(2) K with Mo Kα radiation (λ = 0.71073 Å) using an Oxford Diffraction X-Calibur Diffractometer fitted with an Eos CCD detector, or a Bruker-AXS single crystal diffraction system fitted with an Apex II CCD detector, or with synchrotron radiation (λ = 0.7107 Å) using the Macromolecular Crystallography beamline (MX1) at the Australian Synchrotron.[98] Crystals of **4.10a** and **4.11a** were extremely sensitive to solvent loss and manipulation or removal from solvent rapidly led to loss of crystallinity. Thus, large crystals were used, as noted in Tables 4.1 and 4.2, but, due to the beam size, the data collection was only conducted on a small portion of the crystal. The data sets were corrected for absorption using a multi-scan method, and structures were solved by direct methods using SHELXS-97 [99] and refined by full-matrix least squares on F^2 by SHELXL-97,[100] interfaced through the program X-Seed.[101] All non-hydrogen atoms were refined anisotropically and hydrogen atoms were included as invariants at geometrically estimated positions, unless otherwise stated.

4.5.4. Crystallographic Data

Table 4.1. Crystal data and X-ray experimental data for **4.7**, **4.8**, **4.9**, **4.10a** and **4.10b**.

Compound	**4.7**	**4.8**	**4.9**	**4.10a**	**4.10b**
Empirical formula	$C_{50}H_{30}N_8O_4AgBF_4$	$C_{50}H_{30}N_8O_4AgSbF_6$	$C_{49}H_{27}N_7O_{14}Ag_3Cl_3$	$C_{116}H_{108}N_{32}O_{40}Cu_2B_2F_8$	$C_{50}H_{30}N_8O_4CuBF_4$
Formula weight	1001.50	1150.44	1367.74	2891.04	957.17
Radiation source	Mo Kα	Synchrotron	Synchrotron	Synchrotron	Synchrotron
Crystal system	Triclinic	Triclinic	Orthorhombic	Orthorhombic	Triclinic
Space group	*P*-1	*P*-1	*Pnna*	*Pbca*	*P*-1
a (Å)	9.3749(6)	9.6360(19)	28.799(6)	23.470(5)	9.6110(19)
b (Å)	15.3886(11)	15.622(3)	30.905(6)	22.051(4)	14.831(3)
c (Å)	17.2299(11)	17.308(3)	15.631(3)	52.645(10)	16.740(3)
α (°)	112.269(7)	110.70(3)	90	90	74.76(3)
β (°)	98.944(5)	101.45(3)	90	90	75.04(3)
γ (°)	102.439(6)	103.66(3)	90	90	81.55(3)
Volume ($Å^3$)	2167.6(2)	2251.5(7)	13912(5)	27246(9)	2216.2(8)
Z	2	2	8	8	2
D_{calc} (mg/m^3)	1.534	1.697	1.306	1.410	1.434
Absorption coefficient (mm^{-1})	0.540	1.117	1.006	0.414	0.566
F(000)	1012	1140	5392	11904	976
Crystal size (mm^3)	0.30 × 0.16 × 0.09	0.25 × 0.13 × 0.05	0.10 × 0.03 × 0.01	1.8 × 1.4 × 1.2	0.42 × 0.25 × 0.20
Theta range for data (°)	2.65 to 29.35	1.32 to 29.10	1.46 to 24.19	1.16 to 25.00	1.30 to 27.83
Reflections collected	48646	35950	150585	310511	67800
Independent reflections [R(int)]	10494 [0.0604]	10215 [0.0498]	11121 [0.0937]	23961 [0.0644]	10293 [0.0652]
Completeness to theta full (%)	99.5	91.7	99.5	99.8	99.2
Observed reflections [I>2σ(I)]	7506	7930	7088	20159	9118
Data / restraints / parameters	10494 / 3 / 665	10215 / 10 / 705	11121 / 0 / 515	23961 / 30 / 1131	10293 / 1 / 681
Goodness-of-fit on F2	1.041	1.063	1.287	1.021	1.050
R_1 [I>2σ(I)]	0.0660	0.0652	0.1107	0.0765	0.0738
wR_2 (all data)	0.1944	0.2090	0.3522	0.2338	0.1909
Largest diff. peak and hole ($e.Å^{-3}$)	1.39 and -0.80	1.32 and -1.59	1.53 and -0.91	0.85 and -0.85	1.11 and -1.84

Table 4.2. Crystal data and X-ray experimental data for **4.11a**, **4.11b**, **4.12**, **4.13** and **4.14**.

Compound	**4.11a**	**4.11b**	**4.12**	**4.13**	**4.14**
Empirical formula	$C_{110}H_{90}N_{26}O_{28}Cu_2P_2F_{12}$	$C_{50}H_{30}N_8O_4CuPF_6$	$C_{50}H_{32}N_8O_5Cu_{0.5}PF_6$	$C_{97}H_{73}N_{13}O_{29}Fe_2Cl_4$	$C_{61}H_{39}N_{19}O_{14}Ag_2P_2F_{12}$
Formula weight	2641.10	1015.33	1001.58	2138.18	1767.79
Radiation source	Synchrotron	Synchrotron	Mo Kα	Mo Kα	Mo Kα
Crystal system	Orthorhombic	Triclinic	Triclinic	Triclinic	Monoclinic
Space group	*Pbca*	*P*-1	*P*-1	*P*-1	$P2_1/n$
a (Å)	23.653(5)	9.776(2)	10.9396(6)	14.250(3)	14.5254(6)
b (Å)	23.737(4)	15.018(3)	13.3432(6)	15.020(3)	23.2500(7)
c (Å)	51.930(10)	16.673(3)	16.5754(10)	24.235(5)	23.5325(8)
α (°)	90	74.51(3)	91.011(4)	78.021(12)	90
β (°)	90	76.80(3)	106.488(5)	79.013(12)	98.941(3)
γ (°)	90	78.27(3)	93.026(4)	85.109(16)	90
Volume ($Å^3$)	29156(10)	2270.0(8)	2315.4(2)	4975.6(16)	7850.7(5)
Z	8	2	2	2	4
D_{calc} (mg/m^3)	1.203	1.485	1.437	1.427	1.496
Absorption coefficient (mm^{-1})	0.399	0.597	0.365	0.484	0.637
F(000)	10816	1032	1023	2196	3528
Crystal size (mm^3)	1.6 × 1.3 × 1.1	0.40 × 0.22 × 0.18	0.20 × 0.13 × 0.04	0.25 × 0.20 × 0.11	0.41 × 0.23 × 0.11
Theta range for data (°)	1.16 and 28.86	1.29 to 28.89	2.47 to 25.06	0.87 to 22.00	2.48 to 29.26
Reflections collected	174567	77974	34119	50989	70232
Independent reflections [R(int)]	25220 [0.1581]	11750 [0.0411]	8184 [0.0823]	11901 [0.0590]	18949 [0.0655]
Completeness to theta full (%)	96.2	99.4	99.9	97.6	99.7
Observed reflections [I>2σ(I)]	13060	10609	5332	8938	117685
Data / restraints / parameters	25220 / 3 / 901	11750 / 3 / 652	8184 / 3 / 647	11901 / 0 / 1261	18949 / 0 / 920
Goodness-of-fit on F2	1.086	1.035	1.045	1.104	1.029
R_1 [I>2σ(I)]	0.1336	0.0499	0.0724	0.0775	0.0756
wR_2 (all data)	0.3590	0.1325	0.2004	0.2221	0.2359
Largest diff. peak and hole ($e.Å^{-3}$)	1.09 and -1.18	1.04 and -1.18	0.987 and -0.546	1.56 and -1.48	1.87 and -1.70

Additional refinement details for 4.7. There is disorder of the tetrafluoroborate anion, the silver(I) metal atom, and one nitromethane solvate molecule. All are modelled over two major positions. Three restraints were used to maintain chemically sensible bond lengths within the tetrafluoroborate anion.

Additional refinement details for 4.8. There is disorder of the hexafluoroantimonate anion and the silver(I) metal atom. Both are modelled over two major positions. Four restraints were used to maintain chemically sensible bond lengths in the nitromethane solvate molecules and ISOR commands (six restraints) were used to allow two atoms of a nitromethane solvate molecule to be refined anisotropically. Complex **4.8** was weakly diffracting and as such the data was omitted above 50° to provide a reasonable completeness for the data.

Additional refinement details for 4.9. The structure has large solvent accessible voids. These contained a number of diffuse electron density peaks that could not be adequately identified and refined as solvent. The SQUEEZE routine of PLATON[102] was applied to the collected data, which resulted in significant reductions in R_1 and wR_2 and an improvement in the GOF. R_1, wR_2 and GOF before SQUEEZE routine: 23.5%, 64.3% and 3.18; after SQUEEZE routine: 11.1%, 35.2% and 1.29. The contents of the solvent region calculated from the result of the SQUEEZE routine (3 ClO_4^- and 1 CH_3NO_2 per asymmetric unit) are represented in the unit cell contents in crystal data.

Additional refinement details for 4.10a. The structure has large solvent accessible voids. These contained a number of diffuse electron density peaks that could not be adequately identified and refined as solvent. The SQUEEZE routine of PLATON[102] was applied to the collected data, which resulted in significant reductions in R_1 and wR_2 and an improvement in the GOF. R_1, wR_2 and GOF before SQUEEZE routine: 30.3%, 69.2% and 3.78; after SQUEEZE routine: 7.7%, 23.4% and 1.02. The contents of the solvent region calculated from the result of the SQUEEZE routine (20 CH_3NO_2 per asymmetric unit) are represented in the unit cell contents in crystal data.

Additional refinement details for 4.10b. There is disorder of the tetrafluoroborate anion and one of the nitromethane solvent molecules. Both are modelled over two major positions. One restraint was used to maintain a chemically sensible bond length for one N-O bond in the nitromethane molecule.

Additional refinement details for 4.11a. The structure has large solvent accessible voids. These contained a number of diffuse electron density peaks that could not be adequately identified and refined as solvent. The SQUEEZE routine of PLATON[102] was applied to the collected data, which resulted in significant reductions in R_1 and wR_2 and an

improvement in the GOF. R_1, wR_2 and GOF before SQUEEZE routine: 37.9%, 74.2% and 3.16; after SQUEEZE routine: 13.4%, 35.9% and 1.09. The contents of the solvent region calculated from the result of the SQUEEZE routine (2 PF_6^- and 32 CH_3NO_2 per asymmetric unit) did not correspond with the crystal solvent determined via ^1H NMR digestion (14 CH_3NO_2 per asymmetric unit). In this case the ^1H NMR digestion value is represented in the unit cell contents of the crystal data as it correlates better with that of the isomorphous structure **4.10a**. Three restraints were used to maintain chemically sensible bond lengths within the [3]radialene core. Complex **4.11a** was very weakly diffracting and as such the data was omitted above 42° to provide a reasonable completeness for the data. As a consequence, limited discussion of the structural parameters will be made.

Additional refinement details for 4.11b. There is disorder of one of the nitromethane solvent molecules and this is modelled over two major positions. Three restraints were used to maintain chemically sensible bond lengths within the nitromethane molecule.

Additional refinement details for 4.12. Three restraints were used to maintain chemically sensible bond lengths within one nitromethane solvate molecule. The hydrogen atoms of the water molecule coordinated to the copper(II) were found in the electron difference map.

Additional refinement details for 4.13. The structure contained a number of diffuse electron density peaks that could not be adequately identified and refined as solvent. The SQUEEZE routine of PLATON[102] was applied to the collected data, which resulted in significant reductions in R_1 and wR_2 and an improvement in the GOF. R_1, wR_2 and GOF before SQUEEZE routine: 14.8%, 43.8% and 3.13; after SQUEEZE routine: 7.8%, 22.2% and 1.10. The contents of the solvent region calculated from the result of the SQUEEZE routine (one CH_3NO_2 and two H_2O per asymmetric unit) are represented in the unit cell contents in crystal data. There is disorder of one perchlorate anion and this is modelled over two positions with one oxygen atom refined isotropically. The hydrogen atoms of the coordinated water molecules were unable to be located in the electron difference map but were included in the formula of the structure. Complex **4.13** was weakly diffracting and as such the data was omitted above 44° to provide a reasonable completeness for the data.

Additional refinement details for 4.14. Four nitromethane solvate molecules were able to be located in full in the electron difference map; however the structure contained a number of diffuse electron density peaks that could not be adequately identified and refined as solvent. The SQUEEZE routine of PLATON[102] was applied to the collected data, which resulted in significant reductions in R_1 and wR_2 and an improvement in the GOF. R_1, wR_2 and GOF before SQUEEZE routine: 11.3%, 37.9% and 1.31; after SQUEEZE routine: 7.6%,

23.6% and 1.03. The contents of the solvent region calculated from the result of the SQUEEZE routine (three CH_3NO_2 molecules per asymmetric unit) are represented in the unit cell contents in crystal data.

4.6. References

1 S. R. Batten, S. M. Neville, and D. R. Turner, *Coordination Polymers: Design, Analysis and Application*, RSC Publishing, Cambridge, 2009.

2 A. Y. Robin and K. M. Fromm, *Coord. Chem. Rev.*, **2006**, *250*, 2127.

3 L. Brammer, *Chem. Soc. Rev.*, **2004**, *33*, 476.

4 D. Braga, L. Brammer, and N. R. Champness, *CrystEngComm*, **2005**, *7*, 1.

5 G. Marinescu, M. Andruh, F. Lloret, and M. Julve, *Coord. Chem. Rev.*, **2011**, *255*, 161.

6 H. Miyasaka, A. Saitoh, and S. Abe, *Coord. Chem. Rev.*, **2007**, *251*, 2622.

7 N. Guillou, C. Livage, and G. Férey, *Eur. J. Inorg. Chem.*, **2006**, *2006*, 4963.

8 R. Peng, M. Li, and D. Li, *Coord. Chem. Rev.*, **2010**, *254*, 1.

9 S. Noro, *Phys. Chem. Chem. Phys.*, **2010**, *12*, 2519.

10 A. Erxleben, *Coord. Chem. Rev.*, **2003**, *246*, 203.

11 P. J. Steel and C. M. Fitchett, *Coord. Chem. Rev.*, **2008**, *252*, 990.

12 L. Brammer, C. S. Rodger, A. J. Blake, N. R. Brooks, N. R. Champness, J. W. Cunningham, P. Hubberstey, S. J. Teat, C. Wilson, and M. Schroder, *J. Chem. Soc., Dalton Trans.*, **2002**, *0*, 4134.

13 A. G. Young and L. R. Hanton, *Coord. Chem. Rev.*, **2008**, *252*, 1346.

14 M. Abdul-Kadir, L. R. Hanton, and C. J. Sumby, *Dalton Trans.*, **2011**, *40*, 12374.

15 C. L. Cahill, D. T. de Lill, and M. Frisch, *CrystEngComm*, **2007**, *9*, 15.

16 R. J. Hill, D.-L. Long, N. R. Champness, P. Hubberstey, and M. Schröder, *Acc. Chem. Res.*, **2005**, *38*, 335.

17 X. Gu, D. Xue, and H. Ratajczak, *J. Mol. Struct.*, **2008**, *887*, 56.

18 Y. Zhou, M. Hong, and X. Wu, *Chem. Commun.*, **2006**, 135.

19 M. Andruh, J.-P. Costes, C. Diaz, and S. Gao, *Inorg. Chem.*, **2009**, *48*, 3342.

20 C. J. Sumby, *Coord. Chem. Rev.*, **2011**, *255*, 1937.

21 N. N. Adarsh and P. Dastidar, *Chem. Soc. Rev.*, **2012**, *41*, 3039.

22 W. Ouellette, S. Jones, and J. Zubieta, *CrystEngComm*, **2011**, *13*, 4457.

23 B. Therrien, *J. Organomet. Chem.*, **2011**, *696*, 637.

24 T. C. Stamatatos, C. G. Efthymiou, C. C. Stoumpos, and S. P. Perlepes, *Eur. J. Inorg. Chem.*, **2009**, *2009*, 3361.

25 C. J. Milios, T. C. Stamatatos, and S. P. Perlepes, *Polyhedron*, **2006**, *25*, 134.

26 D. J. Tranchemontagne, J. L. Mendoza-Cortes, M. O'Keeffe, and O. M. Yaghi, *Chem. Soc. Rev.*, **2009**, *38*, 1257.

27 Y. D. Lampeka and L. V. Tsymbal, *Theor. Exp. Chem.*, **2004**, *40*, 345.

28 M. Eddaoudi, D. B. Moler, H. Li, B. Chen, T. M. Reineke, M. O'Keeffe, and O. M. Yaghi, *Acc. Chem. Res.*, **2001**, *34*, 319.

29 R. S. Crees, M. L. Cole, L. R. Hanton, and C. J. Sumby, *Inorg. Chem.*, **2010**, *49*, 1712.

30 T.-F. Liu, J. Lu, and R. Cao, *CrystEngComm*, **2010**, *12*, 660.

31 S. M. Hawxwell, G. M. Espallargas, D. Bradshaw, M. J. Rosseinsky, T. J. Prior, A. J. Florence, J. van de Streek, and L. Brammer, *Chem. Commun.*, **2007**, *0*, 1532.

32 S. Benmansour, C. Atmani, F. Setifi, S. Triki, M. Marchivie, and C. J. Gomez-Garcia, *Coord. Chem. Rev.*, **2010**, *254*, 1468.

33 F. Thetiot, S. Triki, J. S. Pala, and C. J. Gomez-Garcia, *Synth. Met.*, **2005**, *153*, 481.

34 F. Thetiot, S. F. Triki, and J. S. Pala, *Polyhedron*, **2003**, *22*, 1837.

35 D. R. Turner, A. S. R. Chesman, K. S. Murray, G. B. Deacon, and S. R. Batten, *Chem. Commun.*, **2011**, *47*, 10189.

36 C. Janiak, *Dalton Trans.*, **2003**, 2781.

37 C. B. Aakeroy, N. R. Champness, and C. Janiak, *CrystEngComm*, **2010**, *12*, 22.

38 C. Janiak and J. K. Vieth, *New J. Chem.*, **2010**, *34*, 2366.

39 W. L. Leong and J. J. Vittal, *Chem. Rev.*, **2011**, *111*, 688.

40 K. R. Dunbar, *Angew. Chem. Int. Ed. Engl.*, **1996**, *35*, 1659.

41 B. F. Hoskins and R. Robson, *J. Am. Chem. Soc.*, **1989**, *111*, 5962.

42 W. Kaim and M. Moscherosch, *Coord. Chem. Rev.*, **1994**, *129*, 157.

43 D. Venkataraman, G. B. Gardner, S. Lee, and J. S. Moore, *J. Am. Chem. Soc.*, **1995**, *117*, 11600.

44 L. Carlucci, G. Ciani, D. W. von Gudenberg, and D. M. Proserpio, *New J. Chem.*, **1999**, *23*, 397.

45 Y. B. Dong, G. X. Jin, M. D. Smith, R. Q. Huang, B. Tang, and H. C. zur Loye, *Inorg. Chem.*, **2002**, *41*, 4909.

46 T. Kuroda-Sowa, T. Horino, M. Yamamoto, Y. Ohno, M. Maekawa, and M. Munakata, *Inorg. Chem.*, **1997**, *36*, 6382.

47 G. B. Gardner, D. Venkataraman, J. S. Moore, and S. Lee, *Nature*, **1995**, *374*, 792.

48 M. Munakata, G. L. Ning, T. Kuroda-Sowa, M. Maekawa, Y. Suenaga, and T. Horino, *Inorg. Chem.*, **1998**, *37*, 5651.

49 C. A. Hollis, L. R. Hanton, J. C. Morris, and C. J. Sumby, *Cryst. Growth Des.*, **2009**, *9*, 2911.

50 A. M. Kutasi, D. R. Turner, B. Moubaraki, S. R. Batten, and K. S. Murray, *Dalton Trans.*, **2011**, *40*, 12358.

51 A. M. Kutasi, D. R. Turner, P. Jensen, B. Moubaraki, S. R. Batten, and K. S. Murray, *Inorg. Chem.*, **2011**, *50*, 6673.

52 P. J. Steel and C. J. Sumby, *Inorg. Chem. Commun.*, **2002**, *5*, 323.

53 K. Matsumoto, Y. Harada, N. Yamada, H. Kurata, T. Kawase, and M. Oda, *Cryst. Growth Des.*, **2006**, *6*, 1083.

54 A. G. Blackman, *C.R. Chim.*, **2005**, *8*, 107.

55 J. K. Clegg, J. M. Harrowfield, Y. Kim, Y. H. Lee, A. Madalan, P. Thuéry, and A. Woo, *Aust. J. Chem.*, **2012**, *65*, 734.

56 B. Akermark, J. Bjernemose, A. Borje, P. J. Chmielewski, H. Paulsen, O. Simonsen, P. C. Stein, H. Toftlund, and J. A. Wolny, *Dalton Trans.*, **2004**, 1215.

57 D. A. McMorran, S. Pfadenhauer, and P. J. Steel, *Inorg. Chem. Commun.*, **2002**, *5*, 449.

58 P. J. Steel and C. J. Sumby, *Chem. Commun.*, **2002**, 322.

59 A. N. Khlobystov, A. J. Blake, N. R. Champness, D. A. Lemenovskii, A. G. Majouga, N. V. Zyk, and M. Schroder, *Coord. Chem. Rev.*, **2001**, *222*, 155.

60 C. L. Chen, B. S. Kang, and C. Y. Su, *Aust. J. Chem.*, **2006**, *59*, 3.

61 R. Meijboom, R. J. Bowen, and S. J. Berners-Price, *Coord. Chem. Rev.*, **2009**, *253*, 325.

62 C. Carruthers, T. K. Ronson, C. J. Sumby, A. Westcott, L. P. Harding, T. J. Prior, P. Rizkallah, and M. J. Hardie, *Chem. Eur. J.*, **2008**, *14*, 10286.

63 M. D. Stephenson and M. J. Hardie, *Dalton Trans.*, **2006**, 3407.

64 C. J. Sumby, J. Fisher, T. J. Prior, and M. J. Hardie, *Chem. Eur. J.*, **2006**, *12*, 2945.

65 M. J. Hardie and C. L. Raston, *Cryst. Growth Des.*, **2001**, *1*, 53.

66 A. Berkessel, J. A. Adrio, D. Hüttenhain, and J. M. Neudörfl, *J. Am. Chem. Soc.*, **2006**, *128*, 8421.

67 A. Westcott, C. J. Sumby, R. D. Walshaw, and M. J. Hardie, *New J. Chem.*, **2009**, *33*, 902.

68 L. Yang, D. R. Powell, and R. P. Houser, *Dalton Trans.*, **2007**, 955.

69 C. J. Sumby, M. J. Carr, A. Franken, J. D. Kennedy, C. A. Kilner, and M. J. Hardie, *New J. Chem.*, **2006**, *30*, 1390.

70 M. R. A. Al-Mandhary, C. M. Fitchett, and P. J. Steel, *Aust. J. Chem.*, **2006**, *59*, 307.

71 D. M. D'Alessandro, F. R. Keene, P. J. Steel, and C. J. Sumby, *Aust. J. Chem.*, **2003**, *56*, 657.

72 A. Avellaneda, C. A. Hollis, X. He, and C. J. Sumby, *Beil. J. Org. Chem.*, **2012**, *8*, 71.

73 A. Bondi, *J. Phys. Chem.*, **1964**, *68*, 441.

74 R. D. Shannon, *Acta Crystallogr., Sect. A*, **1976**, *32*, 751.

75 K. Biradha and M. Fujita, *Angew. Chem. Int. Ed.*, **2002**, *41*, 3392.

76 Y. Han, Z. H. Zhang, Y. Y. Liu, Y. Y. Niu, D. G. Ding, B. L. Wu, H. W. Hou, and Y. T. Fan, *Cryst. Growth Des.*, **2011**, *11*, 3448.

77 J. J. Jiang, R. Yang, Y. Xiong, L. Li, M. Pan, and C. Y. Su, *Sci. China, Chem.*, **2011**, *54*, 1436.

78 Y.-F. Zhou, B.-Y. Lou, D.-Q. Yuan, Y.-Q. Xu, F.-L. Jiang, and M.-C. Hong, *Inorg. Chim. Acta*, **2005**, *358*, 3057.

79 O. M. Yaghi and H. Li, *J. Am. Chem. Soc.*, **1996**, *118*, 295.

80 S. Deibele, J. Curda, E.-M. Peters, and M. Jansen, *Chem. Commun.*, **2000**, 679.

81 C.-M. Liu, S. Gao, D.-Q. Zhang, Y.-H. Huang, R.-G. Xiong, Z.-L. Liu, F.-C. Jiang, and D.-B. Zhu, *Angew. Chem. Int. Ed.*, **2004**, *43*, 990.

82 H.-Z. Kou, B. Chuan Zhou, and R.-J. Wang, *J. Organomet. Chem.*, **2004**, *689*, 369.

83 M. S. Chen, M. Chen, S. Takamizawa, T. Okamura, J. A. Fan, and W. Y. Sun, *Chem. Commun.*, **2011**, *47*, 3787.

84 Y. Q. Lan, S. L. Li, Y. M. Fu, Y. H. Xu, L. Li, Z. M. Su, and Q. Fu, *Dalton Trans.*, **2008**, 6796.

85 P. W. Atkins and D. F. Shriver, *Shriver & Atkins' Inorganic Chemistry*, 5th ed., Oxford University Press, Oxford, 2010.

86 Q. T. Zhang and J. M. Tour, *J. Am. Chem. Soc.*, **1997**, *119*, 9624.

87 I. Feinsteinjaffe and S. E. Maisuls, *J. Organomet. Chem.*, **1988**, *350*, 57.

88 S. R. Batten, A. R. Harris, P. Jensen, K. S. Murray, and A. Ziebell, *J. Chem. Soc., Dalton Trans.*, **2000**, 3829.

89 M. O'Keeffe, M. A. Peskov, S. J. Ramsden, and O. M. Yaghi, *Acc. Chem. Res.*, **2008**, *41*, 1782.

90 I.-H. Park, H. J. Kim, and S. S. Lee, *CrystEngComm*, **2012**, *14*, 4589.

91 H. A. Jahn and E. Teller, *Proc. R. Soc. London, Ser. A*, **1937**, *161*, 220.

92 S. R. Batten, B. F. Hoskins, and R. Robson, *Inorg. Chem.*, **1998**, *37*, 3432.

93 S. R. Batten, R. Robson, P. Jensen, B. Moubaraki, and K. S. Murray, *Chem. Commun.*, **1998**, 439.

94 S. R. Batten, B. F. Hoskins, B. Moubaraki, K. S. Murray, and R. Robson, *J. Chem. Soc., Dalton Trans.*, **1999**, 2977.

95 L. Xie, S. Liu, B. Gao, C. Zhang, C. Sun, D. Li, and Z. Su, *Chem. Commun.*, **2005**, 2402.

96 C. Qin, X.-L. Wang, E.-B. Wang, and Z.-M. Su, *Inorg. Chem.*, **2005**, *44*, 7122.

97 D. B. Cordes and L. R. Hanton, *Inorg. Chem.*, **2007**, *46*, 1634.

98 T. M. McPhillips, S. E. McPhillips, H.-J. Chiu, A. E. Cohen, A. M. Deacon, P. J. Ellis, E. Garman, A. Gonzalez, N. K. Sauter, R. P. Phizackerley, S. M. Soltis, and P. Kuhn, *J. Synchrotron Radiat.*, **2002**, *9*, 401.

99 G. M. Sheldrick, *Acta Crystallogr., Sect. A*, **1990**, *46*, 467.

100 G. M. Sheldrick, *SHELXL-97*, University of Gottingen, Gottingen, Germany 1997.

101 L. J. Barbour, *J. Supramol. Chem.*, **2001**, *1*, 189.

102 A. L. Spek, *Acta Crystallogr., Sect. A*, **1990**, *46*, 34.

Chapter 5

Anion Interactions of [3]Radialenes

Chapter 5

5. Anion Interactions of [3]Radialenes

5.1. Introduction

5.1.1. Anion-π Interactions

Over the past decade the field of anion coordination chemistry has experienced a period of rapid expansion. As a consequence of this a large number of reviews regarding the subject have been published.[1-7] Still a relatively new field, this intense interest has arisen due to the ubiquity of anions in both environmental and biological settings. For example the DNA double helix is a polyanion and more than two thirds of enzyme substrates and cofactors are anionic.[1,8-10] Simple anions, such as phosphate and nitrate, are a requirement for plant, and subsequently animal, life but can have a detrimental impact on the environment when present in excessive quantities; generally as a result of the over use of fertilisers.[11-13] Compounds which effectively and selectively bind and isolate, detect, or transport anions could have a wide range of application in such areas including the pharmaceutical industry, environmental remediation (removal of nitrate and phosphate anions from fertiliser run off), and nuclear waste treatment (sequestration of sulfate anions to improve the vitrification process).[11,14,15]

Approaches to selectively complex anionic species using non-covalent interactions have been described for a large range of anions including monoatomic halides,[16-21] small polyatomic anions including phosphate, nitrate and sulfate,[16,20,22,23] as well as larger aromatic anions.[24,25] Receptors have been reported which utilise a number of different supramolecular motifs to promote anion association such as hydrogen bonding donor groups,[2,5-7] Lewis acid moieties,[1,26] and electrostatic interactions with cations.[1,27] In addition to these often exploited and well understood interactions, electron deficient π-systems have been observed to interact with anions.[28-31] Weak interactions between polarisable aryl systems and anions were first reported by Schneider in the early 1990's.[32] This early work was supported by further theoretical studies which showed that binding energies of anions and electron deficient aryl rings were in the vicinity of 20-50 kJ.mol^{-1}, comparable in strength to weak to moderate hydrogen bonds.[33,34] These anion-π interactions are defined by electrostatic attraction and anion-induced polarisation of the π-system; similar to that of cation-π interactions (Figure 5.1).[35,36]

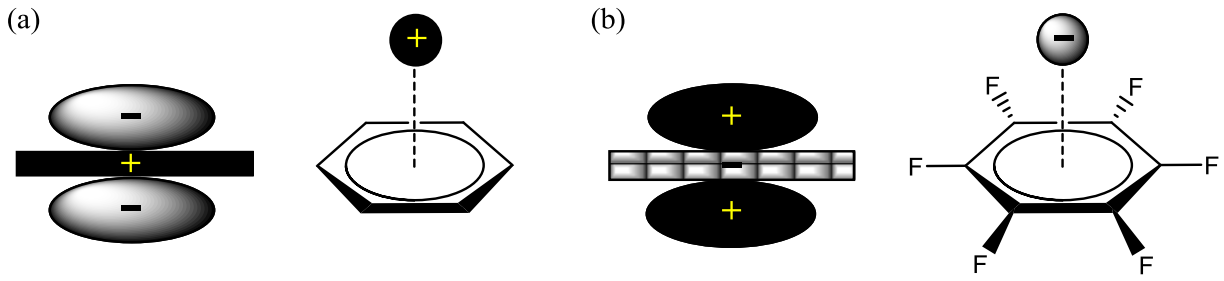

Figure 5.1. Representations of the quadropole moments and ion-π interactions of (a) benzene and (b) hexafluorobenzene.

It has been shown by Deyà and colleagues that the quadropole moment of a ring system is of high importance to the formation of anion-π interactions.[37] The quadropole moment is a product of the aspherical symmetry of charge distribution around the ring (Figure 5.2). If electrons are distributed in a perfectly symmetrical manner the quadropole moment along the z-axis, Q_{zz}, is equal to zero. In electron rich π-systems, such as benzene, the electrons are distributed in a prolate fashion resulting in a negative Q_{zz}, which is favourable for interacting with cations. Conversely, in electron deficient π-systems with electron withdrawing substituents, such as hexafluorobenzene, the electrons are distributed in an oblate fashion. This results in a positive value of Q_{zz} which is favourable for interacting with anions.

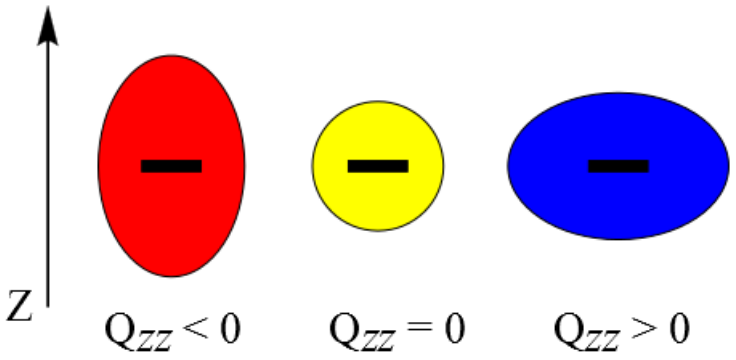

Figure 5.2. Quadropole moments of spherical and aspherical electron distributions.

As well as computational evidence, instances of anion-π interactions have been observed in the gas phase,[38] in solution[19,39] and in the solid-state.[40-42] A recent study by Matile and co-workers into the use of naphthalenediimides (NDIs) as π-slides, molecules with π-acidic surfaces which can span a lipid bilayer membrane allowing anions to effectively pass thorough it by moving along the surface of the slide, used mass spectrometry to demonstrate anion-π interactions within these systems.[38] A series of simplified NDI monomers (generally a rigid-rod oligomer of at least three NDI units is required to span a lipid bilayer) were

synthesised (Figure 5.3) and equimolar solutions of these monomers with halides and small polyatomic anions were analysed via electrospray ionisation Fourier-transform ion cyclotron resonance tandem mass spectrometry. Weakly bound NDI-anion complexes were observed for **5.1**-**5.4** and nitrate, chloride, and bromide anions. A selectivity sequence of **5.4** > **5.3** > **5.2** > **5.1** was determined which demonstrated that anion affinity increases with the π-acidity of the NDI. This sequence also correlated well with gas phase computational results, which shows that mass spectrometry is a useful tool for identifying anion-π complexes in the gas phase.

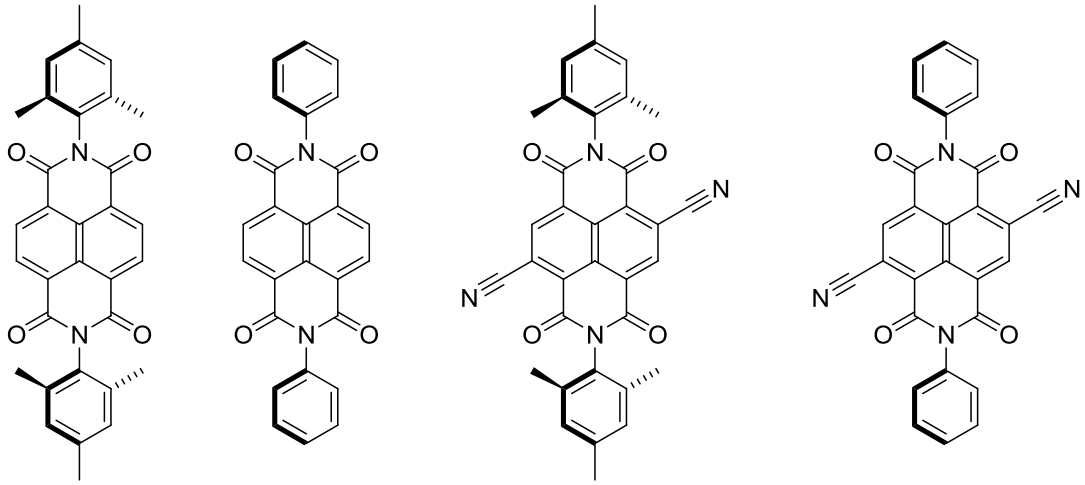

5.1 **5.2** **5.3** **5.4**

Figure 5.3. Simplified naphthalenediimide (NDI) π-slides studied by Matile.[38]

Anion-π interactions have also been observed in solution as shown by Johnson and colleagues who developed an anion receptor, **5.5**, with an electron deficient pentafluorophenyl group (Figure 5.4).[19] A second receptor, **5.6**, with an electron rich phenyl group was also synthesised to allow comparison to the fluorinated derivative (Figure 5.4). ^{1}H NMR titration experiments in $CDCl_3$ were performed for each receptor with (^{n}Bu)$_4$NCl, (^{n}Bu)$_4$NBr and (^{n}Bu)$_4$NI and the downfield shifts of the N-H peaks were monitored. Both receptors **5.5** and **5.6** have the potential to establish hydrogen bonds between the N-H protons and the halide anions but only **5.5** can be involved in anion-π interactions. Association constants for **5.5** were modest ranging from 20-34 M^{-1} however those for **5.6** were too weak to be measured via ^{1}H NMR titration experiments demonstrating the existence of the anion-π interaction in solution.

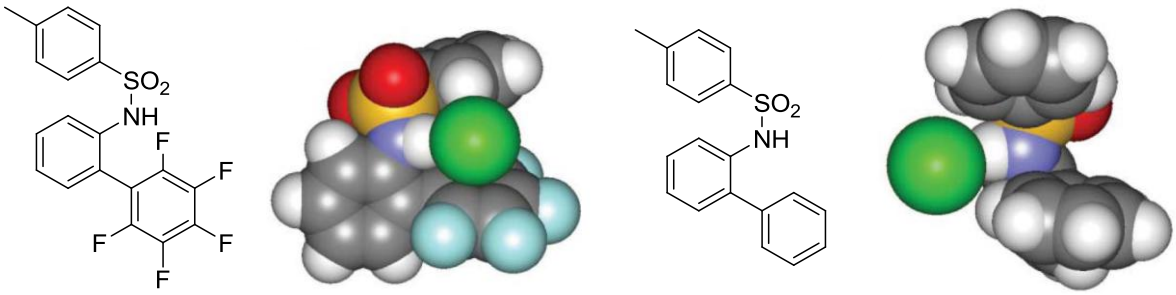

5.5 **5.6**

Figure 5.4. Receptor molecules with, **5.5**, and without, **5.6**, an electron deficient pentafluorophenyl ring and optimised models of their interaction with chloride (images sourced from reference 19).

The frequency of anion-π interactions in solid-state structures present in the Cambridge Structural Database (CSD) has been a contested subject with publications stating that these contacts are quite common[43] and others purporting the rarity of true instances of anion-π interactions.[44,45] These arguments are a product of varying methods of identifying significant anion-π interactions within solid-state structures. The first canvassing of the CSD by Samuelson used the following criteria: (a) any atom of the anion is ≤ 3.5 Å from the arene centroid and (b) all six atom-centroid-arene angles are within 90 ±10°.[44] This search produced a total of 17 hits for C_6 rings and 152 hits for C_5N rings which demonstrated that anion-π interactions were relatively rare. The second investigation by Reedijk and Gamez used less strict criteria which identified an anion-π interaction when the anion was within 4.0 Å of all six ring atoms.[43] This search produced a total of 659 hits for C_6 rings and 3227 hits for C_5N rings which indicated that perhaps anion-π interactions were more common than first thought.

A third study regarding the issue of solid-state anion-π interactions was recently published by Hay and Custelcean.[45] They contend that the contact constraint of ≤ 4.0 Å between the anion and all six ring atoms, used by Reedijk and Gamez, does not provide evidence of an anion-π interaction as most of the structures bear little resemblance to the expected geometries; in other words the anions do not predominantly locate above the core centroid. As anion-π interactions are primarily electrostatic in nature, as shown by computational studies,[36] it is expected that they should have a clear directionality associated with them. On the basis of these observations, it was proposed by Hay and Custelcean, that real examples of solid-state anion-π interactions should fulfil the following guiding principles: (a) exhibit a geometry corresponding to electronic structure calculations; (b) have the anion located above the core centroid; and (c) involve a charge neutral organic compound (or the organic component of a metal-ligand complex or coordination polymer).

An example of a solid-state structure which meets these criteria is a copper(II) complex of 2,4,6-(dipyridin-2-ylamino)[1,3,5]triazine (**5.7**) with the formula $[(\mathbf{5.7})_2(CuCl)_3][CuCl_4]Cl$ (**5.8**) reported by Meyer.[40] The cationic moiety of **5.8** consists of two molecules of **5.7** that are stacked parallel to one another and are bound by three copper(II) ions in a $[(\mathbf{5.7})_2(CuCl)_3]^{3+}$ carousel-type structure (Figure 5.5). The free chloride anion, which is located above the uppermost triazine ring in Figure 5.4, exhibits a distance of 3.17 Å between the anion and the triazine centroid and an angle of $Cl^{-}\cdots$centroid axis of 87° to the plane of the ring. This anion-π interaction correlates well with the equilibrium distance between a triazine ring centroid and a chloride anion calculated by Mascal and co-workers to be 3.2 Å with an angle of 90°.[33] The opposite triazine ring also experiences a close contact with a chlorine atom of the $[CuCl_4]^{2-}$ anion at an even shorter distance of 3.11 Å and an angle of 88°. Yet this would not classify as a true anion-π interaction, according to Hay and Custelcean, as the calculated geometry of a tetrahedral anion would be such that the anion centroid was located over the triazine core centroid with three of the chlorine atoms in close contact with atoms of the ring.[45] However, it is apparent from the space filling diagram of **5.8** (Figure 5.5) that it would be impossible for the $[CuCl_4]^{2-}$ anion to adopt this geometry due the steric bulk of the ligand.

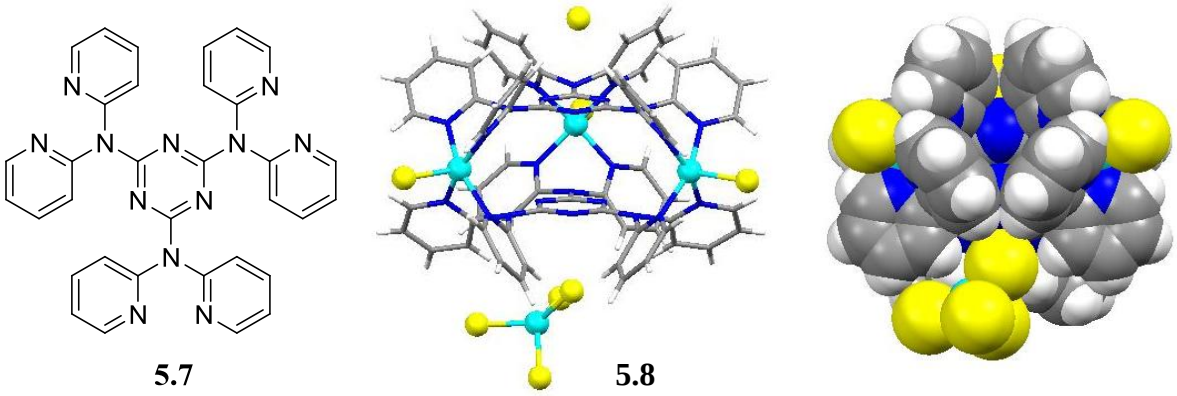

5.7 **5.8**

Figure 5.5. The structure of 2,4,6-(dipyridin-2-ylamino)[1,3,5]triazine (**5.7**); a perspective view of the coordination polymer $[(\mathbf{5.7})_2(CuCl)_3][CuCl_4]Cl$ (**5.8**); and a spacefilling view of **5.8** showing the angle of approach of the $[CuCl_4]^{2-}$ anion.

5.1.2. Analysis of Known Solid-State Radialene Structures

As discussed above, examples of anion-π interactions generally involve electron deficient heterocyclic rings, such as triazine, or aryl rings with electron withdrawing substituents, like fluorine, and because of this, research into anion-π interactions has been focused on aromatic systems. Within solid-state systems anion-π interactions have been classified as significant when the anion centroid is located over the aryl centroid with a tilt angle of 90 ± 10° and

close contacts are observed between the anion and aryl ring which are within the sum of the van der Waals radii of the atoms plus 0.2 Å ($\sum_{vdw}$ + 0.2 Å; ≤ 3.42 Å for oxygen and ≤ 3.37 Å for fluorine). As the [3]radialene core is a constitutional isomer of benzene these guidelines will be used to examine possible anion-π interactions in solid-state structures reported herein. (Note that default CSD van der Waals radii have been used here: H 1.20 Å, C 1.70 Å, O 1.52 Å, and F 1.47 Å.)

It was observed by Reedijk and Gamez that anion-π interactions are almost always accompanied by anion hydrogen bonding due to the tendency of acidic hydrogen atoms in a molecule to interact with anions which are within close proximity.[43] In keeping with the method above, of defining anion-π interactions, anion hydrogen bonds will be classified as significant if the close contacts between the aryl hydrogen atoms and the anions are within $\sum_{vdw}$ + 0.2 Å (≤ 2.92 Å for oxygen and ≤ 2.87 Å for fluorine). These interactions will be further graded according to strength, with a distance between $\sum_{vdw}$ + 0.2 Å and 2.20 Å indicating a weak interaction, from 1.50 to 2.20 Å indicating a moderate interaction and less than 1.5 Å indicating a strong interaction.

A search of the CSD (version 5.33, November 2011 and updates February and May 2012) for the [3]radialene core resulted in 42 hits. Twelve of those were hexaaryl- or hexaheteroaryl[3]radialenes and of those four exhibited proximal anion to radialene π-system contacts. Two of these structures were reported by our group and will be discussed in section 5.4.1. The other two structures discussed here will be referred to by the numbers assigned to them in Chapter 4.

The structure of **4.4** (CSD code MIGQEY), reported by Steel and Sumby, is a M_6L_2F prismate composed of six silver metal atoms, two hexa(2-pyridyl)[3]radialene (**1.3**) ligands, and one fluoride atom (Figure 5.6 (a)). The ligands lie parallel to each other and are bridged by the six silver atoms; each silver atom is bound to one nitrogen donor from each ligand. The fluoride anion resides within the centre of the cage structure and exhibits [3]radialene core centroid···F distances of 2.67 Å and 2.69 Å and core plane to anion angles of 88.5-90.8°. However, these short interactions are supported by coordination of the fluoride anion to three of the silver atoms which in turn are sandwiched between the two radialene ligands. Nevertheless, this discrete complex was the first observation of close contacts between anions and the electron deficient [3]radialene π-system and it prompted further investigation into these systems. Due to the positioning of the fluoride anion encapsulated within the structure no anion hydrogen bonds are observed as it is not adjacent to the outer surface. There are other tetrafluoroborate anions present in the extended structure which exhibit interactions with the peripheral aryl hydrogen atoms, however these will not be discussed here.

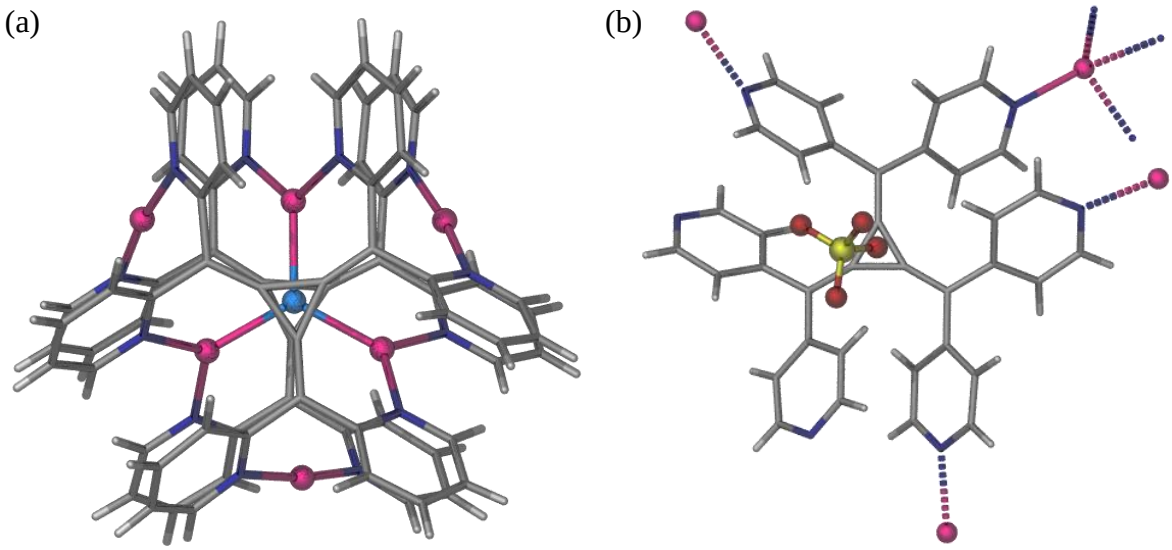

Figure 5.6. (a) A perspective view of the cage structure of **4.4**. (b) A perspective view of structure **4.3**. The dashed bonds are symmetry generated. In both structures other anions and solvate molecules have been removed for clarity.

The structure of **4.3** (CSD code NEHLOC), reported by Oda and colleagues, is a 3-D coordination polymer composed of metal-ligand units containing one silver(I) metal atom and one hexa(4-pyridyl)[3]radialene ligand (**1.4**) (Figure 5.6 (b)).[46] Each silver(I) atom is coordinated by four nitrogen donor atoms from four separate radialenes, which act as four connecting nodes, to form the 3-D coordination polymer. The structure is complicated but this is not the focus here and is described in detail elsewhere.[46] Perchlorate anions situated within the structure sit above the [3]radialene core with a centroid⋯O distance of 3.25 Å with the closest radialene core C⋯O distance being 3.28 Å. The angles between the anion centroid and the plane of the [3]radialene core range from 74.6-100.5° and is 94.7° at its most perpendicular. These features are positive indications of significant anion-π interactions but it is noted that only one atom of the perchlorate anion is directed towards the [3]radialene core and thus it does not exhibit the expected geometry, where three of the oxygen atoms are within 3.42 Å of the ring. Eight weak anion hydrogen bonds are observed between the perchlorate anion and four surrounding radialene ligands ranging from 2.31 to 2.91 Å.

Two solid-state structures of hexaaryl[3]radialenes exhibiting close anion [3]radialene core contacts have been observed in the literature, however within one structure the anion is supported by interactions with metal cations and in the other the anion does not display the expected geometry. Therefore, this chapter poses the question "do hexaaryl[3]radialenes exhibit significant anion-π interactions?" and will endeavour to answer it via the examination of computational, gas phase and solid-state evidence.

5.2. Computational Studies of Anion Interactions

5.2.1. Optimisation of Hexaaryl[3]radialenes

The computational work discussed in this section was undertaken by Mr Jack Evans, with additional guidance from Mr Alexander Gentleman and Prof. Mark Buntine. A series of increasingly electron deficient and synthetically accessible hexaaryl[3]radialene derivatives, **1.1**, **2.38**, **2.29** and **2.44**,[47-49] (Figure 5.7) were optimised to the HF/6-31G++(d,p) level of theory. Radialenes **2.38**, **2.29** and **2.44** were synthesised during the course of this study.

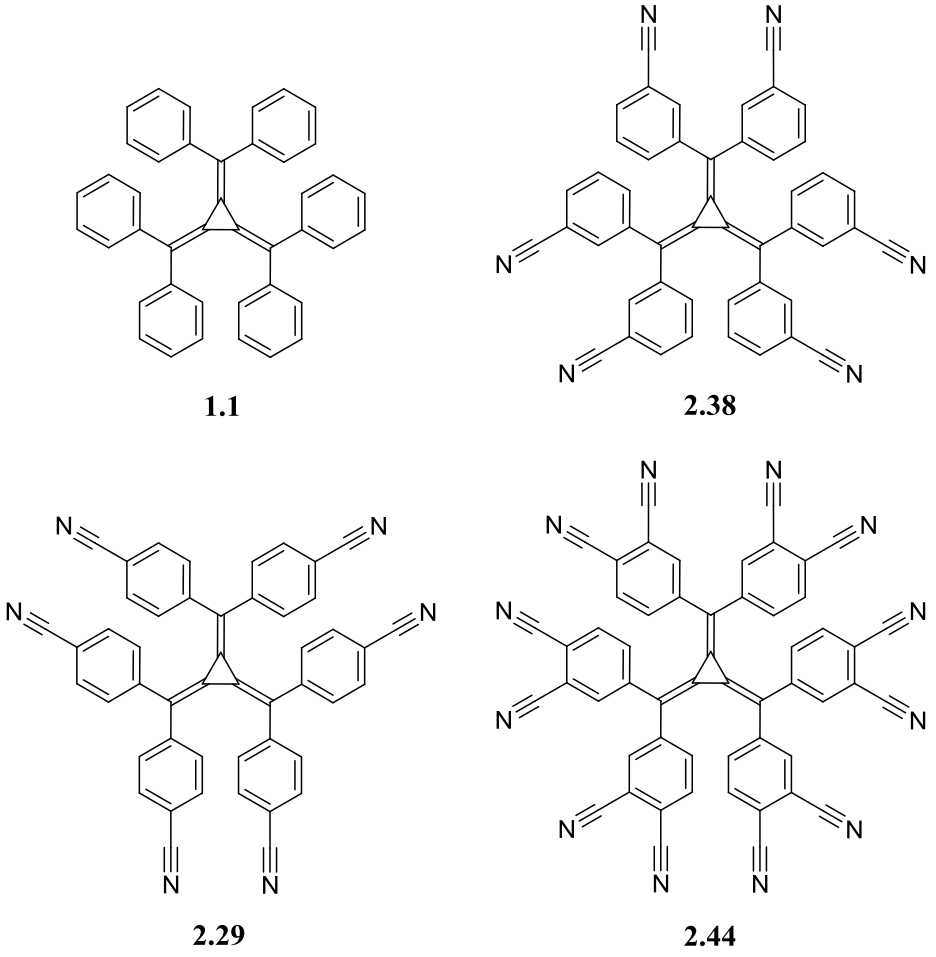

Figure 5.7. Structures of the hexaaryl[3]radialenes investigated via computational means.

The structural parameters of the optimised hexaaryl[3]radialenes correspond well with those observed in crystal structures of these compounds.[46,49-53] The bond lengths of the central cyclopropane ring are consistent across the series at 1.441 Å and the exocyclic double bonds vary minimally ranging from 1.333 to 1.336 Å. The radialenes exhibit the double bladed propeller conformation, as seen in Figure 5.8, which allows the overall energy of the compound to be minimised via increased π-π stacking interactions. This conformation has

been observed numerous times in solid-state structures of hexaaryl- and hexaheteroaryl[3]radialenes.[46,49-53]

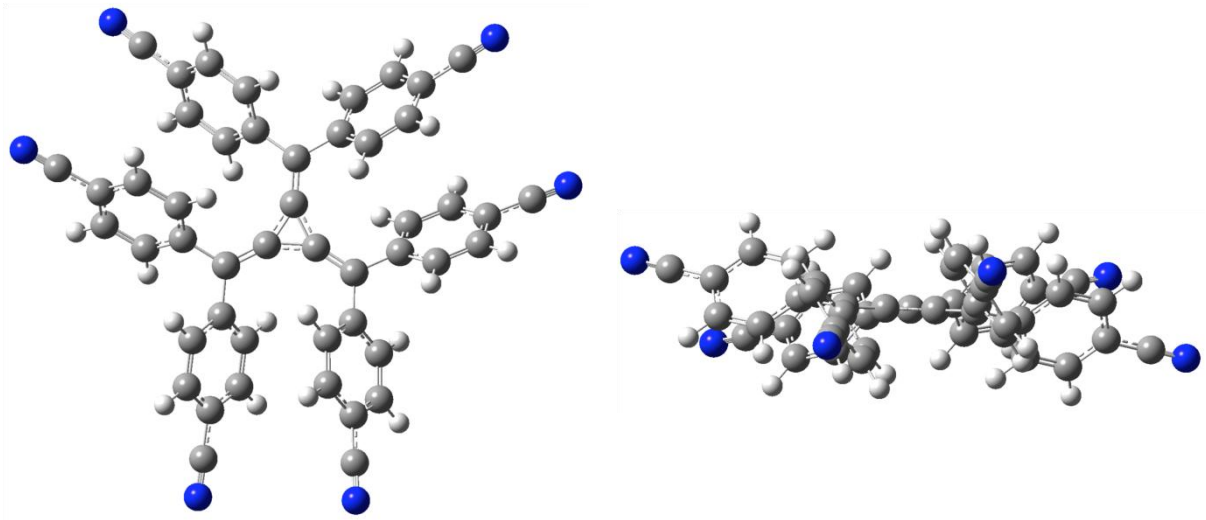

Figure 5.8. Optimised geometry of **2.29**.

When considering the structures of **2.38** and **2.44** it was apparent that there could be a number of different conformers due to free rotation of the phenyl substituents. These could include structures where the *meta* nitrile groups are all aligned on one face of the [3]radialene, **2.38b**, or where they are on alternate sides, **2.38a** (Figure 5.9). In order to determine which conformation best described the structure, these two conformers of **2.38** were optimised. This revealed that the minimum energy configuration was the alternating conformer, **2.38a**. The difference in energy between **2.38a** and **2.38b** was determined to be 10.5 kJ.mol^{-1}, which would allow free rotation between these structures in solution on the NMR timescale.

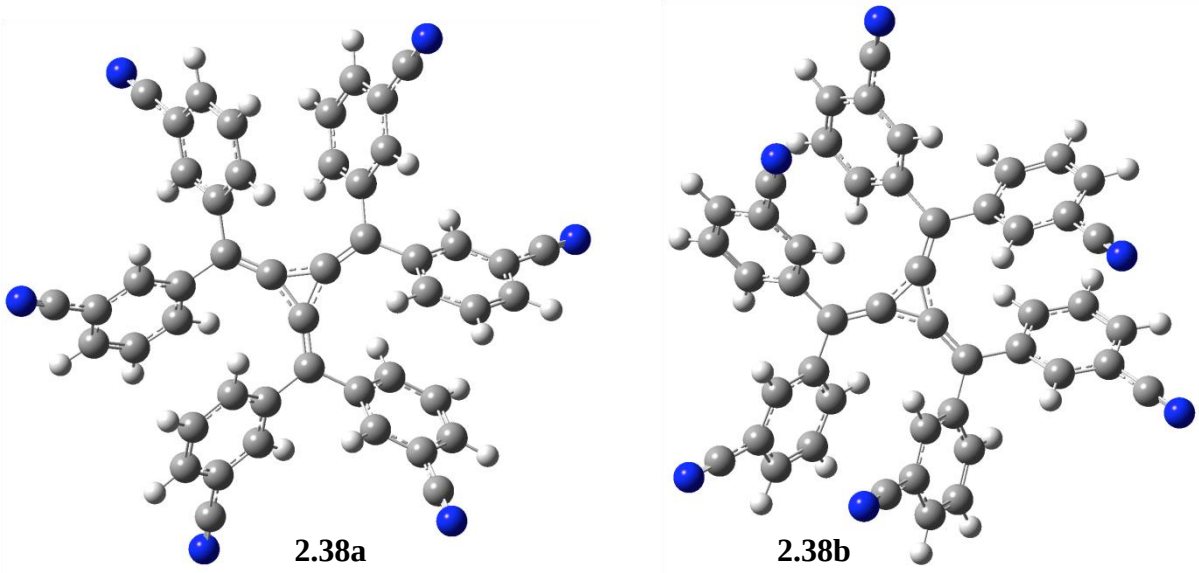

Figure 5.9. Structures of the alternating (**2.38a**) and aligned (**2.38b**) conformers of **2.38**.

Electronic properties of both conformers and their complexes with fluoride are displayed in Table 5.1. Due to the local dipole moments of the nitrile substituents conformer **2.38b** exhibits a molecular dipole moment perpendicular to the [3]radialene core plane; however, alignment of the nitrile substituents also causes the quadropole moment to decrease substantially. Conversely, no dipole moment is observed for conformer **2.38a** as the individual dipole moments of the nitrile substituents cancel due to their alternating configuration and as such the quadropole moment for **2.38a** is much larger than that of **2.38b**. As discussed in section 5.1.1, a large positive quadropole moment is conducive to the formation of anion-π interactions.

Table 5.1. Comparison of dipole moment orthogonal to the molecular plane (*D*, D), quadropole moment (Q_{zz}, B), interaction energy (E_i, kJ.mol^{-1}), and equilibrium distances between the anion and the [3]radialene centroid ($R_{[3]radialene}$, Å) in fluoride complexes of conformers **2.38a** and **2.38b**.

Conformer	***D***	$\mathbf{Q_{zz}}$	$\boldsymbol{E_i}$	$\boldsymbol{R_{[3]radialene}}$
2.38a	0	53	-202	2.745
2.38b	-18	13	-232	2.694

The interaction energies and anion displacements for the complexes of conformers **2.38a** and **2.38b** with fluoride, when the anion is aligned with the dipole moment, are shown in Table 5.1. Due to the interaction with the dipole moment of the radialene, the fluoride complex of the aligned conformer, **2.38b**, is more favourably energetically. However, the alternating conformer, **2.38a**, is more stable than the aligned conformer and so is the configuration that will predominate. As conformer **2.38a** also possesses a larger quadropole moment it was decided to use the alternating configuration of **2.38** and **2.44** in the investigation of anion-π interactions. Hexaaryl[3]radialenes **1.1** and **2.29** do not possess different conformations and so this effect did not have to be considered across the entire series.

The electronic properties of the series of hexaaryl[3]radialenes were analysed in order to determine their propensity to form anion-π interactions. Table 5.2 compares the Q_{zz} quadropole moments and electrostatic potential of each of the radialene species to their reduction potentials. Radialene **1.1** was found not to be conducive to the formation of anion-π interactions as indicated by its negative Q_{zz} quadropole moment, which is a result of its lack of electron withdrawing substituents. The addition of nitrile groups to the *meta* position of the aryl rings, as in **2.38**, causes the Q_{zz} quadropole moment to become positive. This shows that

the [3]radialene itself is not intrinsically electron deficient, as **1.1** has a negative value of Q_{zz}, and that it requires electron withdrawing substituents, in this case nitrile groups, to cause it to become electron deficient.

Table 5.2. Quadropole moments (Q_{zz}, B), maximum electrostatic potential values at the [3]radialene core and aryl hydrogen atoms (ESP, kJ.mol^{-1}) and reduction potentials (E_{red}, V) of hexaaryl[3]radialenes **1.1**, **2.38**, **2.29** and **2.44**.

Compound	Q_{zz}	$ESP_{[3]radialene}$	$ESP_{hydrogens}$	$E_{red(1)}$	$E_{red(2)}$
1.1	-7	91.9	176		
2.38	53	229	306	-0.80	-1.32
2.29	105	238	310	-0.63	-1.03
2.44	140	342	410	-0.06	-0.45

When the nitrile substituents are located in the *para* position of the aryl rings, as in **2.29**, as opposed to the *meta* position the Q_{zz} quadropole moment doubles. This is due to the ability of the nitrile groups in the *para* position to withdraw electron density from the [3]radialene core via resonance and induction, whereas those in the *meta* position can only be involved in inductive electron withdrawal. In addition, withdrawal of electrons via nitrile groups in the *para* position leads to a more oblate electron distribution. The effect on the Q_{zz} quadropole moment of having nitrile substituents in both the *meta* and *para* positions is approximately cumulative as observed for radialene **2.44**.

The electrostatic potential (ESP) for each of the hexaaryl[3]radialenes was mapped onto the electronic density to give the electrostatic potential surfaces shown in Figure 5.10. Within these diagrams areas of positive potential are coloured blue and areas of negative potential are coloured red. The ESP surface of **1.1** displays one area of positive potential, where anions may be attracted, located on the acidic aryl hydrogens, whereas the [3]radialene core is approximately neutral. As electron withdrawing substituents are added, in **2.38**, **2.29** and **2.44**, the positive potential of the acidic aryl hydrogens increases (as seen in Table 5.2) and a new area of localised positive potential is observed on the [3]radialene core. These ESP surfaces also exhibit areas of negative potential on the nitrile nitrogens, which is consistent with nitrogen having a greater electron density than carbon. Overall it can be seen that as the parent structure becomes more electron deficient the intensity of the localised positive potential at the [3]radialene core and the aryl hydrogen atoms increases. Thus, the ESP surface measurements have identified two complementary regions within radialenes **2.38**, **2.29**, and **2.44** amenable to anion binding.

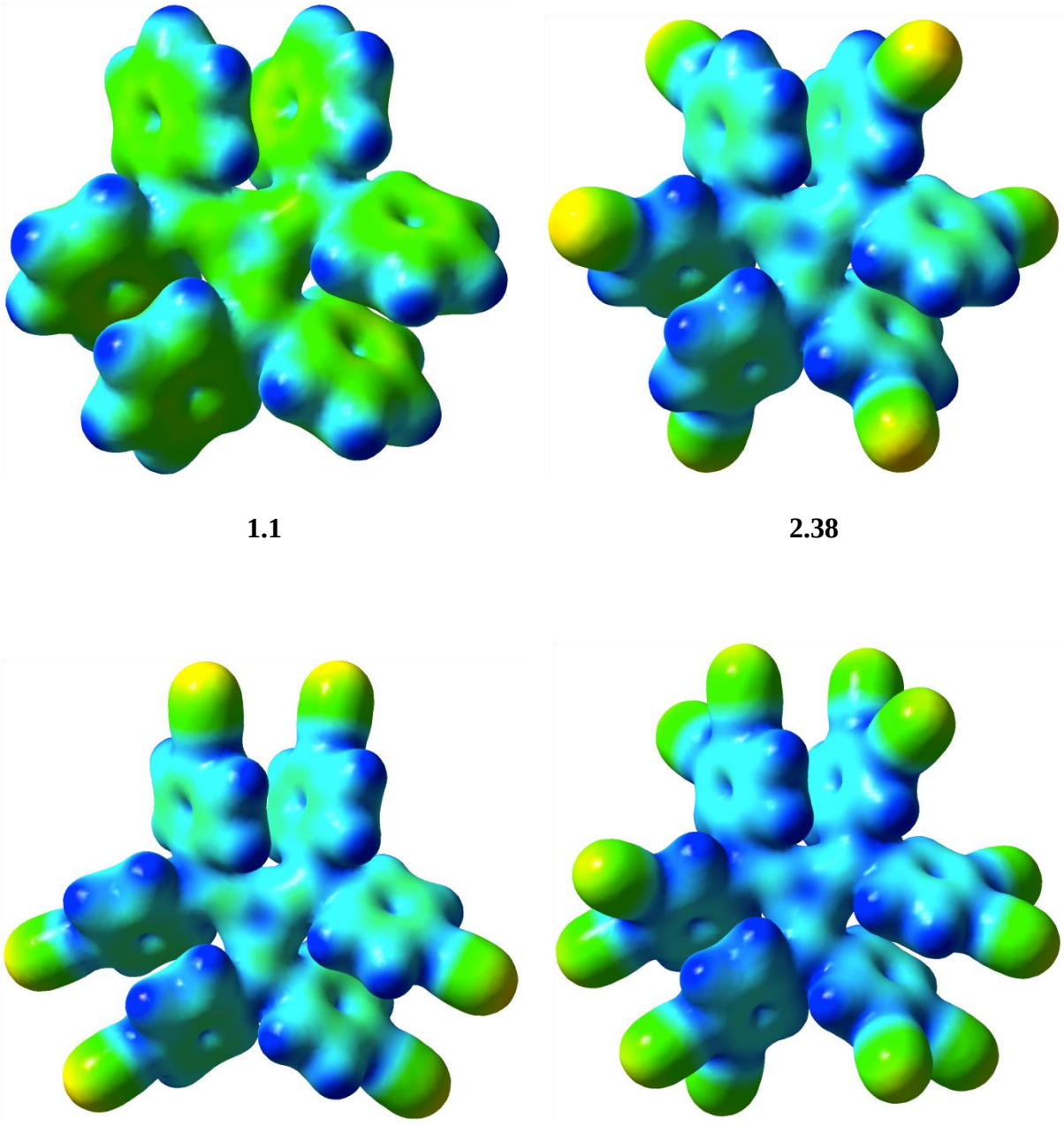

Figure 5.10. Electrostatic potential surfaces (where blue is positive and red is negative) of compounds **1.1**, **2.38**, **2.29**, and **2.44**.

5.2.2. Interaction of Hexaaryl[3]radialenes and Monoatomic Anions

The hexaaryl[3]radialenes **1.1**, **2.38**, **2.29**, and **2.44** were optimised with the halide anions F^-, Cl^- and Br^- using both MO6-2X/6-31++G(d,p) and HF/6-31++G(d,p) levels of theory. These methods both yielded a geometry where the anion is localised above the [3]radialene core on the C_3 axis and provided comparable trends in interaction energy. The MO6-2X functional has been previously used to describe anion-π interactions reliably[54] and so the results using the MO6-2X/6-31++G(d,p) level of theory will be presented. The calculated geometries of compounds **1.1**, **2.38**, **2.29**, and **2.44** with halides F^-, Cl^- and Br^- display weak hydrogen bonding interactions as indicated by close contacts between the anions and three of the aryl hydrogen atoms. The anions are also observed to be in close proximity to the [3]radialene core; as can be seen in the optimised structure of **2.29**-Cl^- (Figure 5.11).

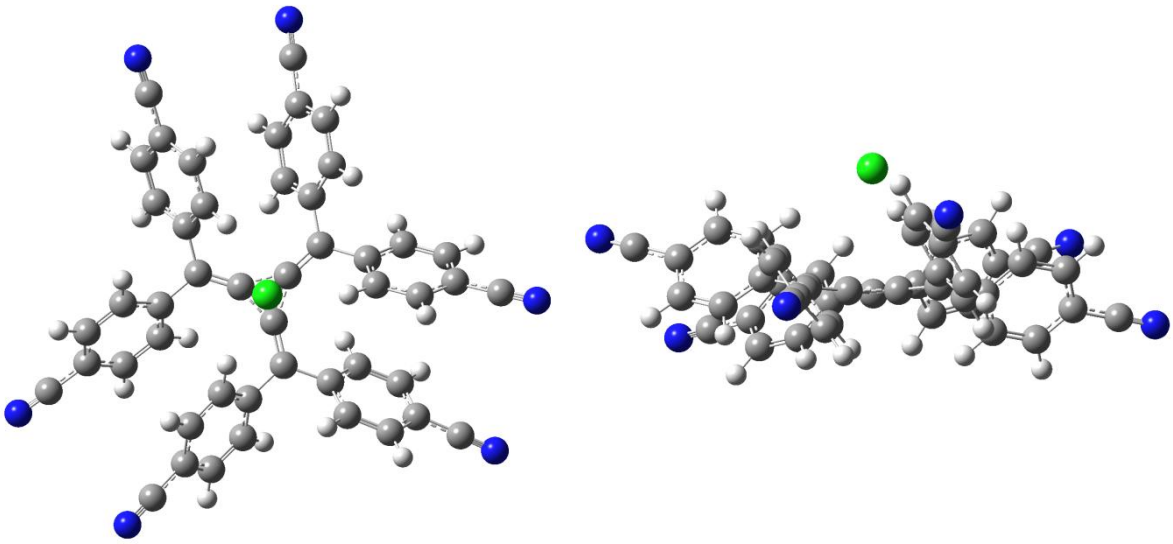

Figure 5.11. Two perspective views of the optimised structure of the **2.29**-Cl^- complex.

When each of the hexaaryl[3]radialenes are bound to fluoride there is a noticeable angle of flex of the exocyclic double bonds of the [3]radialene core towards the anion. This flex is enhanced for electron deficient radialenes (7.3° in **2.44**-F^- compared to 5.4° in **1.1**-F^-) and is due to the attraction between the fluoride anion and the proximal aryl hydrogen atoms. It was noted that the complexes which possess the largest flex angle exhibit the shortest distance between the anion and the proximal hydrogen atoms therby resulting in an improved interaction. The interaction energies and anion displacements for each of the complexes feature in Table 5.3.

Table 5.3. Interaction energies (E_i, kJ.mol^{-1}), equilibrium distances between the anion and the [3]radialene centroid ($R_{[3]radialene}$, Å) and equilibrium distances between the anion and proximal hydrogen atoms (R_H, Å) for halide complexes of **1.1**, **2.38**, **2.29**, and **2.44**.

Complex	$R_{[3]radialene}$	R_H	E_i
1.1-F^-	2.71	2.02	-148
1.1-Cl^-	3.35	2.59	-79.0
1.1-Br^-	3.50	2.79	-67.1
2.38-F^-	2.63	1.95	-249
2.38-Cl^-	3.22	2.50	-190
2.38-Br^-	3.37	2.70	-174
2.29-F^-	2.64	1.96	-279
2.29-Cl^-	3.22	2.51	-192
2.29-Br^-	3.30	2.61	-176
2.44-F^-	2.60	1.90	-354
2.44-Cl^-	3.17	2.47	-279
2.44-Br^-	3.30	2.67	-259

Following analysis of the computational results a number of trends have been identified. Firstly, **1.1**, which has no electron withdrawing groups, was found to exhibit weak anion hydrogen bonding interactions as shown by the equilibrium distances between the anion and proximal hydrogen atoms (R_H) being less than Σ_{vdw} + 0.2 Å. With the addition of electron-withdrawing nitrile substituents, the hydrogen bonding interactions become increasingly favourable as shown by the decreasing R_H distances. This result is not unexpected as the aryl hydrogen atoms become more acidic as the electron deficiency of the arene ring increases. The interaction energies were observed to decrease considerably for the larger anions like bromide and this apparent dependence of the interaction on the charge density of the anions correlates with the electrostatic nature of the anion-π interaction.[55] For the electron deficient compounds, **2.38**, **2.29**, and **2.44**, there is a clear relationship between the interaction energies and the distance of the halide from the [3]radialene core ($R_{[3]radialene}$).

The energies and geometries of the complexes reveal that they are likely to be stabilised by a combination of an anion−π interaction with the [3]radialene core and hydrogen bonding interactions with the proximal aryl hydrogens. This observation of a dual interaction is supported by the *meta* (**2.38**) and *para* (**2.29**) substituted hexaaryl[3]radialenes exhibiting similar binding energies. The electron withdrawing properties of these radialenes dictate that

the *para*-substituted derivative **2.29** should bind halides more strongly as nitrile groups in the *para*-position withdraw electron density more effectively from the core resulting in a larger Q_{zz} quadropole moment. However, the *meta* nitrile groups in **2.38** withdraw electron density from the *ortho* and *para* positions of the aryl rings leading to more acidic hydrogen atoms in these positions. Increased acidity results in an improved hydrogen bonding interaction, which accounts for the enhanced anion binding of **2.38** above what is expected purely on the basis of its Q_{zz} value, as the proximal aryl hydrogens are *ortho* and *para* to the nitrile groups as opposed to **2.29** where the proximal hydrogens are *meta* to nitrile groups.

The valence molecular orbitals of the complexes with electron deficient radialenes, **2.38**, **2.29**, and **2.44**, were calculated in order to further examine the radialene anion interaction. The valence molecular orbitals for **2.29**-F^- and **2.29**-Br^- are shown in Figure 5.12.

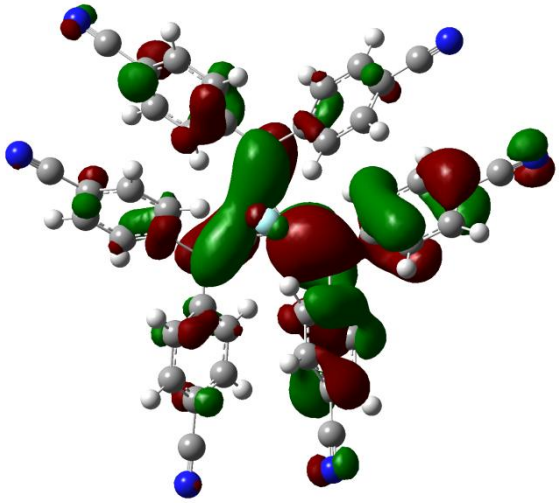

2.29-F^- HOMO

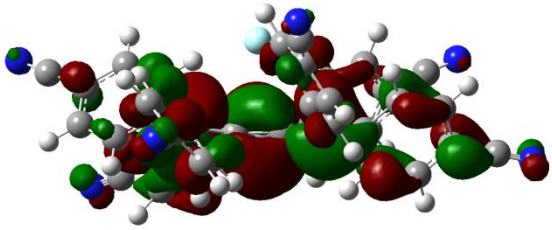

2.29-F^- LUMO

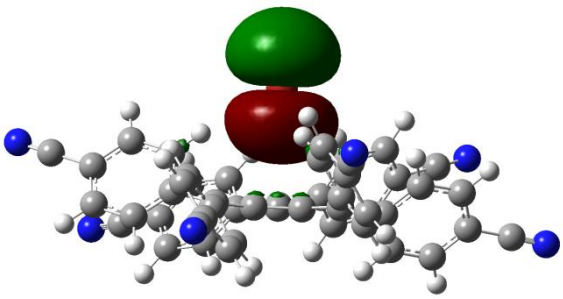

2.29-Br^- HOMO

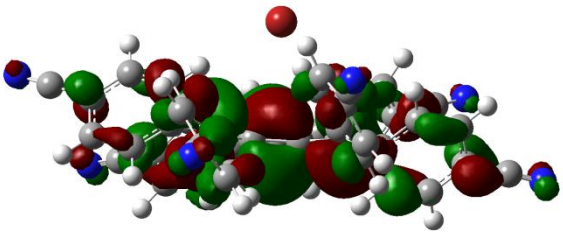

2.29-Br^- LUMO

Figure 5.12. Surface plots of the valence molecular orbitals of hexaaryl[3]radialene halide complexes **2.29**-F^- and **2.29**-Br^-.

The fluoride complexes possess two degenerate HOMOs which contain π-type orbitals distributed on the radialene and a localised p-type orbital on the fluoride anion. The fluoride orbitals associate with the radialene orbitals in a similar fashion to that of anion-π interactions reported by Deyà and colleagues.[56] The degenerate HOMOs reveal an antibonding contribution from both the radialene and anion molecular orbitals. Consequently, the HOMOs signify an electron-electron repulsion that repolarises the π-electron cloud of the radialene which gives rise to a stabilising interaction. This demonstrates that the polarisation effect of the anion-π interaction is observed in these complexes.[56]

In contrast to the fluoride complexes, the chloride and bromide complexes possess a single nondegenerate HOMO which exhibits nonbonding p-type orbitals located predominantly on the anion. This orbital is oriented toward the radialene core and a small amount of density is observed to lie on the carbon atoms of the core forming an antibonding distribution. Due to the increased size of the anion and crowding around the radialene core, it is unsurprising that the radialene and anion orbitals cannot align as they do in the fluoride complexes. This effect explains the lower interaction energies observed for the chloride and bromide complexes.

*5.2.3. Interaction of Hexakis(4-cyanophenyl)[3]radialene (**2.29**) and Polyatomic Anions*

Hexakis(4-cyanophenyl)[3]radialene, **2.29**, was optimised with the polyatomic anions nitrate, perchlorate, tetrafluoroborate and hexafluorophosphate using the HF/6-31++G(d,p) level of theory. This method was shown to produce comparable trends in interaction energy with that of the MO6-2X/6-31++G(d,p) level of theory which has been used to reliably describe anion-π interactions.[54] The optimised structures for each of these **2.29**-anion complexes are displayed in Figure 5.13 and Figure 5.14.

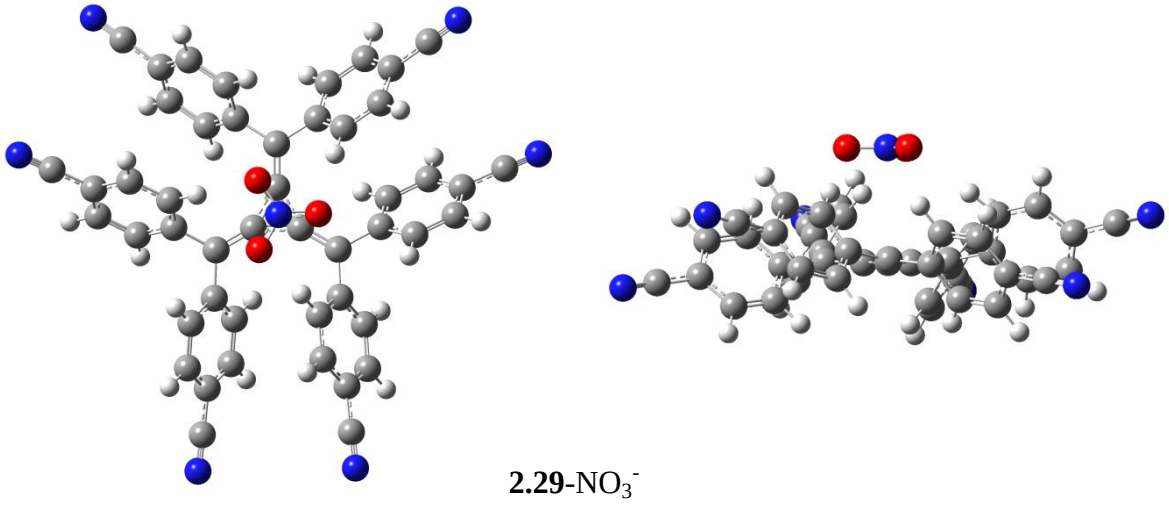

2.29-NO_3^-

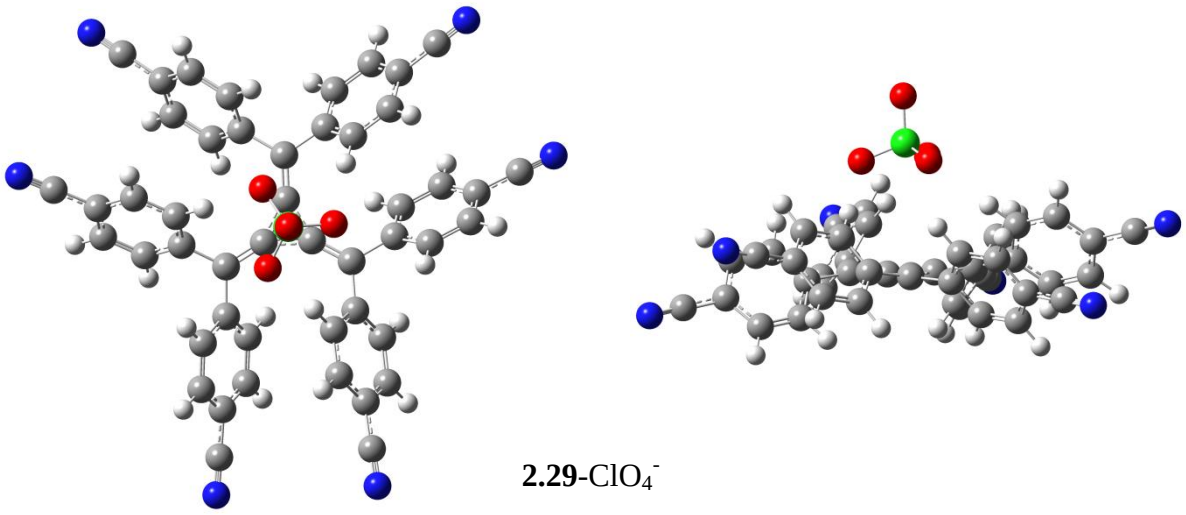

2.29-ClO_4^-

Figure 5.13. Optimised geometries of **2.29** interacting with nitrate and perchlorate anions.

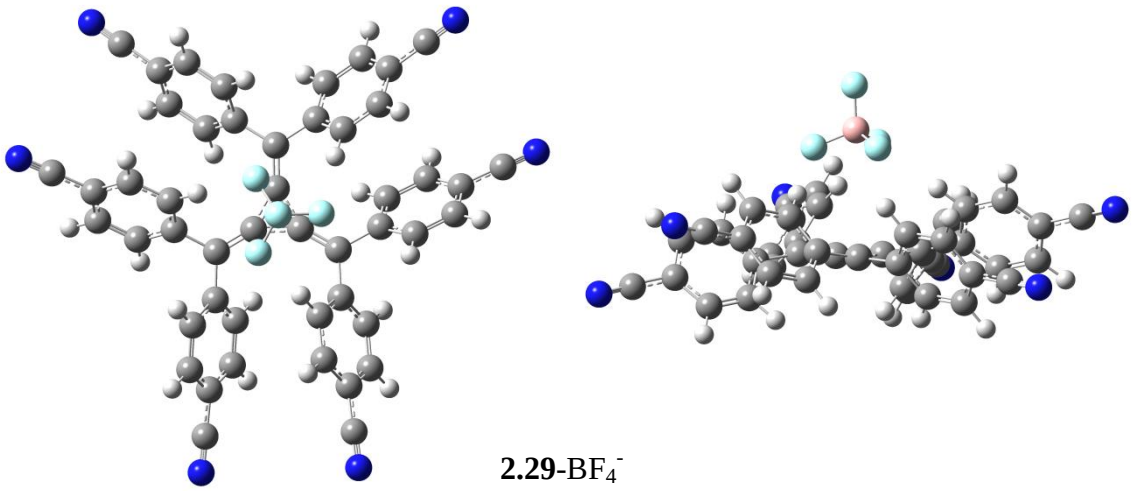

2.29-BF_4^-

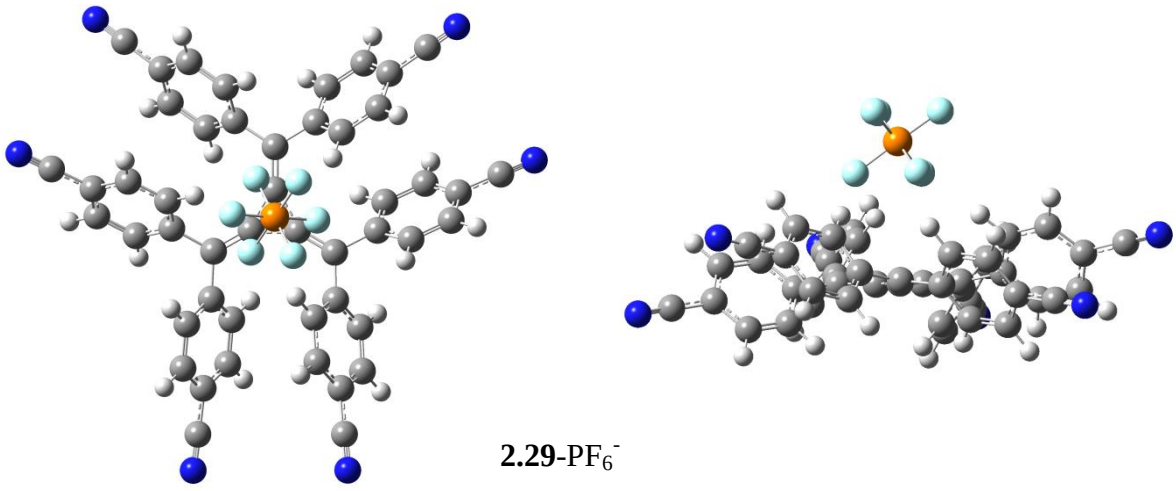

2.29-PF_6^-

Figure 5.14. Optimised geometries of **2.29** interacting with tetrafluoroborate and hexafluorophosphate anions.

The optimised structures of **2.29** with polyatomic anions display very similar geometries to those observed with halide anions. In these cases the centroid of the anion is located directly above the centroid of the [3]radialene core with several aryl hydrogen atoms in close proximity to the peripheral atoms of the anion. A number of different starting geometries were trialled, including a perpendicular nitrate geometry and a perchlorate geometry where one particular oxygen atom was directed towards the core, but each resulted in the geometries pictured. The interaction energies and lengths for these complexes are presented in Table 5.4.

Table 5.4. Interaction energies (E_i, kJ.mol^{-1}), closest distances between the anion and the [3]radialene centroid ($R_{centroid}$, Å), closest distances between the anion and the radialene core ($R_{[3]radialene}$, Å), and closest distances between the anion and proximal hydrogen atoms (R_H, Å) for monoatomic and polyatomic anion complexes of **2.29**.

Complex	$R_{centroid}$	$R_{[3]radialene}$	R_H	E_i
2.29-F^-	2.64	2.64	1.96	-279
2.29-Cl^-	3.22	3.22	2.51	-192
2.29-Br^-	3.30	3.30	2.61	-176
2.29-NO_3^-	3.67	3.53	2.34	-150
2.29-ClO_4^-	3.77	3.60	2.37	-118
2.29-BF_4^-	3.61	3.44	2.28	-132
2.29-PF_6^-	3.62	3.44	2.38	-120

Unlike the radialene halide complexes it was found that there was no relationship between displacement of the polyatomic anions from the [3]radialene core and the interaction energy. This is a result of the different geometries of the polyatomic anions allowing for improved binding when they are in specific conformations. The trigonal planar geometry of the nitrate anion allows all of its atoms to have close contact with anion binding motifs. Each of the peripheral oxygen atoms is directed towards the acidic aryl hydrogens and the central nitrogen atom is directly above the electron deficient [3]radialene core. These combined hydrogen bonding and anion-π interactions provide the **2.29**-NO_3^- complex with the greatest binding energy even though it does not have the shortest anion-radialene contact.

The tetrahedral geometry of both the perchlorate and tetrafluoroborate anions allows three of the peripheral atoms to form anion hydrogen bonds with the aryl hydrogen atoms; however the fourth is directed into space. A similar scenario is observed for the octahedral hexafluorophosphate anion where three of its six fluorine atoms are directed towards the [3]radialene core. The interaction energies follow the trend $NO_3^- > BF_4^- > PF_6^- \approx ClO_4^-$. Even though tetrafluoroborate and perchlorate are both tetrahedral, the size and electronegativity of the peripheral fluorine atoms of tetrafluoroborate compared to oxygen make for a stronger interaction. Thus hexafluorophosphate and perchlorate have similar interaction energies even though a higher proportion of the peripheral atoms in perchlorate are in contact with the radialene than in hexafluorophosphate.

5.3. Gas Phase Anion Interactions

5.3.1. Interaction of Hexakis(cyanophenyl)[3]radialenes and Monoatomic Anions

Negative ion, electrospray ionisation, high-resolution mass spectrometry (ESI-HRMS) was used to validate the computational results. Solution methods of determining binding constants, including ^{1}H NMR and UV-Vis titrations, were attempted but no quantitatively measurable effect was observed upon addition of the anions to the radialene solutions, using either technique. Titration of **2.29** with $(^{n}Bu)_4NF$ in CD_3CN followed by ^{1}H NMR spectroscopy showed no change in chemical shift of the radialene aryl peaks, however the peaks decreased in intensity as the amount of $(^{n}Bu)_4NF$ increased (Figure 5.15). A significant decrease was observed between 0.8 and 1 equivalent of $(^{n}Bu)_4NF$ and by 1.4 equivalents the radialene aryl peaks had vanished. This was due to precipitation which gave qualitative evidence of an interaction between **2.29** and the fluoride anions. Titration of **2.29** with $(^{n}Bu)_4NCl$ in deuterated acetonitrile did not result in precipitation and no shift in the radialene aryl peaks was seen up to 100 equivalents of $(^{n}Bu)_4NCl$. This demonstrated that if there were interactions between **2.29** and the chloride anions they were very weak and unable to be observed in an environment where there were competitive solvent interactions.

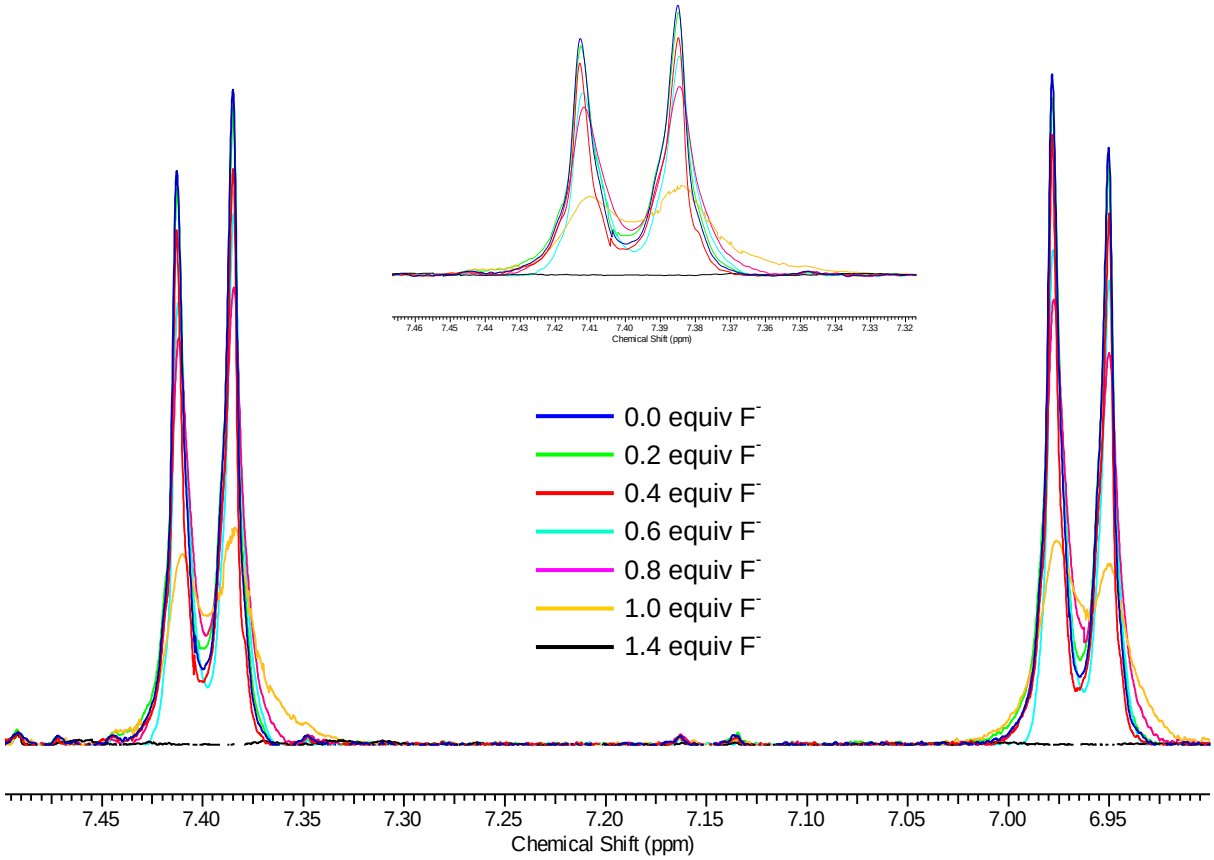

Figure 5.15. Overlayed ^{1}H NMR spectra of **2.29** titrated with $(^{n}Bu)_4NF$ in CD_3CN.

Titration of **2.29** with (^{n}Bu)$_4$NF, (^{n}Bu)$_4$NCl and (^{n}Bu)$_4$NBr in dichloromethane followed by UV-Vis spectroscopy showed a gradual increase in the absorption maxima for **2.29** as the amount of anion added was increased. However, upon plotting the change in absorption versus the number of equivalents of anion present the characteristic sigmoidal curve, representative of significant interactions, was not observed and therefore binding constants could not be determined. This result once again indicated the weakness of these interactions.

Mass spectrometry has an advantage over solution based techniques in the study of weak non-covalent interactions,[57-62] such as the anion-π and anion hydrogen bonding interactions predicted here, due to the removal of solvent effects. Solutions of hexaaryl[3]radialenes **2.38**, **2.29** and **2.44** were prepared with the following anion salts, (^{n}Bu)$_4$NF, (^{n}Bu)$_4$NCl and (^{n}Bu)$_4$NBr in 1:100 ratios. The chloride and bromide complexes were able to be detected in ratios of 1:1, however due to the difficulty in desolvation of the fluoride anion it required a large amount of the anion to be present in order to observe the complex. In order to maintain consistency a high ratio was used across all solutions.

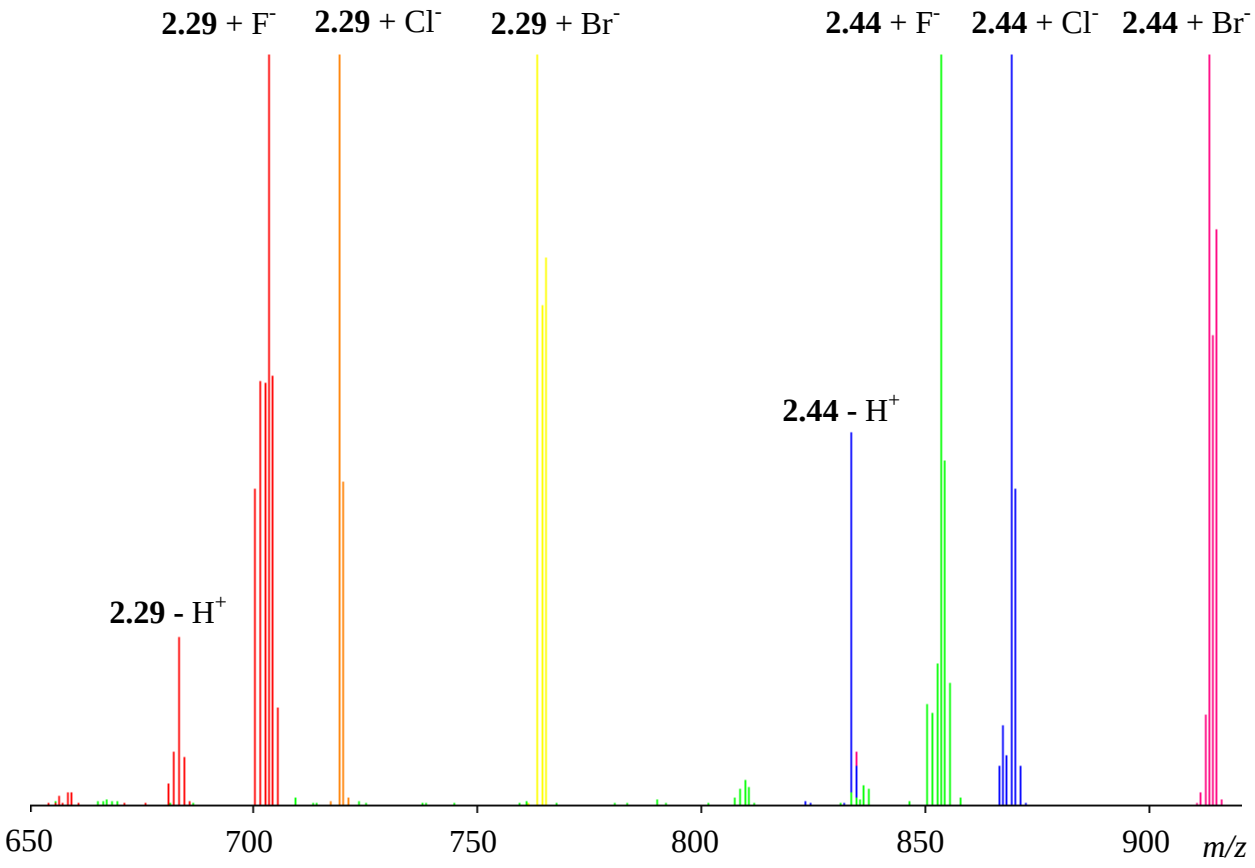

Figure 5.16. Overlaid MS/MS spectra of the fragmentation of halide complexes of [3]radialenes **2.29** and **2.44**.

The solvent was chosen carefully as the radialenes are soluble in methanol and other protic solvents, which could competitively interact with the anions leading to difficulty in desolvation. In order to prevent such problems, acetonitrile was used as the solvent because it is aprotic, easily solubilises all components, and is compatible with the instrumentation. Complexes of **2.38**, **2.29** and **2.44** with each of the halides F^-, Cl^-, and Br^- were detected in the gas phase, mass selected and further examined. Figure 5.16 shows the overlaid MS/MS spectra of the halide complexes of **2.29** and **2.44**.

Each of the halide-radialene complexes is observed to produce the deprotonated molecular ion upon fragmentation. This is due to the complex losing the acid form of the halide conjugate base. The stability of the complexes was examined via comparison of the signal intensities for a particular ion as the normalised collision energy (NCE) was increased incrementally relative to the signal intensity observed at an NCE of zero. This method of comparing intensities at different NCE values is only a qualitative measure; however it has been used previously to infer the stability of other complexes.[63] Naturally, the radialene-halide complexes fragment at a much lower NCE than the radialene molecules themselves as a result of the weaker non-covalent forces that are involved. Table 5.5 summarises the NCE values required to reduce intensity of a particular ion to less than 50% of the intensity of that ion at an NCE of zero.

Table 5.5. Average normalised collision energies (NCE) required to reduce the intensity of a peak for a particular ion below the intensity observed for that peak at an NCE value of 0. All values quoted are an average of 10 scans.

Compound	NCE at which intensity is 50% of intensity of peak at NCE = 0		
	2.38	**2.29**	**2.44**
Radialene	15	22	26
Radialene-F	4	4	10
Radialene-Cl	3	3	3
Radialene-Br	4	4	4
Radialene-Cl-Radialene	2	2	6
Radialene-Br-Radialene	3	3	10

Comparison of the data shows that the radialene-halide complex stability for the most electron deficient [3]radialene, **2.44**, follows a trend where $F^- > Cl^- \approx Br^-$. This is less apparent for hexaaryl[3]radialenes **2.29** and **2.38**. Due to the lack of resolution in incremental increases

of the NCE, the difference between the stability of the chloride and bromide complexes was unable to be determined. The fluoride complexes of all radialenes studied were found to have a lower initial signal intensity (ion counts in the order of 10^4) compared to the chloride and bromide complexes (ion counts in the order of 10^5). This is expected owing to the difficulties associated with the desolvation of fluoride.[64] Conversely, radialene-chloride complexes were easily detected because of the ubiquity of chloride in the environment and its relative ease of desolvation. In fact, chloride complexes were observed in all solutions tested.

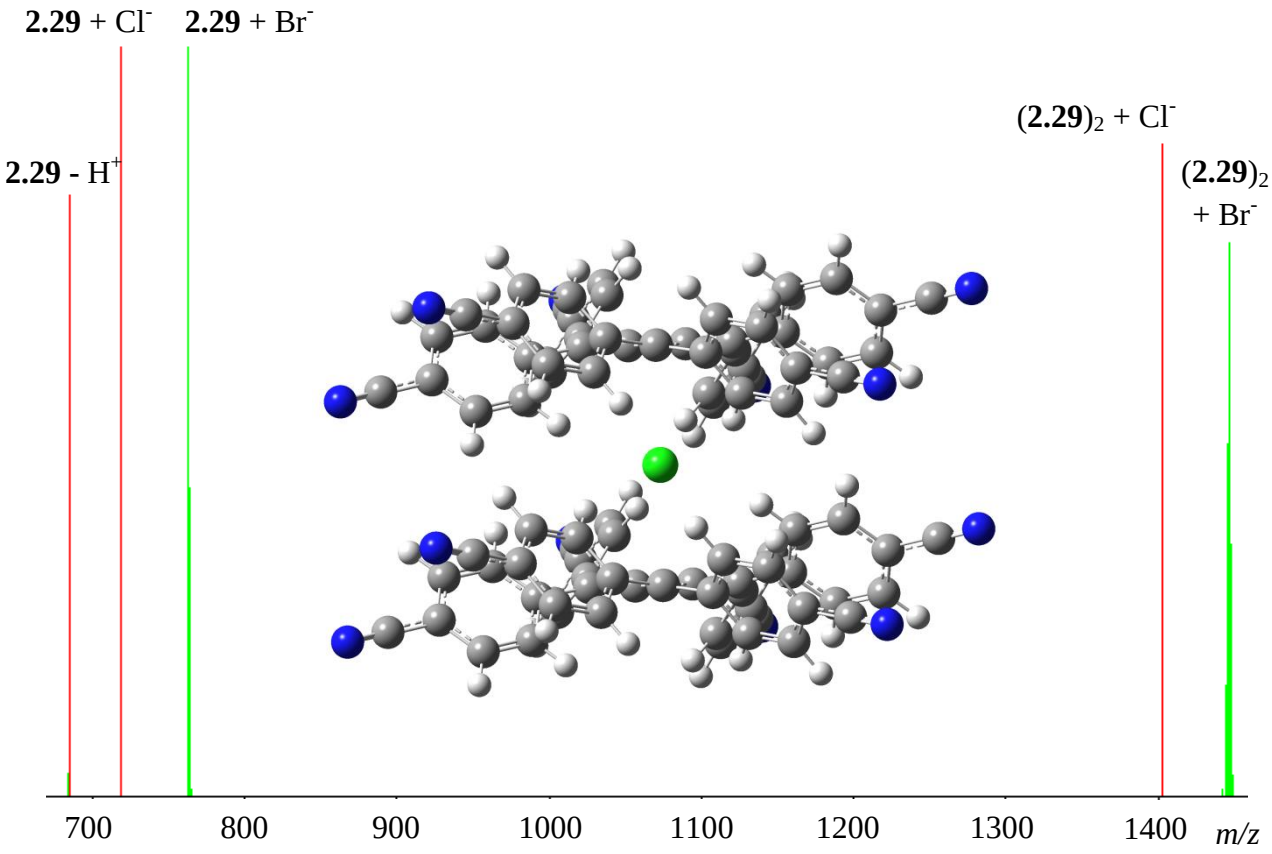

Figure 5.17. Overlaid MS/MS spectra of the fragmentation of sandwich halide complexes (**2.29**)$_2$ + Cl^- and (**2.29**)$_2$ + Br^- and a molecular model of their assumed conformation.

Determining a trend in stability for the different hexaaryl[3]radialene compounds proved difficult. However, the fluoride complexes of radialene **2.44** were significantly more stable than those of radialenes **2.38** and **2.29**. Complexes of **2.38** and **2.29** were found to be of similar stability across the board. This is expected due to an amount of conformer **2.38b** in the population of **2.38**, which may bind to the halides through stronger ion-dipole interactions. Another interesting observation was the appearance of radialene-halide-radialene sandwich complexes in the solutions containing chloride and bromide (Figure 5.17). Each of the dimer complexes were observed to fragment into the monomer complex and also the deprotonated

molecular ion. These complexes appeared to be slightly less stable than the monomers for radialenes **2.38** and **2.29** (Table 5.5). However, the dimer complexes of **2.44** seemed to be more stable than the corresponding monomer complexes (Table 5.5). This may be a result of the increased electron deficiency of the radialene core and acidity of the hydrogen atoms *ortho* and *para* to the nitrile groups.

In summary, negative ion, electrospray ionisation, high-resolution mass spectrometry (ESI-HRMS) of solutions of the radialenes and halide salts has been able to provide physical evidence for each of the complexes predicted by the theoretical calculations. Examination of the strength of each of these complexes involving [3]radialene **2.44**, via changing the normalised collision energy during MS/MS experiments, has shown that the relative stability follows that of the trend predicted. A similar trend in the halide complexes with radialenes **2.29** and **2.38** was expected but unable to be observed due to the lack of resolution in incremental increases of the NCE.

5.3.2. Interaction of Hexakis(cyanophenyl)[3]radialenes and Polyatomic Anions

In an analogous fashion to that described in section 5.3.1, negative ion ESI-HRMS was used to examine complexes of radialenes **2.38**, **2.29** and **2.44** with the polyatomic anions nitrate, tetrafluoroborate and hexafluorophosphate. Figure 5.18 shows the overlaid MS/MS spectra of the polyatomic anion complexes of **2.29** and **2.44**. Each of the polyatomic anion-radialene complexes predicted by the theoretical calculations was observed in the mass spectrum. The polyatomic anion complexes can be seen to produce the molecular ion upon fragmentation unlike the halide-radialene complexes, which produce the deprotonated molecular ion. This is because the softer polyatomic anions are unable to strip a proton from the [3]radialene compounds, whereas the harder halide anions can.[65-67]

As discussed above, the relative stability of each of the complexes was examined via investigating the change in intensity of the peaks as the NCE was increased (Table 5.6). Comparison of Table 5.6 to Table 5.5 shows that the NCE for the radialene compounds, at which the intensity of the peaks is less than 50% of the initial intensity when the NCE is zero, is fairly consistent across the different experiments. Upon further examination of the data it can be seen that the polyatomic anion-radialene complexes of **2.29** follow the stability trend of $NO_3^- > BF_4^- \approx PF_6^-$ as predicted by the theoretical calculations. However, the trends for the other two radialenes, **2.38** and **2.44**, are not as clear. The three polyatomic anion complexes of **2.38** all appear to have a similar stability, even though it would be assumed that the nitrate complex would be the most stable following the trend predicted for radialene **2.29**. It is also noted that the NCE values for the polyatomic anion complexes of **2.29** are greater than the

NCE values for the halide complexes. This contradicts the computational predictions however it may be a result of the polyatomic anions ability to be involved in multi-point interactions.

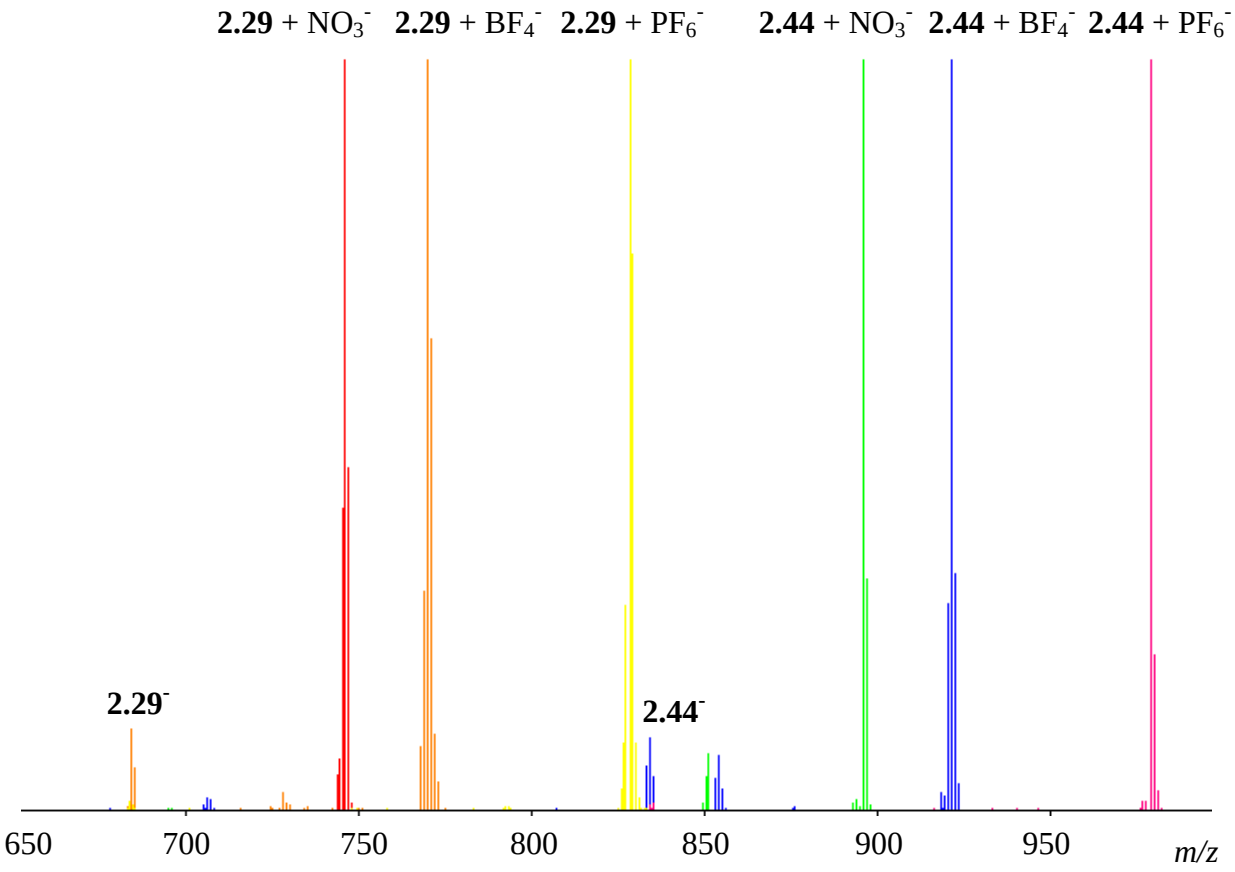

Figure 5.18. Overlaid MS/MS spectra of the fragmentation of polyatomic anion complexes of [3]radialenes **2.29** and **2.44**.

Table 5.6. Average normalised collision energies (NCE) required to reduce the intensity of a peak for a particular ion below the intensity observed for that peak at an NCE value of 0. All values quoted are an average of 10 scans.

Compound	NCE at which intensity is 50% of intensity of peak at NCE = 0		
	2.38	**2.29**	**2.44**
Radialene	15	21	23
Radialene-NO_3	7	10	10
Radialene-BF_4	6	7	16
Radialene-PF_6	5	6	15
Radialene-NO_3-Radialene	7	6	14
Radialene-BF_4-Radialene	10	5	13
Radialene-PF_6-Radialene	8	*	12

* Initial ion count for complex at NCE = 0 was too low to give an accurate measurement

For radialene **2.44** it appears that the complexes with tetrafluoroborate and hexafluorophosphate are more stable than the nitrate complex. As the interaction energies for these complexes have not been calculated we are unable to compare them to the expected trend. The geometries of each of these complexes would be assumed to be consistent with those of **2.29** with polyatomic anions. As such, three of the peripheral atoms of each anion should be able to contact the acidic aryl hydrogen atoms of the radialene. As fluorine is more electronegative than oxygen it is possible that the higher stability is a result of stronger anion-hydrogen bonding interactions with the more acidic hydrogen atoms of **2.44**. In comparision to the halide complexes of **2.44** it appears that the multi-point interactions of the polyatomic anions yield more stable complexes. A trend between the stability of the different radialene complexes of **2.44** > **2.29** ≈ **2.38** is evident, which can once again be explained by the greater electron deficiency of radialene **2.44** and also a certain amount of the **2.38b** conformer being present in solution making the complexes of **2.38** appear equally as stable as those of **2.29** even though it is not as electron deficient. Once again sandwich-like dimer complexes of each of the radialene compounds with the polyatomic anions are observed (Figure 5.19). A similar trend of **2.44** > **2.29** ≈ **2.38** can be observed for the stability of these dimer complexes.

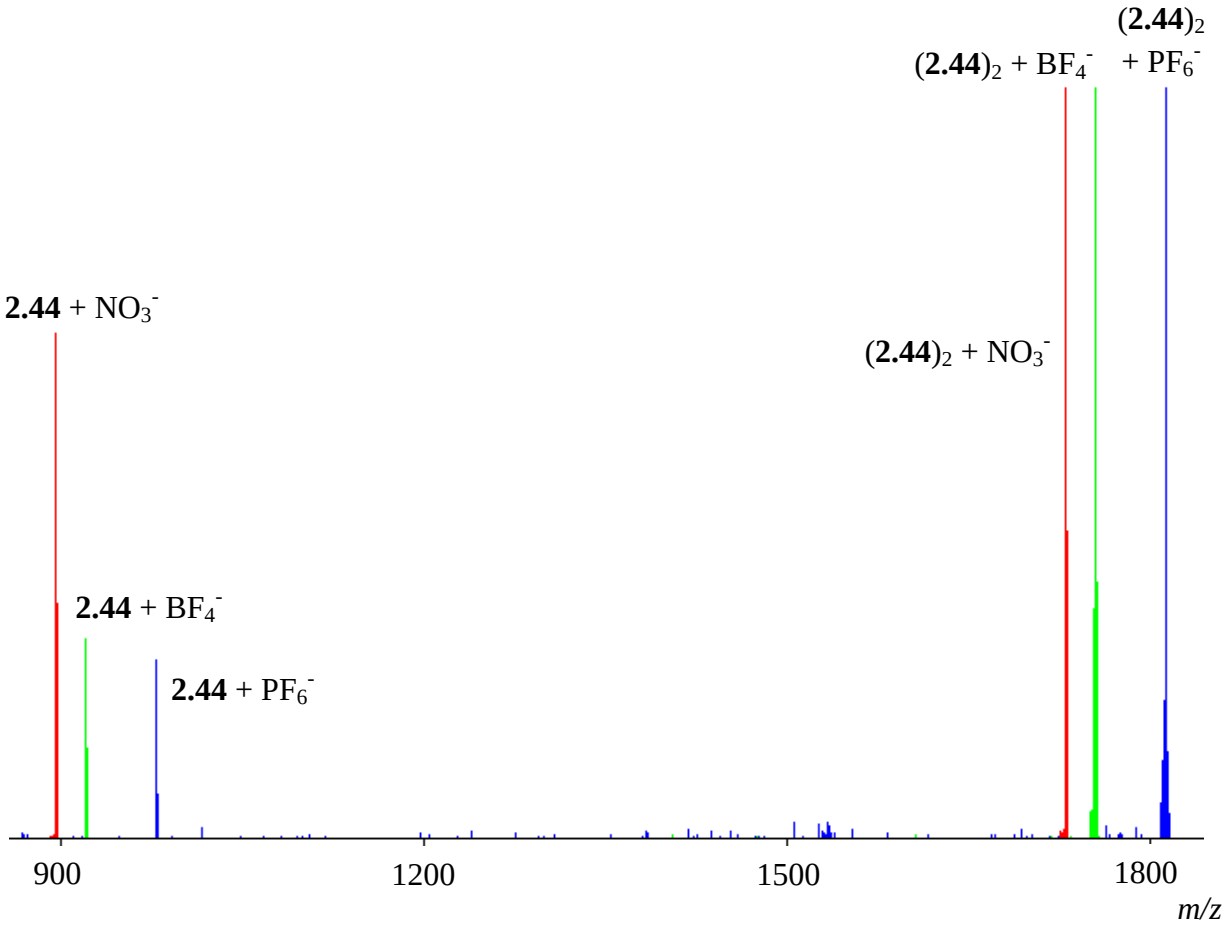

Figure 5.19. Overlaid MS/MS spectra of the fragmentation of sandwich anion complexes (**2.44**)$_2$ + NO_3^-, (**2.44**)$_2$ + BF_4^- and (**2.44**)$_2$ + PF_6^-.

5.4. Solid-State Anion Interactions

*5.4.1 Silver(I) Coordination Polymers of Hexakis(4-cyanophenyl)[3]radialene (**2.29**)*

Of the five coordination polymers of hexakis(4-cyanophenyl)[3]radialene, **2.29**, with silver(I) described in chapter 4, four of them display close contacts with anions. The structures of these complexes, **4.5**, **4.6**, **4.7**, and **4.8**, are 2-D (6,3) networks and they are isomorphous. The only difference between them is the identity of the anion included in the structure. Two of these structures, **4.5** and **4.6**, were located in the CSD search described in section 5.1.2. As previously mentioned, these 2-D (6,3) sheets pack in the extended crystalline lattice in discrete layers which adopt an AB repeating structure (Figure 5.20). The first layer A, shown coloured blue, is followed by layer B, shown in green, which has its [3]radialene units in the opposite orientation, related by a centre of inversion to those of A and is also offset so that its [3]radialene units do not reside directly below those of A. The anions reside between the layers both above and below the [3]radialene core of each ligand in the structure.

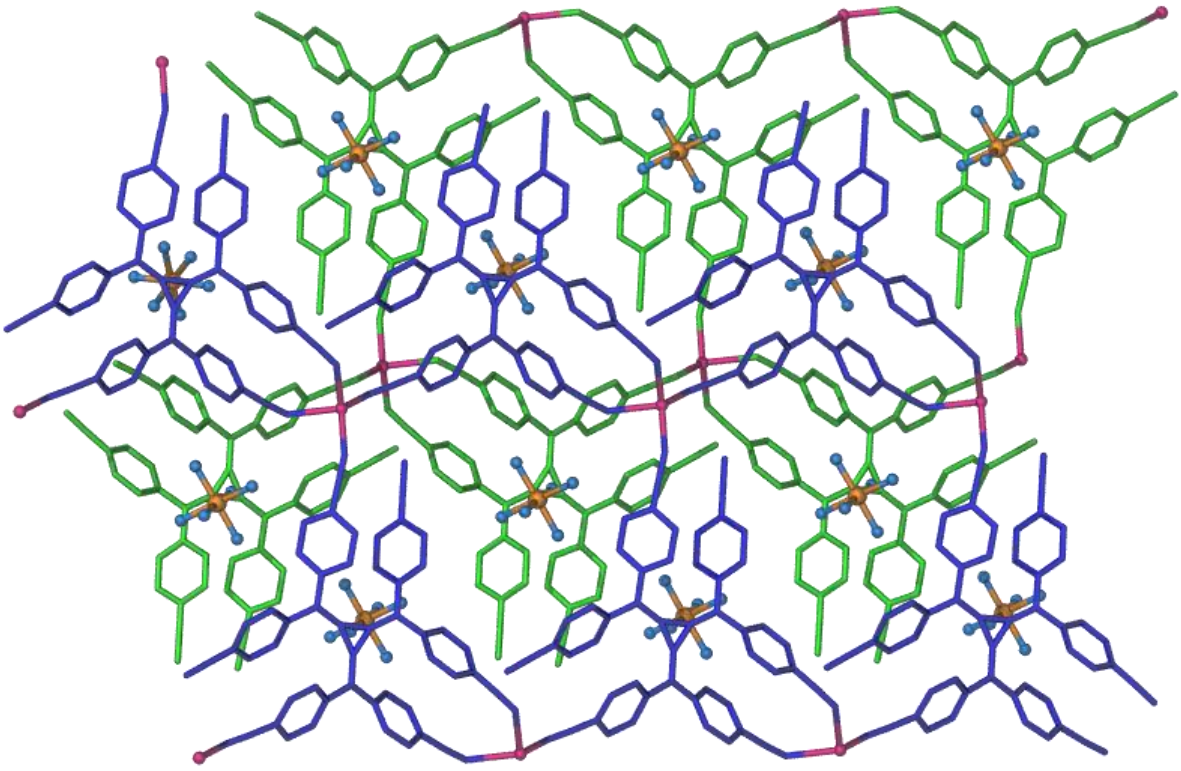

Figure 5.20. A perspective view of two layers of **4.8** showing the crystal packing and the location of the hexafluoroantimonate anion sites in the crystal lattice. Layer A is coloured blue and layer B is shown in green. Nitromethane solvate molecules, hydrogen atoms, and the disorder of the silver(I) atoms and anions have been removed for clarity.

In structure **4.5**, the perchlorate anion lies almost directly over the [3]radialene core (Figure 5.21). The four radialene ligands surrounding the anion generate a cavity which is suitable for an octahedral anion and for this reason the tetrahedral perchlorate anion is disordered over two orientations within the cavity. The shortest contacts between the anion and the ligand are through a number of weak phenyl C-H···O_{anion} hydrogen bonding interactions; this is due to the phenyl protons sitting above and below the plane of the radialene and may prevent the anion from residing closer to the [3]radialene core.

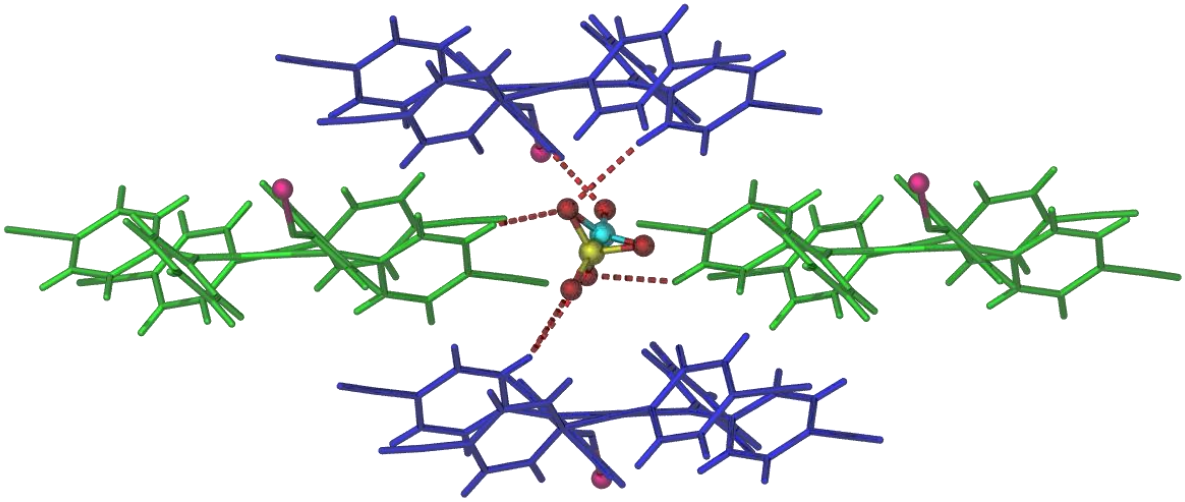

Figure 5.21. A perspective view of the packing of complex **4.5** showing the disordered perchlorate anion in its hydrogen bonding donor pocket. Both disorder components of the perchlorate anion are shown; the chlorine atom of the dominant component is shown in yellow while the minor component is shown in cyan. Radialene phenyl C-H···O_{anion} hydrogen bonds are shown as dashed lines.

The shortest hydrogen bonds involving the two sites occupied by the perchlorate anion are with the radialene ligand situated above the anion in layer A, with C-H···O_{anion} distances of 2.47 and 2.84 Å. The perchlorate anion also forms hydrogen bonds with the radialene ligand situated directly below it in layer A2, with C-H···O_{anion} distances of 2.74 and 2.79 Å. Finally the disordered perchlorate anion interacts with two adjacent radialene ligands, which lie in the same plane as the anion itself, in layer B, with C-H···O_{anion} hydrogen bonding distances of 2.68 and 2.86 Å, respectively.

In this structure, the closest radialene centroid anion distance is 3.35 Å, which occurs between the perchlorate anion (an oxygen atom) and the radialene situated in layer A. The closest radialene core π···O_{anion} distances to the same ligand are 3.41 Å to a ring carbon and 3.61 Å to an exocyclic carbon, respectively. The angles between the centroid of the major

disorder component of the anion and the [3]radialene core plane are 80.41, 93.79 and 95.55°. The major component of the disorder is positioned more perpendicular to the core centroid than the minor component, which displays angles in the range of 74.23-97.96°. These close radialene core-anion contacts provide evidence for the existence of anion-π interactions within this system; however similar to the structure of **4.3**, described in section 5.1.2, the perchlorate anion in complex **4.5** does not display the expected geometry as only one oxygen atom is directed towards the core of the [3]radialene as opposed to three.

In a similar fashion to that observed in structure **4.5**, in complex **4.6** the hexafluorophosphate anions sit almost directly on top of the [3]radialene core (Figure 5.22). The closest contact between the hexafluorophosphate anion and the ligand is through phenyl C-H···F_{anion} hydrogen bonding interactions, due to the propeller configuration of the radialene. The hexafluorophosphate anion forms weak hydrogen bonds with four separate ligand molecules. As previously mentioned, the 2-D coordination polymer and crystal packing generates a cavity, suitable for binding octahedral anions, from these four radialene ligands.

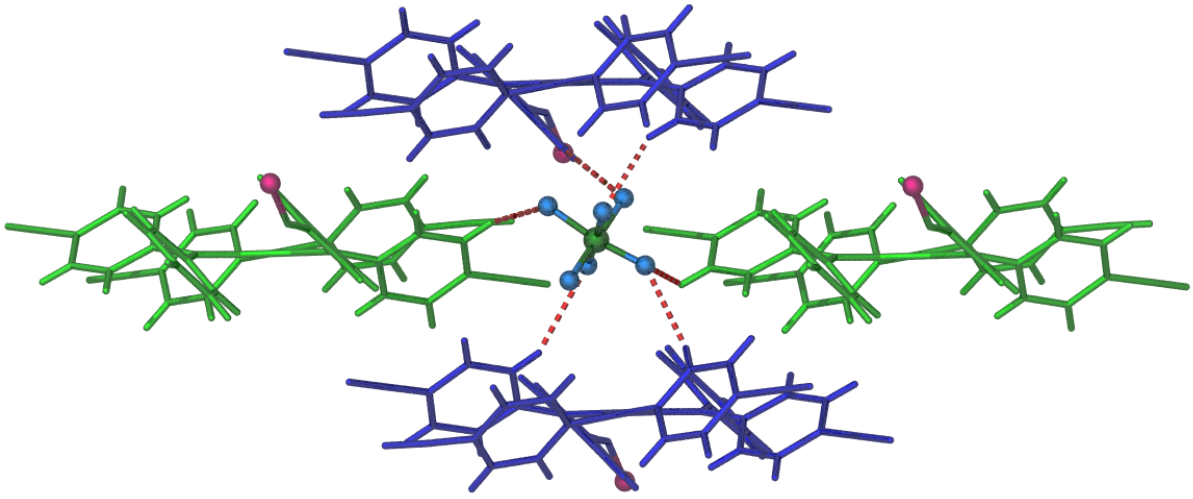

Figure 5.22. A perspective view of the packing of compound **4.6** showing the binding cavity in which the hexafluorophosphate anion is located. Radialene phenyl C-H···F_{anion} hydrogen bonds are shown as dashed lines.

The three fluorine atoms on one face of the hexafluorophosphate anion form two weak phenyl C-H···F_{anion} hydrogen bond interactions, with distances of 2.44 and 2.83 Å, involving the radialene directly above the anion, in layer A. The three fluorine atoms of the opposite face of the anion form two additional weak hydrogen bonds, with distances of 2.60 and 2.80 Å, in layer A2, as well as two further interactions with the two radialene ligands adjacent to the anion, in layer B, with distances of 2.37 and 2.74 Å. The [3]radialene centroid···F_{anion}

distance is 3.47 Å, although the shortest [3]radialene $\pi\cdots F_{anion}$ distances involving the same ligand are 3.26 Å to an exocyclic carbon of the [3]radialene core and 3.37 Å to a ring carbon, respectively. In complex **4.6** the octahedral hexafluorophosphate anion sits comfortably within the binding cavity formed by the four radialene ligands and can easily maintain the six weak C-H$\cdots F_{anion}$ hydrogen bonds.

The angles between the centroid of the hexafluorophosphate anion and the [3]radialene core plane are all within 90 ± 10° at 81.03, 93.07 and 95.86° respectively. Unlike structure **4.5**, the position of the anion in **4.6** closely mirrors the expected geometry with three fluorine atoms directed towards the [3]radialene core and three directed away. The closest radialene core carbon to fluorine atom distance in the optimised structure of **2.29** with hexafluorophosphate is 3.44 Å. This correlates well with the radialene core carbon-anion distances in **4.6** observed for the three fluorine atoms directed towards the core of 3.37, 3.41 and 3.77 Å. Two of these distances are slightly outside the $\sum_{vdw}$ + 0.2 Å (3.37 Å); however closer contacts are observed with exocyclic carbons of the [3]radialene core (3.26 and 3.73 Å). It is worth noting that the [3]radialene core is a cross-conjugated π-system; the π-orbitals are localised in the exocyclic double bonds and not extensively delocalised over the central cyclopropane ring of the [3]radialene.[68]

The tetrahedral tetrafluoroborate anion in structure **4.7** is disordered over two positions like that of the tetrahedral perchlorate anion in complex **4.5**. This is due to the anion residing in a binding pocket which is better suited for octahedral anions. The tetrafluoroborate anion forms six weak C-H$\cdots F_{anion}$ hydrogen bonds with the four radialene ligands surrounding it (Figure 5.23). The anion forms two hydrogen bonds with the radialene ligand directly below it, in layer A, with C-H$\cdots F_{anion}$ distances of 2.59 and 2.61 Å. Two more hydrogen bonding interactions are observed between the anion and the ligand above it, in layer A2, with C-H$\cdots F_{anion}$ distances of 2.49 and 2.76 Å. Lastly, the disordered tetrafluoroborate anion is also involved in hydrogen bonding interactions with the two [3]radialene ligands adjacent to it, in layer B, with C-H$\cdots F_{anion}$ distances of 2.57 and 2.64 Å respectively.

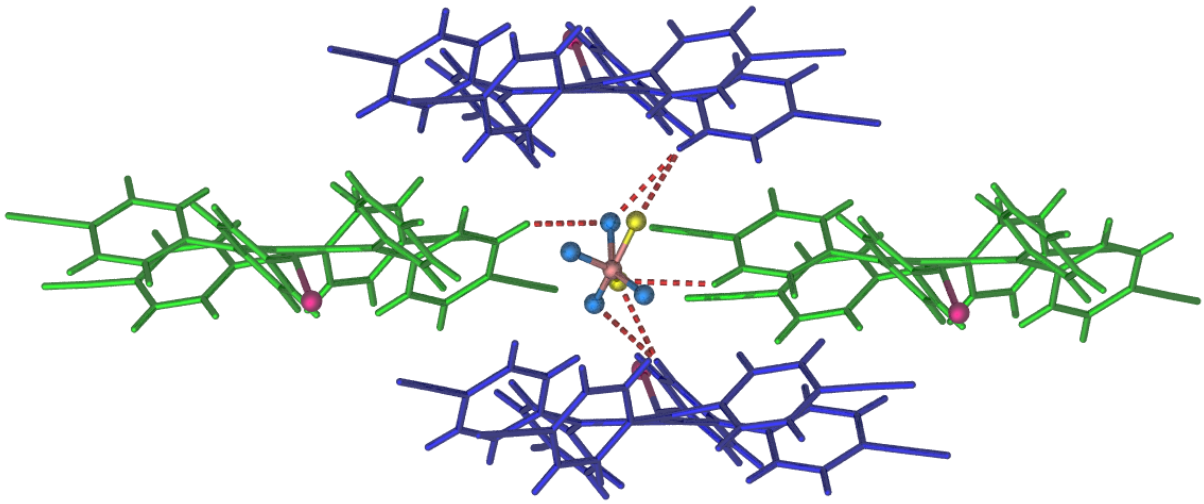

Figure 5.23. A perspective view of the packing of complex **4.7** showing the disordered tetrafluoroborate anion in its hydrogen bonding donor pocket. Both disorder components of the tetrafluoroborate anion are shown; the fluorine atoms of the minor component are shown in yellow. Radialene phenyl C-H···F_{anion} hydrogen bonds are shown as dashed lines.

In structure **4.7** the closest radialene centroid anion distance is 3.42 Å, which occurs between the tetrafluoroborate anion (a fluorine atom) and the radialene situated in layer A. This is slightly outside the $\sum_{vdw}$ + 0.2 Å (3.37 Å) although the closest radialene core $\pi\cdots F_{anion}$ distances to the same ligand are 3.45 Å to a ring carbon and 3.34 Å to an exocyclic carbon, respectively. As previously mentioned, the π-system of the [3]radialene core is localised along the exocyclic double bonds and not delocalised around the core. The angles between the centroid of the anion and the [3]radialene core plane are 74.04, 97.69 and 98.03°, which are outside of the desired range of 90 ± 10°. This shows that the tetrafluoroborate anion is not sitting directly over the core of the [3]radialene. The geometry of the anion is also not as expected with only one peripheral fluorine atom directed toward the core instead of three, similar to complex **4.5**. In this structure it appears that the anion hydrogen bonds are the primary interactions with the radialene ligands as opposed to anion-π interactions.

The final silver(I) coordination polymer of **2.29** that displays close anion-radialene contacts is **4.8**, which includes a hexafluoroantimonate anion. Like structures **4.5** and **4.7**, the anion in **4.8** is disordered over two positions (Figure 5.24). This is of interest as the other structure containing an octahedral anion, **4.6**, does not display any signs of anion disorder. It is possible that this is related to the size of the anion. The hexafluoroantimonate anion is larger than the hexafluorophosphate anion and so can be involved in a greater number of hydrogen bonding interactions, which may confer equal stability for the anion in two different positions. The refined occupancy of the two positions is not vastly different (*ca.* 65:35).

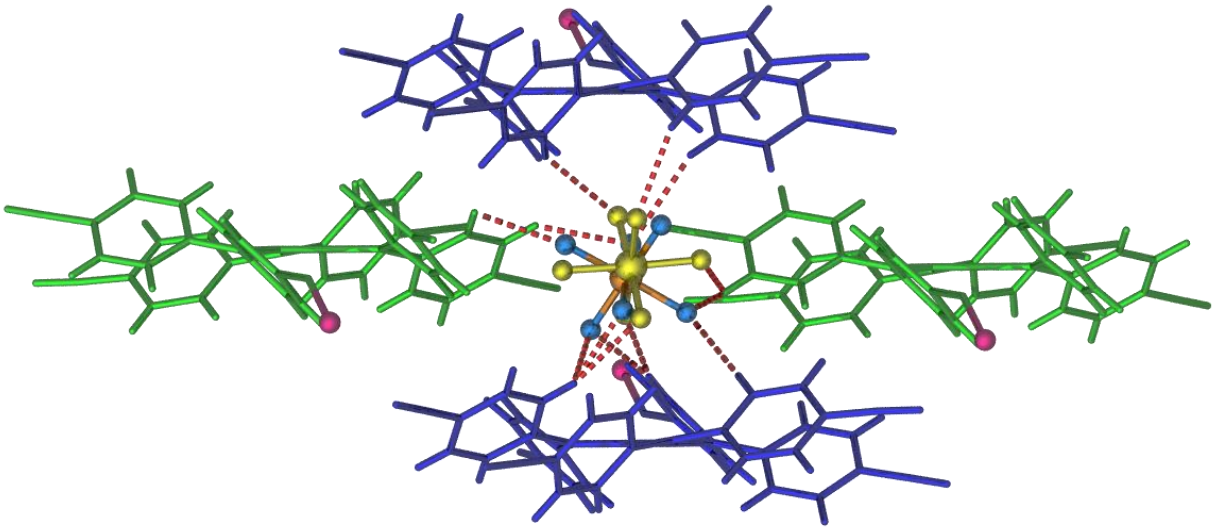

Figure 5.24. A perspective view of the packing of compound **4.8** showing the binding cavity in which the hexafluoroantimonate anion is located. Both disorder components of the tetrafluoroborate anion are shown; with the minor component shown in yellow. Radialene phenyl C-H···F_{anion} hydrogen bonds are shown as dashed lines.

Due to its larger size the hexafluoroantimonate anion exhibits thirteen hydrogen bonding interactions with the four radialene ligands surrounding it in the structure. The closest and most numerous of these interactions involves the radialene ligand directly below the anion, in layer A. Five anion hydrogen bonding interactions with C-H···F_{anion} distances in the range of 2.35-2.84° can be observed. Three hydrogen bonds between the anion and the radialene ligand above it, in layer A2, with C-H···F_{anion} distances of 2.61, 2.74, and 2.86 Å are also present. Four hydrogen bonds between the anion and the adjacent radialene ligands, in layer B, with C-H···F_{anion} distances between 2.67 and 2.86 Å can also be seen in Figure 5.24.

As in previous structures, the hexafluoroantimonate anion sits almost directly over the core of the radialene ligand. Considering the major component of the disordered anion, the closest radialene centroid anion distance is 3.55 Å which occurs between the hexafluroantimonate anion (a fluorine atom) and the radialene situated in layer A. Similar to previous structures with anions containing fluorine, **4.6** and **4.7**, this is slightly outside the limit of the Σ_{vdw} + 0.2 Å of carbon and fluorine (3.37 Å). Closer contacts are observed between the anion and the radialene core with π···F_{anion} distances to the same ligand of 3.21 Å to a ring carbon and 3.08 Å to an exocyclic carbon, respectively. These interactions are the closest so far observed between a fluorine atom of a polyatomic anion and the [3]radialene core.

The angles between the centroid of the major component of the disordered anion and the [3]radialene core plane are 81.48, 93.04, and 95.47° respectively. These are all within the range required for a significant anion-π interaction of 90 ± 10°. In addition to this the major component of the disordered anion is positioned in a geometry very similar to that which would be expected for an octahedral anion with three fluorine atoms directed towards the [3]radialene core and three directed away. As the geometry for **2.29** and a hexafluoroantimonate anion was not optimised it is assumed that the geometry will be similar to that observed for **2.29** and hexafluorophosphate. Table 5.7 summarises the close anion contacts in solid-state structures **4.5**-**4.8** and the distances calculated for the optimised geometries of **2.29** and polyatomic anions in the gas phase.

Table 5.7. Closest distances between the anion and the [3]radialene centroid ($R_{centroid}$, Å), closest distances between the anion and the radialene core ($R_{[3]radialene}$, Å), and closest distances between the anion and proximal hydrogen atoms (R_H, Å) for solid-state structures **4.5**-**4.8** and optimised polyatomic anion complexes of **2.29**.

Radialene 2.29		**Solid-State Structures**			**Optimised Gas Phase Geometries**		
Polymer	**Anion**	$\boldsymbol{R_{centroid}}$	$\boldsymbol{R_{[3]radialene}}$	$\boldsymbol{R_H}$	$\boldsymbol{R_{centroid}}$	$\boldsymbol{R_{[3]radialene}}$	$\boldsymbol{R_H}$
4.5	ClO_4^-	3.35	3.41	2.47	3.77	3.60	2.37
4.7	BF_4^-	3.42	3.34	2.49	3.61	3.44	2.28
4.6	PF_6^-	3.47	3.26	2.37	3.62	3.44	2.38
4.8	SbF_6^-	3.55	3.08	2.35			

It can be noted from Table 5.7 that the closest distances between the anion and the [3]radialene centroid and also the distances between the anion and the closest atom of the [3]radialene core are consistently shorter in the solid-state structures than in the gas phase complexes. Conversely, the hydrogen bond distances are slightly longer in the solid-state structures than in the gas phase complexes. This is likely due to the differing conformations of the anions in the case of the tetrahedral anions ClO_4^- and BF_4^- where one anion atom is directed towards the core, in the solid-state, instead of three, in the gas phase, which allows for a closer approach to the [3]radialene core. However, the octahedral anions PF_6^- and SbF_6^- exhibit similar geometries in the solid-state to those observed in the gas phase with three fluorine atoms directed towards the [3]radialene core and three directed away. In these cases the anion to closest atom of the [3]radialene core distances are especially short and this is likely due to the π-system of the [3]radialene being localised on the exocyclic double bonds and not delocalised around the core.

*5.4.2. Copper(I) Coordination Polymers of Hexakis(4-cyanophenyl)[3]radialene (**2.29**)*

Of the four copper(I) coordination polymers of hexakis(4-cyanophenyl)[3]radialene described in chapter 4, three of them display close contacts with anions. The first two structures, **4.10b** and **4.11b**, are isomorphous 4-connected 2-D coordination polymers. As previously mentioned, in the extended polymer structure each radialene ligand coordinates to four copper cations; with three of these cations it forms a (6,3) net motif, layer A, which is crosslinked by the fourth copper cation to a second (6,3) sheet, layer B, directly below it (Figure 5.25) to create an A-B bilayer. All the 3-connecting nodes are bridged to create a 4-connected 2-D net. Layer B, shown in green, has its [3]radialene units in the opposite orientation, related by a centre of inversion, to those of layer A, shown in blue, and is also offset so that its [3]radialene units do not reside directly below those of layer A. The bilayer, A-B, is then packed in the extended crystalline lattice in additional layers that adopt an A-B A-B repeating structure.

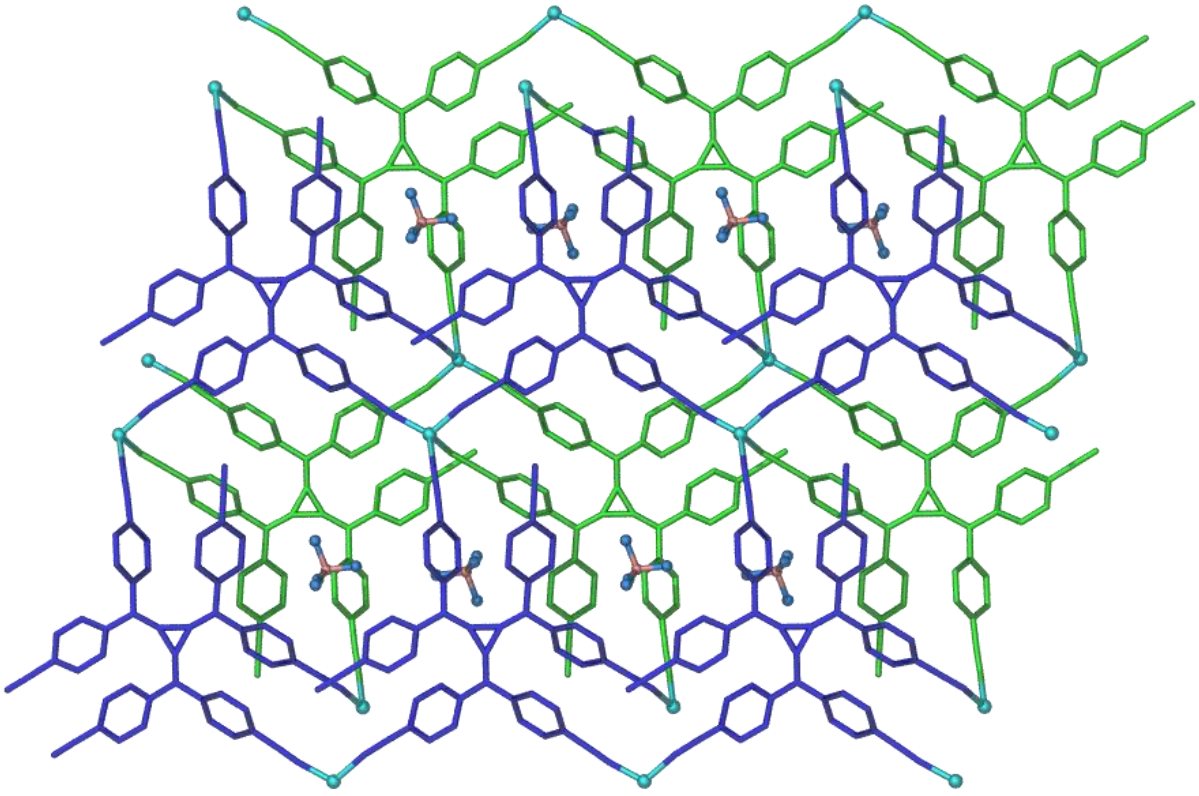

Figure 5.25. The 2-D layered packing of **4.10b** with layer A shown in blue and layer B shown in green. Nitromethane solvate molecules, hydrogen atoms, and the disorder of the anions have been removed for clarity.

The anions reside between the layers A and B but not directly above or below the [3]radialene core of **2.29**. Within the silver polymers, **4.5**-**4.8**, the anions sit almost directly above and below the anion core between 2-D polymer layers which are more separated than layers A and B in the copper polymers. This allows for a closer approach of the anions to the [3]radialene core, such that both radialene π-anion interactions and phenyl C-H···anion hydrogen bonds are observed. Within structure **4.10b** the tetrafluoroborate anion is disordered over two positions with an occupancy of *ca.* 63:37 (Figure 5.26). No short contacts with the [3]radialene core are observed however a number of anion hydrogen bonding interactions are present. The shortest interactions are those between the tetrafluoroborate anion and the radialene ligand directly below it in layer A of the A-B bilayer. There are three anion hydrogen bonds with C-H···F_{anion} distances of 2.35, 2.69 and 2.87 Å respectively. Two anion hydrogen bonds between the anion and the radialene directly above it, which is part of the next A-B bilayer, exhibit C-H···F_{anion} distances of 2.61 and 2.62 Å. Four interactions are also observed with the adjacent [3]radialene ligands with C-H···F_{anion} distances from 2.54-2.63 Å.

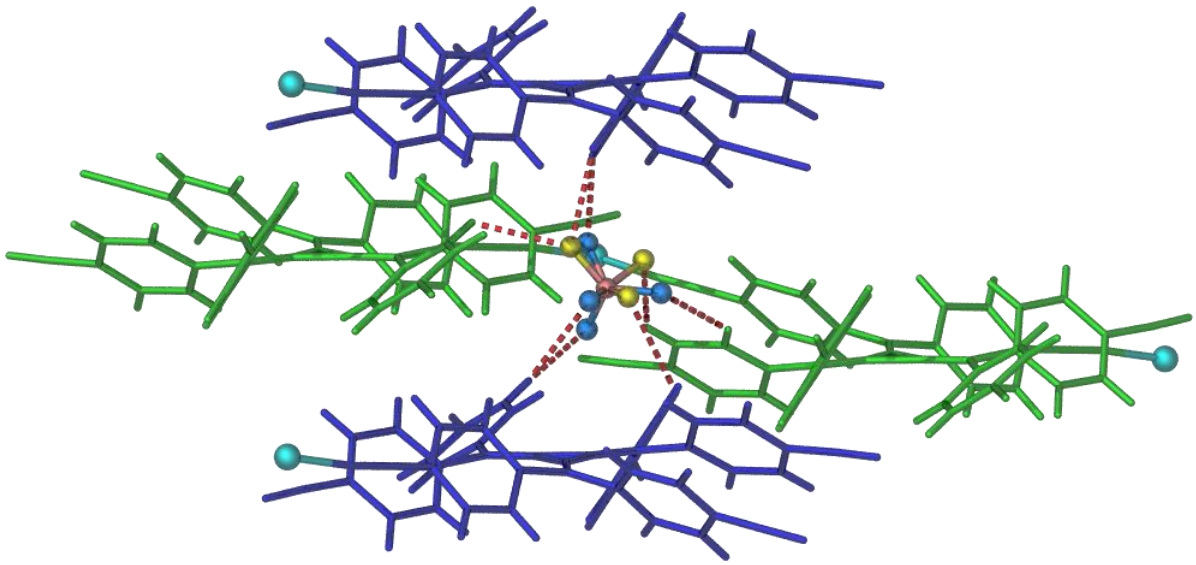

Figure 5.26. A perspective view of **4.10b** showing where the tetrafluoroborate anion resides within the polymer. The major component of the disordered tetrafluoroborate anion is shown in blue and the minor component in yellow. Radialene phenyl C-H···F_{anion} hydrogen bonds are shown as dashed lines.

Similar to structure **4.10b**, the hexafluorophosphate anion in complex **4.11b** does not reside directly above the [3]radialene core and as such no anion-π interactions are observed. However, a number of anion hydrogen bonding interactions are present between the anion and the four radialene ligands which surround it in the polymer (Figure 5.27). Within this

structure three hydrogen bonds are observed between the hexafluorophosphate anion and the radialene below it with C-H···F_{anion} distances of 2.68, 2.84, and 2.85 Å respectively. Another two weak hydrogen bonds are present between the anion and the radialene above it with C-H···F_{anion} distances of 2.37 and 2.80 Å. Finally, the hexafluorophosphate anion is involved in four hydrogen bonding interactions with the radialene ligands adjacent to it with C-H···F_{anion} distances ranging from 2.54-2.64 Å.

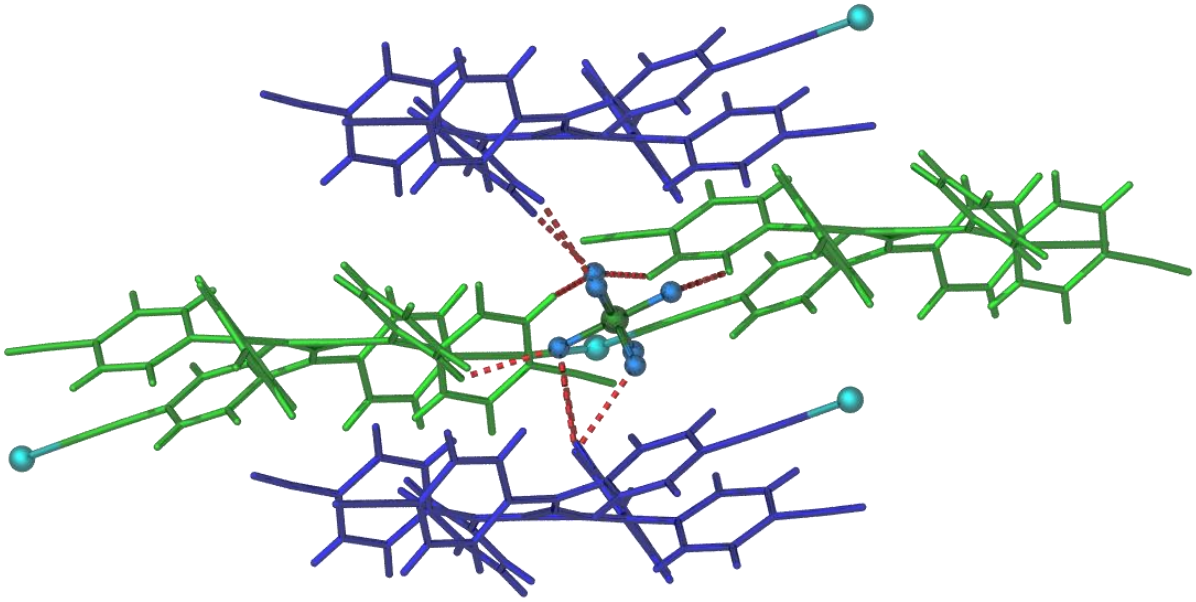

Figure 5.27. A perspective view of **4.11b** showing where the hexafluorophosphate anion resides within the polymer. Radialene phenyl C-H···F_{anion} hydrogen bonds are shown as dashed lines.

The last coordination polymer of copper(I) with [3]radialene **2.29** which displays close radialene anion contacts is that of structure **4.10a**. This structure containes a large number of disordered solvent molecules, however the anions were able to be located in the electron difference map. Structure **4.10a** is a complex 3-D coordination polymer within which the radialene ligand acts as a 3-connecting node and a pair of crystallographically unique copper(I) ions acts as a 6-connecting node; the overall network topology is $(4.6^2)(4^2.6)(4^3.6^6.8^6)$ as there are two inequivalent radialene nodes. This results in large pores which run along the *b*-axis of the structure and contain the disordered solvent molecules and also the anions (Figure 5.28). As such, the crystal packing precludes the approach of the anions towards the [3]radialene core.

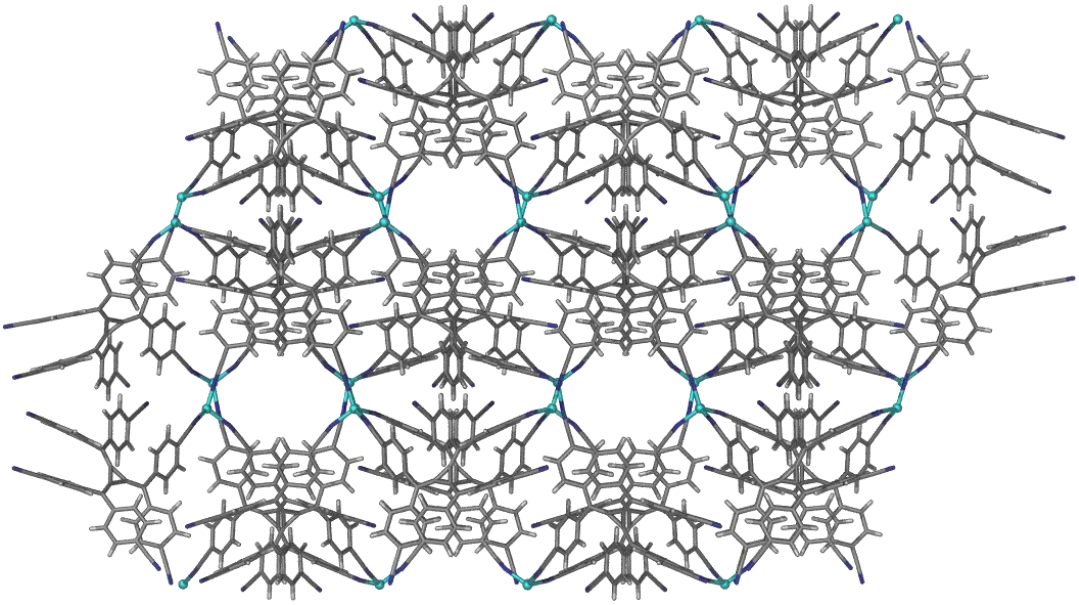

Figure 5.28. A stick representation of **4.10a** showing the channels parallel to the *b*-axis.

Within the asymmetric unit of **4.10a** there are three tetrafluoroborate atoms, two of which are 50% occupied. These anions are surrounded by five different radialene ligands within the structure and form interactions with four of these (Figure 5.29). Yet again no anion-π interactions are observed as the anions do not reside above the core of any of the [3]radialenes. Only a small number of radialene phenyl C-H···F_{anion} hydrogen bonds are seen for each of the tetrafluoroborate anions. This is because they face out into a channel through the polymer which is filled with disordered solvate molecules. The first anion exhibits three radialene phenyl C-H···F_{anion} hydrogen bonds with two different ligands with bond lengths of 2.43, 2.47 and 2.71 Å (Figure 5.29 (a)). The second anion has two hydrogen bonds to the same radialene ligand with C-H···F_{anion} distances of 2.46 and 2.85 Å (Figure 5.29 (b)). Whilst the third anion only has one significant anion hydrogen bond which has a C-H···F_{anion} distance of 2.64 Å (Figure 5.29 (c)). Unlike the silver(I) structures, the copper(I) coordination polymers have not shown any evidence of anion-π interactions.

Table 5.8 summarises the close anion contacts in solid-state structures **4.11a**, **4.11b** and **4.10a** and the distances calculated for the optimised geometries of **2.29** and polyatomic anions in the gas phase. As the anions in these structures were not localised directly above or below the [3]radialene core close contacts between the anions and the [3]radialene centroid or the atoms of the [3]radialene core were not observed. However, anion-hydrogen bonding interactions were observed and these correlate quite closely with the calculated geometries, especially for structures **4.11a** and **4.11b** where the anions are located in the vicinity of the [3]radialene core but slightly off centre. The anions in **4.10a** were located in large channels within the 3-D polymer and so exhibit longer anion-hydrogen bonding interactions.

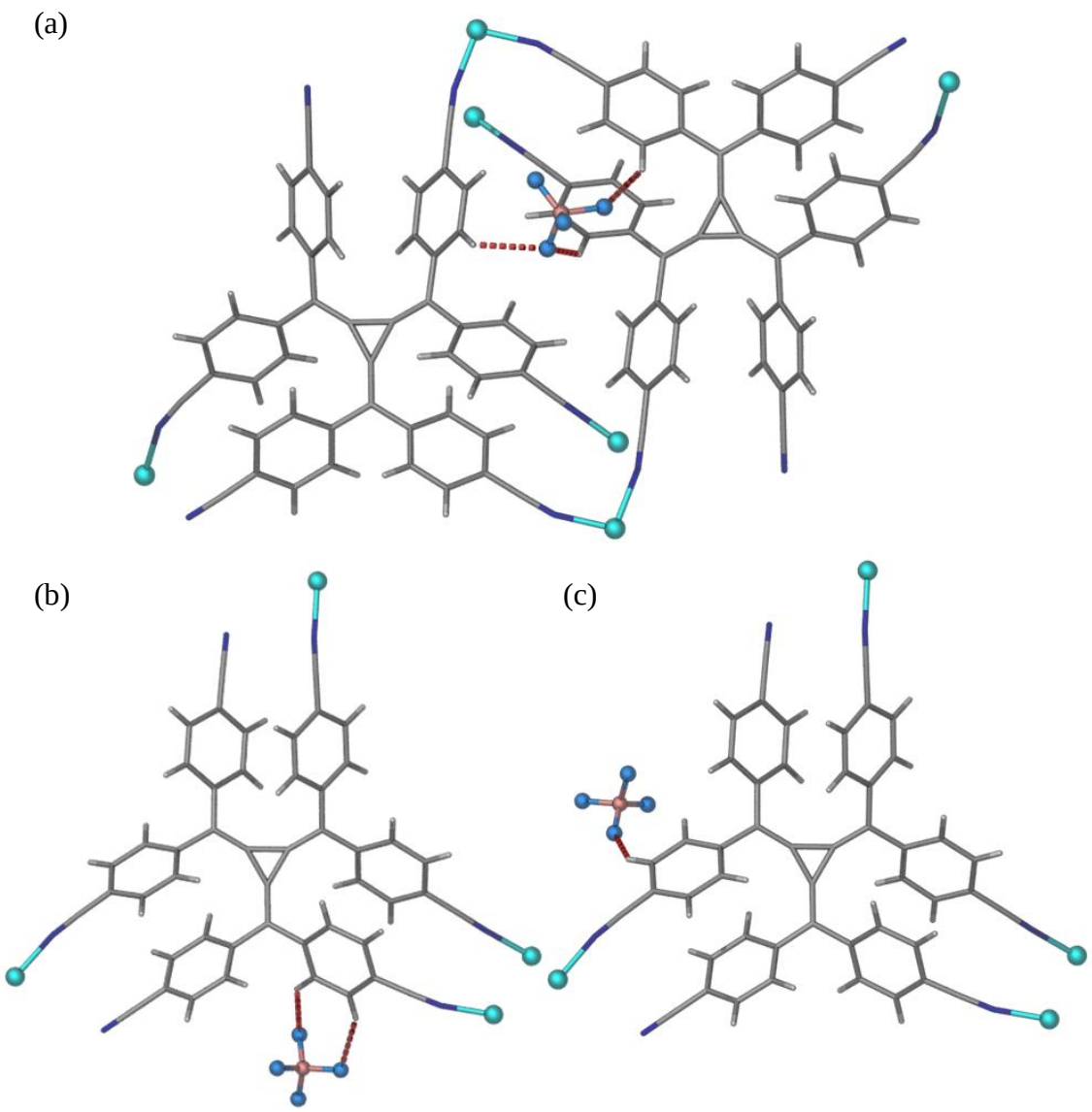

Figure 5.29. Three perspective views showing the environment around the (a) first, (b) second, and (c) third crystallographically unique tetrafluoroborate anions in structure **4.10a**. Radialene phenyl C-H···F_{anion} hydrogen bonds are shown as dashed lines.

Table 5.8. Closest distances between the anion and the [3]radialene centroid ($R_{centroid}$, Å), closest distances between the anion and the radialene core ($R_{[3]radialene}$, Å), and closest distances between the anion and proximal hydrogen atoms (R_H, Å) for solid-state structures **4.11a**, **4.11b** and **4.10a** and optimised polyatomic anion complexes of **2.29**.

Radialene 2.29		**Solid-State Structures**	**Optimised Gas Phase Geometries**		
Polymer	**Anion**	R_H	$R_{centroid}$	$R_{[3]radialene}$	R_H
4.11a	BF_4^-	2.35	3.61	3.44	2.28
4.11b	PF_6^-	2.37	3.62	3.44	2.38
4.10a	BF_4^-	2.43	3.61	3.44	2.28

*5.4.3. Copper(II) and Iron(II) Coordination Polymers of Hexakis(4-cyanophenyl)[3]radialene (**2.29**)*

The coordination polymers of [3]radialene **2.29** with copper(II) and iron(II), described in chapter 4, both exhibit close anion radialene contacts. The copper(II) complex, **4.8**, is a 1-D zigzag polymer which packs in simple layers in the extended structure (Figure 5.30). The hexafluorophosphate anions reside between the layers and are surrounded by four radialene ligands, two above and two below the anion.

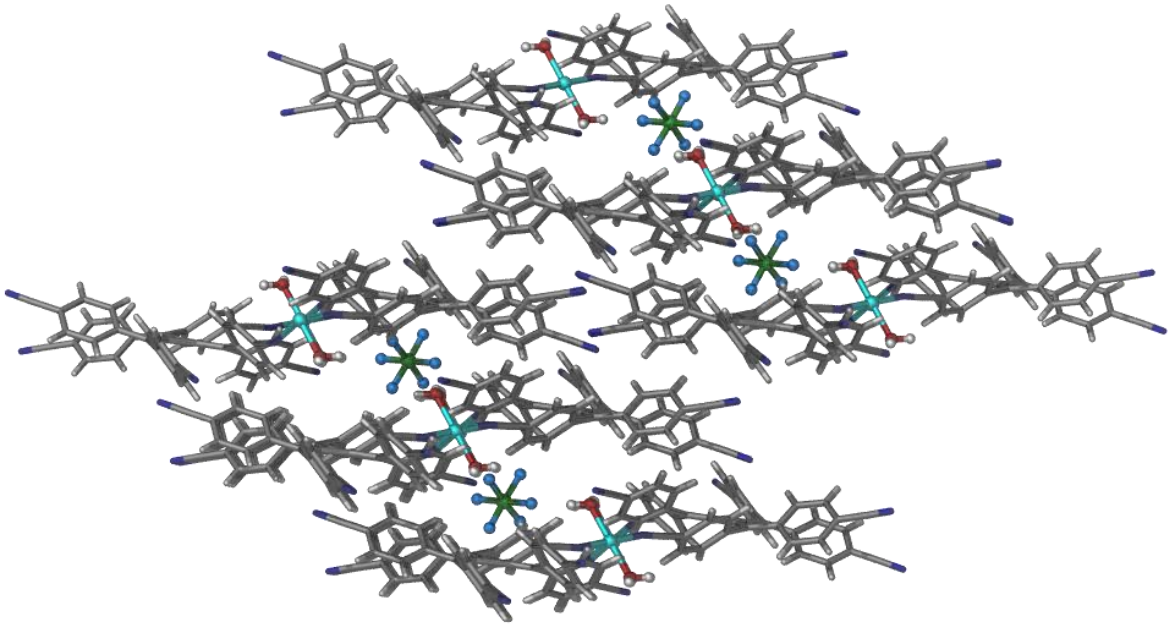

Figure 5.30. The layered packing of **4.12** showing the positions of the hexafluorophosphate anions within the structure. Nitromethane solvate molecules have been removed for clarity.

The hexafluorophosphate anion is involved in anion hydrogen bonding with one of the radialene ligands below it and one above it (Figure 5.31). The shortest contacts are with the radialene directly above the anion with C-H···F_{anion} distances of 2.49 and 2.59 Å. Another two hydrogen bonds are observed between the anion and the radialene directly above it with C-H···F_{anion} distances of 2.54 and 2.59 Å. The anion is not positioned exactly over the centre of the radialene below it, which is demonstrated by the angles between the centroid of the anion and the [3]radialene core plane being 62.00, 88.11, and 120.21° respectively, and the closest radialene centroid to anion distance being 3.92 Å. Despite this, close contacts are still present between carbon atoms of the [3]radialene core and the anion with π···F_{anion} distances to the same ligand of 3.55 Å to a ring carbon and 3.29 Å to an exocyclic carbon, respectively.

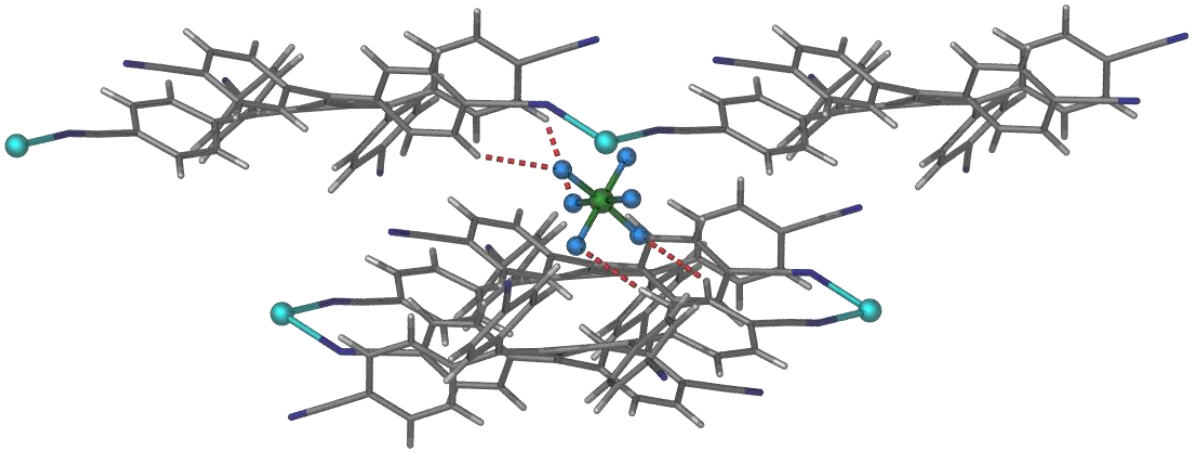

Figure 5.31. A perspective view showing the environment around the hexafluorophosphate anion in structure **4.12**. Radialene phenyl C-H···F_{anion} hydrogen bonds are shown as dashed lines.

The iron(II) complex, **4.13**, is also a 1-D polymer which packs in simple layers in the extended structure (Figure 5.32). The perchlorate anions reside between the layers and are surrounded by three radialene ligands, two either side of the anion and one above or below. There are four different perchlorate anions present in the asymmetric unit and each exhibits anion hydrogen bonding with the surrounding radialene ligands.

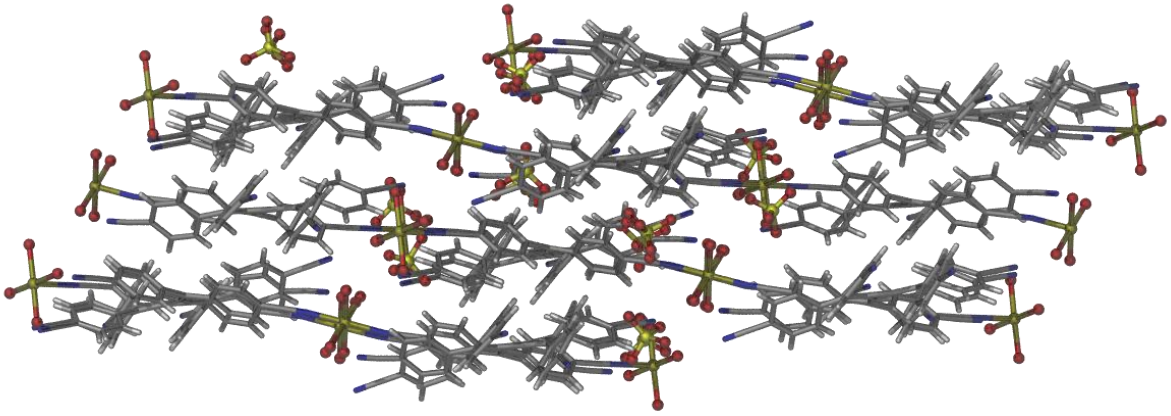

Figure 5.32. The layered packing of **4.13** showing the positions of the perchlorate anions within the structure.

Two of the perchlorate anions are located in pockets near the iron(II) metal atoms adjacent to the radialene ligands, whereas the other two perchlorate anions are located above or below the core of the ligands (Figure 5.33). The perchlorate anions situated near the iron(II) atoms (in the centre of Figure 5.33) are not involved in any anion-π interactions as they are not positioned near the [3]radialene core, although they do exhibit short contacts with the

peripheral aryl hydrogens of adjacent ligands. One of the central perchlorate anions is involved in three anion hydrogen bonds with C-H···O_{anion} distances of 2.63, 2.65 and 2.73 Å. The second central perchlorate also exhibits three anion hydrogen bond interactions but these are slightly longer at 2.76, 2.82, and 2.86 Å respectively.

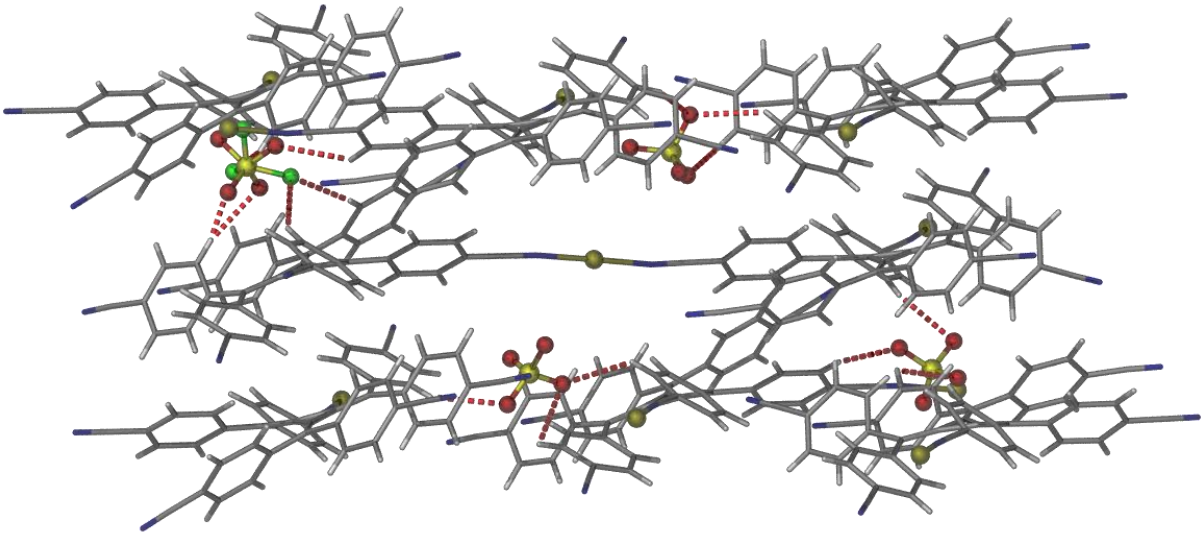

Figure 5.33. A perspective view showing the environment around the perchlorate anions in structure **4.13**. The minor component of the disordered perchlorate anion is shown in green. The coordinated water molecules have been removed for clarity. Radialene phenyl C-H···O_{anion} hydrogen bonds are shown as dashed lines.

The other two perchlorate anions, both situated near the core of a radialene ligand, also exhibit anion hydrogen bonding interactions. One of these anions is disordered over two positions with a refined occupancy of *ca.* 74:26. The disordered anion maintains six hydrogen bonds, two when in the major position with C-H···O_{anion} distances of 2.49 and 2.76 Å and four when in the minor positioning ranging from 2.50-2.71 Å. Four of these hydrogen bonds involve aryl hydrogens of the radialene directly below the anion, as seen in Figure 5.33, and the other two involve aryl hydrogens the two radialene ligands adjacent to the anion. The major component of the disordered perchlorate anion also exhibits a close radialene centroid anion distance of 3.16 Å to the radialene directly below it. This is well within the limit of the Σ_{vdw} + 0.2 Å of carbon and oxygen (3.42 Å). Even closer contacts are observed between the major component of the disordered anion and the radialene core with π···O_{anion} distances to the same ligand of 3.02 Å to a ring carbon and 3.21 Å to an exocyclic carbon, respectively. These interactions are very short and are the closest so far observed between a polyatomic anion and the [3]radialene core. The anion centroid to radialene core plane angles are also within the desired range of 90 ± 10° at 82.89, 89.96, and 97.68° respectively, which shows that the anion

is sitting directly over the core. However, like previous structures the geometry is still not as expected, although this time two oxygen atoms of the major component of the anion are directed towards the core.

The fourth anion sits below the [3]radialene core of another ligand and is involved in one anion hydrogen bond with this ligand with a bond length of 2.61 Å. Two additional hydrogen bonds are present between the fourth perchlorate anion and the two radialene ligands adjacent to it with C-H···O_{anion} distances of 2.72 and 2.75 Å. Similar to the disordered anion, this anion also displays close contacts with the [3]radialene core. The closest radialene centroid to anion distance is 3.18 Å and the closest $\pi\cdots O_{anion}$ distances to the same ligand are 3.25 Å to a ring carbon and 3.63 Å to an exocyclic carbon, respectively. These contacts are slightly longer than those of the disordered ligand and this is because the fourth anion does not sit exactly below the centroid of the [3]radialene core as demonstrated by the anion centroid to [3]radialene core plane angles of 79.61, 93.99 and 95.06°. This anion displays a similar geometry to the major component of the disordered anion.

Table 5.9 summarises the close anion contacts in solid-state structures **4.12** and **4.13** and the distances calculated for the optimised geometries of **2.29** and polyatomic anions in the gas phase. Again it can be noted for both solid-state structures that the closest distances between the anion and the [3]radialene core are much shorter than those in the gas phase whereas the shortest anion-hydrogen bond distances are slightly longer. In the case of structure **4.12** the anion to [3]radialene centroid distance is also longer due to the anion sitting off centre in relation to the [3]radialene core. Conversely, in structure **4.13** the anion to [3]radialene centroid distance is also a lot shorter than that calculated in the gas phase. However, this is likely due to the differing conformation of the anions in **4.13** versus the gas phase. This raises the question of whether observing an anion geometry similar to that seen in gas phase calculations is crucial in assessing the significance of an anion-π interaction in the solid-state.

Table 5.9. Closest distances between the anion and the [3]radialene centroid ($R_{centroid}$, Å), closest distances between the anion and the radialene core ($R_{[3]radialene}$, Å), and closest distances between the anion and proximal hydrogen atoms (R_H, Å) for solid-state structures **4.12** and **4.13** and optimised polyatomic anion complexes of **2.29**.

Radialene 2.29		**Solid-State Structures**			**Optimised Gas Phase Geometries**		
Polymer	**Anion**	$\boldsymbol{R_{centroid}}$	$\boldsymbol{R_{[3]radialene}}$	$\boldsymbol{R_H}$	$\boldsymbol{R_{centroid}}$	$\boldsymbol{R_{[3]radialene}}$	$\boldsymbol{R_H}$
4.12	PF_6^-	3.92	3.29	2.49	3.62	3.44	2.38
4.13	ClO_4^-	3.16	3.02	2.45	3.77	3.60	2.37

*5.4.4. Silver(I) Coordination Polymers of Hexakis(3,4-dicyanophenyl)[3]radialene (**2.44**)*

The structure of one coordination polymer of hexakis(3,4-dicyanophenyl)[3]radialene, **2.44**, with $AgPF_6$ was able to be determined via single crystal X-ray diffraction and is described in detail in chapter 4. Structure **4.14** is a 3-D coordination polymer with a (3,6)-connected rutile network topology, $(4.6^2)_2(4^2.6^{10}.8^3)$, when the radialene ligand is considered a 3-connecting node and a cluster of four silver(I) ions is considered a 6-connecting node. This results in large solvent and anion filled channels which run down the *a*-axis of the unit cell (Figure 5.34).

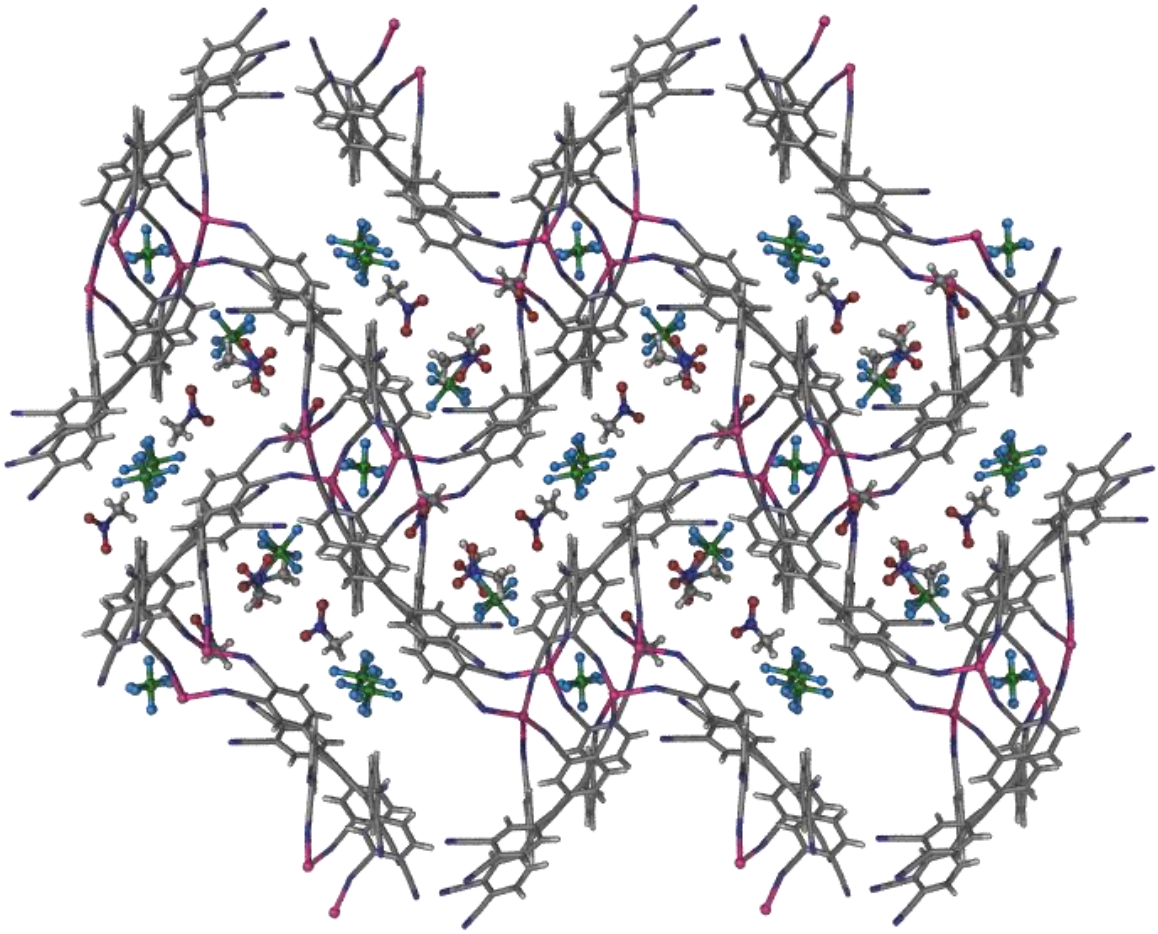

Figure 5.34. A perspective view of **4.14** showing the channels parallel to the *a*-axis.

There are three different hexafluorophosphate anions in the asymmetric unit of this structure, two of which are 50% occupied. Each anion is surrounded by two radialene ligands and are involved in anion-hydrogen bonding interactions with these molecules (Figure 5.35). The first anion is located on a special position near the silver(I) atoms in the structure and displays only one anion hydrogen bond with the radialene ligands which is 2.55 Å in length. This anion is not located over the core of a ligand and thus no anion-π interactions are observed.

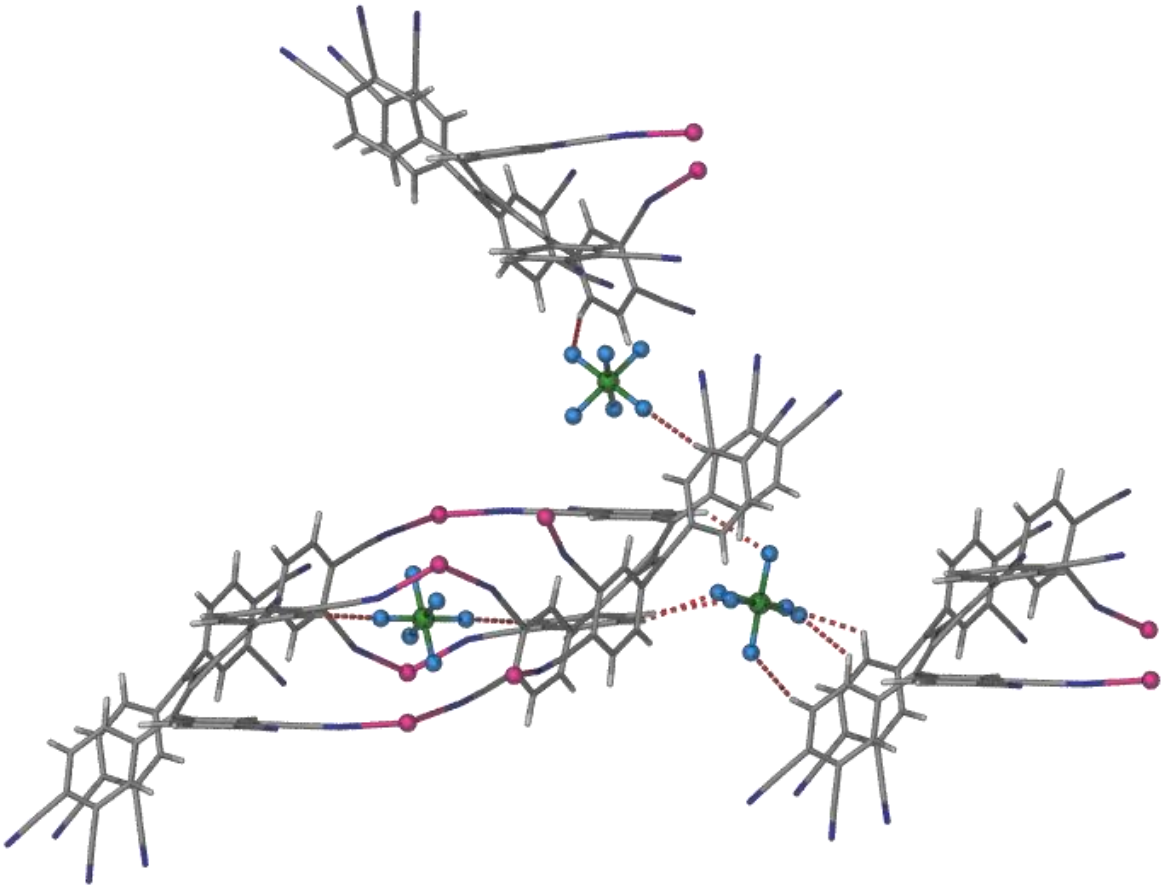

Figure 5.35. A perspective view showing the environment around the hexafluorophosphate anions in structure **4.14**. Solvate molecules have been removed for clarity. Radialene phenyl C-H···F_{anion} hydrogen bonds are shown as dashed lines.

The second hexafluorophosphate anion is also not located over the core of a radialene ligand and instead sits between the peripheral phenyl rings of two such molecules. Two anion hydrogen bonds are observed for this anion, one to each radialene, with C-H···F_{anion} distances of 2.44 and 2.59 Å respectively. The third hexafluorophosphate anion is located below the core of one radialene ligand and above the peripheral phenyl rings of another, as seen in Figure 5.35. This anion exhibits both anion-hydrogen bonding interactions and close contacts with the [3]radialene core.

Three anion hydrogen bonds between the third hexafluorophosphate anion and the radialene directly below it are observed with C-H···F_{anion} distances of 2.35, 2.55 and 2.62 Å. Another three hydrogen bonds are present between this anion and the ligand directly above it which have C-H···F_{anion} distances of 2.41, 2.48 and 2.55 Å. Close contacts are observed between the anion and this radialene ligand with the closest being 3.29 Å to an exocyclic carbon. This is within the limit of the Σ_{vdw} + 0.2 Å for carbon and fluorine of 3.37 Å. However the closest π···F_{anion} contact between the same fluorine atom and a core carbon is

3.53 Å and to the [3]radialene centroid is 3.95 Å. The angles between the plane of the [3]radialene core and the centroid of the anion (49.66, 96.21 and 121.68°) show that the anion is not located directly below the [3]radialene core. The geometry of the anion is similar to that calculated with three peripheral fluorine atoms directed towards the core and three directed away but due to the radialene being off centre this does not constitute a significant anion-π interaction using the guidelines of Hay and Custelcean.[45]

5.5. Summary

Anion-π interactions are weak forces which can occur between polarisable electron deficient aryl rings and anions. They were first observed in the early 1990's by Schneider and colleagues;[32] however the birth of the term 'anion-π interaction' and confirmation of their existence did not occur until as late as 2002.[21,34] Since then anion-π interactions have been shown to exist in the gas phase,[38] in solution,[19] and in the solid-state.[40] Theoretical calculations have further strengthened the case for these interactions by determining that they can exhibit binding energies in the vicinity of 20-50 kJ.mol^{-1}.[33] A similarity throughout these studies is that the anion-π interactions all involve either electron deficient heteroaryl rings or benzene rings with electron withdrawing substituents. The ability of the cross-conjugated structural isomer of benzene, [3]radialene, to form anion-π interactions has garnered less attention with one computational study of hexafluoro[3]radialene being recently published.[69] A few solid-state examples of hexaaryl[3]radialenes displaying close [3]radialene core anion contacts have been reported[46,51,53] and thus it was decided that further study into whether these compounds exhibit significant anion-π interactions was warranted.

A series of increasingly electron deficient and synthetically accessible hexaaryl[3]radialene derivatives, hexaphenyl[3]radialene (**1.1**), hexakis(3-cyanophenyl)-[3]radialene (**2.38**), hexakis(4-cyanophenyl)[3]radialene (**2.29**) and hexakis(3,4-dicyano-phenyl)[3]radialene (**2.44**), were optimised to the HF/6-31G++(d,p) level of theory. The calculations determined that these compounds display increasingly positive Q_{zz} quadropole moments, required for sustaining anion-π interactions, as the number of electron withdrawing groups increased demonstrating that the [3]radialene core itself is not intrinsically electron deficient but requires the addition of electron withdrawing substituents to become so. Two areas of positive potential were identified for the nitrile substituted derivatives **2.38**, **2.29** and **2.44** at the [3]radialene core and on the aryl hydrogen atoms indicating that these two complementary regions are amenable to interacting with anions.

These four hexaaryl[3]radialenes were then optimised with the halide anions F^-, Cl^- and Br^- using both the HF/6-31G++(d,p) and the MO6-2X/6-31++G(d,p) level of theory, which

has been previously shown to model anion-π interactions reliably.[54] Favourable interaction energies were observed with the halide anions and a trend in interaction strength was established across all radialene species of $F^- > Cl^- > Br^-$. This trend was also supported by the examination of the molecular orbitals of these radialene anion complexes, which exhibited a stronger orbital overlap with F^- than with Cl^- or Br^-. It was determined that these complexes were stabilised by a combination of anion hydrogen bonding and anion-π interactions as the *meta* (**2.38**) and *para* (**2.29**) derivatives exhibited similar binding energies. The *meta* derivative possesses more acidic aryl hydrogen atoms whereas the *para* derivative has the more electron deficient [3]radialene core.

Finally radialene **2.29** was also optimised with a series of polyatomic anions (NO_3^-, ClO_4^-, BF_4^-, and PF_6^-) using the HF/6-31G++(d,p) level of theory, which was shown during the halide complex study to give comparable results to MO6-2X/6-31++G(d,p). Favourable interactions energies were also observed for these complexes with the strength of the interaction determinate on the charge density of the peripheral atoms and the proportion of atoms able to form anion-hydrogen bonds with the aryl hydrogens. The resultant geometries were such that the centroid of the anion was above the centroid of the [3]radialene core and the greatest number of peripheral anion atoms were directed towards the aryl hydrogens.

Negative ion, electrospray ionisation, high-resolution mass spectrometry (ESI-HRMS) was used to further validate the computational results. Solutions of **2.38**, **2.29**, and **2.44** were prepared with $(^n Bu)_4NX$ (X = F, Cl, Br, NO_3, BF_4, PF_6) in a 1:100 molar ratio. Hexaaryl[3]radialene anion complexes for all of the anion and radialene combinations tested were observed in the mass spectrum. Some hexaaryl[3]radialene dimer anion complexes were also observed with Cl^-, Br^-, NO_3^-, BF_4^- and PF_6^- and are assumed to adopt a sandwich conformation with the anion situated between the two radialene molecules. The stability of the radialene anion complexes was probed via comparison of the signal intensities for a particular ion as the normalised collision energy (NCE) was increased incrementally, during MS/MS experiments, relative to the signal intensity observed at an NCE of zero. This analysis revealed that the stability of the radialene halide complexes varies such that $F^- > Cl^- \approx Br^-$, which is comparable to the theoretical calculations, and that the complexes of **2.44** are significantly more stable than those of **2.38** and **2.29** which are similar. Also in regard to the polyatomic anions for complexes of **2.29**, the stability varies such that $NO_3^- > BF_4^- \approx PF_6^-$.

Recent studies canvassing the CSD for examples of anion-π interactions have disagreed upon whether they are common[43] or rare[44] depending on the criteria used to identify a significant interaction. As a result of this, Hay and Custelcean published the following guidelines for classifying anion-π interactions in the solid-state: the structure must (a) exhibit

a geometry corresponding to electronic structure calculations; (b) have the anion located above the core centroid; and (c) involve a charge neutral organic compound. These guidelines have been used throughout this report to assess the significance of anion-π interactions. Although a rewording of criterion (c) to "involve a charge neutral organic compound, or the organic component of a metal-ligand complex or coordination polymer" is suggested as metal-ligand complexes and coordination polymers are technically cationic and only the organic parts of these structures are charge neutral.

Weak anion hydrogen bonding was observed in all ten coordination polymers examined in section 5.4. These interactions appear to be ubiquitous whether the anion is positioned above the [3]radialene core or alongside the arms of the radialene within channels in the structure. This is due to the 3-D propeller structure adopted by the hexaaryl[3]radialene compounds which places the aryl hydrogens above and below the plane of the core as well as radiating outwards from the sides of the molecule. These are the only anion interactions observed in structures **4.10a**, **4.10b** and **4.11b** as crystal packing precludes the approach of the anions towards the [3]radialene core.

Close contacts with the [3]radialene core carbons, less than Σ_{vdw} + 0.2 Å of the interacting atoms, were observed in structures **4.5-4.8** and **4.12-4.14**. The majority of these show the anion positioned over the [3]radialene core centroid, with the exception of **4.12**. Although as the π-system of the [3]radialene core is localised along the exocyclic double bonds, due to its cross-conjugation, and not delocalised around the ring it seems sensible that the anions interacting with the π-system would not be perfectly aligned with the core centroid. These structures met the criteria outlined by Hay and Custelcean of involving a charge neutral compound, the hexaaryl[3]radialene, and having the anion located above the core centroid however the geometries of the anions involved in the interactions generally differ to those of the calculated structures. The exception is those structures with octahedral anions, **4.6**, **4.8** and **4.14**, within which the anion has three peripheral atoms directed towards the [3]radialene core and three directed away.

The structures which contain the tetrahedral anions, ClO_4^- or BF_4^-, display an anion conformation with either one or two of the peripheral atoms directed towards the [3]radialene core instead of three atoms an equal distance away from the aryl hydrogens which was observed in the calculated geometries. However, it is one of these structures, **4.13**, that exhibits both the closest anion atom to [3]radialene core carbon distance (3.02 Å) and the closest anion centroid to [3]radialene centroid distance (3.16 Å), which are both well within the Σ_{vdw} + 0.2 Å (for carbon and oxygen of 3.42 Å). This example is similar to the copper(II) complex discussed in section 5.1.1 which displays a close contact (3.11 Å) between a triazine

ring and a tetrahedral $[CuCl_4]^{2-}$ anion, however only one of the peripheral chlorine atoms is directed towards the core.[40] Following the guidelines of Hay and Custelcean these two cases would not classify as instances of true anion-π interactions.[45] This then leads to the question "should comparison to calculated geometries of polyatomic anions with π-systems by used to classify significant anion-π interactions in the solid-state?"

The anion-π contacts observed in the solid-state structures examined here are much shorter than those seen in the calculated geometries, whereas the opposite can be said for anion hydrogen bonds. It is possible that the calculated geometries place too much emphasis on hydrogen bonding to the detriment of anion-π interactions. Or these differences could be due to the isolation of the molecules in gas phase modelling compared to the myriad of packing forces present in the solid-state. However, it cannot be debated that the particularly close anion-radialene core contacts observed in structures **4.6**, **4.8** and **4.13** are significant interactions. Although it is possible that packing forces contributed to the final positioning of the anions above the [3]radialene core it is likely that the attraction between the anion and the electron-deficient radialene also played a role. In the case of the tetrahedral ClO_4^- anion in structure **4.13** having two peripheral oxygen atoms directed towards the [3]radialene core instead of three allows for a closer approach and thus an improved interaction; as such the requirement of having a similar geometry to gas phase calculations in order to classify an anion-π interaction as significant appears to be too restrictive.

Overall the evidence provided by theoretical calculations, mass spectrometry and the examination of solid-state structures has shown that electron deficient, nitrile substituted hexaaryl[3]radialenes are capable of forming, and do in fact exhibit, anion-π interactions. These interactions are accompanied by anion hydrogen bonding with the peripheral aryl hydrogens which are located above and below the [3]radialene core. The detailed understanding of these interactions provided by this work may prove useful in the development of hexaaryl[3]radialenes as anion sensors.

5.6. Experimental

5.6.1. Theoretical Methods

Optimisation, frequency, and quadrupole moment calculations were performed using the Gaussian 09 suite of programs.[70] The hexaaryl[3]radialene ligands **1.1**, **2.38**, **2.29** and **2.44** were fully optimised using default convergence criteria by *ab initio* methods utilising restricted Hartree-Fock theory with the 6-31G++(d,p) basis set. The halide complexes of **1.1**, **2.38**, **2.29** and **2.44** were optimised to the M06-2X/6-31++G(d,p) theory with loose symmetry constraints. The polyatomic anion complexes of **2.29** were optimised to the 6-31++G(d,p) theory with loose symmetry constraints. Frequency calculations were unable to be completed due to the complexity of the structures. All binding energies were calculated with corrections for basis set substitution error (BSSE) using the counterpoise method, as performed in previous studies.[28,55,69] Electrostatic potential surfaces (ESP) were produced by mapping the electrostatic potential onto the electron density surface at a density of 0.005 e·Å^{-3}. Molecular orbitals were also produced at an isovalue of 0.02 a.u. using Gaussview.

5.6.2. Mass Spectrometry

All high resolution mass data were measured with an LTQ Orbitrap XL ETD hybrid mass spectrometer (Thermo Fisher Scientific, Waltham, MA, USA) equipped with an ESI source. Samples were infused at 5 uL min^{-1} using the built-in syringe pump and a spraying voltage of −2.3 kV. A mass resolution of 30,000 (at *m/z* 700) was used. MS/MS experiments were performed in the ion trap with an isolation width of 5 *m/z*. Stability of the complexes were measured by comparing the normalised collision energy (NCE) required to diminish the complex to an intensity signal less than 50% of the initial intensity. Solutions of **2.38**, **2.29**, and **2.44** were prepared with (^{n}Bu)$_4$NX (X = F, Cl, Br, NO_3, BF_4, PF_6) in a 1:100 molar ratio.

5.6.3. CSD Search Details

A search of the CSD (version 5.33, November 2011 and updates February and May 2012) for the [3]radialene core resulted in 42 hits. Twelve of those were hexaaryl[3]radialenes or hexaheteroaryl[3]radialenes and of those four exhibited proximal anion to radialene π-system contacts (CSD codes: GUKTEM, GUKTIQ, MIGQEY, and NEHLOC).

5.7. References

1 P. D. Beer and P. A. Gale, *Angew. Chem. Int. Ed.*, **2001**, *40*, 486.

2 P. A. Gale, *Acc. Chem. Res.*, **2006**, *39*, 465.

3 S. O. Kang, R. A. Begum, and K. Bowman-James, *Angew. Chem. Int. Ed.*, **2006**, *45*, 7882.

4 P. A. Gale, S. E. Garcia-Garrido, and J. Garric, *Chem. Soc. Rev.*, **2008**, *37*, 151.

5 S. Kubik, *Chem. Soc. Rev.*, **2009**, *38*, 585.

6 C. Caltagirone and P. A. Gale, *Chem. Soc. Rev.*, **2009**, *38*, 520.

7 K. Bowman-James, *Acc. Chem. Res.*, **2005**, *38*, 671.

8 P. Bauduin, A. Renoncourt, D. Touraud, W. Kunz, and B. W. Ninham, *Curr. Opin. Colloid Interface Sci.*, **2004**, *9*, 43.

9 E. A. Meyer, R. K. Castellano, and F. Diederich, *Angew. Chem. Int. Ed.*, **2003**, *42*, 1210.

10 S. Kubik In *Anion Coordination Chemistry*, Wiley-VCH Verlag GmbH & Co. KGaA, 2011, p 363.

11 B. A. Moyer, L. H. Delmau, C. J. Fowler, A. Ruas, D. A. Bostick, J. L. Sessler, E. Katayev, G. Dan Pantos, J. M. Llinares, M. A. Hossain, S. O. Kang, and K. Bowman-James In *Advances in Inorganic Chemistry*, Rudi van, E., Kristin, B.-J., Eds., Academic Press, 2006, Vol. Volume 59, p 175.

12 E. P. Hodgkin and B. H. Hamilton, *Fert. Res.*, **1993**, *36*, 95.

13 R. H. Foy and P. J. A. Withers, *The Contribution of Agricultural Phosphorus to Eutrophication*, Fertiliser Society, Peterborough, 1995.

14 C.-C. Tzeng, Y.-Y. Kuo, T.-F. Huang, D.-L. Lin, and Y.-J. Yu, *J. Hazard. Mater.*, **1998**, *58*, 207.

15 J. L. Sessler, E. Katayev, G. D. Pantos, and Y. A. Ustynyuk, *Chem. Commun.*, **2004**, 1276.

16 P. A. Gale, J. L. Sessler, V. Kral, and V. Lynch, *J. Am. Chem. Soc.*, **1996**, *118*, 5140.

17 J. L. Sessler, M. J. Cyr, V. Lynch, E. McGhee, and J. A. Ibers, *J. Am. Chem. Soc.*, **1990**, *112*, 2810.

18 P. Gamez, T. J. Mooibroek, S. J. Teat, and J. Reedijk, *Acc. Chem. Res.*, **2007**, *40*, 435.

19 O. B. Berryman, F. Hof, M. J. Hynes, and D. W. Johnson, *Chem. Commun.*, **2006**, 506.

20 L. H. Uppadine, P. D. Beer, and M. G. B. Drew, *Chem. Commun.*, **2001**, 291.

21 P. de Hoog, P. Gamez, I. Mutikainen, U. Turpeinen, and J. Reedijk, *Angew. Chem. Int. Ed.*, **2004**, *43*, 5815.

22 Z. Qin, M. C. Jennings, and R. J. Puddephatt, *Inorg. Chem.*, **2002**, *41*, 3967.

23 N. L. S. Yue, M. C. Jennings, and R. J. Puddephatt, *Eur. J. Inorg. Chem.*, **2007**, 1690.

24 A. Damsyik, S. F. Lincoln, and K. P. Wainwright, *Inorg. Chem.*, **2006**, *45*, 9834.

25 A. Echavarren, A. Galan, J. M. Lehn, and J. De Mendoza, *J. Am. Chem. Soc.*, **1989**, *111*, 4994.

26 R. Vilar, *Angew. Chem. Int. Ed.*, **2003**, *42*, 1460.

27 J. Yoon, S. K. Kim, N. J. Singh, and K. S. Kim, *Chem. Soc. Rev.*, **2006**, *35*, 355.

28 I. Alkorta, I. Rozas, and J. Elguero, *J. Am. Chem. Soc.*, **2002**, *124*, 8593.

29 D. Quiˆnonero, A. Frontera, and P. M. Deyà In *Anion Coordination Chemistry*, Wiley-VCH Verlag GmbH & Co. KGaA, 2011, p 321.

30 A. Robertazzi, F. Krull, E.-W. Knapp, and P. Gamez, *CrystEngComm*, **2011**, *13*, 3293.

31 P. Ballester In *Recognition of Anions*, Vilar, R., Ed., Springer Berlin Heidelberg, 2008, Vol. 129, p 127.

32 H.-J. Schneider, F. Werner, and T. Blatter, *J. Phys. Org. Chem.*, **1993**, *6*, 590.

33 M. Mascal, A. Armstrong, and M. D. Bartberger, *J. Am. Chem. Soc.*, **2002**, *124*, 6274.

34 D. Quiñonero, C. Garau, C. Rotger, A. Frontera, P. Ballester, A. Costa, and P. M. Deyà, *Angew. Chem. Int. Ed.*, **2002**, *41*, 3389.

35 B. L. Schottel, H. T. Chifotides, and K. R. Dunbar, *Chem. Soc. Rev.*, **2008**, *37*, 68.

36 D. Quiñonero, C. Garau, A. Frontera, P. Ballester, A. Costa, and P. M. Deyà, *Chem. Phys. Lett.*, **2002**, *359*, 486.

37 C. Garau, A. Frontera, D. Quiñonero, P. Ballester, A. Costa, and P. M. Deyà, *ChemPhysChem*, **2003**, *4*, 1344.

38 R. E. Dawson, A. Hennig, D. P. Weimann, D. Emery, V. Ravikumar, J. Montenegro, T. Takeuchi, S. Gabutti, M. Mayor, J. Mareda, C. A. Schalley, and S. Matile, *Nat Chem*, **2010**, *2*, 533.

39 P. Arranz-Mascarós, C. Bazzicalupi, A. Bianchi, C. Giorgi, M.-L. Godino-Salido, M.-D. Gutiérrez-Valero, R. Lopez-Garzón, and M. Savastano, *J. Am. Chem. Soc.*, **2012**, *135*, 102.

40 S. Demeshko, S. Dechert, and F. Meyer, *J. Am. Chem. Soc.*, **2004**, *126*, 4508.

41 C. A. Black, L. R. Hanton, and M. D. Spicer, *Chem. Commun.*, **2007**, *0*, 3171.

42 C. A. Black, L. R. Hanton, and M. D. Spicer, *Inorg. Chem.*, **2007**, *46*, 3669.

43 T. J. Mooibroek, C. A. Black, P. Gamez, and J. Reedijk, *Cryst. Growth Des.*, **2008**, *8*, 1082.

44 R. Ahuja and A. G. Samuelson, *CrystEngComm*, **2003**, *5*, 395.

45 B. P. Hay and R. Custelcean, *Cryst. Growth Des.*, **2009**, *9*, 2539.

46 K. Matsumoto, Y. Harada, N. Yamada, H. Kurata, T. Kawase, and M. Oda, *Cryst. Growth Des.*, **2006**, *6*, 1083.

47 T. Fukunaga, *J. Am. Chem. Soc.*, **1976**, *98*, 610.

48 T. Enomoto, N. Nishigaki, H. Kurata, T. Kawase, and M. Oda, *Bull. Chem. Soc. Jpn.*, **2000**, *73*, 2109.

49 A. Avellaneda, C. A. Hollis, X. He, and C. J. Sumby, *Beil. J. Org. Chem.*, **2012**, *8*, 71.

50 D. M. D'Alessandro, F. R. Keene, P. J. Steel, and C. J. Sumby, *Aust. J. Chem.*, **2003**, *56*, 657.

51 P. J. Steel and C. J. Sumby, *Chem. Commun.*, **2002**, 322.

52 P. J. Steel and C. J. Sumby, *Inorg. Chem. Commun.*, **2002**, *5*, 323.

53 C. A. Hollis, L. R. Hanton, J. C. Morris, and C. J. Sumby, *Cryst. Growth Des.*, **2009**, *9*, 2911.

54 S. E. Wheeler and K. N. Houk, *J. Phys. Chem. A*, **2010**, *114*, 8658.

55 D. Quiñonero, C. Garau, A. Frontera, P. Ballester, A. Costa, and P. M. Deyà, *J. Phys. Chem. A*, **2005**, *109*, 4632.

56 C. Garau, A. Frontera, D. Quiñonero, P. Ballester, A. Costa, and P. M. Deyà, *Chem. Phys. Lett.*, **2004**, *399*, 220.

57 F. Sansone, E. Chierici, A. Casnati, and R. Ungaro, *Organic & Biomolecular Chemistry*, **2003**, *1*, 1802.

58 K. Kavallieratos, A. J. Sabucedo, A. T. Pau, and J. M. Rodriguez, *J. Am. Soc. Mass. Spectrom.*, **2005**, *16*, 1377.

59 W. M. Draper, P. Behniwal, and D. Wijekoon, *Rapid Commun. Mass Spectrom.*, **2008**, *22*, 2613.

60 T. Becherer, D. Meshcheryakov, A. Springer, V. Bohmer, and C. A. Schalley, *Am. J. Mass Spectrom.*, **2009**, 1338.

61 B. Utley and L. A. Angel, *Eur. J. Mass Spectrom.*, **2010**, *16*, 631.

62 Á. Révész, D. Schröder, J. Svec, M. Wimmerová, and V. Sindelar, *J. Phys. Chem. A*, **2011**, *115*, 11378.

63 C. L. Huffman, M. L. Williams, D. M. Benoist, R. E. Overstreet, and E. E. Jellen-McCullough, *Rapid Commun. Mass Spectrom.*, **2011**, *25*, 2299.

64 D. A. Barnett and G. Horlick, *J. Anal. At. Spectrom.*, **1997**, *12*, 497.

65 Y. Cai, M. C. Concha, J. S. Murray, and R. B. Cole, *J. Am. Soc. Mass. Spectrom.*, **2002**, *13*, 1360.

66 I. A. Carasel, C. R. Yamnitz, R. K. Winter, and G. W. Gokel, *J. Org. Chem.*, **2010**, *75*, 8112.

67 E. P. L. Hunter and S. G. Lias, *J. Phys. Chem. Ref. Data*, **1998**, *27*, 413.

68 C. Domene, P. W. Fowler, L. W. Jenneskens, and E. Steiner, *Chem. Eur. J.*, **2007**, *13*, 269.

69 C. Estarellas, A. Frontera, D. Quiñonero, and P. M. Deyà, *J. Phys. Chem. A*, **2011**, *115*, 7849.

70 M. J. Frisch, G. W. Trucks, H. B. Schlegel, G. E. Scuseria, M. A. Robb, J. R. Cheeseman, G. Scalmani, V. Barone, B. Mennucci, G. A. Petersson, H. Nakatsuji, M. L. Caricato, X, H. P. Hratchian, A. F. Izmaylov, J. Bloino, G. Zheng, J. L. Sonnenberg, M. Hada, M. Ehara, K. Toyota, R. Fukuda, J. Hasegawa, M. Ishida, T. Nakajima, Y. Honda, O. Kitao, H. Nakai, T. Vreven, J. A. Montgomery, J. E. Peralta, F. Ogliaro, M. Bearpark, J. J. Heyd, E. Brothers, K. N. Kudin, V. N. Staroverov, R. Kobayashi, J. Normand, K. Raghavachari, A. Rendell, J. C. Burant, S. S. Iyengar, J. Tomasi, M. Cossi, N. Rega, J. M. Millam, M. Klene, J. E. Knox, J. B. Cross, V. Bakken, C. Adamo, J. Jaramillo, R. Gomperts, R. E. Stratmann, O. Yazyev, A. J. Austin, R. Cammi, C. Pomelli, J. W. Ochterski, R. L. Martin, K. Morokuma, V. G. Zakrzewski, G. A. Voth, P. Salvador, J. J. Dannenberg, S. Dapprich, A. D. Daniels, Ö. Farkas, J. B. Foresman, J. V. Ortiz, J. Cioslowski, and D. J. Fox, *Gaussian 09, Revision A.02*, Wallingford CT, 2009.

Chapter 6

Coordination Polymers of Diarylmethanes

Chapter 6

6. Coordination Polymers of Diarylmethanes

6.1. Introduction

6.1.1. Coordination Polymers of Flexible Bridging Ligands

An introduction to coordination polymers has already been given in Chapter 4, section 4.1.1, and so this introductory section will present a short literature review of flexible, diaryl, bridging ligands with simple one atom spacers, which have been previously utilised in the formation of coordination polymers. Simple, flexible, diaryl ligands generally consist of two aryl rings separated by a spacer group which can be, among other things, a methyl, carbonyl, amine, or N-oxime. The aryl rings can possess donor substituents such as nitrile or carboxylic acid groups; however the focus here will be on pyridyl donors as these were present in the majority of the structures discussed in this chapter. In the case of simple, bridging, dipyridyl ligands the pyridyl nitrogen atoms are generally substituted in the 3- or 4-positions, as having the nitrogen atoms in the 2-position more often leads to discrete complexes due to the tendency of such ligands to chelate metal ions.[1,2] A selection of such bridging dipyridyl ligands, which have been shown to form coordination polymers, can be seen in Figure 6.1.

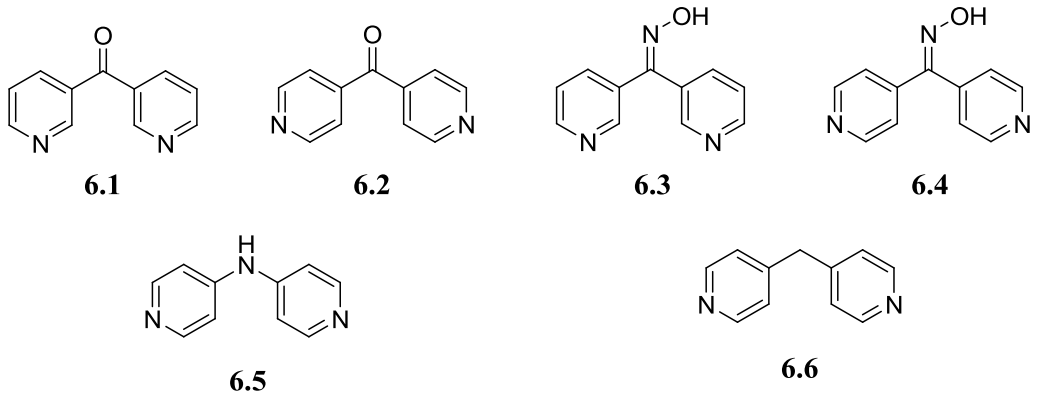

Figure 6.1. Various flexible, dipyridyl, bridging ligands which have been utilised in the formation of coordination polymers.

Di-3-pyridylketone (**6.1**) has been observed to form both 1-D and 2-D networks. Reaction of **6.1** with one equivalent of either $AgBF_4$, $AgClO_4$ or $AgNO_3$ leads to the formation of a series of isomorphous, 1-D helical chains (Figure 6.2 (a)) whereas reaction with $AgCF_3SO_3$ produces a 1-D zigzag chain (Figure 6.2 (b)).[3] The difference in topology between these two

1-D polymers is due to variation in the linking direction of ligand **6.1** and also subtle variations in torsion angle of the two pyridyl rings with respect to the carbonyl group. This results in the torsion angle of three consecutive silver atoms in the zigzag chain being approximately linear, whereas the angle is around 70-75° for the helical chains. Ligand **6.1** has also been shown to form a (4,4)-connected 2-D network (Figure 6.2 (c)) upon reaction with $Cu(ClO_4)_2 \cdot 6H_2O$.[4] Within this structure the square planar copper(II) atoms act as 4-connecting nodes and the ligands are topologically trivial.

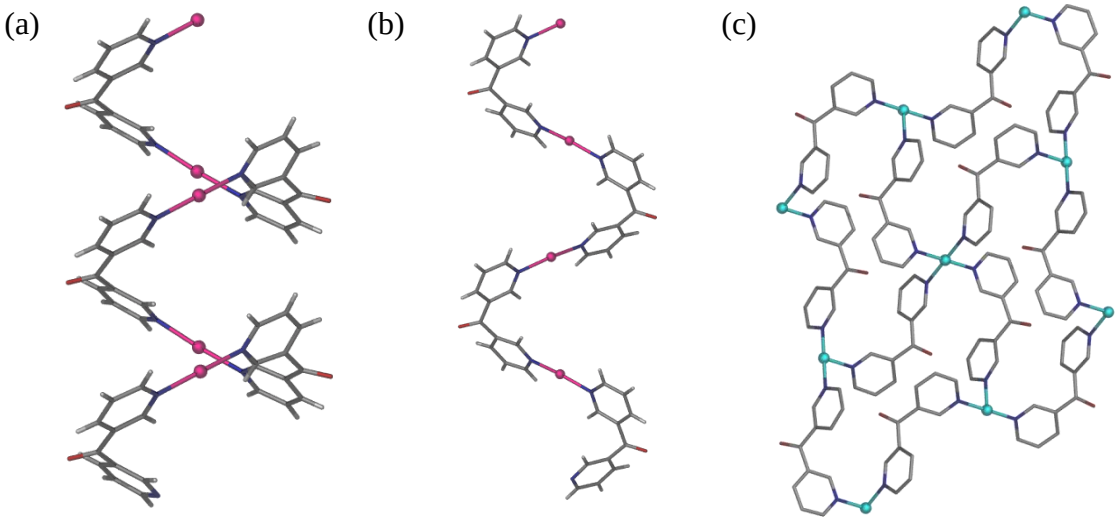

Figure 6.2. Coordination polymers of **6.1** including (a) a 1-D helical chain, (b) a 1-D zigzag chain and (c) a 2-D (4,4)-connected network, with the hydrogen atoms omitted for clarity.

The 4-substituted pyridyl ketone (**6.2**) has also been used to form a complex 3-D structure with copper(II) and phthalic acid.[5] The structure is composed of two helices of copper(II) and **6.2** running parallel to the *c*-axis, which are then connected via phthalate dianions to form a double helical motif. This double helix is then connected to three other helices, with alternate handedness, to form the 3-D network.

The synthesis of a series of dipyridyl ketone oximes, including 3,3'-dipyridyl ketone oxime (**6.3**), 4,4'-dipyridyl ketone oxime (**6.4**), and a number of other asymmetrically substituted derivatives, was very recently reported by Hanton.[6] Reaction of **6.3** with one equivalent of $AgCF_3SO_3$ led to the formation of a 1-D helical chain (Figure 6.3 (a)) similar to that observed with ligand **6.1** (Figure 6.2 (a)). Within this structure the $CF_3SO_3^-$ anions are encapsulated by the helices and hydrogen bonding interactions between these anions and oxime hydroxyl groups of adjacent helices led to a slight helical interdigitatation. Interestingly, the reaction of **6.4** with one equivalent of $AgCF_3SO_3$ did not lead to the formation of a coordination polymer but instead produced a discrete cationic complex where

only one pyridyl nitrogen atom is involved in coordination of a silver(I) cation. The discrete complex is extended into a 2-D hydrogen-bonded network via the second pyridyl nitrogen atom and the oxime hydroxyl group (Figure 6.3 (b)).

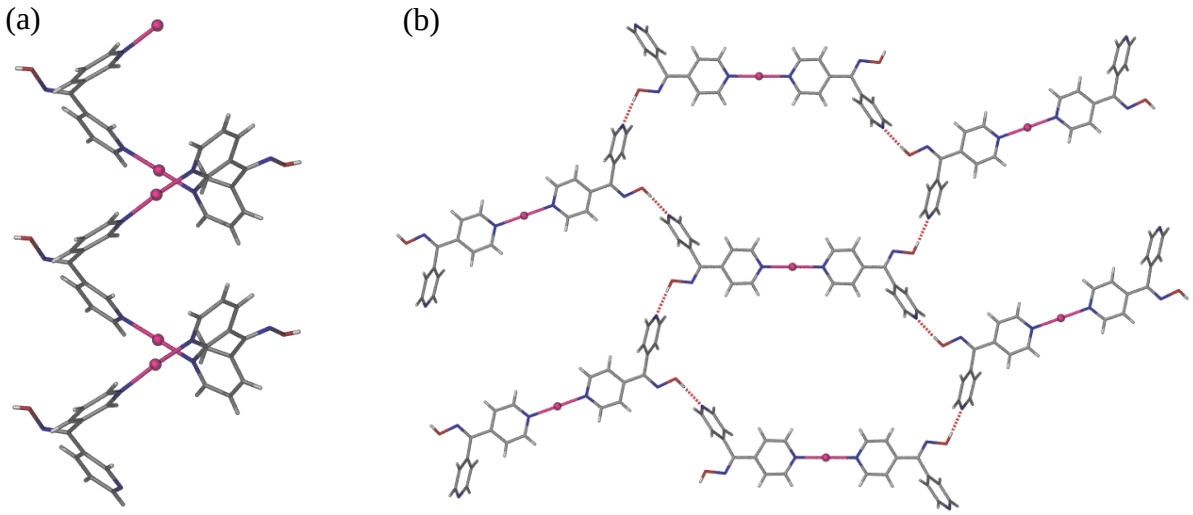

Figure 6.3. (a) The 1-D helical coordination polymer of **6.3** with silver(I) and (b) the 2-D hydrogen bonded network of **6.4** and silver(I) with hydrogen bonds shown as red dotted lines.

The coordination chemistry of a similar ligand, bis(4-pyridyl)amine (**6.5**), has been more widely studied with 1-D, 2-D and 3-D networks being reported.[7-10] As with ligand **6.1**, 1-D helical and zigzag topologies were observed depending on the metal salt used in the reaction. Upon reaction of **6.5** with one equivalent of $AgCF_3SO_3$ a 1-D zigzag polymer is produced where the silver(I) ion has a T-shaped geometry due to coordination by two ligands and one acetonitrile molecule (Figure 6.4 (a)). On the other hand, if $AgNO_3$ is used the result is a 1-D helical polymer with linear silver(I) ions (Figure 6.4 (b)). These polymers are elongated compared to their analogues formed with **6.1** due to the more divergent nature of the 4-pyridyl, as opposed to the 3-pyridyl, substituents.

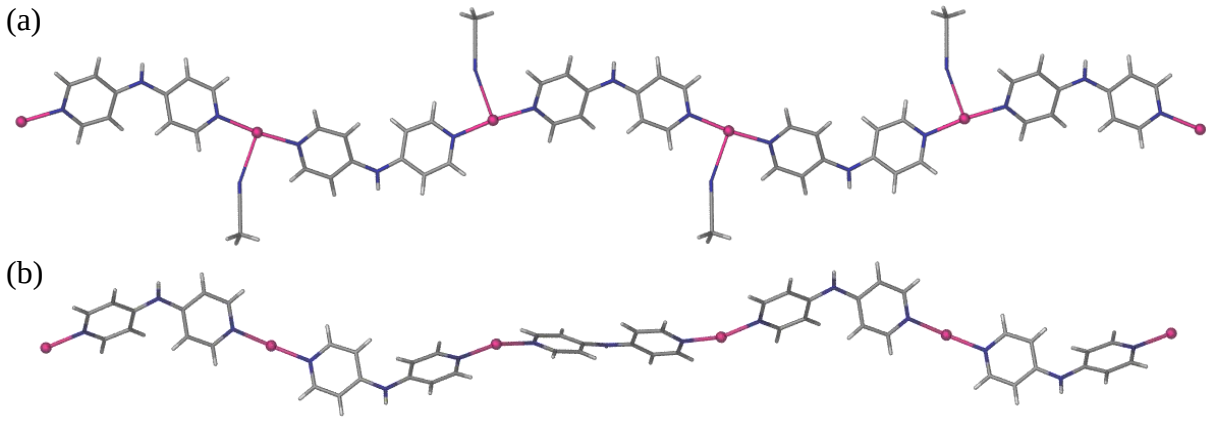

Figure 6.4. The (a) zigzag and (b) helical 1-D coordination polymers of **6.5** with silver(I).

The majority of 2-D and 3-D polymers reported for ligand **6.5** involve either hydrogen bonded networks[7] or an additional ligand[9,10] or anion[7] which results in the increased dimensionality and thus will not be discussed here. An exception is the 3-D pseudo-adamantoid coordination polymer which is formed via the reaction of **6.5** with half an equivalent of $Cd(NO_3)_2.4H_2O$ (Figure 6.5 (a)).[7] Due to the large adamantoid cavities this structure is 4-fold interpenetrated (Figure 6.5 (b)).

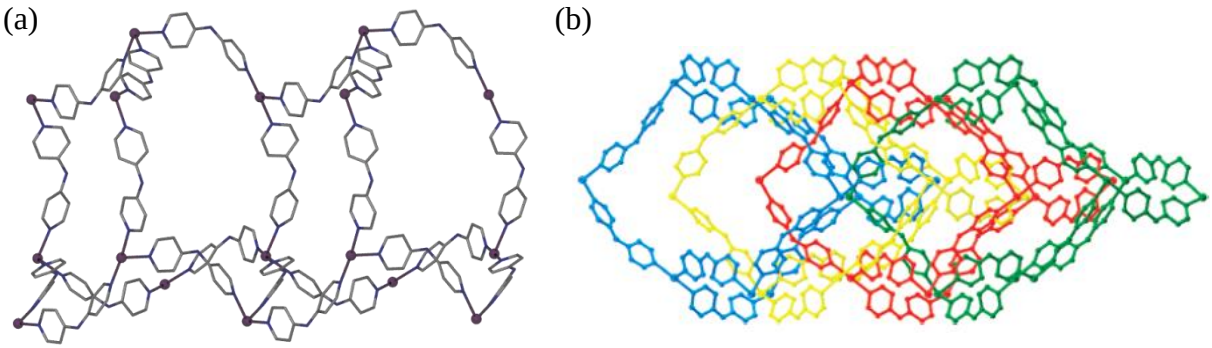

Figure 6.5. (a) The 3-D pseudo-adamantoid motif of **6.5** with cadmium(II) and (b) the four interpenetrated networks present in this structure (image sourced from reference 7).

The final simple, flexible, dipyridyl bridging ligand which will be considered is di-4-pyridylmethane (**6.6**). The coordination chemistry of dipyridyl ligands with methylene groupss has not been studied to as great an extent as those with carbonyl or amine linkers; in fact no coordination polymers containing the 3-subsitituted derivative have been reported. The reaction of **6.6** with 0.25 equivalents of $Cd(NO_3)_2 \cdot 4H_2O$ leads to the formation of a corrugated 2-D (4,4)-connected network (Figure 6.6).[11] Within this structure the octahedral cadmium(II) cations (the apical positions are occupied by two monodentate nitrate anions) act as 4-connecting nodes whereas the ligands are topologically trivial. Like compound **6.6**, the flexible ligands investigated in this chapter possess a methylene group.

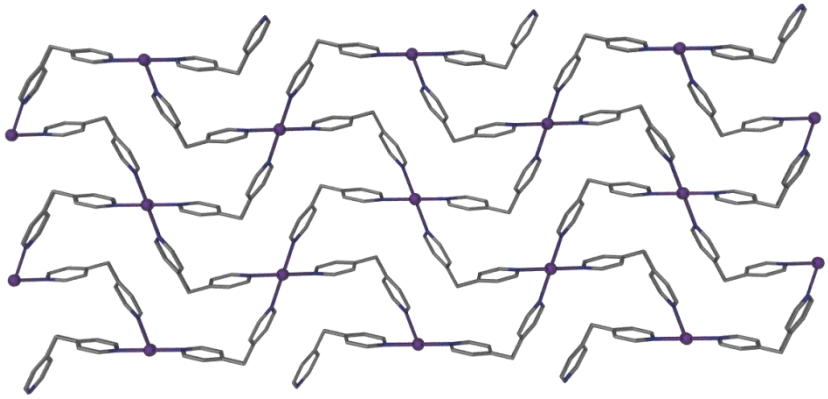

Figure 6.6. The 2-D (4,4)-connected network formed via the reaction of ligand **6.6** and $Cd(NO_3)_2 \cdot 4H_2O$, with the hydrogen atoms and nitrate anions omitted for clarity.

6.1.2. Provenance of the Flexible Ligands Studied and Related Literature Compounds

The flexible dipyridyl ligands examined in this chapter (Figure 6.7) were originally synthesised for use as precursors in the synthesis of extended hexaaryl[3]radialenes. Attempts at synthesising radialenes proved fruitless, as detailed in Chapter 2 section 2.3, however these compounds were subsequently studied as ligands in their own right. It was proposed that the combination of the flexible linker with the extended length of the donor arms may produce structures with dynamic solid-state behaviour.[12] Also the alkyne bonds in compounds **2.51** and **2.52** may provide another site, in addition to the pyridyl donors, for interaction with metal atoms.[13]

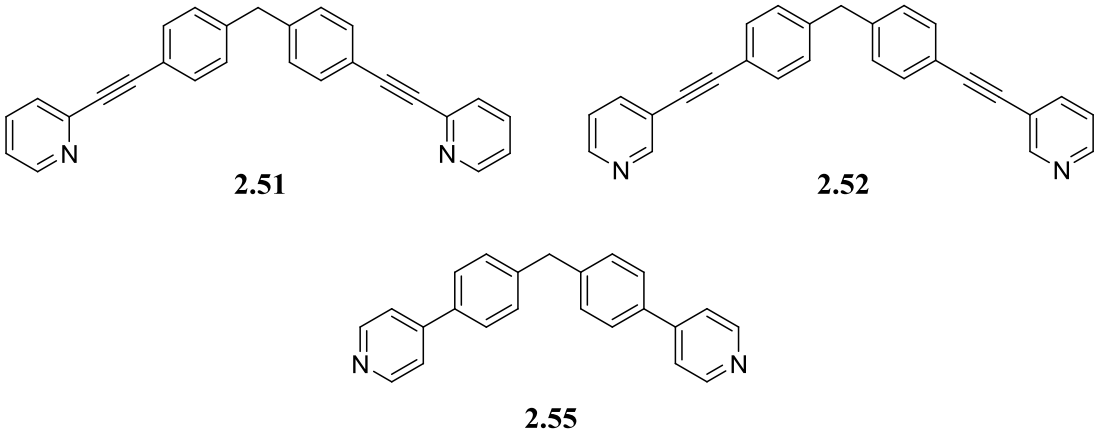

Figure 6.7. The flexible ligands bis(4-(pyridin-2-ylethynyl)phenyl)methane (**2.51**), bis(4-(pyridin-3-ylethynyl)phenyl)methane (**2.52**) and bis(4-(pyridine-4-yl)phenyl)methane (**2.55**).

A number of compounds related to **2.51** and **2.52** have been reported in the literature (Figure 6.8).[14-18] Instead of a flexible diarylmethane linker these structures incorporate either a benzene (**6.7**-**6.9**) or a pyridyl (**6.10**) core and as such they are much more rigid than ligands **2.51** and **2.52**. The pyridyl donor atoms in the literature examples are also a lot closer in space than those in compounds **2.51** and **2.52**. All four of these examples have been observed to form coordination polymers with silver(I).[14-16]

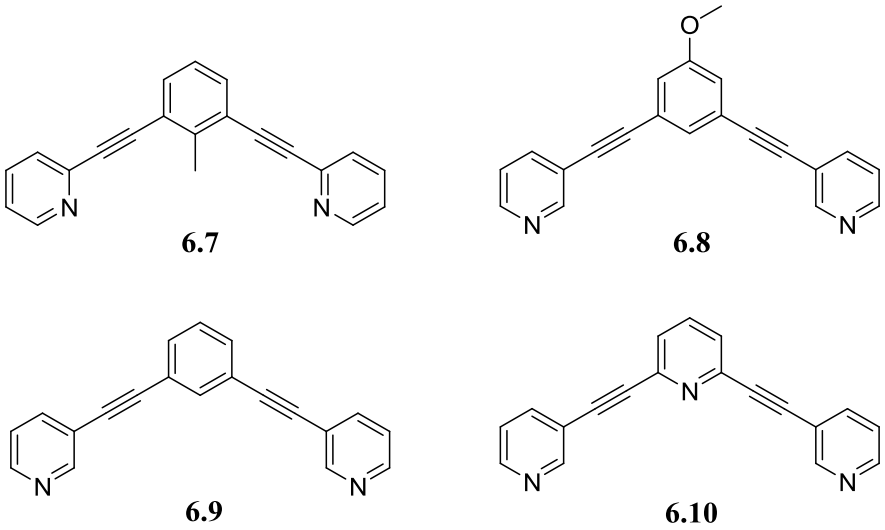

Figure 6.8. Selected literature examples of dipyridyl ligands similar to **2.51** and **2.52**.

1,3-Bis(2-pyridylethynyl)-2-methylbenzene (**6.7**) forms a 1-D helical coordination polymer when reacted with $AgNO_3$ in a metal to ligand ratio of 3:1 (Figure 6.9).[14] The silver(I) atoms act as 2-connecting nodes even though they have a tetrahedral geometry; their coordination sphere is completed via chelation of a nitrate anion or via monodentate binding by one nitrate anion and one water molecule. Within this structure the distance between the nitrogen donor atoms of **6.7** is approximately 10 Å and the angle between the donor atoms and the benzene linker ranges from 132.4-137.8°. In the extended structure π-π stacking is observed between pyridyl rings of adjacent helices with a centroid-centroid distance of 3.6 Å; however no interactions are observed between the alkynes and the silver(I) ions.

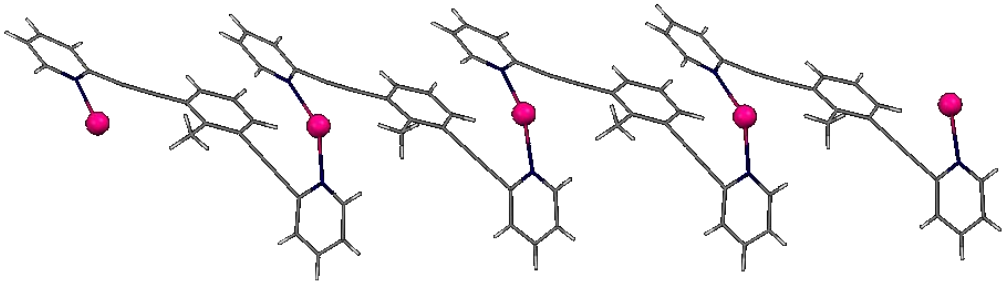

Figure 6.9. A perspective view of the 1-D helical coordination polymer of **6.7** and silver(I). Anions and solvent are not shown.

5-Methoxy-1,3-bis(pyridin-3-ylethynyl)benzene (**6.8**) has also been observed to form 1-D coordination polymers upon reaction with either $AgCF_3SO_3$ or $AgBF_4$.[15] These two structures are similar in the fact that they both have a zigzag topology, however the pyridyl rings of **6.8** in the $AgBF_4$ structure are coplanar with the central benzene ring whereas those in the

$AgCF_3SO_3$ structure have a slight twist. This is due to the difference in packing interactions observed between the two structures. Within the $AgBF_4$ structure (Figure 6.10 (a)) the packing interactions are dominated by π-π stacking between a pyridyl ring and a benzene ring of the ligand **6.8** within adjacent 1-D chains. The distance between the centroids of the interacting rings is 3.51 Å. In the $AgCF_3SO_3$ structure (Figure 6.10 (b)) there are two different interactions present. The first is a Ag-Ag interaction between adjacent chains with Ag-Ag bond lengths of 3.15 Å. The second is a silver-alkyne interaction between the silver(I) ions and the alkyne bonds of ligand **6.8**. The Ag-C_{alkyne} distances range from 3.17-3.24 Å.

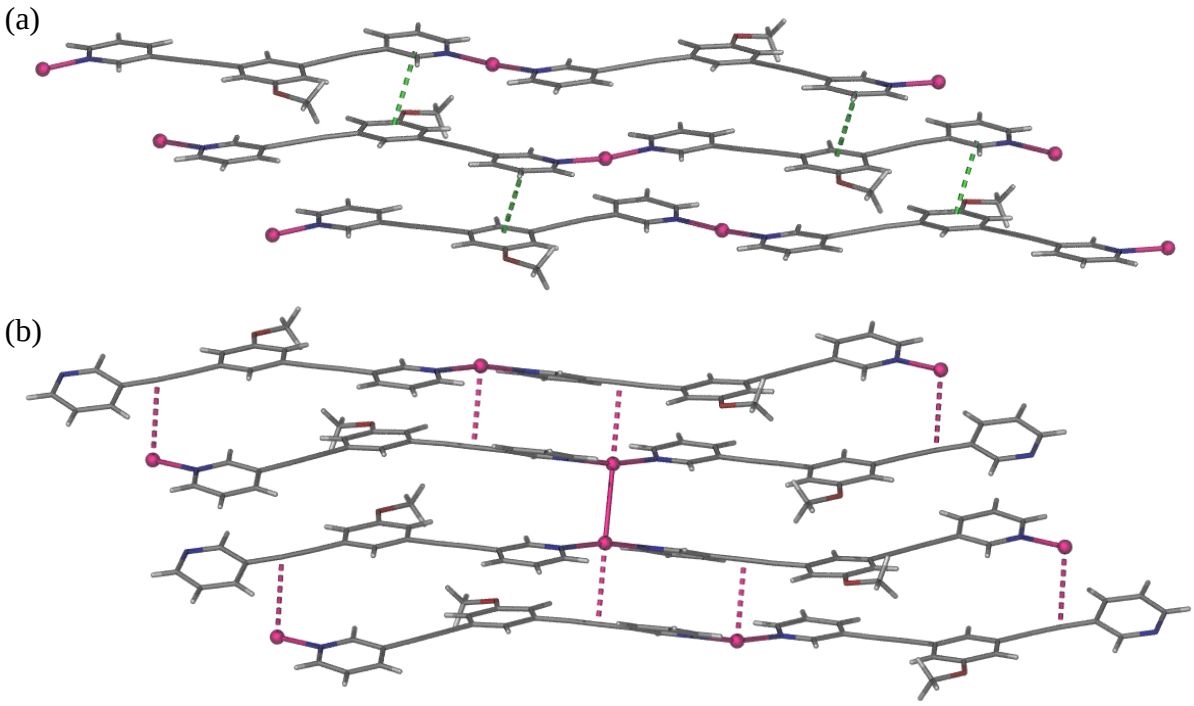

Figure 6.10. A perspective view of the packing of (a) the 1-D polymer of **6.8** and $AgBF_4$ (the π-π interactions are shown as green dotted lines) and (b) the 1-D polymer of **6.8** and $AgCF_3SO_3$ (the Ag-π interactions are shown as pink dotted lines). Anions are not shown.

The final two ligands that will be discussed are 1,3-bis(pyridin-3-ylethynyl)benzene (**6.9**) and 2,6-bis(pyridin-3-ylethynyl)pyridine (**6.10**), the syntheses of which were recently reported by the Crowley group.[16] These ligands were designed for use as components in the synthesis of metal-containing shape-persistent macrocycles, which may pack in the solid-state such that they form 1-D nanotubular structures. The reaction of **6.10** with one equivalent of $AgClO_4$ appeared to form a metallo-macrocycle in solution but upon crystallisation the complex underwent ring-opening to produce a 1-D coordination polymer. The topology of the structure is that of a twisted ladder where the ligands form the sides of the ladder and the silver(I) atoms make up the rungs (Figure 6.11). The central pyridyl ring of ligand **6.10** is involved in

coordination as well as the pyridyl arms and this results in a trigonal planar geometry of the silver(I) ions being coordinated by the donor atoms of two pyridyl arms and one central ring. Like previously discussed 1-D polymers, this structure exhibits π-π stacking interactions between pyridyl rings of adjacent ladders with centroid-centroid distances of 3.65 Å.

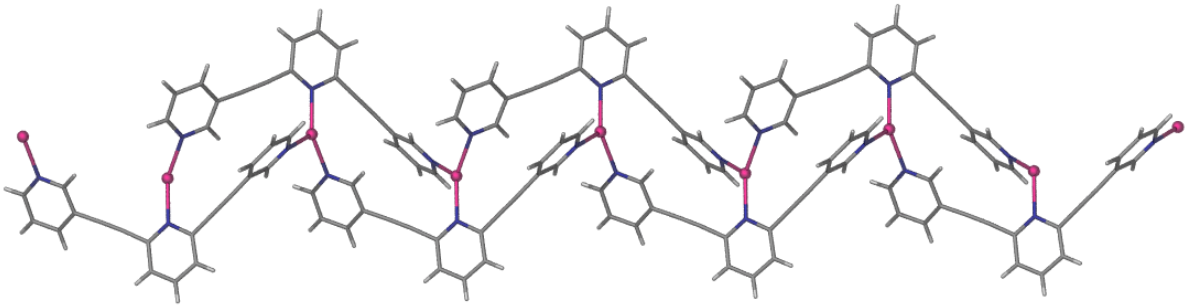

Figure 6.11. A perspective view of the 1-D twisted ladder coordination polymer of **6.10** and silver(I). Anions were omitted for clarity.

The reaction of **6.9** with one equivalent of $AgClO_4$ also produced metallo-macrocycles in solution and this structure was maintained in the solid-state. The 2:2 metallo-macrocycle is composed of two molecules of **6.9** and two linear silver(I) ions and possesses a cavity of approximately 7 × 9 Å in size (Figure 6.12 (a)). Despite its planarity the metallo-macrocycle did not pack in the desired nanotubular fashion and instead exhibited a stepped conformation (Figure 6.12 (b)) stabilised by a combination of Ag-Ag interactions, with a Ag-Ag bond length of 3.15 Å, and π-π stacking interactions between adjacent metallo-macrocycles (with centroid to centroid distances of 3.83 Å).

(a) (b)

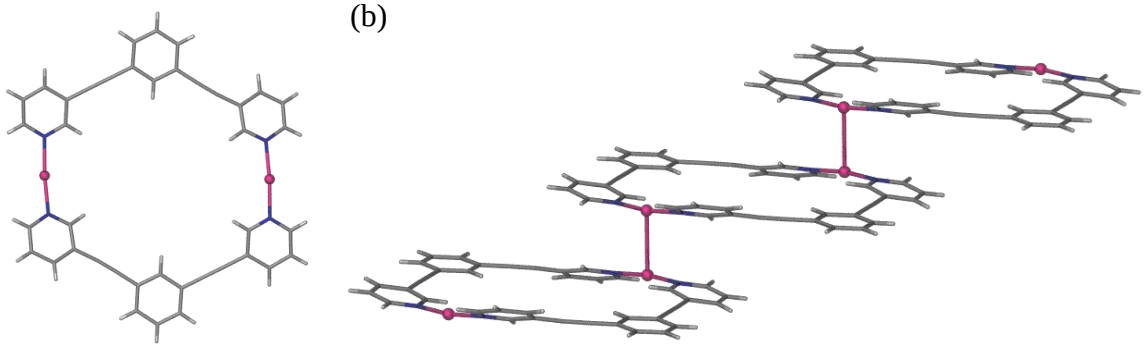

Figure 6.12. A perspective view of (a) the metallomacrocycle of **6.9** and silver(I) and (b) the stepped packing of adjacent metallomacrocycles in the extended polymer structure.

Examination of similar ligands to **2.51** and **2.52** has shown that there is a high probability that they will form 1-D coordination polymers and that it is also likely that π-stacking and possibly Ag-Ag and silver-alkyne interactions will be observed in the extended structures.

6.2. Coordination Polymers of Bis(4-(pyridin-2-ylethynyl)phenyl)methane (2.51)

6.2.1. Silver(I) Coordination Polymers

The coordination chemistry of the ligands discussed in the following sections was investigated via reaction of the ligands with a series of silver(I) and copper(I) salts, including $AgClO_4$, $AgPF_6$, $[Cu(CH_3CN)_4]PF_6$ and $[Cu(CH_3CN)_4]BF_4$. These were conductecd in metal to ligand ratios ranging from 1:2 to 2:1 in either nitromethane or a mixture of methanol and acetonitrile. Compared to the multidentate radialene ligands, the flexible bis-pyridyl ligands examined have only one possible bridging coordination mode, bidentate, in order to produce coordination polymers. Thus the topology of the coordination polymers is determined by the geometry of the metal atoms and the varying conformation of the flexible ligand. A number of coordination polymers of bis(4-(pyridin-2-ylethynyl)phenyl)methane (**2.51**) with silver(I) were able to be obtained (Scheme 6.1).

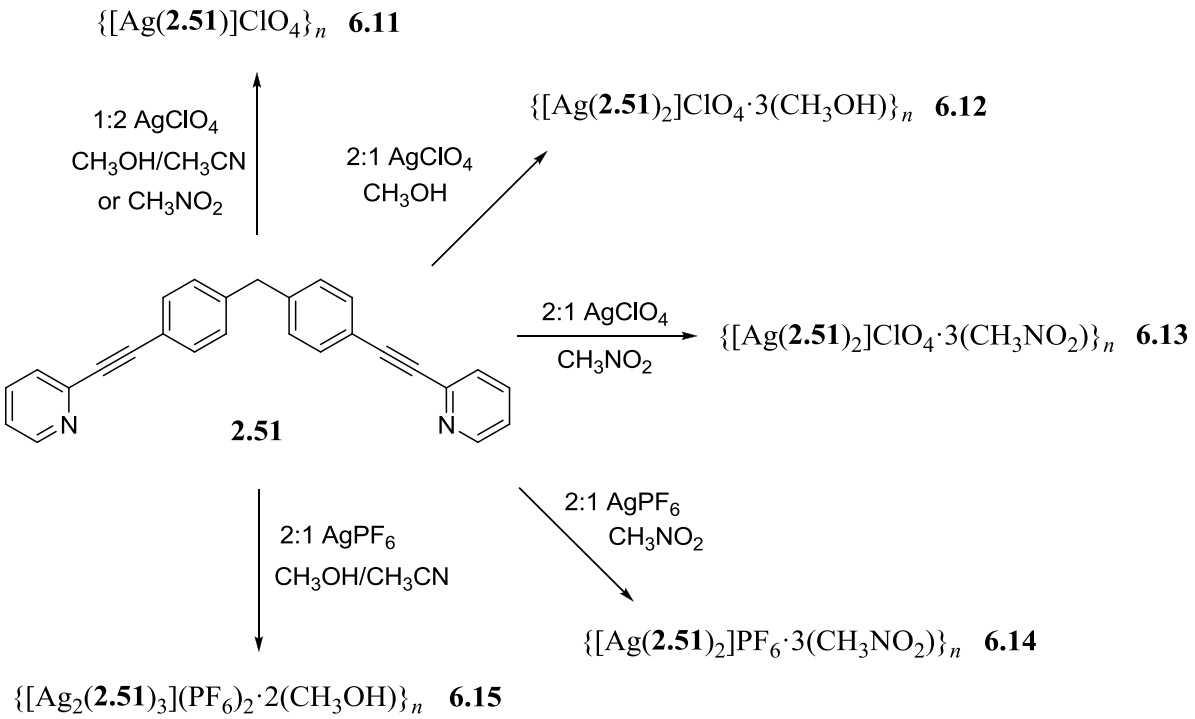

Scheme 6.1

Slow evaporation of a solution of **2.51** and silver perchlorate in a 1:2 ligand to metal ratio from a mixed solvent system of methanol and acetonitrile yielded compound **6.11** as pale yellow plate-like crystals in 67% yield (Scheme 6.1). The crystals were characterised by elemental analysis (analysis calculated for $C_{27}H_{18}N_2Ag_1Cl_1O_4$ C 56.12, H 3.15, N 4.85; found C 55.73, H 3.05, N 4.84) and IR spectroscopy, which exhibited sharp peaks for the C≡C

(2216 cm^{-1}) and Cl-O (1065 cm^{-1}) stretches. The structure, as confirmed by X-ray crystallography, had the formula $\{[Ag(\mathbf{2.51})]ClO_4\}_n$ (**6.11**) and contained no solvate molecules. It was found that this structure could also be obtained via slow evaporation from nitromethane.

Compound **6.11** crystallises in the triclinic space group *P*-1, with an asymmetric unit that contains one molecule of the ligand, one silver(I) atom and one perchlorate anion (Appendix 1, Figure A1.12). The structure was refined with no disorder problems to an R_1 value of 4.11%. The extended structure of **6.11** is a simple 1-D zigzag coordination polymer as both the ligands and the silver(I) atoms act as two-connecting nodes (Figure 6.13). The silver(I) atom has a distorted T-shaped geometry as it is coordinated to two silver(I) atoms, with Ag-N bond lengths of 2.183(3) and 2.188(2) Å, and one oxygen atom of the perchlorate anion with a Ag-O bond length of 2.615(3) Å. The bond angles around the silver(I) atom are 88.24(9)° and 110.90(10)° respectively for the N-Ag-O angles and 151.26(9)° for the N-Ag-N angle. Another point of interest is the slight bend in one of the alkyne linkers connecting the central diarylmethane to the pyridyl rings, which has a C-C-C angle of 175.7(3)° compared to 179.3(4)° for the other, more linear alkyne.

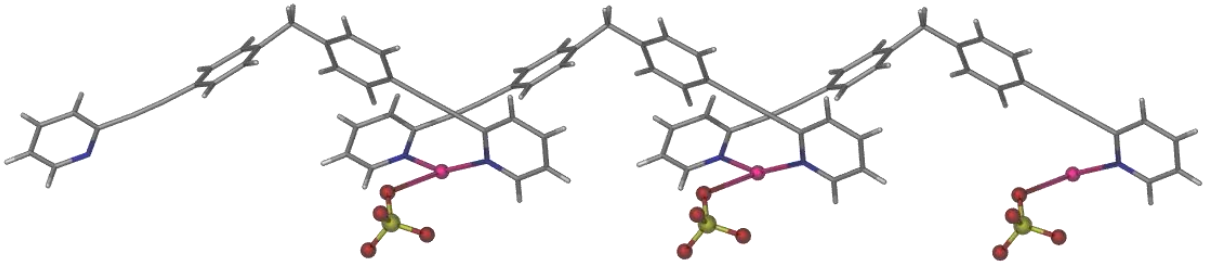

Figure 6.13. A perspective view of the cationic 1-D coordination polymer chain of **6.11**.

Close contacts are exhibited between the silver(I) cations and the two alkyne bonds adjacent to them. The Ag-C_{alkyne} distances are 2.98 and 3.14 Å respectively indicating a weak η^1-Ag-π interaction. Although the average distance of η^1-Ag-π interactions is generally 2.40-2.90 Å,[19-21] examples of similar coordination polymers with Ag-C_{alkyne} distances between 3.17 and 3.30 Å have been reported.[15,22] Complex **6.11** is packed quite tightly in the crystal lattice. Two 1-D polymer chains, one shown in blue and one shown in green in Figure 6.14, are interdigitated with perchlorate anions sandwiched between them. There are no π-stacking interactions present between the pyridyl and aryl rings of the two interdigitated chains.

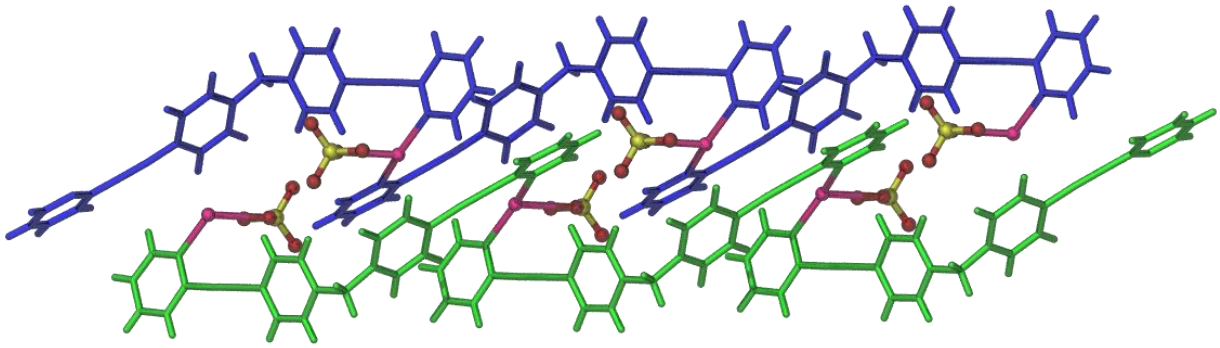

Figure 6.14. A perspective view of **6.11** showing interdigitation of two 1-D polymer chains.

Pairs of interdigitated 1-D polymer chains are then packed around the blue and green chains, as seen in Figure 6.15, to complete the crystal packing. It is between the green and orange chains that weak π-stacking is observed between a pyridyl ring of one ligand and a benzene ring of another. The distance between the centroids of the two interacting rings is 3.88 Å. Another π-stacking interaction is also observed between the layer of 1-D polymer chains observed in Figure 6.15 and those that pack adjacent to them. In this instance the interaction is between two benzene rings and the centroid separation of these rings is 3.64 Å.

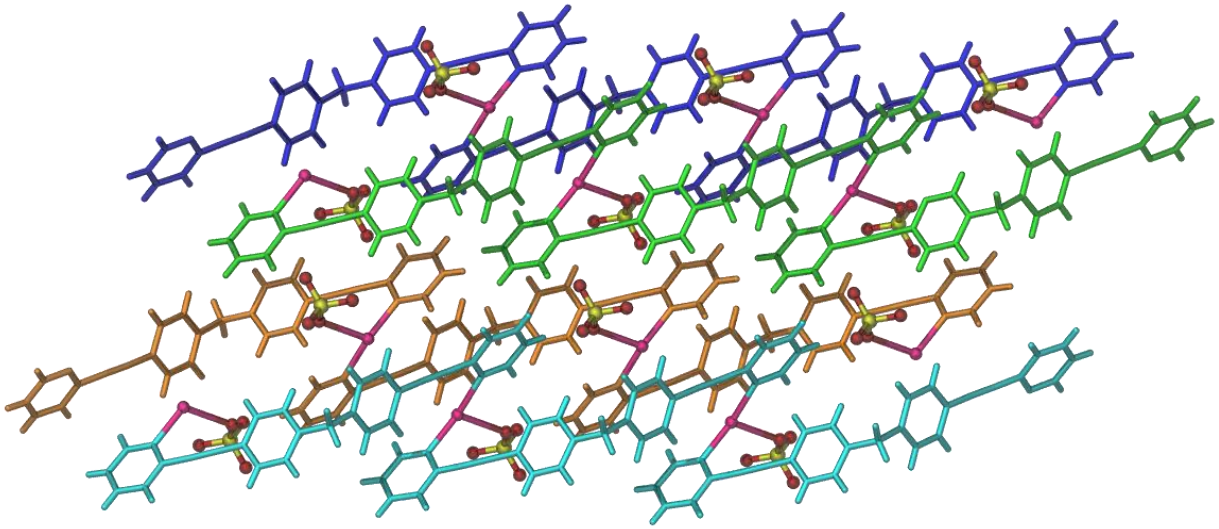

Figure 6.15. A perspective view showing the extended packing of pairs of 1-D polymer chains in the structure of **6.11**.

Slow evaporation of **2.51** and $AgClO_4$ in a ratio of 2:1 from methanol, after an initial beige coloured precipitate was removed, yielded a structure with the formula $\{[Ag(\mathbf{2.51})_2]ClO_4 \cdot 3(CH_3OH)\}_n$ (**6.12**) (Scheme 6.2) as trace quantities of pale yellow blocks. Repeated attempts to reproduce these crystals for IR and elemental analysis were unsuccessful and led to the production of a structure analogous to that of **6.13** instead. Complex **6.12**

crystallises in the triclinic space group *P*-1, with an asymmetric unit that contains two molecules of the ligand, one silver(I) atom and one perchlorate anion (Appendix 1, Figure A1.13). The methanol solvate molecules could not be located completely in the electron difference map and thus the SQUEEZE routine of PLATON was applied to the data. The electron density removed from the asymmetric unit corresponded to three molecules of methanol, which are included in the molecular formula.

The extended structure of **6.12** is also a 1-D coordination polymer except it exhibits a ladder-like topology as the silver(I) atoms act as three connecting nodes. The silver metal centres have a tetrahedral geometry with Ag-N bonds ranging from 2.255(3) to 2.410(3) Å and N-Ag-N angles between 94.62(13) and 138.26(12)°. The tetrahedral silver(I) nodes are slightly distorted from true tetrahedral with a four coordinate geometry index, τ_4, value of 0.78. Each of the silver atoms is connected to the silver(I) atom opposite via two ligands to form the 'rungs' of the ladder structure and then connected via a further two ligands to the two silver(I) atoms either side to form the 'sides' of the ladder (Figure 6.16). The distance between two silver(I) atoms of the same 'rung' is 11.21 Å and between silver(I) atoms on the same side of the ladder is 14.45 Å. The silver(I) nodes are well aligned with those on the same side of the ladder but the 'rungs' are sloped such that the silver nodes making up the same 'rung' are positioned at a 46° angle to each other. As previously mentioned the silver(I) atoms are coordinated by four different ligand molecules however close silver-alkyne contacts are only observed with one of these ligands with a Ag-C_{alkyne} distance of 3.20 Å.

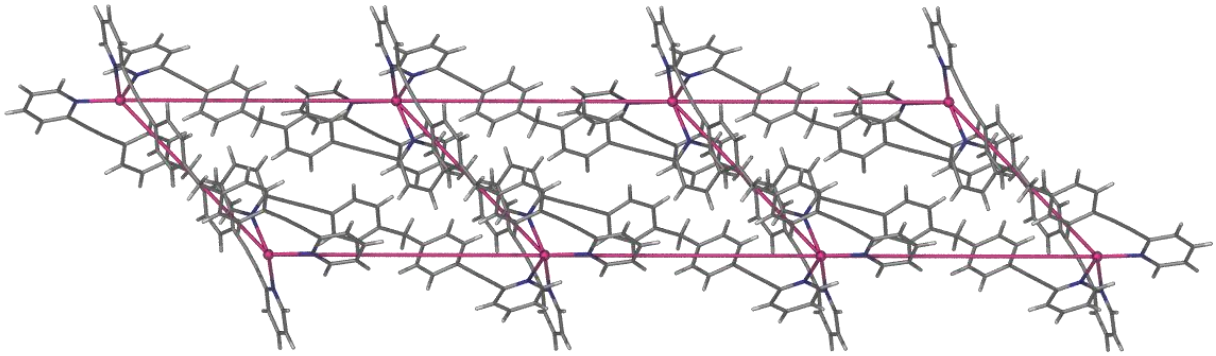

Figure 6.16. A perspective view of the cationic 1-D coordination polymer chain of **6.12**. The silver atoms are connected by pink bonds to highlight the underlying connectivity.

The 1-D ladder polymers pack within the crystal lattice in a layered fashion with the perchlorate anions sandwiched between them (Figure 6.17). Between these layers π-stacking is observed between the benzene and pyridyl rings on one side of the ligand with centroid to centroid distances of 3.77 Å. No silver-alkyne interactions are observed between adjacent

polymer chains as the silver(I) atoms are completely surrounded by the four ligand donor atoms to which they are coordinated.

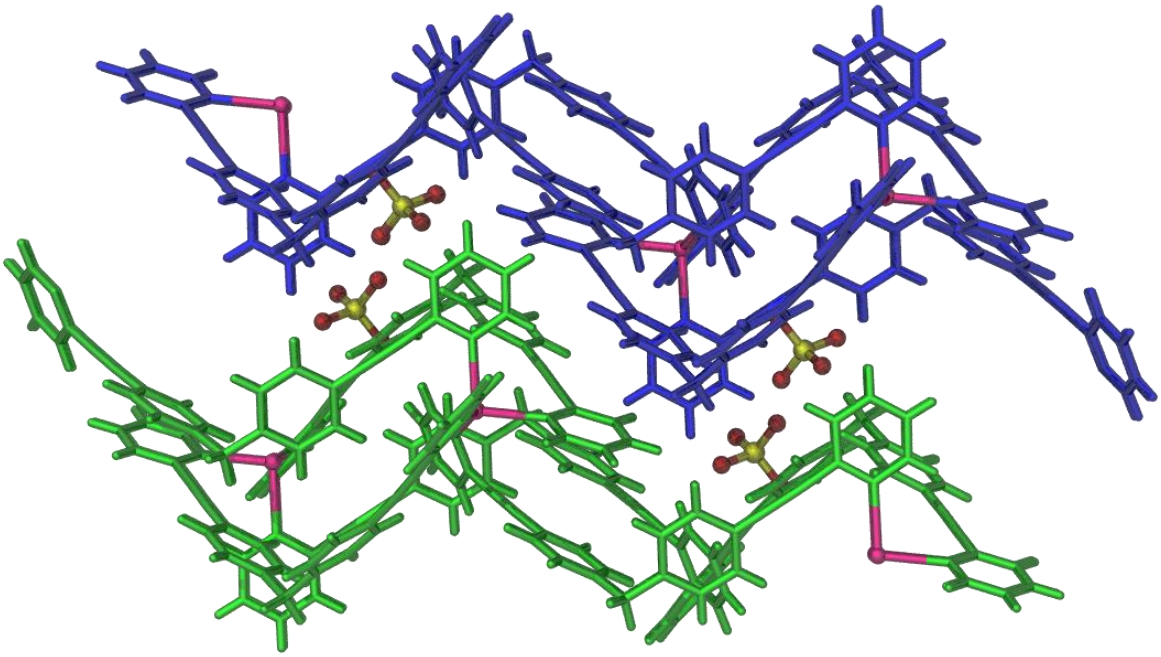

Figure 6.17. A perspective view showing the packing of the 1-D polymer chains in **6.12**.

Similar to structure **6.12**, complexes **6.13** and **6.14** are both 1-D ladder-like coordination polymers. Slow evaporation of a nitromethane solution of **2.51** and $AgClO_4$ in a 2:1 ratio produced a polymer with the formula $\{[Ag(\mathbf{2.51})_2]ClO_4 \cdot 3(CH_3NO_2)\}_n$ (**6.13**) as pale yellow, hexagonal, plate-like crystals in 59% yield. Changing the anion present to hexafluorophosphate via reaction of **2.51** with $AgPF_6$ in a 2:1 ratio led to crystals of a similar morphology with the formula $\{[Ag(\mathbf{2.51})_2]PF_6 \cdot 3(CH_3NO_2)\}_n$ (**6.14**) in 42% yield. Both sets of crystals were analysed via elemental analysis, which were consistent with the X-ray structures but with less solvent due to drying to constant weight under vacuum, and IR spectroscopy, which exhibited the characteristic C≡C and Cl-O or P-F stretches. Compounds **6.13** and **6.14** are isostructural and crystallise in the triclinic space group *P*-1 with two molecules of the ligand, one anion, and three nitromethane solvate molecules in the asymmetric unit (Appendix 1, Figure A1.14 and Figure A1.15). Both polymers were refined with minimal issues (one disordered nitromethane solvate molecule in **6.14** was modelled over two positions) to R_1 values of 5.22 and 5.27% for **6.13** and **6.14** respectively.

Within structures **6.13** and **6.14** the silver(I) atoms act as three connecting nodes with a tetrahedral geometry. The Ag-N bonds in these structures range from 2.349(3) to 2.408(2) Å and N-Ag-N angles are between 94.63(9) and 135.93(9)°. The tetrahedral silver(I) nodes are

slightly distorted with a four coordinate geometry index, τ_4, value of 0.72 for both structures. As seen in structure **6.12**, each of the silver atoms in structures **6.13** and **6.14** are connected to the silver(I) atom opposite via two ligands and then connected via a further two ligands to the two silver(I) atoms either side (Figure 6.18). The distance between two silver(I) atoms of the same 'rung' is 10.79 and 10.90 Å, for **6.13** and **6.14** respectively, and between silver atoms on the same side of the ladder is 14.02 Å for **6.1** and 14.13 Å for **6.14**. In these ladder polymers the distance between the silver(I) atoms of the same 'rung' is shorter than that of structure **6.12** (11.21 Å). Another difference is that in **6.13** and **6.14** the silver(I) nodes are almost perfectly opposite both those on the same side of the ladder structure and those that are on the same 'rung' resulting in a Ag-Ag-Ag angle of 82.72°, as opposed to 133.97° for **6.12**. This opens the polymer up as shown by the large intra-ladder voids in Figure 6.18 compared to the more compressed form in **6.12** (Figure 6.16).

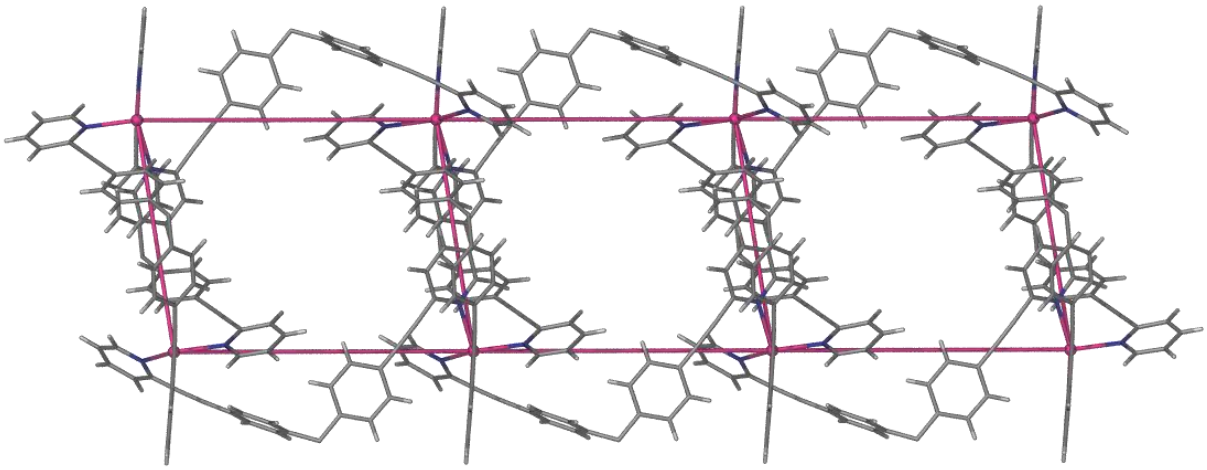

Figure 6.18. A perspective view of the cationic 1-D coordination polymer chain of the isomorphous structures **6.13** and **6.14**. The silver atoms are connected by pink bonds to highlight the underlying connectivity.

It appears that changing the solvent from methanol/acetonitrile to nitromethane, comparing **6.12** to **6.13**, leads to a more open structure likely due to the larger size of the nitromethane molecules (Figure 6.19). These two structures are psuedopolymorphs. Upon repeating the reaction in methanol/acetonitrile, in order to obtain more of complex **6.12** for elemental analysis, it was found that a polymer isomorphous to **6.13** was repeatedly formed. The main difference between these structures is the Ag-Ag-Ag angle, as discussed above, which is a result of subtle changes in the C-CH_2-C angle and rotation of the pyridyl donor arms around the methylene group. Further investigation into **6.12** and **6.13**, regarding possible interconversion upon solvent exchange, may be of interest.

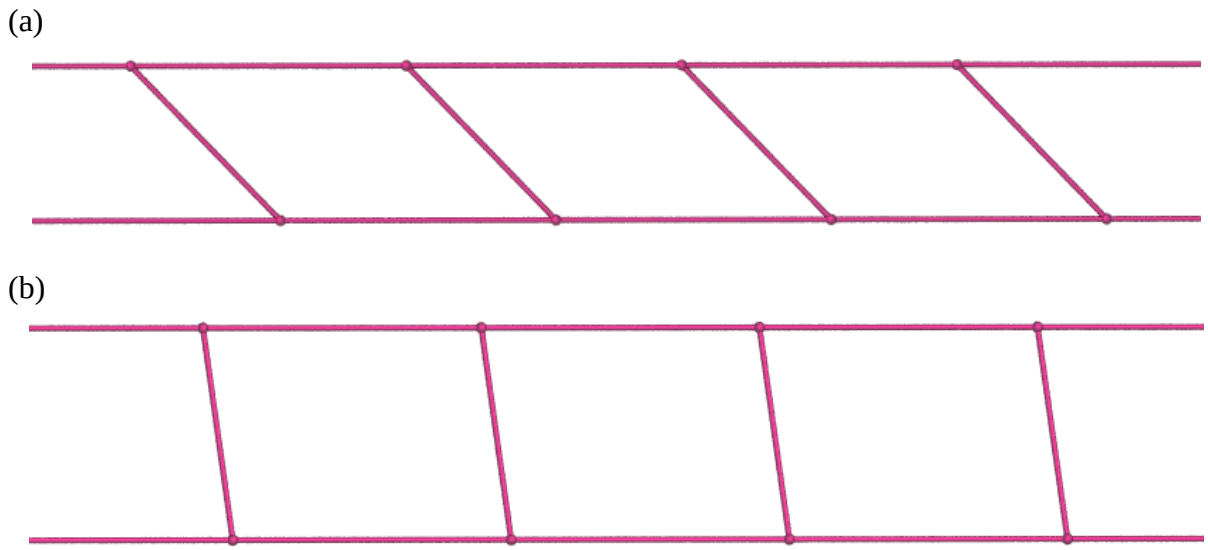

Figure 6.19. The network topologies of structures (a) **6.12** and (b) **6.13**.

The 1-D ladder polymers of structures **6.13** and **6.14** pack within the crystal lattice in layers with the anions and the nitromethane solvate molecules located within the voids in the ladders and also between adjacent layers (Figure 6.20). Very weak π-π stacking interactions are present between pyridyl and benzene rings of different ligands in the same polymer chain with a centroid-centroid distance of 3.79 Å. Stronger C-H···π interactions are observed between pyridyl and benzene rings of adjacent polymer chains with C-H to aryl centroid distances ranging from 2.76 to 3.37 Å.

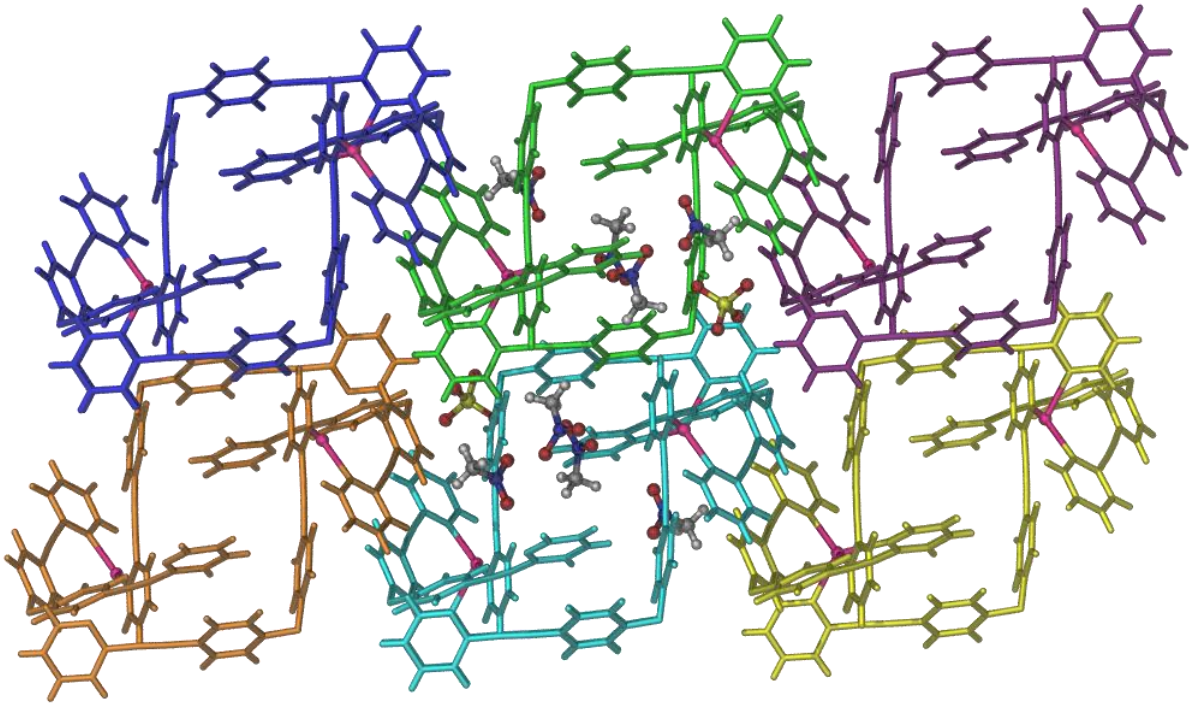

Figure 6.20. A perspective view showing the extended packing of the 1-D polymer chains in structure **6.13**.

Overall, two distinct polymers were obtained via reaction of **2.51** with $AgClO_4$ depending on whether a low ligand to metal ratio was used, 1:2 leads to the 1-D zigzag polymer **6.11**, or a high ligand to metal ratio was used, 2:1 leads to the 1-D open ladder polymer **6.13**. Upon examining the crystallisation of **2.51** with $AgPF_6$ in a similar manner it was discovered that changing the ligand to metal ratio from 2:1, used in the formation of **6.14**, to 1:2 had no effect on the structure produced. In fact reaction of **2.51** with $AgPF_6$ in a 1:2 ratio in either nitromethane or methanol/acetonitrile produced structure **6.14**. This may be a result of the larger hexafluorophosphate anion not allowing the packing of similar 1-D zigzag polymer chains in the same fashion as structure **6.11** (Figure 6.14). Interestingly, keeping the ligand to metal ratio the same as that used in the production of **6.14** (2:1) but changing the solvent from nitromethane to methanol/acetonitrile led to the formation of a new structure, **6.15**, which has the formula $\{[Ag_2(\mathbf{2.51})_3](PF_6)_2 \cdot 2(CH_3OH)\}_n$. Pale yellow, block shaped crystals of **6.15** were produced in 48% yield and were characterised by elemental analysis (analysis calculated for $C_{81}H_{54}N_6Ag_2P_2F_{12} \cdot CH_3OH$ C 59.72, H 3.55, N 5.10; found C 59.37, H 3.29, N 5.14) and IR spectroscopy which exhibited sharp peaks for the characteristic C≡C (2221 cm^{-1}) and P-F (829 cm^{-1}) stretches.

Complex **6.15** crystallises in the triclinic space group *P*-1, with an asymmetric unit that contains three molecules of the ligand, two silver(I) atoms and two perchlorate anions (one fully occupied, one 50% occupied and one on a centre of inversion) (Appendix 1, Figure A1.16). The compound crystallised with significant disorder of the methanol solvate molecules such that they could not be located completely in the electron difference map. The SQUEEZE routine of PLATON was applied to the data and the electron density removed from the asymmetric unit corresponded to two molecules of methanol, which are included in the molecular formula.

In the structure of **6.15** the silver(I) atoms again act as three connecting nodes. Unlike the tetrahedral three-connecting nodes seen in **6.12**, **6.13** and **6.14**, the silver(I) atoms of **6.15** have a trigonal planar geometry. There are two crystallographically unique silver(I) atoms in this structure and their physical parameters are very similar with Ag-N bond lengths ranging from 2.259(4) to 2.272(4) Å and N-Ag-N angles between 117.71(14) and 124.07(14)°. Each of the silver(I) atoms is connected to three other silver(I) atoms via three different ligand molecules, which are topologically trivial. It takes six 3-connecting silver(I) atoms to form the hexagonal motif which is repeated throughout the structure to form a 2-D (6,3) network (Figure 6.21 (a)). This 2-D network is not planar but corrugated (Figure 6.21 (b)) with three silver(I) atoms of one hexagonal motif situated in one plane and three in another (Figure 6.21 (c)).

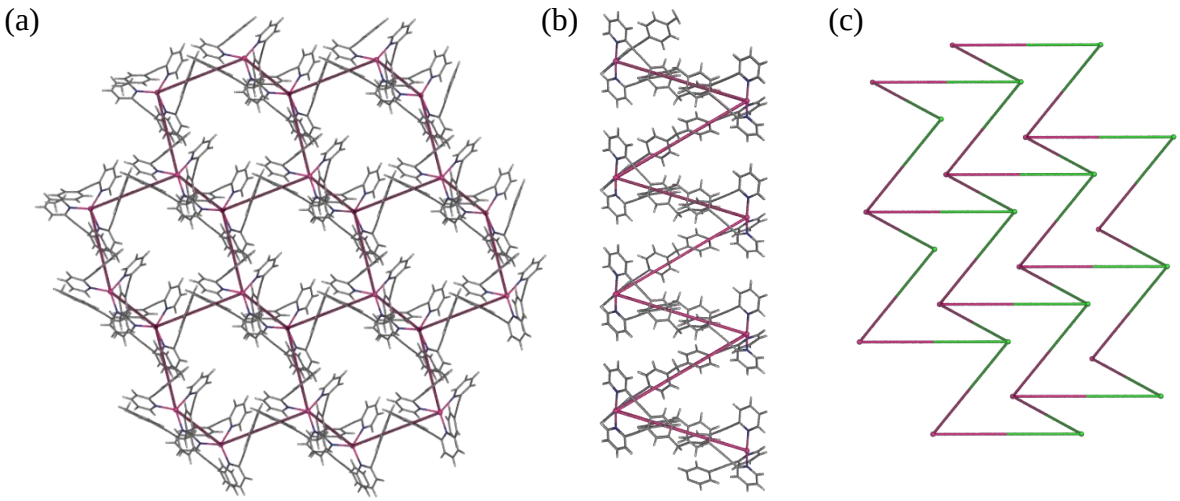

Figure 6.21. Perspective views of (a) the cationic 2-D (6,3) net of structure **6.15** looking down the *c*-axis and (b) looking down the *b*-axis. The 3-connecting silver nodes have been joined by pink bonds to highlight the underlying connectivity. (c) A schematic highlighting the silver(I) atoms within a single 2-D net which reside in different planes.

Each of the two crystallographically unique silver(I) atoms are surrounded by the three ligand molecules to which they are coordinated and exhibit close contacts with the ligand alkyne bonds. The Ag-C_{alkyne} distances for the first silver(I) ion range from 3.12-3.24 Å and for the second silver(I) ion range from 3.16-3.18 Å indicating weak η^1-Ag-π interactions. The trigonal planar geometry of the silver atoms allows closer approach of the ligand alkyne bonds to the metal as opposed to the distorted tetrahedral geometry in structures **6.13** and **6.14** within which no η^1-Ag-π interactions are observed. No π-π stacking or C-H···π interactions are observed between aryl rings within the same 2-D (6,3) sheet.

The voids in the 2-D polymer seen in Figure 6.21 (a) are in fact filled by a second polymer. These two 2-D (6,3) sheets are not interpenetrated but are instead interdigitated, which means the two nets could theoretically be separated without having to break any bonds (Figure 6.22). The pairs of 2-D nets are then packed within the crystal in layers with the hexafluorophosphate anions sandwiched between these layers. No π-π stacking interactions are observed between ligands situated in different 2-D nets. However, there are C-H···π interactions present between pyridyl rings and between pyridyl and benzene rings of ligands situated in different nets with C-H to aryl centroid distances ranging from 2.78 to 3.17 Å.

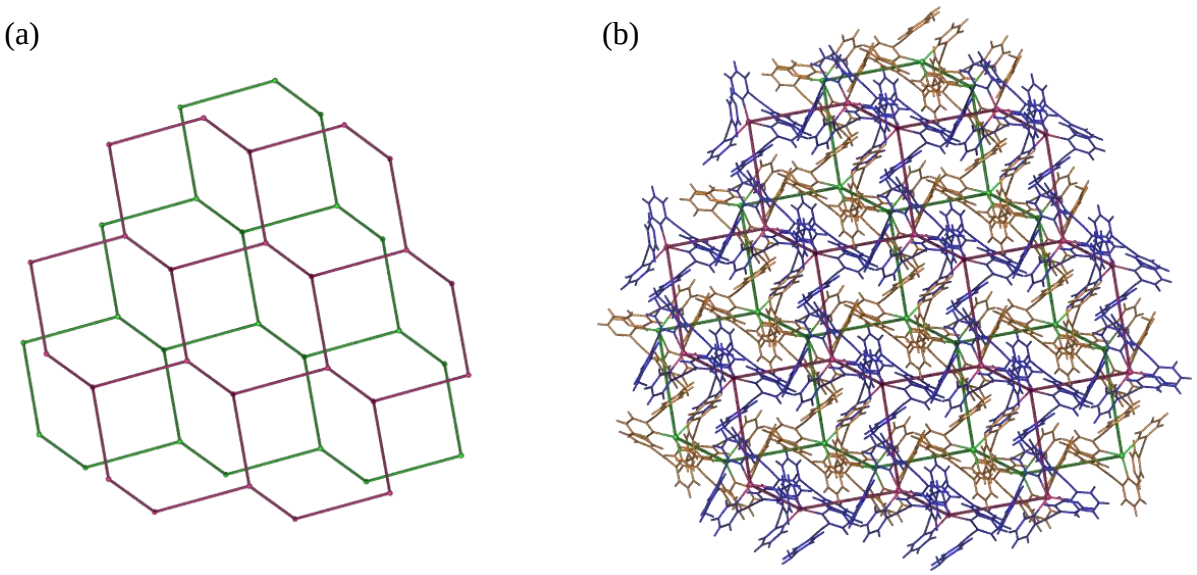

Figure 6.22. (a) A schematic of the two interdigitated networks and (b) a perspective view showing the extended packing of a pair of 2-D (6,3) sheets in structure **6.15**.

A number of 2-D (6,3) nets have already been discussed in Chapter 4, sections 4.1.1 and 4.2.1, including structures **4.5**-**4.8**, which are composed of hexa(4-cyanophenyl)[3]radialene (**2.29**) and silver(I).[23] Within these structures both the ligand and the silver(I) ions act as three connecting nodes to form the hexagonal (6,3) motif, whereas in **6.15** only the metal atoms act as 3-connecting nodes and the ligands are topologically trivial. This is the opposite to what is observed in a 2-D (6,3) network of the hexacyano[3]radialene anion and manganese(II), reported by Murray and Batten, where the ligand acts as a three connecting node and the metal is topologically trivial.[24] These structures, as well as two other examples discussed in Chapter 4,[25,26] are planar and pack in simple layers within the crystal lattice. In this respect the corrugated conformation of **6.15** is more similar to the 2-D (6,3) net of silver tricyanomethanide ($AgC(CN)_3$).[27-29] This structure is also corrugated but exhibits two-fold 2-D → 2-D parallel interpenetration instead of the simple interdigitation as observed in structure **6.15**. Within the silver tricyanomethanide network both the silver(I) ions and the central carbon of the tricyanomethanide anions are considered 3-connecting nodes, however the corrugation is due to the trigonal pyramidal geometry of the silver(I) atoms as the anions are largely planar. This contrasts with the structure of **6.15** where the corrugation is due to the combination of both the trigonal planar geometry of the silver(I) ions and hinged nature of the ligands.

6.2.2. Copper(I) Coordination Polymers

Two different coordination polymers of **2.51** with copper(I) were able to be obtained (Scheme 6.2). Slow evaporation of **2.51** and $[Cu(CH_3CN)_4]PF_6$ in a 1:2 ratio from a solvent mixture of methanol and acetonitrile gave bright yellow, block-shaped crystals with the formula $\{[Cu(\mathbf{2.51})(CH_3CN)_2]PF_6]\}_n$ (**6.16**), as determined by X-ray crystallography, in 51% yield. The crystals were characterised via elemental analysis (analysis calculated for $C_{27}H_{18}N_2Cu_1P_1F_6$ C 56.01, H 3.14, N 4.84; found C 56.28, H 3.19, N 4.92) and IR spectroscopy, which exhibited sharp peaks for the C≡C (2218 cm^{-1}) and P-F (825 cm^{-1}) stretches.

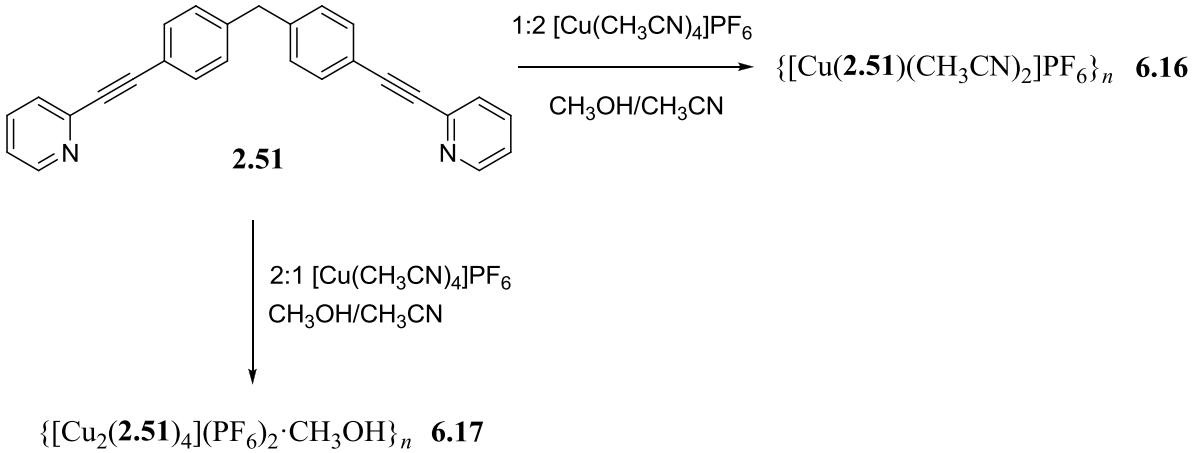

Scheme 6.2

Complex **6.16** crystallises in the monoclinic space group $P2_1/c$, with an asymmetric unit that contains one molecule of the ligand, one copper(I) atom with two coordinated acetonitrile molecules and one hexafluorophosphate anion (Appendix 1, Figure A1.17). The structure was refined with no disorder problems to an R_1 value of 4.69%. The extended structure of **6.16**, very similar to that of **6.11**, is a simple 1-D zigzag coordination polymer as both the ligands and the copper(I) atoms act as two-connecting nodes (Figure 6.23).

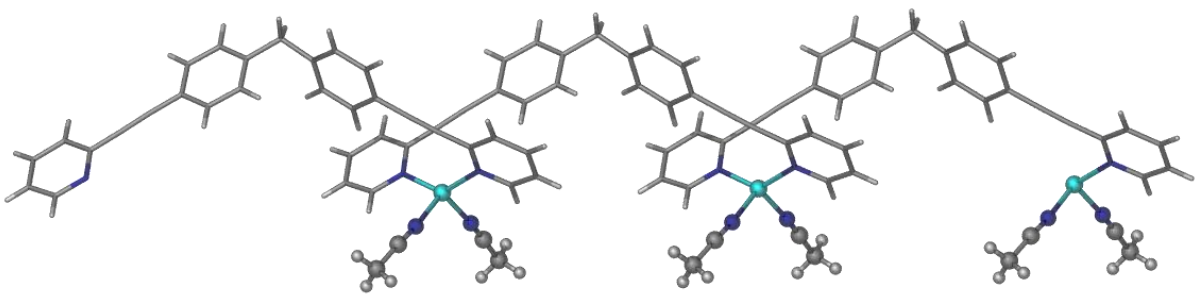

Figure 6.23. A perspective view of the cationic 1-D coordination polymer chain of **6.16**.

The difference between structures **6.16** and **6.11** is that the copper(I) metal atom in **6.16** has a tetrahedral geometry, whereas the silver(I) metal atom of **6.11** has a T-shaped geometry. In fact the copper(I) atom has a slightly distorted tetrahedral geometry as shown by a calculated four coordinate geometry index, τ_4, value of 0.83. The Cu-N bond lengths range from 2.0182(19) to 2.058(2) Å and the N-Cu-N bond angles are between 102.01(9) and 135.21(8)°.

The 1-D polymer chains in structure **6.16** do not pack as tightly as those in structure **6.11** due to two coordinated acetonitrile molecules on the copper(I) metal modes which maintain the preferred tetrahedral geometry of copper(I). Like **6.11**, the 1-D polymer chains in **6.16** pack in pairs, one shown in blue and one shown in green in Figure 6.24, with hexafluorophosphate anions sandwiched between them. It was noted earlier that structure **6.11** could only be obtained when **2.51** was reacted with $AgClO_4$ and that replacing the tetrahedral anion with a larger octahedral anion by reacting with $AgPF_6$ led to a different structure. In this case an analogous structure to **6.11** can be produced due to the coordinated acetonitrile molecules on the copper(I) metal nodes causing the 1-D polymer chains to pack further apart and thus allow for the accommodation of the larger hexafluorophosphate anion.

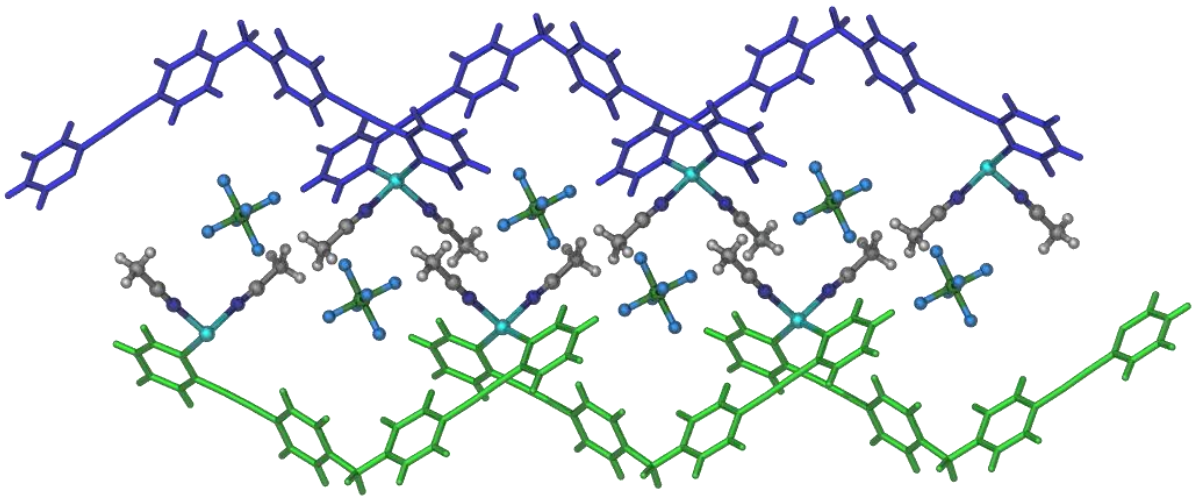

Figure 6.24. A perspective view of **6.16** showing the packing of two 1-D polymer chains.

The 1-D polymer chain pairs are then packed in layers within the crystal where the second chain of the first pair, coloured green in Figure 6.25, is interdigitated with the first chain of the second pair, coloured orange. The closest π-π stacking contacts within this structure are between a pyridyl ring and a phenyl ring within the orange and green polymers as represented in Figure 6.25. However, the distance between the centroids of the two interacting rings is 3.99 Å, which is just outside the limit of a significant interaction.

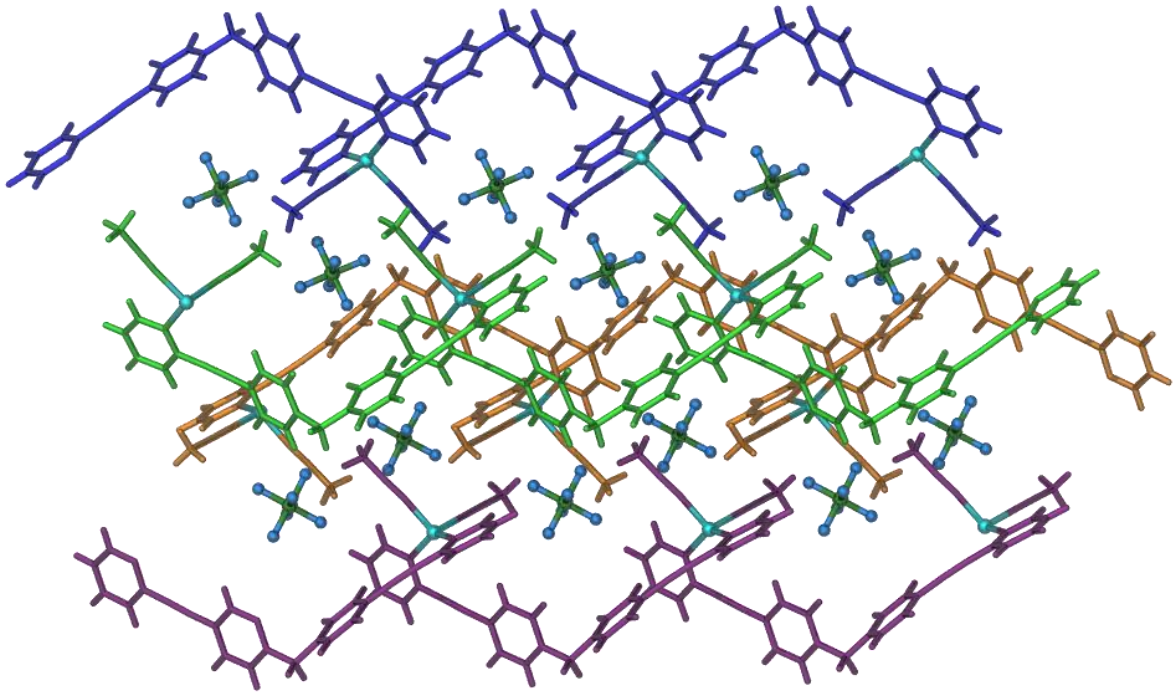

Figure 6.25. A view showing the packing of two pairs of 2-D chains in structure **6.16**.

The final coordination polymer of ligand **2.51** was obtained via slow evaporation of **2.51** and $[Cu(CH_3CN)_4]PF_6$ in a 2:1 ratio from methanol/acetonitrile. The resultant weakly diffracting yellow needles were obtained in 64% yield and required synchrotron radiation in order to solve the structure which has the formula $\{[Cu_2(\mathbf{2.51})_4](PF_6)_2 \cdot CH_3OH\}_n$ (**6.17**). The crystals were also characterised by elemental analysis and IR spectroscopy, which exhibited sharp peaks for the C≡C (2220 cm^{-1}) and P-F (833 cm^{-1}) stretches. Similar issues were encountered with low carbon values in the elemental analysis of this copper compound as were discussed in Chapter 4, section 4.2.2. Complex **6.17** crystallises in the triclinic space group *P*-1 with an asymmetric unit that contains four molecules of the ligand, two copper(I) atoms, two hexafluorophosphate anions (one fully occupied and two 50% occupied) and one methanol solvate molecule (Appendix 1, Figure A1.18). There was disorder of the methanol solvate molecule, which was modelled over two positions, and structure was refined to an R_1 value of 6.79%.

The extended structure of **6.17** is another 1-D polymer chain; even though the copper(I) atoms have a tetrahedral geometry they only act as two connecting nodes like structure **6.16**. Unlike structure **6.16**, the copper(I) metal nodes in structure **6.17** coordinate to four different ligand molecules as opposed to two ligand molecules and two solvent molecules. However, these four ligand molecules only connect the copper(I) nodes to the copper(I) atoms either side and as such form a 1-D polymer chain composed of loops rather than simple links (Figure 6.25).

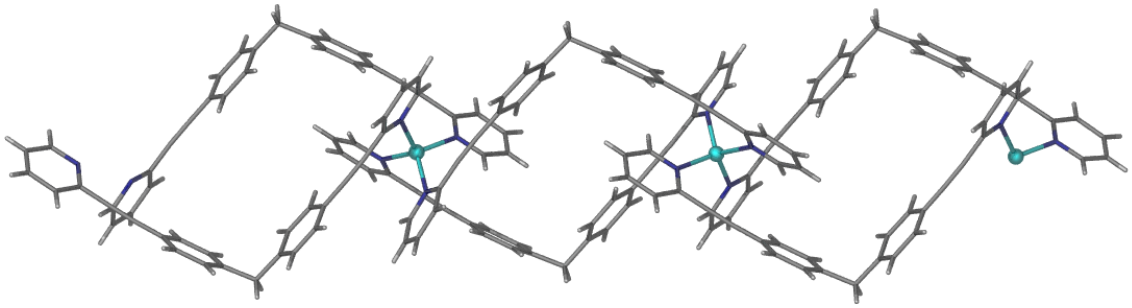

Figure 6.25. A perspective view of the cationic 1-D coordination polymer chain of **6.17**.

The formation of these two different structures is controlled by stoichiometry. When a small amount of ligand is present in the reaction mixture, where the ligand to metal ratio is 1:2, the copper(I) atoms coordinate only two ligand molecules as seen in structure **6.16**. Whereas when a greater amount of ligand is present, i.e. a ligand to metal ratio of 2:1, the copper(I) coordination sphere is completely filled by four ligand molecules as seen in structure **6.17**. There are two crystallographically unique copper(I) atoms in structure **6.17** and their physical parameters are very similar with Cu-N bond lengths ranging from 2.042(3) to 2.077(3) Å and N-Cu-N angles between 101.72(13) and 113.51(13)°. The copper(I) atoms are almost perfectly tetrahedral as shown by the calculated four coordinate geometry index, τ_4, values of 0.95 and 0.96 respectively. The 1-D polymer chains of **6.17** pack in simple layers within the crystal (Figure 6.26). The hexafluorophosphate anions and the methanol solvate molecules are located within the voids formed by the loops which make up the 1-D polymer chain. No π-stacking interactions are present between adjacent polymer chains.

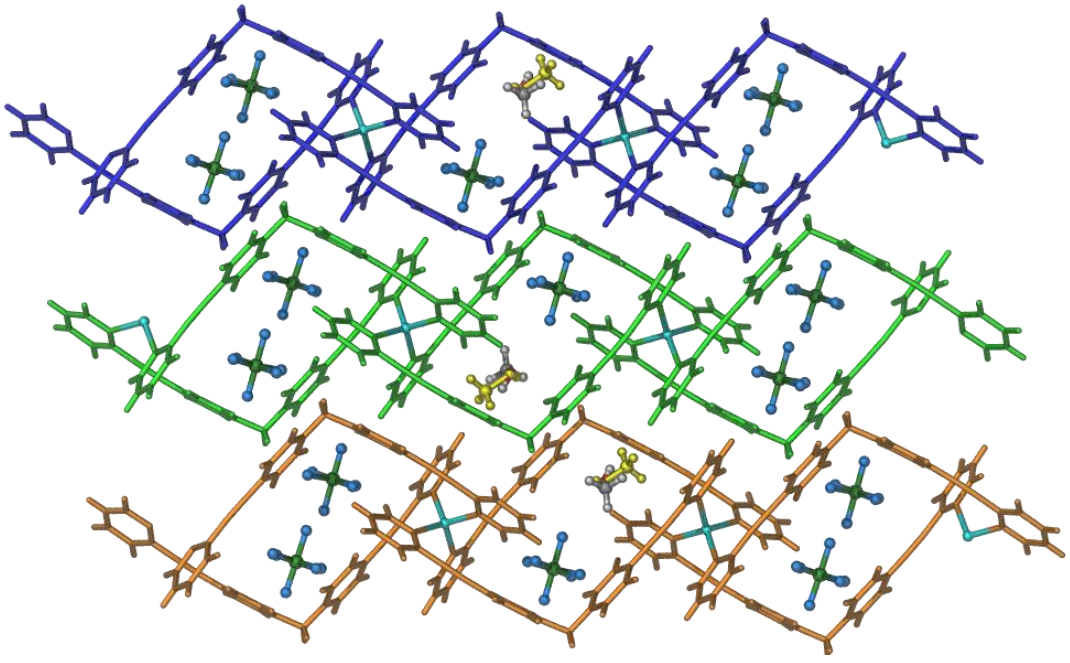

Figure 6.26. A perspective view showing the extended packing of 1-D polymer chains in structure **6.17**. The minor component of the disordered methanol solvate is coloured yellow.

6.3. Coordination Polymers of Bis(4-(pyridin-3-ylethynyl)phenyl)methane (2.52)

6.3.1. Silver(I) Coordination Polymers

As in section 6.2, even though the pyridyl ligand **2.51** only has one possible coordination mode, due to it having just two donor atoms, a range of structures were able to be produced due to the varying geometries of the coordinated metal atoms and the flexibility of the ligand bestowed by the methylene group. Upon changing the 2-pyridyl ring in **2.51** to a 3-pyridyl ring in **2.52** a similar series of structures would be expected. However, compound **2.52** turned out to be more difficult to crystallise than **2.51** and the resultant crystals were of poorer quality and often twinned. Only three coordination polymers of **2.52** with silver(I) were obtained (Scheme 6.3), compared to five for **2.51**, and these do not differ extensively in structure.

The first coordination polymer of **2.52** with silver(I) was obtained via slow evaporation of a solution of **2.52** and $AgSbF_6$ in a 1:1 ratio from acetone (Scheme 6.4). The original aim of this reaction was to produce metallomacrocycles based on those reported by Crowley and colleagues.[16] The ^{1}H NMR spectra of solutions of **2.52** and various silver(I) salts, including nitrate, perchlorate and hexafluoroantimonate, in a 1:1 ratio in deuterated acetone were recorded. These spectra were then compared to that of the ligand alone in order to identify any coordination induced shift of the pyridyl protons which would appear upon the formation of a supramolecular structure in solution. Unfortunately, no coordination induced shifts were observed and in hindsight this is likely due to the flexibility of the ligand favouring formation of polymers over discrete macrocyclic structures. However, crystallisation of the NMR solution containing silver(I) hexafluoroantimonate was observed and this was reproduced under slow evaporation conditions with acetone as the solvent to yield colourless rod-shaped crystals of the formula $\{[Ag(\mathbf{2.52})]SbF_6 \cdot 4(CH_3COCH_3)\}_n$ (**6.18**) in 46% yield. The crystals were characterised via elemental analysis (analysis calculated for $C_{27}H_{18}N_2Ag_1Sb_1F_6$ C 45.42, H 2.55, N 3.92; found C 45.82, H 2.59, N 3.89) and IR spectroscopy, which exhibited sharp peaks for the C≡C (2230 cm^{-1}) and Sb-F (652 cm^{-1}) stretches.

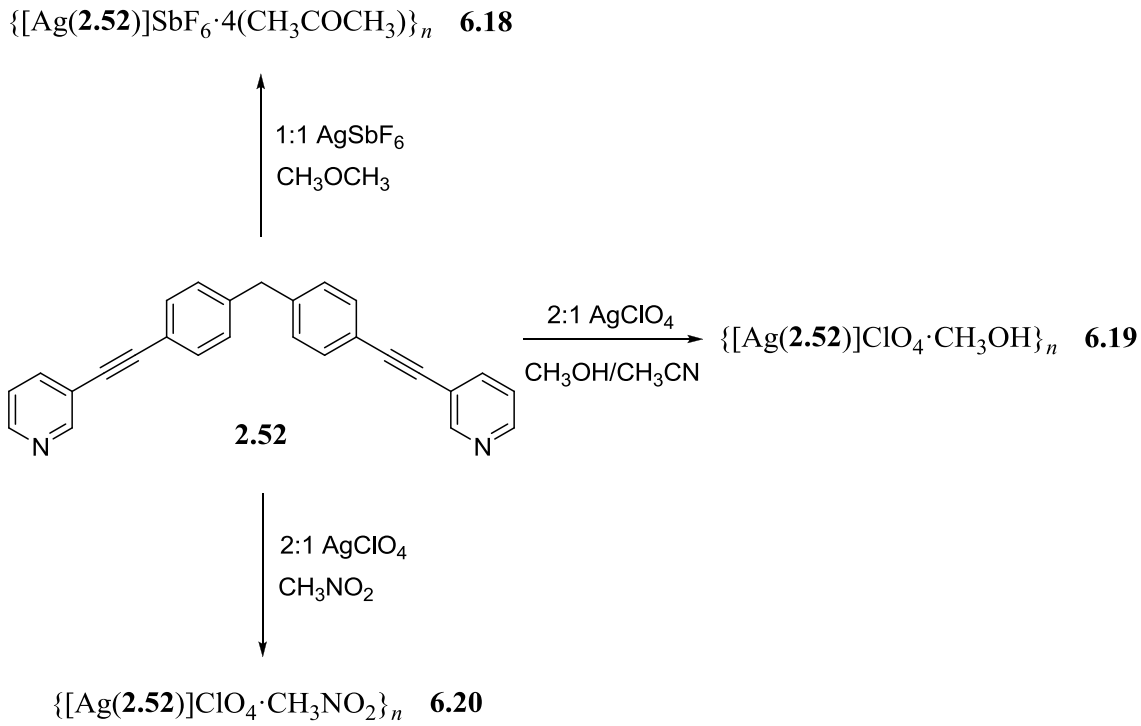

Scheme 6.3

Complex **6.18** crystallises in the monoclinic space group *C*2/*c* with an asymmetric unit that contains half a molecule of the ligand **2.52**, one 50% occupied silver atom, half a hexafluoroantimonate anion and two acetone solvate molecules (Appendix 1, Figure A1.19). The structure was refined with no disorder problems to an R_1 value of 4.01%. The extended structure of **6.18** is a zigzag 1-D coordination polymer (Figure 6.27), similar to **6.11**, as both the ligands and the silver(I) atoms act as two connecting nodes. The silver(I) atom has a near linear geometry with an N-Ag-N angle of 170.03(14)° and Ag-N bond lengths of 2.145(3) Å.

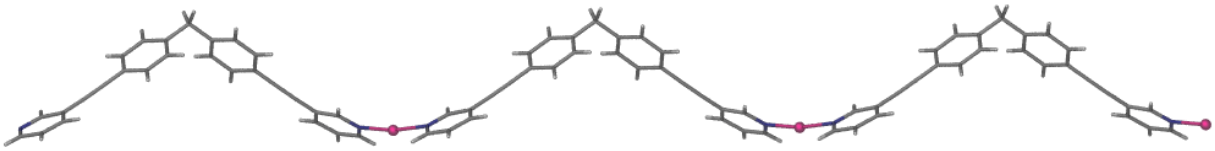

Figure 6.27. A perspective view of the cationic 1-D coordination polymer chain of **6.18**.

The ligand is twisted such that the two pyridyl nitrogen atoms are directed away from each other. The flexibility of the methylene group plays a dominant role in this as it has been observed that similar ligands, which are linked via a rigid phenyl spacer, can form discrete macrocyclic structures,[16] as seen in section 6.1.2. Due to the position of the pyridyl nitrogen atom in ligand **2.52**, a specific section of the 1-D polymer structure of **6.18** is more elongated than that of **6.11**, as can be seen in Figure 6.28. In polymer **6.18** there is no overlap of

adjacent ligands in space, as there is in **6.11**, and as such the distance between neighbouring silver atoms is 21.17 Å, whereas it is nearly half that in polymer **6.11** at 12.41 Å.

(a)

(b)

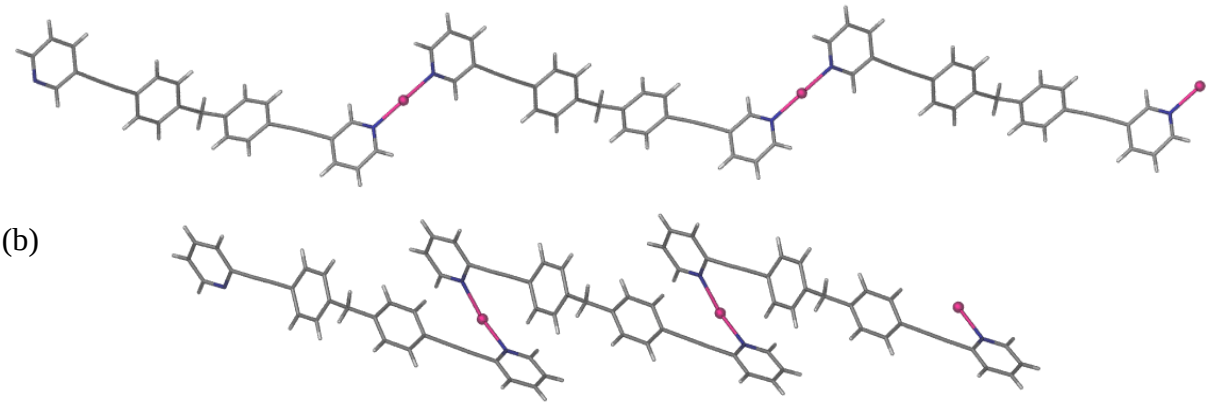

Figure 6.28. Perspective views of (a) the cationic 1-D coordination polymer chain of **6.18** and (b) the cationic 1-D coordination polymer chain of **6.11**.

The 1-D polymer chains of structure **6.18** pack in layers within the crystal lattice as seen in Figure 6.29, which shows two different types of polymer layers coloured blue and green. The ligands in the blue layer are in the opposite orientation to those in the green layer and are offset so that no π-stacking interactions are observed between the layers. Due to the pyridyl nitrogen atoms being in the 3-position there are no Ag-π interactions present between the silver(I) ions and the alkyne bonds within individual polymers as observed in structures **6.11**, **6.12** and **6.15**, which contain the 2-substituted pyridyl ligand. These interactions are also not present between polymer layers as the silver(I) ions pack close to the methylene group within the 'v'-shaped cleft of the ligand.

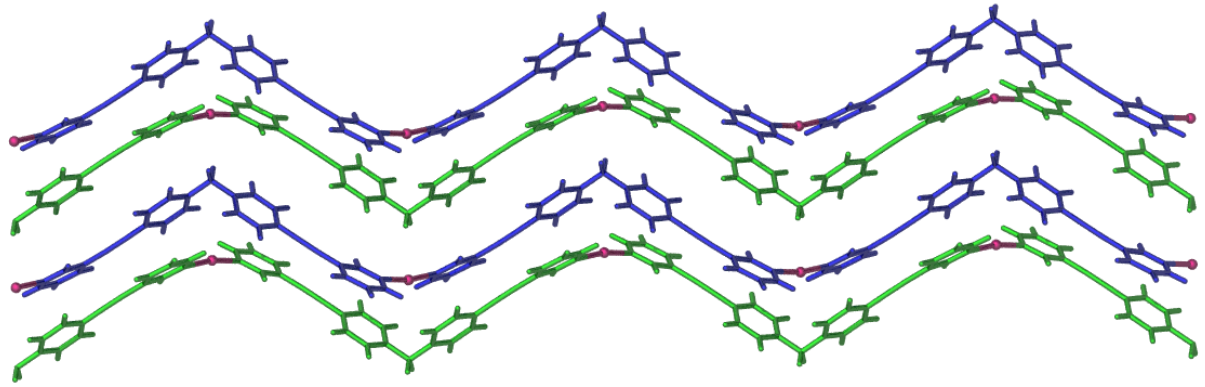

Figure 6.29. A perspective view of **6.18** showing the close packing of four polymer chains.

The stacks of 1-D polymer chains, seen in Figure 6.29, are then further arranged in the extended crystal structure in offset layers which sandwich the hexafluoroantimonate anions and the acetone solvate molecules (Figure 6.30). The channels in which the anions and solvate molecules reside run down the *b*-axis of the structure.

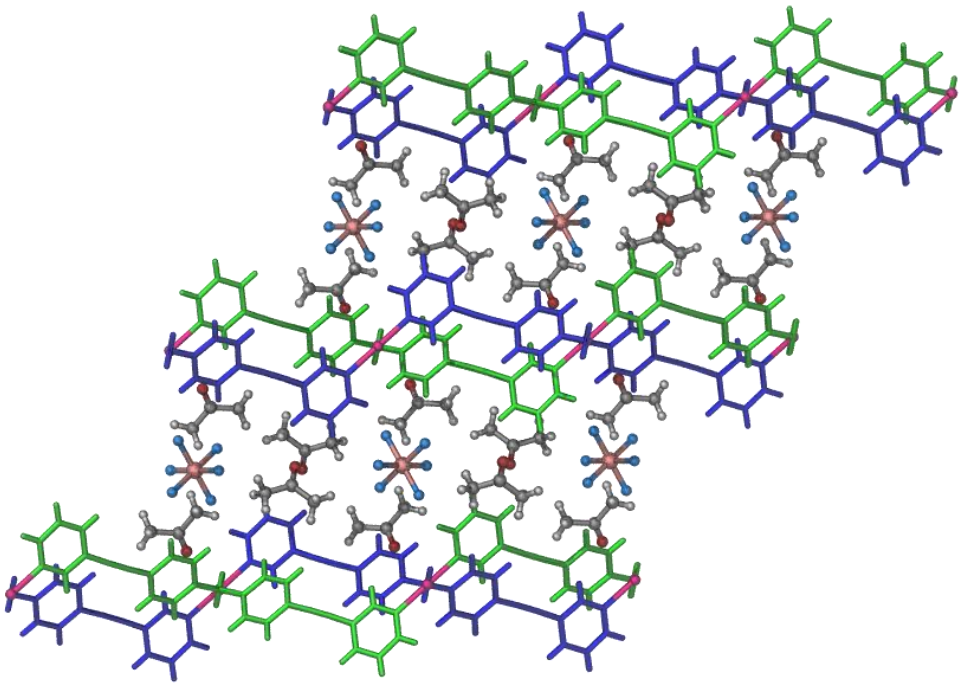

Figure 6.30. A perspective view showing the extended packing of 1-D polymer chains in structure **6.18**.

The second coordination polymer of **2.52**, $\{[Ag(\mathbf{2.52})]ClO_4 \cdot CH_3OH\}_n$ (**6.19**), was obtained via slow evaporation of **2.52** and $AgClO_4$ in a 2:1 ratio from a solvent mixture of methanol and acetonitrile in 68% yield. The colourless needles were characterised via elemental analysis and IR spectroscopy, which exhibited sharp peaks for the C≡C (2222 cm^{-1}) and Cl-O (1050 cm^{-1}) stretches. Compound **6.19** crystallises in the monoclinic space group *C*2/*c* and has an asymmetric unit which contains two molecules of the ligand, two silver(I) atoms, two perchlorate anions and two methanol solvate molecules (Appendix 1, Figure A1.20). The structure was refined with no disorder problems to an R_1 value of 7.11%.

Notably, the change in reactant stoichiometry from a ligand to metal ratio of 1:1 for structure **6.18** to a ligand to metal ratio of 2:1 for **6.19** has not altered the stoichiometry of the resultant polymers - 1:1 ligand to metal content for both structures. Like **6.18**, the extended polymer structure of **6.19** is a 1-D coordination polymer as the silver(I) atoms and the ligands act as 2-connecting nodes. The silver(I) atoms in structure **6.19** have a linear geometry with Ag-N bond lengths ranging from 2.120(5) to 2.160(5) Å and N-Ag-N bond angles of 175.10(14) and 175.35(14)°.

The major difference between **6.18** and **6.19** is that the ligand molecules in a single polymer chain in structure **6.18** are all located on the same side of the axis running through the silver atoms (Figure 6.31 (a)), whereas those in structure **6.19** alternate either side (Figure 6.31 (b)). The distance between adjacent silver atoms in **6.19**, 16.75 Å, is also significantly shorter than that in **6.18**, 21.17 Å. This is due to a more acute C-CH_2-C angle of the methane in structure **6.19** (109.1° versus 112.2° in **6.18**) and less of a twist around the methane bonds; with the average torsion angle around the methylene group being 79.0° in **6.19** compared to 66.3° in **6.18**.

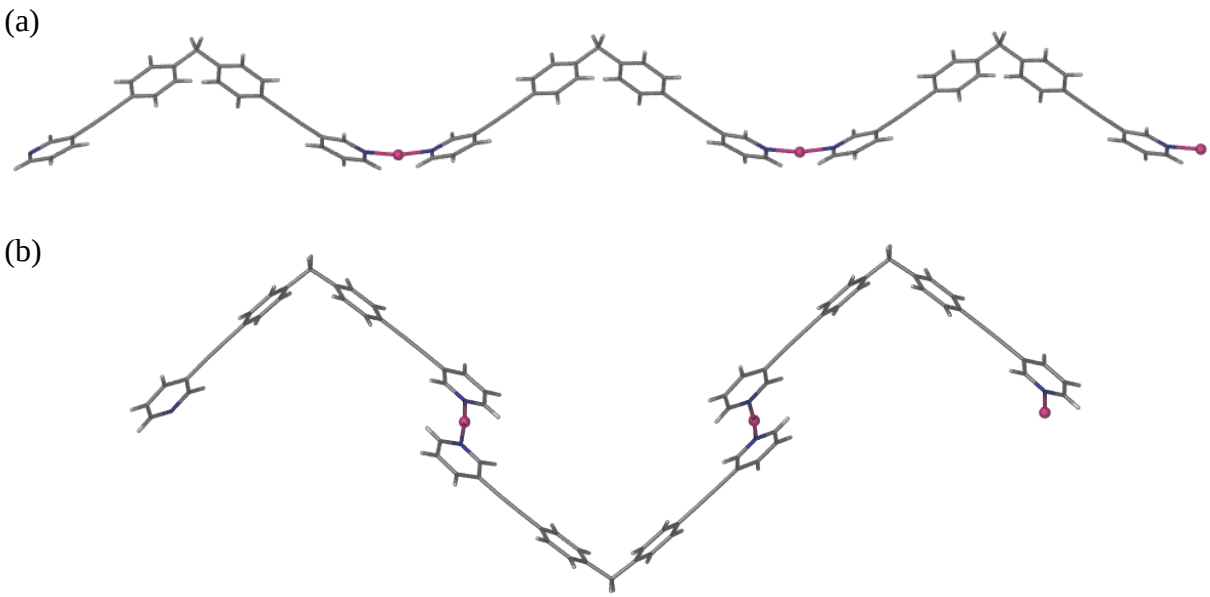

Figure 6.31. Perspective views of (a) the cationic 1-D coordination polymer chain of **6.18** and (b) the cationic 1-D coordination polymer chain of **6.19**.

The difference in conformation of the 1-D polymer chains of these two structures also leads to a difference in the long range packing in the crystal lattice. In structure **6.18** pairs of 1-D polymer stacks pack into layers with solvent and anion filled channels between them, as seen above, whereas the 1-D polymer chains of **6.19** pack tightly in simple layers with small pockets filled with perchlorate anions and methanol solvate molecules between them (Figure 6.32). No π-π stacking or Ag-π interactions were observed between the layers in this structure.

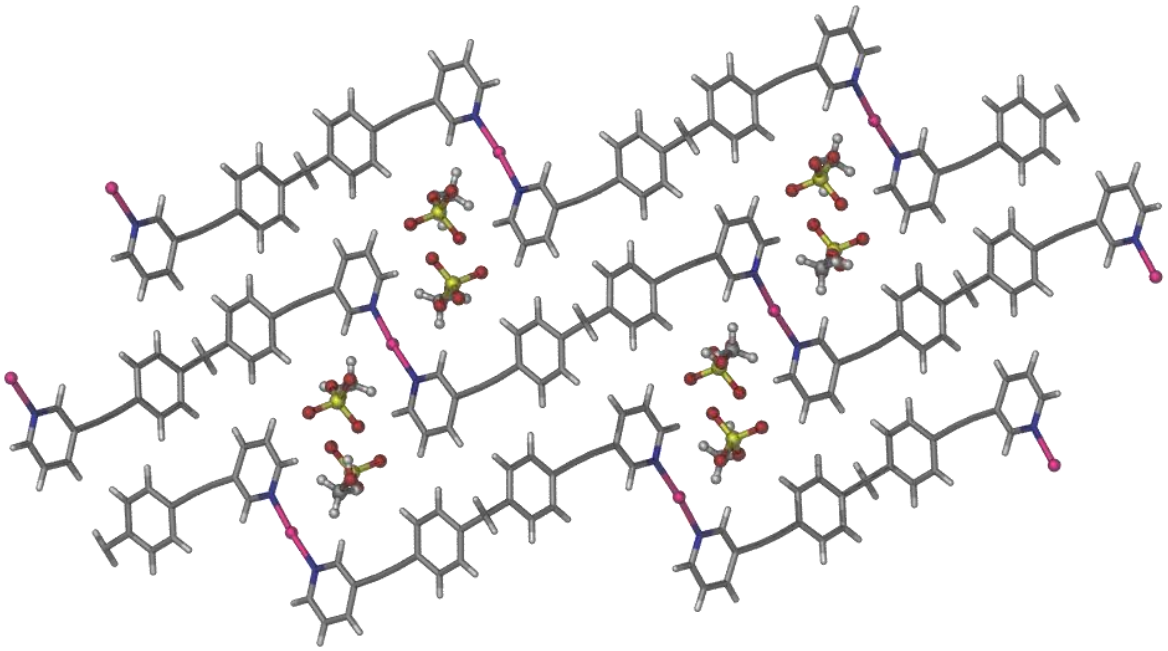

Figure 6.32. A perspective view showing the extended packing of 1-D polymer chains in structure **6.19**.

The final coordination polymer of **2.52** and silver(I) was obtained via slow evaporation of a solution of **2.52** and $AgClO_4$ in a 2:1 ratio from nitromethane to give pale yellow block-shaped crystals with the formula $\{[Ag(\mathbf{2.52})]ClO_4 \cdot CH_3NO_2\}_n$ (**6.20**) in 53% yield. The crystals were characterised via elemental analysis (analysis calculated for $C_{27}H_{18}N_2Ag_1Cl_1O_4 \cdot CH_3NO_2 \cdot H_2O$ C 51.27, H 3.39, N 6.41; found C 50.89, H 3.19, N 5.89) and IR spectroscopy, which exhibited sharp peaks for the C≡C (2222 cm^{-1}) and Cl-O (1050 cm^{-1}) stretches. Structure **6.20** crystallises in the monoclinic space group $P2_1/c$ with an asymmetric unit which contains one molecule of the ligand, one silver(I) atom, one perchlorate anion and one nitromethane solvate molecule (Appendix 1, Figure A1.21). The crystals of **6.20** were twinned and the data was processed taking this into account. Nevertheless, the structure was able to be refined to a reasonable R_1 value of 9.82%.

Structure **6.20** has a similar 1-D polymer chain structure as **6.19** with the ligands acting as two connecting linkers and neighbouring ligands having alternate orientations. However, in structure **6.20** the silver(I) atoms form a bond with another silver(I) atom in adjacent chains to form a 2-D sheet (Figure 6.33). The Ag-Ag bond length is 3.2656(13) Å and this is within both the sum of the van der Waals radii of two silver atoms (3.44 Å) and the accepted range for ligand unsupported Ag-Ag bond distances (2.80-3.30 Å).[30,31] This interaction is accompanied by very weak π-stacking interactions between adjacent polymer chains with centroid to centroid distances between two pyridyl rings of 3.78 and 3.82 Å.

The silver(I) atoms in structure **6.20** have a T-shaped geometry, due to the Ag-Ag bond, and exhibit Ag-Ag-N angles of 73.73(16) and 112.59(18)° and a N-Ag-N angle of 172.2(2)°. The Ag-N bond lengths are 2.110(6) and 2.126(6) Å respectively. The distance between neighbouring silver atoms in the 1-D polymer chain is 18.44 Å, which is approximately the average of that seen in structures **6.18** and **6.19**. A less acute C-CH_2-C methane angle, 113.6°, than structure **6.19** and a more pronounced twist in the methane bonds (average torsion angle around the methane is 57°) allows the closer packing of the 1-D polymer chains of structure **6.20** and subsequent formation of the Ag-Ag bond.

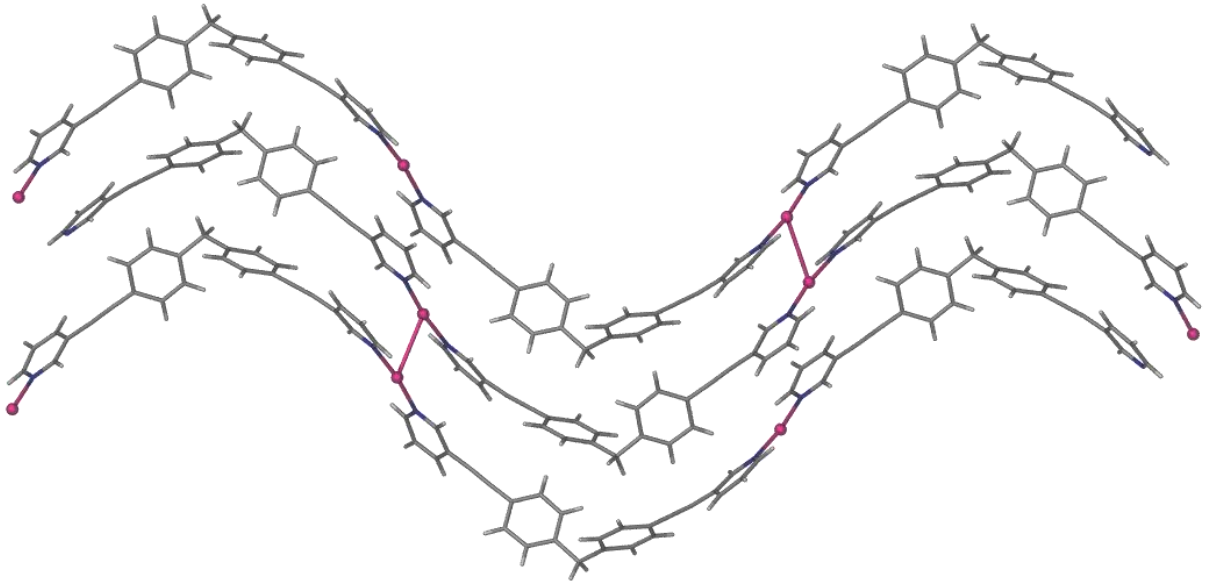

Figure 6.33. A perspective view of the cationic 1-D polymer chains of **6.20** connected by Ag-Ag bonds to form a 2-D coordination polymer.

The 2-D sheets, formed by the connected 1-D polymer chains, pack in the crystal lattice in layers with the perchlorate anions and nitromethane solvate molecules situated in channels between the layers which run down the *a*-*c* plane (Figure 6.34). π-π Stacking interactions are observed between pyridyl rings of adjacent polymer chains with a centroid-centroid distance of 3.55 Å. No Ag-π interactions were observed between the layers in this structure.

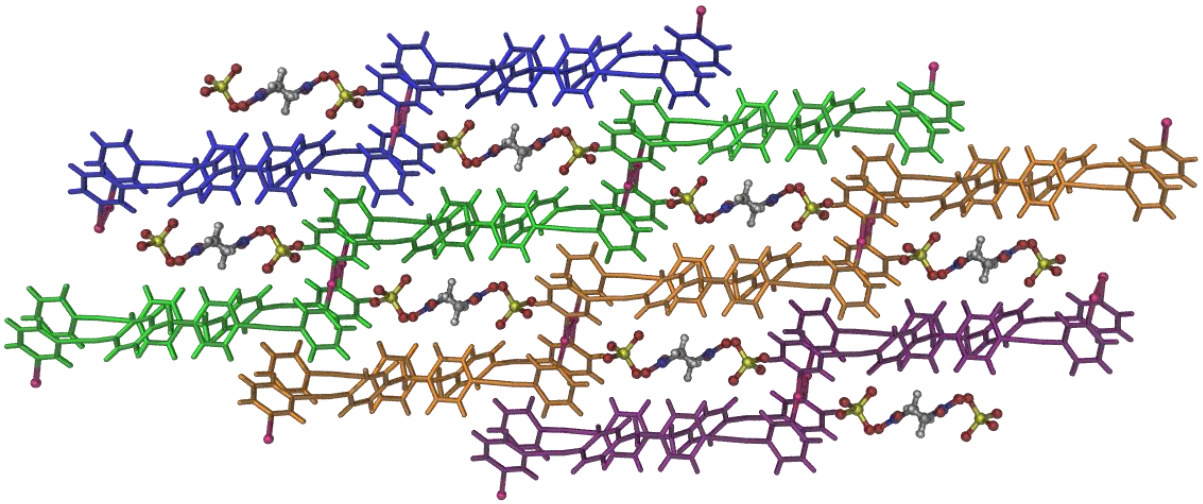

Figure 6.34. A perspective view showing the extended packing of 2-D polymer sheets in structure **6.20**.

It is interesting to note that even though three different geometries were observed for the silver(I) metal nodes in the structures of ligand **2.51** (linear, trigonal planar and tetrahedral) only two geometries were seen in the silver(I) structures of **2.52**. In the case of **2.52** the silver(I) metal has a predominantly linear geometry with only one structure, **6.20**, differing only when a long Ag-Ag bond results in a T-shaped geometry.

6.3.2. Copper(I) Coordination Polymers

The formation of copper(I) coordination polymers with ligand **2.52** proved difficult. Two copper(I) salts, $[Cu(CH_3CN)_4]BF_4$ and $[Cu(CH_3CN)_4]PF_6$, were trialled in slow evaporation reaction conditions with ligand to metal ratios in the range 1:2 to 2:1. Different solvents were investigated too, including nitromethane or mixtures of methanol and acetonitrile. For the most part, neither precipitation nor crystallisation was observed until no solvent remained. Only one coordination polymer of ligand **2.52** and copper was able to be obtained via slow evaporation of **2.52** and $[Cu(CH_3CN)_4]BF_4$ in a 1:2 ratio from nitromethane in 35% yield (Scheme 6.5). The resultant pale yellow block shaped crystals have the molecular formula $\{[Cu(\mathbf{2.52})]PF_6 \cdot CH_3NO_2\}_n$ (**6.21**). These crystals were only able to be isolated once and repeated attempts at regrowing them for elemental analysis led to the precipitation of a blue copper(II) salt. This is possibly due to the low ligand to metal ratio of 1:2 used in this reaction. Similar structures were produced using a higher ligand to metal ratio of 2:1; however upon performing this reaction in such a manner neither crystallisation nor precipitation was observed before the complete evaporation of the solvent.

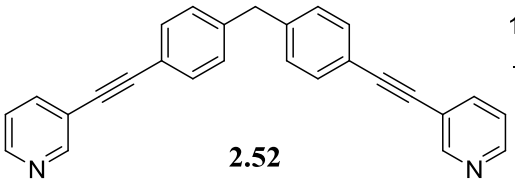

2.52

1:2 $[Cu(CH_3CN)_4]BF_4$

CH_3NO_2

$\{[Cu(\mathbf{2.52})]BF_4 \cdot CH_3NO_2\}_n$ **6.21**

Scheme 6.4

Structure **6.21** crystallises in the monoclinic space group $P2_1/c$ with an asymmetric unit which contains one molecule of the ligand, one copper(I) atom, one tetrafluoroborate anion and one nitromethane solvate molecule (Appendix 1, Figure A1.22). These crystals were consistently twinned and the data was processed taking this into account. The structure was refined with some unresolved disorder of the tetrafluoroborate anion due to the poor quality of the data. As such, the boron atom of the tetrafluoroborate anion was refined isotropically resulting in an R_1 value of 11.41%.

The extended structure of **6.21** is a 1-D polymer chain, which is very similar to that of structure **6.20**. The ligands and the copper(I) metal atoms act as two connecting nodes to form the 1-D polymer chain and adjacent ligands in the chain are in the opposite orientation to each other (Figure 6.35). The distance between the adjacent copper(I) atoms in the 1-D chain is 18.43 Å, which is practically the same as the distance between adjacent silver(I) atoms in structure **6.20** (18.44 Å). Other parameters such as the C-CH_2-C angle around the methane, 112.9° in **6.21** versus 112.2° in **6.20**, and the average torsion angle around the methane, 58.4 in **6.21** versus 57° in **6.20**, are also very similar.

The difference between **6.21** and **6.20** is that an analogous bond to the Ag-Ag bond present in **6.20**, which converts the 1-D polymer chains to a 2-D sheet, does not appear in structure **6.21**. This is likely to be due to the smaller ionic radii of copper(I) compared to silver(I) (91 pm versus 129 pm)[32] preventing significant interaction of the copper(I) atoms. Therefore, the copper(I) atoms in **6.21** have a linear geometry with Cu-N bond lengths of 2.117(7) and 2.121(6) Å and a N-Cu-N angle of 171.8(2)°.

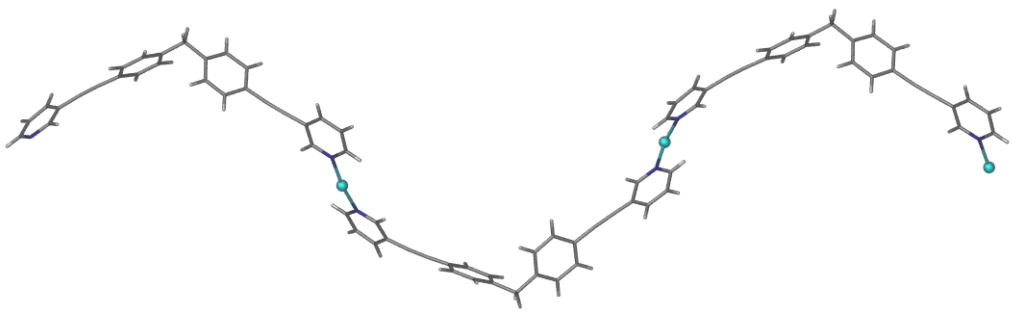

Figure 6.35. A perspective view of the cationic 1-D coordination polymer chain of **6.21**.

The 1-D polymer chains in **6.21** pack in an identical manner to the connected 1-D polymer chains in structure **6.20** (Figure 6.36). The 1-D polymer chains pack in layers with the tetrafluroborate anions and nitromethane solvate molecules situated in channels between the layers which run down the *ac* plane. π-π Stacking is observed between adjacent chains with centroid to centroid distances of 3.77 Å between interacting pyridyl rings. As with structure **6.20**, no Ag-π interactions were observed between the layers in this structure.

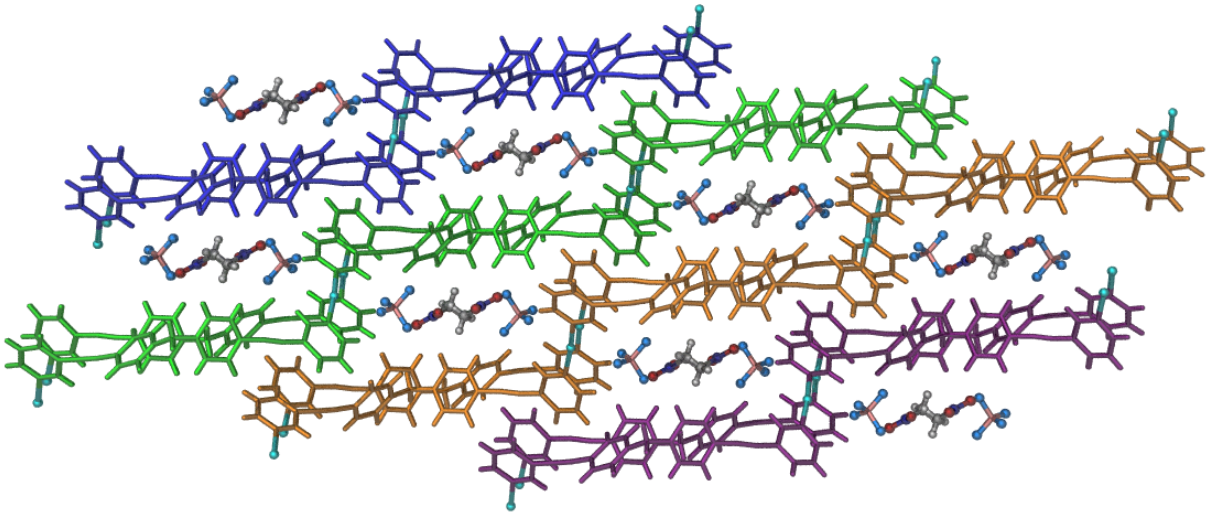

Figure 6.36. A perspective view showing the extended packing of 1-D chains in **6.21**.

6.4. Coordination Polymers of Bis(4-(pyridin-4-yl)phenyl)methane (2.55)

The final flexible pyridyl ligand investigated was bis(4-(pyridine-4-yl)phenyl)methane (**2.55**). This compound does not contain alkyne bonds like **2.51** and **2.52**, instead the pyridyl rings are directly connected to the diarylmethane linker. This results in the nitrogen donor atoms being closer in space, however as they are in the 4-position this ligand will still provide coordination polymers. The coordination chemistry of this ligand was examined, as above for **2.51** and **2.52**, with silver(I) and copper(I) salts using nitromethane and mixtures of methanol and acetonitrile as the solvents. Two coordination polymers of bis(4-(pyridine-4-yl)phenyl)methane (**2.55**) were able to be obtained.

6.4.1. A Copper(I) Coordination Polymer

The first coordination polymer was produced via slow evaporation of a solution of **2.55** and $[Cu(CH_3CN)_4]BF_4$ in a 2:1 ratio from a mixed solvent system of methanol and acetonitrile (Scheme 6.5). The resultant bright yellow, pyramidal crystals have the formula $\{[Cu(\mathbf{2.55})_2]BF_4\}_n$ (**6.22**) and were obtained in 55% yield. The crystals were characterised by elemental analysis (analysis calculated for $C_{46}H_{36}N_4Cu_1B_1F_4$ C 69.47, H 4.57, N 7.05; found

C 69.74, H 4.49, N 7.24) and IR spectroscopy, which exhibited sharp peaks for the C=C (1597 cm^{-1}) and B-F (1051 cm^{-1}) stretches. Structure **6.22** crystallises in the tetragonal space group $I4_1/a$ and has an asymmetric unit which contains two half molecules of the ligand, one 50% occupied copper(I) atom and one 50% occupied tetrafluoroborate anion (Appendix 1, Figure A1.23). The structure was refined with some disorder problems of one of the phenyl rings, which was modelled over two positions with a refined occupancy of *ca.* 61:39, to a reasonable R_1 value of 11.26%.

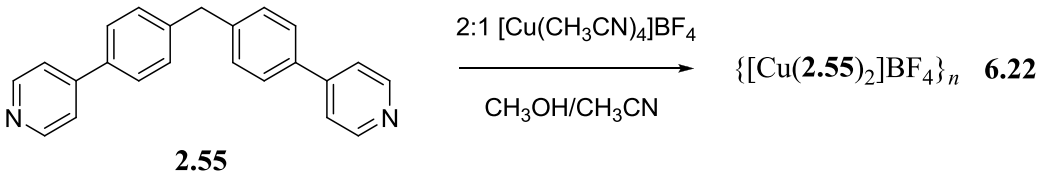

2.55

Scheme 6.5

The extended structure of **6.22** is a 2-D (4,4) coordination polymer as the copper(I) atoms act as 4-connecting nodes and the ligands act as two connecting linkers (Figure 6.37 (a)). It can be seen from Figure 6.37 (b) that the 2-D polymer is not flat but is a corrugated due to the 'v'-shape of the bis(4-(pyridine-4-yl)phenyl)methane ligands. The copper(I) atoms have a tetrahedral geometry and exhibit Cu-N bond lengths of 2.060(6) Å. The Cu-N-Cu bond angles range from 106.43(3) to 117.5(3) and the calculated τ_4 value for the copper(I) atoms is 0.93. This shows that the copper(I) atoms have a fairly regular tetrahedral geometry.

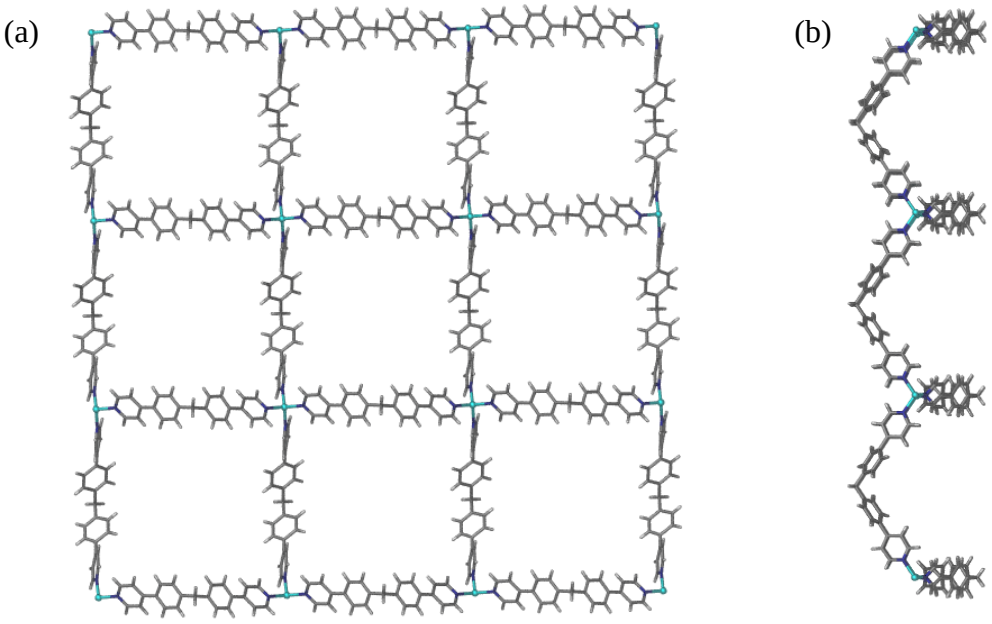

Figure 6.37. Perspective views of (a) the cationic 2-D (4,4) net of **6.22** looking down the *c*-axis and (b) the coordination polymer at 90° to the first.

The 2-D (4,4) nets pack in the extended crystal lattice in pairs of aligned networks as seen in Figure 6.38 (a) showing two pairs of nets, a blue and purple pair and a green and orange pair. These pairs of networks are interpenetrated such that each net of one pair interpenetrates both nets of the other pair but not each other, as they are perfectly aligned it is not possible. For example, it can be seen in Figure 6.38 (b) that the blue network is interpenetrated with the green and the orange networks but not the purple one. Overall this leads to a 3-fold interpenetrated structure as four networks are involved in interpenetration but a single network is only interpenetrated by two others. There are C-H···π interactions present between the two networks within a pair, with a C-H to centroid distance of 2.73 Å between a benzene ring and a pyridyl ring. However, no π-π stacking interactions are observed. There are also no π type interactions present between the network pairs.

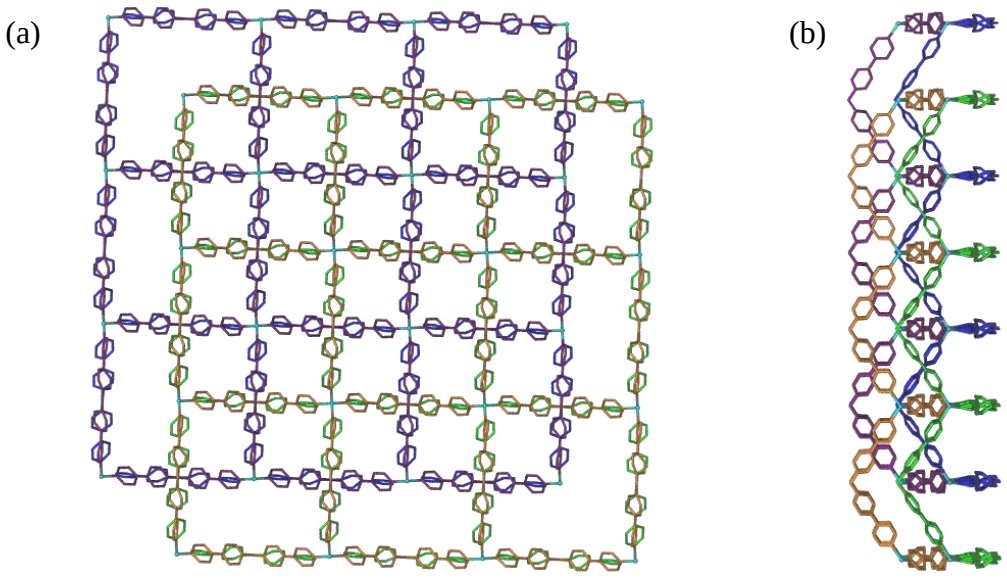

Figure 6.38. Perspective views of (a) two pairs of aligned 2-D (4,4) networks (blue/purple and green/orange) looking down the *c*-axis and (b) the four networks at 90° to the first view showing their interpenetration. Hydrogen atoms have been omitted for clarity.

The two pairs of interpenetrated networks are then further packed in the extended crystal lattice via interdigitation with a second set of four networks (Figure 6.39). Although they appear to pack very closely there are no significant π-type interactions between the two sets. This close packing of multiple networks leads to the preclusion of solvent molecules from the structure.

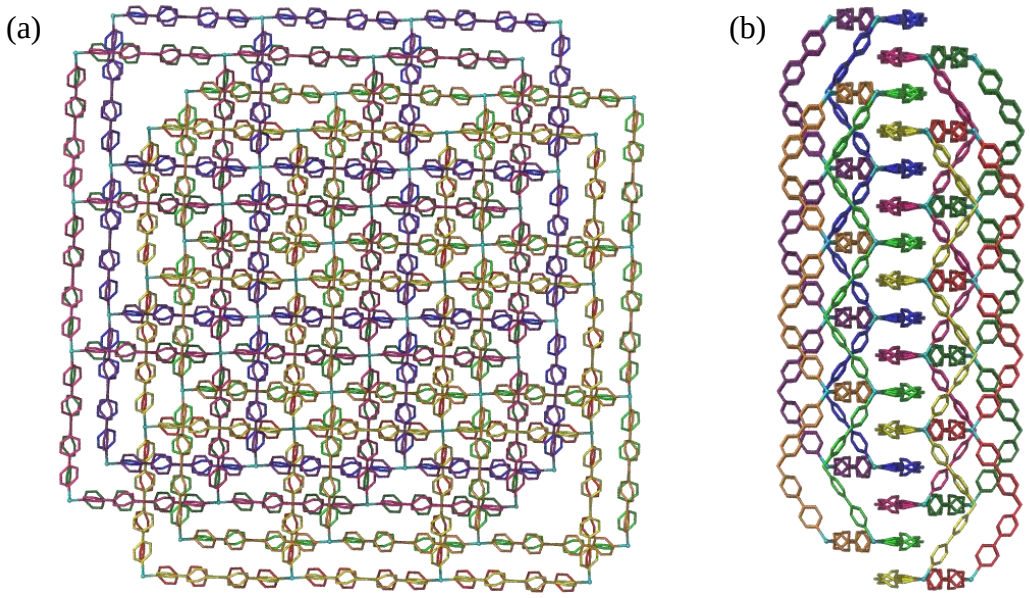

Figure 6.39. Perspective views showing (a) the extended packing of eight (4,4) nets in structure **6.22** looking down the *c*-axis and (b) and looking 90° to the first view.

6.4.2. A Silver(I) Coordination Polymer

The second coordination polymer, **6.23**, was produced via slow evaporation of a solution of **2.55** and $AgClO_4$ in a 2:1 ratio from a mixed solvent system of methanol and acetonitrile (Scheme 6.6). The resultant colourless, octahedral crystals have the formula $\{[Ag(\mathbf{2.55})_2]ClO_4\}_n$ (**6.23**) and were obtained in 67% yield. The crystals were characterised via elemental analysis (analysis calculated for $C_{46}H_{36}N_4Ag_1Cl_1O_4$ C 64.83, H 4.27, N 6.58; found C 65.09, H 4.29, N 6.71) and IR spectroscopy, which exhibited sharp peaks for the C=C (1597 cm^{-1}) and Cl-O (1084 cm^{-1}) stretches. The unit cell of this structure is very large with a volume of 22724(8) $Å^3$. Attempts were made to find a smaller unit cell but the same large cell was repeatedly observed.

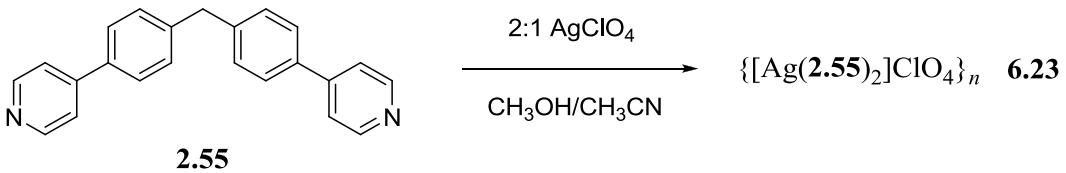

2.55

Scheme 6.6

Complex **6.23** crystallises in the monoclinic space group $P2_1/c$, with an asymmetric unit that contains twelve molecules of **2.55**, six silver(I) atoms and six perchlorate anions (Appendix 1, Figure A1.24). The ADDSYM routine of PLATON was used to search for higher symmetry but none was found. Even though this structure has a very large number of atoms in its asymmetric unit it was able to be refined to an R_1 value of 6.90%. There was

disorder of one of the aryl rings of a ligand molecule, which was modelled over two positions with a refined occupancy of *ca.* 57:43.

Like polymer **6.22**, the extended structure of **6.23** is also a 2-D (4,4) network, as the silver atoms act as four-connecting nodes and the ligands act as two connecting linkers (Figure 6.40 (a)). Again this structure is corrugated (Figure 6.40 (b)) due to the 'v'-shape of the ligand. The silver(I) atoms have a tetrahedral geometry and exhibit Ag-N bond lengths between 2.297(4) and 2.397(4) Å. The Ag-N-Ag bond angles range from 95.22(13) to 126.58(13) and the calculated τ_4 values for each of the six crystallographically unique silver(I) atoms are 0.87, 0.94, 0.88, 0.87, 0.93 and 0.87 respectively. This shows that four of the silver(I) atoms have a slightly more distorted tetrahedral geometry than the other two.

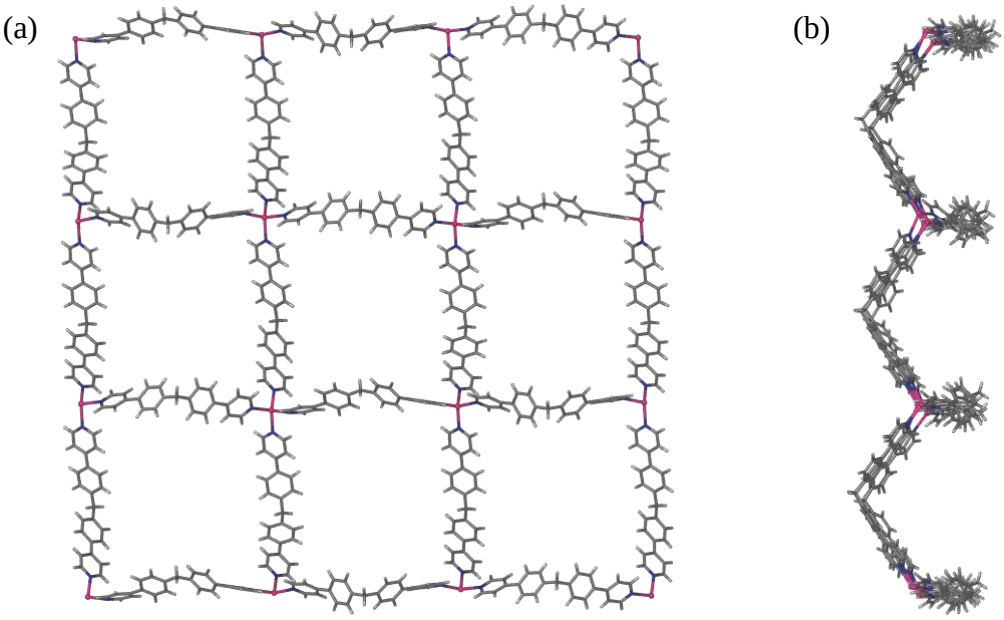

Figure 6.40. Perspective views of (a) the cationic 2-D (4,4) net of **6.23** looking down the *c*-axis and (b) the coordination polymer at 90° to the first.

The ligand molecules that make up the horizontal and vertical struts of the 2-D (4,4) net of **6.22** are all symmetry related and have the exact same orientation, thus the polymer overlays perfectly when viewed from a 90° angle to the *b*-axis (Figure 6.37 (b)). Conversely, the ligands which make up the horizontal and vertical struts of the 2-D (4,4) net of **6.23** have a visible twist so that they are not all in the same orientation (Figure 6.40) which decreases the overall symmetry of the structure, when compared to **6.22**, resulting in a very large asymmetric unit.

Structure **6.23** packs in an identical fashion to structure **6.22**, which is described above in section 6.4.1, and therefore will not be discussed in detail. Similar to **6.22**, the only inter-

network interactions in **6.23** between the network pairs are C-H···π interactions, with C-H to centroid distances from 3.17-3.22 Å, present between two benzene rings.

The majority of interpenetrated (4,4) networks present in the literature are 2-fold 2-D → 2-D parallel interpenetrated.[33-38] This means that the two interpenetrating nets share the same mean plane and that the overall assembly is 2-D. If the two interpenetrating nets are inclined, meaning that they do not share the same plane, this leads to a dimensional increase and the overall structure is 3-D. This is represented as 2-D → 3-D inclined interpenetration. The (4,4) networks of **6.22** and **6.23** are 3-fold 2-D → 2-D parallel interpenetrated. There are only a few examples of 3-fold 2-D → 2-D parallel interpenetrated (4,4) networks within the literature.[39-43]

The first example involves a (4,4) network composed of 3-[2-(4-pyridyl)ethenyl]benzoate (Figure 6.41 (a)) and cadmium(II).[39] The distorted octahedral cadmium(II) metal ion acts as a 4-connecting node with monodentate coordination to the pyridyl groups of two ligands and chelation via the carboxylate groups of two further ligands. This results in a network with large voids, due to the size of the ligand, which are filled via the interpenetration of a further two (4,4) sheets. The main difference between this structure and **6.22**/**6.23** is that 3-[2-(4-pyridyl)ethenyl]benzoate is closer to planar (although it does exhibit a slight twist of the aryl rings) than **2.55** with its methylene group, and thus the resultant coordination polymer exhibits a greater planarity and stacks in parallel sheets within the crystal lattice as opposed to the interdigitation observed in **6.22** and **6.23**.

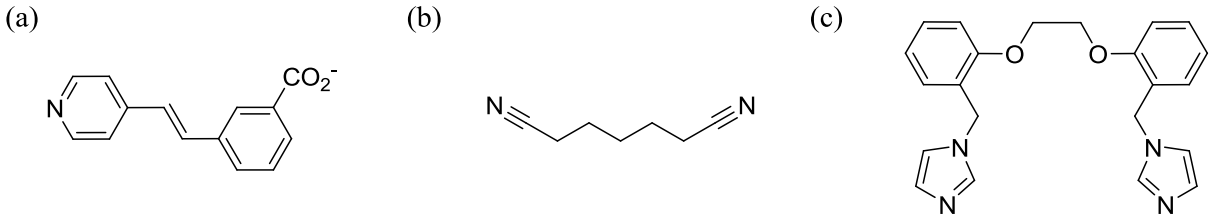

Figure 6.41. The compounds (a) 3-[2-(4-pyridyl)ethenyl]benzoate, (b) 1,7-heptanedinitrile and (c) 1,2-bis[2-(1H-1,3-imidazol-1-ylmethyl)phenoxy]ethane.

The second related (4,4) network was formed via slow evaporation of 1,7-heptanedinitrile (Figure 6.41 (b)) and $AgSbF_6$ or $AgSO_3CF_3$ in a 1:1 ratio from ethanol.[40] Within this structure the silver(I) ions have a distorted tetrahedral geometry and act as 4-connecting nodes whereas the ligands act as 2-connecting linkers, which is the similar to what is observed for structures **6.22** and **6.23**. Again the length of the ligand leads to a (4,4) network with large voids resulting in 3-fold 2-D → 2-D parallel interpenetration. Similar to the first example, the resultant interpenetrated planar sheets pack in parallel layers within the crystal lattice.

The final example, unlike the first two, involves the reaction of two different ligands, benzene-1,4-dicarboxylic acid and 1,2-bis[2-(1H-1,3-imidazol-1-ylmethyl)phenoxy]ethane (Figure 6.41 (c)), with $Cd(NO_3)_2 \cdot 4H_2O$, which was recently reported by Dong and colleagues.[41] The distorted octahedral cadmium(II) metal ion acts as a 4-connecting node, in a similar fashion to the first example, with monodentate coordination to the pyridyl groups of two 1,2-bis[2-(1H-1,3-imidazol-1-ylmethyl)phenoxy]-ethane ligands and chelation via the carboxylate groups of two benzene-1,4-dicarboxylate ligands. Due to the conformational flexibility of 1,2-bis[2-(1H-1,3-imidazol-1-ylmethyl)phenoxy]-ethane the resultant (4,4) net is a wave-like sheet (Figure 6.42 (a)), which is similar to the corrugated structures of **6.22** and **6.23**. This network is then 3-fold 2-D → 2-D parallel interpenetrated, as observed in Figure 6.42 (b). It is presumed that the interpenetrated sheets are then packed in the crystal lattice in an interdigitated fashion similar to **6.22** and **6.23**.

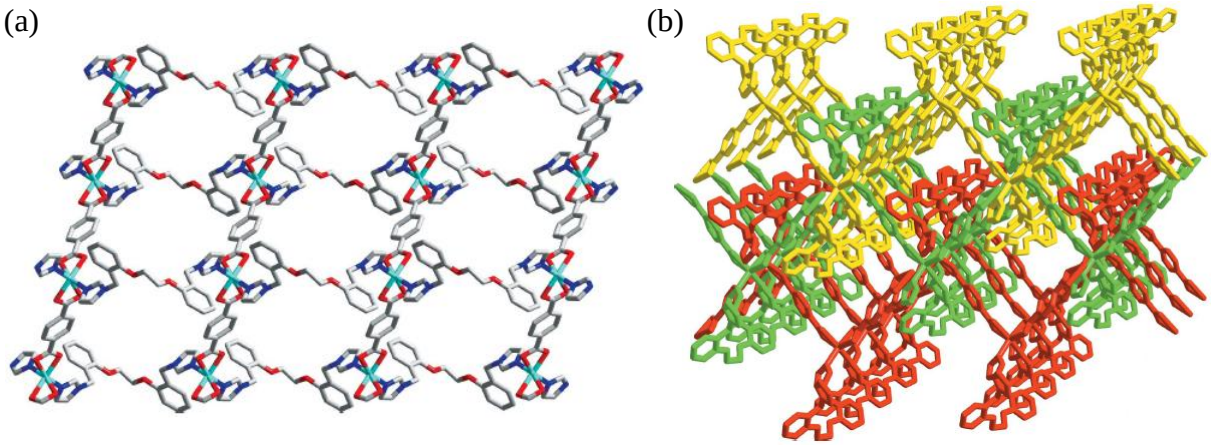

Figure 6.42. Perspective views of (a) the 2-D (4,4) net, recently reported by Dong and colleagues, looking along the *a*-*c* plane and (b) the 3-fold 2-D → 2-D parallel interpenetration of the network (images sourced from reference 41).

Of the examples of 3-fold interpenetrated 2-D (4,4) nets examined none exhibited a similar packing to structures **6.22** and **6.23**, with their parallel pairs of 3-fold interpenetrated sheets, and only one exhibited a similar degree of corrugation; although this example involved the use of two types of ligand with different distances between their donor atoms.

6.5. Coordination Polymers of 4,4'-Methyldiphthalonitrile (2.43)

6.5.1. Silver(I) Coordination Polymers

Aside from the flexible dipyridyl ligands discussed above, the coordination chemistry of the other diarylmethane precursors used to synthesise hexaaryl[3]radialenes was also examined. Multiple attempts to crystallise 4,4'-dicyanodiphenylmethane (**2.25**) and 3,3'-dicyanodiphenylmethane (**2.37**) with salts of silver(I), copper(I) and iron(II) resulted in crystallisation of the ligand alone and only 4,4'-methyldiphthalonitrile (**2.43**) was observed to form a coordination polymer with silver(I). Slow evaporation of a solution of **2.43** and silver perchlorate in a ratio of 1:2 to 1:4 from nitromethane produced **6.24** as colourless rod-shaped crystals in 58% yield (Scheme 6.7). The crystals were characterised by elemental analysis (analysis calculated for $C_{18}H_8N_4Ag_1Cl_1O_4 \cdot CH_3NO_2$ C 40.29, H 2.07, N 13.05; found C 40.00, H 2.13, N 12.76;) and IR spectroscopy, which exhibited sharp peaks for the C≡C (2257 cm^{-1}) and Cl-O (1076 cm^{-1}) stretches. The structure, as obtained by X-ray crystallography, possessed the formula $\{[Ag(\mathbf{2.43})(H_2O)]ClO_4 \cdot CH_3NO_2\}_n$ (**6.24**).

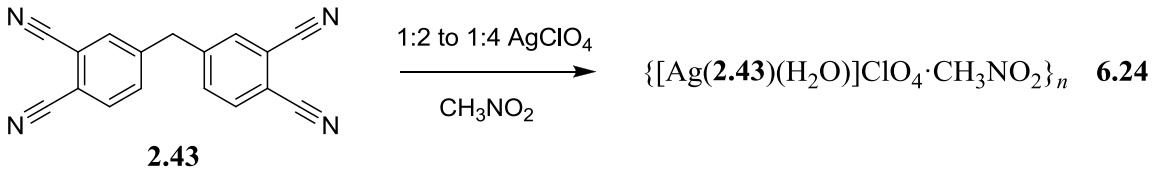

2.43

Scheme 6.7

Compound **6.24** crystallises in the monoclinic space group *P*2/*c*, with an asymmetric unit that contains two half molecules of the ligand, **2.43**, one silver(I) atom with a coordinated water molecule, two 50% occupied perchlorate anions and two 50% occupied nitromethane solvate molecules (Appendix 1, Figure A1.25). The perchlorate anions and the nitromethane molecules occupy the same positions within the structure and constraints were used to keep the chlorine atoms of the perchlorate anions and the nitrogen atoms of the nitromethane molecules in the same position. Constraints were also used to maintain chemically sensible bond lengths in the nitromethane molecules. Despite this disorder, the structure was able to be refined to an R_1 value of 4.69%.

The extended structure of **6.24** is a (3,4)-connected 2-D net with the Schläfli symbol $(4.6^2)_2(4^2.6^2.8^2)$ where the silver(I) atom acts as a 3-connecting node and one of the ligand molecules acts as a 4-connecting node (the other ligand molecule acts as a 2-connecting linker and is topologically trivial) (Figure 6.43). The silver(I) atom has a tetrahedral geometry and is coordinated to three different ligand molecules and one water molecule. The Ag-N bond

lengths are 2.290(4), 2.243(3) and 2.461(3) Å respectively and the Ag-O bond length is 2.380(4) Å. The angles around the silver(I) atom range from 91.53(13) to 140.69(13)° and it has a calculated τ_4 value of 0.77 meaning that the geometry is slightly distorted from true tetrahedral.

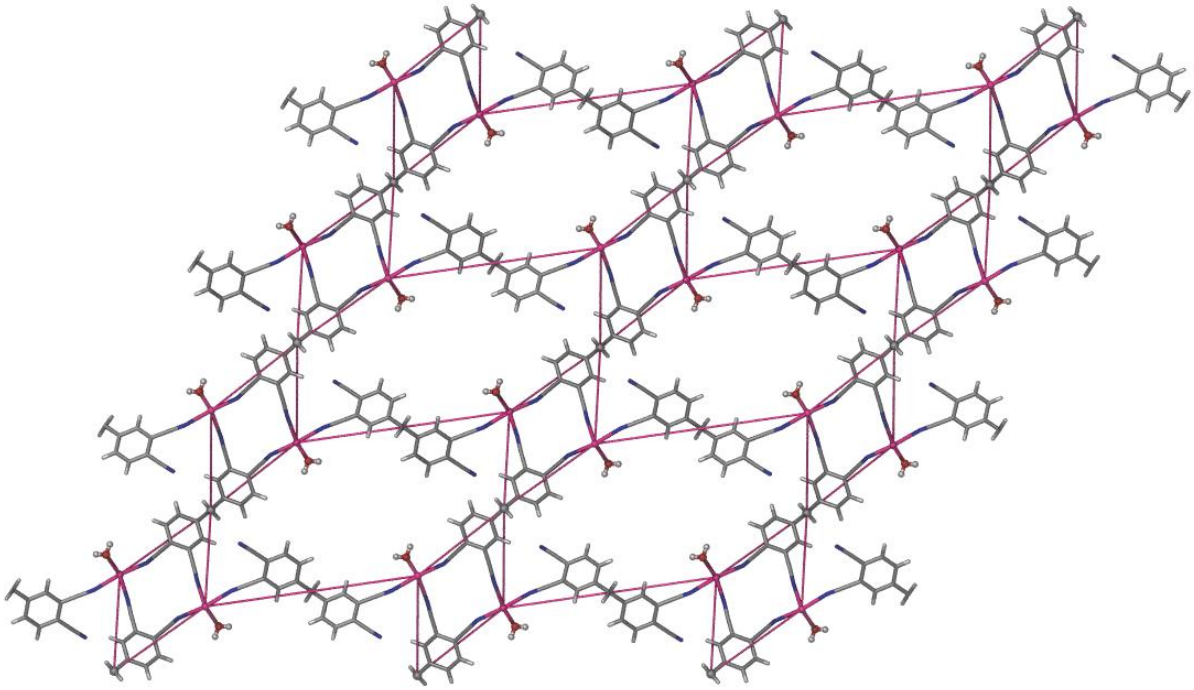

Figure 6.43. A perspective view of structure **6.24** where the 3-connecting silver nodes and the 4-connecting ligand nodes have been joined by pink bonds to highlight the underlying net.

The 2-D polymer packs in layers within the crystal lattice (Figure 6.44). The perchlorate anions and the nitromethane solvate molecules are situated within channels that run through the structure. Each of the voids in the 2-D net contains two perchlorate anions and two nitromethane molecules; however they are disordered over the four available positions. Figure 6.44 shows three separate 2-D polymer layers coloured blue, green and orange. Figure 6.44 (a) shows a perspective view of the polymer looking a few degrees off the *b*-axis to allow the separate layers to be viewed. An image looking exactly down the *b*-axis would show the polymer layers perfectly aligned on top of one another. The distance between the centroids of the overlying aryl rings, 4.06 Å, is slightly outside that used to identify significant π-stacking interactions (3.80 Å). The distance between silver(I) atoms in adjacent layers is also 4.06 Å which is well outside the range of a significant Ag-Ag interaction (3.44 Å). Figure 6.43 (b) shows a perspective view of the polymer looking down the *c*-axis, which shows that the three layers are so tightly packed that they intercalate each other. This is due to the 'v'-shape conformation of the ligands provided by the flexible methylene group.

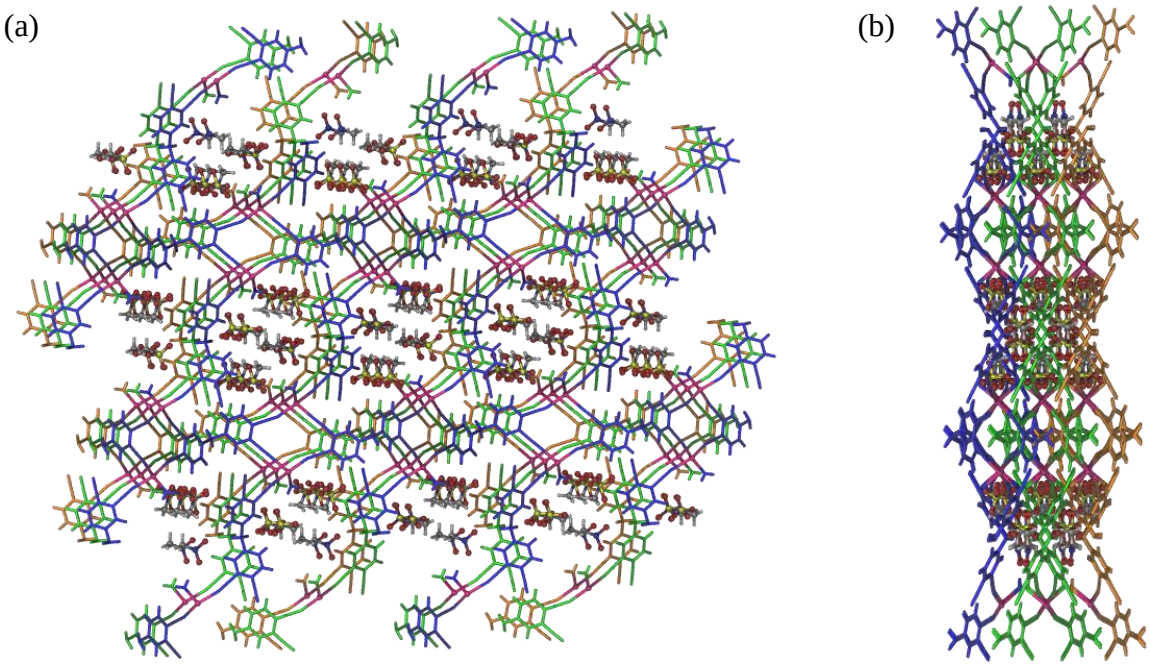

Figure 6.44. A perspective view of (a) of the 2-D net of structure **6.24** showing the packing of the anions and solvate molecules and (b) of the polymer at 90° to the first view showing the very close packing of the 2-D layers.

There are limited examples of 2-D networks in the literature which exhibit this topology.[44,45] The first example was formed from the reaction of 1,8-diphenylocta-1,3,5,7-tetraene (Figure 6.45 (a)) with silver perchlorate in *p*-xylene at 60°C.[44] Within this structure the silver(I) ions link the 1,8-diphenylocta-1,3,5,7-tetraene ligands by interacting with an alkene situated in the linear chain of one ligand and an alkene in an aromatic ring of another ligand. This leads to a 1-D chain which is then bridged through adjacent silver(I) atoms by perchlorate anions to yield the (3,4)-connected 2-D net of $(4.6^2)_2(4^2.6^2.8^2)$ topology.

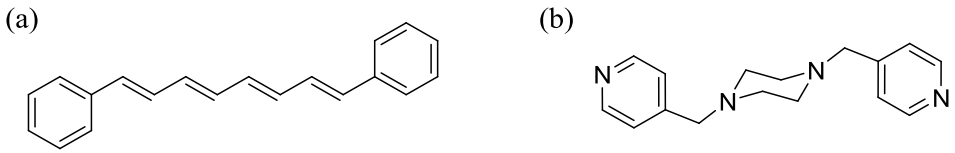

Figure 6.45. The structures of (a) 1,8-diphenylocta-1,3,5,7-tetraene and (b) *N*,*N*'-bis(4-pyridylmethyl)piperazine.

The second example was produced via the reaction of *N*,*N*'-bis(4-pyridylmethyl)piperazine (Figure 6.45 (b)) with $Co(SCN)_2$.[45] Within this structure the cobalt(II) ions act as 2-connecting nodes linking the ligands through their pyridyl donor atoms to form a 1-D polymer. The rest of the coordination sphere of the cobalt(II) ions is taken up by two isothiocyanate anions and two water molecules. The water molecules form hydrogen

bonds with the piperazine nitrogens in adjacent 1-D layers to form the (3,4)-connected 2-D net structure (if each of the piperazine nitrogens is treated as a 3-connecting node and the cobalt(II) ion is treated as a 4-connecting node). The topology of this structure can be further reduced to a simple 2-D (4,4) net if the centroid of the piperazine ring is considered a 4-connecting node.

Even though they exhibit the same network topology, these two examples are quite different to structure **6.24**. It is not simply the cationic polymer formed by the ligand and the metal ion which results in the network topology but coordinating anions, in the case of the first example, and interlayer hydrogen bonds, in the case of the second. The topology of structure **6.24**, on the other hand, is purely a result of the ligands capacity to act as both a 4-connecting node and a 2-connecting linker as well as the versatility of the silver(I) geometry. The coordination chemistry of compound **2.43**, with its four nitrile donor groups, promised to be very interesting however only one coordination polymer containing this ligand was able to be accessed. This is most likely due to the weak nitrile donor groups and is similar to the problems encountered during the investigation of the coordination chemistry of the nitrile substituted hexaaryl[3]radialenes as discussed in Chapter 4.

6.6. Summary

A total of thirteen coordination polymers have been synthesised from the flexible, dipyridyl ligands **2.51**, **2.52**, and **2.55** with silver(I) and copper(I). Three distinct structures were produced from ligand **2.51** with silver(I). The first was a simple 1-D zigzag polymer, the second a ladder-like 1-D polymer and the third an interesting 2-D (6,3) network. The ladder-like polymers **6.12** and **6.13** were found to be isostructural but not isomorphous; **6.12** has a compressed ladder-like structure whereas **6.13** has a more open structure. Structure **6.13** is more readily formed than **6.12** even though their structural differences are due to only subtle changes in the angle around the methylene group of the ligand and resultant distance between the pyridyl donors. Further investigation into whether these two structures can be interconverted upon solvent exchange may be of interest.

A 2-D (6,3) network was also able to be generated because of the adaptable geometry of silver(I); within this structure, **6.15**, it is trigonal planar. Due to the length and flexibility of the ligand this 2-D (6,3) network is highly corrugated instead of being planar, which is commonly observed in these types of structure. This corrugation allows the packing of the polymer nets in pairs of interdigitated sheets, which are further packed in layers sandwiching the counter anions. A similar corrugated structure, silver tricyanomethanide, exhibits 2-fold 2-D → 2-D parallel interpenetration as opposed to the simple interdigitation observed in **6.15**.

Two 1-D coordination polymers were observed upon reaction of **2.51** with copper(I). Due to the preference of copper(I) for a tetrahedral geometry there was not as much structural variation observed in these structures as seen in the silver(I) series. Compound **6.16** is a simple 1-D zigzag polymer where the copper(I) acts as a 2-connecting node and the remaining coordination sites are filled by acetonitrile molecules. Whereas, compound **6.17** is a 1-D polymer composed of loops where the copper(I) ions still act as 2-connecting nodes but all four coordination sites are filled by ligand molecules. The formation of these two structures was controlled by stoichiometry with a lower ligand to metal ratio leading to the first structure and a higher ligand to metal ratio to the latter.

Coordination polymers of ligand **2.52** were a lot more difficult to obtain than those containing **2.51** and the crystals were usually of a poorer quality and often twinned. Even so, three structures with silver(I) and one structure with copper(I) were able to be obtained. This ligand tends to produce 1-D zigzag coordination polymers with both silver(I) and copper(I) adopting 2-coordinate bent geometries in structures **6.18**, **6.19** and **6.21**. There were two different 1-D polymer morphologies observed. The first, seen in structure **6.18**, has all the ligands in the same orientation whilst the second morphology has adjacent ligands in alternate orientations, as seen in structures **6.19** and **6.21**. This is due to changes in the angle around the methylene group placing the nitrogen donor atoms further apart in the first case, 18.15 Å, and closer together in the second case, 15.48 Å for **6.19**. The final structure obtained via reaction of **2.51** with silver perchlorate in nitromethane, **6.20**, is also based on a 1-D zigzag polymer; however the chains are linked via long Ag-Ag bonds (3.27 Å) to form a 2-D net. The 1-D chains within this structure have a similar morphology to those in structures **6.19** and **6.21**, with an alternate orientation of adjacent ligands. Although in this case the nitrogen donor groups are further apart, 17.19 Å, more like those in structure **6.18**.

As both **2.51** and **2.52** possess alkyne groups within their structures it was thought that silver-alkyne interactions may possibly be observed in some of the coordination polymers produced. These interactions were only present in a two structures, **6.11** and **6.15**, and when they were observed the contacts were on the long side, with Ag-C_{alkyne} distances ranging from 2.98 to 3.24 Å, and thus not particularly strong interactions. This may be due to the myriad of other competing interactions present in these structures, in particular interactions with the pyridyl donors as well as the surrounding solvent.

Two isomorphous coordination polymers of **2.55** with copper(I), **6.22**, and silver(I), **6.23**, were obtained. These structures are 2-D with a (4,4) topology and experience an interesting mode of 3-fold 2-D → 2-D parallel interpenetration. Due to the 'v'-shape of the ligands the 2-D structure is corrugated, which allows close packing of the (4,4) sheets in pairs. The two

networks within these pairs are then interpenetrated with two networks of another pair however they do not interpenetrate each other. The resultant 3-fold interpenetrated stack of four sheets is then interdigitated with other stacks within the crystal lattice. A series of examples of 3-fold 2-D → 2-D parallel interpenetration were located in the literature; however none of these structures exhibit a similar unique packing arrangement.

The coordination chemistry of the flexible nitrile ligands **2.25**, **2.38** and **2.44** was also investigated but only one coordination polymer resulted due to the weak nitrile donors. This structure, **6.24**, was produced via reaction of **2.44** with silver perchlorate and exhibited an interesting 2-D (3,4)-connected network with the Schläfli symbol $(4.6^2)_2(4^2.6^2.8^2)$. Only two other examples of this topology were located within the literature; however these structures involved the use of metal-anion interactions and interlayer hydrogen bonds to produce such a network. To the best of our knowledge, structure **6.24** is the only example of this topology based solely on metal-ligand coordinate bonds.

A final conclusion which can be drawn from this study is that, although not often utilised, nitromethane is a very good solvent for the growth of X-ray quality crystals. It has a fairly high boiling point of 101°C and thus a slow evaporation rate which leads to the growth of larger and higher quality crystals. This can be observed via the comparison of those structures produced by slow evaporation from nitromethane (**6.13**, **6.14**, **6.20** and **6.21**) to those produced by slow evaporation from methanol/acetonitrile mixtures (**6.12**, **6.15**, **6.16**, **6.17** and **6.19**), which retained some solvent within the crystal lattice. In all of the structures, which contain nitromethane, the solvate molecules were easily found in the electron difference map and able to be refined anisotropically with only one incidence of solvate disorder in structure **6.14**. In only two of the polymers grown from methanol/acetonitrile were the solvate molecules able to be located and refined, **6.17** and **6.19** (structure **6.17** contained some solvate disorder). In the remaining methanol/acetonitrile grown structures the solvent was unable to be located in its entirety and had to be accounted for via the SQUEEZE routine of PLATON.

Overall the flexible dipyridyl ligands studied have produced some interesting coordination polymers. There is further scope for investigating the structures formed by these ligands upon reaction with metal(II) salts. Due to their length and flexibility they are probably not ideal for use in rigid metal-organic framework structures, targeted towards gas storage or separation, as they will likely be highly interpenetrated. However, there is potential for their use in dynamic coordination polymers as hinted at by the observation of compressed and open polymorphs of the 1-D ladder-like structures **6.12** and **6.13**.

6.7. Experimental

6.7.1. General Experimental

Infrared spectra were recorded using a Perkin Elmer Spectrum 100 FT-IR spectrometer with universal attenuated total reflectance (UATR) sampling accessory. The Campbell microanalytical laboratory at the University of Otago performed elemental analyses. *Perchlorate salts are potentially explosive and should be handled with care in small amounts.*

6.7.2. Crystallisation Procedures

{[Ag(2.51)]ClO_4}$_n$ (6.11). A solution of **2.51** (5.0 mg, 0.013 mmol) in MeOH (2 mL) was combined in a vial with a solution of $AgClO_4$ (5.4 mg, 0.026 mmol) in acetonitrile (0.5 mL). Slow evaporation of the solvent led to precipitation of **6.11** as pale yellow, plate-like crystals (5.0 mg, 67%) that were suitable for X-ray crystallography. Analysis calcd for **6.11**: $C_{27}H_{18}N_2AgClO_4$ C 56.12, H 3.15, N 4.85; found C 55.73, H 3.05, N 4.84; FT-IR υ_{max}/cm^{-1}: 2216 (C≡C str., vs), 1065 (Cl-O str., vs, b).

{[Ag(2.29)$_2$]ClO_4·3(CH_3OH)}$_n$ (6.12). A solution of **2.51** (10.0 mg, 0.026 mmol) in MeOH (3 mL) was combined in a vial with a solution of $AgClO_4$ (10.8 mg, 0.052 mmol) in MeOH (1 mL). Precipitation occurred immediately and the precipitate (11.3 mg) was removed via filtration. Slow evaporation led to precipitation of **6.12** as pale yellow, block-shaped crystals (trace quantities) suitable for X-ray crystallography. Repeated attempts to reproduce these crystals for IR and elemental analysis were unsuccessful and led to the isolation of a structure analogous to that of **6.13** instead.

{[Ag(2.51)$_2$]ClO_4·3(CH_3NO_2)}$_n$ (6.13). A solution of **2.51** (5.0 mg, 0.013 mmol) in nitromethane (2 mL) was combined in a vial with a solution of $AgClO_4$ (1.4 mg, 0.0065 mmol) in nitromethane (0.5 mL). Slow evaporation of the solvent led to precipitation of **6.13** as pale yellow, hexagonal plate crystals (4.3 mg, 59%) that were suitable for X-ray crystallography. Analysis calcd for **6.13**: $C_{54}H_{36}N_4AgClO_4·CH_3NO_2$ C 65.45, H 3.90, N 6.94; found C 65.61, H 4.03, N 6.27; FT-IR υ_{max}/cm^{-1}: 2223 (C≡C str., vs), 1083 (Cl-O str.).

{[Ag(2.51)$_2$]PF_6·3(CH_3NO_2)}$_n$ (6.14). A solution of **2.51** (5.0 mg, 0.013 mmol) in nitromethane (2 mL) was combined in a vial with a solution of $AgPF_6$ (1.7 mg, 0.0065 mmol) in nitromethane (0.5 mL). Slow evaporation of the solvent led to precipitation of **6.14** as pale yellow, hexagonal plate crystals (3.2 mg, 42%) that were suitable for X-ray crystallography. Analysis calcd for **6.14**: $C_{54}H_{36}N_4AgPF_6·½(CH_3NO_2)$ C 63.90, H 3.70, N 5.95; found C 64.26, H 3.85, N 5.95; FT-IR υ_{max}/cm^{-1}: 2221 (C≡C str., vs), 825 (P-F str., vs, b).

{[Ag$_2$(2.51)$_3$](PF_6)$_2$·2(CH_3OH)}$_n$ (6.15). A solution of **2.51** (5.0 mg, 0.013 mmol) in MeOH (2 mL) was combined in a vial with a solution of $AgPF_6$ (1.7 mg, 0.0065 mmol) in

acetonitrile (0.5 mL). Slow evaporation of the solvent led to precipitation of **6.15** as pale yellow, block-shaped crystals (2.6 mg, 48%) that were suitable for X-ray crystallography. Analysis calcd for **6.15**: $C_{81}H_{54}N_6Ag_2P_2F_{12}\cdot CH_3OH$ C 59.72, H 3.55, N 5.10; found C 59.37, H 3.29, N 5.14; FT-IR υ_{max}/cm^{-1}: 2221 (C≡C str., vs), 829 (P-F str., vs, b).

{[Cu(2.51)(CH$_3$CN)$_2$]PF$_6$}$_n$ (6.16). A solution of **2.51** (5.0 mg, 0.013 mmol) in MeOH (2 mL) was combined in a vial with a solution of $[Cu(CH_3CN)_4]PF_6$ (9.7 mg, 0.026 mmol) in acetonitrile (0.5 mL). Slow evaporation of the solvent led to precipitation of **6.16** as bright yellow, needle-like crystals (4.4 mg, 51%) that were suitable for X-ray crystallography. Analysis calcd for **6.16**: $C_{27}H_{18}N_2CuPF_6$ C 56.01, H 3.14, N 4.84; found C 56.28, H 3.19, N 4.92; FT-IR υ_{max}/cm^{-1}: 2218 (C≡C str., vs), 825 (P-F str., vs, b).

{[Cu$_2$(2.51)$_4$](PF$_6$)$_2$·CH$_3$OH}$_n$ (6.17). A solution of **2.51** (5.0 mg, 0.013 mmol) in MeOH (2 mL) was combined in a vial with a solution of $Cu(CH_3CN)_4PF_6$ (2.5 mg, 0.0065 mmol) in acetonitrile (0.5 mL). Slow evaporation of the solvent led to precipitation of **6.17** as bright yellow, needle-like crystals (4.0 mg, 64%) that were suitable for X-ray crystallography. Analysis calcd for **6.17**: $C_{108}H_{72}N_8Cu_2P_2F_{12}\cdot CH_3OH$ C 67.79, H 3.98, N 5.80; found C 65.48, H 3.69, N 5.88; FT-IR υ_{max}/cm^{-1}: 2220 (C≡C str., vs), 833 (P-F str., vs, b).

{[Ag(2.52)]SbF$_6$·4(CH$_3$OCH$_3$)}$_n$ (6.18). A solution of **2.52** (5.0 mg, 0.013 mmol) in acetone (2 mL) was combined in a vial with a solution of $AgSbF_6$ (4.6 mg, 0.013 mmol) in acetone (0.5 mL). Slow evaporation of the solvent led to precipitation of **6.18** as colourless, needle-like crystals (5.7 mg, 46%) that were suitable for X-ray crystallography. Analysis calcd for **6.18**: $C_{27}H_{18}N_2AgSbF_6$ C 45.42, H 2.55, N 3.92; found C 45.82, H 2.59, N 3.89; FT-IR υ_{max}/cm^{-1}: 2230 (C≡C str., vs), 652 (Sb-F str., vs, b).

{[Ag(2.52)]ClO$_4$·(CH$_3$OH)}$_n$ (6.19). A solution of **2.52** (5.0 mg, 0.013 mmol) in MeOH (2 mL) was combined in a vial with a solution of $AgClO_4$ (1.4 mg, 0.0065 mmol) in acetonitrile (0.5 mL). Slow evaporation of the solvent led to precipitation of **6.19** as colourless needles (2.7 mg, 68%) that were suitable for X-ray crystallography. Analysis calcd for **6.19**: $C_{27}H_{18}N_2AgClO_4\cdot$**½(**$CH_3OH)\cdot$½$(CH_3CN)\cdot H_2O$ C 54.13, H 3.75, N 5.54; found C 53.70, H 3.60, N 5.67; FT-IR υ_{max}/cm^{-1}: 2222 (C≡C str., vs), 1050 (Cl-O str., vs, b).

{[Ag(2.52)]ClO$_4$·CH$_3$NO$_2$}$_n$ (6.20). A solution of **2.52** (5.0 mg, 0.013 mmol) in nitromethane (2 mL) was combined in a vial with a solution of $AgClO_4$ (1.4 mg, 0.0065 mmol) in nitromethane (0.5 mL). Slow evaporation of the solvent led to precipitation of **6.20** as pale yellow, block-shaped crystals (2.2 mg, 53%) that were suitable for X-ray crystallography. : $C_{27}H_{18}N_2AgClO_4\cdot CH_3NO_2\cdot H_2O$ C 51.27, H 3.39, N 6.41; found C 50.89, H 3.19, N 5.89;; FT-IR υ_{max}/cm^{-1}: 2222 (C≡C str., vs), 1050 (Cl-O str., vs, b).

{[Cu(2.52)]BF_4·CH_3NO_2}$_n$ (6.21). A solution of **2.52** (5.0 mg, 0.013 mmol) in MeOH (2 mL) was combined in a vial with a solution of [Cu(CH_3CN)$_4$]BF_4 (8.2 mg, 0.026 mmol) in acetonitrile (0.5 mL). Slow evaporation of the solvent led to precipitation of **6.21** as pale yellow, block-shaped crystals (2.7 mg, 35%) that were suitable for X-ray crystallography. Repeated attempts to reproduce these crystals for IR spectroscopy and elemental analysis were unsuccessful and led to the precipitation of a blue copper(II) salt.

{[Cu(2.55)$_2$]BF_4}$_n$ (6.22). A solution of **2.55** (5.0 mg, 0.016 mmol) in MeOH (2 mL) was combined in a vial with a solution of [Cu(CH_3CN)$_4$]BF_4 (2.4 mg, 0.0076 mmol) in acetonitrile (0.5 mL). Slow evaporation of the solvent led to precipitation of **6.22** as bright yellow pyramidal crystals (3.3 mg, 55%) that were suitable for X-ray crystallography. Analysis calcd for **6.22**: $C_{46}H_{36}N_4CuBF_4$ C 69.47, H 4.57, N 7.05; found C 69.74, H 4.49, N 7.24; FT-IR υ_{max}/cm^{-1}: 1597 (C=C str., vs), 1051 (B-F str., vs, b).

{[Ag(2.55)$_2$]ClO_4}$_n$ (6.23). A solution of **2.55** (5.0 mg, 0.016 mmol) in MeOH (2 mL) was combined in a vial with a solution of $AgClO_4$ (1.6 mg, 0.0076 mmol) in acetonitrile (0.5 mL). Slow evaporation of the solvent led to precipitation of **6.23** as colourless octahedral crystals (4.4 mg, 67%) that were suitable for X-ray crystallography. Analysis calcd for **6.23**: $C_{46}H_{36}N_4AgClO_4$ C 64.83, H 4.27, N 6.58; found C 65.09, H 4.29, N 6.71; FT-IR υ_{max}/cm^{-1}: 1597 (C=C str., vs), 1084 (Cl-O str., vs, b).

{[Ag(2.43)(H_2O)]ClO_4·CH_3NO_2}$_n$ (6.24). A solution of **2.43** (5.0 mg, 0.019 mmol) in nitromethane (2 mL) was combined in a vial with a solution of $AgClO_4$ (15.4 mg, 0.037 mmol) in nitromethane (0.5 mL). Slow evaporation of the solvent led to precipitation of **6.24** as colourless, rod-shaped crystals (6.1 mg, 58%) that were suitable for X-ray crystallography. Analysis calcd for **6.24**: $C_{18}H_8N_4AgClO_4$·CH_3NO_2 C 40.29, H 2.07, N 13.05; found C 40.00, H 2.13, N 12.76; FT-IR υ_{max}/cm^{-1}: 2257 (C≡N str., vs), 1076 (Cl-O str., vs, b).

6.7.3. X-Ray Crystallography

Crystals were mounted under oil on a loop and X-ray diffraction data were collected at 150(2) K with Mo Kα radiation (λ = 0.71073 Å) using an Oxford Diffraction X-Calibur Diffractometer fitted with an Eos CCD detector or with synchrotron radiation (λ = 0.7107 Å) using the Macromolecular Crystallography beamline (MX1) at the Australian Synchrotron.[46] The data set was corrected for absorption using a multi-scan method, and structures were solved by direct methods using SHELXS-97 [47] and refined by full-matrix least squares on F^2 by SHELXL-97,[48] interfaced through the program X-Seed.[49] All non-hydrogen atoms were refined anisotropically and hydrogen atoms were included as invariants at geometrically estimated positions, unless otherwise stated.

6.7.4. Crystallographic Data

Table 6.1. Crystal data and X-ray experimental data for **6.11**, **6.12**, **6.13**, **6.14** and **6.15**.

Compound	**6.11**	**6.12**	**6.13**	**6.14**	**6.15**
Empirical formula	$C_{27}H_{18}N_2O_4AgCl$	$C_{57}H_{48}N_4O_7AgCl$	$C_{57}H_{41}N_7O_{10}AgCl$	$C_{57}H_{45}N_7O_6AgPF_6$	$C_{83}H_{62}N_6O_2Ag_2P_2F_{12}$
Formula weight	577.75	1044.32	1127.29	1176.84	1681.07
Radiation source	Mo Kα	Mo Kα	Mo Kα	Mo Kα	Synchrotron
Crystal system	Monoclinic	Triclinic	Triclinic	Triclinic	Triclinic
Space group	$P2_1/c$	P-1	P-1	P-1	P-1
a (Å)	11.8581(7)	11.7920(6)	14.0217(4)	13.8807(4)	14.381(3)
b (Å)	17.6636(6)	14.4527(6)	14.0806(4)	14.1302(4)	14.463(3)
c (Å)	12.4085(8)	16.5994(7)	16.3171(4)	17.0012(4)	21.913(4)
α (°)	90	104.661(4)	75.795(3)	68.047(3)	86.58(3)
β (°)	116.923(8)	96.100(4)	73.676(2)	72.252(3)	80.77(3)
γ (°)	90	105.962(4)	62.915(3)	63.858(3)	60.60(3)
Volume ($Å^3$)	2317.3(2)	2583.9(2)	2726.51(13)	2736.81(13)	3918.3(14)
Z	4	2	2	2	2
D_{calc} (mg/m^3)	1.656	1.342	1.373	1.428	1.371
Absorption coefficient (mm^{-1})	1.023	0.498	0.483	0.475	0.615
F(000)	1160	1076	1152	1200	1628
Crystal size (mm^3)	0.65 × 0.36 × 0.12	0.55 × 0.33 × 0.26	0.53 × 0.36 × 0.15	0.59 × 0.38 × 0.31	0.33 × 0.26 × 0.15
Theta range for data (°)	2.95 to 29.30	2.58 to 27.37	2.52 to 29.36	2.54 to 29.33	1.62 to 28.77
Reflections collected	20948	32580	48853	71212	66396
Independent reflections [R(int)]	5665 [0.0517]	11084 [0.0318]	13219 [0.0483]	13309 [0.0686]	17547 [0.0299]
Completeness to theta full (%)	99.8	97.5	99.5	99.4	91.9
Observed reflections [I>2σ(I)]	4050	8888	10471	10245	15556
Data / restraints / parameters	5665 / 0 / 316	11084 / 0 / 577	13219 / 0 / 688	13309 / 0 / 724	17547 / 21 / 961
Goodness-of-fit on F2	1.040	1.130	1.044	1.053	1.049
R_1 [I>2σ(I)]	0.0411	0.0600	0.0522	0.0527	0.0661
wR_2 (all data)	0.0955	0.1969	0.1485	0.1396	0.2098
Largest diff. peak and hole ($e.Å^{-3}$)	0.950 and -0.599	0.485 and -1.66	1.19 and -0.722	0.977 and -0.918	1.33 and -1.47

Table 6.2. Crystal data and X-ray experimental data for **6.16**, **6.17**, **6.18**, **6.19** and **6.20**.

Compound	**6.16**	**6.17**	**6.18**	**6.19**	**6.20**
Empirical formula	$C_{31}H_{24}N_4CuPF_6$	$C_{109}H_{76}N_8OCu_2P_2F_{12}$	$C_{19.5}H_{21}NO_2Ag_{0.5}Sb_{0.5}F_3$	$C_{56}H_{44}N_4O_{10}Ag_2Cl_2$	$C_{28}H_{21}N_3O_6AgCl$
Formula weight	661.05	1930.80	473.18	1219.59	638.80
Radiation source	Mo Kα	Synchrotron	Mo Kα	Mo Kα	Mo Kα
Crystal system	Monoclinic	Triclinic	Monoclinic	Monoclinic	Monoclinic
Space group	$P2_1/c$	P-1	C2/c	$C2/c$	$P2_1/c$
a (Å)	12.2533(4)	10.700(2)	29.564(4)	37.4980(14)	9.8366(5)
b (Å)	18.3547(6)	17.374(3)	7.8773(5)	9.3907(3)	9.8227(5)
c (Å)	14.0387(6)	25.297(5)	21.169(3)	33.5021(13)	28.1560(14)
α (°)	90	100.95(3)	90	90	90
β (°)	111.966(4)	95.90(3)	124.433(17)	123.099(3)	98.542(5)
γ (°)	90	96.38(3)	90	90	90
Volume ($Å^3$)	2928.17(18)	4551.4(15)	4066.2(7)	9882.8(6)	2690.3(2)
Z	4	2	4	8	4
D_{calc} (mg/m^3)	1.500	1.409	1.546	1.637	1.577
Absorption coefficient (mm^{-1})	0.867	0.584	1.213	0.967	0.896
F(000)	1344	1980	1896	4912	1288
Crystal size (mm^3)	0.43 × 0.23 × 0.13	0.32 × 0.13 × 0.05	0.51 × 0.27 × 0.16	0.91 × 0.14 × 0.08	0.37 × 0.26 × 0.11
Theta range for data (°)	2.72 to 29.26	1.20 to 28.80	2.72 to 29.28	2.45 to 29.29	2.54 to 29.28
Reflections collected	33326	78511	18815	46441	13386
Independent reflections [R(int)]	7212 [0.0334]	20751 [0.0599]	4914 [0.0577]	11915 [0.0454]	13570 [0.0650]
Completeness to theta full (%)	99.8	94.7	99.6	99.5	99.5
Observed reflections [I>2σ(I)]	5825	12468	3578	6625	11616
Data / restraints / parameters	7212 / 0 / 390	20751 / 2 / 1273	4914 / 0 / 246	11915 / 0 / 672	13570 / 0 / 335
Goodness-of-fit on F2	1.026	1.038	1.029	1.045	1.163
R_1 [I>2σ(I)]	0.0469	0.0679	0.0401	0.0711	0.0982
wR_2 (all data)	0.1272	0.2211	0.0943	0.2481	0.2484
Largest diff. peak and hole ($e.Å^{-3}$)	1.01 and -0.630	1.60 and -0.939	1.80 and -0.652	3.04 and -1.10	1.26 and -2.96

Table 6.3. Crystal data and X-ray experimental data for **6.20**, **6.21**, **6.22**, and **6.23**.

Compound	**6.21**	**6.22**	**6.23**	**6.24**
Empirical formula	$C_{28}H_{21}N_3O_2CuBF_4$	$C_{23}H_{18}N_2Cu_{0.5}B_{0.5}F_2$	$C_{276}H_{216}N_{24}O_{24}Ag_6Cl_6$	$C_{18}H_{13}N_5O_7AgCl$
Formula weight	581.83	397.57	5112.65	554.65
Radiation source	Mo Kα	Mo Kα	Synchrotron	Mo Kα
Crystal system	Monoclinic	Tetragonal	Monoclinic	Monoclinic
Space group	$P2_1/c$	$I4_1/a$	$P2_1/c$	$P2/c$
a (Å)	9.8476(4)	12.6136(4)	12.835(3)	19.0917(7)
b (Å)	9.8187(4)	12.6136(4)	44.805(9)	4.05750(10)
c (Å)	28.1656(17)	46.561(2)	39.516(8)	27.0688(8)
α (°)	90	90	90	90
β (°)	98.433(5)	90	90.24(3)	99.547(3)
γ (°)	90	90	90	90
Volume ($Å^3$)	2693.9(2)	7407.9(5)	22724(8)	2067.83(11)
Z	4	16	4	4
D_{calc} (mg/m^3)	1.435	1.426	1.494	1.782
Absorption coefficient (mm^{-1})	0.869	0.650	0.655	1.156
F(000)	1184	3280	10464	1104
Crystal size (mm^3)	0.73 × 0.37 × 0.31	0.34 × 0.21 × 0.13	0.30 × 0.28 × 0.25	1.1 × 0.10 × 0.07
Theta range for data (°)	2.54 to 29.36	2.45 to 24.99	1.04 to 28.80	2.85 to 29.02
Reflections collected	12116	15335	383344	14473
Independent reflections [R(int)]	12460 [0.1250]	3262 [0.0453]	57825 [0.0551]	4810 [0.0489]
Completeness to theta full (%)	99.4	99.9	99.8	99.0
Observed reflections [I>2σ(I)]	10122	2538	50220	3338
Data / restraints / parameters	12460 / 3 / 349	3262 / 6 / 306	57825 / 0 / 3044	4810 / 10 / 364
Goodness-of-fit on F2	1.038	1.124	1.127	1.036
R_1 [I>2σ(I)]	0.1141	0.1126	0.0690	0.0469
wR_2 (all data)	0.3076	0.2085	0.1632	0.1062
Largest diff. peak and hole ($e.Å^{-3}$)	3.80 and -1.86	0.495 and -0.488	1.78 and -1.91	0.808 and -1.32

Additional refinement details for 6.12. The structure has solvent accessible voids. These contained a number of diffuse electron density peaks that could not be adequately identified and refined as solvent. The SQUEEZE routine of PLATON[50] was applied to the collected data, which resulted in significant reductions in R_1 and wR_2 and an improvement in the GOF. R_1, wR_2 and GOF before SQUEEZE routine: 9.4%, 30.7% and 1.20; after SQUEEZE routine: 6.0%, 19.7% and 1.13. The contents of the solvent region calculated from the result of the SQUEEZE routine (3 MeOH per asymmetric unit) are represented in the unit cell contents in crystal data.

Additional refinement details for 6.14. There is disorder of one nitromethane solvate molecule, which was modelled over two major positions.

Additional refinement details for 6.15. The structure has solvent accessible voids. These contained a number of diffuse electron density peaks that could not be adequately identified and refined as solvent. The SQUEEZE routine of PLATON[50] was applied to the collected data, which resulted in significant reductions in R_1 and wR_2 and an improvement in the GOF. R_1, wR_2 and GOF before SQUEEZE routine: 10.7%, 39.8% and 1.96; after SQUEEZE routine: 6.8%, 21.5% and 1.01. The contents of the solvent region calculated from the result of the SQUEEZE routine (2 MeOH per asymmetric unit) are represented in the unit cell contents in crystal data. There is disorder of the half occupied hexafluorophosphate anion. The SAME command was used to model it on the well refined, fully occupied, hexafluorophosphate anion. Complex **6.15** was very weakly diffracting and as such the data was omitted above 42° to provide a reasonable completeness for the data.

Additional refinement details for 6.17. There is disorder of one methanol solvate molecule, which was modelled over two major positions. Two restraints were used to maintain chemically sensible bond lengths within the methanol solvate molecule. Complex **6.17** was very weakly diffracting and as such the data was omitted above 42° to provide a reasonable completeness for the data.

Additional refinement details for 6.20. These crystals were twinned with a ratio of the twin components of 58:42. The data was processed as such and refined using a hklf5 twin refinement.

Additional refinement details for 6.21. These crystals were twinned with a ratio of the twin components of 59:41. The data was processed as such and refined using a hklf5 twin refinement. The structure was refined with significant disorder issues of the tetrafluoroborate anion due to the twinned crystal and, consequently, poor quality of the data. The boron atom of the tetrafluoroborate anion was refined isotropically and three restraints were used to maintain chemically sensible bond lengths within the anion.

Additional refinement details for 6.22. There is disorder of one benzene ring of one of the bis(4-(pyridin-4-yl)phenyl)methane ligands, which was modelled over two major positions. Six restraints were used to maintain chemically sensible bond lengths within the disordered benzene ring.

Additional refinement details for 6.23. There is disorder of one benzene ring of the bis(4-(pyridin-4-yl)phenyl)methane ligand, which was modelled over two major positions.

Additional refinement details for 6.24. The structure contains two 50% occupied perchlorate anions and two 50% occupied nitromethane solvate molecules which occupy the same positions. Two EXYZ and two EADP constraints were used to keep the chlorine atoms of the perchlorate anions and the nitrogen atoms of the nitromethane molecules in the same position and give them the same anisotropic displacement parameters. Five constraints were used to maintain chemically sensible bond lengths within the nitromethane molecules.

6.8. References

1 W. R. McWhinnie, *Coord. Chem. Rev.*, **1970**, *5*, 293.

2 C. J. Sumby, *Coord. Chem. Rev.*, **2011**, *255*, 1937.

3 X.-D. Chen and T. C. W. Mak, *J. Mol. Struct.*, **2005**, *743*, 1.

4 X.-D. Chen, J.-H. Guo, M. Du, and T. C. W. Mak, *Inorg. Chem. Commun.*, **2005**, *8*, 766.

5 M. A. Braverman, J. H. Nettleman, R. M. Supkowski, and R. L. LaDuca, *Inorg. Chem.*, **2009**, *48*, 4918.

6 V. J. Argyle, L. M. Woods, M. Roxburgh, and L. R. Hanton, *CrystEngComm*, **2013**, *15*, 120.

7 D. B. Cordes, L. R. Hanton, and M. D. Spicer, *Cryst. Growth Des.*, **2006**, *7*, 328.

8 D. B. Cordes, L. R. Hanton, and M. D. Spicer, *Inorg. Chem.*, **2006**, *45*, 7651.

9 M. R. Montney, S. Mallika Krishnan, N. M. Patel, R. M. Supkowski, and R. L. LaDuca, *Cryst. Growth Des.*, **2007**, *7*, 1145.

10 M. A. Braverman and R. L. LaDuca, *Cryst. Growth Des.*, **2007**, *7*, 2343.

11 M. J. Plater, M. R. S. J. Foreman, T. Gelbrich, S. J. Coles, and M. B. Hursthouse, *J. Chem. Soc., Dalton Trans.*, **2000**, *0*, 3065.

12 W. M. Bloch and C. J. Sumby, *Chem. Commun.*, **2012**, *48*, 2534.

13 J. Burgess and P. J. Steel, *Coord. Chem. Rev.*, **2011**, *255*, 2094.

14 T. Kawano, C.-X. Du, T. Araki, and I. Ueda, *Inorg. Chem. Commun.*, **2003**, *6*, 165.

15 C. Desmarets, I. Azcarate, G. Gontard, and H. Amouri, *Eur. J. Inorg. Chem.*, **2011**, *2011*, 4558.

16 K. J. Kilpin, M. L. Gower, S. G. Telfer, G. B. Jameson, and J. D. Crowley, *Inorg. Chem.*, **2011**, *50*, 1123.

17 E. Bosch and C. L. Barnes, *J. Coord. Chem.*, **2003**, *56*, 329.

18 W. W. Ellis, M. Schmitz, A. A. Arif, and P. J. Stang, *Inorg. Chem.*, **2000**, *39*, 2547.

19 D. L. Reger, J. R. Gardinier, and M. D. Smith, *Inorg. Chem.*, **2004**, *43*, 3825.

20 M. Munakata, L. P. Wu, T. Kuroda-Sowa, M. Maekawa, Y. Suenaga, T. Ohta, and H. Konaka, *Inorg. Chem.*, **2003**, *42*, 2553.

21 A. N. Khlobystov, A. J. Blake, N. R. Champness, D. A. Lemenovskii, A. G. Majouga, N. V. Zyk, and M. Schroder, *Coord. Chem. Rev.*, **2001**, *222*, 155.

22 E. C. Constable, C. E. Housecroft, B. M. Kariuki, and C. B. Smith, *Aust. J. Chem.*, **2006**, *59*, 30.

23 C. A. Hollis, L. R. Hanton, J. C. Morris, and C. J. Sumby, *Cryst. Growth Des.*, **2009**, *9*, 2911.

24 A. M. Kutasi, D. R. Turner, B. Moubaraki, S. R. Batten, and K. S. Murray, *Dalton Trans.*, **2011**, *40*, 12358.

25 G. B. Gardner, D. Venkataraman, J. S. Moore, and S. Lee, *Nature*, **1995**, *374*, 792.

26 D. Venkataraman, G. B. Gardner, S. Lee, and J. S. Moore, *J. Am. Chem. Soc.*, **1995**, *117*, 11600.

27 J. Konnert and D. Britton, *Inorg. Chem.*, **1966**, *5*, 1193.

28 S. R. Batten, B. F. Hoskins, and R. Robson, *New J. Chem.*, **1998**, *22*, 173.

29 B. F. Abrahams, S. R. Batten, B. F. Hoskins, and R. Robson, *Inorg. Chem.*, **2003**, *42*, 2654.

30 K. Singh, J. R. Long, and P. Stavropoulos, *J. Am. Chem. Soc.*, **1997**, *119*, 2942.

31 H. M. J. Wang and I. J. B. Lin, *Organometallics*, **1998**, *17*, 972.

32 A. Bondi, *J. Phys. Chem.*, **1964**, *68*, 441.

33 S. R. Batten and R. Robson, *Angew. Chem. Int. Ed.*, **1998**, *37*, 1460.

34 S. R. Batten, *CrystEngComm*, **2001**, *3*, 67.

35 S. R. Batten, S. M. Neville, and D. R. Turner, *Coordination Polymers: Design, Analysis and Application*, RSC Publishing, Cambridge, 2009.

36 K. A. Hirsch, S. R. Wilson, and J. S. Moore, *Inorg. Chem.*, **1997**, *36*, 2960.

37 S. R. Batten, A. R. Harris, P. Jensen, K. S. Murray, and A. Ziebell, *J. Chem. Soc., Dalton Trans.*, **2000**, 3829.

38 Z. Ni and J. J. Vittal, *Cryst. Growth Des.*, **2001**, *1*, 195.

39 O. R. Evans and W. Lin, *Chem. Mater.*, **2001**, *13*, 3009.

40 L. Carlucci, G. Ciani, D. M. Proserpio, and S. Rizzato, *CrystEngComm*, **2002**, *4*, 413.

41 N.-N. Yuan, Q.-K. Liu, J.-P. Ma, R.-Q. Huang, and Y.-B. Dong, *Acta Crystallogr., Sect. C*, **2011**, *67*, m119.

42 C.-H. Ge, X.-D. Zhang, P. Zhang, W. Guan, F. Guo, and Q.-T. Liu, *Polyhedron*, **2003**, *22*, 3493.

43 K. L. Gurunatha and T. K. Maji, *Inorg. Chim. Acta*, **2009**, *362*, 1541.

44 J. C. Zhong, M. Munakata, T. Kuroda-Sowa, M. Maekawa, Y. Suenaga, and H. Konaka, *Inorg. Chim. Acta*, **2001**, *322*, 150.

45 D. P. Martin, W. R. Knapp, R. M. Supkowski, and R. L. LaDuca, *Inorg. Chim. Acta*, **2009**, *362*, 1559.

46 T. M. McPhillips, S. E. McPhillips, H.-J. Chiu, A. E. Cohen, A. M. Deacon, P. J. Ellis, E. Garman, A. Gonzalez, N. K. Sauter, R. P. Phizackerley, S. M. Soltis, and P. Kuhn, *J. Synchrotron Radiat.*, **2002**, *9*, 401.

47 G. M. Sheldrick, *Acta Crystallogr., Sect. A*, **1990**, *46*, 467.

48 G. M. Sheldrick, *SHELXL-97*, University of Gottingen, Gottingen, Germany 1997.

49 L. J. Barbour, *J. Supramol. Chem.*, **2001**, *1*, 189.

50 A. L. Spek, *Acta Crystallogr., Sect. A*, **1990**, *46*, 34.

Chapter 7

Conclusion

Chapter 7

7. Conclusion

This thesis has described the synthesis of three nitrile substituted hexaaryl[3]radialenes, **2.29**, **2.38**, and **2.44**, two of which are new compounds. It was noted that having an electron withdrawing group in the 4-position of the aryl rings of the diaryl methane precursor greatly enhanced the yield of the final product. X-ray crystallography and ^{1}H NMR spectroscopy were used to demonstrate that these structures possess a double-bladed propeller conformation with the "arms" of the radialene at an average torsion angle of 39° to the core plane. This pre-organisation makes these structures ideal scaffolds for incorporation into metallo-supramolecular assemblies and coordination polymers.

The increasing electron deficiency of the radialenes along the series **2.38** < **2.29** < **2.44** was shown via the determination of their respective reduction potentials by cyclic voltammetry. Radialene **2.44** was shown to have the lowest reduction potentials (-0.06 and -0.45 V) of any hexaaryl[3]radialene previously reported. The electron deficient [3]radialene core and the acidic aryl protons are favourable motifs for anion interactions, making anions a possible target for radialene-based sensors. These hexaaryl[3]radialenes are also highly fluorescent and exhibit large Stokes shifts; the difference between the excitation and emission maxima. A fluorescent sensor ideally possesses a large Stokes shift as this allows the emission photons to be detected against a low background signal, isolated from the excitation photons, which enhances the sensitivity of the technique.

Despite considerable synthetic effort, the acquisition of extended hexaaryl[3]radialenes, with the aim of utilising these as components in metallo-supramolecular capsules with potential application in sensing and sequestering anions, was unsuccessful. This was largely proposed to be due to the instability of the methane carbanions of **2.51**, **2.52**, and **2.55**. A recent study, published during the course of this work, by Matsumoto and colleagues reported the synthesis of extended hexaaryl[3]radialenes via post-synthetic modification of hexakis(4-bromophenyl)[3]radialene. This was affected via a cross-coupling reaction with various lithium diarylamides according to Hartwig's procedure. Post-synthetic modification of pre-existing hexaaryl[3]radialenes may provide a more effective route for the formation of the desired extended hexaaryl[3]radialenes.

It was proposed that bridging ligands incorporating a cross-conjugated [3]radialene core may enable a metal atom in a multinuclear complex to interact in a facile manner with a

second metal through the linearly conjugated segment of the π-system but not in the same manner with a third due to cross-conjugation. However, the synthesis of multinuclear ruthenium complexes of the radialene ligands **2.29** and **2.38** proved to be problematic. Reaction of these ligands with more than one equivalent of $[RuCp(PPh_3)_2]Cl$ led to the formation of multiple products including the mononuclear species and three isomeric dinuclear species. Dinuclear complexes containing the [3]radialene precursor ligands, 4,4'-dicyanodiphenylmethane (**2.25**) and 3,3'-dicyanodiphenylmethane (**2.37**), were able to be obtained. However, no metal-metal communication was observed for these complexes, as demonstrated by the presence of only one oxidation wave in their cyclic voltammograms, due to the insulating methylene spacer.

Mononuclear complexes of **2.29** and **2.38** containing $[RuCp(PPh_3)_2]$ and [RuCp*(dppe)] moieties were able to be produced via the use of stoichiometric control. It was observed that the radialene reduction potentials were reduced by an average of 0.09 V from the free radialene which indicated that where the radialene was *para*-substituted, there was an interaction between the ruthenium centre and the radialene that allowed the stabilisation of the reduced forms of the radialene. Interestingly, a similar scenario was seen for the complexes where the radialene was *meta*-substituted. This indicated that despite the lack of direct conjugation in the *meta* isomer **2.38**, the ruthenium centre still acted to stabilise the radical and, to a lesser extent, the dianion. These complexes also maintained the fluorescence of the radialene ligands and their large Stokes shifts.

The coordination chemistry of all three nitrile substituted hexaaryl[3]radialenes, **2.29**, **2.38**, and **2.44**, was examined by reaction with a variety of metal salts, particularly silver(I) and copper(I) due to the presence of weak nitrile donors. A total of nine new coordination polymers were synthesised from the hexatopic ligand hexakis(4-cyanophenyl)[3]radialene, **2.29,** with silver(I), copper(I)/(II) and iron(II). Within these structures five different coordination modes were observed for **2.29**, which included two different bidentate binding modes, two different tetradentate binding modes (including the formation of a 17-membered chelate ring via coordination by two nitrile donor groups situated on adjacent radialene arms) and a hexadentate binding mode.

Even though **2.29** has the potential to be hexadentate it generally prefers to be hypodentate, as shown by four of the observed coordination modes. Structure **4.9** is the first example of **2.29** acting as a hexadentate ligand. With low Ag:**2.29** stoichiometries, in the region of 1:1 to 3:1, [3]radialene **2.29** acts as a tetradentate ligand as observed for the 2-D (6,3) sheet topology of structures **4.5-4.8**. Increasing the Ag:**2.29** ratio dramatically to 10:1 allowed the isolation of structure **4.9**, an 8-fold interpenetrated (10,3)-*b* net. It appears that

such high Ag:**2.29** ratios are necessary to facilitate utilisation of all six nitrile donor groups of **2.29**.

Coordination polymers with two distinct topologies, **4.10a**/**4.11a** and **4.10b**/**4.11b**, were formed upon reaction of **2.29** with copper(I) salts. The formation of these structures is not controlled by stoichiometry, as observed for the silver(I) structures, and is instead kinetically controlled with both polymers having the same stoichiometry despite being formed at different stages of the slow evaporation process. In this case the more open, metastable products (**4.10a** and **4.11a**) appear to form first – these are particularly solvent dependent – and over time the denser, close-packed and stable structures of **4.10b** and **4.11b** form. Structures **4.10a**/**4.11a** exhibit a complex 3-D network with large solvent accessible voids, which accounts for their inherent instability. Whereas structures **4.10b**/**4.11b** are 4-connected networks formed by the bridging of (6,3) sheets similar to those seen in structures **4.5**-**4.8**.

Another interesting observation was the production of a copper(II) coordination polymer from the reaction of **2.29** with a copper(I) salt. It was proposed that the oxidation of the copper(I) salt came at the expense of the reduction of some of the radialene, or through a disproportionation reaction of copper(I), as the crystals were only produced in trace quantities. While copper(I) salts are often oxidised *in-situ*, it is relatively uncommon for this to result in the production of X-ray quality crystals as shown by the discovery of only one other example in the literature of the oxidation of copper(I) to copper(II) during crystallisation.

Much synthetic effort was expended in the endeavour to crystallise the two new hexaaryl[3]radialene compounds **2.38** and **2.44**. [3]Radialene **2.38** proved resistant to all crystallisation attempts and not even crystals of the compound itself could be obtained. Finally, success was achieved with the generation of a 3-D coordination polymer, **4.14**, via the reaction of **2.44** with $AgPF_6$ in a ratio of 1:12. Within this structure the potentially dodecatopic ligand is hypodentate with only eight of its twelve nitrile donor groups involved in coordination. The polymer itself appeared complex but the topology could be reduced to that of the rutile network via the treatment of a cluster of four silver(I) atoms as a 6-connecting node and the radialene ligands as 3-connecting nodes.

Within the polymers obtained, close contacts were observed between anions and the [3]radialene core prompting further research into the ability of hexaaryl[3]radialene ligands to exhibit anion-π interactions. Each of the three nitrile substituted radialenes previously mentioned, as well as hexaphenyl[3]radialene (**1.1**), were optimised to the HF/6-31G++(d,p) level of theory. These calculations showed that the [3]radialene core itself was not intrinsically electron deficient but required the addition of electron withdrawing substituents

to become so as only the nitrile substituted compounds showed positive Q_{zz} quadropole moments, required for sustaining anion-π interactions, and two areas of positive potential, at the [3]radialene core and on the aryl hydrogens, amenable to interacting with anions. Optimisation of these radialenes with the halide anions F^-, Cl^- and Br^- revealed a trend in interaction energy across all species of $F^- > Cl^- > Br^-$. Radialene **2.29** was also optimised with a series of polyatomic anions with the resulting geometries exhibiting the anions above the core centroid of the [3]radialene.

Negative ion, electrospray ionisation, high-resolution mass spectrometry (ESI-HRMS) was used to further validate the computational results. The stability of the radialene anion complexes was probed via comparison of the signal intensities for a particular ion as the normalised collision energy (NCE) was increased incrementally, during MS/MS experiments, relative to the signal intensity observed at an NCE of zero. This analysis revealed that the stability of the radialene halide complexes varied such that $F^- > Cl^- \approx Br^-$, which is comparable to the theoretical calculations, and that the complexes of **2.44** were significantly more stable than those of **2.38** and **2.29** which display similar stabilities.

Examination of solid-state structures provided further evidence for the existence of interactions between anions and the [3]radialene core. Close contacts with the [3]radialene core carbons, less than Σ_{vdw} + 0.2 Å of the interacting atoms, were observed in structures **4.5-4.8** and **4.12-4.14**. The majority of these show the anion positioned over the [3]radialene core centroid, with the exception of **4.12**. Although as the π-system of the [3]radialene core is localised along the exocyclic double bonds, due to its cross-conjugation, and not delocalised around the ring it seems sensible that the anions interacting with the π-system would not be perfectly aligned with the core centroid.

The structures which contain the tetrahedral anions, ClO_4^- or BF_4^-, display an anion conformation with either one or two of the peripheral atoms directed towards the [3]radialene core instead of three atoms an equal distance away from the aryl hydrogens which was observed in the calculated geometries. However, guidelines recently published by Hay and Custelcean state that a solid-state example of a true anion-π interaction should exhibit a geometry corresponding to electronic structure calculations. It is one of these structures, **4.13**, that exhibits both the closest anion atom to [3]radialene core carbon distance (3.02 Å) and the closest anion centroid to [3]radialene centroid distance (3.16 Å), which are both well within the Σ_{vdw} + 0.2 Å (for carbon and oxygen 3.42 Å) and as such the requirement of having a similar geometry to gas phase calculations in order to classify a solid-state anion-π interaction as significant appears to be too restrictive.

Overall the evidence provided by theoretical calculations, mass spectrometry and the examination of solid-state structures has shown that electron deficient, nitrile substituted hexaaryl[3]radialenes are capable of forming, and do in fact exhibit, anion-π interactions. These interactions are accompanied by anion hydrogen bonding with the peripheral aryl hydrogens which are located above and below the [3]radialene core. The detailed understanding of these interactions provided by this work may prove useful in the development of hexaaryl[3]radialenes as anion sensors.

Further to the principal study of the synthesis, coordination chemistry, and anion interactions of nitrile substituted hexaaryl[3]radialenes, an examination of the coordination chemistry of a series of flexible, dipyridyl ligands **2.51**, **2.52**, and **2.55**, produced as [3]radialene precursors, was also undertaken. A total of thirteen coordination polymers were synthesised from **2.51**, **2.52**, and **2.55** with silver(I) and copper(I). A particularly interesting structure formed was a 2-D (6,3) network produced via reaction of **2.51** with $AgPF_6$ (**6.15**). Due to the length and flexibility of the dipyridyl ligand the 2-D (6,3) network is highly corrugated instead of being planar, which is commonly observed in these types of structures. This corrugation allowed for the packing of the polymer nets in pairs of interdigitated sheets, which are further packed in layers sandwiching the counter anions. This structure also exhibited weak silver-alkyne interactions, which were only present in two of the eleven structures containing dipyridyl alkyne ligands. This was likely due to the myriad of other competing interactions present in these structures, in particular interactions with the pyridyl donors as well as the surrounding solvent.

Other structures of note included the ladder-like polymers **6.12** and **6.13**, which were found to have an identical connectivity but are not isomorphous; **6.12** has a compressed ladder-like structure whereas **6.13** has a more open structure. Structure **6.13** is more readily formed than **6.12** even though their morphological differences are due to only subtle changes in the angle around the methylene group of the ligand and the resultant distance between the pyridyl donors. Also two isomorphous coordination polymers of **2.55** with copper(I), **6.22**, and silver(I), **6.23**, which exhibit the common 2-D (4,4) topology, experience an interesting mode of 3-fold 2-D → 2-D parallel interpenetration. Due to the 'v'-shape of the ligands the 2-D structure is corrugated, which allows close packing of the (4,4) sheets in pairs. The two networks within these pairs are then interpenetrated with two networks of another pair however they do not interpenetrate each other. The resultant 3-fold interpenetrated stack of four sheets is then interdigitated with other stacks within the crystal lattice.

Overall the flexible dipyridyl ligands studied have produced some interesting coordination polymers. There is further scope for investigating the structures formed by these ligands upon

reaction with metal(II) salts. Due to their length and flexibility these ligands are probably not ideal for use in rigid metal-organic framework structures, targeted towards gas storage and other properties that are dependent on high surface areas and large pore volumes, as they will likely be highly interpenetrated. However, there is potential for their use in dynamic coordination polymers as hinted by the compressed and open polymorphs of the 1-D ladder-like structures **6.12** and **6.13**. Both the flexible dipyridyl compounds and the hexaaryl[3]radialenes reported herein make interesting ligands for use in metallo-supramolecular complexes and coordination polymers. Such structures have potential for application in the areas of catalysis, conductivity, luminescence and magnetism.

Appendices

Appendix 1: Views of the Asymmetric Units

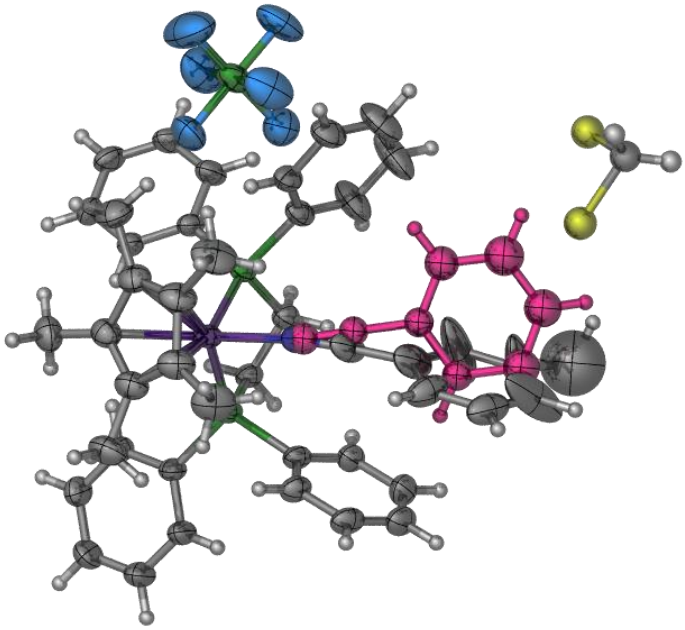

Figure A1.1. Asymmetric unit of [{RuCp*(dppe)}$_2$(**2.37**)](PF$_6$)$_2$ (**3.6**) with anisotropic displacement parameters represented as ellipsoids at the 50% probability level. The minor component of the disordered ligand is highlighted in pink. The disordered DCM molecule is represented as spheres.

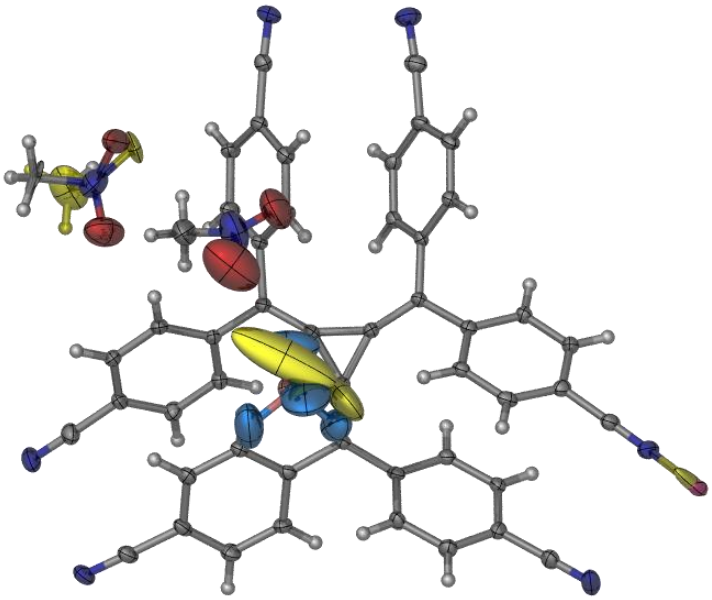

Figure A1.2. Asymmetric unit of **{**[Ag(**2.29**)]BF$_4$·2(CH$_3$NO$_2$)}$_n$ (**4.7**) with anisotropic displacement parameters represented as ellipsoids at the 50% probability level. The minor component of the disorder of the silver(I) cation, BF$_4^-$ anion and one nitromethane solvate molecule is shown in yellow.

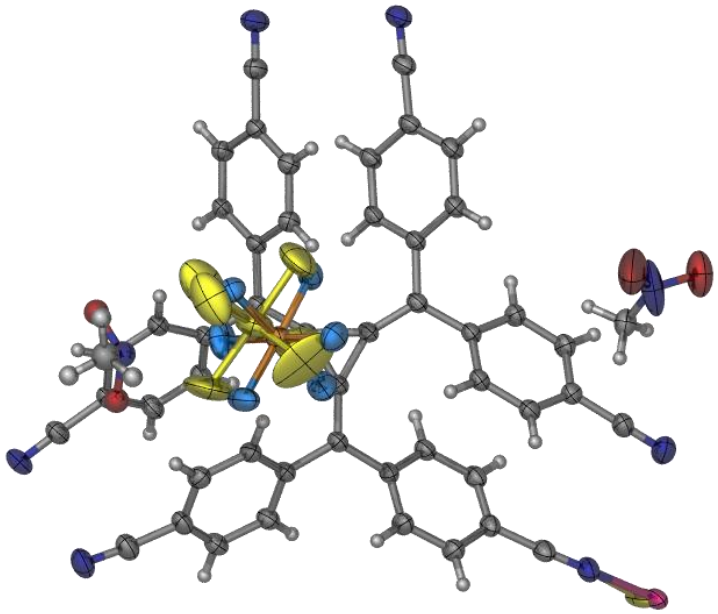

Figure A1.3. Asymmetric unit of {[Ag(**2.29**)]SbF_6·2(CH_3NO_2)}$_n$ (**4.8**) with anisotropic displacement parameters represented as ellipsoids at the 50% probability level. The minor component of the disorder of the silver(I) cation and SbF_6^- anion is shown in yellow. One disordered CH_3NO_2 molecule is represented as spheres.

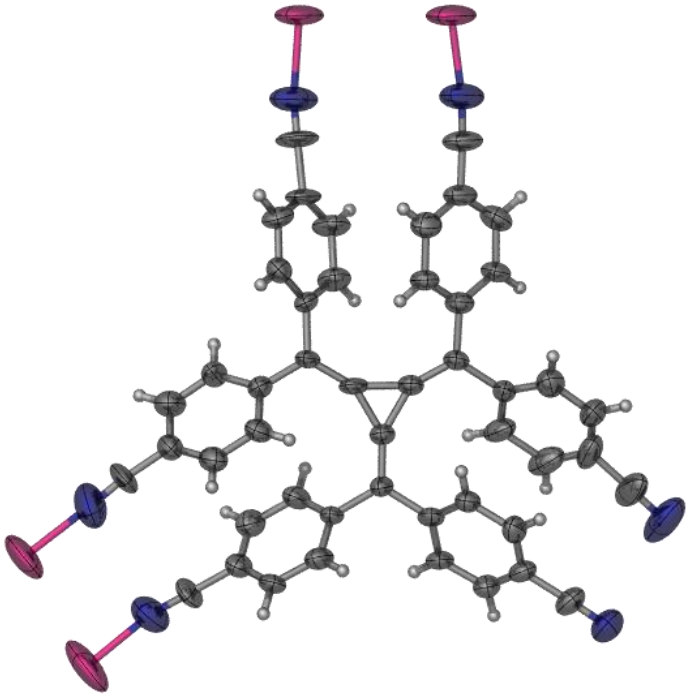

Figure A1.4. Asymmetric unit of {[Ag_3(**2.29**)](ClO_4)$_3$·CH_3NO_2}$_n$ (**4.9**) with anisotropic displacement parameters represented as ellipsoids at the 50% probability level.

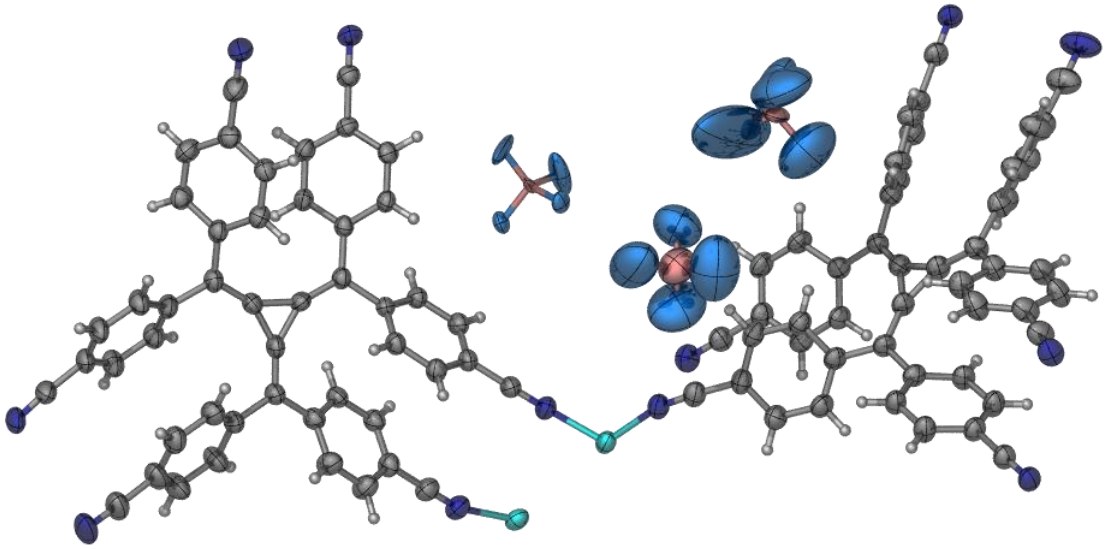

Figure A1.5. Asymmetric unit of $\{[Cu_2(\mathbf{2.29})_2](BF_4)_2 \cdot 20(CH_3NO_2)\}_n$ (**4.10a**) with anisotropic displacement parameters represented as ellipsoids at the 50% probability level.

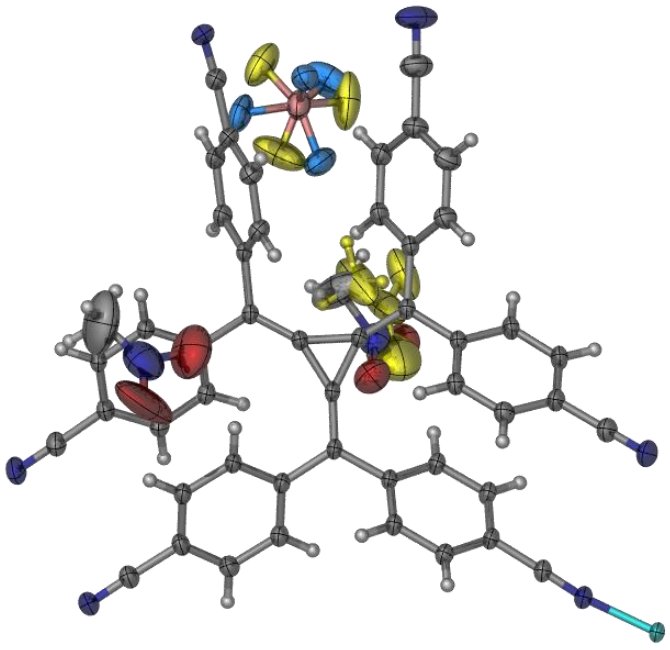

Figure A1.6. Asymmetric unit of $\{[Cu(\mathbf{2.29})]BF_4 \cdot 2(CH_3NO_2)\}_n$ (**4.10b**) with anisotropic displacement parameters represented as ellipsoids at the 50% probability level. The minor components of the disorder of the BF_4^- anion and one CH_3NO_2 solvate molecule are shown in yellow.

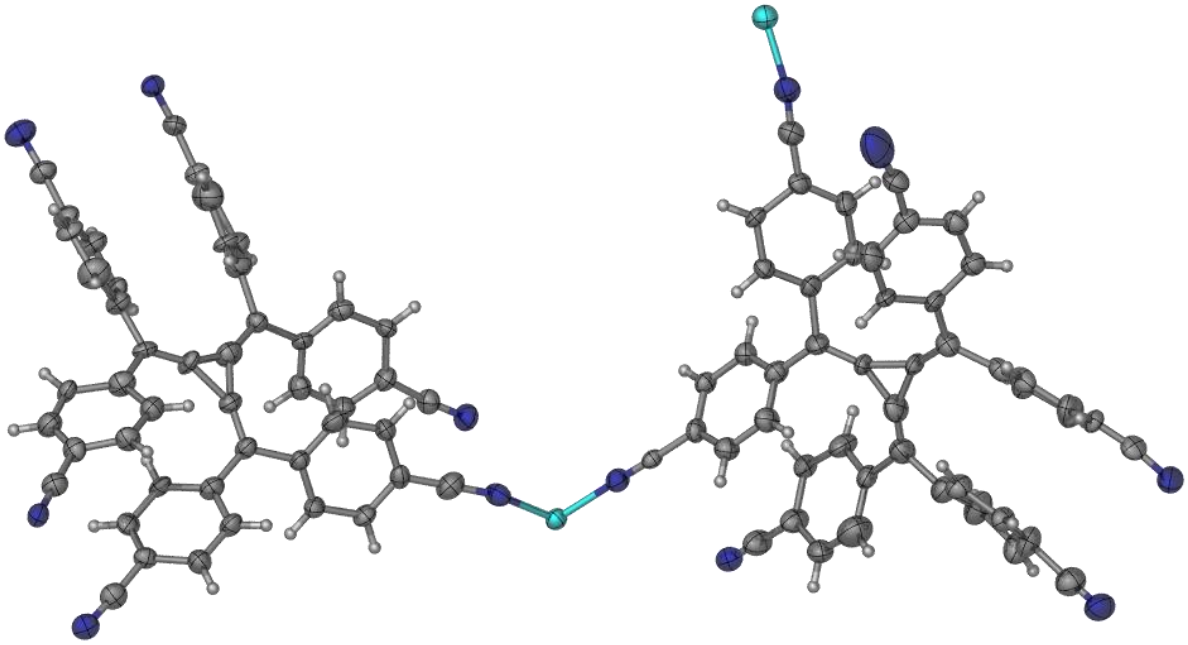

Figure A1.7. Asymmetric unit of $\{[Cu_2(\mathbf{2.29})_2](PF_6)_2 \cdot 14(CH_3NO_2)\}_n$ (**4.11a**) with anisotropic displacement parameters represented as ellipsoids at the 50% probability level.

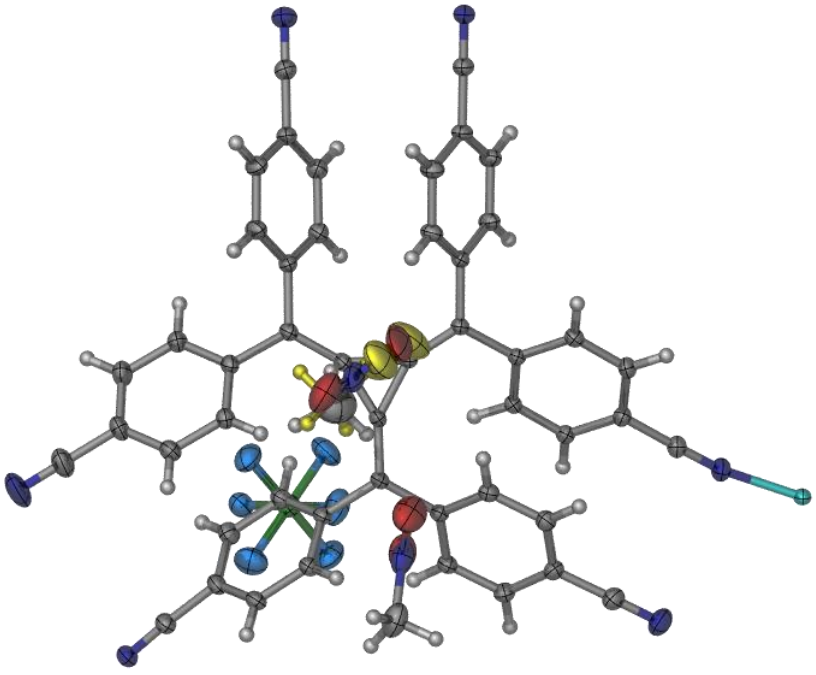

Figure A1.8. Asymmetric unit of $\{[Cu(\mathbf{2.29})]PF_6 \cdot 2(CH_3NO_2)\}_n$ (**4.11b**) with anisotropic displacement parameters represented as ellipsoids at the 50% probability level. The minor component of the disorder of one CH_3NO_2 solvate molecule is shown in yellow.

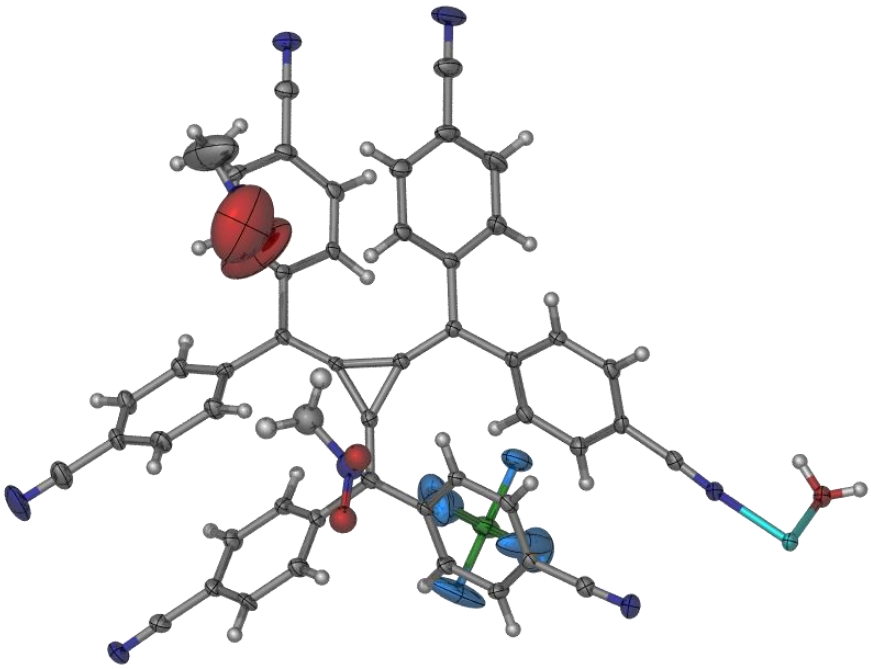

Figure A1.9. Asymmetric unit of $\{[Cu(\mathbf{2.29})_2(H_2O)_2](PF_6)_2 \cdot 4(CH_3NO_2)\}_n$ (**4.12**) with anisotropic displacement parameters represented as ellipsoids at the 50% probability level. One disordered CH_3NO_2 molecule is represented as spheres.

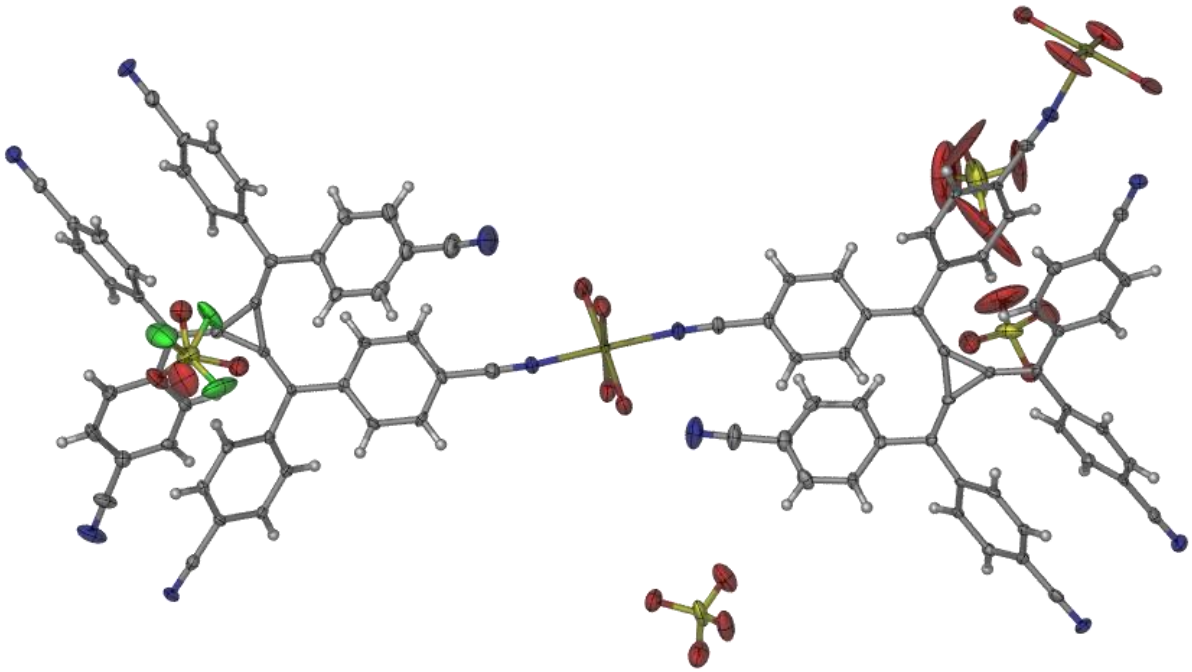

Figure A1.10. Asymmetric unit of $\{[Fe_2(\mathbf{2.29})_2(H_2O)_8](ClO_4)_4 \cdot CH_3NO_2 \cdot 2H_2O\}_n$ (**4.13**) with anisotropic displacement parameters represented as ellipsoids at the 50% probability level. The minor component of the disorder of one ClO_4^- anion is shown in green. Due to unresolved disorder one oxygen atom of the disordered ClO_4^- anion is represented as a sphere.

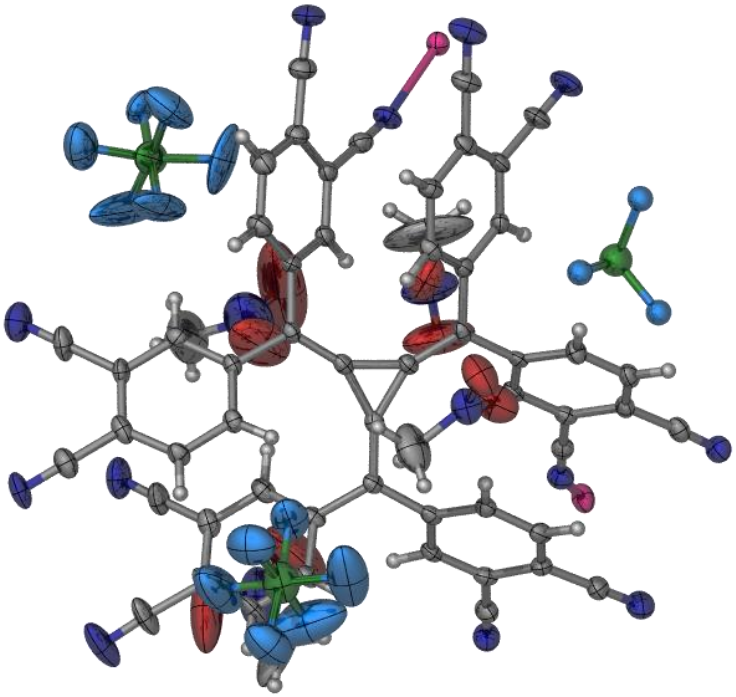

Figure A1.11. Asymmetric unit of $\{[Ag_2(\mathbf{2.44})](PF_6)_2 \cdot 7(CH_3NO_2)\}_n$ (**4.14**) with anisotropic displacement parameters represented as ellipsoids at the 50% probability level. The PF_6^- anion on the special position is represented as spheres.

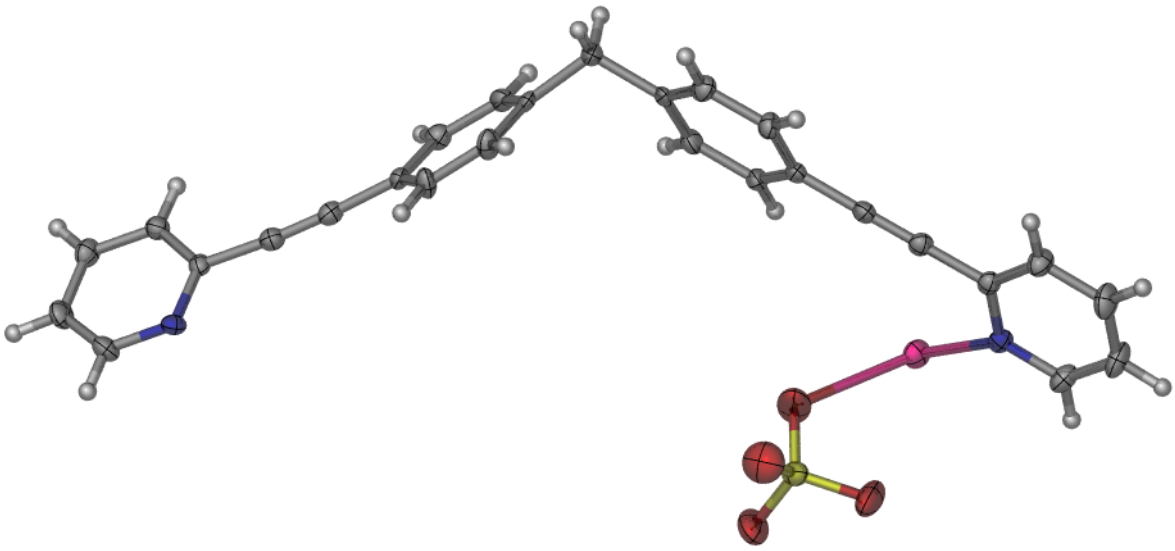

Figure A1.12. Asymmetric unit of $\{[Ag(\mathbf{2.51})]ClO_4\}_n$ (**6.11**) with anisotropic displacement parameters represented as ellipsoids at the 50% probability level.

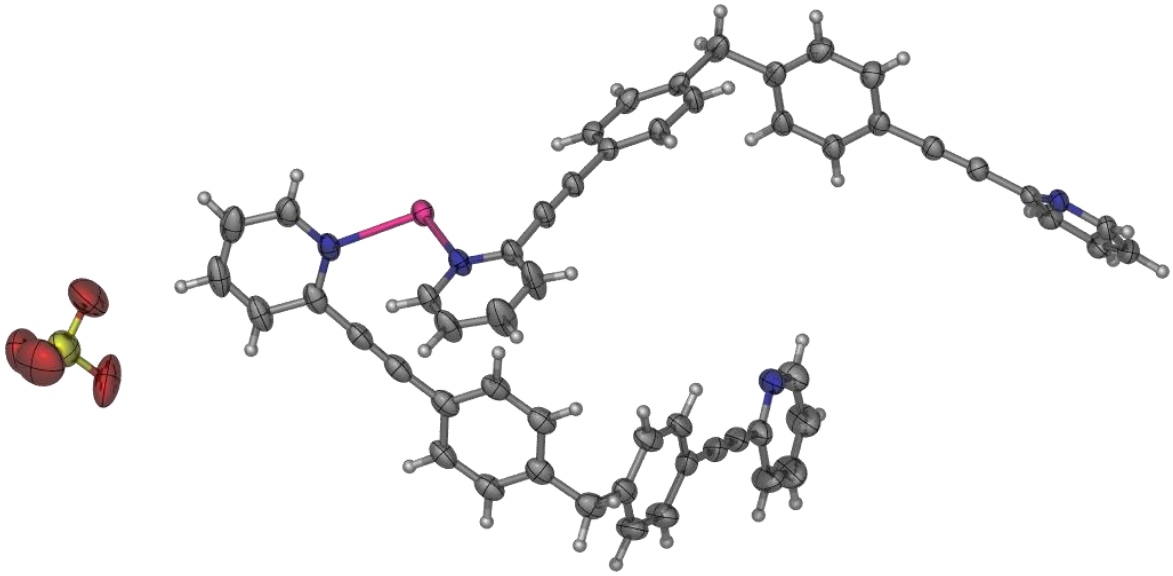

Figure A1.13. Asymmetric unit of {[Ag(**2.29**)$_2$]ClO_4·3(CH_3OH)} (**6.12**) with anisotropic displacement parameters represented as ellipsoids at the 50% probability level.

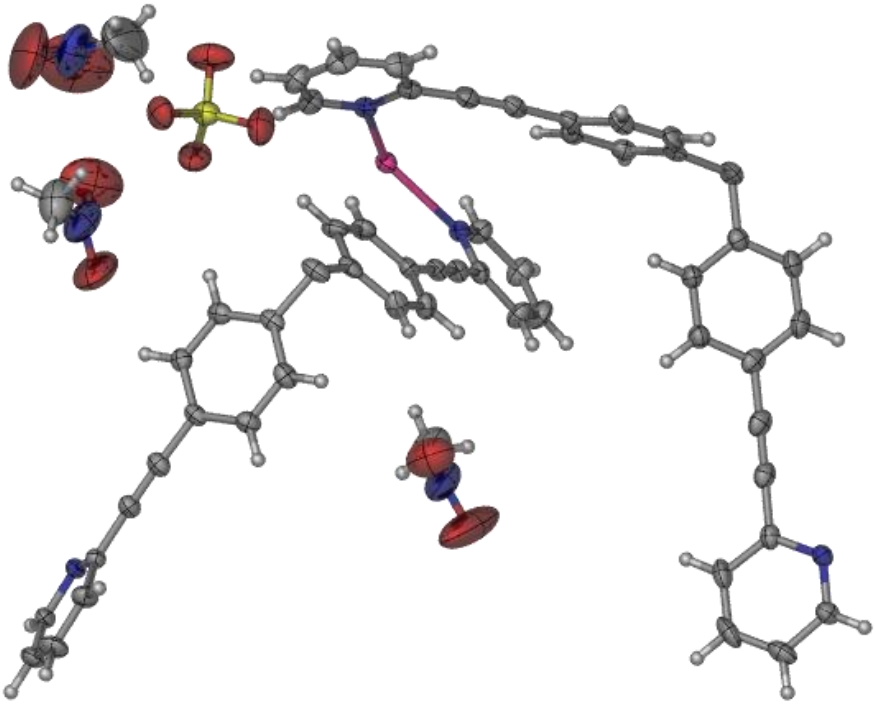

Figure A1.14. Asymmetric unit of {[Ag(**2.51**)$_2$]ClO_4·3(CH_3NO_2)}$_n$ (**6.13**) with anisotropic displacement parameters represented as ellipsoids at the 50% probability level.

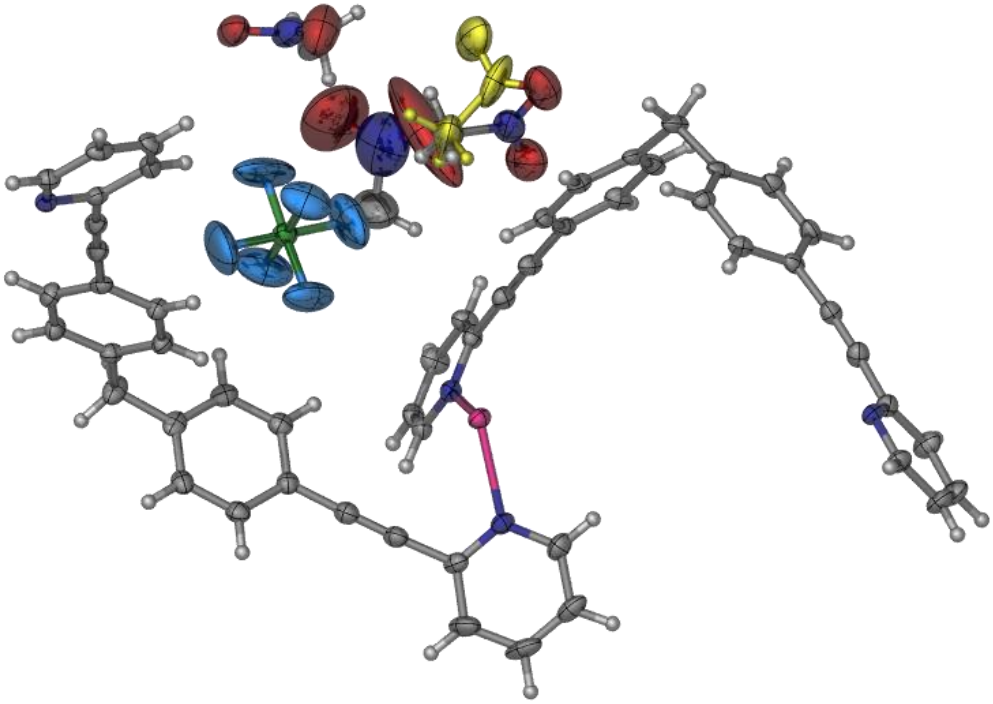

Figure A1.15. Asymmetric unit of $\{[Ag(\mathbf{2.51})_2]PF_6 \cdot 3(CH_3NO_2)\}_n$ (**6.14**) with anisotropic displacement parameters represented as ellipsoids at the 50% probability level. The minor component of the disordered CH_3NO_2 solvate molecule is shown in yellow.

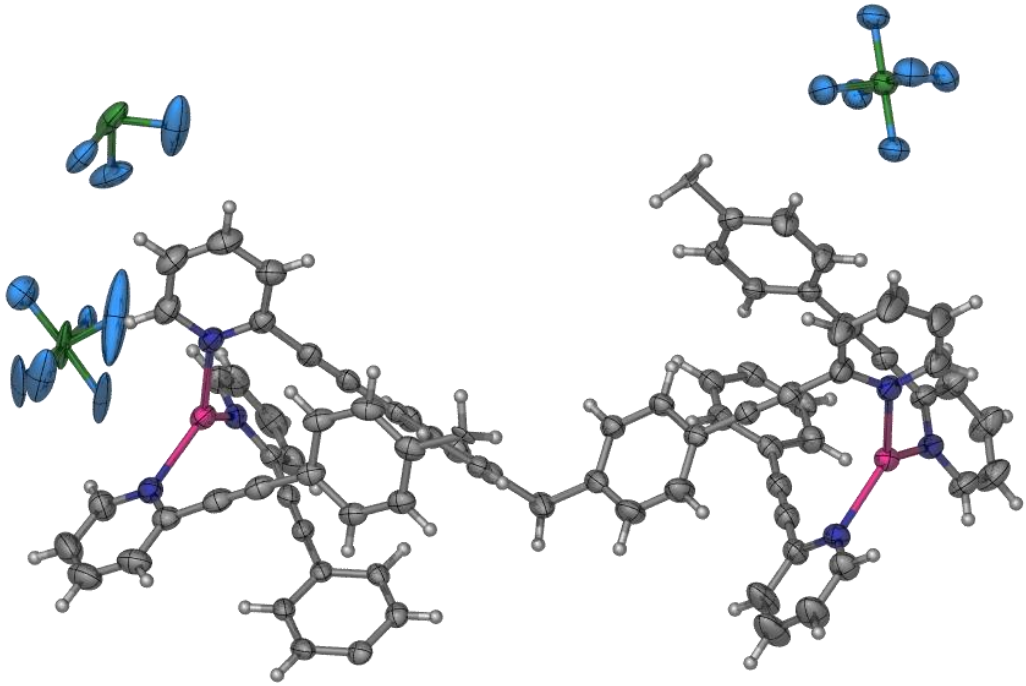

Figure A1.16. Asymmetric unit of $\{[Ag_2(\mathbf{2.51})_3](PF_6)_2 \cdot 2(CH_3OH)\}_n$ (**6.15**) with anisotropic displacement parameters represented as ellipsoids at the 50% probability level. The two PF_6^- anions to the left of the image are represented as ellipsoids at the 20% probability level due to disorder.

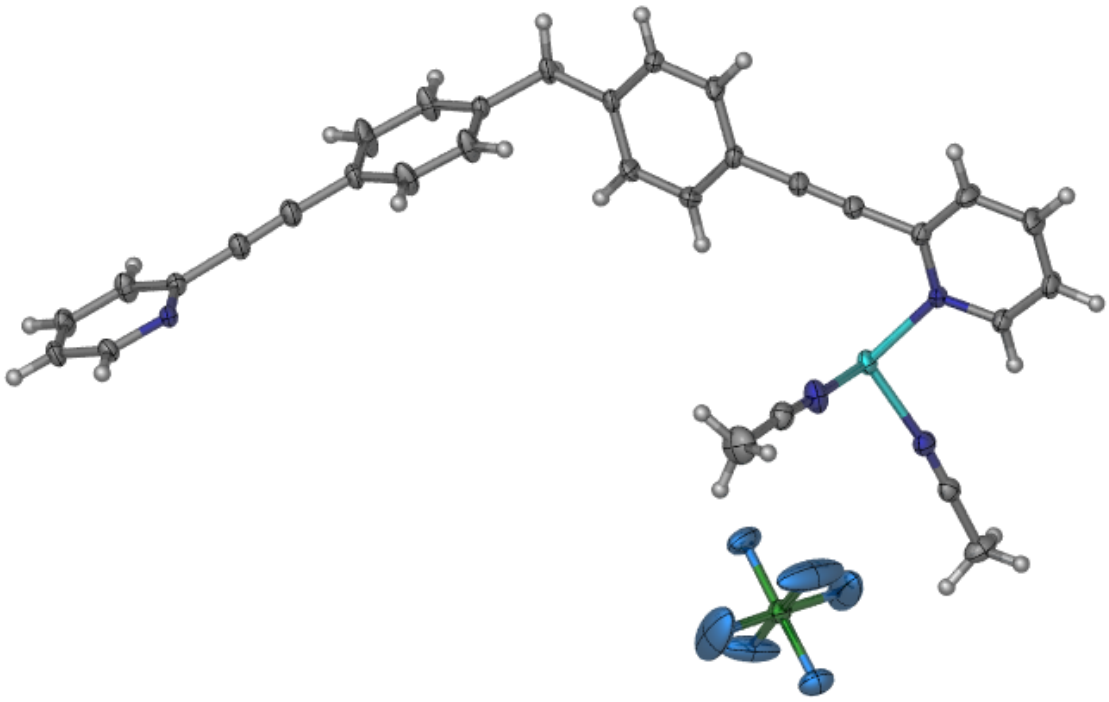

Figure A1.17. Asymmetric unit of $\{[Cu(\mathbf{2.51})(CH_3CN)_2]PF_6\}_n$ (**6.16**) with anisotropic displacement parameters represented as ellipsoids at the 50% probability level.

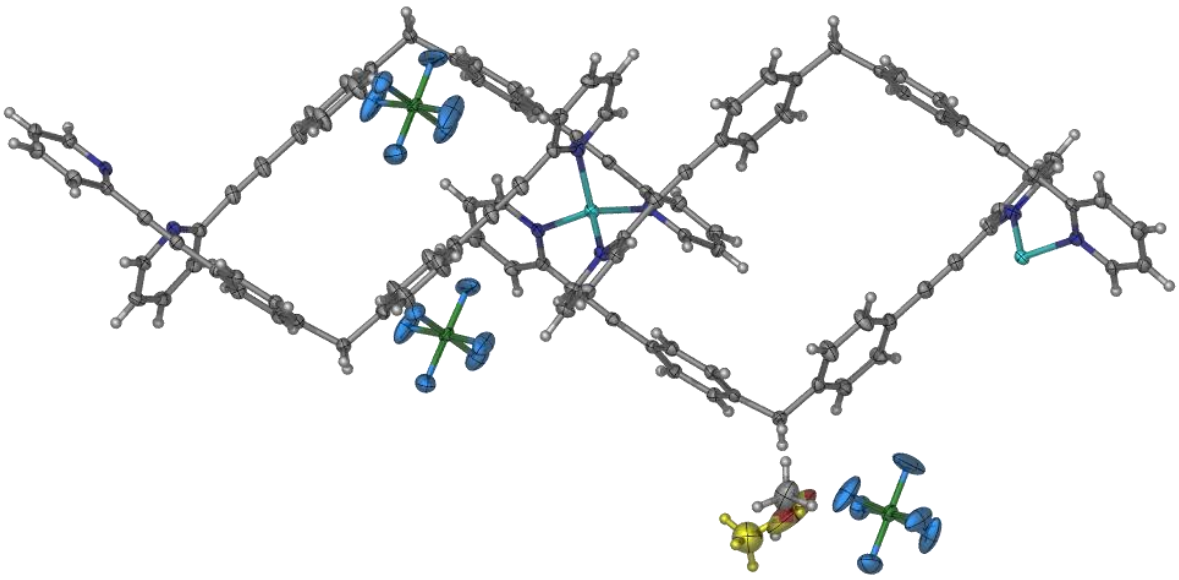

Figure A1.18. Asymmetric unit of $\{[Cu_2(\mathbf{2.51})_4](PF_6)_2 \cdot CH_3OH\}_n$ (**6.17**) with anisotropic displacement parameters represented as ellipsoids at the 50% probability level. The minor component of the disordered MeOH solvate molecule is shown in yellow.

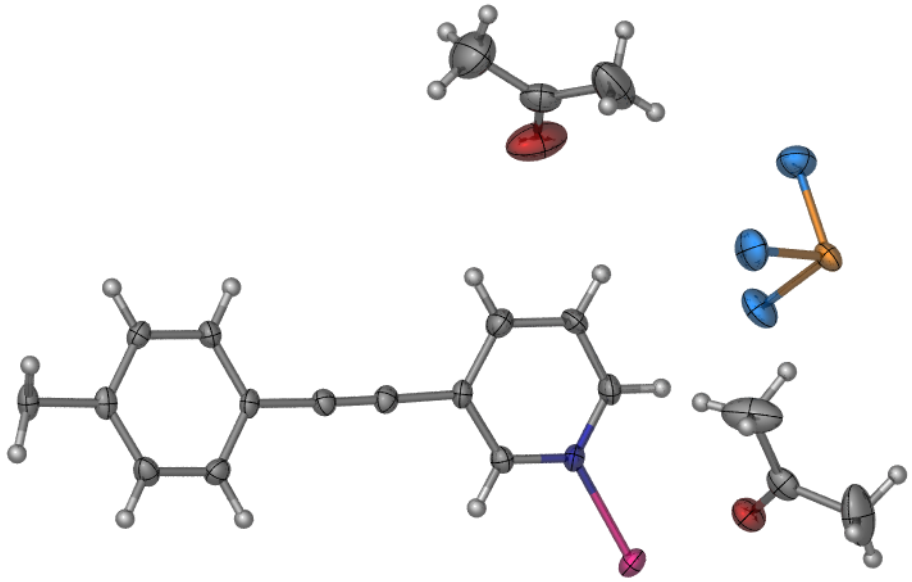

Figure A1.19. Asymmetric unit of {[Ag(**2.52**)]SbF_6·4(CH_3OCH_3)}$_n$ (**6.18**) with anisotropic displacement parameters represented as ellipsoids at the 50% probability level. The SbF_6^- anion is on a special position.

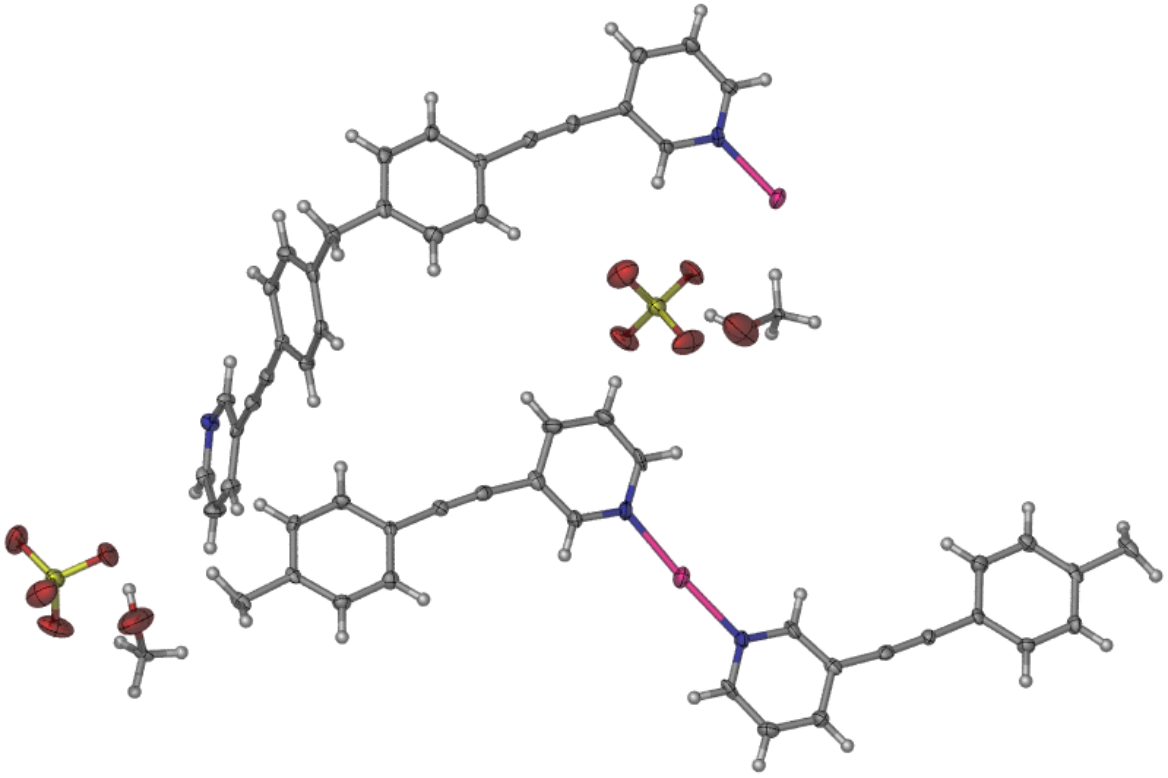

Figure A1.20. Asymmetric unit of {[Ag(**2.52**)]ClO_4·(CH_3OH)}$_n$ (**6.19**) with anisotropic displacement parameters represented as ellipsoids at the 50% probability level.

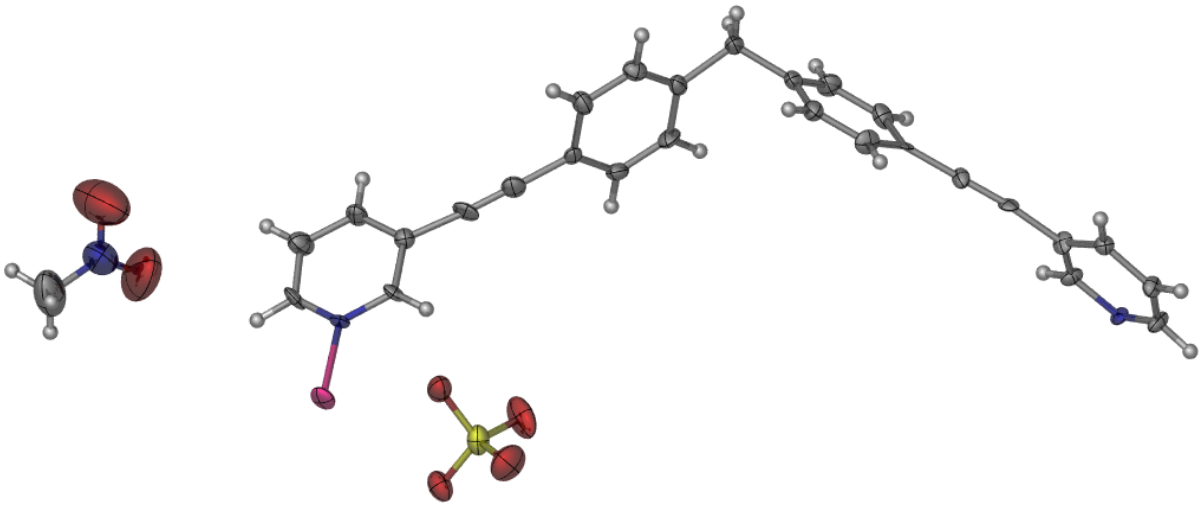

Figure A1.21. Asymmetric unit of {[Ag(**2.52**)]$ClO_4 \cdot CH_3NO_2$}$_n$ (**6.20**) with anisotropic displacement parameters represented as ellipsoids at the 50% probability level.

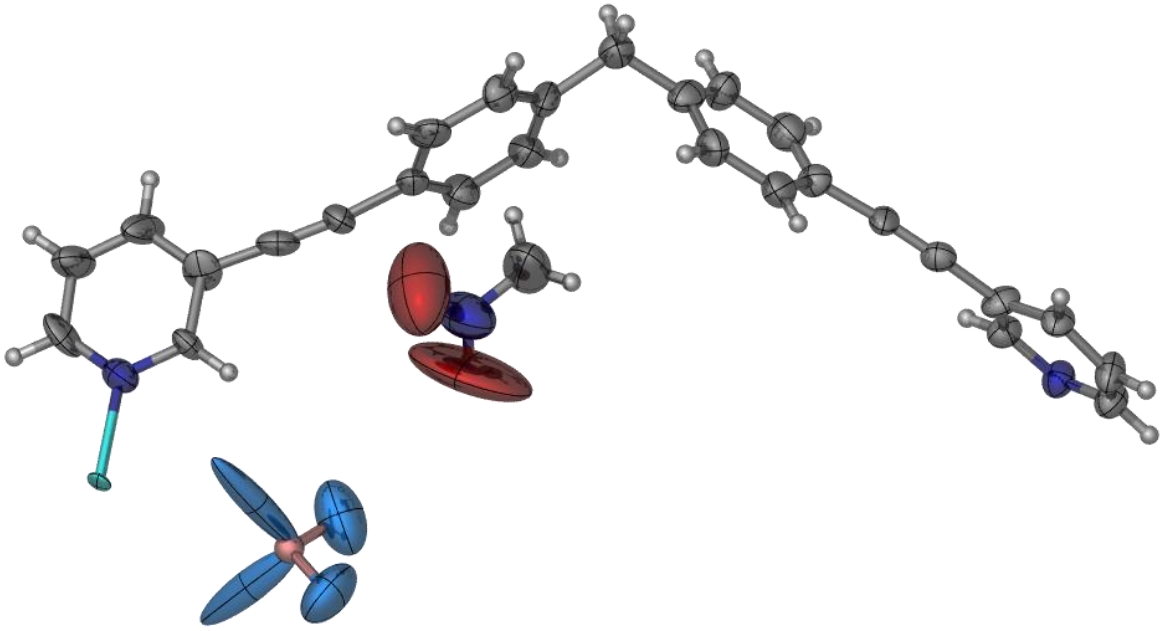

Figure A1.22. Asymmetric unit of {[Cu(**2.52**)]$BF_4 \cdot CH_3NO_2$}$_{\boldsymbol{n}}$ (**6.21**) with anisotropic displacement parameters represented as ellipsoids at the 50% probability level. Due to unresolved disorder the boron atom is represented as a sphere.

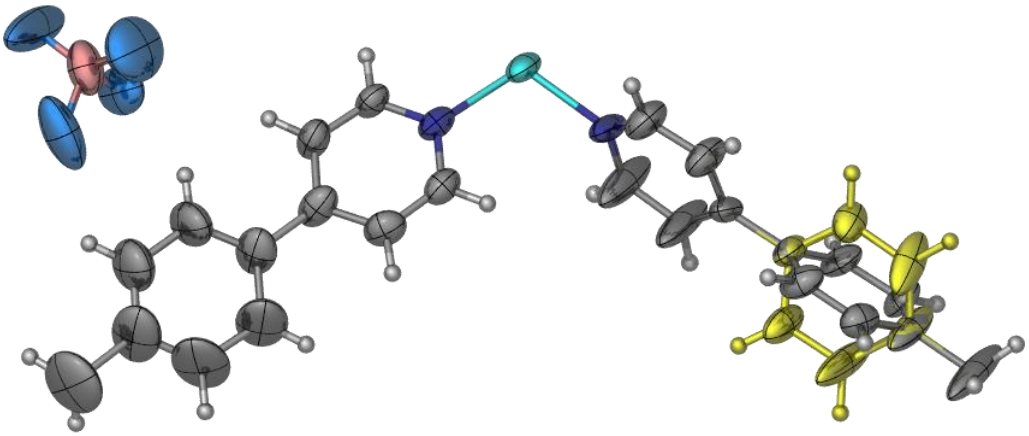

Figure A1.23. Asymmetric unit of {[Cu(**2.55**)$_2$]BF_4}$_n$ (**6.22**) with anisotropic displacement parameters represented as ellipsoids at the 50% probability level. The minor component of the disordered benzene ring is shown in yellow.

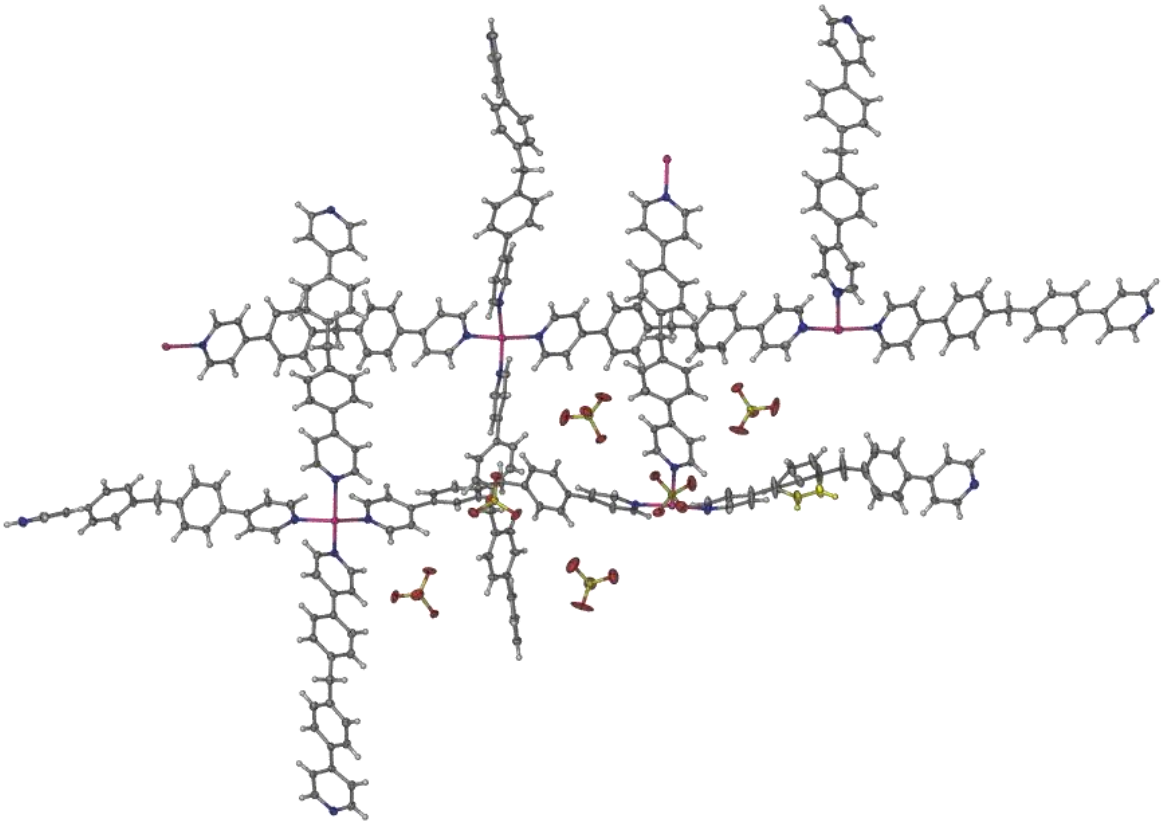

Figure A1.24. Asymmetric unit of {[Ag(**2.55**)$_2$]ClO_4}$_n$ (**6.23**) with anisotropic displacement parameters represented as ellipsoids at the 50% probability level. The minor component of the disordered benzene ring is shown in yellow.

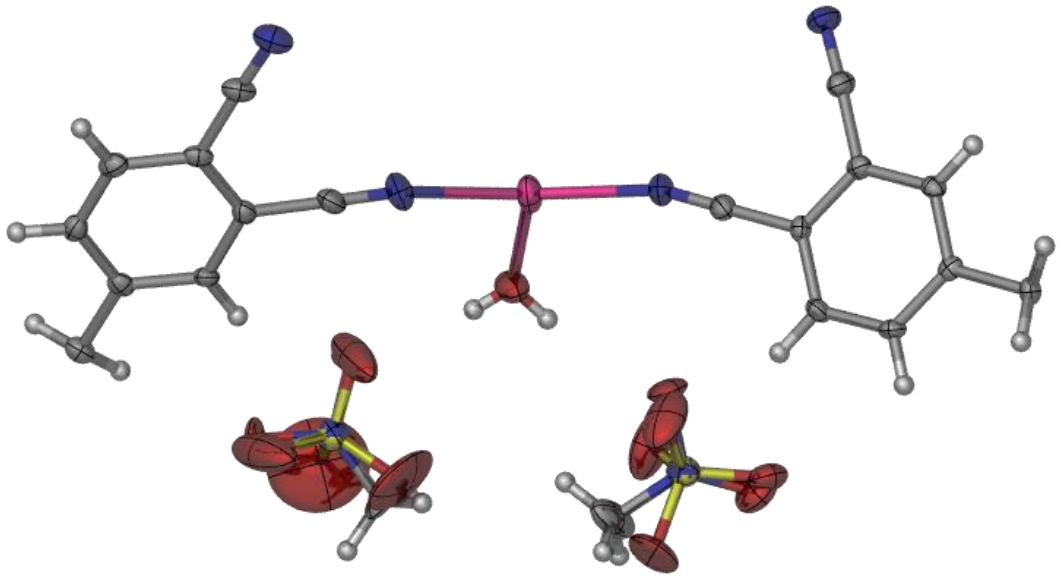

Figure A1.25. Asymmetric unit of $\{[Ag(\mathbf{2.43})(H_2O)]ClO_4 \cdot CH_3NO_2\}_n$ (**6.24**) with anisotropic displacement parameters represented as ellipsoids at the 50% probability level.

Appendix 2: Cyclic Voltammograms

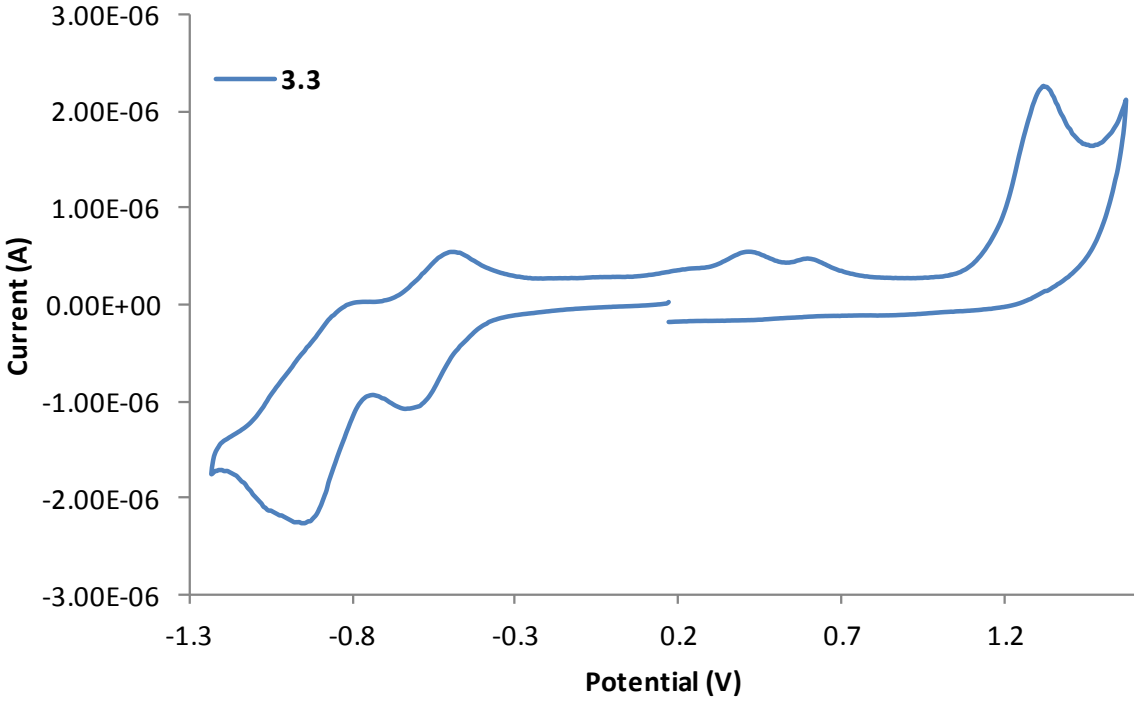

Figure A2.1. Cyclic voltammogram of complex **3.3** (1mM in dichloromethane/0.1M $[(n\text{-}C_4H_9)_4]NPF_6$, platinum working electrode and ferrocene internal standard).

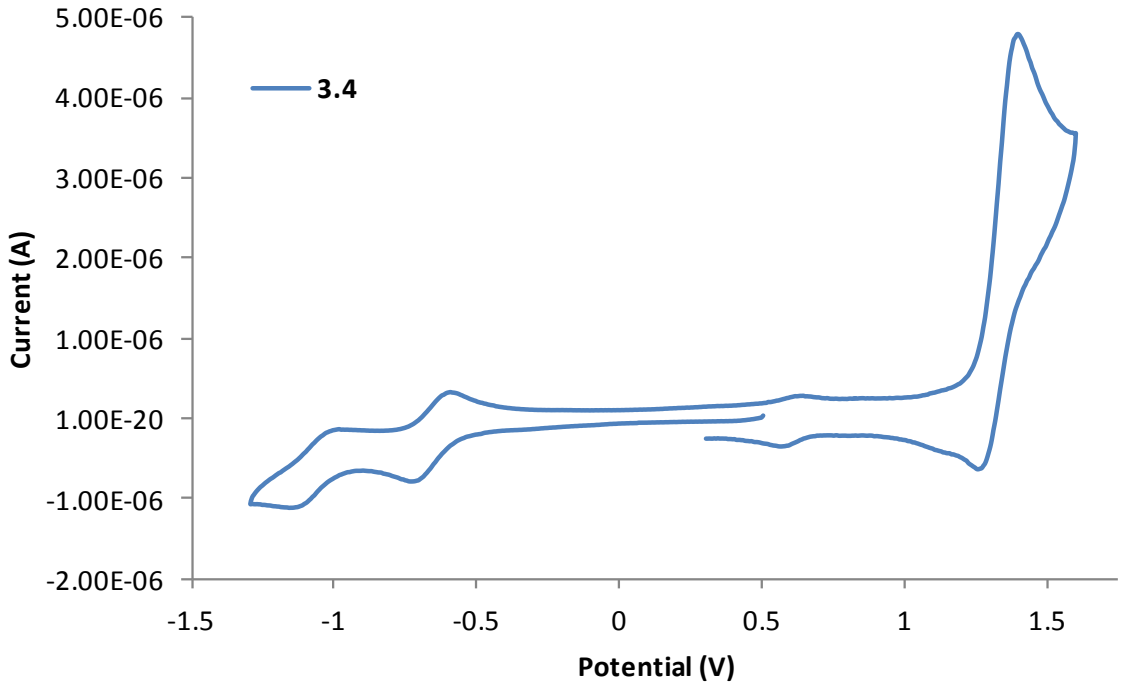

Figure A2.2. Cyclic voltammogram of complex **3.4** (1mM in dichloromethane/0.1M $[(n\text{-}C_4H_9)_4]NPF_6$, platinum working electrode and ferrocene internal standard).

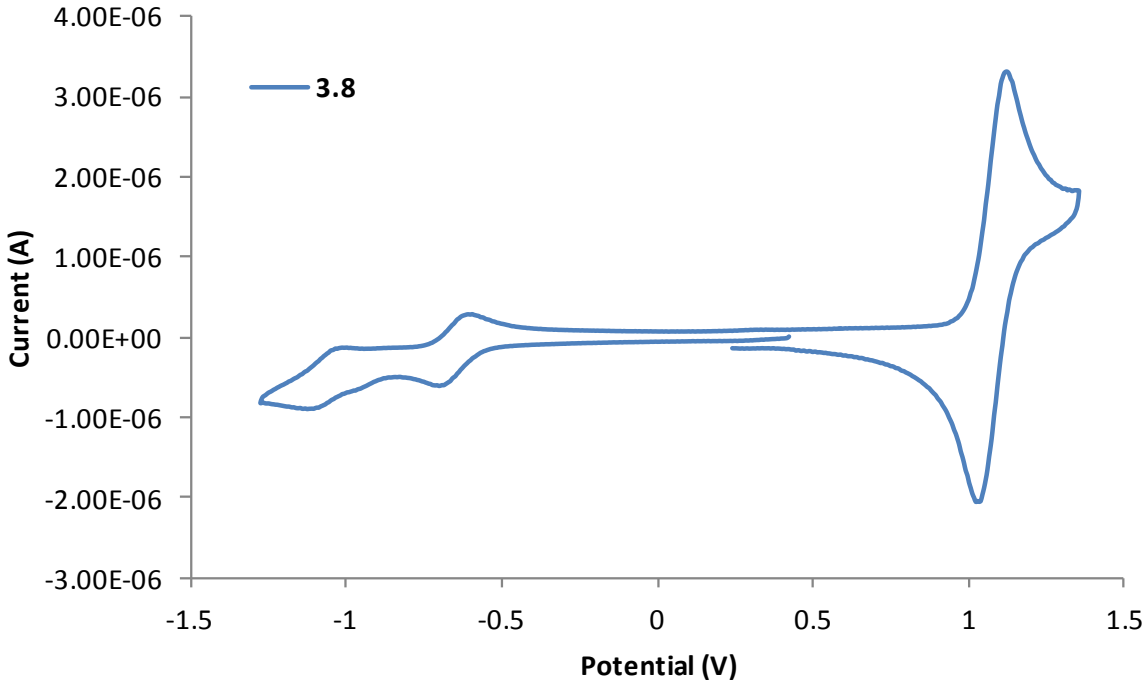

Figure A2.3. Cyclic voltammogram of complex **3.8** (1mM in dichloromethane/0.1M $[(n\text{-}C_4H_9)_4]NPF_6$, platinum working electrode and ferrocene internal standard).

Appendix 3: List of Publications

The following is a list of publications that have resulted from the research work described in this thesis.

1. Antonio Avellaneda, Courtney A. Hollis, Xin He and Christopher J. Sumby, Fluorescent hexaaryl- and hexa-heteroaryl[3]radialenes: Synthesis, structures, and properties, *Beil. J. Org. Chem.*, *8*, **2012**, 71-80.
2. Jack D. Evans, Courtney A. Hollis, Sandra Hack, Alexander S. Gentleman, Peter Hoffman, Mark A. Buntine and Christopher J. Sumby, Anion-π Interactions of Hexaaryl[3]radialenes, *J. Phys. Chem. A.*, *116*, **2012**, 8001-8007.
3. Courtney A. Hollis, Stuart R. Batten and Christopher J. Sumby, Two-Dimensional and Three-Dimensional Coordination Polymers of Hexakis(4-cyanophenyl)[3]radialene: The Role of Stochiometry and Kinetics, *Cryst Growth Des.*, *13*, **2013**, 2350-2361.